School of Earth and Planetary Sciences

SEDIMENTOLOGY AND PROVENANCE OF NE AUSTRALIAN PROTEROZOIC BASINS WITH RELEVANCE TO THE FORMATION OF THE SUPERCONTINENT NUNA

Adam Richmond Nordsvan

This thesis is presented for the Degree of

Doctor of Philosophy - Applied Geology

Curtin University

July 2019

Declaration

To the best of my knowledge, this thesis contains no material previously published by any other person except where due acknowledgment has been made. This thesis contains no material which has been accepted for the award of any other degree or diploma in any university.

I acknowledge that the copyright of published works contained within this thesis rest with the copyright holders of those works. Where necessary, I have obtained permission from the copyright holders to use any material reproduced in this thesis, including the use of my own published works (journal articles) which are held by another party (e.g. publishers).

Adam R. Nordsvan 04/07/2019

Abstract

The tectonic evolution of North Australian Craton (NAC) throughout the Paleo- to Mesoproterozoic is intimately tied to the amalgamation of supercontinent Nuna. In NE Australia at the eastern margin of the NAC, Proterozoic rocks occur in five main inliers, the Mount Isa Inlier in western Queensland, and further to the east, the Georgetown, Dargalong, Coen and Yambo inliers. The geological relationship between the eastern inliers and the NAC has always been questionable, however, most authors suggest they share a similar history from at-least ca. 1.75 Ga. This study focusses on the sedimentological and (detrital zircon) geochronological evolution between the Mount Isa and Georgetown inliers, both of which consist of Paleo- to Mesoproterozoic sedimentary rocks that have experienced relatively complex deformational and metamorphic histories. The aim of this thesis is to better understand the tectonic evolution of the NAC and its position in the supercontinent Nuna.

Detrital zircon geochronology is an important technique for reconstructing ancient supercontinents. The method aids in tying sedimentary rocks with their potential source regions and allows for a wide range of geological questions to be addressed. Statistical methods to compare detrital zircon samples is imperative for investigating large datasets, such is often the case when studying past supercontinents. One such method, multidimensional scaling (MDS) has become the most prominent technique utilised, however, it is not without limitations. These limitations become accentuated when comparing datasets obtained from different studies, or when comparing

detrital zircon data with potential source regions. These limitations can be overcome by a new resampling method developed within this thesis. The utility of this method is demonstrated on the Roper Group of the McArthur Basin and on detrital zircon samples from the Mount Isa Inlier.

Within the supercontinent Nuna, NE Australia occupies a position juxtaposed with western Laurentia. Critical links between Australia and Laurentia are observed in the detrital zircon record from the Georgetown Inlier that show two distinct changes in provenance. The lowermost units (depositional age ca. 1700–1650 Ma) have a detrital zircon provenance that strongly resembles Laurentian source rock ages and the similar-aged Wernecke Supergroup of northwest Laurentia. Up-sequence, sediments deposited from ca. 1650 to 1600 Ma show a unimodal proximal signature thought to have been sourced locally, and sediments deposited after ca. 1550 Ma have detrital zircon age spectra similar to the Mount Isa Inlier. This new and existing detrital zircon data, along with new paleocurrent measurements, strongly suggest that the Georgetown Inlier was an allochthonous block that collided with the Mount Isa Inlier and the NAC during the amalgamation of Nuna.

To examine the basin history of the Mount Isa Inlier leading to the amalgamation of Nuna, the oldest sequence was targeted. Sedimentology, sequence stratigraphy and detrital zircon geochronology are utilised to challenge previously correlated units from the central and eastern belts of the inlier. The results indicate that sediments of the Mary Kathleen Group in the central belt correlate with the Myally Supersequence in the western belt rather than the Quilalar Supersequence, as previously suggested.

In addition, contrasting sedimentology and stratigraphy suggest that the Mitakoodi Quartzite of the eastern belt do not correlate with the Ballara Quartzite (central belt) as previously proposed. These spurious correlations have been used as evidence to propose that the entire Mount Isa Inlier evolved collectively from ca. 1.85 to 1.5 Ga. However, the contrasting stratigraphy between the Mitakoodi to Ballara quartzites might suggest that the eastern belt of the inlier evolved allochthonous from the NAC ca. 1.75 Ga. Furthermore, detrital zircon from the Mitakoodi Quartzite is statistically dissimilar from all other samples from the Mount Isa Inlier, largely due to the addition of a ca. 2.58 Ga population. Zircon populations of this age (ca. 2.58 Ga) are uncommon in the NAC but common in Laurentian sedimentary rocks deposited at a similar age, hinting at a possible link between the eastern belt of the Mount Isa Inlier and Laurentia at ca. 1.75 Ga. If indeed the eastern belt of the Mount Isa Inlier has a true affinity with Laurentia than either it was an exotic terrane accreted to the eastern margin of the NAC at ca. 1.72 Ga or Laurentia was more proximal to Australia during this period.

Several crustal-scale breaks observed from seismic profiles between the Mount Isa and Georgetown inliers have been interpreted as possible sutures. However, other than geophysical images, basement rocks between the two inliers are relatively unknown. To examine the nature of the intermediate basement, zircon from granitic samples intersected by drill core were analysed for U-Pb ages Lu-Hf isotope geochemistry. The granites, from approximately 100 km west of the Georgetown Inlier (outcrop extent) have an I-type affinity and ages of ca. 1.54 Ga. In contrast, granites in the Georgetown Inlier are predominantly S-type and have ca. 1.56 Ga

ages. The Lu-Hf composition from zircon in the basement granites are slightly more enriched and have younger model ages than those from the granites in the Georgetown Inlier. On the other hand, these granites from the basement are similar in age and composition with the Maramungee Granite from the eastern belt of the Mount Isa Inlier. Comparing the zircon Lu-Hf composition of the basement granites with limited data from both the eastern Mount Isa and Georgetown inliers indicates they are more similar with zircon from the eastern Mount Isa Inlier. The trends in Lu-Hf composition for the region might reflect ongoing subduction post-1.6 Ga or might reflect changes in the composition of the basement they intruded. From the western Mount Isa Inlier eastward to the Georgetown Inlier there are two distinct changes in the whole rock Sm-Nd and Lu-Hf two-stage model ages that could be related to the different terranes accreted to the eastern margin of the NAC during the amalgamation of Nuna. The first, possibly the eastern belt of the Mount Isa Inlier and the second, the Georgetown Inlier. Ultimately, these new findings suggest that the connection between Australia and Laurentia was relatively dynamic leading to the final amalgamation of the supercontinent. Nevertheless, further work is required to fully understand the tectonic evolution of this complex region.

"No amount of experimentation can ever prove me right;
a single experiment can prove me wrong."
– Albert Einstein

Acknowledgments

First and foremost, I would like to express my sincere appreciation to my primary supervisors Professors Zheng-Xiang Li, and Bill Collins, thank you for your patience, guidance and sound advice. To my supervisor Dr Amaury Pourteau, it has been great to get to know you, thanks for all the support, the assistance in the field, and challenging discussions. I also appreciate supervision from Dr Chris Spencer. To every member of the Earth Dynamics Research Group, past and present. You guys have made the last three years extremely entertaining; it has been very stimulating and an absolute pleasure discussing science with all of you. A special mention to Dr Uwe Kirscher and Dr Ross Mitchell. I think you guys became damn good Aussies over the last few years, it has been a pleasure to get to know you both, and I'm happy to call you good mates. It is hard to express how much gratitude I have for Ian Withnall from the Geological Survey of Queensland. He went out of his way to help on numerous occasions, and everything would have been much harder without his support, thank you. I would also like to thank Professor Pete Betts for taking the time to share his extensive knowledge of Proterozoic Australia, you're a bloody legend. To my PhD siblings, Jiangyu Li, and Silvia Volante, thanks for the assistance in the field and the long discussions about all things NE Australia. You guys are great, and I truly believe you will both succeed in any endeavour you take, and I wish you all the best.

I must also thank my amazing family for supporting me through this decision to chase my passion for science. I know it was tough to watch me reset my life, thanks for everything. And finally, to my amazing partner Erin. It might have appeared to go unnoticed, but I've got it all here in my heart. Did you ever know that you're my hero? You are the wind beneath my wings.

"I was not proud of what I had learned,
but I never doubted that it was worth knowing."
– Hunter S. Thompson

Table of Contents

Declaration ..... **ii**

Abstract ..... **iii**

Acknowledgments ..... **vii**

Table of Contents ..... **viii**

List of figures ..... **xiii**

List of tables ..... **xxii**

Chapter 1: Introduction **1**

1.1 NE Australia in Nuna reconstructions 2

1.2 Geological Background 6

1.3 Thesis structure 9

1.4 References 11

Chapter 2: Resampling (detrital) zircon age distributions for accurate Multidimensional Scaling solutions **18**

2.1 Abstract 18

2.2 Introduction 19

2.3 Multidimensional Scaling in detrital zircon geochronology 22

2.3.1 Method 1: Bootstrap resampling and Procrustes rotation (BoPR) 30

2.3.2 Method 2: Error resampling MDS (ERM) 36

2.4 Real-world case study: The Proterozoic Roper Group, Australia 37

2.4.1 Methods 38

2.4.2 Results 39

2.4.3 Discussion 45

2.5 Conclusions 46

2.6 Acknowledgements 47

2.7 References 47

Chapter 3: Laurentian crust in northeast Australia: Implications for the assembly of the supercontinent Nuna 52

3.1 Abstract 52

3.2 Introduction 53

3.3 Geological Setting 54

3.4 Methods and Results 56

3.5 Discussion of the Provenance Results 57

3.6 Tectonic Reconstruction 58

3.7 Implications for Nuna Assembly 60

3.8 Acknowledgments 62

3.9 References 63

Chapter 4: Contrasting stratigraphy and provenance in the Mount Isa Inlier: Implications for the Nuna supercontinent 67

4.1 Abstract 67

4.2 Introduction 68

4.3 Stratigraphic context and study regions 71

4.4 Methodology 77

4.4.1 Sedimentology and stratigraphy 77

4.4.2 Detrital zircon geochronology 78

4.5 Sedimentology 80

4.5.1 Facies Associations 80

4.5.2 Measured sections 82

4.5.3 Basin evolution 96

4.6 Detrital zircon sampling and results 102

4.6.1 BAL1701 102

4.6.2 BAL1703 105

4.6.3 BAL1706 106

4.6.4 COR1701 107

4.6.5 COR1702e 107

4.6.6 MQ02 108

4.6.7 MQ01 109

4.6.8 MIT1701 110

4.6.9 MIT1705A 111

4.6.10 Multidimensional scaling (MDS) 112

4.7 Discussion 113

4.7.1 Timing of deposition, and correlations 113

4.7.2 Detrital Zircon Provenance 116

4.7.3 Tectonic implications 126

4.8 Conclusions 128

4.9 References 129

Chapter 5: New U-Pb ages and Lu-Hf isotope data from Mesoproterozoic granites in NE Australia 145

5.1 Abstract 145

5.2 Introduction 146

5.3 Geological Setting 149

5.4 Methods 151

5.5 Samples and Results 154

5.5.1 Forsayth Granite (FOG01) (UTM54: 760190 / 7975926) 154

5.5.2 Macartneys Granite (PGE01) (UTM54: 706725 / 7974131) 156

5.5.3 Esmeralda Granite (CUG01) (UTM54: 706725 / 7974131) 158

5.5.4 Cudgee Creek Granite (042) (Drill hole: HBPD001, UTM54: 556804/7922330) 160

5.5.5 Cudgee Creek Granite (045) (Drill hole: HBPD002, UTM54: 556533 /7821948) 162

5.6 Discussion 164

5.6.1 Georgetown Inlier granites 164

5.6.2 Cudgee Creek Granite drill-core samples: basement west of the Georgetown Inlier 168

5.6.3 Lu-Hf data 168

5.6.4 Tectonic implications 175

5.7 Conclusion 177

5.8 References 177

Chapter 6: Conclusion 183

6.1 References 190

Chapter 7: Bibliography 193

Appendix A: Statement of Authorship 216

Chapter 2: SOA 216

Chapter 3: SOA 217

Appendix B: Chapter 2, supplementary file 219

Appendix C: Chapter 3, supplementary file 228

Appendix D: Chapter 4, supplementary file 255

Appendix E: Chapter 5, supplementary file 359

List of figures

Figure 1.1: Map of Australia outlining the study area. NAC: North Australian Craton. WAC: Western Australian Craton. SAC: South Australian Craton. The box corresponds to the box in Figure 1.2. Beige are the cratons, and grey are the younger rocks.

Figure 1.2: ca. 1.5 Ga Nuna reconstruction taken from Kirscher et al. (2018). Black box corresponds to Figure 1.1.

Figure 2.1: The Kolmogorov-Smirnov 2-sample test measures the maximum difference between the two samples empirical cumulative functions whereas the Kuiper test sums the greatest positive and negative distances. Sample 1 has a single population of 150 synthetic ages of 500 Ma with 0.5% uncertainty, sample 2 is the same but has 2.5% uncertainty.

Figure 2.2: Comparison of age uncertainty of detrital zircon grains obtained with different analytical procedures and igneous grains obtained by all procedures. Detrital zircon data are from the McArthur Basin and the igneous data are from nearby potential source regions. Uncertainties are from 207Pb/206Pb ages taken directly from reports. They are 2σ for the LA-ICP-MS data and 1σ for the shrimp and igneous data. Analyses >10% discordant are excluded. Data compilation and sources are listed in Appendix Table 2.1 and in the supplementary file. SHRIMP: sensitive high-resolution ion microprobe. LA-ICP-MS: laser ablation inductively coupled plasma mass spectrometry.

Figure 2.3: Linear relationship associated with measuring the dissimilarities between samples with different uncertainties. Un1 is the mean uncertainty of sample 1 and Un2 the mean uncertainty of sample 2.

Figure 2.4: MDS plots resulting from A) K-S test, B) Kuiper test and C) KFE. Blue text denotes source area zircon samples and red text denotes detrital zircon samples from the basin strata. The solid line represents the nearest neighbour and dashed lines the second closest.

Figure 2.5: A) S1 is sample 1 from Figure 2.1 (n=150, 500 Ma grains with 0.5% uncertainty), S2 is the same but with 3% uncertainty. S1 resampled is the result of resampling S1 to match the uncertainty of S2. B) are the cumulative distribution functions of S1 following KFE smoothing with 10 Ma bandwidth, S2 with 10 Ma smoothing and S1 with 30 Ma smoothing to demonstrate how KFE smoothing produces similar results to the resampling method and vice versa.

Figure 2.6: The results from simulating 8000 K-S and Kuiper test D- and V-values. A) With 0.5% uncertainty B) 3% uncertainty C) 0.5% uncertainty vs. 3% uncertainty. D) 0.5% samples resampled to match the 3% uncertainty.

Figure 2.7: Methods for utilising Procrustes rotation. M = Method. D = MDS coordinates. P = Procrustes coordinates.

Figure 2.8: Results of testing the bootstrap resampling and Procrustes method for handling different uncertainties. A) standard K-S based MDS plot. B) Standard Kuiper based MDS plot. C) K-S based MDS following the bootstrap resampling and Procrustes method. D) Kuiper following the bootstrap resampling and Procrustes method.

Figure 2.9: Regional map showing the McArthur Basin and potential source regions and simplified stratigraphic column of the Roper Group. Yellow circles are sample locations with the first three letters of each sample. See Table 2.3 for an overview of the samples.

Figure 2.10: Results of the K-S based MDS analysis. A) Standard MDS plot not accounting for different uncertainties. B) MDS plot following bootstrap resampling and Procrustes method. C) MDS plot following the resampling method. Red text denotes detrital samples, whereas blue text is the source regions. The colours of the ellipses are for illustrative purpose.

Figure 2.11: Results of the Kuiper based MDS analysis. A) Standard MDS plot not accounting for different uncertainties. B) MDS plot following bootstrap resampling and Procrustes method. C) MDS plot following the resampling method. Red text denotes detrital samples, whereas blue text is the source regions. The colours of the ellipses are for illustrative purpose.

Figure 3.1: A: NE Australian Proterozoic terrains. B: Stratigraphic column outlining the main sedimentary groups and events in the Georgetown Inlier.

Figure 3.2: Probability density plots show two distinct provenance shifts in the U–Pb detrital zircon from the Georgetown Inlier. Rose diagrams show paleocurrent data from primary sedimentary structures in the Georgetown Inlier.

Figure 3.3: Tectonic and paleogeographic reconstructions for the amalgamation of the Georgetown Inlier with the NAC. Corresponding paleocurrent data and detrital zircon age spectra from the Georgetown Inlier in comparison with age equivalents from the Mt. Isa Inlier of northeast Australia and the Wernecke Supergroup of the Yukon, northwest Canada (Carson, 2013; Furlanetto et al., 2016; Neumann et al., 2009; Neumann et al., 2006). A and E:

ca. 1700 Ma: Sediments in the Georgetown Inlier were initially deposited in a passive margin whilst sediments in Mt. Isa were deposited in a back-arc basin to a possible west-dipping subduction zone (Betts et al., 2016). B and F: ca. 1650–1620 Ma: Development of an east-dipping subduction zone off the western margin of Laurentia promoted back-arc rifting between the Georgetown Inlier and Laurentia causing complete separation by ca. 1650 Ma. C and G: Continued subduction leads to collision of the Georgetown Inlier and the NAC (Isan–Jana Orogeny) and the thin-skinned Racklan Orogeny in west Laurentia. D and H: Post 1550 Ma: Detrital zircon age spectra from the Inorunie Group strongly resembles the Constance Sandstone of the Mt. Isa Inlier suggesting a correlation and further indicating a connection post-1580 Ma. Laurentia: He = Hearne Carton, Sl = Slave Craton, Australia: NAC = North Australia Craton, SAC = South Australia Craton, WAC = West Australia Craton.

Figure 4.1: A) Map of the Mount Isa Inlier illustrating the geographical extent of the three superbasin sequences and the granitic suites. B) Mount Isa Inlier domain map highlighting the 15 fault bound domains and the western, central and eastern belts (Day, 1983; Withnall and Hutton, 2013). Different colours represent different domains (Withnall and Hutton, 2013). The green with a thick border is the Camooweal-Murphy Domain (CMD) (see discussion for significance).

Figure 4.2: Overview of the Leichhardt Superbasin stratigraphy highlighting the problems with the proposed correlations based on geochronology. References: 1) Magee et al. (2012) 2) Neumann et al. (2009b), 2), 3) Page (1983), 4) Pearson et al. (1992). *Age reported as Argylla Formation, however, recent mapping defines the unit as Bulonga Volcanics.

Figure 4.3: Geological map of the Mary Kathleen Group study area. See Figure 4.1 for location within the Mount Isa Inlier. A) Overview of the area. B) Location B1. C) Locations B2 and B3. D) Locations B4 and B5. DZ = Detrital zircon. Maps generated using data from the Queensland Geological Survey. Bedding measurements are from this study.

Figure 4.4: Geology map of the Malbon Group study area. See Figure 4.1 for location within the Mount Isa Inlier. A) Overview of the area. B) Location M1. C) Location M2. DZ = Detrital zircon. Maps generated using data from the Queensland Geological Survey. Bedding measurements are from this study.

Figure 4.5: Stratigraphic columns from locations B1, B2, and B3. BQ=Ballara Quartzite. CF=Corella Formation. Contacts between BQ and CF are from geological maps for reference (Figure 4.3). See Table 4.2 for descriptions of the facies association.

Figure 4.6: Outcrop photos of the Mary Kathleen Group. a) FA1, coarse-grained sandstone sheet flood deposits from Location B1. b) FA2, trough cross-bedding in medium-grained wavy bedded sandstones at location B5b. c) FA2, Wave ripples on the tops of fine to medium-grained sandstones at location B3. d) FA3, Hummocky cross-stratification in fine to medium-grained sandstones. e) FA4, cleaved mudstones interbedded with fine-grained sandstones at location B4. Bedding is sub-horizontal f) FA6, Laminated calcareous mudstone at location B5. g) FA7, scapolitic limestone at location B1. h) FA8, fine to medium-grained calcareous sandstones interbedded with calcareous mudstone featuring convoluted bedding at location B4. The pen is 14 cm in length. Hammer is 40 cm.

Figure 4.7: Stratigraphic columns from locations B4 and B5. BQ=Ballara Quartzite. CF=Corella Formation. Contacts between BQ and CF are from geological maps for reference (Figure 4.3). See Table 4.2 for the facies and facies associations.

Figure 4.8: Stratigraphic columns from locations M1 and M2. MSM = Mount Star Member. MQ = Mitakoodi Quartzite. WB = Wakefield Metabasalt. OJ = Overhang Jaspilite. Contacts between units are from geological maps for reference (Figure 4.4). See Table 4.2 for facies association.

Figure 4.9: Outcrop photos of the Malbon Group. a) FA3, Low-angle planar cross-beds in fine-grained sandstones featuring erosional surface at location M1b. b) FA2, Herringbone style cross-bedding in medium-grained sandstone at location M2a. c) FA2, Planar cross-beds and horizontally laminated medium-grained sandstones at location M1a. d) Coarsening up-ward parasequences at location M2a, the base is approximately 400 m on the stratigraphic column M2 (Figure 4.9). e) FA3, medium-grained sandstones featuring wavy bedding and horizontal laminations at location M2b. f) FA5, Folded jaspilite interbedded with mudstone at location M2b.

Figure 4.10: Simple cartoon illustrating the depositional model for the Mary Kathleen Group. Blue dashed line is relative sea-level. a) General N-S extension at ca. 1.77 Ga creates a significant gradient change at a rift shoulder allowing for deposition of the alluvial fans in location B1. At the same time, the southern locations (B4 and B5), are uplifted and actively

eroding. b) Rift-related subsidence provides accommodation for deposition of shallow marine deposits in the north. At this time in the south, non-marine sediments might start to fill the low-stand erosional incisions. c) The active rift propagates further to the south generating a significant flooding surface in the north, in the south, there is also a flooding surface, however, the low-stand deposits show a higher frequency of parasequences indicative of a proximal location to the shoreline. d) the rift propagates further to the south flooding the entire basin, the north becomes starved of sediment, resulting in precipitation of limestone. In the south, the maximum flooding surface is marked in the middle part of the mudstone. e) Hypothetical distal section (B1). f) Hypothetical proximal section (B4 and B5).

Figure 4.11: Sequence stratigraphic interpretation for the Mary Kathleen Group measured sections, aligned with north to the left. Each colour represents a parasequence. Note that parasequences cut major system tract boundaries, contrary to typically sequence stratigraphic models. See text for discussion. LST: Lowstand system tract. TST: Transgressive system tract. HST: Highstand system tract. MRS: Maximum regressive surface. MFS: Maximum flooding surface. Terms from Catuneanu (2006).

Figure 4.12: Concordia plots for all detrital zircon samples from this study.

Figure 4.13: Detrital zircon data <5% discordant. A) KDE plots from the Mary Kathleen Group samples. B) KDE plots from the Mitakoodi Quartzite (Malbon Group) samples. C) MDS plots show that the detrital zircon samples from the Mary Kathleen Group are statistical dissimilar from the Mitakoodi Quartzite. D) KDE plots of samples grouped based on unit names. The Mitakoodi Quartzite samples lack the <1800 Ma population that are observed in all Mary Kathleen Group samples as well as have a significant ca. 2580 Ma population. Ages are calculated from $^{207}Pb/^{206}Pb$.

Figure 4.14: Mary Kathleen Group detrital zircon samples ε_{Hf} vs age. A) All data with 1σ error bars. B) Zoomed in plots for individual samples. Depleted mantle from Vervoort and Blichert-Toft (1999). CHUR is CHondritic Uniform Reservoir (Blichert-Toft and Albarède, 1997). Dashed lines are crustal evolution lines.

Figure 4.15: Mitakoodi Quartzite detrital zircon samples εHf vs age. A) All data with 1σ error bars. B) Zoomed in plots for individual samples. Depleted mantle from Vervoort and Blichert-Toft (1999). CHUR is CHondritic Uniform Reservoir (Blichert-Toft and Albarède, 1997). Dashed lines are crustal evolution lines.

Figure 4.16: A) Detrital zircon KDE plots from the studied samples in comparison with Mount Isa Inlier igneous ages >1700 Ma from

http://www.ga.gov.au/geochron-sapub-web/geochronology/shrimp/search.htm

B) Comparison of the detrital zircon from Mitakoodi Quartzite with Mount Isa Inlier igneous grains and every all igneous zircon grains in the NAC.

Figure 4.17: MDS analysis, following methods of Nordsvan et al. (Chapter 2) comparing all detrital zircon samples from the Mount Isa Inlier (Carson et al., 2008; Magee et al., 2012; Neumann et al., 2009a; Neumann et al., 2009b; Neumann et al., 2006). Lines denote most similar samples, dashed lines denote seconded closest.

Figure 4.18: A) Comparison of the Mitakoodi Quartzite detrital zircon samples with the Westmoreland Conglomerate and the Wire Creek Sandstone from the Camooweal-Murphy Domain. All data is less <5% discordant. B) Comparison of the Mitakoodi Quartzite detrital zircon samples with previously obtained Malbon Group samples (shown in yellow) (Neumann, 2016a, b). C) All Malbon Group samples compared with all samples from the Westmoreland Conglomerate and the Wire Creek Sandstone.

Figure 4.19: Two dimensional KDE plots show the ε_{Hf} data density from the samples analysed in this study. A) Mitakoodi Quartzite data. B) Corella Formation data. C) Ballara Quartzite data. D) 90th, 50th and 10th percentile lines between 1700–2100 Ma for comparison between the three samples.

Figure 4.20: A) MDS plot using the K-S test following the methods outlined in Nordsvan et al. (Chapter 2). B) Kuiper based MDS plot. C) Dendrogram of the K-S distances highlights the significant difference in the Mitakoodi Quartzite samples. D) Similar to C, the dendrogram of Kuiper distances have the same results. All source region data is from http://www.ga.gov.au/geochron-sapub-web/geochronology/shrimp/search.htm Only ages within uncertainty >1750 Ma were used for the analysis.

Figure 5.1: Aeromagnetic image of total magnetic intensity for northeast Australia (modified from Withnall and Hutton, 2013). Black lines outline the outcrop extent of the Mount Isa (MII) and Georgetown (GTI) inliers. Yellow stars are sample locations. White dots are towns. NAC: North Australian Craton. WAC: Western Australian Craton. SAC: South Australian Craton. Numbers correspond samples analysed in this study: 1) 042, basement sample. 2)

045, basement sample. 3) CUG01, Esmeralda Granite. 4) PGE01, Macartneys Granite. 5) FOG01, Forsayth Granite. And previously analysed samples in the Georgetown Inlier: 6) Mistletoe Granite, 7) Mount Hogan Granite, 8) Unnamed granitic gneiss, 9) Digger Creek Granite, 10) Unnamed monzogranite, 11) Mywyn Granite, 12) Lighthouse Granite, 13) Brandy Hot Granodiorite, 14) Forest Home Trondhjemite. See table 1 for the references. Pink overlay in eastern Mount Isa Inlier is the ca. 1.55 to 1.49 Ga Williams Batholith and the Maramungee Granite.

Figure 5.2: Overview of the data from the Forsayth Granite (FOG01). Zircon images are transmitted light and cathodoluminescence SEM where the circles represent the laser ablation spot. The difference in uncertainties reflects the different analytical sessions. The (zoomed) Concordia plot on the right includes all data utilised in the mean weighted age.

Figure 5.3: ε_{Hf} vs U-Pb age (Ma) plots for the analysed samples. A) ε_{Hf} values calculated with the weighted mean age of the granites. B) ε_{Hf} values calculated with the individual grain age. Macartneys Granite = PGE01, Esmeralda Granite = CUG01, Forsayth Granite = FOG01, 042 and 045 = Cudgee Creek granites.

Figure 5.4: Overview of the geochronology data from the Macartneys Granite (PGE01). Zircon images are transmitted light and cathodoluminescence SEM, the circles represent the location of the laser ablation spots. Larger uncertainties in the mean weighted age correspond with zircon analysed using LASS.

Figure 5.5: Overview of the data from the Esmeralda Granite (CUG01). Zircon images are transmitted light and cathodoluminescence SEM, the circles represent the location of the laser ablation spots. Larger uncertainties in the mean weighted age correspond with zircon analysed using LASS.

Figure 5.6: Overview of the data from the Cudgee Creek granite (042). Zircon images are transmitted light and cathodoluminescence SEM, the circles represent the location of the laser ablation spots. Larger uncertainties in the mean weighted age correspond with zircon analysed using LASS.

Figure 5.7: Overview of the data from the Cudgee Creek granite (045). Zircon images are transmitted light and cathodoluminescence SEM, the circles represent the location of the laser ablation spots. Larger uncertainties in the mean weighted age correspond with zircon analysed using LASS.

Figure 5.8 (next page): Overview of the Georgetown Inlier geochronology following this study. Height of each box represents the age uncertainty of the sample References: 1) This study. 2) Neumann and Kositcin (2011). 3) Black and Withnall (1993). 4) Black and McCulloch (1990). 5) Black et al. (1998). 6) Pourteau et al. (2018) 7) Lambeck et al. (2012). 8) Black et al. (2005). Granite names: ESG: Esmeralda, MCG: Macartneys, FHT: Forest Home Trondhjemite: BHG: Brandy Hot, FSG: Forsayth, LHT: Lighthouse, DCG: Digger Creek, MTG: Mistletoe, MHG: Mount Hogan, UMG, Unnamed Monzogranite, MYG: Mywyn, UGG: Unnamed granitic gneiss, 045 and 042, Cudgee Creek basement granites. Ages within the plutons are reported crystallisation ages. Corresponding two-stage depleted mantle model ages are reported at the bottom of the figure. ε_{Nd} two-stage model ages are in black text and ε_{Hf} two-stage model ages are in red. ε_{Nd} two-stage model ages were calculated using formulas outlined in Champion (2013), when possible against the new ages reported in this study. Locations of the granites can be seen in Figure 5.1.

Figure 5.9: A) ε_{Hf} values vs age for the granite analysed in this study. B) ε_{Hf} value vs longitude. PGE) Macartneys Granite, CUG) Esmeralda Granite, FOG) Forsayth Granite, 042 and 045) Cudgee Creek basement granites. Black lines on (A) represent the ε_{Hf} uncertainties. Outliers have been removed from these plots.

Figure 5.10: Georgetown Inlier (n=155) (Murgulov et al., 2007), and eastern Mount Isa Inlier (n=250) (Griffin et al., 2006) Age vs ε_{Hf} bivariate kernel density estimate (2dKDE) plots from modern stream sediments, overlain with the ε_{Hf} values from the granites analysed in this study. A) Georgetown Inlier stream sediment 2dKDE plots overlain with the granite ε_{Hf} values calculated to the mean weighted age. B) Georgetown Inlier stream sediment overlain by ε_{Hf} values of the granites calculated to individual grain age. C) ε_{Hf} density plot calculated including Murgulov et al. (2007) stream sediments plus the Georgetown Inlier granites from this study, overlain with the ε_{Hf} values from the basement granites calculated to the mean weighted age. D) 2dKDE plot same as (C) overlain with ε_{Hf} values from the basement granites calculated to the individual grain age. E) ε_{Hf} value 2dKDE plots of stream sediments from the eastern belt of the Mount Isa Inlier (Griffin et al., 2006), overlain with the ε_{Hf} values calculated to the mean weighted age. E) 2dKDE stream sediment plot of Mount Isa data overlain with ε_{Hf} values calculated to the individual grain age.

Figure 5.11: KDE plots of zircon ε_{Hf} two-stage model ages from the granites analysed in this study. A) Basement granite data grouped together. B) The Esmeralda Granite. C) Macartneys Granite. D) Forsayth Granite. E) Ungrouped basement granites.

Figure 5.12: Kernel density estimate plots of zircon ε_{Hf} two-stage model ages from modern stream sediments of the eastern Mount Isa Inlier and the Georgetown Inlier (Griffin et al., 2006; Murgulov et al., 2007). Model ages are shown for grains with crystallisation ages between 1.48 and 1.61 Ga.

List of tables

Table 2.1: Input data to test the resampling methods ability to replicate D-and V-values.

Table 2.2: Input data for testing i) the bootstrap resampling and Procrustes method (Figure 2.8) and ii) the resampling method (Figure 2.9).

Table 2.3: Detrital zircon samples used in the case study, taken from Munson et al. (2018).

Table 4.1: Analytical days. LASS: Laser ablation split stream.

Table 4.2: Facies and facies associations from this study for sediments of the Mary Kathleen and Malbon groups.

Table 5.1: Review of all previous ages obtained for granites in the Georgetown Inlier. *Granites redated in this study. [†]Granite age revised by a later study. 1) Black and McCulloch (1990), 2) Black and Withnall (1993), 3) Neumann and Kositcin (2011). Uncertainty is 1σ as reported by the references.

Table 5.2: Summary of analytical days. Zircon Standard known ages: GJ1: 608.5 Ma (Wiedenbeck et al., 1995). 91500: 1062.4 Ma (Jackson et al., 2004). OG1: 2465.4 Ma (Stern et al., 2009).

Table 5.3: New U-Pb Proterozoic granite ages from NE Australia.

Chapter 1: Introduction

Over the last 2 billion years the continents have amassed to form at least three distinct supercontinents. The idea that the assembly and break-up of these supercontinents are cyclic is nothing new (Nance et al., 1988); however, the mechanism for such cyclicity and the geodynamic significance is still widely debated (Li and Zhong 2009; Nance et al., 2014). Advancing our knowledge of the supercontinent cycle is imperative for comprehending Earths evolution, and understanding such cycles requires precise and accurate paleogeographic reconstructions that can account for numerous geological observations. Under that light, the aim of this thesis is to understand a key component of the oldest supercontinent, Nuna.

Of the three supercontinents, Pangea, Rodina and Nuna/Columbia (in increasing age), it should come as no surprise that the oldest, the Paleo- to Mesoproterozoic supercontinent Nuna is the least well-constrained. Just over twenty years ago, Hoffman (1997) conceptualised a Paleoproterozoic supercontinent Nuna correlating orogenic belts in Laurentia and Baltic and propose their extent into Australia and Siberia. The existence of the supercontinent is now supported by multiple lines of geological evidence, but a number of important connections still require further clarification. One such region is NE Australia, where several different connections with Laurentia, Siberia and North China have been proposed.

Proterozoic rocks in NE Australia can be identified in five main inliers, Mount Isa, Georgetown, Dargalong, Coen and Yambo. The two most prominent, the Mount Isa

and Georgetown inliers are the focus of this thesis (Figure 1.1). The aim is to understand the sedimentological evolution of these two inliers in terms of local and global plate tectonics, to assess Nuna reconstructions

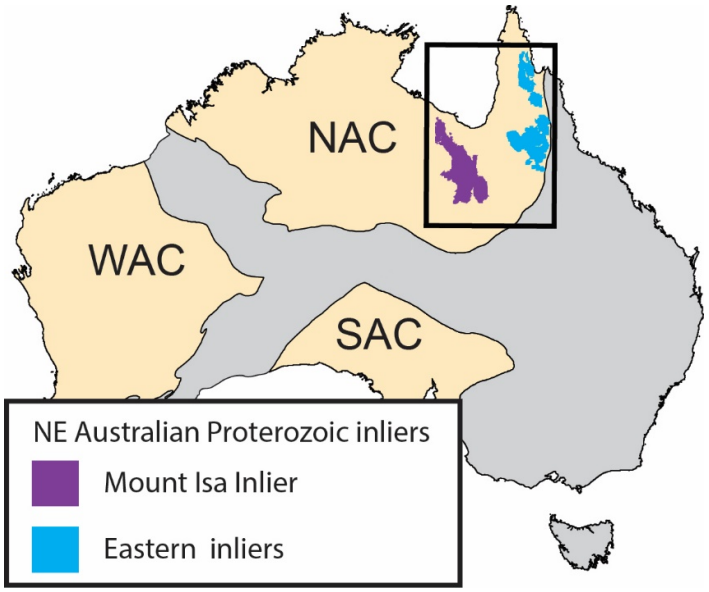

Figure 1.1: Map of Australia outlining the study area. NAC: North Australian Craton. WAC: Western Australian Craton. SAC: South Australian Craton. The box corresponds to the box in Figure 1.2. Beige are the cratons, and grey are the younger rocks.

1.1 NE Australia in Nuna reconstructions

The first global reconstructions of the Nuna supercontinent (Figure 1.2) were based on correlating ca. 2.1 to 1.8 Ga orogenic belts across the continents (Rogers and Santosh, 2002; Zhao et al., 2002; Zhao et al., 2004). In these early reconstructions, Australia occupies a proto-SWEAT (South West United States East Antarctica; Moores (1991)) or a modified SWEAT position in respect to Laurentia; i.e., where NE Australia is connected to NW Laurentia. A lack of geochronological constraints meant that the connection between Australia and Laurentia, which was mainly based on stratigraphic correlations of Tonian sedimentary rocks (Bell and Jefferson, 1987; Jefferson, 1978), was highly speculative. Nevertheless, Hoffman (1991) had noted similarities between the Wopmay orogeny of northern Canada and the Barramundi

Orogeny of the Mount Isa Inlier and tentatively suggested a ca. 1.85 Ga correlation between the two continents. Additionally, Idnurm and Giddings (1995) showed from ca. 1.7 to 1.6 Ga, Australia and Laurentia have a similar apparent polar wander path that was compatible with a SWEAT like configuration throughout that period.

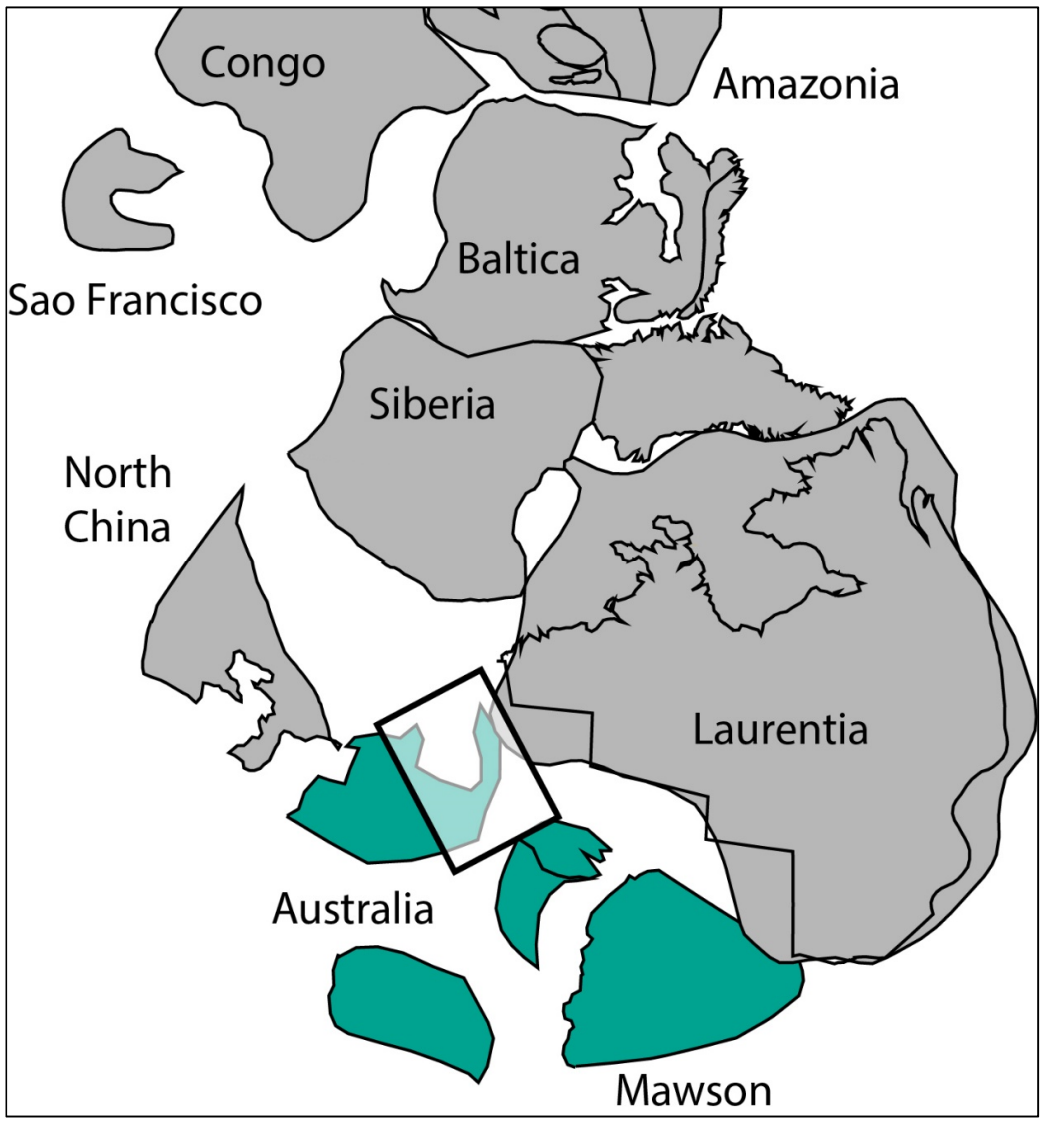

Figure 1.2: ca. 1.5 Ga Nuna reconstruction taken from Kirscher et al. (2018). Black box corresponds to Figure 1.1.

In NW Laurentia, Thorkelson et al. (2001b) correlated ca. 1.6 Ga hydrothermal megabreccias of the Yukon region with similarly aged hydrothermal breccias in the

Gawler Craton of South Australia (Jagodzinski, 2005; Johnson and Cross, 1995). Thorkelson et al. (2001a) also correlated the Wernecke Supergroup of NW Laurentia with the sedimentary rocks in the Mount Isa Inlier and made comparisons between the ca. 1.6 Ga Racklan and Isan orogenies of Laurentia and NE Australia, respectively. Betts et al. (2008) undertook a comprehensive review of the possible correlations between Australia and Laurentia ca. 1.8 to 1.6 Ga and provided a geodynamic model consistent with paleomagnetic data. In their reconstruction, Australia is in a rotated SWEAT like position with respect to Laurentia, a configuration also suggested by Payne et al. (2009), termed proto-SWEAT. Betts et al. (2008) correlated the ca. 1.78–1.65 Ga Yavapai and Mazatzal accretionary orogens of south Laurentia to similarly aged accretionary orogens in central and south Australia. In both reconstructions (Betts et al., 2008; Payne et al., 2009), NE Australia is juxtaposed to NW Laurentia occupying an intracontinental position broadly consistent with the reconstructions of Thorkelson et al. (2001a). However, Thorkelson et al. (2005) pointed out that the Wernecke Supergroup of the Yukon region was likely associated with a passive margin setting rather than an intracontinental one throughout that period, and that the ca. 1.6 Ga Racklan Orogeny might be a result of far-field stresses related to continental collision.

In the Yukon region of NW Canada, sedimentary rocks of the Wernecke Supergroup were deposited ca. 1.67 to 1.6 Ga and subjected the Racklan Orogeny at ca. 1.6 Ga (Furlanetto et al., 2016). The sediments are approximately 14 Km thick and consist of fine-grained sandstones, mudstone and dolomite interpreted to have been deposited on a passive margin at the western margin of the newly assembled Laurentian

continent (Furlanetto et al., 2016; Hoffman, 1989; Whitmeyer and Karlstrom, 2007). The ca. 1.6 Ga Racklan Orogeny is thought to be the thin-skinned expression of the Forward Orogeny to the east, which is characterised by two compressional events: the early event resulted in east-verging overturned folds associated with greenschist facies metamorphism and the second event is defined by overturned south-verging folds (Furlanetto et al., 2013; Thorkelson et al., 2005). Hydrothermal megabreccias that cut the Racklan deformational features, dated at ca. 1.59 Ga, have volcanic clasts within them, which are assigned to the ca. 1.7 Ga Bonnetia Arc (Nielsen et al., 2013; Thorkelson and Laughton, 2015). Put simply, these arc rocks are thought to have been thrust over the Wernecke Supergroup during the Racklan Orogeny and subsequently incorporated into the hydrothermal megabreccias (Nielsen et al., 2013). The consequence of the Bonnetia Arc model is that not only was there an ocean between Australia and Laurentia at ca. 1.7 Ga, but also a magmatic arc and accompanying subduction zone.

Evans and Mitchell (2011) used paleomagnetic data to validate the existence of a ca. 1.9–1.3 Ga Nuna core consisting of Laurentia, Baltica and Siberia. In their full plate reconstruction, based mainly on previous studies, Australia was placed in the proto-SWEAT configuration with respect with Laurentia (Betts et al., 2008; Evans and Mitchell, 2011; Payne et al., 2009). In a review of the global paleomagnetic data, Zhang et al. (2012) concluded that the proto-SWEAT configuration was indeed viable for ca. 1.75 Ga, where Australia occupies a position juxtaposed with Laurentia and Siberia to the east, and the North China Craton and India to the north (Zhang et al., 2012). In a later review of the paleomagnetic data, Pisarevsky et al. (2014) showed

that Australia can be shifted further from Laurentia to account for the Bonnetia Arc and associated ocean. Most recently, Kirscher et al. (2019) provided new paleomagnetic data from the ca. 1.79 Ga Hart Dolerite of the North Australian Craton (NAC), which showed that Australia and Laurentia could have been in a proto-SWEAT configuration by ca. 1.78 Ga but would require a relative motion between ca. 1.78 to 1.6 Ga to reach their final position in the Nuna supercontinent.

The correlation between Australia and Laurentia is strongly supported by detrital zircon studies from Mesoproterozoic sedimentary basins of western Laurentia (Doe et al., 2013; Doe et al., 2012; Medig et al., 2014; Ross et al., 1992; Ross and Villeneuve, 2003), which contain ca. 1.6 to 1.5 Ga zircon grains largely absent from source terranes in Laurentia and typically thought to have come from Australia. Indeed, ca. 1.5 to 1.6 Ga aged source terranes are particularly abundant in NE Australia.

1.2 Geological Background

The Mount Isa Inlier of NE Australia is the exposed part of a much larger province that can be clearly identified in geophysical images (Betts et al., 2006; Withnall and Hutton, 2013). O'Dea et al. (1997) discussed the geological evolution of the Mount Isa Inlier in terms of global tectonics, suggesting that the ca. 1.9–1.87 Ga Barramundi Orogeny might be contiguous with the either the Trans Hudson or Wopmay orogenies of Laurentia. The Barramundi Orogeny in the Mount Isa Inlier is characterised by an intense bedding-parallel gneissic foliation and north south-trending upright folds interpreted to have developed during east-west directed shortening (Betts et al., 2006; Blake, 1992; Blake, 1987; Etheridge et al., 1987). The orogen is widespread

throughout the NAC and was originally interpreted to have resulted from intraplate processes (Etheridge et al., 1987). However, heterogeneities in whole rock and isotope geochemistry across the Mount Isa Inlier, corresponding with distinct north-south trending metallogenic boundaries, have been used to argue forth the operation of active plate tectonic processes during orogenic development (Bierlein et al., 2011). Furthermore, an east-west seismic profile across the Mount Isa Inlier in combination with magnetotelluric data was used to argue that the orogen was the result of the Mount Isa Inlier (terrane) colliding with the proto-NAC (Betts et al., 2016; Korsch et al., 2012). Overlying the Barramundi Orogeny basement rocks in the Mount Isa Inlier are three successive "superbasin" sedimentary sequences that span about 400 million years. They have (all) been interpreted to have been deposited in either a passive margin, an intraplate epicontinental rift or a back-arc basin to a subduction zone to either the east or the south (Betts and Giles, 2006; Blake, 1992; Blake, 1987; Eriksson et al., 1993; Gibson et al., 2018; Gibson et al., 2012; Giles et al., 2002; Jackson and Southgate, 2000; Neumann et al., 2009; Neumann et al., 2006; Scott et al., 2000; Southgate et al., 2013).

Located approximately 500 km to the east of the Mount Isa Inlier, the Georgetown Inlier consists of ca. 1.7 to 1.6 Ga sedimentary rocks, which have been highly deformed and variably metamorphosed during the ca. 1.6 Ga Jana Orogeny (Withnall and Henderson, 2012). Based on a seismic transect from Mount Isa to Georgetown, Korsch et al. (2012) suggested that the inlier overlay two allochthonous blocks (termed the Numil and Abingdon seismic provinces) that they suggested were accreted to the eastern margin of the NAC during the Barramundi Orogeny at ca. 1.85

Ga and at ca. 1.7 Ga, respectively. The potential suture for the first event, associated with accretion of the Numil Terrane, is the west-dipping Gidyea Suture located to the east of the Mount Isa Inlier under Phanerozoic cover rocks (Betts et al., 2016; Korsch et al., 2012). Betts et al. (2016) argued that the Numil Terrane was accreted during a continental collision with Laurentia. In both models (Betts et al., 2016; Korsch et al., 2012), the Georgetown Inlier is considered to have been part of the NAC by at least ca. 1.7 Ga. Nevertheless, how exactly the Georgetown Inlier relates to the Mount Isa Inlier and the rest of the NAC has always been enigmatic (Withnall et al., 1988). This is partly due to the absence of ca. 1.9 to 1.8 Ga basement rocks in the Georgetown Inlier that are so prominent throughout the NAC, and partly due to the substantial amount of younger cover between Georgetown and Mount Isa. But the main reason the relationship between the Georgetown and Mount Isa inliers is so poorly understood is because of the substantial geological differences between them.

Following the proposed collision between Laurentian and Australia at ca. 1.85 Ga, Betts et al. (2016) hypothesised that the two continents drifted apart and re-amalgamated at ca. 1.55 Ga, constituting a full Wilson cycle. In NE Australia the superbasins of the Mount Isa Inlier and the sedimentary rocks in the Georgetown Inlier are thought to represent the development of the passive margin, whereas in Laurentia the conjugate margin is thought to be sedimentary rocks of the Wernecke Supergroup. The Isan and Jana orogenies in the Mount Isa and Georgetown inliers, respectively, and the Racklan and Forward orogenies in the northern Canadian Cordillera, are thought to represent the closure of the ocean between the NAC and Laurentia (Betts et al., 2016). Alternatively, Gibson et al. (2018) suggest a similar

model, although they considered that the sedimentary rocks in the Mount Isa and Georgetown inliers were deposited in a back-arc basin rather than in a passive margin, and that ocean closure was driven by subduction occurring on the Australian margin, rather than on both margins as suggested by Betts et al., 2016.

This thesis constitutes an examination of NE Australia in the context of Nuna formation. Throughout the following chapters, a number of geological data are reported to assess the validity of the models discussed above and to further understand NE Australia within the Nuna supercontinent.

1.3 Thesis structure

The thesis is structured into 6 chapters of which chapter 3 is published in *Geology* and chapter 2 is currently under review at *Earth-Science Reviews*. Two chapters are in the late stage of preparation to be submitted to scientific journals. The other two chapters constitute the introduction and the conclusion.

Chapter One: The Introduction

In this chapter, the reader is introduced to the Nuna supercontinent, the Australian and Laurentian connection within Nuna and the tectonic models for the evolution of NE Australia within Nuna. As each chapter in the thesis is formatted as if it were a manuscript, they each have an introduction and a geological setting that will delve deeper into the scientific issues addressed throughout the thesis.

Chapter Two: Resampling (detrital) zircon age distributions for accurate Multidimensional Scaling solutions (under review at Earth-Science Reviews)

The aim of this chapter is to introduce, review and critique an emerging method being utilised in detrital zircon geochronology. Multidimensional scaling (MDS) is a statistical method that allows one to visualise the dissimilarities between multiple detrital zircon datasets. In this chapter, multiple issues with the method are discussed with the aim to firstly clarify, and secondly quantify the significance of the issues. New tools are provided to aid with MDS, which is then demonstrated with a case study from the Proterozoic McArthur Basin of north Australia.

Chapter Three: Laurentian crust in northeast Australia: Implications for the assembly of the supercontinent Nuna (Published in Geology)

In this chapter previous and newly obtained detrital zircon data along with new paleocurrent data is utilised to put forth the hypothesis that the Georgetown Inlier is an allochthonous terrane, sourced from Laurentia and transferred to Australia during Nuna amalgamation at ca. 1.6 Ga.

Chapter Four: Contrasting stratigraphy and provenance in the Mount Isa Inlier: Implications for Nuna amalgamation

In this chapter, new sedimentological field observations and stratigraphic columns along with detrital zircon U-Pb/Lu-Hf data are presented from the Mount Isa Inlier to challenge long-standing correlations. Demonstrating that these previously correlated units were deposited at different ages under different conditions with different source regions disproves the simple hypothesis that the Mount Isa Inlier sedimentary rocks represent an east-west extensional basin that deepened to the east.

Chapter Five: New U-Pb ages and Lu-Hf isotope data from Mesoproterozoic granites in NE Australia

This chapter reports the first ages from newly identified granitic plutons from the basement rocks between the Georgetown and Mount Isa inliers. Furthermore, new ages from granites in the Georgetown Inlier and the zircon Lu-Hf isotopic composition from all the samples are used to discuss the origin and significance of these newly identified Proterozoic granites.

Chapter Six: The conclusion

Chapter six summaries the data and ideas presented in this thesis, newly identified issues, and recommendations for future work.

1.4 References

Bell, R. T., and Jefferson, C. W., An hypothesis for an Australian-Canadian connection in the Late Proterozoic and the birth of the Pacific Ocean, in Proceedings Proceedings, Pacific Rim Congress1987, Volume 87, p. 39-50.

Betts, P. G., Armit, R. J., Stewart, J., Aitken, A. R. A., Ailleres, L., Donchak, P., Hutton, L., Withnall, I. W., and Giles, D., 2016, Australia and Nuna: Geological Society, London, Special Publications, v. 424, p. SP424. 422.

Betts, P. G., and Giles, D., 2006, The 1800–1100 Ma tectonic evolution of Australia: Precambrian Research, v. 144, no. 1-2, p. 92-125.

Betts, P. G., Giles, D., Mark, G., Lister, G. S., Goleby, B. R., and Ailleres, L., 2006, Synthesis of the Proterozoic evolution of the Mt Isa Inlier: Australian Journal of Earth Sciences, v. 53, no. 1, p. 187-211.

Betts, P. G., Giles, D., and Schaefer, B. F., 2008, Comparing 1800–1600Ma accretionary and basin processes in Australia and Laurentia: possible

geographic connections in Columbia: Precambrian Research, v. 166, no. 1, p. 81-92.

Bierlein, F. P., Maas, R., and Woodhead, J., 2011, Pre-1.8 Ga tectono-magmatic evolution of the Kalkadoon–Leichhardt Belt: implications for the crustal architecture and metallogeny of the Mount Isa Inlier, northwest Queensland, Australia: Australian Journal of Earth Sciences, v. 58, no. 8, p. 887-915.

Blake, D. H., 1987, Geology of the Mount Isa inlier and environs, Queensland and Northern Territory, Australian Govt. Pub. Service.

Blake, D. H., and Stewart, A. J., 1992, Stratigraphic and tectonic framework, Mount Isa inlier, in Stewart, A. J., and Blake, D. H., eds., Detailed study of the Mount Isa Inlier, Volume 243: Canberra, Australia, AGSO Bulletin, p. 1-12.

Doe, M. F., Jones, J. V., Karlstrom, K. E., Dixon, B., Gehrels, G., and Pecha, M., 2013, Using detrital zircon ages and Hf isotopes to identify 1.48–1.45 Ga sedimentary basins and fingerprint sources of exotic 1.6–1.5 Ga grains in southwestern Laurentia: Precambrian Research, v. 231, p. 409-421.

Doe, M. F., Jones, J. V., Karlstrom, K. E., Thrane, K., Frei, D., Gehrels, G., and Pecha, M., 2012, Basin formation near the end of the 1.60–1.45 Ga tectonic gap in southern Laurentia: Mesoproterozoic Hess Canyon Group of Arizona and implications for ca. 1.5 Ga supercontinent configurations: Lithosphere, v. 4, no. 1, p. 77-88.

Eriksson, K. A., Simpson, E. L., and Jackson, M. J., 1994, Stratigraphical Evolution of a Proterozoic Syn-Rift to Post-Rift Basin: Constraints on the Nature of Lithospheric Extension in the Mount Isa Inlier, Australia, in A, F. K., and J, S. R., eds., Tectonic controls and signatures in sedimentary successions: London, UK, The International Associtation of Sedimentologists, p. 203-221.

Etheridge, M. A., Rutland, R. W. R., and Wyborn, L. A. I., 1987, Orogenesis and tectonic process in the Early to Middle Proterozoic of northern Australia: Proterozic Lithospheric Evolution, p. 131-147.

Evans, D. A. D., and Mitchell, R. N., 2011, Assembly and breakup of the core of Paleoproterozoic–Mesoproterozoic supercontinent Nuna: Geology, v. 39, no. 5, p. 443-446.

Furlanetto, F., Thorkelson, D. J., Gibson, H. D., Marshall, D. D., Rainbird, R. H., Davis, W. J., Crowley, J. L., and Vervoort, J. D., 2013, Late Paleoproterozoic terrane accretion in northwestern Canada and the case for circum-Columbian orogenesis: Precambrian Research, v. 224, p. 512-528.

Furlanetto, F., Thorkelson, D. J., Rainbird, R. H., Davis, W. J., Gibson, H. D., and Marshall, D. D., 2016, The Paleoproterozoic Wernecke Supergroup of Yukon, Canada: Relationships to orogeny in northwestern Laurentia and basins in North America, East Australia, and China: Gondwana Research, v. 39, p. 14-40.

Gibson, G. M., Champion, D. C., Withnall, I. W., Neumann, N. L., and Hutton, L. J., 2018, Assembly and breakup of the Nuna supercontinent: Geodynamic constraints from 1800 to 1600 Ma sedimentary basins and basaltic magmatism in northern Australia: Precambrian Research, v. 313, p. 148-169.

Gibson, G. M., Henson, P. A., Neumann, N. L., Southgate, P. N., and Hutton, L. J., 2012, Paleoproterozoic-earliest Mesoproterozoic basin evolution in the Mount Isa region, northern Australia and implications for reconstructions of the Nuna and Rodinia supercontinents: Episodes, v. 35, no. 1, p. 131-141.

Giles, D., Betts, P. G., and Lister, G. S., 2002, Far-field continental backarc setting for the 1.80–1.67 Ga basins of northeastern Australia: Geology, v. 30, no. 9, p. 823-826.

Hoffman, P. F., 1989, Precambrian geology and tectonic history of North America, in Albert W. Bally, and Palmer, A. R., eds., The Geology of North America—An Overview: Boulder, United States of America, Geological Society of America, Inc., p. 447-512.

-, 1991, Did the breakout of Laurentia turn Gondwanaland inside-out: Science, v. 252, no. 5011, p. 1409-1412.

Hoffman, P. F., 1997, Tectonic genealogy of North America, in Marshak, S., and Van der Pluijm, B. A., eds., Earth structure: An introduction to structural geology and tectonics.: New York, United States of America, McGraw-Hill, p. 459-464.

Idnurm, M., and Giddings, J. W., 1995, Paleoproterozoic-Neoproterozoic North America–Australia link: new evidence from paleomagnetism: Geology, v. 23, no. 2, p. 149-152.

Jackson, M. J., and Southgate, P. N., 2000, Evolution of three unconformity-bounded sandy carbonate successions in the McArthur River region of northern Australia: The Lawn, Wide and Doom Supersequences in a proximal part of the Isa Superbasin: Australian Journal of Earth Sciences, v. 47, no. 3, p. 625-635.

Jagodzinski, E. A., 2005, Compilation of SHRIMP U-Pb geochronological data, Olympic Domain, Gawler Craton, South Australia, 2001-2003.

Jefferson, C. W., Correlation of Middle and Upper Proterozoic strata between northwestern Canada and south and central Australia, in Proceedings Geological Association of Canada: Abstracts1978, Volume 13, p. 429.

Johnson, J. P., and Cross, K. C., 1995, U-Pb geochronological constraints on the genesis of the Olympic Dam Cu-U-Au-Ag deposit, South Australia: Economic Geology, v. 90, no. 5, p. 1046-1063.

Kirscher, U., Liu, Y., Li, Z., Mitchell, R., Pisarevsky, S., Denyszyn, S., and Nordsvan, A., 2019, Paleomagnetism of the Hart Dolerite (Kimberley, Western Australia)–A two-stage assembly of the supercontinent Nuna?: Precambrian Research, v. 329, p. 170-181.

Kirscher, U., Mitchell, R., Liu, Y., Li, Z., Cox, G., Nordsvan, A., Wang, C., and Pisarevsky, S., Long lived supercontinent Nuna-updated paleomagnetic constraints from Australia, in Proceedings AGU Fall Meeting Abstracts2018.

Korsch, R. J., Huston, D. L., Henderson, R. A., Blewett, R. S., Withnall, I. W., Fergusson, C. L., Collins, W. J., Saygin, E., Kositcin, N., and Meixner, A. J., 2012, Crustal architecture and geodynamics of North Queensland, Australia: insights from deep seismic reflection profiling: Tectonophysics, v. 572, p. 76-99.

Li, Z.-X., and Zhong, S., 2009, Supercontinent–superplume coupling, true polar wander and plume mobility: plate dominance in whole-mantle tectonics: Physics of the Earth and Planetary Interiors, v. 176, no. 3, p. 143-156.

Medig, K. P. R., Thorkelson, D. J., Davis, W. J., Rainbird, R. H., Gibson, H. D., Turner, E. C., and Marshall, D. D., 2014, Pinning northeastern Australia to northwestern Laurentia in the Mesoproterozoic: Precambrian Research, v. 249, p. 88-99.

Moores, E. M., 1991, Southwest US-East Antarctic (SWEAT) connection: a hypothesis: Geology, v. 19, no. 5, p. 425-428.

Nance, R. D., Murphy, J. B., and Santosh, M., 2014, The supercontinent cycle: a retrospective essay: Gondwana Research, v. 25, no. 1, p. 4-29.

Nance, R. D., Worsley, T. R., and Moody, J. B., 1988, The supercontinent cycle: Scientific American, v. 259, no. 1, p. 72-79.

Neumann, N. L., Southgate, P. N., and Gibson, G. M., 2009, Defining unconformities in Proterozoic sedimentary basins using detrital geochronology and basin analysis—An example from the Mount Isa Inlier, Australia: Precambrian Research, v. 168, no. 3, p. 149-166.

Neumann, N. L., Southgate, P. N., Gibson, G. M., and McIntyre, A., 2006, New SHRIMP geochronology for the Western Fold Belt of the Mt Isa Inlier: developing a 1800–1650 Ma event framework∗: Australian Journal of Earth Sciences, v. 53, no. 6, p. 1023-1039.

Nielsen, A. B., Thorkelson, D. J., Gibson, H. D., and Marshall, D. D., 2013, The Wernecke igneous clasts in Yukon, Canada: fragments of the Paleoproterozoic volcanic arc terrane Bonnetia: Precambrian Research, v. 238, p. 78-92.

O'Dea, M. G., Lister, G. S., MacCready, T., Betts, P. G., Oliver, N. H. S., Pound, K. S., Huang, W., and Valenta, R. K., 1997, Geodynamic evolution of the Proterozoic Mount Isa terrain: Geological Society, London, Special Publications, v. 121, no. 1, p. 99-122.

Payne, J. L., Hand, M., Barovich, K. M., Reid, A., and Evans, D. A. D., 2009, Correlations and reconstruction models for the 2500-1500 Ma evolution of the Mawson

Continent: Geological Society, London, Special Publications, v. 323, no. 1, p. 319-355.

Pisarevsky, S. A., Elming, S. Å., Pesonen, L. J., and Li, Z.-X., 2014, Mesoproterozoic paleogeography: supercontinent and beyond: Precambrian Research, v. 244, p. 207-225.

Rogers, J. J. W., and Santosh, M., 2002, Configuration of Columbia, a Mesoproterozoic supercontinent: Gondwana Research, v. 5, no. 1, p. 5-22.

Ross, G. M., Parrish, R. R., and Winston, D., 1992, Provenance and U-Pb geochronology of the Mesoproterozoic Belt Supergroup (northwestern United States): Implications for age of deposition and pre-Panthalassa plate reconstructions: Earth and Planetary Science Letters, v. 113, no. 1-2, p. 57-76.

Ross, G. M., and Villeneuve, M., 2003, Provenance of the Mesoproterozoic (1.45 Ga) Belt basin (western North America): Another piece in the pre-Rodinia paleogeographic puzzle: Geological Society of America Bulletin, v. 115, no. 10, p. 1191-1217.

Scott, D. L., Rawlings, D. J., Page, R. W., Tarlowski, C. Z., Idnurm, M., Jackson, M. J., and Southgate, P. N., 2000, Basement framework and geodynamic evolution of the Palaeoproterozoic superbasins of north-central Australia: An integrated review of geochemical, geochronological and geophysical data: Australian Journal of Earth Sciences, v. 47, no. 3, p. 341-380.

Southgate, P. N., Neumann, N. L., and Gibson, G. M., 2013, Depositional systems in the Mt Isa Inlier from 1800 Ma to 1640 Ma: Implications for Zn–Pb–Ag mineralisation: Australian Journal of Earth Sciences, v. 60, no. 2, p. 157-173.

Thorkelson, D. J., Abbott, J. G., Mortensen, J. K., Creaser, R. A., Villeneuve, M. E., McNicoll, V. J., and Layer, P. W., 2005, Early and middle Proterozoic evolution of Yukon, Canada: Canadian Journal of Earth Sciences, v. 42, no. 6, p. 1045-1071.

Thorkelson, D. J., and Laughton, J. R., 2015, Paleoproterozoic closure of an Australia–Laurentia seaway revealed by megaclasts of an obducted volcanic arc in Yukon, Canada: Gondwana Research, v. 33, p. 115-133.

Thorkelson, D. J., Mortensen, J. K., Creaser, R. A., Davidson, G. J., and Abbott, J. G., 2001, Early Proterozoic magmatism in Yukon, Canada: constraints on the evolution of northwestern Laurentia: Canadian Journal of Earth Sciences, v. 38, no. 10, p. 1479-1494.

Thorkelson, D. J., Mortensen, J. K., Davidson, G. J., Creaser, R. A., Perez, W. A., and Abbott, J. G., 2001, Early Mesoproterozoic intrusive breccias in Yukon, Canada: the role of hydrothermal systems in reconstructions of North America and Australia: Precambrian Research, v. 111, no. 1-4, p. 31-55.

Whitmeyer, S. J., and Karlstrom, K. E., 2007, Tectonic model for the Proterozoic growth of North America: Geosphere, v. 3, no. 4, p. 220-259.

Withnall, I. W., Bain, J. H. C., Draper, J. J., MacKenzie, D. E., and Oversby, B. S., 1988, Proterozoic stratigraphy and tectonic history of the Georgetown Inlier, northeastern Queensland: Precambrian Research, v. 40, p. 429-446.

Withnall, I. W., and Henderson, R. A., 2012, Accretion on the long-lived continental margin of northeastern Australia: Episodes, v. 35, no. 1, p. 166-176.

Withnall, I. W., and Hutton, L. J., 2013, Proterozoic–North Australian Craton, in Jell, P. A., ed., Geology of Queensland: Brisbane, Australia, Geological Survey of Queensland, p. 23-112.

Zhang, S., Li, Z.-X., Evans, D. A. D., Wu, H., Li, H., and Dong, J., 2012, Pre-Rodinia supercontinent Nuna shaping up: a global synthesis with new paleomagnetic results from North China: Earth and Planetary Science Letters, v. 353, p. 145-155.

Zhao, G., Cawood, P. A., Wilde, S. A., and Sun, M., 2002, Review of global 2.1–1.8 Ga orogens: implications for a pre-Rodinia supercontinent: Earth-Science Reviews, v. 59, no. 1, p. 125-162.

Zhao, G., Sun, M., Wilde, S. A., and Li, S., 2004, A Paleo-Mesoproterozoic supercontinent: assembly, growth and breakup: Earth-Science Reviews, v. 67, no. 1, p. 91-123.

Chapter 2: Resampling (detrital) zircon age distributions for accurate Multidimensional Scaling solutions

In round two of revisions at Earth-Science Reviews

Adam R. Nordsvan[1], Uwe Kirscher[1,2], Chris Kirkland[3], Milo Barham[3], Daniel T. Brennan[1]

[1]Earth Dynamics Research Group and The Institute for Geoscience Research (TIGeR), School of Earth and Planetary Sciences, Curtin University, Bentley, WA 6845, Australia

[2]Department of Geosciences, University of Tübingen, Tübingen, 72074, Germany

[3]Centre for Exploration Targeting – Curtin Node, School of Earth and Planetary Sciences, Curtin University, Bentley, WA 6845, Australia

2.1 Abstract

Multidimensional scaling (MDS) has become an important tool in detrital zircon geochronology for discriminating and comparing multiple samples, especially where large datasets are concerned. However, the non-parametrical statistical tests used in MDS (e.g., Kolmogorov–Smirnov [K-S] or Kuiper) to calculate differences between detrital zircon samples are sensitive to differences in grain age uncertainty. We illustrate the effect of differing age uncertainties on comparison metrics and MDS analysis using synthetic populations. Additionally, we introduce two techniques that reduce these limitations: bootstrap resampling and Procrustes rotation (BoPR) and error resampling MDS (ERM). These methods are used to show that results can be

significantly altered by up to 50% when comparing detrital samples with potential source areas. Resampling techniques reduce these limitations which can be shown on a case study comparing detrital samples from the Mesoproterozoic Roper Group of Northern Australia with nearby potential source regions. Mitigating the limitations of MDS, and the underlying statistics by employing resampling techniques makes MDS a more potent means of addressing source to sink relationships in detrital zircon studies.

2.2 Introduction

Detrital zircon (DZ) geochronology is a staple method for investigating sedimentary rocks (Fedo et al., 2003; Gehrels, 2011). The method relies on compiling individual zircon grain ages from a sedimentary sample, either modern or ancient, to capture a snapshot of the basin provenance. The method is most often utilised to link sediments (or sedimentary rocks) to potential source regions, make stratigraphic correlations, constrain maximum depositional ages and understand broader tectonic histories (Gehrels, 2014; Nordsvan et al., 2018; Rainbird and Davis, 2007). At its core, DZ geochronology often relies on making comparisons between different detrital samples and/or potential source regions, which is often achieved by plotting the data using probability density plots or kernel density estimations for subsequent visual comparison (Alonso-Torres et al., 2018). This approach is useful for quick assessments and local geological questions but is inefficient, inaccurate, and prone to subjective bias as compilations increase in size. To overcome the limitations of visual comparisons in DZ geochronology numerous statistical treatments have been proposed. Simply put, the aim of using statistical methods in detrital zircon studies is

to subjectively calculate and efficiently visualise the differences (dissimilarity) between multiple samples (Armistead et al., 2018; Barham et al., 2019; Kirkland et al., 2008; Satkoski et al., 2013; Saylor et al., 2012; Saylor and Sundell, 2016; Saylor et al., 2019; Sircombe and Hazelton, 2004; Vermeesch, 2013; Wissink et al., 2018).

Following Vermeesch (2013), Multidimensional Scaling (MDS) has become one of the more prevalent statistical procedures in DZ geochronology. In essence, MDS is a means of visualising (dis)similarity in multivariate datasets (Borg and Groenen, 2003; Cox and Cox, 2000; Kruskal, 1964; Torgerson, 1952). In DZ geochronology MDS encompasses the process of evaluating the difference between samples using a non-parametrical statistical test to create a dissimilarity matrix that can be visualised on a "map." The MDS map can consist of multiple dimensions; however, two dimensions are generally sufficient and most often used in DZ studies. Two of the most appropriate (Vermeesch, 2018), and utilised distance measures in DZ-MDS are the two-sample Kolmogorov-Smirnov (K-S) test (Massey, 1951; Vermeesch, 2013), and the Kuiper test (Kuiper, 1960; Saylor and Sundell, 2016). The K-S test measures the greatest absolute vertical difference between the empirical cumulative distribution functions (ECDF) of two samples, whereas the Kuiper test sums the greatest positive and negative vertical distance between the two samples (Figure 2.1). Importantly, in either test, results can be biased when comparing samples with different age uncertainties (Figure 2.1 and 2.2). These comparisons using either statistical test can lead to spurious correlations that are based more on the differences in age uncertainty than the differences in the given datasets. To resolve this issue, in this chapter, we develop two simple resampling and bootstrapping techniques that

address age uncertainties and allow us to plot confidence ellipses on two-dimensional MDS solutions.

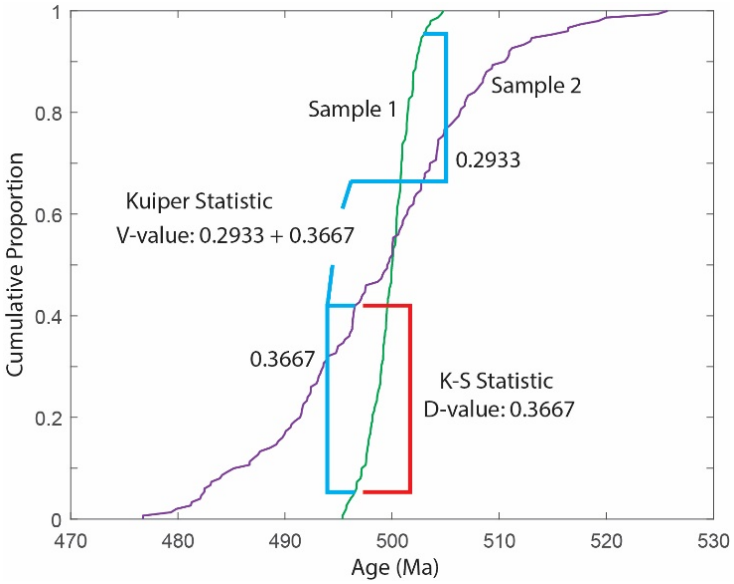

Figure 2.1: The Kolmogorov-Smirnov 2-sample test measures the maximum difference between the two samples empirical cumulative functions whereas the Kuiper test sums the greatest positive and negative distances. Sample 1 has a single population of 150 synthetic ages of 500 Ma with 0.5% uncertainty, sample 2 is the same but has 2.5% uncertainty.

Throughout the manuscript, we use various synthetic datasets along with previously published DZ data from the Mesoproterozoic Roper Group of the McArthur Basin in Northern Australia and nearby potential source regions (Munson et al., 2018). The DZ data from the Roper Group were obtained from laser ablation inductively coupled plasma mass spectrometry (LA-ICP-MS) with a median (2σ) uncertainty of 34 Ma, whereas the data from potential source regions were obtained using various different methods (including secondary ionization mass spectrometry; SIMS) but with a have a significantly lower median (1σ) age uncertainty of 10 Ma (Figure 2.2). Figure 2.2 highlights the difference in age uncertainty between the potential source regions (Igneous zircon) and the DZ data obtained with LA-ICP-MS (Figure 2.2; red and purple,

respectively). It is also interesting to note that source region data have a lower median 1σ age uncertainty than DZ data obtained with SIMS (SHRIMP).

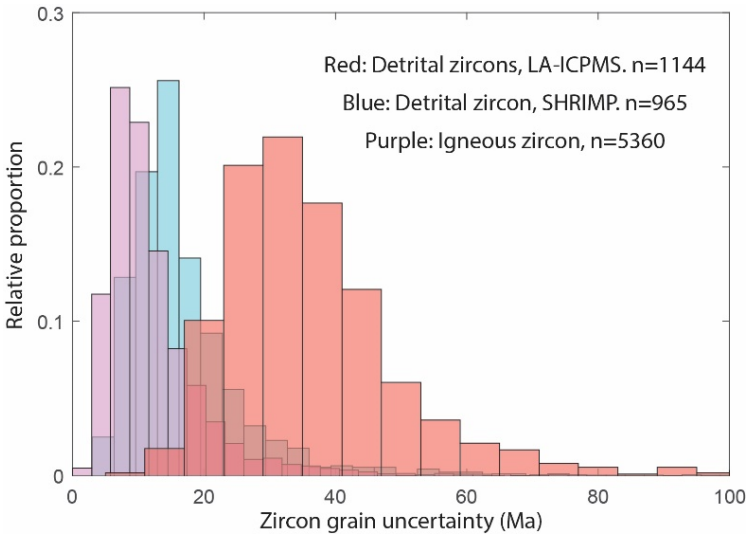

Figure 2.2: Comparison of age uncertainty of detrital zircon grains obtained with different analytical procedures and igneous grains obtained by all procedures. Detrital zircon data are from the McArthur Basin and the igneous data are from nearby potential source regions. Uncertainties are from 207Pb/206Pb ages taken directly from reports. They are 2σ for the LA-ICP-MS data and 1σ for the shrimp and igneous data. Analyses >10% discordant are excluded. Data compilation and sources are listed in Appendix Table 2.1 and in the supplementary file. SHRIMP: sensitive high-resolution ion microprobe. LA-ICP-MS: laser ablation inductively coupled plasma mass spectrometry.

2.3 Multidimensional Scaling in detrital zircon geochronology

The standard workflow of MDS in DZ geochronology can be broken down into two steps: i) pairwise comparison of input samples using a statistical test (e.g., K-S, Kuiper) to create a dissimilarity matrix; and ii) use the dissimilarity matrix to create an MDS "map" where the distances between the samples on the map correspond to the dissimilarities (calculated by the statistical test) between the samples (Vermeesch, 2013; Vermeesch, 2018). In MDS, the most common and appropriate methods for measuring the dissimilarity between DZ samples are the K-S and Kuiper tests (see

Vermeesch, 2018 for a review). Other nonparametric tests might be suitable for DZ geochronology, such as the Cramér–von Mises but have not received the same attention as the K-S or Kuiper tests. The two-sample K-S test is formally used to test if two samples come from the same distribution and is defined as:

$$D(1,2) = \max|E1(i) - E2(i)| \quad (1)$$

where E1 and E2 are the ECDF for the two samples and the resulting D-value is the maximum (absolute) distance between them. If the D-value (K-S statistic) exceeds a critical value than the null hypothesis (H0), that both samples come from the same population and have the same distribution, is rejected. Despite continued use (Ibañez-Mejia et al., 2018), the resulting P-value associated with the K-S test is not suited (Vermeesch, 2018) for DZ geochronology as the relevant question is: how different the two samples are, not how significant is the difference between the samples. In contrast to the P-value, the D-value of the K-S test is a dissimilarity measure and has been widely applied in DZ-MDS with significant and meaningful results. The two-sample Kuiper test is also appropriate for detrital geochronology and is defined as:

$$V = D1 + D2 = \max|E1(i) - E2(i)| + \max|E2(i) - E1(i)| \quad (2)$$

where E1 and E2 are the ECDF for the two samples. The Kuiper test is similar to the two-sample K-S test but sums the greatest positive and negative values between the two sample ECDFs to produce the V-value (Figure 2.1). Like the K-S test, the resulting P-value from the Kuiper test is not appropriate for detrital geochronology, but the V-value is. The Kuiper test is more sensitive to minor populations when compared with

the K-S test, as it takes two points of difference between the samples rather than a single point.

Results of the K-S and Kuiper tests may be affected by the uncertainty of ages within each sample population (Vermeesch, 2018). Take Figure 2.1 as an example. Sample 1 consists of 150 synthetic (zircon) ages taken from a 500 Ma population with 0.5% age uncertainty, whereas, Sample 2 is taken from the same population but has a 2.5% age uncertainty. These age uncertainties are realistic for data obtained from sensitive high-resolution ion microprobe (SHRIMP) and quadrupole laser ablation inductively coupled plasma mass spectrometry (LA-ICP-MS), respectively. Increasing the age uncertainty of a sample decreases the "slope" of the line in the respective ECDF and causes a significant offset so as to affect the result of both the K-S and Kuiper tests. Differences in uncertainty between samples will affect the K-S and Kuiper results mostly when comparing DZ samples with the same, single population consisting of over 70% of the sample.

It is not entirely clear how different any age uncertainties [of two samples derived from the same parent populations] need to be before D- and V- values are significantly degraded. Given their value in DZ provenance investigations, improvements to the K-S and Kuiper statistical tests in MDS are of particular interest. To better understand how the D- and V values can be impacted when comparing samples with different uncertainties, we produce 40,000 measurements of each (D- and V-values) using randomly generated age populations between 1 and 3000 Ma (N=500) and random level uncertainties between 1 and 50 Ma. For each case, the

random age populations are the same but each uncertainty between the samples different. Figure 2.3 shows the relationship for both the Kuiper V-value and the K-S D-Value with changing uncertainty between samples. No matter what the age of the population, the effect of comparing samples with different uncertainties is similar in terms of the D- and V-values. This relationship between uncertainty and the D- or V-value can be modelled by linear regression (Figure 2.3).

For the K-S test:

$$D = 0.4693x + 0.0035 \quad (3)$$

And, for the Kuiper:

$$V = 0.932x + 0.0428 \quad (4)$$

wherein both cases:

$$x = |Un1 - Un2| / Un1 + Un2 \quad (5)$$

Where, Un1 equals the mean uncertainty from sample 1 and Un2, the mean uncertainty from sample 2. This relationship allows one to input the observed uncertainties to better understand the effect that the different uncertainties could have on the statistical values. For the Kuiper test, the intercept should be subtracted from the result and taken as an approximate maximum percentage of difference that could be attributed to the dissimilar uncertainties. This relationship shows that the Kuiper test is more sensitive to variable uncertainties and also that small differences in the uncertainties can have a significant impact on the results when comparing precise samples. For example, a precise sample with 4 Ma average uncertainty

compared to a sample with 10 Ma uncertainty can change the K-S D-value by up to 20% and the Kuiper V-value up to 38%. Using real-world examples from Figure 2.2, comparing source regions (Mdn: 10) to the DZ data obtained by LA-ICP-MS (Mdn: 34) can alter the statistical values by up to 25% for the K-S test and 50% for the Kuiper test. This emphasises the crucial need to develop a method to account for different uncertainties when utilising the K-S or Kuiper tests in DZ-MDS. It should also be stated that decreasing sample size produces the same trend but increases the spread of the data.

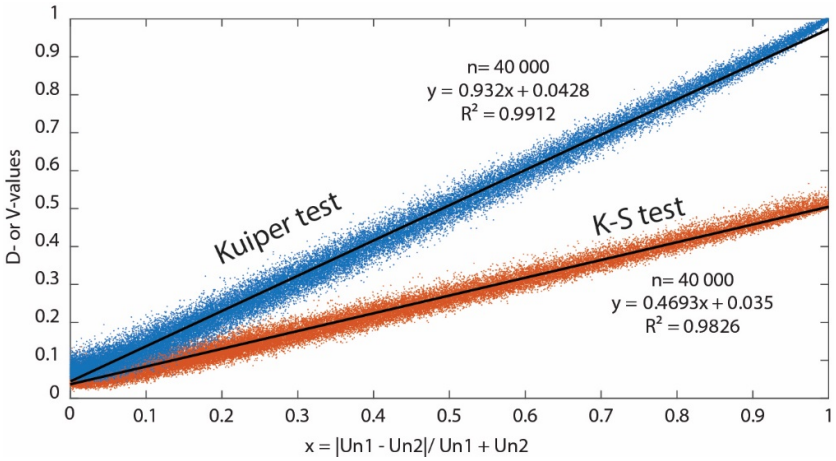

Figure 2.3: Linear relationship associated with measuring the dissimilarities between samples with different uncertainties. Un1 is the mean uncertainty of sample 1 and Un2 the mean uncertainty of sample 2.

Accounting for the difference in age uncertainties between samples has been a major challenge in DZ geochronology for a considerable period of time. To compare samples obtained with different analytical procedures, Sircombe and Hazelton (2004) developed the kernel function estimation (KFE) method. Ultimately, KFE uses a variable bandwidth to smooth samples so that the precision of each sample becomes equivalent across the entire dataset. Following this procedure, neither the K-S or

Kuiper tests can be utilised as a dissimilarity measurement as they require numerical data, however, the L2 norm distance between the samples is thought to be sufficient for MDS (Vermeesch, 2018). Figure 2.4 shows examples of “standard” MDS plots created using the K-S, Kuiper and the KFE as the dissimilarity measurements for data from the Mesoproterozoic Roper Group of the Mcarthur Basin in northern Australia and the surrounding potential source regions.

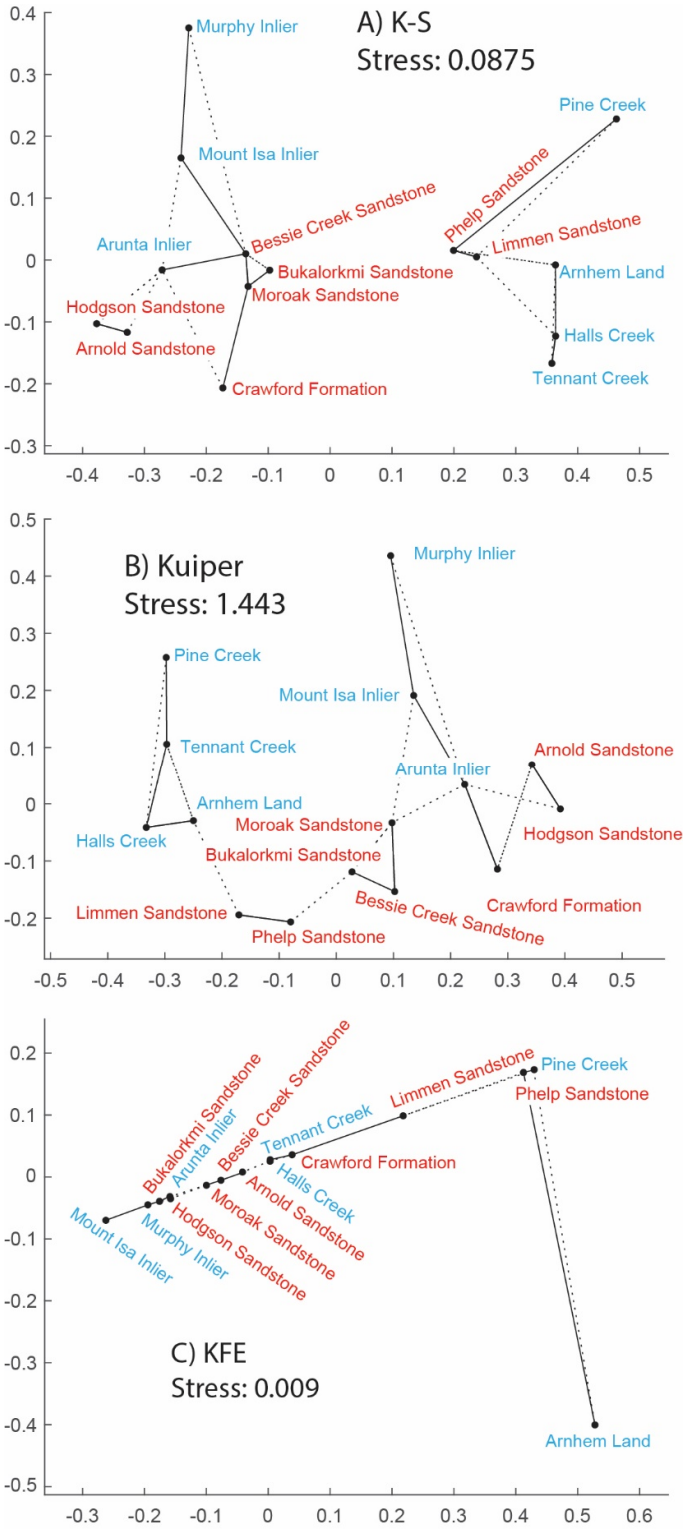

Figure 2.4: MDS plots resulting from A) K-S test, B) Kuiper test and C) KFE. Blue text denotes source area zircon samples and red text denotes detrital zircon samples from the basin strata. The solid line represents the nearest neighbour and dashed lines the second closest.

The only MDS plot in Figure 2.4 that considers the age uncertainties associated with the samples is the KFE (Figure 2.4C). Nevertheless, the stress value associated with the KFE-MDS plot is extremely low and the resulting plot suggests the data are "overfitting" and would be more suitable for unidimensional scaling (Meara et al., 2000). In this case, KFE has over smoothed the data, suggesting that important information is lost. The stress in MDS is a goodness of fit measurement where lower values indicate a better fit between the distances on the MDS plot and the measured dissimilarities between the samples. While typically stress below 0.15 is desirable, depending on the data, stress values higher than 0.15 can be appropriate and stress values too low (as in Figure 2.4C) indicate the data are overfitted and potentially meaningless (Borg and Groenen, 2003). We have found similar overfitting problems associated with KFE-MDS plots across numerous real-world datasets and recommended it be utilised with caution and tested against other methods.

Samples in MDS plots represent a single point on a "map" for which the distances to the other points represent the individual relationship to that specific sample (i.e. the dissimilarities). For straight forward multivariant data, this is adequate, but the standard MDS map does not display confidence or uncertainty with the input data or the (goodness of fit, stress) quality of the plot. One way to rectify this is by using the maximum likelihood estimation, which accounts for the uncertainty of the stress on the MDS plots but does not represent the uncertainty associated with the input data (Ramsay, 1977). Similarly, the stress per point method provides an uncertainty on the configuration of the MDS plot but not the input data (Mair et al., 2016). While these methods could be applied to DZ-MDS analysis and would provide another level of

detail they will not account for the uncertainty of the dissimilarity measurement or the age uncertainties. Another approach to handle confidence in MDS is to apply resampling strategies to the input values, such as jackknife (De Leeuw and Meulman, 1986) or bootstrap (Jacoby and Armstrong, 2014). Jacoby and Armstrong (2014) developed a bootstrap resampling strategy for constructing confidence regions in 2D MDS solutions for political science data. This algorithm integrates data with uncertainty by i) resampling the multivariant data to create bootstrap replicates for the complete dissimilarity matrix. ii) Perform MDS on each bootstrapped matrix, and iii) compare the replicated MDS solutions to the original MDS solution to assess the stability. A similar approach can be used in DZ-MDS to account for age uncertainties.

In this manuscript, we propose two solutions to limit the problems regarding age uncertainty in DZ-MDS. The first, inspired by Jacoby and Armstrong (2014) utilises bootstrap resampling and Procrustes rotation, the second uses a resampling technique and compares synthetic samples directly.

2.3.1 Method 1: Bootstrap resampling and Procrustes rotation (BoPR)

The bootstrap resampling and Procrustes rotation (BoPR) method require five steps. The first step is to produce a range of values that define the dissimilarity between each sample to account for the uncertainties. Following similar principles to the KFE method, every sample should be smoothed to the same uncertainty level, but ideally, the data remain numerical so to proceed with the K-S or Kuiper test. This is achieved by resampling the individual ages of the more precise samples to match the uncertainty of the less-precise data by adding the mean percentage uncertainty of

the less precise sample multiplied with a normal distributed random number between -1 and 1:

$$\vec{x}' = \vec{x} + (\vec{x} * P) * Rn \quad (6)$$

where $\vec{x}$ is the higher precision sample vector with individual grain ages. $\vec{x}'$ is the modified sample after resampling to the sample with higher precision. P is the mean percentage of age uncertainty of the sample(s) with the higher uncertainty (i.e. P=0.4 for 40%) and Rn is a normally distributed random value between -1 and 1. This error resampling method (ER) emulates KFE or kernel density estimate (KDE; Vermeesch, 2012) smoothing but maintains the numerical nature of the data so the K-S and Kuiper tests can still be utilised as the dissimilarity measurements (Figure 2.5). Figure 2.5A shows an example of the results of this procedure. S1 is a synthetic sample consisting of n=150 at 500 Ma with an uncertainty of 0.5% and S2 the same sample but with an uncertainty of 3%. S1 resampled (Figure 2.5A) is the result of the resampling procedure performed twice on S1. Figure 2.5B shows how the method emulates KFE smoothing. The resampling method resolves the problems associated with comparing samples with different age uncertainties with both the K-S and Kuiper tests. Table 2.1 and Figure 2.6 show the results from simulating 8000 K-S and Kuiper test D- and V-values for samples with 0.5% uncertainty (Figure 2.6A), 3% uncertainty (Figure 2.6B), comparing them against each other (Figure 2.6C), and for samples with 0.5% resampled to match the 3% uncertainty (Figure 2.6D). These results show that the amount of uncertainty does not impact the results of either the K-S or Kuiper tests when comparing samples with the same uncertainty (Figure 2.6A and 2.6B).

Also, they indicate that the resampling technique is appropriate to handle differences in uncertainty between the samples (Figure 2.6D).

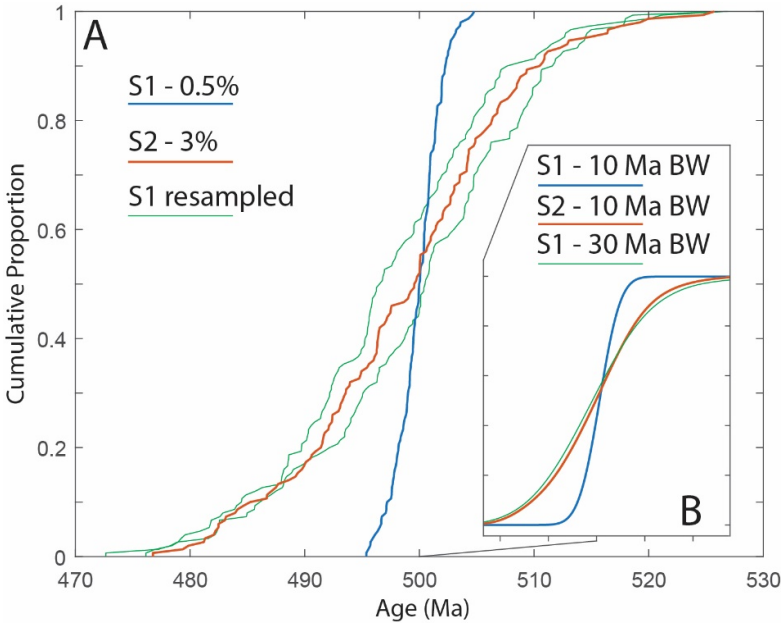

Figure 2.5: A) S1 is sample 1 from Figure 2.1 (n=150, 500 Ma grains with 0.5% uncertainty), S2 is the same but with 3% uncertainty. S1 resampled is the result of resampling S1 to match the uncertainty of S2. B) are the cumulative distribution functions of S1 following KFE smoothing with 10 Ma bandwidth, S2 with 10 Ma smoothing and S1 with 30 Ma smoothing to demonstrate how KFE smoothing produces similar results to the resampling method and vice versa.

Table 2.1: Input data to test the resampling methods ability to replicate D-and V-values.

Example	N	Age	Un (%)	Un (Ma)	K-S	Kuiper
a	500	1000	0.5	5	Mdn: 0.052	Mdn: 0.076
b	500	1000	3	30	Mdn: 0.052	Mdn: 0.074
c		a vs c			Mean: 0.42	Mean: 0.81
d		a(resampled) vs c			Mdn: 0.052	Mdn: 0.076

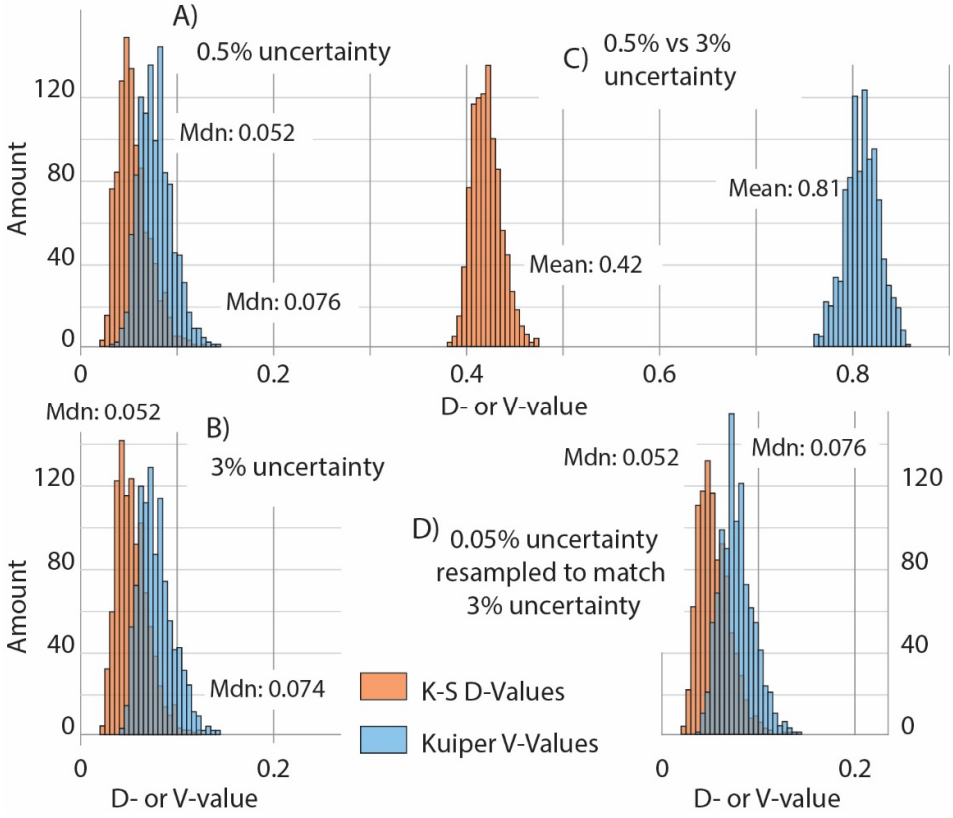

Figure 2.6: The results from simulating 8000 K-S and Kuiper test D- and V-values. A) With 0.5% uncertainty B) 3% uncertainty C) 0.5% uncertainty vs. 3% uncertainty. D) 0.5% samples resampled to match the 3% uncertainty.

The resampling technique is applied X amount of times on the samples with higher precision (low uncertainty) to match the samples with the higher uncertainties. The second step requires that all samples, including the resampled ones, are compared using the K-S or Kuiper tests to produce a set of D-or V-values (dissimilarity values). Where there are multiple D-or V-values representing the dissimilarity, such as when comparing samples with different uncertainties, (the third step) the values are bootstrapped Y amount of times so as to create Z amount of MDS plots. Each MDS plot is generated by randomly re-sampling the dissimilarity values from Y populations.

In the fourth step, the Z MDS plots are then compared using Procrustes rotation (Borg and Groenen, 2003). Procrustes rotation is a method used to compare the configuration of two plots by rotating and scaling. This is mathematically achieved by superimposing one plot on the other to reduce the sum of squared differences between the points. The minimum sum of squares is called the root mean square error (RMSE) and the smaller the RMSE, the more similar the two configurations are. The configurations are considered to have converged when the RMSE is less than 0.01, and no single residual value exceeds 0.005. Procrustes rotation can be used to compare any MDS plot with another (or a resulting Procrustes plot) in a number of different ways since the method is valid on any 2D configuration. We attempted four different approaches of utilising Procrustes rotation (Figure 2.7) and while all produced valid results in certain cases, M4 produced the most reliable results in the most often cases. The final step is to fit 90% confidence ellipses to each sample in the MDS solution.

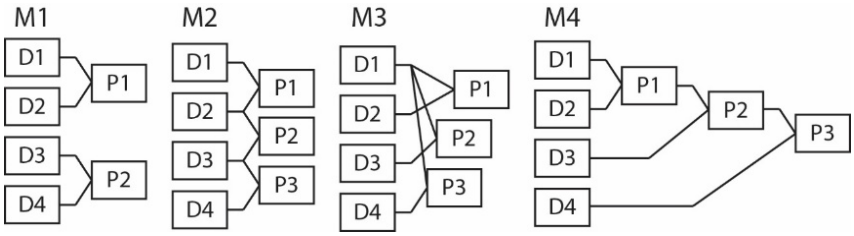

Figure 2.7: Methods for utilising Procrustes rotation. M = Method. D = MDS coordinates. P = Procrustes coordinates.

To illustrate the effectiveness of the bootstrap resampling and Procrustes method in limiting problems associated with comparing samples with different uncertainties we provide an example using synthetic data. In the example, we use four different samples and apply three different levels of uncertainty on each (low, medium, and

high). The sample populations can be observed in Table 2.2. The appropriate response for the MDS plot should be that samples A cluster together, as well as samples S, and so forth. As seen in Figure 2.8A and 2.8B, the standard K-S and Kuiper MDS plots fail to group the samples based on their populations and rather plot them based on their similarities in uncertainty. Importantly, as seen in Figure 2.8C and 2.8D, utilising BoPR amends the MDS plots and groups the samples based on their similar age populations. The MDS plots also distinguish both sample populations as the X-axis is sorting the samples by their primary populations (80%) and the Y-axis their secondary (20%) populations.

Table 2.2: Input data for testing i) the bootstrap resampling and Procrustes method (Figure 2.8) and ii) the resampling method (Figure 2.9).

	Age populations (Ma)		
Sample	80%	20%	(%)
AL	500	800	0.4
AM	500	800	1
AH	500	800	3
SL	500	700	0.4
SM	500	700	1
SH	500	700	3
DL	600	700	0.4
DM	600	700	1
DH	600	700	3
FL	600	800	0.4
FM	600	800	1
FH	600	800	3

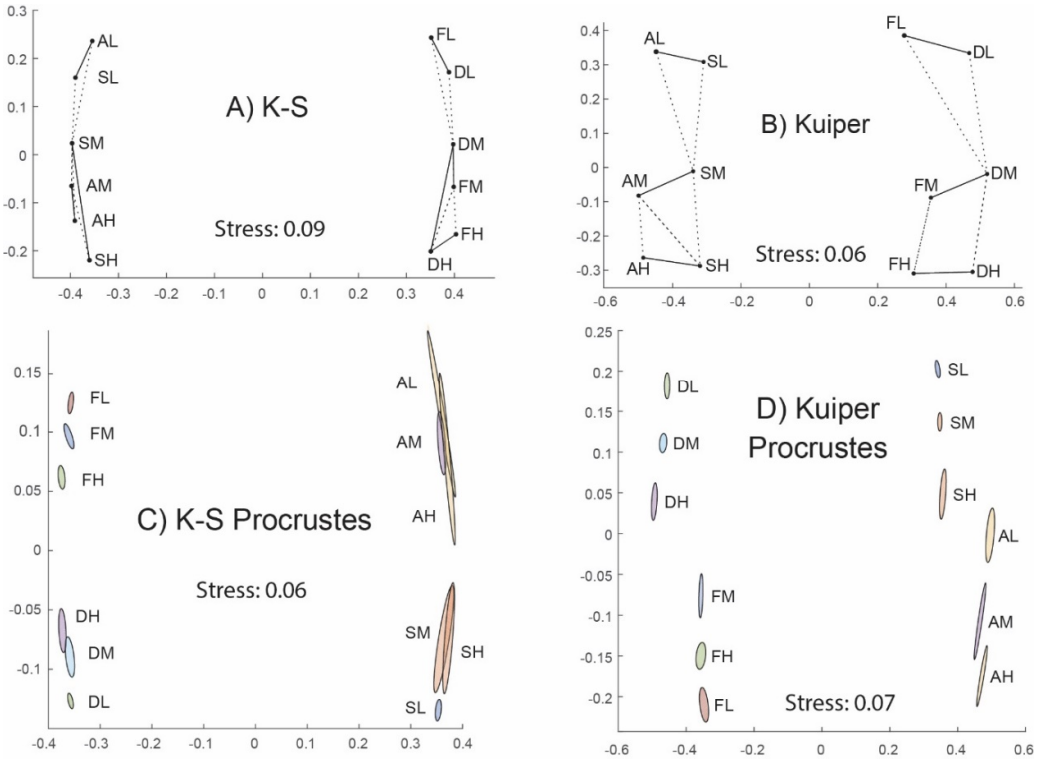

Figure 2.8: Results of testing the bootstrap resampling and Procrustes method for handling different uncertainties. A) standard K-S based MDS plot. B) Standard Kuiper based MDS plot. C) K-S based MDS following the bootstrap resampling and Procrustes method. D) Kuiper following the bootstrap resampling and Procrustes method.

2.3.2 Method 2: Error resampling MDS (ERM)

The alternative method used to account for different uncertainties in DZ-MDS is similar to the previous method in using the ER method but much simpler. In this method, the resampling strategy (ER, equation 6) is used on the more precise data to match that of the less precise data. Subsequently, all the samples, including those resampled, are compared using the K-S or Kuiper test and are all plotted on a single MDS map. Points that represent data obtained with higher uncertainty denote a single point on the resulting MDS plot and the higher precision data many points. For ease of interpretation, 90% confidence ellipses are fitted to the resampled higher precision data. Figure 2.9 shows the results of this method using the same data from

the previous synthetic example (Table 2.2 and Figure 2.8). The results indicate this method is just as useful as the BoPR method

2.4 Real-world case study: The Proterozoic Roper Group, Australia

Both methods proposed here are valuable for identifying source regions of the Mesoproterozoic Roper Group, McArthur Basin, Northern Territory (Ahmad et al., 2013; Rawlings and Scott, 2002; Scott et al., 2000). The McArthur Basin is exposed over an area of 180 000 km^2 in northern Australia where it overlies Paleoproterozoic orogenic terranes; the Pine Creek Orogen to the west, the Arnhem Province to the northeast and the Murphy Inlier to the southeast (Figure 2.9) (Ahmad et al., 2013). The basin is characterised by unmetamorphosed and reasonably undeformed deep to shallow marine siliciclastic and carbonate facies, with minor fluvial and volcanic rocks that are up to ~15 km thick (Rawlings, 1999). Stratigraphically, the basin is sub-divided into five disconformity-bound "packages" that are mostly correlated using lithofacies, age dating and stratigraphic position (Figure 2.9) (Rawlings, 1999). Stratigraphically, the Wilton package occurs towards the top of the basin and the Roper Group is the sequence that occurs in the southern region. The Roper Group is roughly 1500 m thick and consists of six coarsening upward sequences that are dived into two subgroups, the lower Collara Subgroup and the upper Maiwok Subgroup (Abbott and Sweet, 2000; Abbott et al., 2001). The Collara Subgroup is characterised by shallow marine sandstones and deeper marine mudstones. The Maiwok Subgroup disconformably overlies the Collara Subgroup and consists of similar depositional facies but has notable less sandstone. Detrital zircon data are readily available from

the Roper Group along with igneous zircon ages from the adjacent potential source regions. Furthermore, the data were obtained using different analytical procedures and have different uncertainties. Thus, the Roper Group provides an excellent case study to utilise the resampling techniques discussed herein. We take eight DZ samples that span the entire Roper Group sequence to access the provenance of the sediments and the validity of our methods.

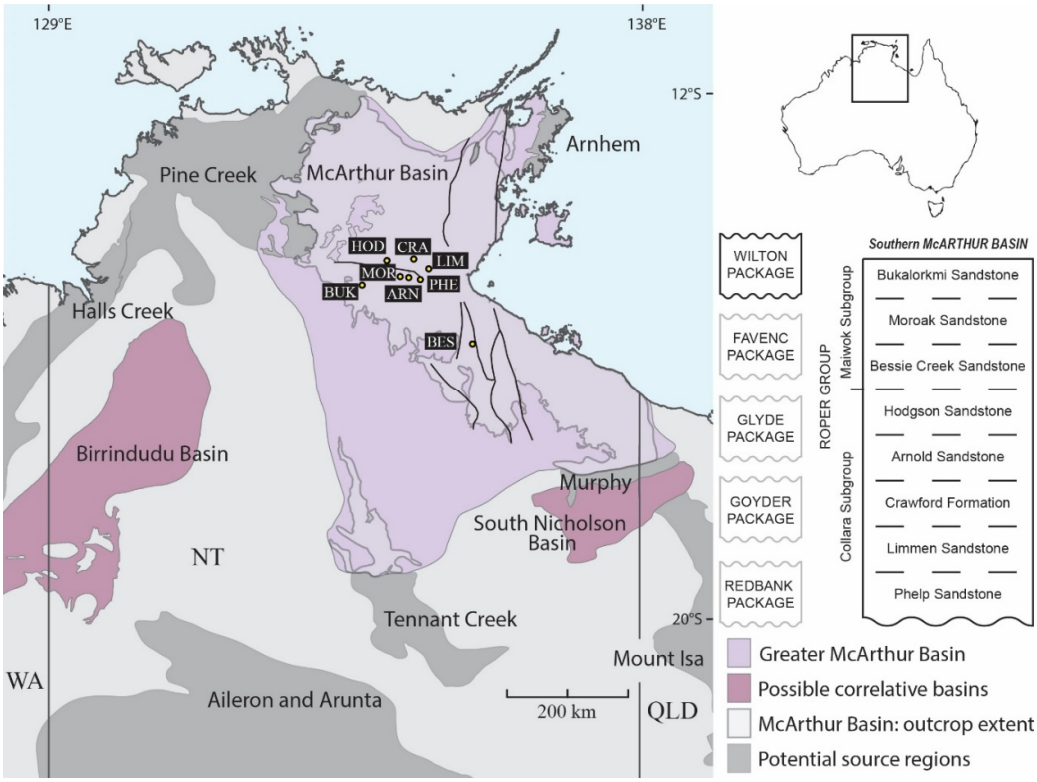

Figure 2.9: Regional map showing the McArthur Basin and potential source regions and simplified stratigraphic column of the Roper Group. Yellow circles are sample locations with the first three letters of each sample. See Table 2.3 for an overview of the samples.

2.4.1 Methods

Detrital zircon U-Pb age data were obtained from Munson et al. (2018) (Table 2.3). Only data within 10% of concordia are considered. All MDS plots were generated using our new methods with newly developed scripts in Matlab that were inspired by the MuDisc script

(Vermeesch, 2013). The data for the source regions were obtained from the Geoscience Australia Geochron Delivery system (http://www.ga.gov.au/geochron-sapub-web/geochronology/shrimp/search.htm). To avoid bias related to source area data and depositional age, source area data were limited to ages older than 1300 Ma to match the depositional age of the sediments (ca. 1450 to 1300 Ma). For the BoPR method we resampled the higher precision data (source regions) 20 (X) times for each sample using 2.2% uncertainties to match the lower precision data. We bootstrapped those results 300 (Y) times on each D- or V-value and produced 50 (Z) MDS plots for the subsequent Procrustes rotation. For the resampling method (ReM; Method 2) we resampled the higher precision data (source regions) 20 times for each sample. All MDS plots are non-classical and use non-metric scaling, i.e. the stress is normalised by the sum of squares of the inter-point distances rather than the dissimilarities.

Table 2.3: Detrital zircon samples used in the case study, taken from Munson et al. (2018).

Sample (sub-group)	Location (GPS Coordinate)	Analytical Method	Number of analysis	Average uncertainty (myr)
Phelp Sandstone (Collara)	MGA94 Zone 53 463247mE 8360755mN	LA-ICP-MS	77	37.0
Limmen Sandstone (Collara)	MGA94 Zone 53 477151mE 8379039mN	LA-ICP-MS	29	37.5
Crawford Formation (Collara)	MGA94 Zone 53 452370mE 8395579mN	LA-ICP-MS	18	33.2
Arnold Sandstone (Collara)	MGA94 Zone 53 444475mE 8364049mN	LA-ICP-MS	84	39.7
Hodgson Sandstone (Collara)	MGA94 Zone 53 408460mE 8392580mN	LA-ICP-MS	59	34.2
Bessie Creek Sandstone (Maiwok)	MGA94 Zone 53 548465mE 8252458mN	LA-ICP-MS	75	42.2
Moroak Sandstone (Maiwok)	MGA94 Zone 53 430184mE 8365941mN	LA-ICP-MS	86	36.2
Bukalorkmi Sandstone (Maiwok)	MGA94 Zone 53 368075mE 8350979mN	LA-ICP-MS	29	34.5

2.4.2 Results

The standard K-S based MDS plot suggests that the sedimentary samples can be placed into three groups (Figure 2.10A), the Phelp and Limmen sandstones in the first,

the Hodgson and Arnold sandstones in the second, and the Bessie Creek, Bukalorkmi and Moroak sandstones in the third. One sample, the Crawford Formation does not appear to group with any of the other samples in the standard K-S plot (Figure 2.10A), however, in other plots, this sample is proximal to the "group 2" samples (Figure 2.10C). The groups correlate with the stratigraphic position, from the oldest (Group 1) to youngest (Group 3). The results of the standard K-S MDS plot suggest that the older samples were sourced from either the Pine Creek Orogen to the northwest, the Arnhem Province to the north/northeast or a combination of both. The "Group 2" samples from the middle part of the succession were sourced from the Arunta Inlier to the south, and the uppermost sediments from the Arunta- and/or Mount Isa inliers from the south and south-east, respectively.

When considering the limitations of comparing samples with different uncertainties by utilising the methods introduced in this manuscript the results are altered to a level significantly for scientific questions of the data sets. For example, using the BoPR method (1) the sedimentary samples maintain their groupings (Figure 2.10B), but the probable source regions shift and the DZ samples plot more proximal to their potential source regions. Thus, justifying the need to account for the difference in uncertainties between DZ samples and the source regions. By considering the sample method uncertainty the results are more robust and therefore more decisive. The BoPR MDS suggests that the lowermost sediments (group 1) were sourced from the Arnhem Province, with perhaps a slight influence from the Pine Creek Orogen. Group 2 samples and the Crawford Formation are inconclusive, suggesting none of the potential source regions in the plot can adequately explain their respective age

spectra. Finally, the uppermost sediments (group 3) were most likely sourced from the Arunta Inlier to the south. The resampling method (method 2) produces similar results to the BoPR method, confirming that this approach is a suitable means to mitigate against DZ comparison issues caused by sample uncertainty (Figure 2.10C). Interestingly, the larger size of the ellipse for the Murphy Inlier data may correspond with the small sample size N=91. The size of the uncertainty ellipse appears related to N for method 2 (resampling) but does not occur for BoPR.

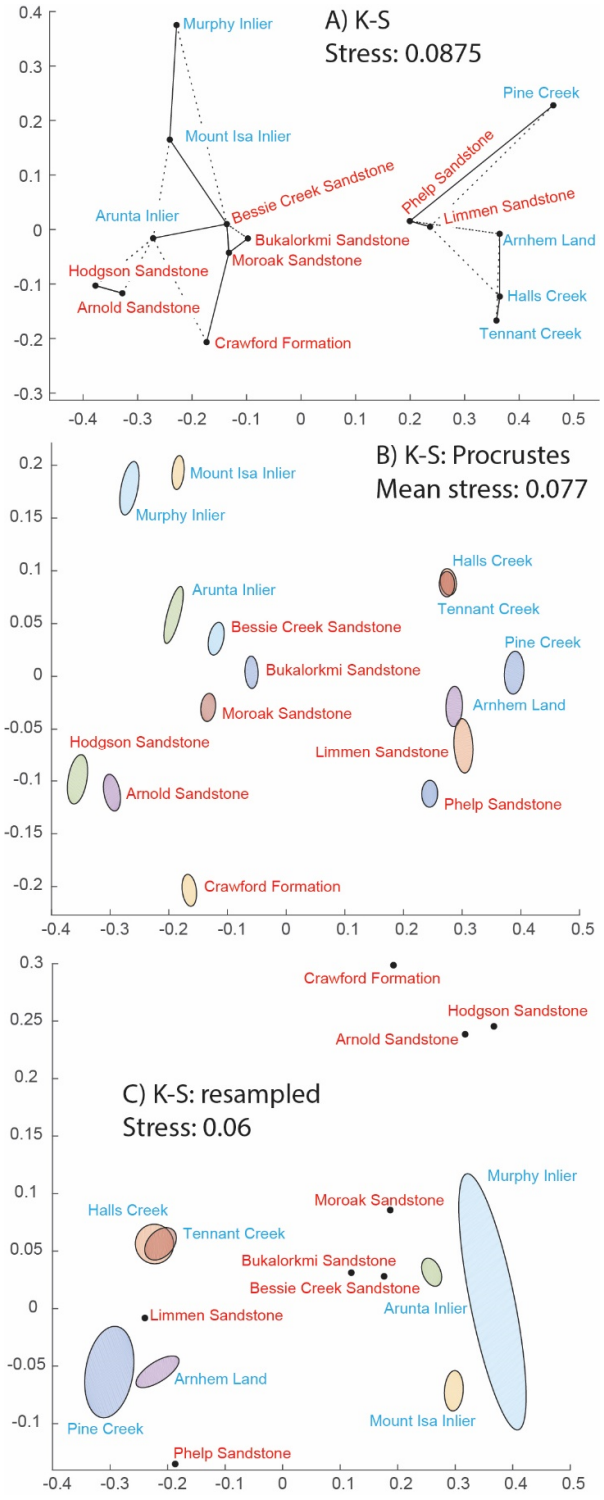

Figure 2.10: Results of the K-S based MDS analysis. A) Standard MDS plot not accounting for different uncertainties. B) MDS plot following bootstrap resampling and Procrustes method. C) MDS plot following the resampling method. Red text denotes detrital samples, whereas blue text is the source regions. The colours of the ellipses are for illustrative purpose.

As expected, the standard Kuiper test based MDS plot (Figure 2.11A) does a poor job of grouping the sediments with potential source regions as the V-value is highly sensitive when comparing samples with different uncertainties. Applying the BoPR and ReM methods has significantly improved the results for the Kuiper based MDS plots (Figure 2.11B and 2.12C). The BoPR (method 1) Kuiper MDS plot has similar results to the K-S based plots, suggesting the lowest units (group 1) were sourced from the Arnhem Province and that group 2 samples are unresolved (Figure 2.11B). Also similar to the K-S based plots, the uppermost sediments (group 3) plot nearest the Arunta Inlier, however, the Bessie Creek Sandstone is slightly more proximal with the Mount Isa Inlier (Figure 2.11B). The results utilising ReM (method 2) for the Kuiper MDS plot are the most different from the other three (resampling) plots (Figure 2.10 and 2.12). The resampled MDS plot shows one (Phelp Sandstone) of the samples from the lowermost units (group 1) plotting nearest the Arnhem Province, whereas the other (Limmen Sandstone) plots nearest Halls Creek. The group 2 samples plot far away from all other samples and hence remain uncertain. The samples from the upper part of the sequence plot nearest to the Mount Isa Inlier and second nearest to the Arunta Inlier (Figure 2.11C).

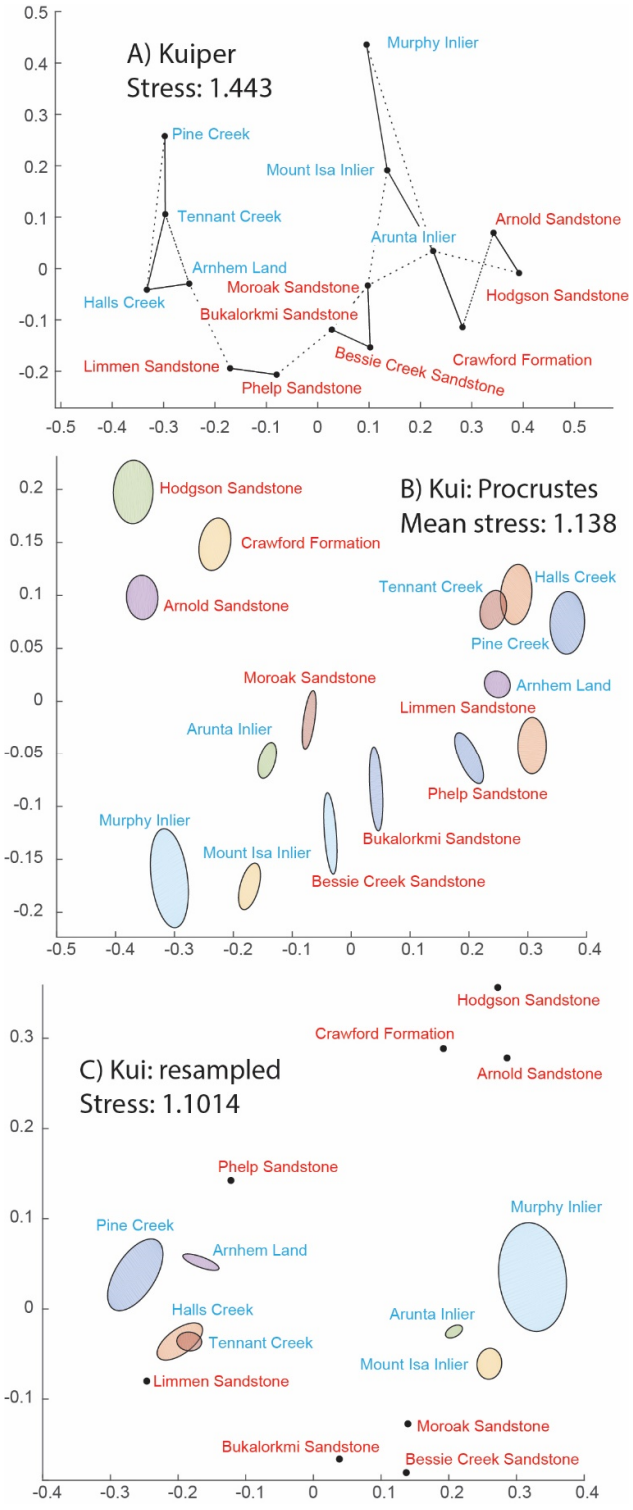

Figure 2.11: Results of the Kuiper based MDS analysis. A) Standard MDS plot not accounting for different uncertainties. B) MDS plot following bootstrap resampling and Procrustes method. C) MDS plot following the resampling method. Red text denotes detrital samples, whereas blue text is the source regions. The colours of the ellipses are for illustrative purpose.

2.4.3 Discussion

All the MDS plots that account for uncertainties suggest the basal units of the Roper Group were sourced from northern terranes (Arnhem, Pine Creek, etc.) whereas the uppermost units were sourced from southernly terranes (Arunta, Mount Isa, etc.). Group 2 samples from the middle of the sequence were unresolved in MDS space. This could suggest that these samples were sourced from an exotic terrane, or that extra steps are needed when attempting to resolve source regions with MDS. Two possible solutions to these unresolved provenance signatures in group 2 could be to combine the detrital samples, and/or to break the source regions up into time slices (i.e. remove ages younger than 1500 Ma, 1600 Ma, and so on). We refrain from attempting that here as it is beyond the scope of this manuscript and requires substantial explanation. Recently, based on a DZ study from drill core intersecting the Roper Group south of the exposed sequence, Yang et al. (2018) suggested that the Bessie Creek Sandstone (upper part, group 3) was sourced from the Mount Isa Inlier broadly consistent with our results. Yang et al. (2018) also suggest a provenance shift occurs directly above the Bessie Creek Sandstone, however, the results here are in contrast with that finding and suggest a similar provenance for the units overlying the Bessie Creek Sandstone. This contrast could be due to local DZ variations, or the provenance shift occurred at different times in different parts of the basin. Alternatively, it may be that the MDS analysis of Yang et al. (2018) had lost resolving power as the differences in uncertainty between the samples were not accounted for.

Whereas, the results of the standard K-S and Kuiper based MDS plots were ambiguous, both the PoBR method and the ReM method provide more resolving power for linking the potential source regions with the samples. A key part of both methods is the resampling procedure to emulate KDE/KFE smoothing to match the uncertainties. This can be achieved

by resampling to the mean uncertainty of the less precise sample or to the percentage of the age uncertainty. This decision could have implications if resampling to samples that include both $^{206}U/^{238}Pb$ and $^{206}Pb/^{207}Pb$ ages as there is a substantial difference in the age uncertainty with each system (which is in part a function of the detrital age itself).

Another factor we found important for the Procrustes rotation (BoPR) was adjusting the starting configuration of the MDS plots. The final configuration of any MDS plot is dictated by its starting position. Typically, (like in Matlab) MDS plots start at a classical scaling solution. The data are then adjusted to reach the best fit (limit the stress). These adjustments can occur in multiple ways and the resulting MDS plots can achieve minimal stress having a number of different configurations. Often MDS plots will have the same configuration but just be reflected or inverted. This spatial arrangement can cause problems with the Procrustes method. To account for this, the starting configuration of every MDS plot can be configured to reflect the previous Procrustes coordination that resulted from comparing the previous two MDS plots. Finally, it is worth mentioning that adjusting the number of times the individual samples were resampled, the D-/V-values bootstrapped, or the quantity of MDS plots did not have a significant impact on the results. For the BoPR method, we resampled each (more precise) sample 20 (X) times, bootstrapped those results 300 (Y) times and produced 50 (Z) MDS plots for this Procrustes rotation. These variables can be adjusted with ease in the associated Matlab script but typically have a very little impact above roughly: X = 10, Y=100, and Z=25.

2.5 Conclusions

DZ geochronology is a widely used technique that can address a range of earth-science questions. This approach is strengthened using robust statistical methods that aid correlation, such as MDS. Although MDS analysis is becoming an essential

tool to evaluate DZ geochronology, some nuances of its application remain untested in certain situations. Comparing samples with different uncertainties can significantly alter the results up to 25% when using the K-S test, or and 50% when the Kuiper test as the dissimilarity measure. While this might be seen to discredit those tests, it more so reflects the complications associated with comparing DZ datasets with different uncertainties. In any statistical test, or else wise (even visual comparison), if the uncertainties between samples are not sufficiently accounted for then miscorrelations can occur. Addressing issues related to comparing samples with different age uncertainties is a high priority as we demonstrate correlation metrics may be produced simply due to age uncertainty alone. In this work, we provide two methods, both based on resampling techniques, that address this issue. These provide an opportunity to robustly link DZ samples to source regions in MDS plots. The Roper Group case study demonstrates that uncertainty-based resampling enables better source to sink correlations indicating that basal units were sourced from northernly regions, whereas younger sediments were sourced from the south.

2.6 Acknowledgements

This chapter has benefitted significantly from reviews at the scientific journal *Earth-Science Reviews* by Pieter Vermeesch, Tom Andersen, Joel Saylor, and Daniel Coutts.

2.7 References

Abbott, S.T. and Sweet, I.P., 2000. Tectonic control on third-order sequences in a siliciclastic ramp-style basin: an example from the Roper Superbasin (Mesoproterozoic), northern Australia. Australian Journal of Earth Sciences, 47(3): 637-657.

Abbott, S.T., Sweet, I.P., Plumb, K.A., Young, D.A., Cutovinos, A., Ferenczi, P.A., Brakel, A.T. and Pietsch, B.A., 2001. Roper Region: Urapunga - Roper River, Northern Territory : combined explanatory notes.

Ahmad, M., Dunster, J.N. and Munson, T.J., 2013. Chapter 15: McArthur Basin. In: A. M and M. T.J. (Editors), Geology and mineral resources of the Northern Territory. Northern Territory Geological Survey: Special Publication, Darwin, Australia.

Alonso-Torres, D., Beauchamp, B., Guest, B., Hadlari, T. and Matthews, W., 2018. Late Paleozoic to Triassic arc magmatism north of the Sverdrup Basin in the Canadian Arctic: Evidence from detrital zircon U-Pb geochronology. Lithosphere, 10(3): 426-445.

Armistead, S.E., Collins, A.S., Payne, J.L., Foden, J.D., De Waele, B., Shaji, E. and Santosh, M., 2018. A re-evaluation of the Kumta Suture in western peninsular India and its extension into Madagascar. Journal of Asian Earth Sciences, 157: 317-328.

Barham, M., Kirkland, C.L. and Hollis, J., 2019. Spot the difference: Zircon disparity tracks crustal evolution. Geology, 47(5): 435–439.

Borg, I. and Groenen, P., 2003. Modern multidimensional scaling: Theory and applications. Journal of Educational Measurement, 40(3): 277-280.

Cox, T.F. and Cox, M.A.A., 2000. Multidimensional scaling. Chapman and hall/CRC, Boca Raton, FL.

De Leeuw, J. and Meulman, J., 1986. A special jackknife for multidimensional scaling. Journal of Classification, 3(1): 97-112.

Fedo, C.M., Sircombe, K.N. and Rainbird, R.H., 2003. Detrital zircon analysis of the sedimentary record. Reviews in Mineralogy and Geochemistry, 53(1): 277-303.

Gehrels, G., 2011. Detrital zircon U-Pb geochronology: Current methods and new opportunities, Tectonics of sedimentary basins: Recent advances. Blackwell Publishing Ltd, pp. 45-62.

Gehrels, G., 2014. Detrital zircon U-Pb geochronology applied to tectonics. Annual Review of Earth and Planetary Sciences, 42: 127-149.

Ibañez-Mejia, M., Pullen, A., Pepper, M., Urbani, F., Ghoshal, G. and Ibañez-Mejia, J.C., 2018. Use and abuse of detrital zircon U-Pb geochronology—A case from the Río Orinoco delta, eastern Venezuela. Geology, 46(11): 1019-1022.

Jacoby, W.G. and Armstrong, D.A., 2014. Bootstrap confidence regions for multidimensional scaling solutions. American Journal of Political Science, 58(1): 264-278.

Kirkland, C.L., Strachan, R.A. and Prave, A.R., 2008. Detrital zircon signature of the Moine Supergroup, Scotland: Contrasts and comparisons with other Neoproterozoic successions within the circum-North Atlantic region. Precambrian Research, 163(3-4): 332-350.

Kruskal, J.B., 1964. Nonmetric multidimensional scaling: a numerical method. Psychometrika, 29(2): 115-129.

Kuiper, N.H., 1960. Tests concerning random points on a circle, Nederl. Akad. Wetensch. Proc. Ser. A, pp. 38-47.

Mair, P., Borg, I. and Rusch, T., 2016. Goodness-of-fit assessment in multidimensional scaling and unfolding. Multivariate behavioral research, 51(6): 772-789.

Massey, F.J., 1951. The Kolmogorov-Smirnov test for goodness of fit. Journal of the American statistical Association, 46(253): 68-78.

Meara, K., Robin, F. and Sireci, S.G., 2000. Using multidimensional scaling to assess the dimensionality of dichotomous item data. Multivariate Behavioral Research, 35(2): 229-259.

Munson, T.J., Thompson, J.M., Zhukova, I., Meffre, S., Beyer, E.E., Woodhead, J.D. and Whelan, J.A., 2018. Summary of results. NTGS laser ablation ICP-MS U-Pb and Lu-Hf geochronology project: Roper Group (McArthur Basin), overlying ungrouped units (Beetaloo Sub-basin), Renner Group (Tomkinson Province), and Tijunna Group (Birrindudu Basin). 1443-1149, Darwin, Australia.

Nordsvan, A.R., Collins, W.J., Li, Z.-X., Spencer, C.J., Pourteau, A., Withnall, I.W., Betts, P.G. and Volante, S., 2018. Laurentian crust in northeast Australia:

Implications for the assembly of the supercontinent Nuna. Geology, 46(3): 251-254.

Rainbird, R.H. and Davis, W.J., 2007. U-Pb detrital zircon geochronology and provenance of the late Paleoproterozoic Dubawnt Supergroup: Linking sedimentation with tectonic reworking of the western Churchill Province, Canada. Geological Society of America Bulletin, 119(3-4): 314-328.

Ramsay, J.O., 1977. Maximum likelihood estimation in multidimensional scaling. Psychometrika, 42(2): 241-266.

Rawlings, D.J., 1999. Stratigraphic resolution of a multiphase intracratonic basin system: the McArthur Basin, northern Australia. Australian Journal of Earth Sciences, 46(5): 703-723.

Rawlings, D.J. and Scott, D., 2002. Geodynamics of the Redbank package, basal McArthur Basin, Annual geoscience exploration seminar (AGES),. Northern Territory Geological Survey.

Satkoski, A.M., Wilkinson, B.H., Hietpas, J. and Samson, S.D., 2013. Likeness among detrital zircon populations—An approach to the comparison of age frequency data in time and space. Bulletin, 125(11-12): 1783-1799.

Saylor, J.E., Stockli, D.F., Horton, B.K., Nie, J. and Mora, A., 2012. Discriminating rapid exhumation from syndepositional volcanism using detrital zircon double dating: Implications for the tectonic history of the Eastern Cordillera, Colombia. Bulletin, 124(5-6): 762-779.

Saylor, J.E. and Sundell, K.E., 2016. Quantifying comparison of large detrital geochronology data sets. Geosphere, 12(1): 203-220.

Saylor, J.E., Sundell, K.E. and Sharman, G.R., 2019. Characterizing sediment sources by non-negative matrix factorization of detrital geochronological data. Earth and Planetary Science Letters, 512: 46-58.

Scott, D.L., Rawlings, D.J., Page, R.W., Tarlowski, C.Z., Idnurm, M., Jackson, M.J. and Southgate, P.N., 2000. Basement framework and geodynamic evolution of the Palaeoproterozoic superbasins of north-central Australia: An integrated

review of geochemical, geochronological and geophysical data. Australian Journal of Earth Sciences, 47(3): 341-380.

Sircombe, K.N. and Hazelton, M.L., 2004. Comparison of detrital zircon age distributions by kernel functional estimation. Sedimentary Geology, 171(1-4): 91-111.

Torgerson, W.S., 1952. Multidimensional scaling: I. Theory and method. Psychometrika, 17(4): 401-419.

Vermeesch, P., 2013. Multi-sample comparison of detrital age distributions. Chemical Geology, 341: 140-146.

Vermeesch, P., 2018. Dissimilarity measures in detrital geochronology. Earth-Science Reviews, 178: 310-321.

Wissink, G.K., Wilkinson, B.H. and Hoke, G.D., 2018. Pairwise sample comparisons and multidimensional scaling of detrital zircon ages with examples from the North American platform, basin, and passive margin settings. Lithosphere, 10(3): 478-491.

Yang, B., Smith, T.M., Collins, A.S., Munson, T.J., Schoemaker, B., Nicholls, D., Cox, G., Farkas, J. and Glorie, S., 2018. Spatial and temporal variation in detrital zircon age provenance of the hydrocarbon-bearing upper Roper group, Beetaloo sub-basin, Northern Territory, Australia. Precambrian Research, 304: 140-155.

Chapter 3: Laurentian crust in northeast Australia: Implications for the assembly of the supercontinent Nuna

Published in GEOLOGY

Laurentian crust in northeast Australia: Implications for the assembly of the supercontinent Nuna: *GEOLOGY*, v. 46, no. 3, p. 251-254.

Adam R. Nordsvan[1], William J. Collins[1], Zheng-Xiang Li[1], Christopher J. Spencer[1], Amaury Pourteau[1], Ian W. Withnall[2], Peter G. Betts[3] and Silvia Volante[1]

[1]Earth Dynamics Research Group, ARC Centre of Excellence for Core to Crust Fluid Systems (CCFS) and The Institute for Geoscience Research (TIGeR), School of Earth and Planetary Sciences, Curtin University, GPO Box U1987, WA 6845, Australia

[2]Geological Survey of Queensland, Department of Natural Resources and Mines, PO Box 15216, City East, QLD 4002, Australia

[3]School of Earth, Atmosphere and Environment, Monash University, 9 Rainforest Walk, Clayton Campus, VIC 3800, Australia

3.1 Abstract

The Georgetown Inlier of northeast Australia provides critical links between Australia and Laurentia during the late Paleoproterozoic and the early Mesoproterozoic. Detrital zircon age spectra from sedimentary strata within the Inlier show two distinct changes in sedimentary provenance: (1) The lowermost units (depositional age ca. 1700–1650 Ma) have detrital zircon age spectra that strongly resemble Laurentian magmatic ages and detrital zircon age spectra of the similar-aged Wernecke

Supergroup of northwest Laurentia; (2) Sediments deposited from ca. 1650 to 1610 Ma show a unique proximal signature, and (3) sediments deposited post-1550 Ma have zircon age spectra like the Mt. Isa Inlier of the North Australian Craton (NAC). Along with new paleocurrent measurements, the detrital age data challenge current models that suggest the Georgetown Inlier was part of Australia before ca. 1700 Ma. Rather, we argue it was a continental ribbon rifted from west Laurentia during slab-rollback at approximately 1690 Ma, by 1650 Ma the Georgetown Inlier had completely rifted from Laurentia and at ca. 1600 Ma was colliding with Australia during Nuna amalgamation.

3.2 Introduction

Speculation about a Proterozoic connection between Australia and Laurentia was originally based on similarities between sedimentary sequences in South Australia and NW Canada (Jefferson, 1978). This connection was key in early reconstructions of the Neoproterozoic supercontinent Rodinia (Dalziel, 1991; Hoffman, 1991; Moores, 1991) and Hoffman (1991) proposed that the connection might even extend back to the Paleoproterozoic noting similarities between the Barramundi Orogen in NE Australia and the Wopmay Orogen in NW Canada. The connection between the two continents during the Proterozoic has been strengthened by numerous data sets; however, debate remains about the nature and timing of this connection, particularly in the Paleo- to Mesoproterozoic supercontinent Nuna.

In the Nuna supercontinent; debate remains about the timing and configuration of the connection between NE Australia and west Laurentia. Paleomagnetic data has

proven essential in constraining the positions of continents in Nuna (Pisarevsky et al., 2014); however, to better comprehend and constrain supercontinent amalgamation processes, a more multifaceted approach is required. Most global Nuna reconstructions based on paleomagnetic data show the eastern margin of the North Australian Craton (NAC) juxtaposed with northwest Laurentia at ca. 1800 or 1600 Ma (Pehrsson et al., 2016; Pisarevsky et al., 2014). Possible Laurentian correlatives with the NAC during the late Paleoproterozoic are the Wernecke Supergroup in the Yukon region and the Muskwa assemblage in northern British Columbia (Betts et al., 2008; Ross et al., 2001; Thorkelson et al., 2001). This positions the Proterozoic Georgetown Inlier (Figure 3.1A) of NE Australia close to Laurentia, however, the terrane has not been used to directly test Nuna models. Here we utilise paleocurrent data with U-Pb detrital zircon geochronology from sedimentary sequences of the Georgetown Inlier to test NE Australia's position within the supercontinent Nuna.

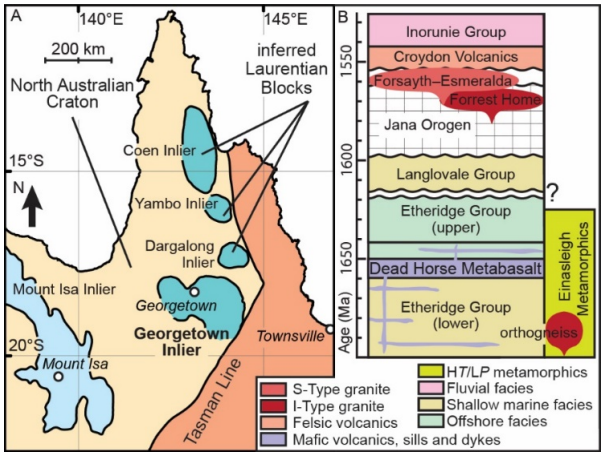

Figure 3.1: A: NE Australian Proterozoic terrains. B: Stratigraphic column outlining the main sedimentary groups and events in the Georgetown Inlier.

3.3 Geological Setting

The Georgetown Inlier consists of the lower Etheridge, the upper Etheridge, the Langlovale and the Inorunie groups (Figure 3.1B). Sediments of the lower Etheridge

Group range from offshore mudstone to wave and tidally influenced lower shoreface and wave-dominated upper shoreface facies deposited during the sag phase of a passive margin or intracontinental rift (Withnall and Hutton, 2013). This was followed by the eruption of the tholeiitic Deadhorse Metabasalt (ca. 1665 Ma) and emplacement of tholeiitic Cobbold Metadolerite sills and dykes (Black et al., 1998). A deepening of the basin occurred simultaneously with the mafic magmatism, resulting in deposition of the overlying offshore mudstones of the uppermost part of the lower Etheridge Group and the upper Etheridge Group (Withnall and Hutton, 2013). A possible unconformably separates the Etheridge Group from the overlying Langlovale Group, however recent field observations suggest this boundary may be conformable; thus, in this paper, we will treat the upper Etheridge and Langlovale groups as one and the same.

The inlier records a complex deformation and metamorphic history, with successive north-south, east-west, and finally northwest-southeast horizontal shortening events associated with lower greenschist to upper amphibolite facies metamorphism from ca. 1620 to 1550 Ma during the Jana Orogeny (Boger and Hansen, 2004; Cihan et al., 2006; Withnall and Hutton, 2013). The tectonometamorphic evolution culminated ca. 1560–1550 Ma with the generation of extensive S-type granites, and the orogen was capped by sediments of the Inorunie Group (Figure 3.1B) (Withnall and Hutton, 2013).

3.4 Methods and Results

New and existing detrital zircon data (Neumann and Kositcin, 2011), and new paleocurrent measurements from the Georgetown Inlier are presented in Figure 3.2 (data and detailed methods can be found in the appendix).

The observed age spectra show three distinct provenances (Figure 3.2): Detrital zircon age spectra from the lower Etheridge Group show a major peak at 2600 Ma and subordinate peaks at 1845, 1920,2350, 2495 and 2710 Ma. The upper Etheridge and Langlovale group age spectra have a major peak at 1655 Ma, whereas the Inorunie Group shows a major peak at 1740 Ma, with subordinate populations at 1600 Ma and 2400–2500 Ma. Paleocurrent measurements taken from lower shoreface hummocky cross-stratification and current ripples the lower Etheridge Group indicate a general westward paleoflow direction; whereas those taken from deltaic and fluvial trough cross-stratification in the Inorunie Group indicate an eastward paleoflow direction.

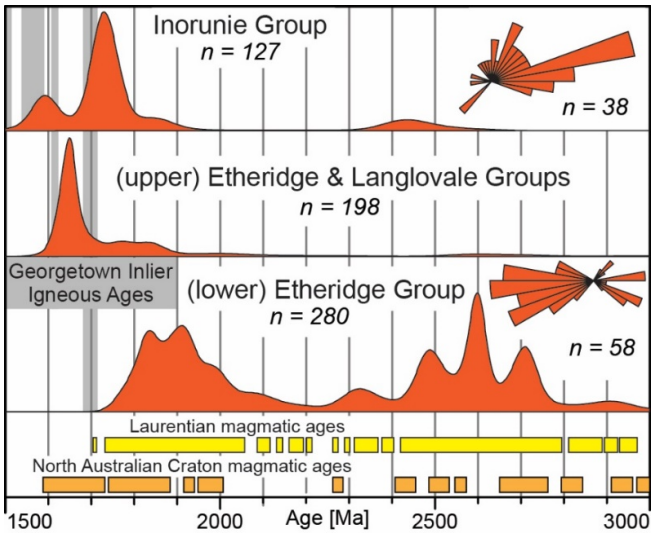

Figure 3.2: Probability density plots show two distinct provenance shifts in the U–Pb detrital zircon from the Georgetown Inlier. Rose diagrams show paleocurrent data from primary sedimentary structures in the Georgetown Inlier.

3.5 Discussion of the Provenance Results

The lower Etheridge Group zircon age spectrum shows a closer affinity to basement ages from Laurentian cratonic blocks than to those from cratonic Australia. There is no magmatic source for the ca. 2600, 2300 and 1900 Ma zircon ages in north Australia (Neumann and Fraser, 2007). Rather, these ages correspond to magmatic events in Laurentia cratonic blocks (e.g. Rae, Slave, Hearne, etc.) and surrounding orogens (e.g. the Taltson-Thelon orogen) (Eglington et al., 2013). This age spectrum strongly resembles those from Paleoproterozoic sediments in north Laurentia (e.g., the Wernecke Supergroup, the Athabasca Group, the Muskwa assemblage, etc.) (Furlanetto et al., 2016; Rainbird et al., 2007; Ross et al., 2001).

The switch to a predominant 1655 Ma age population from the lower to upper Etheridge Group suggests disconnection from Laurentian sources at ca. 1640 Ma (Figure 3.2). The upper Etheridge Group detrital zircon age spectrum contrasts with contemporaneous sediments from the Mt. Isa inlier (Neumann et al., 2009) (Figure 3.3b), also suggesting a disconnection from cratonic Australia. Possible 1655 Ma magmatic sources are known in both Laurentia and Australia (Eglington et al., 2013; Neumann and Fraser, 2007), but would require that the zircons are far-travelled and have bypassed more proximal sedimentary basins. Zircon ages have been obtained from numerous igneous rocks in the Georgetown Inlier and its northern counterparts (the Yambo, Coen & Dargalong inliers) (Figure 3.1A) that span the age peak (ca. 1690–1620 Ma) (Neumann and Fraser, 2007), suggesting that these zircons could be from a proximal source.

A further provenance change in the Georgetown Inlier is evident in the post-orogenic Inorunie Group (Figure 3.2). The detrital zircon age spectra from these sediments have age peaks of 1740, 1600, and 2450 Ma that correspond to magmatic events from the Mt. Isa Inlier (Neumann and Fraser, 2007; Neumann et al., 2006). Furthermore, the Constance Sandstone in the Mt. Isa Inlier has an almost identical age spectrum to the Inorunie Group (Carson, 2013) (Figure 3.3D) suggesting a connection between the NAC and the Georgetown Inlier post ca. 1550 Ma.

3.6 Tectonic Reconstruction

The detrital zircon age spectrum from the lower Etheridge Group shows sediments were derived from northern Laurentian terranes. These sediments were deposited in the sag phase of an epicontinental rift or on a passive margin (Baker et al., 2010). Either way, westerly paleocurrents and detrital zircon data suggest a Laurentian source of the sediments rather than derivation from Australia (Figure 3.3A and 3E). Emplacement of Deadhorse and Cobbold tholeiites (Figure 3.1) suggests active rifting and the change in zircon provenance from the lower to the upper Etheridge Group indicates the Georgetown Inlier had completely separated from Laurentia by ca. 1640 Ma (Figure 3.3B). This shift in the provenance is mirrored by a change in the εNd values which become more juvenile from the lower to the upper Etheridge Group (Lambeck et al., 2012).

In our model, rifting from ca. 1680 to 1650 Ma is explained by the development of a juvenile arc associated with east-dipping subduction off the west Laurentian margin (Figure 3.3B). The occurrence of 1690–1685 Ma trondhjemitic and I-type orthogneiss

in the Georgetown Inlier (Black et al., 1998; Neumann and Kositcin, 2011) indicates likely arc magmatism pre-dating the rift event. We suggest the arc migrated outboard from Laurentia during slab rollback, causing the Georgetown Inlier to rift from the margin producing active subsidence and the eruption of ca. 1665 Ma rift-related tholeiites (Figure 3.1). This speculated arc not only provides a source for the ca. 1655 Ma zircons but would also supply large quantities of juvenile material as indicated by the bulk-rock ƐNd values of these sedimentary rocks (Lambeck et al., 2012). With ongoing subduction, the ocean between Laurentia and Australia would have closed causing the subsequent accretion of the Georgetown Inlier to the NAC by ca. 1600 Ma (Figure 3.3C).

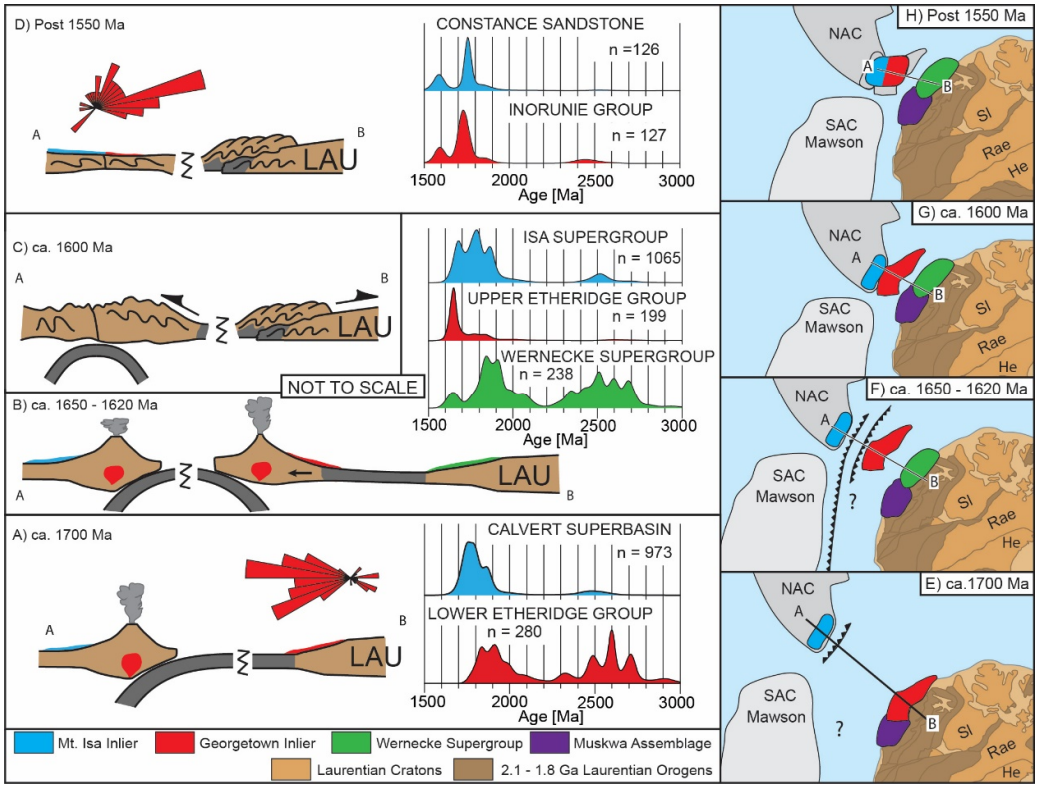

Figure 3.3: Tectonic and paleogeographic reconstructions for the amalgamation of the Georgetown Inlier with the NAC. Corresponding paleocurrent data and detrital zircon age spectra from the Georgetown Inlier in comparison with age equivalents from the Mt. Isa Inlier

of northeast Australia and the Wernecke Supergroup of the Yukon, northwest Canada (Carson, 2013; Furlanetto et al., 2016; Neumann et al., 2009; Neumann et al., 2006). A and E: ca. 1700 Ma: Sediments in the Georgetown Inlier were initially deposited in a passive margin whilst sediments in Mt. Isa were deposited in a back-arc basin to a possible west-dipping subduction zone (Betts et al., 2016). B and F: ca. 1650–1620 Ma: Development of an east-dipping subduction zone off the western margin of Laurentia promoted back-arc rifting between the Georgetown Inlier and Laurentia causing complete separation by ca. 1650 Ma. C and G: Continued subduction leads to collision of the Georgetown Inlier and the NAC (Isan–Jana Orogeny) and the thin-skinned Racklan Orogeny in west Laurentia. D and H: Post 1550 Ma: Detrital zircon age spectra from the Inorunie Group strongly resembles the Constance Sandstone of the Mt. Isa Inlier suggesting a correlation and further indicating a connection post-1580 Ma. Laurentia: He = Hearne Carton, Sl = Slave Craton, Australia: NAC = North Australia Craton, SAC = South Australia Craton, WAC = West Australia Craton.

Both the Georgetown and Mt Isa inliers were subjected to orogenesis between ca. 1620–1550 Ma. Earliest deformation in the Mt. Isa Inlier was characterised by north-south to northwest-southeast crustal shortening with peak metamorphic conditions at ca. 1600–1580 Ma (Giles and Nutman, 2002). Later stages of orogenesis in the Mt. Isa Inlier are characterised by crustal-scale upright to steeply inclined folds during east-west to northwest-southeast crustal shortening (MacCready et al., 1998; O'Dea et al., 2006). In the Georgetown Inlier, north-south compression was followed by the development of a dominant east-west foliation accompanied by medium- to high T metamorphism between ca. 1600 – 1550 Ma (Boger and Hansen, 2004; Cihan et al., 2006). Both inliers have a complex deformational and metamorphic history, however, each shows a similar evolution between ca. 1600 – 1550 Ma (see Betts et al., 2009 for a summary).

3.7 Implications for Nuna Assembly

Preliminary Nuna reconstructions were based on correlating global ca. 2.1 – 1.8 Ga orogenic events that were proposed to have recorded the amalgamation of the

supercontinent (Zhao et al., 2002). More recent reconstructions show Nuna amalgamation was incomplete until ca. 1600 Ma, when east Australia and west Laurentia were amalgamated (Pehrsson et al., 2016; Pisarevsky et al., 2014). Generally, this amalgamation is facilitated by a west-dipping subduction zone off the east coast of NAC, where the Georgetown Inlier is considered part of the NAC (Furlanetto et al., 2016; Gibson et al., 2017).

Sediments of the Wernecke Supergroup in the Yukon region of Canada are interpreted to have deposited in passive margin from ca. 1700 to 1610 Ma, that were later deformed during the ca. 1600 Ma Racklan Orogeny (Furlanetto et al., 2016). This orogeny was associated with east and south (craton) verging folds and thrusts that culminated in the obduction of mafic igneous rocks, remnants of an exotic arc terrane termed Bonnetia (Furlanetto et al., 2016; Nielsen et al., 2013). The similarity in the detrital zircon age spectra between the lower Etheridge Group and the Wernecke Supergroup (Figure 3A and 3B) suggests a shared provenance. In our model, the Wernecke Supergroup sediments were deposited on the continental side of a back-arc basin as the Georgetown Inlier was rifted from Laurentia (Figures 3B and 3F). Modern passive margins can show similar features back-arc basins (Jolivet et al., 2015), particularly on the continental side as we propose for the Wernecke Supergroup. During the amalgamation of the Georgetown Inlier with Australia at ca. 1600 Ma, the Racklan Orogeny recorded the closure of that back-arc basin as the inlier accreted to the NAC (Figure 3.3C and 3G). Bonnetia volcanic rocks obducted onto west Laurentia during the closure of the back-arc basin likely correlate with the arc that rifted the Georgetown Inlier from the west Laurentian margin.

Orogenesis recorded in the eastern NAC inliers suggests the Georgetown Inlier was accreted to the NAC between ca. 1600 Ma and 1550 Ma. S-type magmatism and high-T low-P metamorphism in the Georgetown Inlier, until at least 1550 Ma, indicates a protracted tectono-magmatic event. Sediments deposited in Laurentia Post-1550 Ma were likely sourced from the NAC (Doe et al., 2012; Medig et al., 2014), further indicating a correlation between the ca.1600 Ma Racklan Orogeny and the NAC orogenesis (Thorkelson et al., 2001). Previous authors have highlighted both differences and similarities (Boger and Hansen, 2004; Cihan et al., 2006) in NAC orogenesis during this period, however, the regional context of the amalgamation events in either craton remains uncertain and requires further investigation

The Georgetown Inlier is an important part of the connection between west Laurentia and the North Australian Craton. Although the exact location of the NAC along western Laurentia is not well constrained by the data presented here, this work nevertheless provides a strong link between the NAC and Laurentia in the Paleoproterozoic. In our model, subduction occurring on the eastern margin of the NAC and the western margin of Laurentia during the Paleoproterozoic provides a mechanism that accounts for the evolution of the Georgetown and Mt. Isa inliers whilst supporting current Nuna reconstructions that indicate Nuna assembly was uncomplete until ca. 1600–1550 Ma (Pehrsson et al., 2016; Pisarevsky et al., 2014).

3.8 Acknowledgments

ARN is supported by an Australian Postgraduate Award and a Curtin Research Scholarship. This study was supported by an Australian Research Council grant to ZXL

(FL150100133). WJC acknowledges the support of ARC DP 120104004. We gratefully thank Professors Brendan Murphy and Paul Hoffman for clarifying discussions. Reviews by Sally Pehrsson, Alan Collins and Derek Thorkelson helped refine the manuscript.

3.9 References

Betts, P.G., Armit, R.J., Stewart, J., Aitken, A.R.A., Ailleres, L., Donchak, P., Hutton, L., Withnall, I.W., and Giles, D., 2016, Australia and Nuna: Geological Society, London, Special Publications, v. 424, p. SP424. 422.

Betts, P.G., Giles, D., and Schaefer, B.F., 2008, Comparing 1800–1600Ma accretionary and basin processes in Australia and Laurentia: possible geographic connections in Columbia: Precambrian Research, v. 166, no. 1, p. 81-92.

Black, L.P., Gregory, P., Withnall, I.W., and Bain, J.H.C., 1998, U-Pb zircon age for the Etheridge Group, Georgetown region, north Queensland: Implications for relationship with the Broken Hill and Mt Isa sequences*: Australian Journal of Earth Sciences, v. 45, no. 6, p. 925-935.

Boger, S.D., and Hansen, D., 2004, Metamorphic evolution of the Georgetown Inlier, northeast Queensland, Australia; evidence for an accreted Palaeoproterozoic terrane?: Journal of Metamorphic Geology, v. 22, no. 6, p. 511-527.

Carson, C., 2013, GA Sample No - 1987412: Geoscience Australia Geochron Delivery System, Geoscience Australia.

Cihan, M., Evins, P., Lisowiec, N., and Blake, K., 2006, Time constraints on deformation and metamorphism from EPMA dating of monazite in the Proterozoic Robertson River Metamorphics, NE Australia: Precambrian research, v. 145, no. 1, p. 1-23.

Dalziel, I.W., 1991, Pacific margins of Laurentia and East Antarctica-Australia as a conjugate rift pair: Evidence and implications for an Eocambrian supercontinent: Geology, v. 19, no. 6, p. 598-601.

Doe, M.F., Jones, J.V., Karlstrom, K.E., Thrane, K., Frei, D., Gehrels, G., and Pecha, M., 2012, Basin formation near the end of the 1.60–1.45 Ga tectonic gap in southern Laurentia: Mesoproterozoic Hess Canyon Group of Arizona and implications for ca. 1.5 Ga supercontinent configurations: Lithosphere, v. 4, no. 1, p. 77-88.

Eglington, B., Pehrsson, S., Ansdell, K., Lescuyer, J.-L., Quirt, D., Milesi, J.-P., and Brown, P., 2013, A domain-based digital summary of the evolution of the Palaeoproterozoic of North America and Greenland and associated unconformity-related uranium mineralization: Precambrian Research, v. 232, p. 4-26.

Furlanetto, F., Thorkelson, D.J., Rainbird, R.H., Davis, W.J., Gibson, H.D., and Marshall, D.D., 2016, The Paleoproterozoic Wernecke Supergroup of Yukon, Canada: Relationships to orogeny in northwestern Laurentia and basins in North America, East Australia, and China: Gondwana Research, v. 39, p. 14-40.

Gibson, G.M., Hutton, L.J., and Holzschuh, J., 2017, Basin inversion and supercontinent assembly as drivers of sediment-hosted Pb–Zn mineralization in the Mount Isa region, northern Australia: Journal of the Geological Society, p. jgs2016-2105.

Giles, D., and Nutman, A.P., 2002, SHRIMP U–Pb monazite dating of 1600–1580 Ma amphibolite facies metamorphism in the southeastern Mt Isa Block, Australia: Australian Journal of Earth Sciences, v. 49, no. 3, p. 455-465.

Hoffman, P.F., 1991, Did the breakout of Laurentia turn Gondwanaland inside-out: Science, v. 252, no. 5011, p. 1409-1412.

Jefferson, C.W., Correlation of Middle and Upper Proterozoic strata between northwestern Canada and south and central Australia, in Proceedings Geological Association of Canada: Abstracts1978, Volume 13, p. 429.

Jolivet, L., Gorini, C., Smit, J., and Leroy, S., 2015, Continental breakup and the dynamics of rifting in back-arc basins: The Gulf of Lion margin: Tectonics, v. 34, no. 4, p. 662-679.

Lambeck, A., Barovich, K., Gibson, G., Huston, D., and Pisarevsky, S., 2012, An abrupt change in Nd isotopic composition in Australian basins at 1655Ma: Implications for the tectonic evolution of Australia and its place in NUNA: Precambrian Research, v. 208, p. 213-221.

MacCready, T., Goleby, B.R., Goncharov, A., Drummond, B.J., and Lister, G.S., 1998, A framework of overprinting orogens based on interpretation of the Mount Isa deep seismic transect: Economic Geology, v. 93, no. 8, p. 1422-1434.

Medig, K.P.R., Thorkelson, D.J., Davis, W.J., Rainbird, R.H., Gibson, H.D., Turner, E.C., and Marshall, D.D., 2014, Pinning northeastern Australia to northwestern Laurentia in the Mesoproterozoic: Precambrian Research, v. 249, p. 88-99.

Moores, E.M., 1991, Southwest US-East Antarctic (SWEAT) connection: a hypothesis: Geology, v. 19, no. 5, p. 425-428.

Neumann, N.L., and Fraser, G.L., 2007, Geochronological synthesis and time-space plots for Proterozoic Australia, Geoscience Australia.

Neumann, N.L., and Kositcin, N., 2011, New SHRIMP U-Pb zircon ages from north Queensland, 2007-2010: Geoscience Australia, 1921954450.

Neumann, N.L., Southgate, P.N., and Gibson, G.M., 2009, Defining unconformities in Proterozoic sedimentary basins using detrital geochronology and basin analysis—An example from the Mount Isa Inlier, Australia: Precambrian Research, v. 168, no. 3, p. 149-166.

Neumann, N.L., Southgate, P.N., Gibson, G.M., and McIntyre, A., 2006, New SHRIMP geochronology for the Western Fold Belt of the Mt Isa Inlier: developing a 1800–1650 Ma event framework∗: Australian Journal of Earth Sciences, v. 53, no. 6, p. 1023-1039.

Nielsen, A.B., Thorkelson, D.J., Gibson, H.D., and Marshall, D.D., 2013, The Wernecke igneous clasts in Yukon, Canada: fragments of the Paleoproterozoic volcanic arc terrane Bonnetia: Precambrian Research, v. 238, p. 78-92.

O'Dea, M.G., Betts, P.G., MacCready, T., and Aillères, L., 2006, Sequential development of a mid-crustal fold-thrust complex: evidence from the

Mitakoodi Culminationin the eastern Mt Isa Inlier, Australia: Australian Journal of Earth Sciences, v. 53, no. 1, p. 69-90.

Pehrsson, S.J., Eglington, B.M., Evans, D.A.D., Huston, D., and Reddy, S.M., 2016, Metallogeny and its link to orogenic style during the Nuna supercontinent cycle: Geological Society, London, Special Publications, v. 424, no. 1, p. 83-94.

Pisarevsky, S.A., Elming, S.Å., Pesonen, L.J., and Li, Z.X., 2014, Mesoproterozoic paleogeography: supercontinent and beyond: Precambrian Research, v. 244, p. 207-225.

Rainbird, R.H., Stern, R.A., Rayner, N., and Jefferson, C.W., 2007, Age, provenance, and regional correlation of the Athabasca Group, Saskatchewan and Alberta, constrained by igneous and detrital zircon geochronology: BULLETIN-GEOLOGICAL SURVEY OF CANADA, v. 588, p. 193.

Ross, G.M., Villeneuve, M.E., and Theriault, R.J., 2001, Isotopic provenance of the lower Muskwa assemblage (Mesoproterozoic, Rocky Mountains, British Columbia): New clues to correlation and source areas: Precambrian Research, v. 111, no. 1, p. 57-77.

Thorkelson, D.J., Mortensen, J.K., Creaser, R.A., Davidson, G.J., and Abbott, J.G., 2001, Early Proterozoic magmatism in Yukon, Canada: constraints on the evolution of northwestern Laurentia: Canadian Journal of Earth Sciences, v. 38, no. 10, p. 1479-1494.

Withnall, I.W., and Hutton, L.J., 2013, Proterozoic–North Australian Craton, in Jell, P. A., ed., Geology of Queensland, p. 23-112.

Zhao, G., Cawood, P.A., Wilde, S.A., and Sun, M., 2002, Review of global 2.1–1.8 Ga orogens: implications for a pre-Rodinia supercontinent: Earth-Science Reviews, v. 59, no. 1, p. 125-162.

Chapter 4: Contrasting stratigraphy and provenance in the Mount Isa Inlier: Implications for the Nuna supercontinent

4.1 Abstract

Previously correlated sedimentary units in the western, central and eastern belts of the Proterozoic Mount Isa Inlier are interpreted to have been deposited in an east-facing passive margin, or on the continental side of a back-arc basin. Here, we provide new measured sections, facies analysis, and detrital zircon geochronology to test the correlations between the Mary Kathleen Group of the central belt and the Malbon Group of the western belt. Sedimentological data from the Mary Kathleen Group indicate the sediments were deposited during N-S extension in contrast to the existing model. New detrital zircon geochronology along with previous extrusive volcanic ages indicate that the Mary Kathleen Group is likely older than previously thought and correlates with the Myally Supersequence of the western belt rather than the (younger) Quilalar Supersequence. The Malbon Group of the eastern belt has a ca. 2.58 Ga detrital zircon population exotic to most North Australian Craton sedimentary rocks, which cannot be identified in any potential source area Australia wide. Rather, this population can be identified in multiple regions in Laurentia. While not definitive, if this ca. 2.58 Ga detrital zircon population identified in ca. 1.75 Ga sedimentary rocks in Australia was sourced from Laurentia then it suggests that two continents could have been together as early as ca. 1.85 Ga and the amalgamation of the supercontinent Nuna more dynamic.

4.2 Introduction

The periodic assembly and reorganization of continents to form supercontinents is the inferred surface reflection of mantle processes (Li and Zhong, 2009; Nance et al., 1988). Understanding the driving mechanisms for such processes requires accurate plate reconstructions for the ancient supercontinents, such as the timing of amalgamation, the duration of tenure, and the configuration. While paleomagnetic studies provide constraints on the latitudinal position of each continental block, precise reconstructions require accurate geological correlations.

The supercontinent Nuna (also known as Columbia) was initially thought to have assembled between ca. 2.1 to 1.8 Ga corresponding with a period of global orogenesis (Hoffman, 1997; Zhao et al., 2002). More recently, however, geological constraints have established that the supercontinent might not have completely amalgamated until at-least ca. 1.6 Ga, when eastern margin of proto-Australia collided with west Laurentia (Betts et al., 2016; Furlanetto et al., 2013; Nielsen et al., 2013; Nordsvan et al., 2018; Pourteau et al., 2018; Verbaas et al., 2018). The Proterozoic Mount Isa Inlier of NE Australia was affected by the ca. 1.6 Ga amalgamation event and is, therefore, a key piece to understanding the assembly processes. However, leading to this final amalgamation event, two similar but contrasting models have been proposed for the tectonic significance of ca. 1.8 to 1.6 Ga sedimentary deposits in the Mount Isa Inlier, as discussed below (Betts et al., 2016; Gibson et al., 2018).

The Mount Isa Inlier is the largest Proterozoic terrane in NE Australia. The Inlier is subdivided into 15 geologically distinct domains (GSQ, 2011) that for simplicity can be broadly divided into three N-S oriented belts; the west, central and east (Figure 3.1) (Day, 1983; Withnall and Hutton, 2013). Sedimentation in the western belt of the inlier occurred in three main basin forming episodes that have been categorised into superbasins; namely, the Leichhardt (ca. 1800–1740 Ma), Calvert (ca. 1720–1680 Ma) and Isa (ca. 1665–1580 Ma) (Domagala et al., 2000; Jackson et al., 2000; Jackson and Southgate, 2000; Jackson et al., 2005; Neumann et al., 2006; Page et al., 2000; Withnall and Hutton, 2013). The three superbasins recorded roughly 200 million years of sedimentation separating two major orogenic events, the ca. 1.9–1.85 Ga Barramundi Orogeny, and the ca. 1.6–1.55 Ga Isan Orogeny (Etheridge et al., 1987; O'Dea et al., 1997b). Betts et al. (2016) suggested that the inlier records a full Wilson cycle between ca. 1.74 to 1.6 Ga and that Laurentia and proto-North Australia were connected at ca. 1.8 Ga in a proto-SWEAT configuration (Betts et al., 2008; Payne et al., 2009). At ca. 1.74 Ga the continents then drift apart and sediments in the Mount Isa Inlier are deposited in a passive margin deepening to the east. Subsequent west and east-dipping subduction zones develop on the western margin of Australia, and the eastern margin of Laurentia, respectively, and drive the closure of this newly formed ocean (Betts et al., 2016; Murphy and Nance, 2003). Gibson et al. (2018) proposed a similar model to Betts et al. (2016); however, they suggest that following the initial phase of rifting between Laurentia and Australia, sediments of the Leichardt Superbasin are deposited in a back-arc formed by a west-dipping subduction zone off the eastern margin of proto-Australia and ultimately drive the

closure of the newly formed ocean between Australia and Laurentia. A major point of difference between the models is the timing and mechanism regarding the initial stage of rifting recorded in the Leichhardt Superbasin.

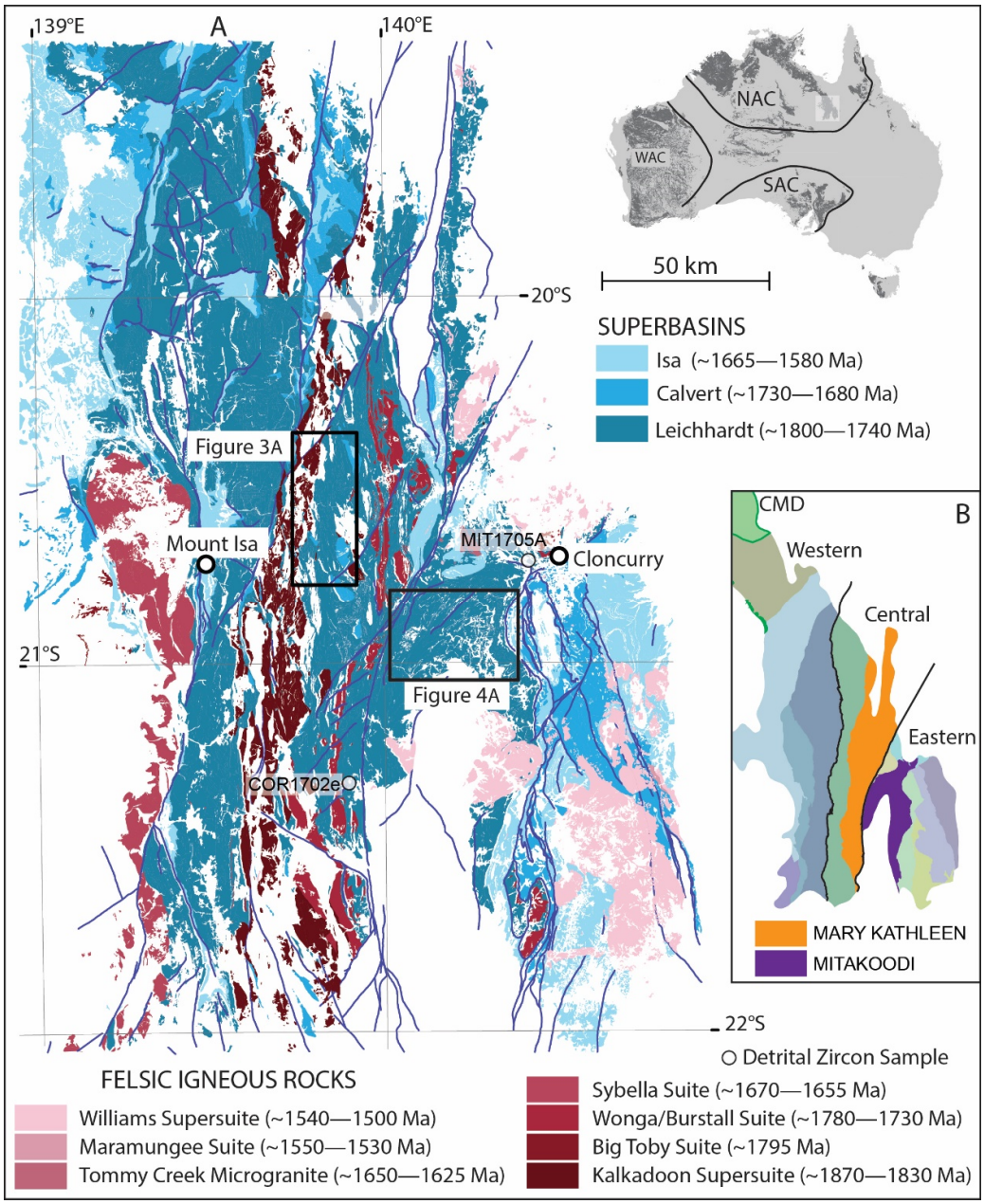

Figure 4.1: A) Map of the Mount Isa Inlier illustrating the geographical extent of the three superbasin sequences and the granitic suites. B) Mount Isa Inlier domain map highlighting the 15 fault bound domains and the western, central and eastern belts (Day, 1983; Withnall and Hutton, 2013). Different colours represent different domains (Withnall and Hutton,

2013). The green with a thick border is the Camooweal-Murphy Domain (CMD) (see discussion for significance).

To evaluate the tectonic significance of the Leichhardt Superbasin and test proposed correlations throughout the Mount Isa Inlier, new sedimentological data is provided from the Mary Kathleen Group in the central belt of the Mount Isa Inlier and the previously correlated Malbon Group in the eastern belt. Furthermore, new detrital zircon U-Pb/Lu-Hf data are presented to understand the provenance of the sediments, test current tectonic models, and better constrain Nuna reconstructions.

4.3 Stratigraphic context and study regions

The Leichhardt Superbasin is best defined in the western belt of the Mount Isa Inlier where the sequence is divided into three second-order, rift-sag associated "supersequences"; the Guide, Myally and Quilalar (Figure 4.2) (Jackson et al., 2000; Neumann et al., 2006). Confined to the Leichhardt Domain (western belt), the oldest sedimentary rocks, assigned to the Guide Supersequence overlie ca. 1.79 Ga felsic volcanics and were deposited during a period of east-west extension (and the associated sag phase) (Eriksson et al., 1993; Jackson et al., 2000). Renewed extension was accompanied by the eruption of extensive continental flood basalts (Eastern Creek Volcanics) up to 8km thick along N-S trending normal faults (Bain et al., 1992; O'Dea et al., 1997a; Wilson et al., 1984). The overlying Myally Supersequence is confined to the western belt and was deposited during N-S extension (Neumann et al., 2006; O'Dea et al., 1997a). Conformably to disconformably overlying the Myally Supersequence is the Quilalar Supersequence, which in the western belt of the inlier was deposited during E-W extension. Sediments are thought to correlate across the

whole inlier, during the sag phase of the Quilalar Supersequence (Jackson et al., 1990; Neumann et al., 2006; Southgate et al., 2013). However, several different depositional models have been presented.

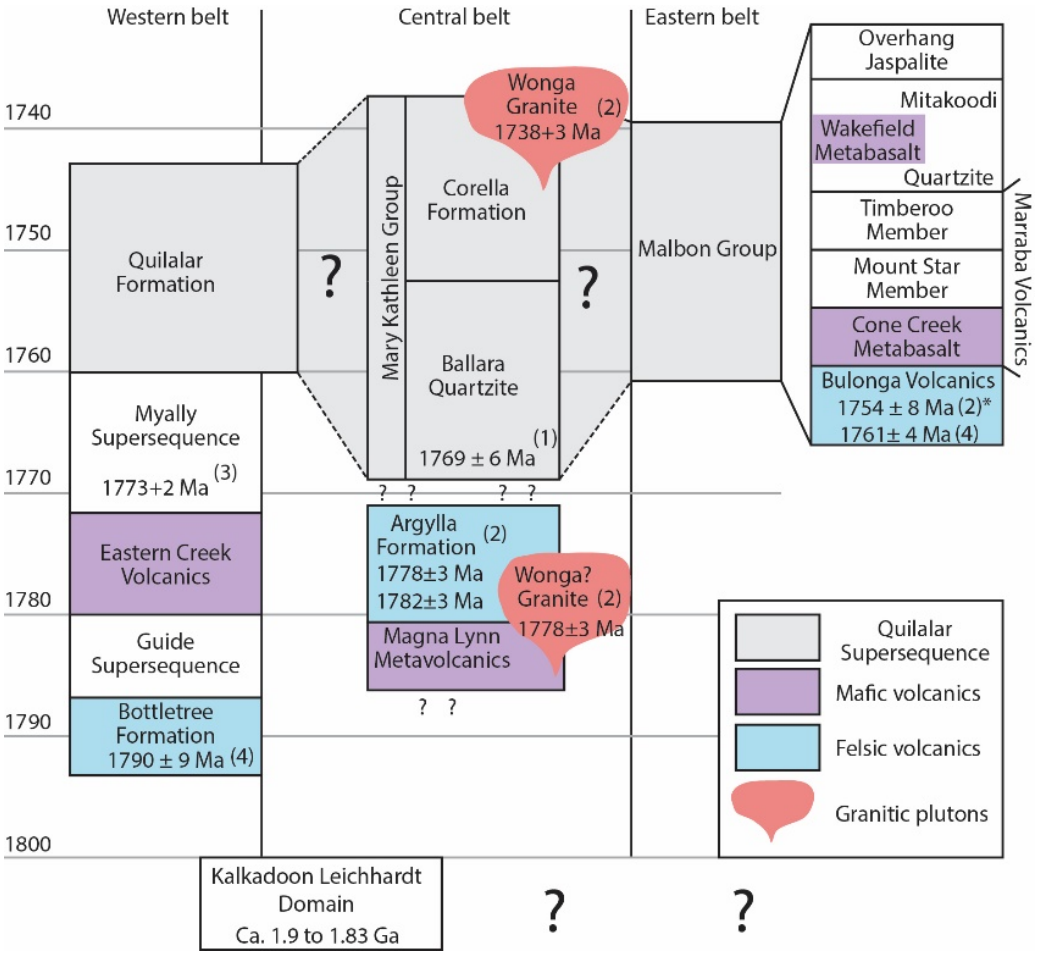

Figure 4.2: Overview of the Leichhardt Superbasin stratigraphy highlighting the problems with the proposed correlations based on geochronology. References: 1) Magee et al. (2012) 2) Neumann et al. (2009b), 2), 3) Page (1983), 4) Pearson et al. (1992). *Age reported as Argylla Formation, however, recent mapping defines the unit as Bulonga Volcanics.

Derrick et al. (1980) first proposed that the Quilalar Formation of the western belt was correlative to the Mary Kathleen Group (Ballara Quartzite and Corella Formation) in the central belt based on similarities between the lower Quilalar Formation sandstones and those of the Ballara Quartzite, and the carbonate units of the upper

Quilalar and those of the Corella Formation. Derrick et al. (1980) also noted similarities between the underlying "Argylla Formation" volcanics between the two areas; however, recent dating has revealed that the "Argylla Formation" underlying the Quilalar Formation (in the western belt) is not the same volcanic unit (Argylla Formation) that underlie the Mary Kathleen Group (in the central belt), but rather older Leichhardt Volcanics (Figure 4.2; Withnall and Hutton, 2013). Jackson et al. (1990) further interrogated the proposed correlation between the Quilalar Formation and the Mary Kathleen Group and put forward a model where the Ballara Quartzite represented the eastern margin of an elongate north-south trending trough, and the Quilalar Formation represented both the deeper, central part of the trough and the opposing margin located to the west. The correlation between the Quilalar Formation and the Ballara Quartzite can be further supported by detrital zircon geochronology, which has shown some of the easternmost samples from the Quilalar Formation share a ca. 1780 Ma population with the Ballara Quartzite (Neumann et al., 2009a; Neumann et al., 2009b).

In the eastern belt, the Mitakoodi Quartzite (of the Malbon Group) is suggested to be correlative with the Ballara Quartzite (Figure 4.2) (Foster and Austin, 2008; Gibson et al., 2012; Southgate et al., 2013). Gibson et al. (2012) proposed that the Marraba Volcanics (undated), that underlie the Mitakoodi Quartzite, are correlative with the Eastern Creek Volcanics (undated); however, the felsic Bulonga Volcanics that underlie the Marraba Volcanics have an eruption age of 1761 ± 3 Ma, roughly 30 Myr younger than the proposed age for the Eastern Creek Volcanics (Figure 4.2) (Neumann et al., 2009a; Neumann and Fraser, 2007). Southgate et al. (2013)

suggested that both the Mitakoodi and Ballara quartzites represent a retrograding transgressive systems tract (TST) in a thermally relaxing basin; however, no detailed sedimentological data has been presented to support this concept. Moreover, previous authors have suggested a rift setting for these sedimentary rocks (Gibson et al., 2008; Potma and Betts, 2006).

To test some of the issues raised above regarding the proposed correlations; the Mary Kathleen Group of the central belt and the Malbon Group of the eastern belt were targeted utilising sedimentology and detrital geochronology. Primarily, the sediments of the Ballara and Mitakoodi quartzites were focused on as they outcrop most prominently, have experienced the least amount of metamorphism, and are not as weathered as other units. Nonetheless, numerous attempts at characterising the Corella Formation in the central region and the other units of the Malbon Group in the western fold belt were made.

The Ballara Quartzite is the basal unit of the Mary Kathleen Group and is confined to the N-S trending the Mary Kathleen Domain in the central belt of the Mount Isa Inlier (Figure 4.2 and 4.3). The Mary Kathleen Domain is multiply-deformed and underwent in parts, up to high-grade metamorphism (Holcombe et al., 1992). The earliest deformation event recorded in the Mary Kathleen Domain is associated with a mid-crustal detachment zone associated with emplacement of the ca. 1758–1729 Ma Wonga granites, gabbro, and dolerite (Holcombe et al., 1992; Neumann et al., 2009a; Page and Sun, 1998). Sedimentary rocks of the Mary Kathleen Group vary in thickness and metamorphic grade in different locations throughout the domain (Blake and

Stewart, 1992; Holcombe et al., 1992; Withnall and Hutton, 2013). In the eastern part of the domain, the Ballara Quartzite has undergone higher-grade metamorphism, is typically thinner, and directly overlies the high-grade Boomarra Metamorphics that are probably equivalent to the Argylla Formation (Withnall and Hutton, 2013). To avoid the sedimentary rocks that have been affected by high-grade metamorphism, in this study, we focus on the western part of the Mary Kathleen Domain; where the ca. 1.85 Ga Leichhardt Volcanics and Kalkadoon Granodiorite basement rocks of the Kalkadoon-Leichhardt Domain are unconformably overlain by the Magna Lynn Metabasalt that up-sequence is interbedded with the felsic volcanics of the Argylla Formation (Figure 4.2 and 4.3). The Magna Lynn Metabasalt is characterised by amygdaloidal pillow basalts interbedded with non-marine and shallow marine quartzites and minor mudstones (Withnall and Hutton, 2013). The Argylla Formation consists of felsic extrusive and high-level intrusive rocks interbedded with non-marine sedimentary rocks. The contact between the Argylla Formation with the overlying Ballara Quartzite has been suggested by different authors to be either unconformable or conformable (Blake and Stewart, 1992; Neumann et al., 2009a; Stewart, 1992).

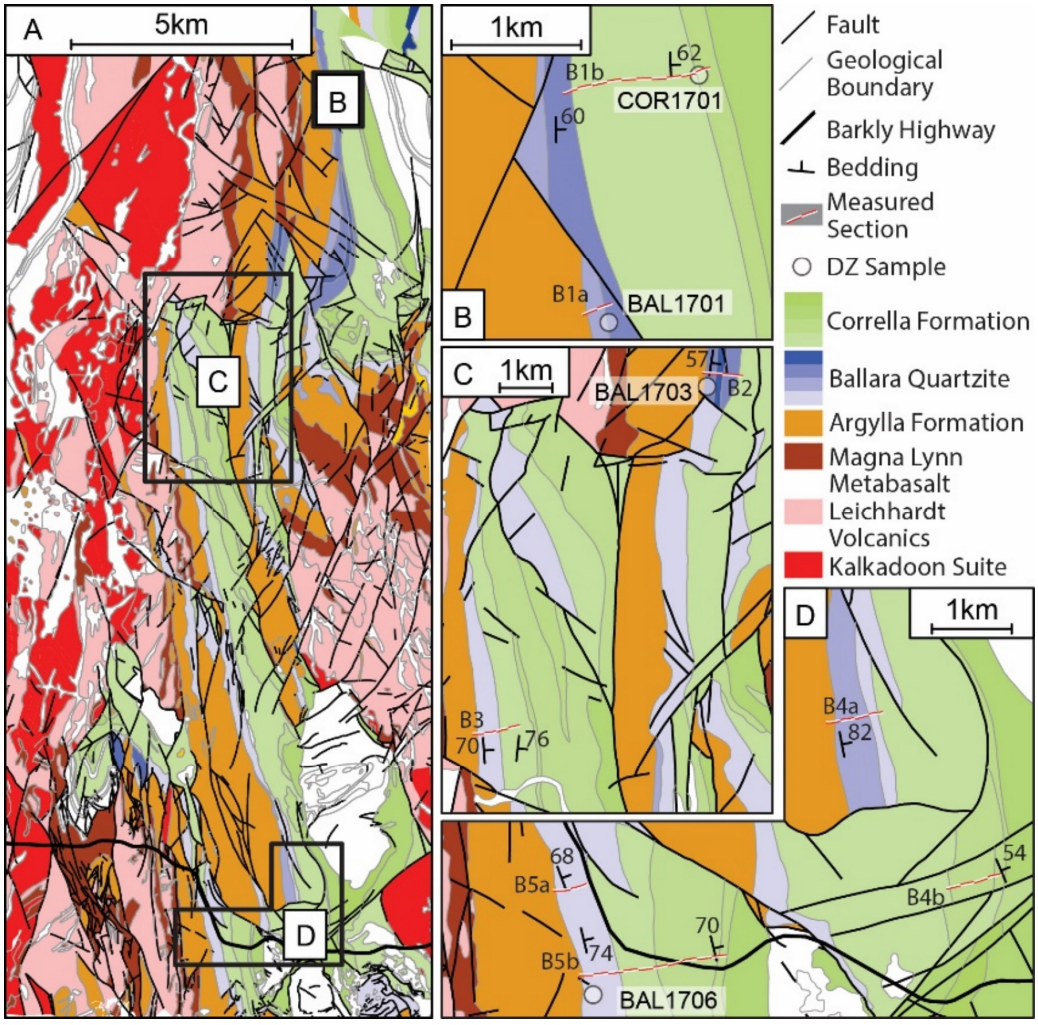

Figure 4.3: Geological map of the Mary Kathleen Group study area. See Figure 4.1 for location within the Mount Isa Inlier. A) Overview of the area. B) Location B1. C) Locations B2 and B3. D) Locations B4 and B5. DZ = Detrital zircon. Maps generated using data from the Queensland Geological Survey. Bedding measurements are from this study.

The Malbon Group is confined to the Mitakoodi Domain, a north to northeast plunging anticlinorium that is faulted against the Mary Kathleen Domain to the west, the Tommy Creek Domain to the northwest and the Marimo-Staveley Domain to the east (Figure 4.2 and 4.4). The oldest rocks in the Mitakoodi Domain are the ca. 1.76 Ga felsic Bulonga Volcanics which are overlain by the tholeiitic basalts of the Marraba Volcanics (Derrick et al., 1980; Foster and Austin, 2008). The Bulonga Volcanics are interpreted to be the early rift-phase sequence, whereas the Marraba Volcanics are

thought to represent a major period of basaltic magmatism and mature rifting (Beardsmore et al., 1988; Potma and Betts, 2006). Potma and Betts (2006) noted angular unconformities associated with normal faulting, block rotations, and conglomerate in the upper part of the Mitakoodi Quartzite, they interpreted as indicating an active rift setting.

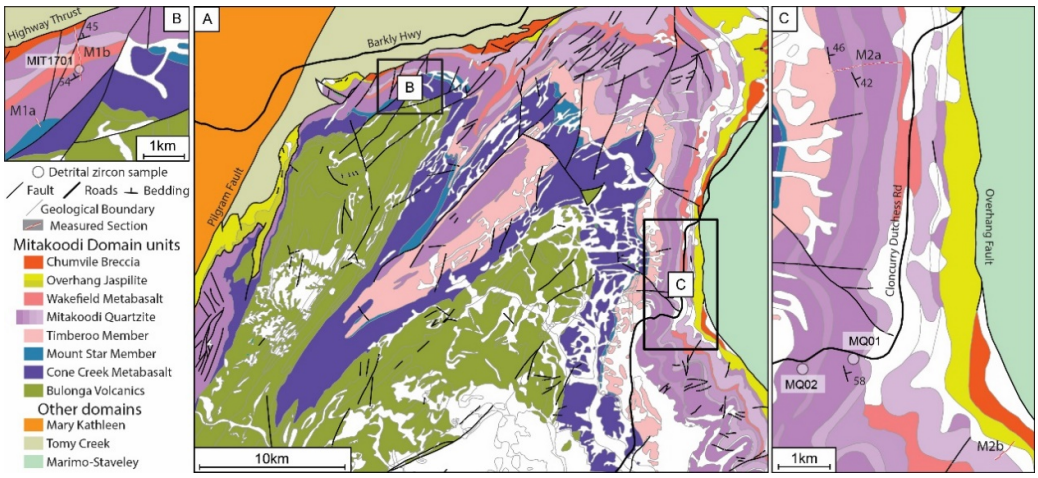

Figure 4.4: Geology map of the Malbon Group study area. See Figure 4.1 for location within the Mount Isa Inlier. A) Overview of the area. B) Location M1. C) Location M2. DZ = Detrital zircon. Maps generated using data from the Queensland Geological Survey. Bedding measurements are from this study.

4.4 Methodology

4.4.1 Sedimentology and stratigraphy

Facies analysis and stratigraphy were completed at eight locations for the Ballara Quartzite and Corella Formation (Mary Kathleen Group) and five locations for the Malbon Group. The aim was to measure multiple stratigraphic sections across the strike of bedding for both areas, and for the Mary Kathleen Group across different fault blocks. In this manner, the intent was to reconstruct basin-scale depositional trends. Locations were selected based on previous mapping, the ability to access the land, and the quality of outcrop. In cases where poor outcrop inhibited the ability to

make accurate descriptions and measurements, sections were measured along strike. Consequently, a total of five “composite sections” are presented for the Mary Kathleen Group sections, whereas a total of two composite sections are presented for the Malbon Group. Sequence stratigraphic interpretations are used to discuss the basin evolution.

4.4.2 Detrital zircon geochronology

Samples were collected from different sites and different stratigraphic heights to fully characterise the detrital zircon signature from each location. Samples were cleaned and crushed using conventional methods. Zircon grains were separated and concentrated using a Wilfley table, LST heavy-liquid, and a Frantz magnetic separator. The grains were mounted on double-sided tape, set in epoxy resin, ground down to expose the grains, and polished using polycrystalline diamond suspension. Zircon grains were imaged using standard light microscopy. The resin discs were carbon-coated for backscattered, secondary electron and cathodoluminescence (CL) imaging on MIRA3 VP-FESEM scanning electron microscope (SEM) at John de Laeter Centre, Curtin University.

The isotopic composition of the zircon grains was measured using laser ablation inductively coupled plasma mass spectrometry (LA-ICP-MS) at the John de Laeter Centre, Curtin University. Samples were analysed on five separate days (Table 4.2), using a Resonetics M-50 193 nm ArF excimer laser and a laser ablation split stream (LASS) setup with an Agilent 7700s quadrupole for U-Pb and a Nu Plasma II multi-collector for Lu-Hf. Zircon standards GJ1 (608.5 Ma), 91500 (1062.4 Ma) and OG1

(2465.4 Ma) were the analysed as the U-Pb standards (Jackson et al., 2004; Stern et al., 2009; Wiedenbeck et al., 1995). Additionally, Mud Tank zircon grains were analysed as the hafnium standard. For each sample between 131 to 227 individual zircon grains were analysed. The data were reduced using Iolite with the VizualAge addon (Paton et al., 2011; Petrus and Kamber, 2012). Initial $^{177}Hf/^{176}Hf$ values were calculated using the ^{176}Lu decay constant = 1.865×10^{-11} yr^{-1} (Scherer et al., 2001). Chondritic values follow Bouvier et al. (2008): $^{176}Hf/^{177}Hf$ CHUR = 0.282785 and $^{176}Lu/^{177}Hf$ CHUR = 0.0336, where CHUR is the chondritic uniform reservoir. Hafnium data are reported in epsilon units (ε), where one εHf unit represents one part per 10,000 deviations of $^{177}Hf/^{177}Hf$ from CHUR composition at the time defined by the crystallisation age of the zircon or the weighted mean age of the granite (Kinny and Maas, 2003).

Table 4.1: Analytical days. LASS: Laser ablation split stream.

DAY	DATE	Samples analysed	Method	Spot size	U-Pb Standard ($^{206}Pb/^{238}Pb$ age MA)	Secondary standard ($^{206}Pb/^{238}Pb$ age MA)	Secondary standard ($^{207}Pb/^{206}Pb$ age MA)
1	6/04/2017	BAL1701, MQ01, MQ02	LASS	50 µm	GJ1 (602.2)	91500 (1062.7)	OG1 (3456.9)
2	7/04/2017	MQ01, MQ02	LASS	50 µm	GJ1 (601.83)	91500 (1061.6)	OG1 (3466.3)
3	28/11/2017	BAL1706, COR1701, MIT1701	LASS	50 µm	91500 (1602)	GJ1 (604.7)	OG1 (3483.5)
4	29/11/2017	BAL01701, BAL1703, BAL1706, COR1701, MIT1705A	LASS	50 µm	GJ1 (601)	91500 (1048)	OG1 (3466)
5	30/11/2017	BAL1703, COR1702e	LASS	50 µm	GJ1 (600.4)	91500 (1063.2)	OG1 (3460)

Individual zircon grain U-Pb ages were calculated using Isoplot R (Vermeesch, 2018b), which was also used to generate the Concordia diagrams. To compare the samples,

only detrital zircon grains less than 5% discordant were plotted using kernel density estimates (KDE) with a bandwidth of 20 myr for visual comparison (Vermeesch, 2012). Multidimensional scaling using both the Kolmogorov-Smirnov (K-S) and Kuiper statistical tests were used to compare the detrital zircon samples with each other, and with potential source regions (Vermeesch, 2013, 2018a). Lu-Hf isotopes in detrital zircon less than 10% discordant was also used for comparison between the samples.

4.5 Sedimentology

4.5.1 Facies Associations

Summarised in Table 4.2, eight facies associations are recognised in this study that represents deposition from non-marine to sediment starved off-shelf environments.

Table 4.2: Facies and facies associations from this study for sediments of the Mary Kathleen and Malbon groups.

Facies Association	Description	Depositional environment	Locations
FA1: Basal conglomerate interbedded with sandstone	Poorly to moderately sorted, lenticular conglomerates interbedded with coarse to very coarse tabular sandstones. Conglomerates are thick to very thickly bedded and generally massive, clast-supported with rare graded bedding and coarse to very coarse lithic matrix. Clasts are subrounded to well-rounded and range in size from granule to boulder with a mean size of roughly 60 mm. The base of the conglomerate with the interbedded sandstone is commonly erosional. The sandstone is moderately sorted and typically consists of angular to sub-angular lithic fragments. Sandstone beds are medium to thickly bedded and commonly feature horizontal laminations with common 10 to 15 cm thick planar crossbedding with granules on the forests. Discontinuous 5 to 10 cm thick lenses of poorly sorted conglomerate uncommonly occur interbedded with the sandstones	Non-marine debris flows and sheet floods.	B1, B4, and B5
FA2: Medium to coarse-grained sandstone plus/minus fine-grained sandstone	Laterally continuous, medium to coarse-grained sandstones, featuring abundant trough and planar crossbedding with minor hummocky cross-stratification (HCS) interbedded with parallel laminated fine-grained sandstones with wave ripples. Planar cross-beds are up to 50 cm high, low angled, and commonly feature reactivation surfaces. Trough cross-beds are 10 to 20 cm high and are commonly associated with climbing ripples and herringbone cross-bedding. HCS is noted on the tops of sandstone beds and is typically an erosional feature that is overlain by fine-grained sandstones.	Shallow marine, upper shoreface. Above fair-weather wave base.	All
FA3: Fine to medium-grained sandstone	Laterally continuous, commonly fine to medium-grained sandstones in the Ballara sections but coarser in the Mitakoodi. Common horizontal laminations and abundant wave ripples. Some beds contain small scale HCS and swaley cross-stratification common. Contacts are sharp to wavy and commonly erosional.	Shallow marine, lower shoreface. Below fair-weather wave base, above storm wave base.	All
FA4: Fine-grained sandstone interbedded with mudstone	Fine-grained laterally continuous generally massive to laminated sandstones with minor heterolithic facies interbedded with mudstones.	Off-shore transitional zone. Below storm wave base	All
FA5: Massive mudstone	Poorly outcropping, highly weathered and cleaved mudstones.	Off-shore distal.	All
FA6: Laminated calcareous mudstone	Buff coloured laminated calcareous mudstones with minor fine-grained sandstone in some locations. Often scapolitic.	Off-shore. Below storm wave base, sediment starved.	B1, B4, and B5
FA7: Limestone	Commonly laminated limestone with minor wave ripples, less often massive. Often scapolitic.	Off-shore, sediment starved.	B1 and B3
FA8: Syn-sedimentary deformed calcareous mudstone and fine-grained sandstone	Calcareous mudstone with interbedded fine-grained sandstones featuring chaotic and convolute bedding.	Unknown, possible reef front/edge?	B1

4.5.2 Measured sections

4.5.2.1 Mary Kathleen Group

4.5.2.1.1 Section B1

Section B1 is the most northerly section of the Mary Kathleen Group presented in this study and is a composite of three high-resolution measured sections (Figure 4.3B and 4.5A). Basal units of section B1 are characterised by roughly 110 m of FA1, interpreted to be alluvial fan facies (Table 4.2). The contact with the underlying Argylla Formation outcrops poorly but when traced laterally appears to be undulating. Numerous volcanic to volcaniclastic units interbedded with the conglomerates suggest the contact might be transitional. The discontinuous nature of the outcrop and vegetation inhibit a complete characterisation of the unit. Nevertheless, the lenticular, poorly sorted conglomerates are likely the product of debris flows whereas the very coarse-grained, cross-bedded sandstones can be attributed to sheet flood events (Nilsen 1982) (Figure 4.6a). Numerous sections of FA1 were measured along strike across a previously mapped fault (mapped from aerial photography) for section B1 composite (Figure 4.5A). FA1 was roughly 30 m thicker on the northern side of the mapped fault which can be accounted for by either along strike facies variations, or activity along the fault (Figure 4.3B). Paleocurrent measurements from the sheet flood deposits are generally north to northeast (Figure 4.5). The contact with the overlying marine deposits is not exposed but they consist of massive to laminated fine-grained sandstone interbedded with minor mudstones approximately 30m thick. These deposits coarsen upwards to upper shoreface coarse-grained sandstones

featuring HCS and planar cross-bedding. Overlying these shoreface facies the sediments fine upwards to mudstone facies indicative decreasing depositional energy which is interpreted as gradual shoreline transgression (Figure 4.5A). The mudstone progressively becomes more calcareous up-sequence and is capped by a limestone unit likely reflecting sediment starvation in a distal setting (Figure 4.6g). Up-sequence a calcareous mudstone interbedded with limestone featuring chaotic and convoluted bedding might be the result of syn-sedimentary deformation. The overlying units gradually coarsen upwards to shallow marine sandstones reflecting normal regression of the shoreline.

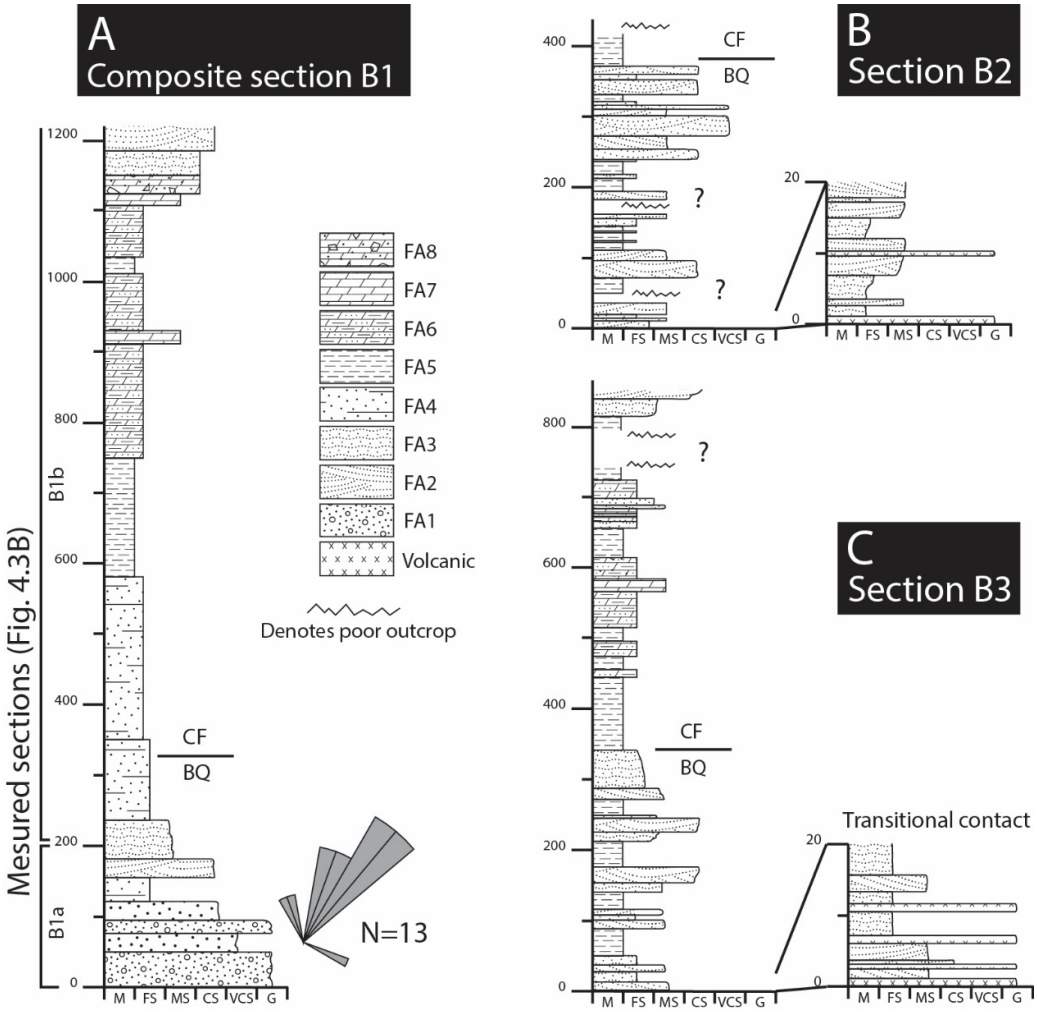

Figure 4.5: Stratigraphic columns from locations B1, B2, and B3. BQ=Ballara Quartzite. CF=Corella Formation. Contacts between BQ and CF are from geological maps for reference (Figure 4.3). See Table 4.2 for descriptions of the facies association.

4.5.2.1.2 Section B2

Section B2 is roughly 8km south-southwest from section B1 but is located on a more westerly fault block (Figure 4.3C). Section B2 is the result of numerous measured sections across strike trying to best characterise poorly outcropping units, particularly finer-grained units. The base of the Ballara Quartzite with the underlying Argylla Formation at section B2 is transitional (Figure 4.5B). Basal units consist of FA3, thin to medium bedded, fine to medium-grained sandstones with wave-ripples,

interbedded with felsic volcanic rocks that have a similar composition to the underlying Argylla Formation. Over 380 m the sequence consists of four coarsening upwards sequences that are characterised by either basal mudstones or fine-grained sandstones, (FA4 and 5) that coarsen upwards to medium or coarse-grained sandstones of FA1. Sharply overlying the coarsening upwards parasequences are mudstones of the Corella Formation which are highly foliated and weathered (Figure 4.5B).

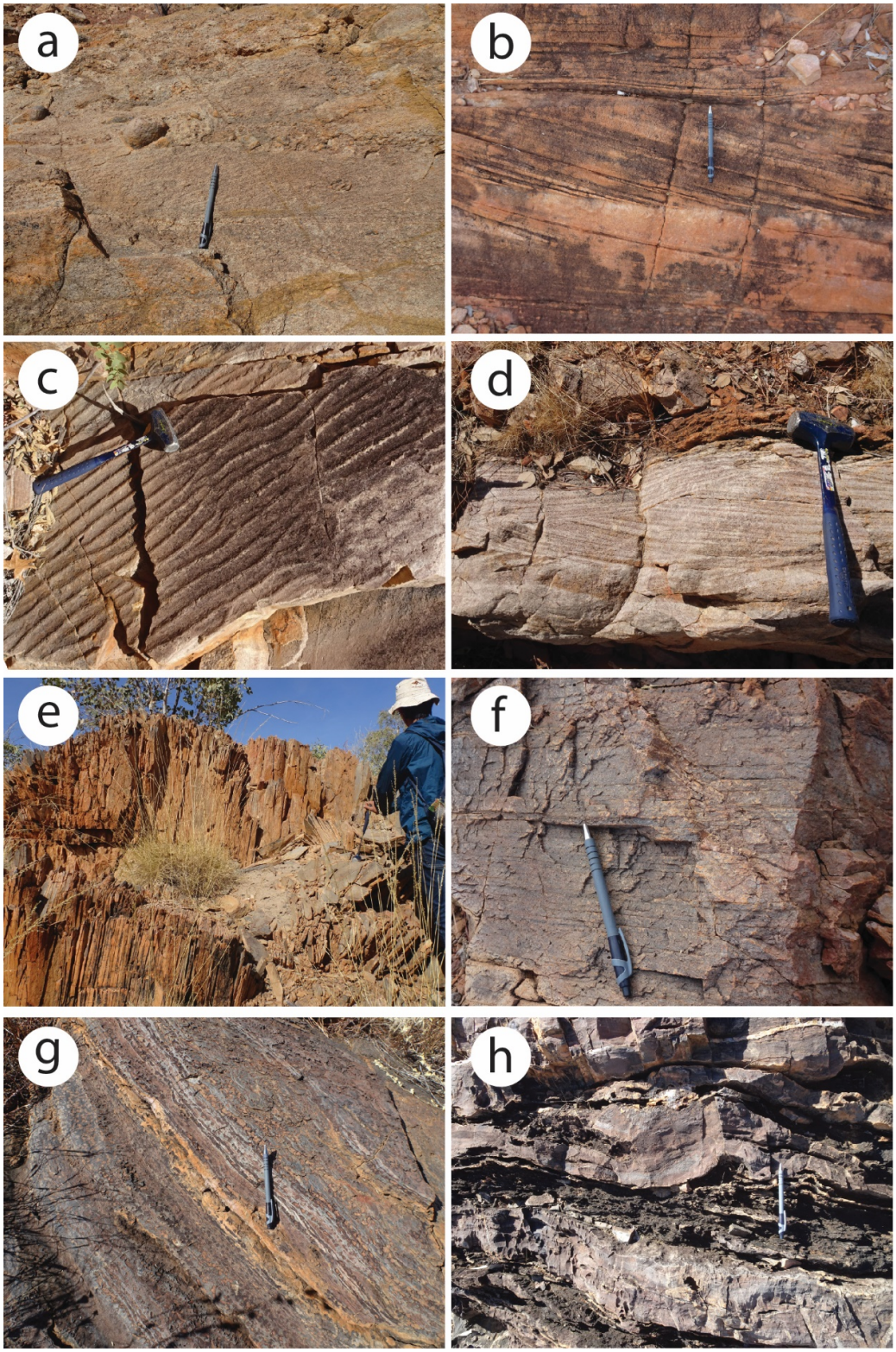

Figure 4.6: Outcrop photos of the Mary Kathleen Group. a) FA1, coarse-grained sandstone sheet flood deposits from Location B1. b) FA2, trough cross-bedding in medium-grained wavy bedded sandstones at location B5b. c) FA2, Wave ripples on the tops of fine to medium-

grained sandstones at location B3. d) FA3, Hummocky cross-stratification in fine to medium-grained sandstones. e) FA4, cleaved mudstones interbedded with fine-grained sandstones at location B4. Bedding is sub-horizontal f) FA6, Laminated calcareous mudstone at location B5. g) FA7, scapolitic limestone at location B1. h) FA8, fine to medium-grained calcareous sandstones interbedded with calcareous mudstone featuring convoluted bedding at location B4. The pen is 14 cm in length. Hammer is 40 cm.

4.5.2.1.3 Section B3

Section B3 was measured at a location approximately 8 km southwest of section B2 on a fault block further to the west (Figure 4.3C). Section B3 is the composite product of a single measured section and numerous observations along the strike of the bedding (Figure 4.5C). In this location the contact of the Ballara Quartzite with the underlying Argylla Formation is transitional. Basal units are fine to medium-grained sandstones with HCS, wave ripples (Figure 4.6C), and low angled trough cross-bedding deposited in shallow marine settings (Table 4.2). The Ballara Quartzite in this location is approximately 270 m thick and characterised by four sequences that consist of sharp based mudstone facies that coarsen upwards to FA3 and FA2 shallow marine facies (Figure 4.5C). Intriguingly, bedding measurements from the shallow marine sandstones of sequence two (and above) strike differently and appear to onlap the underlying sandstones towards the north. This could be the result of either post-deposition deformation or syn-depositional faulting. Unfortunately, the contact between the sandstone units is concealed by vegetation. Satellite imagery, taken from Google Earth (TM) indicates there is a degree of lateral variation in the sandstone units at this location but it is not clear if this is due to syn or post-depositional faulting. If syn-depositional, the structural relationship would suggest a clockwise rotation of the lower units. The overlying Corella Formation consists of

basal mudstones that have a sharp contact with the underlying sandstone. Up-section the mudstones become more calcareous and three coarsening upwards sequences of mudstone interbedded with calcareous fine to medium-grained sandstones are observed.

4.5.2.1.4 Section B4

Section B4 was taken roughly 20 km south of B3 from the same fault block (Figure 4.3D). For the lower part (Ballara Quartzite), the section is a composite of 3 high-resolution sections measured along strike (bedding). The upper part of the section (Corella Formation) was based on multiple small measured sections (Some less than <15 m), field observations, and the previous geological mapping as outcrop was sporadic and discontinuous. The contact with the Argylla Formation volcanics at this location is locally erosional. The erosional surface occurs near the base of the previously mapped contact between the Ballara Quartzite and the Argylla Formation. However, numerous volcanic units, both mafic and felsic occur above this erosional surface which could be attributed to the Argylla Formation (Figure 4.7A), suggesting the hiatus in sedimentation might not have occurred for a significant period. Section B4 starts roughly 5m below this disconformity. The erosional surface has roughly 10 m relief with the underlying volcanics, the incision is filled with conglomerate interbedded with very coarse-grained volcaniclastic sandstones. The conglomerate is massive and consists of moderately sorted pebble to boulder-sized clasts, of felsic volcanics. The interbedded sandstones have planar crossbedding with paleocurrent measurements towards the NE. Only one shoulder of the incision can be mapped accurately so its width is uncertain. Overlying the basal conglomerate and sandstones

are thin to medium bedded fine-grained sandstones with trough cross-bedding and swaley cross-stratification attributed to FA3 deposited in lower shoreface conditions (Table 4.2). Within these fine-grained sediments are multiple occurrences of structureless laterally continuous mafic volcanics roughly 0.8 m thick that have rare angular blocks of cohesive sedimentary clasts at their bases up to 30 cm in diameter interpreted as volcanic flows with sedimentary rip-up clasts. Over roughly 350 m the sequence coarsens upward featuring five coarsening upward sequences (Figure 4.7A). This is overlain by a laterally continuous very poorly sorted conglomerate that is commonly clast supported but has lenses of matrix-supported conglomerate and very coarse sandstones. The conglomerate consists of sub-rounded to angular, mostly pebble to cobble in size but some boulder-sized clasts. The lithology of the clasts is both sedimentary and volcanic and likely sourced from the Ballara Quartzite and underlying Argylla Formation. This conglomerate unit might be non-marine, or the result of subaqueous debris flows due to tectonic forces. The conglomerate unit is overlain by thickly bedded mudstone interbedded with fine-grained sandstones of FA4, interpreted to have been deposited in off-shore transitional environments that ultimately coarsen upward to medium and coarse-grained sandstones. Another sequence overlies this unit which is in turn overlain by poorly outcropping mudstones of the Corella Formation. Based on the previous mapping, the mudstones might be 1 km thick at this location; however, they do not outcrop and are largely covered by modern sediment. Up-sequence, at location B5b (Figure 4.3D), the lowermost sediments observed are calcareous mudstones (Figure 4.6f), that are overlain by fine

to medium-grained calcareous sandstones that are convoluted, have wavy contacts and are interbedded with mudstone (Figure 4.6h).

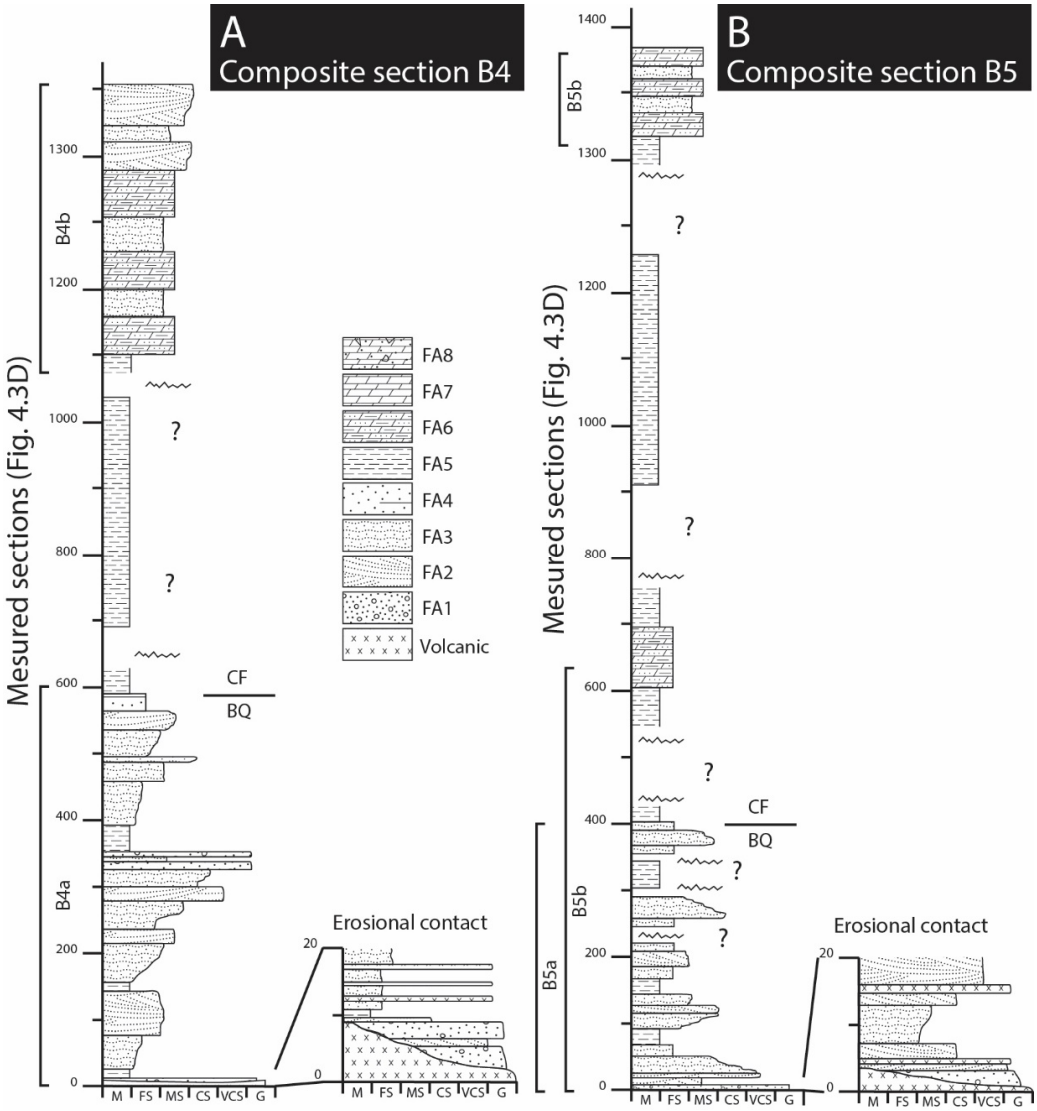

Figure 4.7: Stratigraphic columns from locations B4 and B5. BQ=Ballara Quartzite. CF=Corella Formation. Contacts between BQ and CF are from geological maps for reference (Figure 4.3). See Table 4.2 for the facies and facies associations.

4.5.2.1.5 Section B5

Section B5 is located roughly 4 km west of section B4 on a fault block further to the west (Figure 4.3D). For the Ballara Quartzite, the composite section was constructed from 2 measured sections roughly 1.5 km along strike and numerous observations

between them. The upper part of the section consists of a single measured section, the middle part of the section is largely inferred from previous geological maps and only a few observations. The contact with the underlying Argylla Formation outcrops poorly but is undulating and erosional with up to 5 m relief. Basal units consist of laterally discontinuous poorly sorted FA1 conglomerates and very coarse-grained sandstone units (Figure 4.7B). Poor outcrop makes it is difficult to tell if the conglomerates are confined to erosional incisions, but that seems likely. The conglomerate consists of some sedimentary and mafic volcanic clasts, but most are felsic volcanics indistinguishable from those of the Argylla Formation. These sedimentary rocks are envisaged to have been deposited in non-marine sheet-flood settings. The overlying units consist or sharp based shallow marine sandstones of FA2 interbedded with fine-grained sandstones of FA3 that coarsen upwards over 20 m (Figure 4.6b). The sequence consists of five coarsening upwards cycles towards the contact with the basal mudstone unit of the Corella Formation (Figure 4.7B). In the lowest ca. 50 m four felsic volcanic units ranging from 0.2 to 0.7 m thick are observed. In the next ca. 200 m of stratigraphy, 2 mafic units roughly 1 m thick are noted interbedded within the mudstone units. These mafic units are conformable, but their contacts are obscured, so it is not possible to ascertain whether they are flows or sills.

4.5.2.2 Malbon Group

4.5.2.2.1 Section M1

Section M1 is a composite section comprising of one measured section through the Mitakoodi Quartzite and Wakefield Metabasalt and observations from the basal

Mount Star Member (Derrick et al., 1976) (Figure 4.4B). The contact between the Mount Star Member and the underlying Cone Creek Metabasalt (Derrick et al., 1976) is obscured at this location but was previously mapped as a fault contact (Figure 4.4). The Mount Star Member consists of highly weathered fine-grained sandstones of FA3 interbedded with calcareous fine-grained sandstones and cleaved mudstones. At the base of the measured section, the Mitakoodi Quartzite consists of fine-grained sandstones of FA3 with minor interbedded heterolithic fine-grained sandstone and mudstone that coarsen upwards over two ca. 40 m cycles to medium to coarse-grained sandstones of FA1 (Figure 4.8A). These lower units have very similar characteristics of the uppermost units observed in the Mount Star Member to the south and from satellite imagery (Google Earth) look to be broadly coeval (Figure 4.4B). Up-section, the sequence coarsens upwards to fine to medium-grained sandstones of FA2 (Figure 4.9a), that are overlain by medium to coarse-grained sandstones of FA1. The sequence then consists of roughly 500 m predominately medium to coarse-grained sandstones of FA1 with common erosional contacts interbedded with rare fine-grained laterally continuous sandstones. The Wakefield Metabasalt rarely outcrops and is mostly identifiable from basaltic boulders on the ground, neither the lower or upper contact with the Mitakoodi Quartzite was observed at this location. The overlying upper Mitakoodi Quartzite consists of fine-grained sandstones and interbedded mudstones of FA2 and FA3 that ultimately coarsen upward over three cycles to medium-grained sandstones of FA1. The overlying mudstone and fine-grained sandstone indicate a return to deep-water

environments. In this location, the Overhang Jaspilite (Derrick et al., 1976) is absent, likely a result of the Highway Thrust to north-northeast (Figure 4.4).

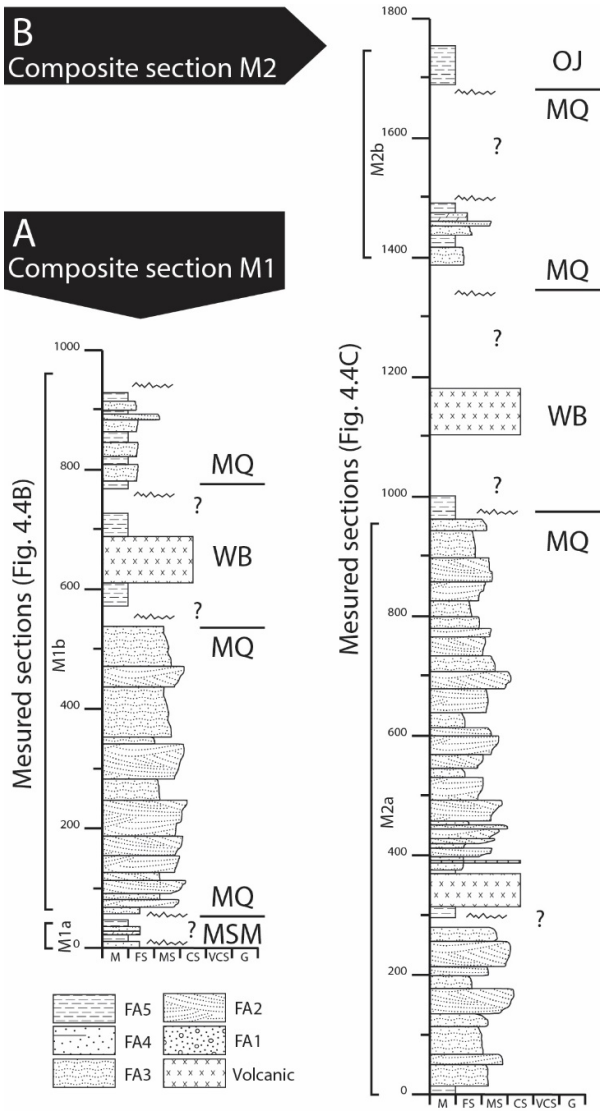

Figure 4.8: Stratigraphic columns from locations M1 and M2. MSM = Mount Star Member. MQ = Mitakoodi Quartzite. WB = Wakefield Metabasalt. OJ = Overhang Jaspilite. Contacts between units are from geological maps for reference (Figure 4.4). See Table 4.2 for facies association.

4.5.2.2.2 Section M2

Section M2 is a composite of a measured section from the basal Mitakoodi Quartzite to the upper Mitakoodi Quartzite and through the upper Mitakoodi Quartzite and the Overhang Jaspilite further to the south (Figure 4.4C). The upper Timberoo Member (Derreck et al., 1976) underlying the Mitakoodi Quartzite outcrops poorly and

consists of calcareous mudstone interbedded with felsic volcanics and fine-grained sandstones. The contact between the Timberoo Member with the basal medium-grained sandstones of the Mitakoodi Quartzite is concealed. Lower units of the Mitakoodi Quartzite are white to grey, medium to coarse-grained sandstones of FA1 and FA2 (Figure 4.9b and 4.9c). The sandstones are typically medium to thickly bedded, have sharp erosional bases and commonly consist of coarsening upwards bundles roughly 5m thick. Over ca. 250 m the succession broadly coarsens upwards and is overlain by fine-grained sandstone interbedded with mudstone and basalt. The context of the basalt is uncertain. The contact between the mudstone with the overlying sandstones is gradational. The overlying three coarsening-upward cycles become progressively thinner towards the top (Figure 4.9d) and are part of a larger coarsening upwards sequence that is capped by a thinly bedded, coarse to very coarse-grained sandstone, featuring parallel laminations interbedded with fine-grained sandstones and mudstones, possibly deposited in marginal marine environments. This unit is overlain by approximately 600 m thick, medium to thickly bedded, fine to medium-grained sandstones of FA1 and FA2 with minor occurrences of fine-grained sandstones and mudstones of FA3 and FA4. The contact between the Mitakoodi Sandstone and overlying Wakefield Metabasalt is concealed and the basalt is only known from boulder scree. Similarly, the contact between the Wakefield Metabasalt and the overlying upper Mitakoodi Quartzite in concealed. The upper Mitakoodi Quartzite at location M2b further to the south consists of fine to medium-grained sandstones interbedded with mudstones of FA3 and FA4 (Figure 4.9e), with uncommonly interbedded mudstones of FA4. The contact with the overlying

Overhang Jaspilite is conformable. The Overhang Jaspilite is highly deformed jaspilite beds interbedded with calcareous mudstone and fine-grained sandstones (Figure 4.9f). This unit is considered to have been deposited in a distal sediment starved environment.

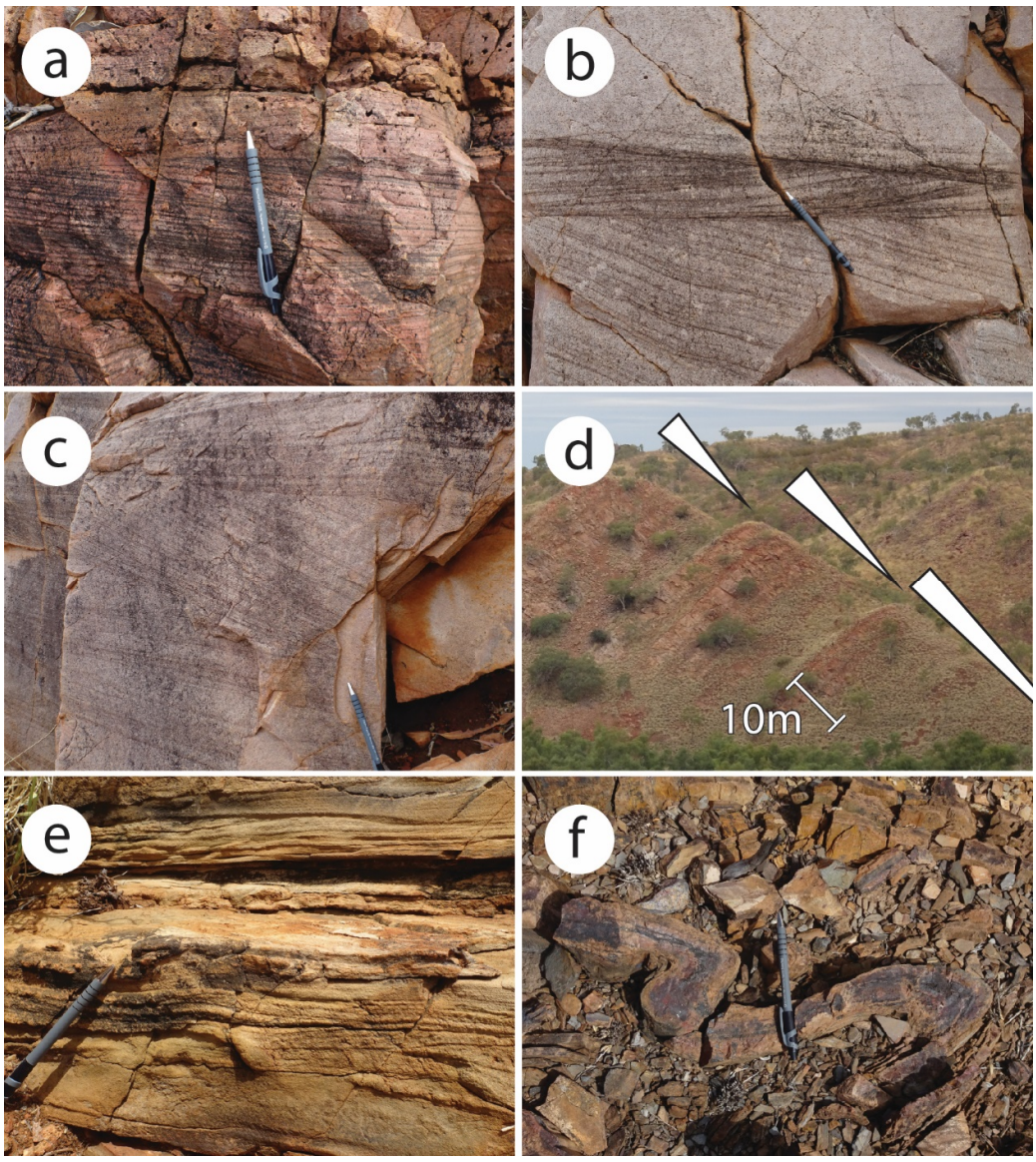

Figure 4.9: Outcrop photos of the Malbon Group. a) FA3, Low-angle planar cross-beds in fine-grained sandstones featuring erosional surface at location M1b. b) FA2, Herringbone style cross-bedding in medium-grained sandstone at location M2a. c) FA2, Planar cross-beds and horizontally laminated medium-grained sandstones at location M1a. d) Coarsening up-ward parasequences at location M2a, the base is approximately 400 m on the stratigraphic column

M2 (Figure 4.9). e) FA3, medium-grained sandstones featuring wavy bedding and horizontal laminations at location M2b. f) FA5, Folded jaspilite interbedded with mudstone at location M2b.

4.5.3 Basin evolution

4.5.3.1 Mary Kathleen Group

The stratigraphic evolution of the Mary Kathleen Group is notably different from north to south. Section B1, the most northerly measured section, consists of basal alluvial fan deposits largely absent from all other sections (Figure 4.5 and 4.6). Alluvial fans develop where there is a notable change in the gradient of the topography and are generally associated with active tectonic regimes, such as rifted margins (Blair, 1987; Nilsen, 1982). At location B1, a previously mapped NW-SE striking fault cuts and offsets the Ballara Quartzite and underlying Argylla Formation normally but not the overlying Corella Formation (Figure 3B), indicating it was likely active during this interval. Furthermore, the alluvial fan deposits to the north of this fault are roughly 30 m thicker, as would be expected in the hanging wall of the fault. Nevertheless, given the occurrence of alluvial fan deposit either side of this fault, it seems unlikely it was the major control for these basal deposits. The absence of alluvial fan deposits in the sections measured further to the south (section B2 and B3) (Figure 4.3C and 4.5), suggests that the fault that controlled the deposition of the alluvial fan deposits at northern section occurs between location B1 and B2. Numerous faults striking both NE-SW and NW-SE cross-cutting the Ballara Quartzite deposits can be seen from the geological map and aerial images (Figures 4.1 and 4.3). Field observations are needed to confirm if any of these faults were syn-depositional and a main controlling fault responsible for the topographic gradient change needed to deposit the alluvial fans.

Another major point of difference from section B1 to sections further south is the thickness of the low-stand deposits, and the occurrence of more coarsening up-ward parasequences in the south (Figure 4.5, 4.7 and 4.10). This suggests that B1 was deposited in a more distal location than the sections to the south and is consistent with the occurrence of relatively pure limestone further up-sequence at B1, whereas the sections to the south are typically associated with more terrigenous material (Figure 4.5 and 4.7).

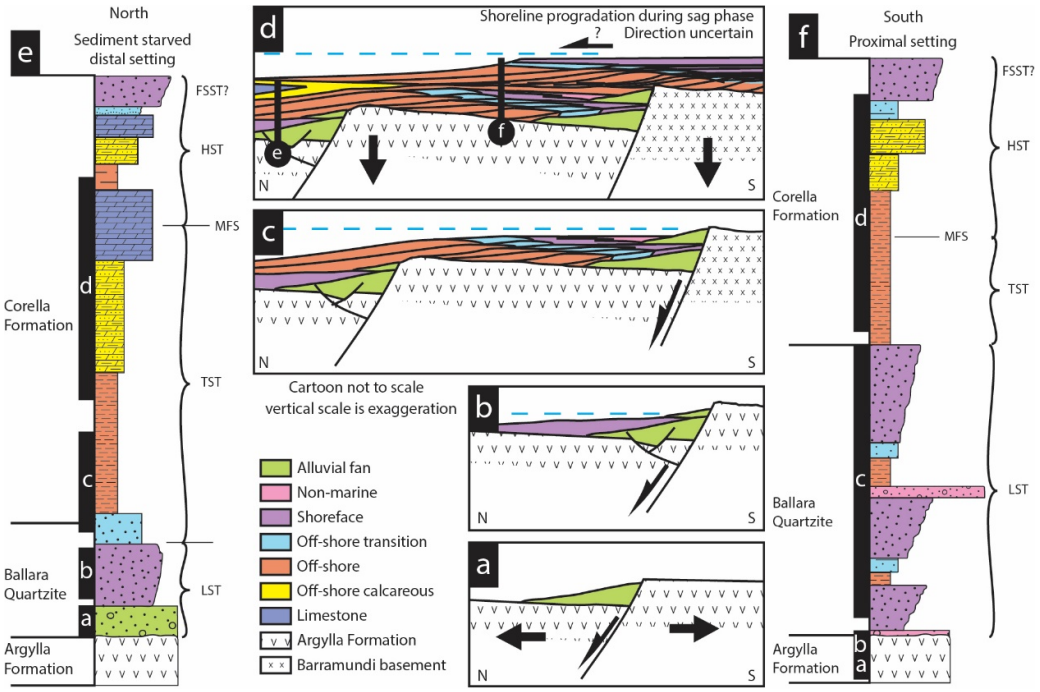

Figure 4.10: Simple cartoon illustrating the depositional model for the Mary Kathleen Group. Blue dashed line is relative sea-level. a) General N-S extension at ca. 1.77 Ga creates a significant gradient change at a rift shoulder allowing for deposition of the alluvial fans in location B1. At the same time, the southern locations (B4 and B5), are uplifted and actively eroding. b) Rift-related subsidence provides accommodation for deposition of shallow marine deposits in the north. At this time in the south, non-marine sediments might start to fill the low-stand erosional incisions. c) The active rift propagates further to the south generating a significant flooding surface in the north, in the south, there is also a flooding surface, however, the low-stand deposits show a higher frequency of parasequences indicative of a proximal location to the shoreline. d) the rift propagates further to the south flooding the entire basin, the north becomes starved of sediment, resulting in precipitation

of limestone. In the south, the maximum flooding surface is marked in the middle part of the mudstone. e) Hypothetical distal section (B1). f) Hypothetical proximal section (B4 and B5).

Section B4 and B5, the most southerly sections measured for the Mary Kathleen Group locally both have erosional contacts with the underlying Argylla formation (Figure 4.7). The erosional surface or subaerial unconformity was likely developed synchronously with the deposition of the alluvial fans at location B1 (Figure 4.10a). Volcanic units observed in basal portion at all Mary Kathleen Group locations suggests that the unconformity (at B4 and B5) was probably not associated with a significant break in sedimentation. At location B2 and B3, the contact with the underlying Argylla Formation is transitional suggesting a gradual transition to the basal shallow marine deposits of the Ballara Quartzite (Figure 4.5B and 4.5C). Further south at locations B4 and B5 the contact is locally erosional to transitional (Figure 4.7). At B4, the erosional relief is almost 10 m whereas at B5 the relief is about 5 m. A model where locations B4 and B5 were uplifted and eroding, providing material deposited at B1 is consistent with the sedimentology from those sections (Figure 4.10a) but does not reconcile the transitional contacts observed at B2 and B3. Perhaps these locations were also uplifted and eroded, but not to the same extent as the locations further to the south. Thus, only localised channels were developed, or the erosional surface was located stratigraphically below where the measured sections started. Nevertheless, alluvial fans in the north corresponding to an erosional surface to the south, along with well-developed and more numerous parasequences to the south, are indicative of a general north-south extension associated with deposition of the Ballara Quartzite (Figure 4.10).

In sequence stratigraphy, the lowstand systems tract (LST) is relative to the occurrence of the overlying transgressive systems tract (TST) and the highstand system tract (HST) (Catuneanu, 2006; Posamentier, 1988; Van Wagoner et al., 1988). In some rift settings, the lowstand system tract might be poorly developed or completely absent due to rapid subsidence (Martins-Neto and Catuneanu, 2010). Rapid subsidence results in the shoreline retreating quickly landward not allowing for the development of the TST. Therefore, the maximum regressive surface (MRS, the surface marking the change from the LST to the TST) might be condensed with the subaerial unconformity. The deposits overlying this condensed surface would then be the HST. This sequence stratigraphic interpretation would be appropriate if the rifting was a single event, however, all rift systems are a culmination of numerous events (Chorowicz, 2005). Typically, the maximum regressive surface should be synchronous (Helland-Hansen and Martinsen, 1996; Zecchin and Catuneanu, 2013); however, the interpretation in this study that is compatible with the data, indicates that the MRS is diachronous, and stepping landward as tectonic subsidence allows the base-level to rise and overcome each fault block (Figure 4.11). In this scenario one blocks LST correlates with another blocks HST. Herein, we interpret the LST as those units typified by coarsening upwards parasequences underlying a significant flooding surface, for which the units above show either no effect from the shoreline (i.e. parasequences) or are deepening upwards. The units overlying the flooding surface are interpreted as the TST. In the TST, the shoreline may be under regression or transgression but from these units, it is impossible to tell from field observations. Using this method in this study can account for the sections further to the south

(landward), having thicker LSTs and have more coarsening upwards parasequences (Figure 4.11). In this fashion, the LST and the TST encompass the active rifting (Ballara Quartzite and lower Corella Formation), and the HST is interpreted as the sag phase (Corella Formation).

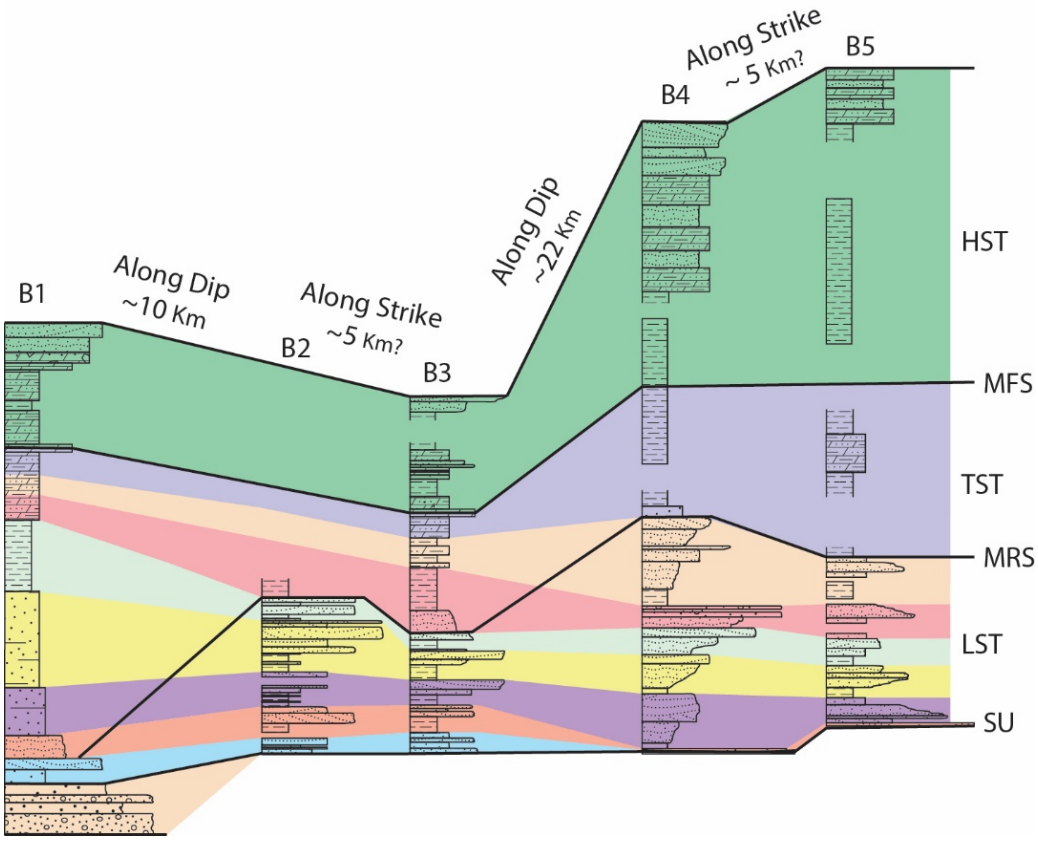

Figure 4.11: Sequence stratigraphic interpretation for the Mary Kathleen Group measured sections, aligned with north to the left. Each colour represents a parasequence. Note that parasequences cut major system tract boundaries, contrary to typically sequence stratigraphic models. See text for discussion. LST: Lowstand system tract. TST: Transgressive system tract. HST: Highstand system tract. MRS: Maximum regressive surface. MFS: Maximum flooding surface. Terms from Catuneanu (2006).

4.5.3.2 Malbon Group

The contact between the Mitakoodi Quartzite and the underlying Timberoo Member at section M2 was concealed but is thought to be conformable (Derrick et al., 1976).

At section M2 the lower Mitakoodi Quartzite consists of coarsening upwards

parasequences of amalgamated shallow marine sandstones with common erosional contacts (Figure 4.8B). This suggests slow sedimentation rates, a lack of accommodation space, and high wave energy (Hampson and Storms, 2003). Sediment in these systems is largely reworked, accommodation space is generated by sediment compaction and thermal subsidence, and parasequences are generated by both climate- and auto-cyclic processes rather than tectonic activity (Catuneanu, 2006; Helland-Hansen and Hampson, 2009; Muto and Steel, 2001). Up-sequence, the occurrence of tholeiitic basalts interbedded with mudstones and fine-grained sandstones suggest renewed rifting and a deepening of the basin. The overlying upper Mitakoodi Quartzite commonly consists of fined grained units and coarsening up-wards bundles which are sharp based but have transitional contacts up sequence, indicative of increased accommodation space. In line with the tholeiitic basalts, this suggests the upper Mitakoodi Quartzite was deposited during a period of renewed rifting, which is also evident from the Wakefield Basalt that overlies the upper part of the Mitakoodi Quartzite.

In the Mitakoodi Domain, notable differences in the stratigraphy occur in the eastern (M2) and western (M1) sections, however, most of those differences could be due to structural complexities (Potma and Betts, 2006; Williams, 1989). The eastern part of the Mitakoodi Domain has undergone a much higher degree of folding and faulting owing in part to the proximity with the Pilgrim Fault (Figure 4.1 and 4.4) (Williams, 1989). In the east, two basaltic units are observed, whereas in the western section there is only one. However, Derrick et al. (1976) noted that further south in the eastern part there was another basaltic unit, probably correlative with the lower

basaltic unit in the east. Potma and Betts (2006) described a fault in the eastern part of the Mitakoodi Domain south of location M2b, that they interpreted to be extensional, hanging wall to the south-east, thus suggesting the basin deepened in that direction. At first glance, it seems plausible that the western section was a more proximal location, however, the geology is complicated and further work is required.

4.6 Detrital zircon sampling and results

4.6.1 BAL1701

Sample BAL1701 consists of two different samples, 01a, and 01b (Figure 4.3B). Sample 01b was a very coarse-grained poorly sorted sandstone from the sheet flow facies within the alluvial fan deposits at location B1. 01a was taken approximately 20 m up-section from a medium-grained sandstone of the shoreface facies. Zircon from the alluvial fan facies are euhedral, highly angular to angular, mostly translucent and have abundant inclusions and fractures. In CL images the zircons are mostly homogeneous with rare occurrences of oscillatory zoning that are more common in larger grains. Some of the zircons from the overlying shoreface facies (01a) are similar to 01b but are slightly more rounded. Otherwise, under plain light, most zircons from 01a are rounded to well-rounded and some are very spherical. In transmitted light, the grans are typically translucent and less often have a yellowish tint and are often fractured. Grains range from those with oscillatory zoning, with and without inherited cores, some are homogeneous and others rarely metamict. From sample 01b, 66 grains analysed in two different sessions resulted in a total of 30 grains <5% discordant (Figure 4.12 and 4.13A). These 30 concordant grains form a unimodal

population at ca. 1775 Ma (Figure 4.13A). From sample 01a, 98 grains analysed over a single session resulted in 50 concordant analyses (<5%) that form the main population centred at ca. 1880 Ma with a younger shoulder population (Figure 4.13A). In total, sample BAL1701 contains 80 concordant analysis that has the main population at 1770 Ma and a subordinate population at 1880 Ma (Figure 4.12 and 4.12A). The ε_{Hf} values from 78 grains ranging in age from ca. 1730 to 1950 Ma, <10% discordant, range from -9.56 to 1.79, excluding one outlier at -14.59 (Figure 4.13). The zircon grains with ages older than ca. 1830 Ma are more negative and show higher variability in ε_{Hf} than those younger than ca. 1830 Ma.

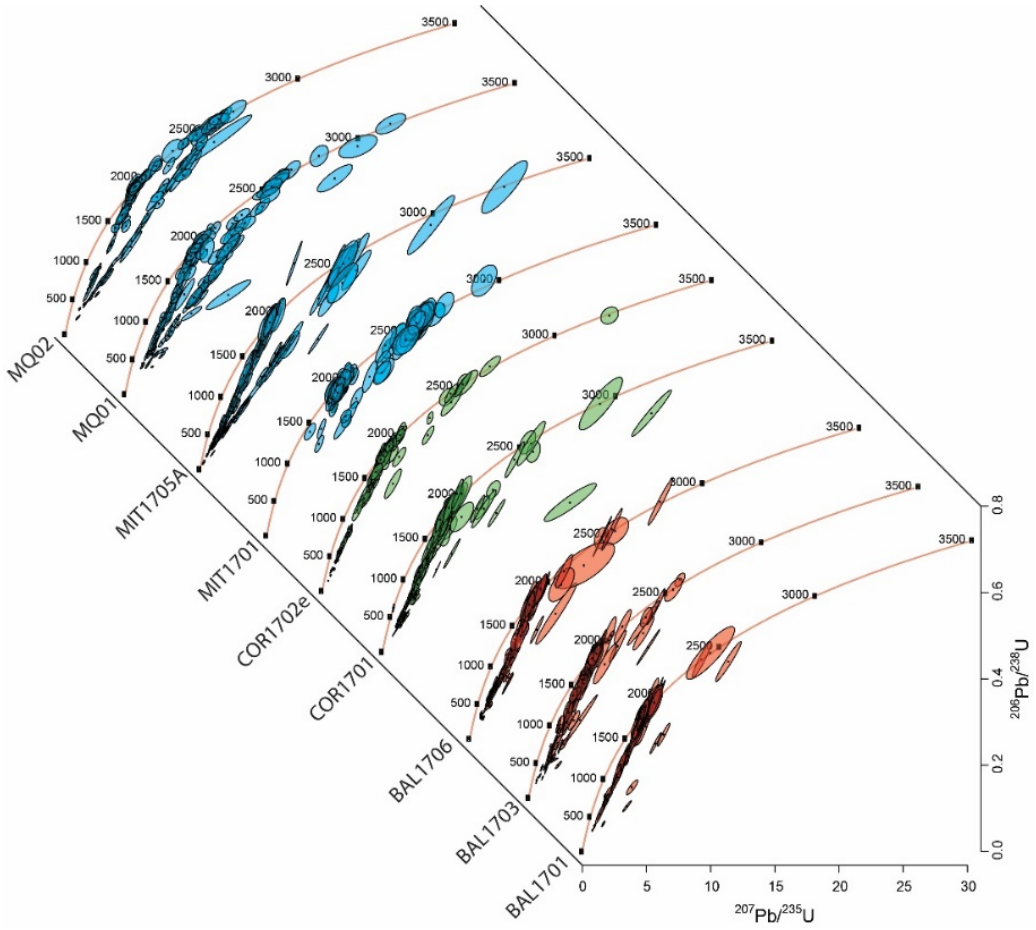

Figure 4.12: Concordia plots for all detrital zircon samples from this study.

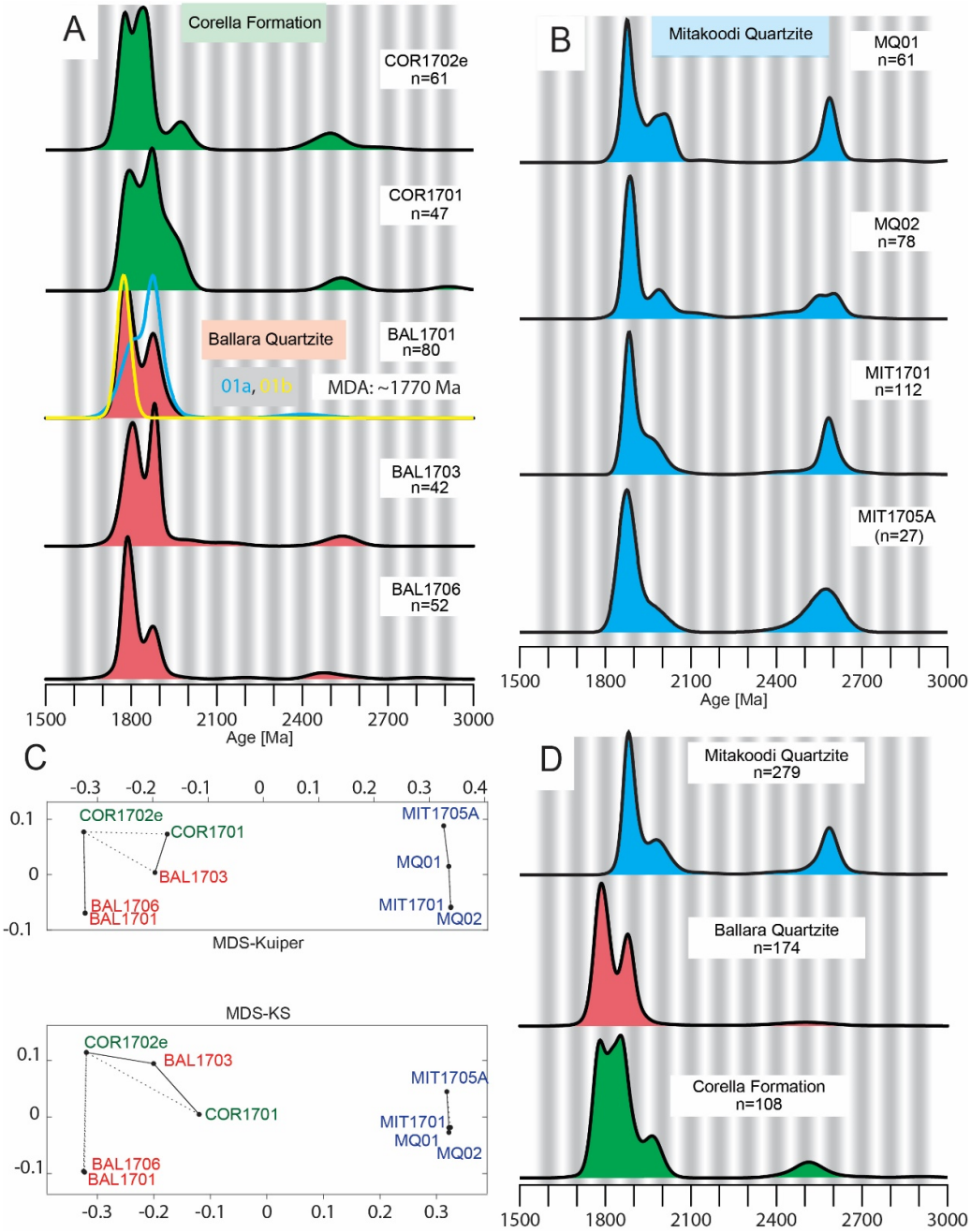

Figure 4.13: Detrital zircon data <5% discordant. A) KDE plots from the Mary Kathleen Group samples. B) KDE plots from the Mitakoodi Quartzite (Malbon Group) samples. C) MDS plots show that the detrital zircon samples from the Mary Kathleen Group are statistical dissimilar from the Mitakoodi Quartzite. D) KDE plots of samples grouped based on unit names. The Mitakoodi Quartzite samples lack the <1800 Ma population that are observed in all Mary

Kathleen Group samples as well as have a significant ca. 2580 Ma population. Ages are calculated from $^{207}Pb/^{206}Pb$.

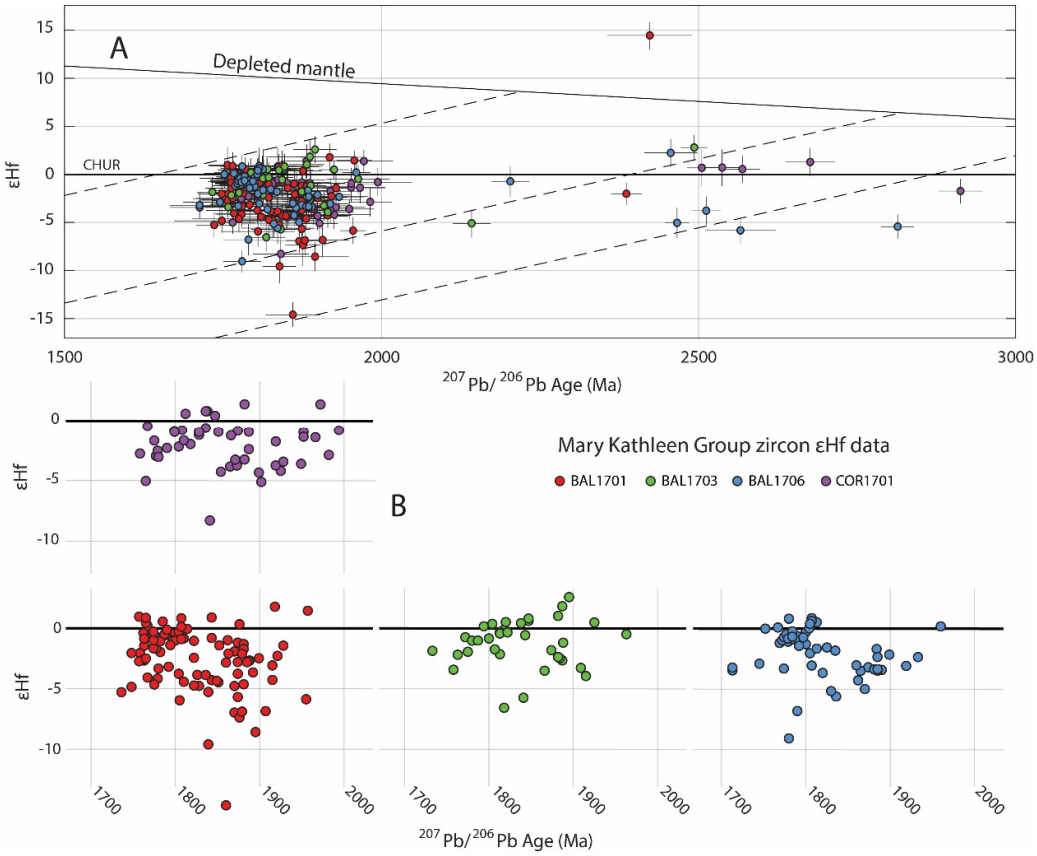

Figure 4.14: Mary Kathleen Group detrital zircon samples ε_{Hf} vs age. A) All data with 1σ error bars. B) Zoomed in plots for individual samples. Depleted mantle from Vervoort and Blichert-Toft (1999). CHUR is CHondritic Uniform Reservoir (Blichert-Toft and Albarède, 1997). Dashed lines are crustal evolution lines.

4.6.2 BAL1703

Sample BAL1703 is a medium-grained sandstone from location B2 approximately 130 m up-sequence from the base of the measured section (Figure 4.3C and 4.5B). This unit is mapped as Argylla Formation; however, the highest volcanic unit is lower in the sequence and the quartzite at the sample location is indistinguishable from what is typically mapped as Ballara Quartzite. The sample consists of two blocks, one taken at the base of the bed and another taken from the top. Zircon grains are rounded to

well-rounded and under transmitted light microscopy are typically clear and/or dark grey with an orange to yellow tint. In CL the zircon most often feature oscillatory zoning or are less commonly homogeneous or metamict. From 137 grains targeted on two sessions, 42 grains are <5% discordant (Figure 4.13A). The detrital zircon spectra for sample BAL1703 features two main populations centred on ca. 1800 and 1880 Ma with a small population defined by three grains at ca. 2530 Ma (Figure 4.13A). The ε_{Hf} values from 36 grains aged from ca. 1730 to 1960 Ma, <10% discordant, range from -6.5 to 2.8 (Figure 4.14). Zircon grains with ages older than ca. 1850 Ma show higher variability in ε_{Hf} than those younger than ca. 1850 Ma.

4.6.3 BAL1706

Sample BAL1706 is combined from two distinct samples, 06a and 06b from location B5 (Figure 4.3D and 4.7B). Sample 06a is a medium-grained sandstone taken about 70m up-sequence from the contact with the underlying Argylla Formation, whereas, sample 06b was taken about 80m up-sequence from sample 06a and roughly 180m south along strike (Figure 4.7B). The zircons from both samples have the same characteristics and results, and thus, both samples will be discussed together. Most grains are rounded to well rounded. Under transmitted light microscopy, the zircon grains are clear to dark grey and often fractured. CL images show most grains have oscillatory zoning, very few have inherited cores or are metamict. Over three sessions a total of 137 grains were analysed resulting in 52 grains <5% discordant (Figure 4.12). The detrital zircon KDE plot for sample BAL1706 has a main population centred on ca. 1790 Ma, a subordinate population at ca. 1840 Ma and a few grains at ca. 2500 Ma

(Figure 4.13A). The ε_{Hf} values from 52 grains aged from ca. 1710 to 1950 Ma, <10% discordant, range from -9.0 to 0.9 (Figure 4.14). Zircon grains with ages older than ca. 1810 Ma have a more negative ε_{Hf} than those younger than ca. 1810 Ma.

4.6.4 COR1701

Sample COR1701 is the result of two combined samples that were taken from medium-grained sandstones roughly 60 m along strike from one and other at location B1b (Figure 4.3B). Zircon grains from both samples have a similar appearance and similar results, and so will be discussed as a single sample. Under transmitted light the zircons of COR1701 are commonly clear with a yellowish tint, larger grains are typically dark red to orange and have abundant fractures. Most grains are well rounded except for a few small grains that are slightly angular. In CL, the zircon are mostly homogeneous or have oscillatory zoning and very few have inherited cores or are metamict. From 142 analysis a total of 47 grains are <5% discordant (Figure 4.12). The concordant grains form a broad population with ages ranging from ca. 1750 to 1980 Ma with most ages between ca. 1800 and 1860 Ma, and a minor population at ca. 2530 Ma (Figure 4.13A). The ε_{Hf} values from 46 grains aged from ca. 1760 to 1970 Ma, <10% discordant, range from -8.4 to 1.4 (Figure 4.14). Zircon grains with ages older than ca. 1850 Ma have slightly more negative ε_{Hf} values than those younger than ca. 1850 Ma.

4.6.5 COR1702e

Sample COR1702e was taken roughly 70 km to the south of the closest measured section of the Corella Formation (Figure 4.1). The sampled unit is medium to coarse-

grained sandstone with large scale low angle cross-beds and wave ripples that would be in a similar stratigraphic position as sample COR1701. Under transmitted light, the zircon are clear with a yellowish to orange tint and larger grains are typically darker orange. Most grains are well rounded and fractured, very few small grains are angular. In CL, most grains have well developed oscillatory zoning with very few having metamict textures. From 131 grains analysed 61 grains <5% discordant form a main population that encompasses ages from ca. 1720 to 1900 Ma with peaks at ca. 1790 and 1840 Ma and a minor population at ca. 2500 Ma (Figure 4.13A). No Lu-Hf zircon data was recovered for this sample due to instrument failures.

4.6.6 MQ02

MQ02 is from a medium to coarse-grained sandstone sampled ca. 6.5 km south of the location of where the measured section M2a was taken. Stratigraphically, the sample is in the "lower" Mitakoodi Quartzite ca. 150 m below the first occurrence of mafic volcanics (Figure 4.4C and 4.8B). Most grains appear clear to light pink under transmitted light microscopy and larger grains are typically darker and more well-rounded and spherical. Some smaller grains are slightly angular and more fractured. In CL, most grains feature well developed oscillatory zoning, some are homogeneous, very rarely do grains have inherited cores or are metamict. Over two sessions 140 grains were analysed resulting in 78 grains <5% discordant (Figure 4.12). The detrital zircon spectra for MQ02 features a prominent population at ca. 1890 Ma with a smaller population at ca. 1990 Ma, and a broad subordinate population defined by a spread of ages from ca. 2510 to 2630 Ma (Figure 4.13B). The ε_{Hf} values from 61 grains

aged from ca. 1830 to 2150 Ma, <10% discordant, range from -7.51 to 4, excluding one very isotopically enriched analysis (1983 Ma, -24.38) (Figure 4.14). Whereas, the ε_{Hf} values from 24 grains aged from ca. 2280 to 2695 Ma, <10% discordant, range from -13.2 to 4.3 but most grains have ε_{Hf} values between -4 and 1.5. From the younger population (1850–2100 Ma), zircon grains older than ca. 1930 Ma are typically closer to the depleted mantle values, whereas those younger than 1930 Ma are more variable and more enriched.

4.6.7 MQ01

MQ01 was sampled approximately 1 km east of MQ02, or stratigraphically about 800 m up-section, considered the "upper" Mitakoodi Quartzite (Figure 4.4C and 4.8B). The sample was from a massive pinkish medium-grained sandstone. Under transmitted light microscopy the grains are mostly clear with a slightly pink hue. Most grains a rounded to well-rounded, but a few are spherical, and most have a high aspect ratio. In the CL images, most grains show oscillatory zoning or are homogeneous, some have small inherited cores, and a few are metamict. Sample MQ01 was analysed over two sessions, from 171 grains analysed a total of 61 grains are <5% discordant. The detrital zircon spectra show the main population centred on ca. 1890 Ma with a broad ca. 1990 Ma population and a well-defined subordinate population at ca. 2580 Ma (Figure 4.13B). The ε_{Hf} values from 52 grains aged from ca. 1840 to 2140 Ma, <10% discordant, range from -9.2 to 7.1, but most grains have ε_{Hf} values between -4 and 5 (Figure 4.15). The ε_{Hf} values from 21 grains aged from ca. 2370 to 3122 Ma, <10% discordant, range from -4.1 to 3.7.

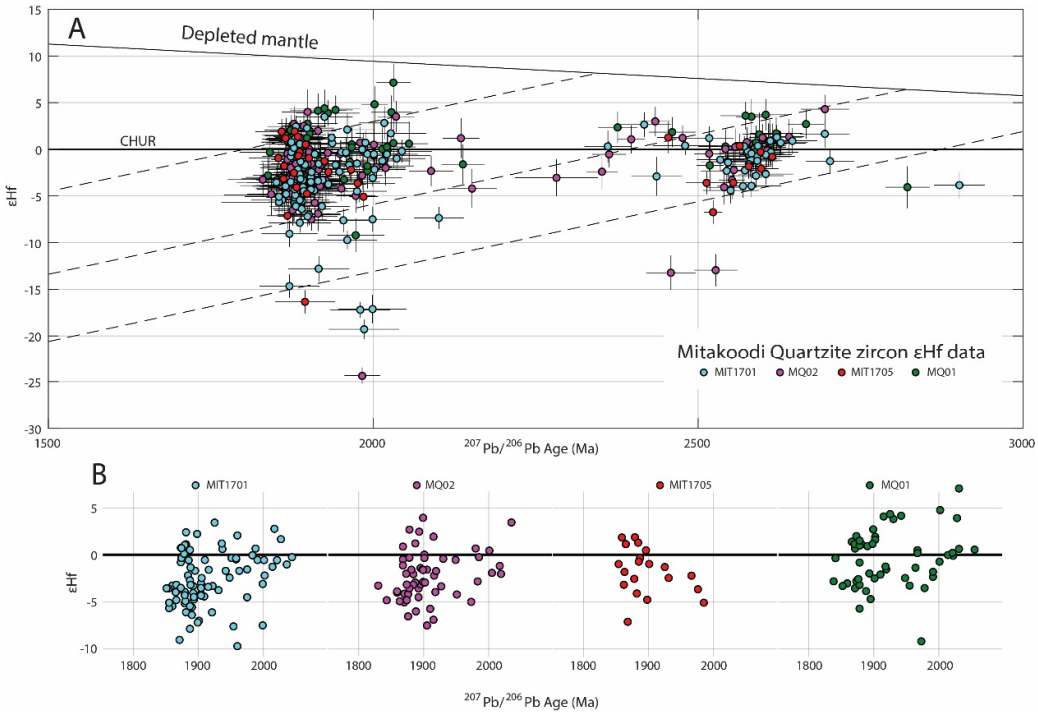

Figure 4.15: Mitakoodi Quartzite detrital zircon samples ε_{Hf} vs age. A) All data with 1σ error bars. B) Zoomed in plots for individual samples. Depleted mantle from Vervoort and Blichert-Toft (1999). CHUR is CHondritic Uniform Reservoir (Blichert-Toft and Albarède, 1997). Dashed lines are crustal evolution lines.

4.6.8 MIT1701

Sample MIT1701 was taken at location M1 approximately 140 m up-sequence from the base of the measured section (Figure 4.4B and 4.8A). The sample is a composite resulting from sampling two distinct medium to coarse-grained sandstone beds, stratigraphically 2 m apart. The appearance of the zircon from both samples is indistinguishable and the analytical results the same, and therefore will be discussed as a single sample. Under transmitted light microscopy the zircons are most commonly clear with some having a yellowish tint. Larger grains are typically darker, more well-rounded and more spherical. In CL the grains have well developed oscillatory zoning or are homogeneous. Very few grains have inherited cores or are metamict. In total, 140 grains from MIT1701 were analysed on a single day resulting

in 111 analysis <5% discordant (Figure 4.12). The detrital zircon age spectra for MIT1701 has the main population that is centred on ca. 1880 Ma that encompasses ages from ca. 1850 to 2220 Ma and a subordinate population at ca. 2580 Ma (Figure 4.13B). The ε_{Hf} values from 83 grains aged from ca. 1850 to 2100 Ma, <10% discordant, range from -9.72 to 3.48, along with 5 grains have ε_{Hf} values between -12.8 to -19.3 (Figure 4.15). The ε_{Hf} values from 38 grains aged from ca. 2360 to 2900 Ma, <10% discordant, range from -4.4 to 2.7.

4.6.9 MIT1705A

Sample MIT1705A was taken from a massive, medium bedded, medium-grained sandstone about 21 km to the NE of location M2a (Figure 4.1). This location is mapped as Mitakoodi Quartzite which is interbedded with calc-silicates mapped as Corella Formation. The stratigraphic context is uncertain, but the sample was collected to further test the proposed correlations. Under transmitted light microscopy most grains appear grey to yellow and a few are clear with a yellowish tint. Most grains are well rounded, and a small proportion is very spherical. In CL, most grains are homogeneous or feature oscillatory zoning, but there is a large proportion that has inherited cores, and a few are metamict. Analysed over a single day, 142 grains were targeted resulting in 28 analysis <5% discordant (Figure 4.12). The detrital zircon spectra from sample MIT1705A has the main population at ca. 1880 Ma and a subordinate population at ca. 2570 Ma (Figure 4.13B). The ε_{Hf} values from 20 grains aged from ca. 1850 to 1980 Ma, <10% discordant, range from -7.12 to 1.92, and a

single grain has ε_{Hf} values of -16.34 (Figure 4.15). The ε_{Hf} values from 11 grains aged from ca. 2450 to 3262 Ma, <10% discordant, range from -6.74 to 1.26.

4.6.10 Multidimensional scaling (MDS)

Both the Kolmogorov–Smirnov (K-S) and Kuiper statistical tests were used to assess the similarities between the individual samples. Put simply, the K-S test is a measurement of greatest absolute distance between two samples empirical cumulative frequency distributions (eCDF), whereas the Kuiper test is the sum of the greatest positive and negative distance between two eCDF's (Vermeesch, 2013, 2018a). In MDS, every sample is compared using the statistical test and plotted in MDS space based on their dissimilarities so that samples more similar plot closer together. The MDS plots generated using both the K-S and Kuiper tests show that the samples analysed in this study can be statistically grouped in two (Figure 13C). The first is the Ballara Quartzite and the Corella Formation of the Mary Kathleen Group and the second is the all the Mitakoodi Quartzite. In Figure 13D, the samples are grouped based on the results of the MDS analysis and their stratigraphic nomenclature as to visualise the difference between the samples. The differences between the Mary Kathleen Group samples and the Mitakoodi Quartzite is the absence of the <1850 Ma population and the addition of a ca. 2580 Ma population that is observed in all the Mitakoodi Quartzite samples.

4.7 Discussion

4.7.1 Timing of deposition, and correlations

North-south extension as indicated by the sedimentological observations is consistent with previous structural based interpretations from the Mary Kathleen Domain (Figure 4.1) (Gibson et al., 2008; Holcombe et al., 1992; Oliver et al., 1991; Stewart, 1992). Although the timing of extension is questionable, the structural evolution of the eastern part of the Mary Kathleen Domain is interpreted as being a mid-crustal, sub-horizontal detachment formed during north-south crustal extension with the top to the north (Holcombe et al., 1992). In the Little Beauty Syncline of the eastern part of the domain, faulting has primarily affected the Argylla Formation and the Ballara Quartzite, which Holcombe et al. (1992) suggested was due to brittle extension between two ductile layers. Thus, in this interpretation, the detachment post-dated deposition of the Mary Kathleen Group. However, Gibson et al. (2008) suggested the faulting was syn-depositional and suggested, based on the fault geometry, the basin was deepening southward. Foliated granites of the Wonga Batholith related to the detachment have ages ranging from ca. 1778 to 1738 Ma (Neumann et al., 2009a; Page and Sun, 1998), and were therefore emplaced concurrently with deposition of the Mary Kathleen Group. Thus, if the faults in the Little Beauty Syncline that indicate the basin was deepening to the south were syn-depositional, and the Ballara Quartzite at that location was deposited during the extension associated with the detachment, then there might be a transfer fault situated between the east (Little Beauty Syncline) and the west (this study location), separating an upper plate to the north from an upper plate to the south, respectively.

This is highly speculative, but would resolve some of the outstanding problems with current models, such as, why if the extension was N-S is there so much variability in the stratigraphy and the basement rocks east-west across the Mary Kathleen Domain (Blake, 1996)?

The sedimentological analysis here indicates that the Ballara Quartzite, in the western part of the Mary Kathleen Domain was deposited during a phase of active rifting broadly directed north-south (Figure 4.10). In the south of the study area, the Ballara Quartzite is characterised by a higher number of parasequences compared to the northernly sections suggesting the basin deepened to the north (Figure 4.11). The north-south extension is consistent with structural data from other areas in the Mary Kathleen Domain (Gibson et al., 2008; Holcombe et al., 1992; Oliver et al., 1991; Pearson et al., 1992). The timing of deposition for the Ballara Quartzite is constrained by U-Pb ages from volcanic units in the underlying Argylla Formation at ca. 1780 Ma (Neumann et al., 2009a), volcanic units in the lower part of the Ballara Quartzite at ca. 1770 Ma, and the maximum depositional ages from the detrital zircon at ca. 1767 Ma (Neumann et al., 2009a) and from this study ca. 1775 Ma (Figure 4.13A). These results suggest that the Ballara Quartzite has a depositional age between ca. 1780 and 1765 Ma. Foliated granites of the Wonga Batholith typically associated with the north-south detachment zone have ages from ca. 1780 to ca. 1740 Ma overlapping with the depositional age of the Ballara Quartzite (Gibson et al., 2008; Neumann et al., 2009a; Oliver et al., 1991).

In the western belt of the Mount Isa Inlier, basal units of the Quilalar Formation typically thought to correlate with the Mary Kathleen Group have maximum depositional ages of ca. 1750, and 1760 Ma (Neumann et al., 2006), notably younger than the depositional age for the Ballara Quartzite. Every depositional model for the Mary Kathleen Group is strongly based on the assumption that these sediments correlate with the Quilalar Formation and were therefore deposited during a sag phase of basin formation. Given that the Ballara Quartzite (Mary Kathleen Group) was deposited during N-S extension and has slightly older depositional ages than the Quilalar Formation, it more likely correlates with the older Myally Supersequence (Neumann et al., 2009a). The Quilalar Formation might be correlative with the sag phase in the Mary Kathleen Group, i.e. the HST of the Corella Formation. However, the timing of deposition for the Corella Formation is not well constrained, the maximum depositional ages from the detrital zircon in this study are consistent with previous findings at ca. 1775 Ma (Neumann et al., 2009a).

The maximum depositional age from the Mitakoodi Quartzite (Malbon Group) detrital zircon data is ca. 1810 Ma (Figure 4.13B). However, the underlying Bulonga Volcanics has a crystallisation age of ca. 1760 Ma (Neumann et al., 2009a), and a rhyolitic unit located at the top of the lower Mitakoodi Quartzite has a crystallisation age of ca. 1755 Ma (Neumann et al., 2009a; Page et al., 1997; Pearson et al., 1992; Potma and Betts, 2006). These ages provide a more robust depositional age of ca. 1760 to ca. 1750 Ma for the Malbon Group. The Timberoo Member underlying the Mitakoodi Quartzite is characterised by mudstone and chert interbedded with minor basaltic units (Withnall and Hutton, 2013). This unit is thought to correspond to a

regional deepening associated with mature rifting (Beardsmore et al., 1988; Derrick et al., 1980; Potma and Betts, 2006).

In contrast to the Mary Kathleen Group, where the Ballara Quartzite was deposited syn-rift during N-S extension, the lower units of Mitakoodi Quartzite were probably deposited in the HST at a mature or post rifting phase (Potma and Betts, 2006). Furthermore, the only evidence of north-south directed extension occurred post-Malbon Group (Mitakoodi Quartzite) deposition (Williams, 1989). Therefore, it is highly unlikely that the Mitakoodi Quartzite is correlative with the Ballara Quartzite based on sedimentological grounds.

4.7.2 Detrital Zircon Provenance

The detrital zircon spectra from all Ballara Quartzite samples in the central belt have a population at ca. 1770–1780 Ma and ca. 1880 Ma suggesting the same source region for all areas (Figure 4.13). At location B1, a provenance shift is observed between the alluvial fan and overlying shallow marine deposits, which is consistent with the proposed sedimentological model, where the southern locations were eroding material to source the basal units in the north (Figure 4.13A and Figure 4.10). The alluvial fan spectra primarily consist of Argylla Formation aged grains (ca. 1775 Ma) whereas the overlying shallow marine deposits have a more prominent Barramundi Orogen-aged population (ca. 1880 Ma), typical of the NAC. The ca. 1775 Ma population provides a maximum depositional age that is consistent (within uncertainty) with previous results (ca. 1767 Ma) (Figure 4.16) (Neumann et al., 2009a). The detrital zircon age spectra from the Corella Formation have similar

populations to the Ballara Quartzite but also have an additional small population at ca. 2000 Ma and a more significant population at ca. 2500 Ma (Figure 4.16). The 1750 to 1900 Ma grains that dominate all samples from all Mary Kathleen Group can be accounted for from granitic and metamorphic rocks of the Mount Isa Inlier (Figure 4.16A) (Withnall and Hutton, 2013). No source rocks with ages between ca. 1.9 to 2 Ga or 2.5 Ga have been identified in Mount Isa, however, numerous inherited grains of that age have been reported from igneous rocks in the central and western belts of the Mount Isa Inlier, and both Lu-Hf in zircon and whole-rock Nd model ages also support the idea that these zircon were sourced locally (Betts et al., 2006; Bierlein et al., 2011; McDonald et al., 1997). In contrast to the Mary Kathleen Group samples, ca. 2000 and 2580 Ma detrital zircon populations from the Mitakoodi Quartzite samples cannot be accounted from known source rock ages in the Mount Isa Inlier or the entire NAC (Figure 4.16B).

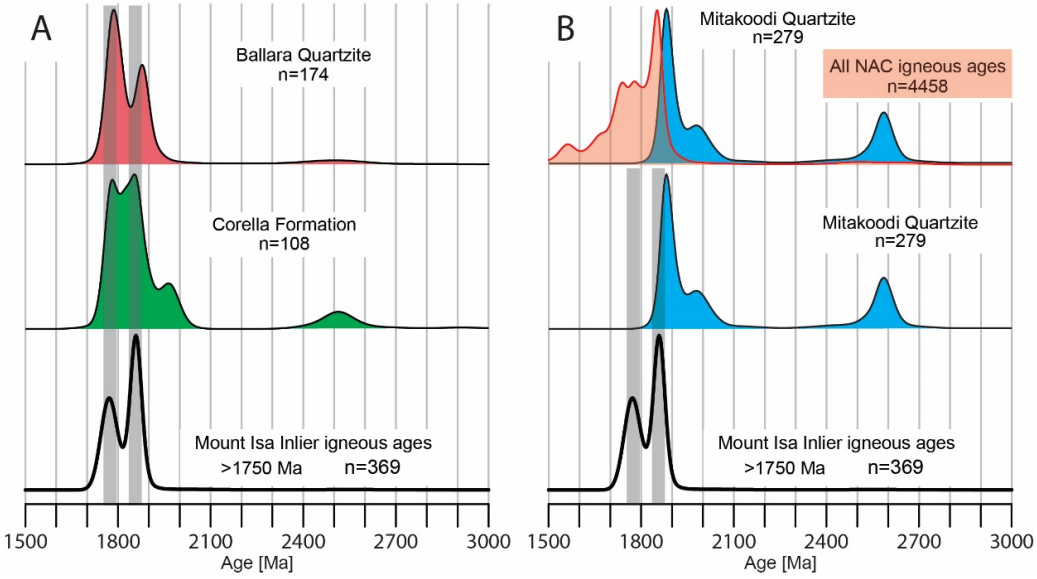

Figure 4.16: A) Detrital zircon KDE plots from the studied samples in comparison with Mount Isa Inlier igneous ages >1700 Ma from http://www.ga.gov.au/geochron-sapub-web/geochronology/shrimp/search.htm

B) Comparison of the detrital zircon from Mitakoodi Quartzite with Mount Isa Inlier igneous grains and every all igneous zircon grains in the NAC.

Using methods to address the differences in uncertainties outlined in Nordsvan et al. (Chapter 2), all detrital zircon samples from this study and previous studies from the Mount Isa Inlier were compared using MDS with the both the K-S and Kuiper statistically tests (Carson et al., 2008; Magee et al., 2012; Neumann et al., 2009a; Neumann et al., 2009b; Neumann et al., 2006). With the K-S test, the Mitakoodi Quartzite samples plot separately, but not surprisingly close to previously obtained samples from the Mitakoodi Quartzite and the Mount Star Member (Figure 4.17A) (Neumann, 2016a, 2016b). Similar results are observed in the Kuiper based MDS plot (Figure 4.17B). The samples from the Mary Kathleen Group plot in the centre, the most data-dense area of the MDS plots in proximity to sediments thought to be both correlative, older (Lena Quartzite) and younger (Surprise Creek Formation). Perhaps the most intriguing feature of the MDS plots is the proximity of the Mitakoodi Quartzite Samples with the Wire Creek Sandstone (Figure 4.17).

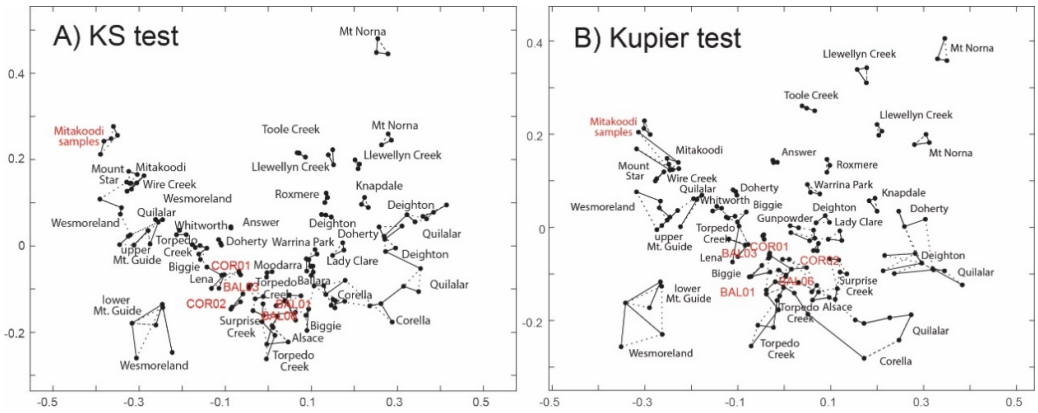

Figure 4.17: MDS analysis, following methods of Nordsvan et al. (Chapter 2) comparing all detrital zircon samples from the Mount Isa Inlier (Carson et al., 2008; Magee et al., 2012; Neumann et al., 2009a; Neumann et al., 2009b; Neumann et al., 2006). Lines denote most similar samples; dashed lines denote seconded closest.

The Wire Creek Sandstone is the basal unit from Camooweal-Murphy Domain, the most northernly domain in the Mount Isa Inlier (Figure 4.1) (Withnall and Hutton, 2013). The Wire Creek Sandstone was deposited ca. 1.8 Ga and consists of immature fluvial sandstones that unconformably overlie Murphy Inlier (NW of Mount Isa) basement rocks. The Wire Creek Sandstone is thought to be correlative with the Westmoreland Conglomerate also of the Camooweal-Murphy Domain, which based on sedimentological data was likely sourced from the northeast (Wygralak et al., 1988). Detrital zircon spectrum from the Westmoreland Conglomerate (Magee et al., 2012) and the Wire Creek Sandstone (Hollis et al., 2010) show overlapping populations with the Mitakoodi Quartzite (Figure 4.18A). However, comparing all the data from the Mitakoodi Quartzite (including the Mount Star Member) with the northern samples (Westmoreland Conglomerate and the Wire creek Sandstone) illustrates there are substantial differences (Figure 4.18B and 4.18C). This highlights that samples plotting close to each other in MDS does not mean they are similar, just most similar to the samples being compared. Hence, while the Wire Creek Sandstone has the most similar detrital zircon populations to the Mitakoodi Quartzite samples, it is notably different, most importantly, it lacks the ca. 2580 Ma population.

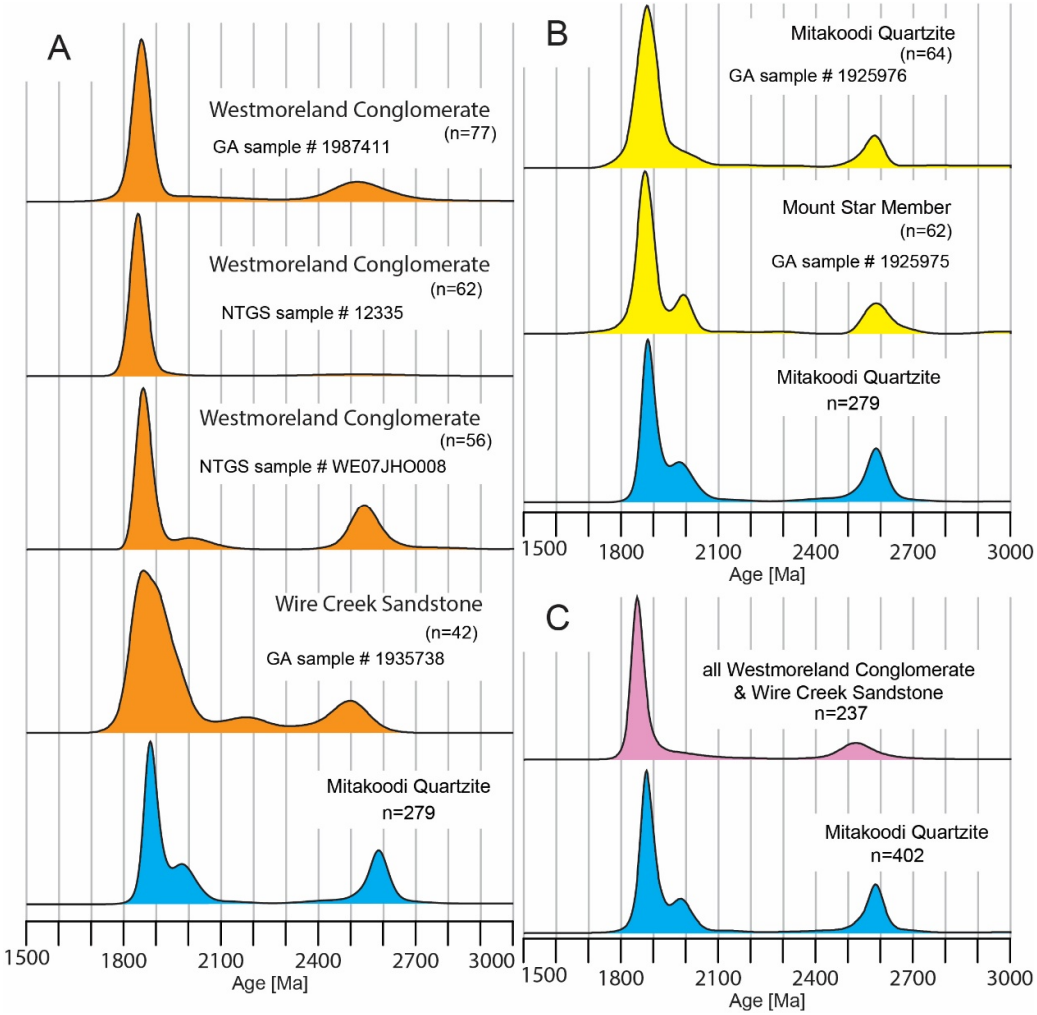

Figure 4.18: A) Comparison of the Mitakoodi Quartzite detrital zircon samples with the Westmoreland Conglomerate and the Wire Creek Sandstone from the Camooweal-Murphy Domain. All data is less <5% discordant. B) Comparison of the Mitakoodi Quartzite detrital zircon samples with previously obtained Malbon Group samples (shown in yellow) (Neumann, 2016a, b). C) All Malbon Group samples compared with all samples from the Westmoreland Conglomerate and the Wire Creek Sandstone.

The detrital zircon data from the Mitakoodi Quartzite is unique from all other detrital zircon samples elsewhere in the Mount Isa Inlier (Figure 4.17); however, the prominent population, ca. 1880 Ma is not so uncommon and overlaps with populations observed in the Mary Kathleen Group samples. The ε_{Hf} values for this population in the Mitakoodi Quartzite samples range from -24.38 to 4.82, but most grains have ε_{Hf} values around -3 (Figure 4.15 and 4.19A). Similarly aged zircon grains

in the Mary Kathleen Group samples have ε_{Hf} values overlapping with the most data-dense area of Mitakoodi Quartzite samples (Figure 4.19B, 4.19C and 4.19D), suggesting that the ca. 1.89 Ga population observed in the Mitakoodi Quartzite could have come from the same source for all the samples. Nevertheless, while there are similarities between the Mitakoodi Quartzite and the Mary Kathleen Group within this population, there are also variations within this population and the other populations (Figure 4.14, 4.15 and 4.19). The Mitakoodi Quartzite has a larger spread of ε_{Hf} values for the ca. 1890 Ma population when compared with the Mary Kathleen Group samples (Figure 4.19). Furthermore, the Mitakoodi Quartzite samples have more negative values for the ca. 1990 Ma population (Figure 4.14 and 4.15). Therefore, while there are overlaps in the ε_{Hf} values between the Mitakoodi Quartzite and Mary Kathleen Group samples, overall the data suggests they were likely sourced from different terranes.

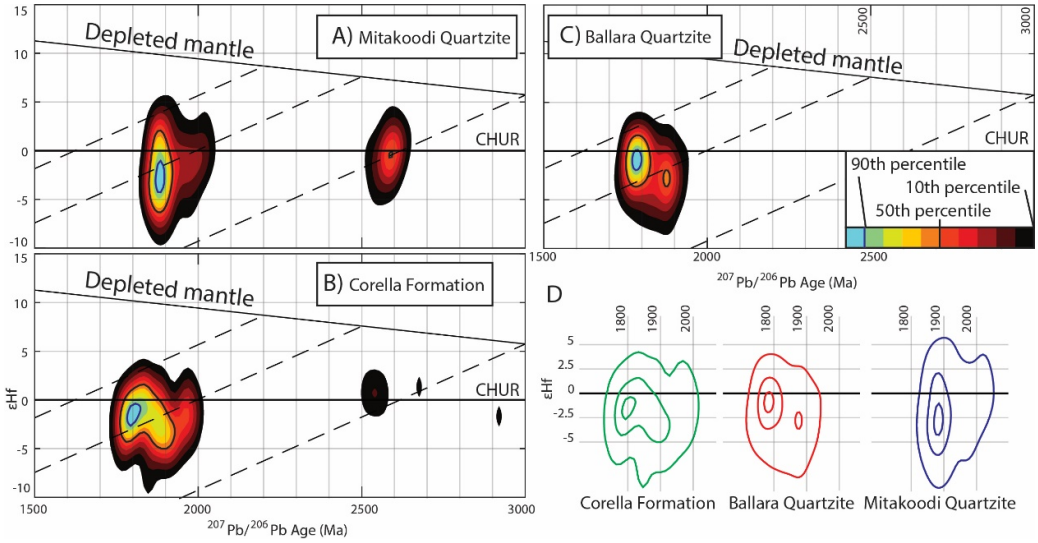

Figure 4.19: Two dimensional KDE plots show the ε_{Hf} data density from the samples analysed in this study. A) Mitakoodi Quartzite data. B) Corella Formation data. C) Ballara Quartzite data. D) 90th, 50th and 10th percentile lines between 1700–2100 Ma for comparison between the three samples.

While the detrital zircon in the Mary Kathleen Group was probably sourced locally from the Mount Isa Inlier (Figure 4.16), to further evaluate this proposal, and test the source region for the Mitakoodi Quartzite, the grouped samples from this study were statistically compared with potential source regions in the NAC using MDS (Figure 4.20). Following the methods outlined in Nordsvan et al. (Chapter 2), to account for the depositional age, source area data were limited to analyses, within uncertainty, older than 1750 Ma. From both MDS plots, the K-S and Kuiper tests indicate that detrital zircon from the Ballara Quartzite is statistically most likely sourced from the Mount Isa Inlier (Figure 4.20). In the Kuiper MDS plot, the Corella Formation is most likely sourced from the Mount Isa Inlier, whereas in the K-S-MDS plot, it is most similar to the Halls Creek Orogen in northern Western Australia. The Halls Creek Orogen as a source region for detrital zircon in the Mount Isa Inlier during this period is not impossible but would imply, they are far-travelled and have bypassed the

McArthur Basin, to the west, which was likely sourced from the Arnhem Province to the north throughout this period.

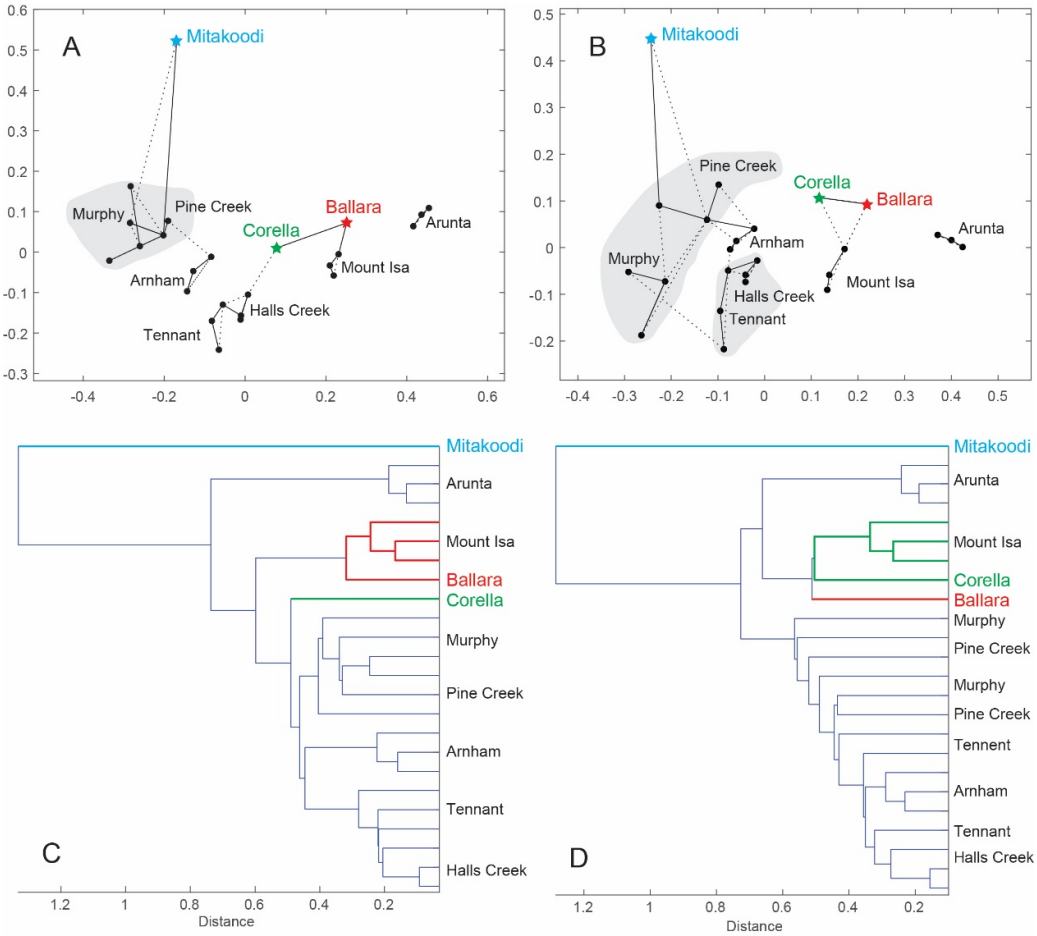

Figure 4.20: A) MDS plot using the K-S test following the methods outlined in Nordsvan et al. (Chapter 2). B) Kuiper based MDS plot. C) Dendrogram of the K-S distances highlights the significant difference in the Mitakoodi Quartzite samples. D) Similar to C, the dendrogram of Kuiper distances have the same results. All source region data is from http://www.ga.gov.au/geochron-sapub-web/geochronology/shrimp/search.htm Only ages within uncertainty >1750 Ma were used for the analysis.

A NAC provenance for the Mitakoodi Quartzite is unlikely (Figure 4.20). Statistically, the Mitakoodi Quartzite samples are the most dissimilar with all other detrital zircon samples from the Mount Isa Inlier (Figure 4.17). Likewise, when statistically

compared with the source regions from the NAC, the Mitakoodi Quartzite detrital zircon samples are the most dissimilar, suggesting an exotic source region (Figure 4.20). While the ca. 1850 to 1900 Ma population could have been sourced from several NAC terranes, ca. 1900 to 2100 Ma source terranes are rare in the NAC, and the ca. 2580 Ma population is completely absent from any potential NAC source terranes. Furthermore, a review of 25 detrital zircon samples from the McArthur Basin, with a total of 1855 individual grain analysis, have less than 2% of grain ages between 2550 and 2650 Ma (Beyer et al., 2012; Kositcin et al., 2017; Kositcin et al., 2015; Munson et al., 2018). Similarly, from the Mount Isa Inlier retracting the Mitakoodi Quartzite samples, a total of 3127 zircon grains have less than 2% of ages between 2550 and 2650 Ma (Carson et al., 2008; Magee et al., 2012; Neumann et al., 2009a; Neumann et al., 2009b; Neumann et al., 2006). From the entire NAC, only sedimentary rocks from the Pine Creek Orogen (Cahill Formation (Hollis et al., 2010, 2014)) and the Georgetown Inlier (lower Etheridge Group (Neumann and Kositcin, 2011)) have more than 5% of zircon grains aged between 2550 and 2650 Ma. The Cahill Formation of the Pine Creek Orogen was deposited in an allochthonous setting between ca. 1.85 and 1.87 Ga and subsequently affected by convergent tectonism ca. 1.85 Ga (Hollis et al., 2014). The Cahill Formation possibly would have been uplifted by ca. 1.83 Ga during the Pine Creek Orogen and thus, the ca. 2.58 Ga zircon population seen in the Malbon Group could have been sourced from this uplifted terrane. However, this is highly unlikely given how for the zircon would have to travel and how many more proximal basins they would have to bypass (i.e. the McArthur Basin). From the Malbon Group samples, 17% of detrital zircon grains have ages

between 2550 and 2650 Ma. Furthermore, the Malbon Group detrital zircon from a coherent population centred on ca. 2580 Ma, whereas those from the McArthur Basin and the other samples from the Mount Isa Inlier do not. This ca. 2580 Ma population observed in the Malbon Group cannot be reconciled with any known source terrane in the NAC, or elsewhere in Australia (Neumann and Fraser, 2007). These source rocks might be undercover; however, considering the absence of these detrital zircon ages from most other sedimentary rocks in the NAC it seems more reasonable to consider an exotic source terrane.

The enigmatic ca. 2580 Ma detrital zircon population observed in the Mitakoodi Quartzite is common in many sedimentary rocks deposited around the same period in western Laurentia, including the Muskwa Assemblage, Wernecke Supergroup and Hornby Bay Group (Betts et al., 2008; Furlanetto et al., 2016; Hahn et al., 2013; Ross et al., 2001), and further to the east, the Athabasca and Thelon Basins (Rainbird et al., 2003; Rainbird and Davis, 2007; Rainbird et al., 2007). These Proterozoic Laurentian sediments were likely deposited in a single system, where deeper marine deposits are typically noted in the west and shallow marine to non-marine sediments in the east (Hahn et al., 2013). Furthermore, as with the ca. 2580 Ma population, most detrital zircon samples from Laurentia that have similar ca. 1800 to 2100 Ma zircon ages, and all the age populations observed in the Mitakoodi Quartzite detrital zircon samples can be accounted for from Laurentian source terranes (Davis et al., 2014; Davis et al., 2015; Eglington et al., 2013; Foster et al., 2006; Jackson et al., 2013; Ootes et al., 2015; Thériault et al., 2001). Although there are other zircon populations common in the Laurentian sediments absent in the Mitakoodi Quartzite, such as ca.

2300 or 2700 Ma, they are not always present in Laurentian sediments (Rainbird et al., 2007). It is plausible that the Mitakoodi Quartzite was sourced from Laurentia, but further evidence is required, such as correlating the Lu-Hf zircon data, which at present is relatively rare for the Laurentian basins of that age. Furthermore, many of the Laurentian basins that share a similar detrital zircon provenance are from central or eastern parts of the continent rather than the western margin as required.

4.7.3 Tectonic implications

Recent tectonic models favour a dominantly east-west extensional model to explain the Paleoproterozoic tectonic evolution in the Mount Isa Inlier (Gibson et al., 2018; Gibson et al., 2017). Indeed, the earliest manifestation of post-Barramundi Orogen (ca. 1.85 Ga) rifting at ca. 1.79 Ga was directed east-west (Eriksson et al., 1993; Jackson et al., 2000; O'Dea et al., 1997a), however, subsequent to that event there is substantial evidence indicating that north-south directed extension played a critical role in the evolution of the Mount Isa Inlier, particularly during the emplacement of the Wonga Batholith (Gibson et al., 2008; Holcombe et al., 1992; O'Dea et al., 1997a; O'Dea et al., 1997b; Oliver et al., 1991; Pearson et al., 1992).

Giles et al. (2002) proposed a model where north-dipping subduction along the southern margin of the NAC produced back-arc basins in the Mount Isa Inlier continuous with the McArthur Basin to the west. Regardless of whether subsidence in the McArthur Basin was driven by lithospheric down-warping or subduction roll-back (Giles et al., 2002; Rawlings and Scott, 2002; Scott et al., 2000), the Redbank package of the McArthur Basin was deposited at a similar time to the Mary Kathleen

Group and likewise was associated with north-south extension (Rawlings and Scott, 2002; Scott et al., 2000). According to Betts et al. (2016) and Giles et al., (2002), north-south extension at ca. 1.78–1.74Ga occurred when the Gawler Craton rifted from the NAC due to the retreat of the north-dipping subduction zone. It is proposed that this roll-back event is associated with the N-S extension reported in this study. In contrast to the western and central belt, the ca. 1.76 Ga rift-related Marraba and Bulonga volcanics in the eastern belt preserve no direct evidence of N-S extension, further suggesting that the eastern Mount Isa Inlier might be an allochthonous terrane.

If Australia and Laurentia were proximal at ca. 1.85 Ga, as many have suggested (Betts et al., 2006; Betts et al., 2016; Betts et al., 2008; Gibson et al., 2008; Gibson et al., 2012; Hoffman, 1997; Hoffman, 1991; O'Dea et al., 1997b; Payne et al., 2009), than to account for numerous geological observations from both Laurentia and Australia, they must have separated and re-amalgamated between ca. 1.8 to 1.6 Ga (Betts et al., 2016; Furlanetto et al., 2013; Furlanetto et al., 2016; Gibson et al., 2018; Gibson et al., 2017; Medig et al., 2014; Nordsvan et al., 2018; Payne et al., 2009; Pourteau et al., 2018; Thorkelson and Laughton, 2015; Verbaas et al., 2018). To account for the lack of evidence for N-S directed extension in the eastern belt, the separation would have to occur during the first major east-west extensional event at ca. 1.79 Ga (Jackson and Southgate, 2000; O'Dea et al., 1997a). Alternatively, Laurentia and Australia were apart at ca. 1.85 Ga, and the Barramundi Orogen does not correlate with orogenesis in Laurentia, in this case, the eastern belt of the Mount Isa Inlier would be considered an allochthonous terrane, perhaps sourced from Laurentia and accreted to the NAC post-1.75 Ga.

Following the north-south extensional events in the western and central belts of the Mount Isa Inlier, ca. 1.73 to 1.74 Ga large scale east-west directed shortening inverted the Leichhardt Superbasin sediments (Blaikie et al., 2017). Blaikie et al. (2017) correlated this event with the mid-Tawallah inversion in the McArthur Basin (Bull and Rogers, 1996), the Kimban Orogeny in the Gawler Craton (Hand et al., 2007), and the Late Strangways Orogeny in the Arunta Inlier (Collins and Shaw, 1995). This indicates that the entire eastern part of the NAC, and the SAC (Gawler craton), were subjected to a continental-scale event which was associated with E-W compression in the Mount Isa Inlier and E-W directed extension further to the south. Succeeding the ca. 1.74 Ga basin inversion in the Mount Isa Inlier, broadly east-west directed extension accommodates deposition of the Calvert Superbasin which has been correlated across the entire Mount Isa Inlier (Neumann et al., 2006; Betts et al., 2016). If the Calvert Superbasin is truly correlative across the entire Mount Isa Inlier than the ca. 1.73 Ga E-W directed shortening event is likely related to a collision between the eastern Mount Isa Inlier and the NAC.

4.8 Conclusions

Sedimentary rocks in the western Mary Kathleen Group are characterised by basal non-marine facies that deepen to the north deposited during a period of broadly north-south directed extension. Higher frequency LST parasequences in the south correspond to a thicker TST in the north and more facies associated with sediment starvation. This suggests that in rifted settings correlating system tract bounding surfaces along depositional dip might be problematic, as proximal locations will be deposited during the LST, whereas in distal sections, the TST.

The detrital zircon provenance data along with a review of previous geochronology suggest that the Mary Kathleen Group could be older than previously reported and probably correlates with the Myally Supersequence of the western belt rather than the Quilalar Supersequence. Thus, the Myally Supersequence north-south extensional event is likely correlative with the north-south extension reported from the Mary Kathleen domain associated with emplacement of the Wonga Batholith. The sedimentological data from the Malbon Group indicates that it is not correlative with the Mary Kathleen Group, but more data would be required to fully understand the evolution of the basin. Detrital zircon from Mary Kathleen Group is likely sourced locally from the Mount Isa Inlier and other NAC terranes, whereas the detrital zircon from the Malbon Group was not likely sourced from Australia but rather Laurentia. If this is substantiated, then it suggests that the eastern belt of the Mount Isa Inlier is an exotic terrane. Large scale E-W directed compression at ca. 1.74 Ga recognised in the eastern Mount Isa Inlier might be related to the juxtaposition of the eastern belt of the Mount Isa Inlier with the NAC.

4.9 References

Bain, J. H. C., Heinrich, C. A., and Henderson, G. A. M., 1992, Stratigraphy, structure, and metasomatism of the Haslingden Group, east Moondarra area, Mount Isa: a deformed and mineralised Proterozoic multistage rift-sag sequence, *in* Stewart, A. J., and Blake, D. H., eds., Detailed Studies of the Mount Isa Inlier, Volume 243: Canberra, Australia, AGSO Bulletin, p. 125-136.

Beardsmore, T. J., Newbery, S. P., and Laing, W. P., 1988, The Maronan Supergroup: an inferred early volcanosedimentary rift sequence in the Mount Isa Inlier, and its implications for ensialic rifting in the Middle Proterozoic of northwest Queensland: Precambrian Research, v. 40, p. 487-507.

Bennett, V. C., and DePaolo, D. J., 1987, Proterozoic crustal history of the western United States as determined by neodymium isotopic mapping: Geological Society of America Bulletin, v. 99, no. 5, p. 674-685.

Betts, P. G., Armit, R. J., Stewart, J., Aitken, A. R. A., Ailleres, L., Donchak, P., Hutton, L., Withnall, I. W., and Giles, D., 2016, Australia and Nuna: Geological Society, London, Special Publications, v. 424, p. SP424. 422.

Betts, P. G., Giles, D., Mark, G., Lister, G. S., Goleby, B. R., and Ailleres, L., 2006, Synthesis of the Proterozoic evolution of the Mt Isa Inlier: Australian Journal of Earth Sciences, v. 53, no. 1, p. 187-211.

Betts, P. G., Giles, D., and Schaefer, B. F., 2008, Comparing 1800–1600Ma accretionary and basin processes in Australia and Laurentia: possible geographic connections in Columbia: Precambrian Research, v. 166, no. 1, p. 81-92.

Beyer, E. E., Hollis, J. A., Whelan, J. A., Glass, L. M., Donnellan, N., Yaxley, G., Armstrong, R., Allen, C., and Scherstén, A., 2012, Summary of results. NTGS laser ablation ICPMS and SHRIMP U-Pb, Hf and O geochronology project: Pine Creek Orogen, Arunta Region, Georgina Basin and McArthur Basin, July 2008–May 2011.

Bickford, M. E., and Hill, B. M., 2007, Does the arc accretion model adequately explain the Paleoproterozoic evolution of southern Laurentia?: An expanded interpretation: Geology, v. 35, no. 2, p. 167-170.

Bierlein, F. P., Maas, R., and Woodhead, J., 2011, Pre-1.8 Ga tectono-magmatic evolution of the Kalkadoon–Leichhardt Belt: implications for the crustal architecture and metallogeny of the Mount Isa Inlier, northwest Queensland, Australia: Australian Journal of Earth Sciences, v. 58, no. 8, p. 887-915.

Blaikie, T. N., Betts, P. G., Armit, R. J., and Ailleres, L., 2017, The ca. 1740–1710 Ma Leichhardt Event: Inversion of a continental rift and revision of the tectonic evolution of the North Australian Craton: Precambrian Research, v. 292, p. 75-92.

Blair, T. C., 1987, Tectonic and hydrologic controls on cyclic alluvial fan, fluvial, and lacustrine rift-basin sedimentation, Jurassic-Lowermost Cretaceous Todos Santos Formation, Chiapas, Mexico: Journal of Sedimentary Research, v. 57, no. 5, p. 845-862.

Blake, D. H., 1996, Structural interpretations of the Wonga Belt in the Proterozoic Mount Isa Inlier of northwest Queensland-A review: AGSO Journal of Australian Geology and Geophysics, v. 16, no. 4, p. 609.

Blake, D. H., and Stewart, A. J., 1992, Stratigraphic and tectonic framework, Mount Isa inlier, *in* Stewart, A. J., and Blake, D. H., eds., Detailed study of the Mount Isa Inlier, Volume 243: Canberra, Australia, AGSO Bulletin, p. 1-12.

Blichert-Toft, J., and Albarède, F., 1997, The Lu-Hf isotope geochemistry of chondrites and the evolution of the mantle-crust system: Earth and Planetary Science Letters, v. 148, no. 1-2, p. 243-258.

Borg, S. G., and DePaolo, D. J., 1994, Laurentia, Australia, and Antarctica as a Late Proterozoic supercontinent: constraints from isotopic mapping: Geology, v. 22, no. 4, p. 307-310.

Bouvier, A., Vervoort, J. D., and Patchett, P. J., 2008, The Lu–Hf and Sm–Nd isotopic composition of CHUR: constraints from unequilibrated chondrites and implications for the bulk composition of terrestrial planets: Earth and Planetary Science Letters, v. 273, no. 1-2, p. 48-57.

Bull, S. W., and Rogers, J. R., Recognition and significance of an early compressional deformation event in the Tawallah Group, McArthur Basin, NT, *in* Proceedings MIC'96: New developments in metallogenyic research1996, Volume 55, p. 28-32.

Carson, C. J., Hutton, L. J., Withnall, I. W., and Perkins, W. G., 2008, Joint GSQ-GA-NGA geochronology project Mount Isa region, 2007–2008: Geological Survey of Queensland.

Catuneanu, O., 2006, Principles of sequence stratigraphy, Amsterdam, The Netherlands, Elsevier Science, v. 1st, 386 p.:

Champion, D. C., 2013, Neodymium depleted mantle model age map of Australia: explanatory notes and user guide, Canberra, Australia, Geoscience Australia, Geoscience Australia Record: 2013/44.

Chorowicz, J., 2005, The east African rift system: Journal of African Earth Sciences, v. 43, no. 1-3, p. 379-410.

Collins, W. J., and Shaw, R. D., 1995, Geochronological constraints on orogenic events in the Arunta Inlier: a review: Precambrian Research, v. 71, no. 1-4, p. 315-346.

Davis, B. J., Berman, R. G., Nadeau, L., and Percival, J. A., 2014, U-Pb Zircon Geochronology of a Transect Across Thelon Tectonic Zone, Queen Maud Region, and Adjacent Rae Craton, Kitikmeot Region, Nunavut: Natural Resources Canada.

Davis, B. J., Pehrsson, S. J., and Percival, J. A., 2015, Results of a U-Pb zircon geochronology transect across the southern Rae craton, Northwest Territories, Canada: Geological Survey of Canada.

Day, R. W., 1983, Queensland Geology: A companion volume to the 1: 2,500,000 scale geological map (1975), Geological Survey of Queensland, v. 383.

Derrick, G. M., Wilson, I. H., and Hill, R. M., 1976, Revision of stratigraphic nomenclature in the Precambrian of northwestern Queensland, IV: Malbon Group: Queensl. Gov. Min. J., v. 77, p. 515-517.

Derrick, G. M., Wilson, I. H., and Sweet, I. P., 1980, The Quilalar and Surprise Creek Formations—new Proterozoic units from the Mount Isa inlier: Their regional sedimentology and application to regional correlation: BMR Journal of Australian Geology & Geophysics, v. 5, p. 215-223.

Domagala, J., Southgate, P. N., McConachie, B. A., and Pidgeon, B. A., 2000, Evolution of the Palaeoproterozoic Prize, Gun and lower Loretta Supersequences of the Surprise Creek Formation and Mt Isa Group: Australian Journal of Earth Sciences, v. 47, no. 3, p. 485-507.

Eglington, B. M., Pehrsson, S. J., Ansdell, K. M., Lescuyer, J.-L., Quirt, D., Milesi, J.-P., and Brown, P., 2013, A domain-based digital summary of the evolution of the

Palaeoproterozoic of North America and Greenland and associated unconformity-related uranium mineralization: Precambrian Research, v. 232, p. 4-26.

Eriksson, K. A., Simpson, E. L., and Jackson, M. J., 1994, Stratigraphical Evolution of a Proterozoic Syn-Rift to Post-Rift Basin: Constraints on the Nature of Lithospheric Extension in the Mount Isa Inlier, Australia, *in* A, F. K., and J, S. R., eds., Tectonic controls and signatures in sedimentary successions: London, UK, The International Associtation of Sedimentologists, p. 203-221.

Etheridge, M. A., Rutland, R. W. R., and Wyborn, L. A. I., 1987, Orogenesis and tectonic process in the Early to Middle Proterozoic of northern Australia: Proterozic Lithospheric Evolution, p. 131-147.

Foster, D. A., Mueller, P. A., Mogk, D. W., Wooden, J. L., and Vogl, J. J., 2006, Proterozoic evolution of the western margin of the Wyoming craton: Implications for the tectonic and magmatic evolution of the northern Rocky Mountains: Canadian Journal of Earth Sciences, v. 43, no. 10, p. 1601-1619.

Foster, D. R. W., and Austin, J. R., 2008, The 1800–1610 Ma stratigraphic and magmatic history of the Eastern Succession, Mount Isa Inlier, and correlations with adjacent Paleoproterozoic terranes: Precambrian Research, v. 163, no. 1-2, p. 7-30.

Furlanetto, F., Thorkelson, D. J., Gibson, H. D., Marshall, D. D., Rainbird, R. H., Davis, W. J., Crowley, J. L., and Vervoort, J. D., 2013, Late Paleoproterozoic terrane accretion in northwestern Canada and the case for circum-Columbian orogenesis: Precambrian Research, v. 224, p. 512-528.

Furlanetto, F., Thorkelson, D. J., Rainbird, R. H., Davis, W. J., Gibson, H. D., and Marshall, D. D., 2016, The Paleoproterozoic Wernecke Supergroup of Yukon, Canada: Relationships to orogeny in northwestern Laurentia and basins in North America, East Australia, and China: Gondwana Research, v. 39, p. 14-40.

Gibson, G. M., Champion, D. C., Withnall, I. W., Neumann, N. L., and Hutton, L. J., 2018, Assembly and breakup of the Nuna supercontinent: Geodynamic

constraints from 1800 to 1600 Ma sedimentary basins and basaltic magmatism in northern Australia: Precambrian Research, v. 313, p. 148-169.

Gibson, G. M., Henson, P. A., Neumann, N. L., Southgate, P. N., and Hutton, L. J., 2012, Paleoproterozoic-earliest Mesoproterozoic basin evolution in the Mount Isa region, northern Australia and implications for reconstructions of the Nuna and Rodinia supercontinents: Episodes, v. 35, no. 1, p. 131-141.

Gibson, G. M., Hutton, L. J., and Holzschuh, J., 2017, Basin inversion and supercontinent assembly as drivers of sediment-hosted Pb–Zn mineralization in the Mount Isa region, northern Australia: Journal of the Geological Society, p. jgs2016-2105.

Gibson, G. M., Rubenach, M. J., Neumann, N. L., Southgate, P. N., and Hutton, L. J., 2008, Syn-and post-extensional tectonic activity in the Palaeoproterozoic sequences of Broken Hill and Mount Isa and its bearing on reconstructions of Rodinia: Precambrian Research, v. 166, no. 1-4, p. 350-369.

Giles, D., Betts, P. G., and Lister, G. S., 2002, Far-field continental backarc setting for the 1.80–1.67 Ga basins of northeastern Australia: Geology, v. 30, no. 9, p. 823-826.

Hahn, K., Rainbird, R., and Cousens, B., 2013, Sequence stratigraphy, provenance, C and O isotopic composition, and correlation of the late Paleoproterozoic–early Mesoproterozoic upper Hornby Bay and lower Dismal Lakes groups, NWT and Nunavut: Precambrian Research, v. 232, p. 209-225.

Hampson, G. J., and Storms, J. E. A., 2003, Geomorphological and sequence stratigraphic variability in wave-dominated, shoreface-shelf parasequences: Sedimentology, v. 50, no. 4, p. 667-701.

Hand, M., Reid, A., and Jagodzinski, L., 2007, Tectonic framework and evolution of the Gawler Craton, Southern Australia: Economic Geology, v. 102, no. 8, p. 1377-1395.

Helland-Hansen, W., and Hampson, G. J., 2009, Trajectory analysis: concepts and applications: Basin Research, v. 21, no. 5, p. 454-483.

Helland-Hansen, W., and Martinsen, O. J., 1996, Shoreline trajectories and sequences: description of variable depositional-dip scenarios: Journal of Sedimentary Research, v. 66, no. 4.

Hoffman, P. F., 1991, Did the breakout of Laurentia turn Gondwanaland inside-out: Science, v. 252, no. 5011, p. 1409-1412.

Hoffman, P. F., 1997, Tectonic genealogy of North America, *in* Marshak, S., and Van der Pluijm, B. A., eds., Earth structure: An introduction to structural geology and tectonics.: New York, United States of America, McGraw-Hill, p. 459-464.

Holcombe, R. J., Pearson, P. J., and Oliver, N. H. S., 1992, Structure of the Mary Kathleen fold belt, *in* Stewart, A. J., and Blake, D. H., eds., Detailed Studies of the Mount Isa Inlier: Canberra, Australia, AGSO Bulletin, p. 257-287.

Hollis, J. A., Carson, C. J., Glass, L. M., Kositcin, N., Scherstén, A., Worden, K. E., Armstrong, R. A., Yaxley, G. M., and Kemp, A. I. S., 2014, Detrital zircon U–Pb–Hf and O isotope character of the Cahill Formation and Nourlangie Schist, Pine Creek Orogen: Implications for the tectonic correlation and evolution of the North Australian Craton: Precambrian Research, v. 246, p. 35-53.

Jackson, M. J., Scott, D. L., and Rawlings, D. J., 2000, Stratigraphic framework for the Leichhardt and Calvert Superbasins: review and correlations of the pre-1700 Ma successions between Mt Isa and McArthur River: Australian Journal of Earth Sciences, v. 47, no. 3, p. 381-403.

Jackson, M. J., Simpson, E. L., and Eriksson, K. A., 1990, Facies and sequence stratigraphic analysis in an intracratonic, thermal-relaxation basin: the Early Proterozoic, Lower Quilalar Formation and Ballara Quartzite, Mount Isa Inlier, Australia: Sedimentology, v. 37, no. 6, p. 1053-1078.

Jackson, M. J., and Southgate, P. N., 2000, Evolution of three unconformity-bounded sandy carbonate successions in the McArthur River region of northern Australia: The Lawn, Wide and Doom Supersequences in a proximal part of the Isa Superbasin: Australian Journal of Earth Sciences, v. 47, no. 3, p. 625-635.

Jackson, M. J., Southgate, P. N., Black, L. P., Blake, P. R., and Domagala, J., 2005, Overcoming Proterozoic quartzite sand-body miscorrelations: integrated sequence stratigraphy and SHRIMP U–Pb dating of the Surprise Creek Formation, Torpedo Creek and Warrina Park Quartzites, Mt Isa Inlier: Australian Journal of Earth Sciences, v. 52, no. 1, p. 1-25.

Jackson, S. E., Pearson, N. J., Griffin, W. L., and Belousova, E. A., 2004, The application of laser ablation-inductively coupled plasma-mass spectrometry to in situ U–Pb zircon geochronology: Chemical Geology, v. 211, no. 1, p. 47-69.

Jackson, V. A., van Breemen, O., Ootes, L., Bleeker, W., Bennett, V., Davis, W. J., Ketchum, J. W. F., and Smar, L., 2013, U–Pb zircon ages and field relationships of Archean basement and Proterozoic intrusions, south-central Wopmay Orogen, NWT: implications for tectonic assignments: Canadian Journal of Earth Sciences, v. 50, no. 10, p. 979-1006.

Jessup, M. J., Karlstrom, K. E., Connelly, J., Williams, M., Livaccari, R., Tyson, A., Rogers, S. A., and Keller, G., 2005, Complex Proterozoic crustal assembly of southwestern North America in an arcuate subduction system: The Black Canyon of the Gunnison, southwestern Colorado: Lithospheric structure and evolution of the Rocky Mountains: American Geophysical Union Geophysical Monograph, v. 154, p. 21-38.

Kinny, P. D., and Maas, R., 2003, Lu–Hf and Sm–Nd isotope systems in zircon: Reviews in mineralogy and geochemistry, v. 53, no. 1, p. 327-341.

Kositcin, N., Munson, T. J., and Whelan, J. A., 2017, Summary of results. Joint NTGS-GA geochronology project: greater McArthur Basin, July 2016-June 2017.

Kositcin, N., Whelan, J. A., and Edgoose, C. J., 2015, Summary of results. Joint NTGS-GA geochronology project: McArthur Basin, July 2014-June 2015: Northern Territory Geological Survey, 0724572988.

Lambeck, A., Barovich, K., Gibson, G., Huston, D., and Pisarevsky, S., 2012, An abrupt change in Nd isotopic composition in Australian basins at 1655Ma: Implications for the tectonic evolution of Australia and its place in NUNA: Precambrian Research, v. 208, p. 213-221.

Li, Z.-X., and Zhong, S., 2009, Supercontinent–superplume coupling, true polar wander and plume mobility: plate dominance in whole-mantle tectonics: Physics of the Earth and Planetary Interiors, v. 176, no. 3, p. 143-156.

Magee, C. W., Withnall, I. W., Hutton, L. J., Perkins, W. G., Donchak, P. J. T., Parson, A., Blake, P. R., Sweet, I. P., and Carson, C. J., 2012, Joint GSQ–GA geochronology project, Mount Isa Region, 2008–2009: Queensland Geological Record 2012/07.

Martins-Neto, M. A., and Catuneanu, O., 2010, Rift sequence stratigraphy: Marine and Petroleum Geology, v. 27, no. 1, p. 247-253.

McDonald, G. D., Collerson, K. D., and Kinny, P. D., 1997, Late Archean and early Proterozoic crustal evolution of the Mount Isa block, northwest Queensland, Australia: Geology, v. 25, no. 12, p. 1095-1098.

Medig, K. P. R., Thorkelson, D. J., Davis, W. J., Rainbird, R. H., Gibson, H. D., Turner, E. C., and Marshall, D. D., 2014, Pinning northeastern Australia to northwestern Laurentia in the Mesoproterozoic: Precambrian Research, v. 249, p. 88-99.

Munson, T. J., Thompson, J. M., Zhukova, I., Meffre, S., Beyer, E. E., Woodhead, J. D., and Whelan, J. A., 2018, Summary of results. NTGS laser ablation ICP-MS U-Pb and Lu-Hf geochronology project: Roper Group (McArthur Basin), overlying ungrouped units (Beetaloo Sub-basin), Renner Group (Tomkinson Province), and Tijunna Group (Birrindudu Basin), 1443-1149.

Murphy, J. B., and Nance, R. D., 2003, Do supercontinents introvert or extrovert?: Sm-Nd isotope evidence: Geology, v. 31, no. 10, p. 873-876.

Muto, T., and Steel, R. J., 2001, Autostepping during the transgressive growth of deltas: results from flume experiments: Geology, v. 29, no. 9, p. 771-774.

Nance, R. D., Worsley, T. R., and Moody, J. B., 1988, The supercontinent cycle: Scientific American, v. 259, no. 1, p. 72-79.

Neumann, N., 2016, GA Sample No - 1925975: Geoscience Australia Geochron Delivery System, Geoscience Australia.

-, 2016, GA Sample No - 1925976: Geoscience Australia Geochron Delivery System, Geoscience Australia.

Neumann, N. L., and Fraser, G. L., 2007, Geochronological synthesis and time-space plots for Proterozoic Australia, Canberra, Australia, Geoscience Australia.

Neumann, N. L., Gibson, G. M., and Southgate, P. N., 2009, New SHRIMP age constraints on the timing and duration of magmatism and sedimentation in the Mary Kathleen Fold Belt, Mt Isa Inlier, Australia: Australian Journal of Earth Sciences, v. 56, no. 7, p. 965-983.

Neumann, N. L., and Kositcin, N., 2011, New SHRIMP U-Pb zircon ages from north Queensland, 2007-2010: Geoscience Australia, 1921954450.

Neumann, N. L., Southgate, P. N., and Gibson, G. M., 2009, Defining unconformities in Proterozoic sedimentary basins using detrital geochronology and basin analysis—An example from the Mount Isa Inlier, Australia: Precambrian Research, v. 168, no. 3, p. 149-166.

Neumann, N. L., Southgate, P. N., Gibson, G. M., and McIntyre, A., 2006, New SHRIMP geochronology for the Western Fold Belt of the Mt Isa Inlier: developing a 1800–1650 Ma event framework∗: Australian Journal of Earth Sciences, v. 53, no. 6, p. 1023-1039.

Nielsen, A. B., Thorkelson, D. J., Gibson, H. D., and Marshall, D. D., 2013, The Wernecke igneous clasts in Yukon, Canada: fragments of the Paleoproterozoic volcanic arc terrane Bonnetia: Precambrian Research, v. 238, p. 78-92.

Nilsen, T. H., 1982, Alluvial fan deposits, *in* Scholle, P. A., and Spearing, D., eds., Sandstone Depostional Environments: Tulsa, United States of America, American Association of Petroleum Geologists, p. 49-86.

Nordsvan, A. R., Collins, W. J., Li, Z.-X., Spencer, C. J., Pourteau, A., Withnall, I. W., Betts, P. G., and Volante, S., 2018, Laurentian crust in northeast Australia: Implications for the assembly of the supercontinent Nuna: Geology, v. 46, no. 3, p. 251-254.

O'Dea, M. G., Lister, G. S., Betts, P. G., and Pound, K. S., 1997, A shortened intraplate rift system in the Proterozoic Mount Isa terrane, NW Queensland, Australia: Tectonics, v. 16, no. 3, p. 425-441.

O'Dea, M. G., Lister, G. S., MacCready, T., Betts, P. G., Oliver, N. H. S., Pound, K. S., Huang, W., and Valenta, R. K., 1997, Geodynamic evolution of the Proterozoic Mount Isa terrain: Geological Society, London, Special Publications, v. 121, no. 1, p. 99-122.

Oliver, N. H. S., Holcombe, R. J., Hill, E. J., and Pearson, P. J., 1991, Tectono-metamorphic evolution of the Mary Kathleen Fold Belt, northwest Queensland: a reflection of mantle plume processes?: Australian Journal of Earth Sciences, v. 38, no. 4, p. 425-455.

Ootes, L., Davis, W. J., Jackson, V. A., and van Breemen, O., 2015, Chronostratigraphy of the Hottah terrane and Great Bear magmatic zone of Wopmay Orogen, Canada, and exploration of a terrane translation model: Canadian Journal of Earth Sciences, v. 52, no. 12, p. 1062-1092.

Page, R. W., 1983, Timing of superposed volcanism in the Proterozoic Mount Isa inlier, Australia: Precambrian Research, v. 21, no. 3-4, p. 223-245.

Page, R. W., Jackson, M. J., and Krassay, A. A., 2000, Constraining sequence stratigraphy in north Australian basins: SHRIMP U–Pb zircon geochronology between Mt Isa and McArthur River: Australian Journal of Earth Sciences, v. 47, no. 3, p. 431-459.

Page, R. W., and Sun, S. S., 1998, Aspects of geochronology and crustal evolution in the Eastern Fold Belt, Mt Isa Inlier: Australian Journal of Earth Sciences, v. 45, no. 3, p. 343-361.

Page, R. W., Sun, S.-S., and MacCready, T. C., New Geochronological Results in the Central and Eastern Mount Isa Inlier & Implications for Mineral Exploration, *in* Proceedings Geodynamics and Ore Deposits Conference1997.

Paton, C., Hellstrom, J., Paul, B., Woodhead, J., and Hergt, J., 2011, Iolite: Freeware for the visualisation and processing of mass spectrometric data: Journal of Analytical Atomic Spectrometry, v. 26, no. 12, p. 2508-2518.

Payne, J. L., Hand, M., Barovich, K. M., Reid, A., and Evans, D. A. D., 2009, Correlations and reconstruction models for the 2500-1500 Ma evolution of the Mawson

Continent: Geological Society, London, Special Publications, v. 323, no. 1, p. 319-355.

Pearson, P. J., Holcombe, R. J., and Page, R. W., 1992, Synkinematic emplacement of the Middle Proterozoic Wonga batholith into a midcrustal extensional shear zone, Mount Isa Inlier, Queensland, Australia, *in* Stewart, A. J., and Blake, D. H., eds., Detailed Studies of the Mount Isa Inlier: Canberra, Australia, AGSO Bulletin, p. 289-328.

Petrus, J. A., and Kamber, B. S., 2012, VizualAge: A novel approach to laser ablation ICP-MS U-Pb geochronology data reduction: Geostandards and Geoanalytical Research, v. 36, no. 3, p. 247-270.

Posamentier, H. W., Jervey, M. T., and Vail, P. R., 1988, Eustatic controls on clastic deposition I—conceptual framework, *in* Wilgus, C. K., Hastings, B. S., Posamentier, H. W., Van Wagoner, J. C., Ross, C. A., and Kendall, C. G. S. C., eds., Sea-Level Changes: An Integrated Approach, Volume 42: Oklahoma, United States of America, Society of Economic Paleontologists and Mineralogists (SEPM), p. 110–124.

Potma, W. A., and Betts, P. G., 2006, Extension-related structures in the Mitakoodi Culmination: implications for the nature and timing of extension, and effect on later shortening in the eastern Mt Isa Inlier: Australian Journal of Earth Sciences, v. 53, no. 1, p. 55-67.

Pourteau, A., Smit, M. A., Li, Z.-X., Collins, W. J., Nordsvan, A. R., Volante, S., and Li, J., 2018, 1.6 Ga crustal thickening along the final Nuna suture: Geology, v. 46, no. 11, p. 959-962.

Rainbird, R. H., and Davis, W. J., 2007, U-Pb detrital zircon geochronology and provenance of the late Paleoproterozoic Dubawnt Supergroup: Linking sedimentation with tectonic reworking of the western Churchill Province, Canada: Geological Society of America Bulletin, v. 119, no. 3-4, p. 314-328.

Rainbird, R. H., Hadlari, T., Aspler, L. B., Donaldson, J. A., LeCheminant, A. N., and Peterson, T. D., 2003, Sequence stratigraphy and evolution of the Paleoproterozoic intracontinental Baker Lake and Thelon basins, western

Churchill Province, Nunavut, Canada: Precambrian Research, v. 125, no. 1-2, p. 21-53.

Rainbird, R. H., Stern, R. A., Rayner, N., and Jefferson, C. W., 2007, Age, provenance, and regional correlation of the Athabasca Group, Saskatchewan and Alberta, constrained by igneous and detrital zircon geochronology, *in* W, J. C., and G, D., eds., EXTECH IV - geology and uranium EXploration TECHnology of the Proterozoic Athabasca Basin, Saskatchewan and Alberta, Volume 588, Geological Survey of Canada Bulletin, p. 193–209.

Rawlings, D. J., and Scott, D., Geodynamics of the Redbank package, basal McArthur Basin, *in* Proceedings Annual geoscience exploration seminar (AGES),2002, Northern Territory Geological Survey.

Ross, G. M., Villeneuve, M. E., and Theriault, R. J., 2001, Isotopic provenance of the lower Muskwa assemblage (Mesoproterozoic, Rocky Mountains, British Columbia): New clues to correlation and source areas: Precambrian Research, v. 111, no. 1, p. 57-77.

Scherer, E., Münker, C., and Mezger, K., 2001, Calibration of the lutetium-hafnium clock: Science, v. 293, no. 5530, p. 683-687.

Scott, D. L., Rawlings, D. J., Page, R. W., Tarlowski, C. Z., Idnurm, M., Jackson, M. J., and Southgate, P. N., 2000, Basement framework and geodynamic evolution of the Palaeoproterozoic superbasins of north-central Australia: An integrated review of geochemical, geochronological and geophysical data: Australian Journal of Earth Sciences, v. 47, no. 3, p. 341-380.

Southgate, P. N., Neumann, N. L., and Gibson, G. M., 2013, Depositional systems in the Mt Isa Inlier from 1800 Ma to 1640 Ma: Implications for Zn–Pb–Ag mineralisation: Australian Journal of Earth Sciences, v. 60, no. 2, p. 157-173.

Stern, R. A., Bodorkos, S., Kamo, S. L., Hickman, A. H., and Corfu, F., 2009, Measurement of SIMS instrumental mass fractionation of Pb isotopes during zircon dating: Geostandards and Geoanalytical Research, v. 33, no. 2, p. 145-168.

Stewart, A. J., 1992, Stratigraphy, extension, and contraction in the Ballara-Mount Frosty area, Mount Isa Inlier, Queensland, *in* Stewart, A. J., and Blake, D. H., eds., Detailed Studies in the Mount Isa Inlier, Volume 243: Canberra, Australia, AGSO Bulletin, p. 209-228.

Tapani Rämö, O., and Calzia, J. P., 1998, Nd isotopic composition of cratonic rocks in the southern Death Valley region: Evidence for a substantial Archean source component in Mojavia: Geology, v. 26, no. 10, p. 891-894.

Thériault, R. J., St-Onge, M. R., and Scott, D. J., 2001, Nd isotopic and geochemical signature of the Paleoproterozoic Trans-Hudson Orogen, southern Baffin Island, Canada: implications for the evolution of eastern Laurentia: Precambrian Research, v. 108, no. 1-2, p. 113-138.

Thorkelson, D. J., and Laughton, J. R., 2015, Paleoproterozoic closure of an Australia–Laurentia seaway revealed by megaclasts of an obducted volcanic arc in Yukon, Canada: Gondwana Research, v. 33, p. 115-133.

Van Wagoner, J. C., Posamentier, H. W., Mitchum, R. M. J., Vail, P. R., Sarg, J. F., Loutit, T. S., and Hardenbol, J., 1988, An overview of the fundamentals of sequence stratigraphy and key definitions.

Verbaas, J., Thorkelson, D. J., Crowley, J., Davis, W. J., Foster, D. A., Gibson, H. D., Marshall, D. D., and Milidragovic, D., 2018, A sedimentary overlap assemblage links Australia to northwestern Laurentia at 1.6 Ga: Precambrian Research, v. 305, p. 19-39.

Vermeesch, P., 2012, On the visualisation of detrital age distributions: Chemical Geology, v. 312, p. 190-194.

-, 2013, Multi-sample comparison of detrital age distributions: Chemical Geology, v. 341, p. 140-146.

-, 2018, Dissimilarity measures in detrital geochronology: Earth-Science Reviews, v. 178, p. 310-321.

-, 2018, IsoplotR: A free and open toolbox for geochronology: Geoscience Frontiers, v. 9, no. 5, p. 1479-1493.

Vervoort, J. D., and Blichert-Toft, J., 1999, Evolution of the depleted mantle: Hf isotope evidence from juvenile rocks through time: Geochimica et Cosmochimica Acta, v. 63, no. 3-4, p. 533-556.

Whitmeyer, S. J., and Karlstrom, K. E., 2007, Tectonic model for the Proterozoic growth of North America: Geosphere, v. 3, no. 4, p. 220-259.

Wiedenbeck, M., Alle, P., Corfu, F., Griffin, W. L., Meier, M., Oberli, F. v., Quadt, A. v., Roddick, J. C., and Spiegel, W., 1995, Three natural zircon standards for U-Th-Pb, Lu-Hf, trace element and REE analyses: Geostandards newsletter, v. 19, no. 1, p. 1-23.

Williams, P. R., 1989, Nature and timing of early extensional structures in the Mitakoodi Quartzite, Mount Isa Inlier, northwest Queensland: Australian Journal of Earth Sciences, v. 36, no. 2, p. 283-296.

Wilson, I. H., Derrick, G. M., and Perkin, D. J., 1984, Eastern Creek Volcanics-their geochemistry and possible role in copper mineralization at Mount Isa, Queensland: BMR Journal of Australian Geology & Geophysics, v. 9, no. 4, p. 317-328.

Withnall, I. W., and Hutton, L. J., 2013, Proterozoic–North Australian Craton, *in* Jell, P. A., ed., Geology of Queensland: Brisbane, Australia, Geological Survey of Queensland, p. 23-112.

Wygralak, A. S., Ahmad, M., and Hallenstein, C. P., 1988, Sedimentology of the Westmoreland Conglomerate, southern McArthur Basin, Northern Territory, Australia: Journal of the Geological Society of Australia, v. 35, no. 2, p. 195-207.

Zecchin, M., and Catuneanu, O., 2013, High-resolution sequence stratigraphy of clastic shelves I: units and bounding surfaces: Marine and Petroleum Geology, v. 39, no. 1, p. 1-25.

Zhao, G., Cawood, P. A., Wilde, S. A., and Sun, M., 2002, Review of global 2.1–1.8 Ga orogens: implications for a pre-Rodinia supercontinent: Earth-Science Reviews, v. 59, no. 1, p. 125-162.

Chapter 5: New U-Pb ages and Lu-Hf isotope data from Mesoproterozoic granites in NE Australia

To be submitted to Precambrian Research.

Adam R. Nordsvan[1], Erin Martin[1], Silvia Volante[1], William J. Collins[1], Simon Beams[2], Amaury Pourteau[1], Jiangyu Li[1], Ian W. Withnall[3], and Zheng-Xiang Li[1]

[1]Earth Dynamics Research Group, ARC Centre of Excellence for Core to Crust Fluid Systems (CCFS) and The Institute for Geoscience Research (TIGeR), School of Earth and Planetary Sciences, Curtin University, GPO Box U1987, WA 6845, Australia

[2]Terra Search Pty Ltd, PO Box 981, Castletown, Hyde Park, QLD 4812, Australia

[3]Geological Survey of Queensland, Department of Natural Resources and Mines, PO Box 15216, City East, QLD 4002, Australia

5.1 Abstract

New crystallisation ages obtained from Mesoproterozoic granites in the Georgetown Inlier, NE Australia, indicate that magmatism following the amalgamation of the supercontinent Nuna occurred simultaneously across the inlier at ca. 1.56 Ga. Approximately 100 km west of the Georgetown Inlier, two newly identified Proterozoic granites were sampled by drill core from below thick Cenozoic and Mesozoic cover sequences. The granites termed the “Cudgee Creek Granites”, have a crystallisation age of ca. 1.54 Ga, roughly 10–20 Myr younger than the Georgetown Inlier granites and are similar in age and composition to some granites in the eastern belt of the Mount Isa Inlier. Within the Georgetown Inlier, zircon Lu-Hf isotopes from

the granites differ between the Esmeralda Batholith in the west and the Forsayth Granite to the east. Whereas, the Lu-Hf values from the Cudgee Creek granites are similar to those from the Esmeralda Batholith. The east to west variation in Lu-Hf composition from the granites in this study either reflects a variation in the basement across the region, an increasing degree of a juvenile crustal (or mantle) component westward, or a combination of both.

5.2 Introduction

In NE Australia Proterozoic rocks can be identified in five main inliers (Mount Isa, Georgetown, Dargalong, Yambo and Coen) but the geological relationship between them remains speculative. This ambiguity is due to lack of exposure, with the region between the Mount Isa and Georgetown inliers covered by Mesozoic and Cenozoic sedimentary rocks (Figure 5.1). Although geophysical images have revealed several structural discontinuities and possible exotic terranes (Betts et al., 2016; Korsch et al., 2012), the relationship between the eastern inliers and the Mount Isa Inlier (North Australian Craton (NAC)) is still enigmatic (Boger and Hansen, 2004; Cihan et al., 2006; Withnall et al., 1988).

The eastern Proterozoic inliers (Georgetown, Dargalong, Yambo and Coen) are thought to be continental ribbons, accreted to the NAC by either ca. 1.75 Ga (Betts et al., 2016; Gibson et al., 2018; Korsch et al., 2012), or ca. 1.6 Ga (Boger and Hansen, 2004; Nordsvan et al., 2018; Pourteau et al., 2018). While central to the debate, the origin and tectonic evolution of the Georgetown inlier has always been uncertain. Withnall et al. (1988) first questioned the relationship of the Georgetown Inlier with

tectonic models put forward for the NAC (Etheridge et al., 1987), noting that the Georgetown Inlier differed in stratigraphy, deformation, and the tectonic evolution. Based on thermodynamic modelling, Boger and Hansen (2004) suggested that the inlier had a different metamorphic evolution compared with other NAC terranes until the Isan Orogeny at ca. 1.6 Ga. With newer age constraints, both Black et al. (2005) and Cihan et al. (2006) suggested that the metamorphic history of the Mount Isa and Georgetown inliers was broadly correlative between ca. 1.65 to 1.5 Ga and argued they were part of a single orogenic system during that period. A deep seismic profile from the Mount Isa Inlier to the Georgetown Inlier, was interpreted by Korsch et al. (2012) as showing potential exotic terranes: the Numil Province, interpreted to have been accreted to the NAC at ca. 1.85 Ga; and the Abingdon Province, interpreted to have initially rifted from the NAC at ca. 1.8 Ga due to roll back of west-dipping subduction and re-accreted at ca. 1.7 Ga. However, recent work by Nordsvan et al. (2018) strongly suggests that the oldest sediments in the Georgetown Inlier were sourced from Laurentia, and Pourteau et al. (2018) used garnet geochronology and thermodynamic modelling to document contrasting, albeit simultaneous, metamorphic evolution between the eastern Mount Isa and Georgetown inliers at ca. 1.6 Ga, corresponding to an upper and lower plate, respectively. Thus, both papers argued the Georgetown Inlier was a part of Laurentia, which accreted to the NAC during the Isan Orogeny at ca. 1.6 Ga (Nordsvan et al., 2018; Pourteau et al., 2018). Alternatively, Gibson et al. (2018) presented geochemical data from mafic rocks in the Mount Isa Inlier to argue that the sediments deposited in the Georgetown Inlier (Etheridge Group) were the distal equivalent (turbidites) of the

more proximal sedimentary facies reported in the Mount Isa Inlier. However, no sedimentological evidence has been presented to support this, and in contrast, any work that has been done indicates they were deposited in more shallow marine environments.

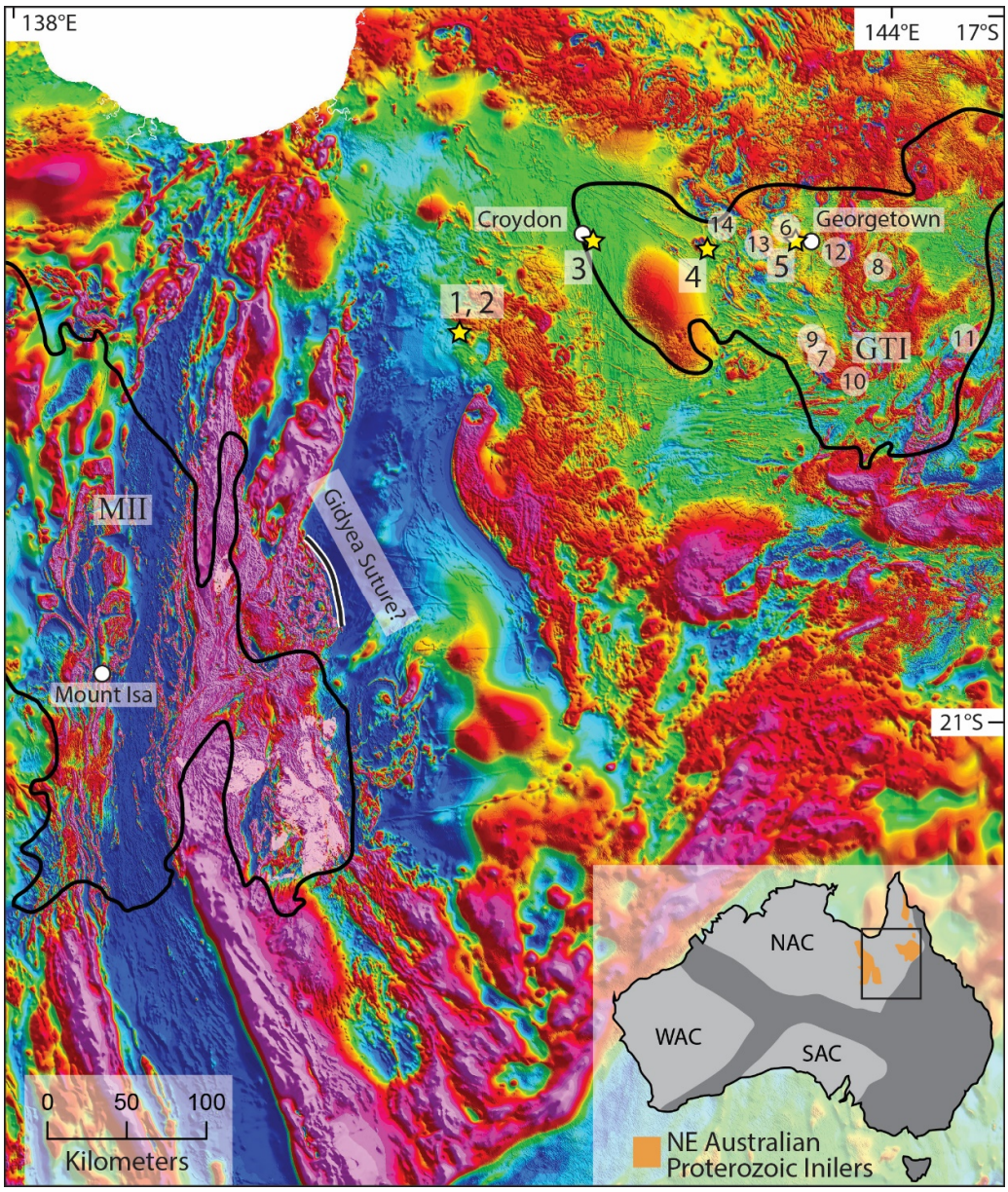

Figure 5.1: Aeromagnetic image of total magnetic intensity for northeast Australia (modified from Withnall and Hutton, 2013). Black lines outline the outcrop extent of the Mount Isa (MII) and Georgetown (GTI) inliers. Yellow stars are sample locations. White dots are towns.

NAC: North Australian Craton. WAC: Western Australian Craton. SAC: South Australian Craton. Numbers correspond samples analysed in this study: 1) 042, basement sample. 2) 045, basement sample. 3) CUG01, Esmeralda Granite. 4) PGE01, Macartneys Granite. 5) FOG01, Forsayth Granite. And previously analysed samples in the Georgetown Inlier: 6) Mistletoe Granite, 7) Mount Hogan Granite, 8) Unnamed granitic gneiss, 9) Digger Creek Granite, 10) Unnamed monzogranite, 11) Mywyn Granite, 12) Lighthouse Granite, 13) Brandy Hot Granodiorite, 14) Forest Home Trondhjemite. See table 1 for the references. Pink overlay in eastern Mount Isa Inlier is the ca. 1.55 to 1.49 Ga Williams Batholith and the Maramungee Granite.

This study aims to use Lu-Hf in zircon from granites in the Georgetown Inlier, and newly identified granites from the basement between the Georgetown and Mount Isa inliers to determine if they have a Laurentian (Georgetown Inlier) or Australian (NAC, western Mount Isa Inlier) affinity. Basement samples 042 and 045 (Figure 5.1) were obtained by Terra Search Pty Ltd who were operating for Real (Aust) Holdings Pty Ltd, an exploration company who targeted two major magnetic and gravity anomalies. In this paper, these newly identified Proterozoic granites are referred to informally as the Cudgee Creek granites.

5.3 Geological Setting

The Georgetown Inlier consists of Paleo- to Mesoproterozoic sedimentary rocks that have been regionally deformed and metamorphosed up to granulite facies locally (Withnall and Hutton, 2013). The oldest sedimentary rocks, termed the lower Etheridge Group were deposited between ca. 1700 to 1655 Ma and have a detrital zircon provenance that strongly resembles that of sediments deposited at the same time in Laurentia (Neumann and Kositcin, 2011; Nordsvan et al., 2018). The sediments are interbedded with ca. 1665 Ma tholeiitic basalts (Baker et al., 2010), and intruded by dolerite dykes and sills at ca. 1660 Ma (Black et al., 1998). Up-sequence, the upper Etheridge Group is characterised by fine-grained sediments that

are not intruded by the dolerite dykes or sills (Withnall et al., 1988; Black et al., 1998). These sediments have a different zircon provenance from the lower Etheridge Group (Neumann and Kositcin, 2011; Nordsvan et al., 2018) and more juvenile ε_{Nd} values (Lambeck et al., 2012). The inlier has undergone a complex history of metamorphism and deformation and was intruded by numerous 1.56–1.55 Ga granitic plutons (Withnall and Hutton, 2013).

The Georgetown Inlier was intruded by voluminous Mesoproterozoic granites that have been dated by several previous studies (Table 5.1). They range in age and composition from an I-type orthogneiss at ca. 1.69 Ga to ca. 1.54 Ga S-type granites. Typically, the Georgetown Inlier granites are assigned to one of three petrological groups; the Forsayth Supersuite, Forest Home Supersuite, and Esmeralda Supersuite (Champion, 1991; Withnall and Hutton, 2013). The Forsayth Supersuite is the largest accumulation of Mesoproterozoic S-type granites in northern Australia and consists of about 30 individual plutons (Champion, 1991; Budd et al., 2001; Withnall and Hutton, 2013). The Forest Home Supersuite consists of the Forest Home and Talbot Creek trondhjemites, and most likely the Brandy Hot Granite, a series of I-type plutons (Champion, 1991). The westernmost granites in the Georgetown Inlier, the Esmeralda Supersuite, are generally classified as S-type; most plutons are peraluminous, have an abundance of muscovite, biotite, with garnet reported in some samples, locally they record a reduced oxidation state, have a particular trend of P2O5, and have an association with tin mineralisation. However, Budd et al. (2002) suggested that parts of the Esmeralda Supersuite could be classed as I-type because some samples contain hornblende and several of the granites are oxidised. Graphitic

sedimentary xenoliths are common, and assimilation of such material by the magma may have produced the reduced granites of the Supersuite and peraluminous geochemistry.

While most granites in the Georgetown Inlier are categorised into one of these three supersuites, many plutons have remained undated and have only minimal lithological and geochemical descriptions (Withnall and Hutton, 2013).

Table 5.1: Review of all previous ages obtained for granites in the Georgetown Inlier. *Granites redated in this study. [†]Granite age revised by a later study. 1) Black and McCulloch (1990), 2) Black and Withnall (1993), 3) Neumann and Kositcin (2011). Uncertainty is 1σ as reported by the references.

Name	Suite	Reported Age (Ma)	Reported Uncertainty (± Ma)	Reference
Mistletoe Granite	Forsayth Batholith	1544	7	1
Mount Hogan Granite[†]	Forsayth Batholith	1549	25	2
Forsayth Granite*	Forsayth Batholith	1550	7	1
Unnamed granitic gneiss	Forsayth Batholith?	1554	4	3
Digger Creek Granite	Forsayth Batholith	1554	10	2
Hogan Granite	Forsayth Batholith	1558	2	3
Esmeralda Granite*	Esmeralda Supersuite	1558	4	1
Unnamed monzogranite	Forrest Home Supersuite?	1559	2	3
Mywyn Granite	Forsayth Batholith	1559	3	3
Lighthouse Granite	Forsayth Batholith	1561	10	2
Brandy Hot Granodiorite	Forrest Home Supersuite	1563	3	3
Forest Home Trondhjemite	Forrest Home Supersuite	1564	7	3

5.4 Methods

Thee granite samples were collected along an east-west transect between Georgetown and Croydon, and two from drill core that intersected the basement east of the Georgetown Inlier (Figure 5.1). Approximately 1 kg of each sample was cleaned and crushed at Curtin University, zircon grains were concentrated using a Wilfley table and LST heavy-liquid for density separation, and Frantz for magnetic separation.

Zircon grains were mounted on double-sided tape and set in epoxy resin, which was ground down to expose the grans and then polished. The zircon grains were imaged using standard light microscopy. The resin discs were carbon-coated for backscattered, secondary electron and cathodoluminescence (CL) imaging on MIRA3 VP-FESEM scanning electron microscope (SEM) at John de Laeter Centre (JdL), Curtin University.

The isotopic composition of the zircons grains was measured using laser ablation inductively coupled plasma mass spectrometry (LA-ICP-MS) at JdL. Samples were analysed on six separate occasions (Table 5.2), using a Resonetics M-50 193 nm ArF excimer laser doing laser ablation split stream with an Agilent 7700s quadrupole for U-Pb and a Nu Plasma II multi-collector for Lu-Hf. For more precise ages, samples were later analysed using a Resonetics M-50 193 nm ArF excimer laser with a Nu Plasma II multi-collector mass spectrometer. Zircon GJ1 (608.5 Ma), 91500 (1062.4 Ma) and OG1 (2464 Ma) were then analysed as U-Pb standards (Jackson et al., 2004; Stern et al., 2009; Wiedenbeck et al., 1995). Additionally, Mud Tank zircon grains were analysed as the hafnium standard (Woodhead and Hergt, 2005). The data were reduced using Iolite with the VizualAge addon (Paton et al., 2011; Petrus and Kamber, 2012). The propagated uncertainty of each grain was directly taken from the Iolite output. Weighted mean ages were calculated for each session separately to test their validity, then presented together because the weighted mean ages for every session are within the uncertainty of the higher precision data (single-stream Nu Plasma II multi-collector). Individual zircon grain ages and weighted mean ages were calculated

using Isoplot R (Vermeesch, 2018), which was also used to generate the U-Pb data plots. For weighted mean ages, a discordance limit of <5% was set.

For ε_{Hf} calculations, a Discordance limit of <10% was applied to increase the number of viable analyses per sample. Possible effects of variation in ages associated with the larger discordia allowance were avoided by recalculating ε_{Hf} values to the weighted mean ages, interpreted as the crystallisation ages of the granites. Initial $^{177}Hf/^{176}Hf$ values were calculated using the ^{176}Lu decay constant = 1.865×10^{-11} yr^{-1} (Scherer et al., 2001). Chondritic values follow Bouvier et al. (2008): $^{176}Hf/^{177}Hf$ CHUR = 0.282785 and $^{176}Lu/^{177}Hf$ CHUR = 0.0336, where CHUR is chondritic uniform reservoir. Hafnium data are reported in epsilon units (ε), where one εHf unit represents one part per 10,000 deviations of $^{176}Hf/^{177}Hf$ from CHUR composition at the time defined by the crystallisation age of the zircon or the weighted mean age of the granite (Kinny and Maas, 2003).

Table 5.2: Summary of analytical days. Zircon Standard known ages: GJ1: 608.5 Ma (Wiedenbeck et al., 1995). 91500: 1062.4 Ma (Jackson et al., 2004). OG1: 2465.4 Ma (Stern et al., 2009).

Date	Samples	Method	Spot size (μm)	U–pb Standard ($^{206}Pb/^{238}Pb$ age MA)	Secondary standard ($^{206}Pb/^{238}Pb$ age MA)	Secondary standard ($^{207}Pb/^{206}Pb$ age MA)
8/04/17	FOG01, PGE01	LASS	50	GJ1 (601.83)	91500 (1061.6)	OG1 (3466.3)
28/02/18	CUG01, FOG01	LASS	50	91500 (1063)	GJ1 (609.5)	OG1 (3456.5)
7/03/18	FOG01	LASS	39	GJ1 (602)	91500 (1054.3)	OG1 (3465)
22/03/18	042, 045	LASS	50	GJ1 (601.82)	91500 (1061.8)	OG1 (3470.7)
18/07/18	CUG01, PGE01, 042, 045	Multi collector	33	GJ1 (601.5)	91500 (1060.3)	OG1 (3465.1)
3/12/18	CUG01, 042	LASS	39	GJ1 (602)	91500 (1066.4)	OG1 (3459.6)

5.5 Samples and Results

5.5.1 Forsayth Granite (FOG01) (UTM54: 760190 / 7975926)

The Forsayth Granite sample was collected from an outcrop alongside the Gulf Development Road approximately 10 km west from Georgetown (Figure 5.1). This granite is characteristically grey, medium to coarse-grained, generally porphyritic, weakly foliated, with prismatic 5 cm K-feldspar megacrysts. Biotite schlieren and nebulitic streaks are commonly aligned parallel to the weak foliation. The foliation is defined by recrystallised biotite and quartz grains which wrap the magmatic K-feldspar megacrysts. Migmatitic metasedimentary xenoliths are locally abundant, along with rare amphibolite and lumps of white quartz. The xenoliths are interpreted as restite from the original metamorphic protolith. Pegmatite veins and dykes are common throughout the batholith, while mafic microgranular enclaves are rare.

Zircon grains extracted from sample FOG01 are generally light to dark brown or slightly orange with little transparency, less commonly grains are colourless (Figure 5.2). Most grains are prismatic, have preserved crystal faces, are generally subhedral and fewer euhedral. The dimensions of 40 zircon grains were measured and range from 141 to 239 µm long, and from 52 to 125 µm wide, with an aspect ratio ranging from 1.8 to 4.32 (averaging 2.9) (Figure 5.2). In cathodoluminescence images, most grains are extremely dark and showed common oscillatory zoning when the brightness was increased significantly. Three grains imaged had inherited cores that were too small to be targeted for laser ablation.

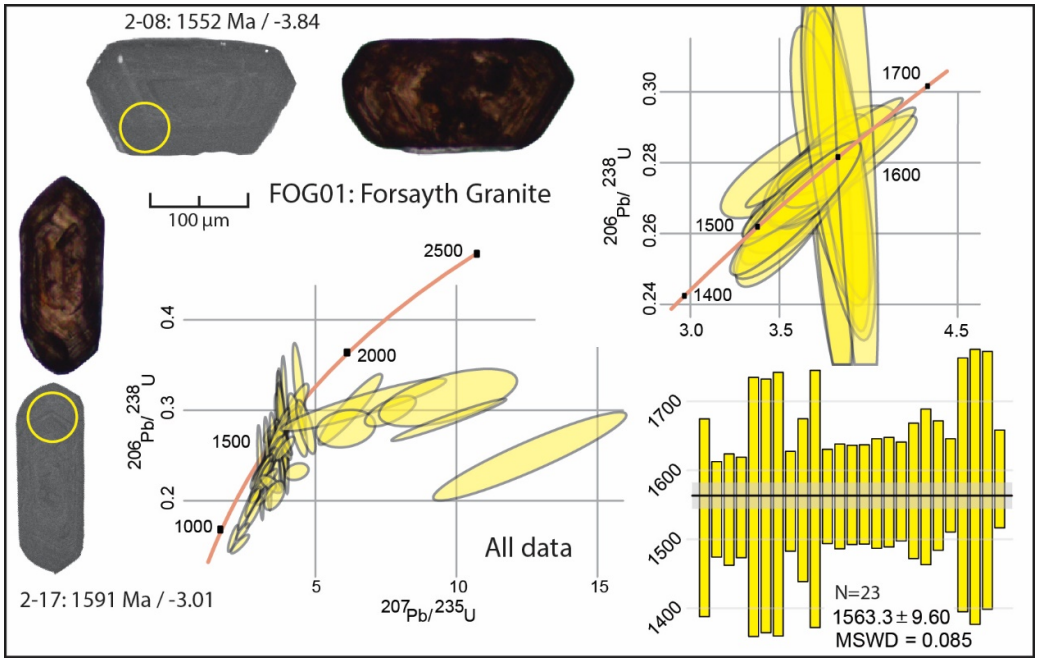

Figure 5.2: Overview of the data from the Forsayth Granite (FOG01). Zircon images are transmitted light and cathodoluminescence SEM where the circles represent the laser ablation spot. The difference in uncertainties reflects the different analytical sessions. The (zoomed) Concordia plot on the right includes all data utilised in the mean weighted age.

The Forsayth Granite sample was analysed on three separate days (1, 2 and 3; Table 5.2). In total, 71 grains were analysed for U-Pb isotopes, of which two are interpreted as being inherited (FOG01-3-05: 1642 ± 61 Ma; FOG01-1-25: 1656 ± 47), and 44 grains were discordant (>5%). From 25 grains at <5% discordance, a single population has a $^{207}Pb/^{206}Pb$ weighted mean age of 1563.3 ± 9.6 Ma (MSWD = 0.085) (Table 5.3, Figure 5.2). From 37 grains <10 % discordant, the hafnium data has ε_{Hf} values from -4.7 to +0.3 with a mean value of -2.6 when calculated against the U-Pb grain age. Excluding outliers (inherited grains) and recalculating the ε_{Hf} values against the weighted mean age (1563.3 Ma) results in ε_{Hf} values ranging from -4 to -0.7 with a mean value of -2.9 (Figure 5.3). Using these recalculated ε_{Hf} values, two-stage depleted mantle model ages from the Forsayth Granite range from 2.3 to 2.5 Ga with an average of 2.5 Ga.

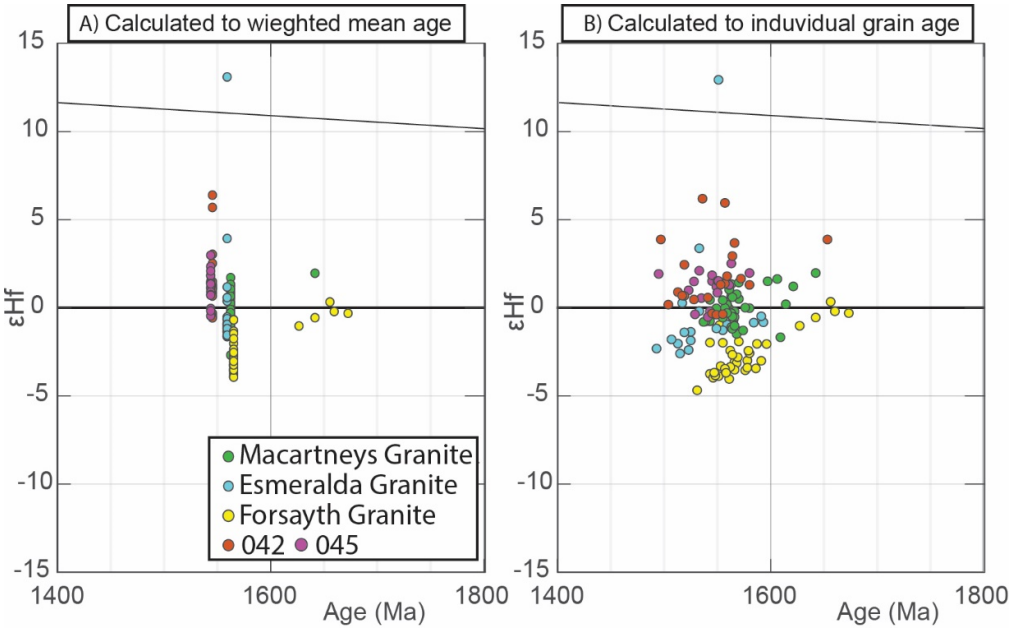

Figure 5.3: ε_{Hf} vs U-Pb age (Ma) plots for the analysed samples. A) ε_{Hf} values calculated with the weighted mean age of the granites. B) ε_{Hf} values calculated with the individual grain age. Macartneys Granite = PGE01, Esmeralda Granite = CUG01, Forsayth Granite = FOG01, 042 and 045 = Cudgee Creek granites.

Table 5.3: New U-Pb Proterozoic granite ages from NE Australia.

Granite	Sample	$^{207}Pb/^{206}Pb$ Age (Ma)	Uncertainty (Ma)	MSWD	ε_{Hf} (mean)	ε_{Hf} 2TDM age (mean, Ga)
Forsyth Granite	FOG01	1563.3	9.6	0.085	-2.91	2.46
Macartneys Granite	PGE01	1562.9	4.1	0.29	-0.14	2.28
Esmeralda Granite	CUG01	1559.6	4.6	0.54	-0.55	2.3
Cudgee Creek granites	042	1545.9	3.4	0.51	+1.71	2.15
	045	1544.2	3.7	0.52	+1.22	2.18

5.5.2 Macartneys Granite (PGE01) (UTM54: 706725 / 7974131)

The Macartneys Granite is part of the Esmeralda Supersuite and was collected from bedrock alongside Paddy's Road (Figure 5.1). The sample is a slightly porphyritic garnet-biotite-bearing granite with abundant metasedimentary, carbonaceous

xenoliths, and graphite inclusions. The abundance of enclaves and graphite increases towards the west (Withnall and Hutton, 2013). No age or geochemistry has previously been reported from the Macartneys Granite.

Zircons from the PGE01 sample are elongated, commonly euhedral with minor subhedral grains and are between 133 to 355 µm long and 36 to 85 µm wide, having an average aspect ratio of 3.77 (Figure 5.4). Grains are generally translucent and colourless with some grains having a minor pink hue. Cathodoluminescence images show the grains have a large, commonly structureless core, with faint oscillatory zoning on the rim (Figure 5.4).

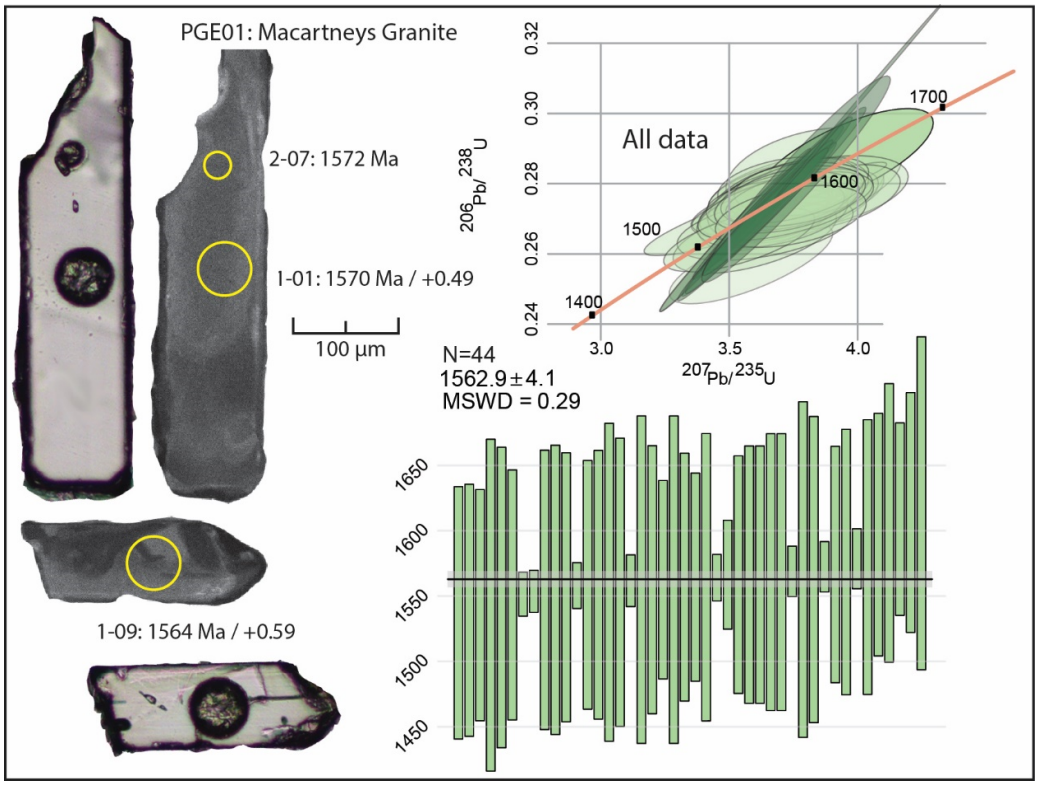

Figure 5.4: Overview of the geochronology data from the Macartneys Granite (PGE01). Zircon images are transmitted light and cathodoluminescence SEM, the circles represent the location of the laser ablation spots. Larger uncertainties in the mean weighted age correspond with zircon analysed using LASS.

Of the 48 grains analysed for U-Pb isotopes, 44 with <5% discordance have a $^{207}Pb/^{206}Pb$ weighted mean age of 1562.9 ± 4.1 Ma (MSWD = 0.29) (Figure 5.4). A single analysis considered to be inheritance was excluded as an outlier (PGE01-1-08: 1642 ± 46 Ma).

From 36 grains <10 % discordant, ε_{Hf} values are -1.68 to +1.96 with a mean value of +0.02 when calculated against the individual U-Pb grain ages. Excluding the inherited grains ε_{Hf} values recalculated against the weighted mean age (1562.9 Ma) range from -2.68 to +1.71 and have a mean of -0.14 (Figure 5.3). Using these recalculated ε_{Hf} values, two-stage depleted mantle model ages from the Macartneys Granite range from 2.16 to 2.44 Ga with an average of 2.28 Ga.

5.5.3 Esmeralda Granite (CUG01) (UTM54: 706725 / 7974131)

The Esmeralda Granite is the largest pluton of the Esmeralda Supersuite. The sample was collected from a boulder alongside the Gulf Development Road, roughly 5 km east of Croydon. This granite has a phaneritic texture with medium-grained biotite, orthoclase, plagioclase, quartz and secondary muscovite. The Esmeralda Granite was previously dated by Black and McCulloch (1990) using the 'conventional' multigrain U-Pb zircon method to obtain an age of 1558 ± 4 Ma. They also reported an age of 1552 ± 2 Ma from the Croydon Volcanic Group, which is intruded by the Esmeralda Granite and thought to be comagmatic (Withnall et al., 1988).

Zircon grains from CUG01 are commonly clear to light brown with very few dark brown grains. Most grains are elongate, euhedral, and preserve crystal faces (Figure 5.5). The average grain is 228 µm long and 72 µm wide with a mean aspect ratio of 3.22. The dark brown grains are shorter, more rounded and typically show inherited

cores in cathodoluminescence images. Cathodoluminescence images of the dominant grains have well developed oscillatory zoning and are rarely structureless.

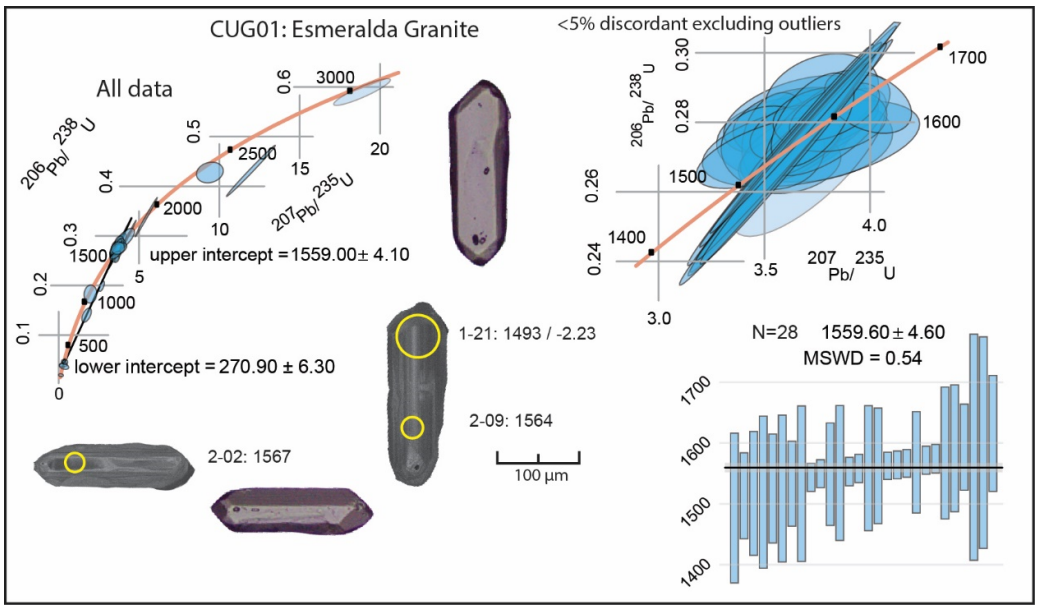

Figure 5.5: Overview of the data from the Esmeralda Granite (CUG01). Zircon images are transmitted light and cathodoluminescence SEM, the circles represent the location of the laser ablation spots. Larger uncertainties in the mean weighted age correspond with zircon analysed using LASS.

From 59 analyses for U-Pb isotopes, 41 grains are <5% discordant. From the concordant grains, a single population of 28 grains have a $^{207}Pb/^{206}Pb$ weighted mean age of 1559.6 ± 4.6 Ma (MSWD = 0.54). 9 grains are younger than 1100 Ma, and four are considered inherited (CUG01-2-06: 1912 ± 12 Ma; CUG01-2-07: 1709 ± 11 Ma; CUG01-1-16: 2424 ± 65 Ma; CUG01-3-2: 3073 ± 36 Ma). The 9 concordant grains with ages less than 1100 Ma do not form a single population, eight grains have a spread of ages between 255 – 314 Ma, and one is 1083 ± 40 Ma. A discordia line fitted through the data (excluding outliers, interpreted as inheritance older than 2 Ga) gives a lower intercept of 270 ± 6.3 Ma with an upper intercept of 1559 ± 4.1 Ma (MSWD = 1.7) (Figure 5.5).

Of the 22 grains <10 % discordant, three analyses are excluded as outliers: one has an age of 2424 ± 65 Ma and two have outlier ε_{Hf} values (CUG01-1-18: 1568 Ma, ε_{Hf} -69.9; CUG01-1-07: 1553 Ma, ε_{Hf} 12.95). For the remaining 19 grains, the ε_{Hf} values range from -2.6 to +3.4 and have a mean value of -0.9 when calculated against each U-Pb grain age. Recalculating the ε_{Hf} values against the weighted mean age (1559.6 Ma) yields values from -1.6 to +3.9 with a mean of -0.6. Using these recalculated ε_{Hf} values (Figure 5.3), two-stage depleted mantle model ages from the Esmeralda Granite range from 2.0 to 2.4 Ga with an average of 2.3 Ga.

5.5.4 Cudgee Creek Granite (042) (Drill hole: HBPD001, UTM54: 556804/7922330)

This sample was taken from drill core HBP001 that reached the basement between the Mt Isa and Georgetown inliers (Figure 5.1). The hole was drilled to a depth of 419.6 m and intersected the basement at 252.47 m. The analysed sample was cored from 350.27 to 351.1 m. The granite sample is coarse-grained, weakly foliated, and composed by K-feldspar, quartz, plagioclase, biotite, titanate, minor hornblende, and accessory phases such as zircon, apatite and monazite. The presence of hornblende and titanite indicates that the granite is an I-type.

Zircon grains from sample 042 are generally transparent to translucent and colourless and rarely light brown. The largest grains are dark brown to black, have abundant inclusions, and are typically associated with a high degree of fracturing (Figure 5.6). Most grains are euhedral, showing well developed and preserved crystal faces. In cathodoluminescence imaging about one-third of the observed zircon grains have

inherited cores; which are often metamict and well rounded, or when subhedral have convoluted zoning. The rims commonly show well-developed oscillatory zoning or are less commonly structureless. Zircon grains that have no observable cores also have well-developed oscillatory zoning. Zircon grains are 230 to 540 µm long and 47 to 250 µm wide and have a mean aspect ratio of 3.07.

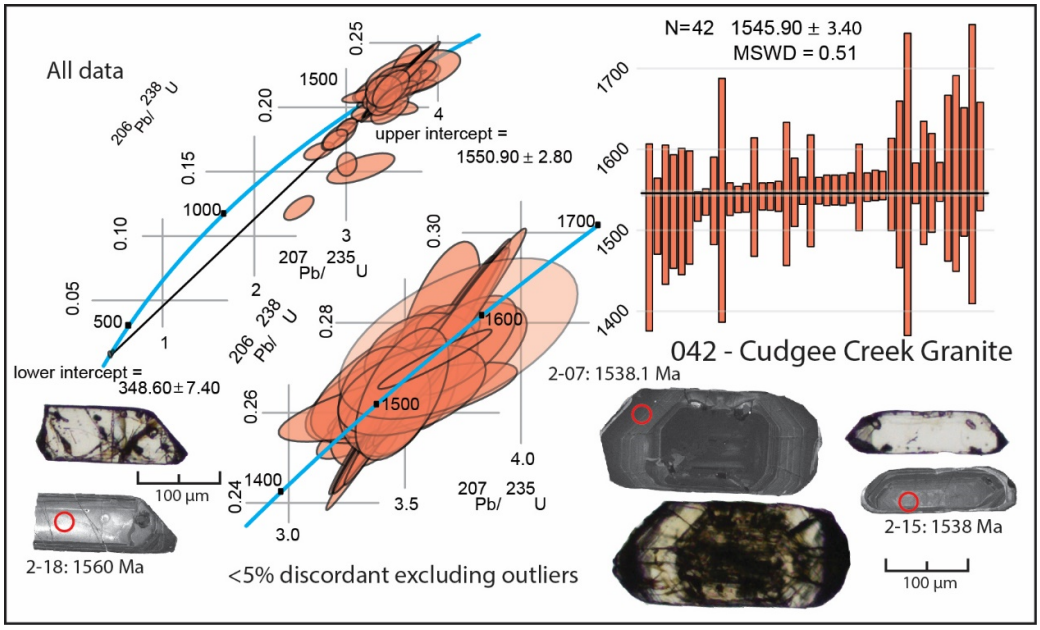

Figure 5.6: Overview of the data from the Cudgee Creek granite (042). Zircon images are transmitted light and cathodoluminescence SEM, the circles represent the location of the laser ablation spots. Larger uncertainties in the mean weighted age correspond with zircon analysed using LASS.

From 57 grains analysed for U-Pb isotopes, excluding 2 grains that had Phanerozoic ages (042-2-16: 343.5 ± 5.8 Ma, 042-2-25: 364.1 ± 6.1 Ma) considered contamination, 42 grains have < 5% discordance and form a single population with a mean $^{207}Pb/^{206}Pb$ weighted age of 1545.9 ± 3.4 Ma (MSWD = 0.51) (Table 5.3; Figure 5.6). A discordia line fitted through the data reveals a lower intercept of 348.6 ± 7.4 Ma and an upper intercept of 1550.9 ± 2.8 Ma (MSWD = 1.3).

From 16 grains at <10 % discordance utilised for Lu-Hf isotopes, one analysis is excluded as an outlier (042-1-10: 1527 Ma, ε_{Hf} 28.79). For the other 15 grains, ε_{Hf} values range from -0.4 to +6.17 with a mean value of +1.66 when calculated against the U-Pb grain age (Figure 5.3). Excluding the outliers, ε_{Hf} values recalculated against the weighted mean age (1545.9 Ma) for the granite, are -0.57 to +6.39 with a mean of +1.71. Using the recalculated ε_{Hf} values, two-stage depleted mantle model ages for sample 042 range from 1.85 to 2.3 Ga with an average of 2.15 Ga.

5.5.5 Cudgee Creek Granite (045) (Drill hole: HBPD002, UTM54: 556533 /7821948)

This sample was taken from core HBPD002 drilled into the basement between the Mt Isa and Georgetown inliers (Figure 5.1). The hole was drilled to a depth of 455 m and intersected the basement at 267.96 m. The analysed sample was cored from 316.85 to 317.9 m. The sample is a weakly foliated coarse to very coarse-grained monzogranite, with foliation wrapping feldspar megacrysts. Titanite and allanite are common accessory minerals and suggest the granite is an I-type.

Zircon grains extracted from sample 045 are remarkably similar to sample 042. They are generally colourless to light brown, highly fractured, and have abundant inclusions (Figure 5.7). Cathodoluminescence imaging indicates they share many of the characteristics of sample 042; but there is noticeably less inherited and metamict cores. Zircon grains are 241 to 596 µm long and 70 to 317 µm wide with a mean aspect ratio of 3.22.

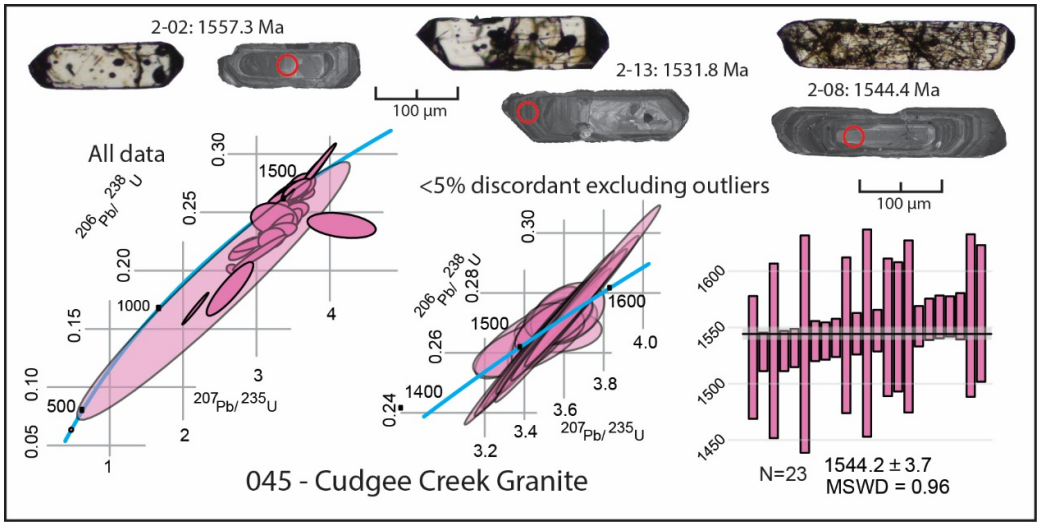

Figure 5.7: Overview of the data from the Cudgee Creek granite (045). Zircon images are transmitted light and cathodoluminescence SEM, the circles represent the location of the laser ablation spots. Larger uncertainties in the mean weighted age correspond with zircon analysed using LASS.

Of the 51 grains targeted for U-Pb isotopes, excluding one Phanerozoic aged grain (045-2-08: 397 ± 4.4 Ma) that is considered contamination, 23 grains with <5% discordance form a single population with a mean $^{207}Pb/^{206}Pb$ weighted age of 1544.2 ± 3.7 Ma (MSWD = 0.96) (Figure 5.7).

For 17 grains with <10 % discordance analysed for Lu-Hf, ε_{Hf} values are -0.53 to +2.5 with a mean value of +1.18 when calculated against the U-Pb grain age. Excluding the outlier, ε_{Hf} values recalculated against the weighted mean age (1544.2 Ma), for the granite, are -0.46 to +2.98 with a mean of +1.22 (Figure 5.3). Using these recalculated ε_{Hf} values, two-stage depleted mantle model ages for granite 045 range from 2.07 to 2.29 Ga with an average of 2.18 Ga.

5.6 Discussion

5.6.1 Georgetown Inlier granites

The age reported here for the Forsayth Granite (1563.3 ± 9.6 Ma) is slightly older (yet within uncertainty) than the previously reported age of 1550 ± 7 Ma (Black and McCulloch, 1990), and is consistent with recent ages reported from other Georgetown Inlier granites interpreted to be part of the Forsayth Supersuite (Neumann and Kositcin, 2011). Neumann and Kositcin (2011) reported 1559 ± 3 Ma for the Mywyn Granite, and a revised age of 1558 ± 2 Ma for the Mount Hogan Granite, that was previously dated at 1549 ± 25 Ma by Black and Withnall (1993). Thus, all Forsayth Batholith granites dated have mean crystallisation ages between ca. 1554 and 1564 Ma, except for the Mistletoe Granite which has an age of 1544 ± 7 Ma, obtained using 'conventional' multigrain zircon dating (Black and McCulloch, 1990). It is likely that this younger 1544 ± 7 Ma age for the Mistletoe Granite is incorrect as every other age reported from the same study has been revised and found to be at least 10 Myr older. It is recommended that the Mistletoe Granite be redated using modern analytical methods, and until the ca. 1544 Ma age is reproduced it should remain questionable.

Figure 5.8 (next page): Overview of the Georgetown Inlier geochronology following this study. Height of each box represents the age uncertainty of the sample References: 1) This study. 2) Neumann and Kositcin (2011). 3) Black and Withnall (1993). 4) Black and McCulloch (1990). 5) Black et al. (1998). 6) Pourteau et al. (2018) 7) Lambeck et al. (2012). 8) Black et al. (2005). Granite names: ESG: Esmeralda, MCG: Macartneys, FHT: Forest Home Trondhjemite: BHG: Brandy Hot, FSG: Forsayth, LHT: Lighthouse, DCG: Digger Creek, MTG: Mistletoe, MHG: Mount Hogan, UMG, Unnamed Monzogranite, MYG: Mywyn, UGG: Unnamed granitic gneiss, 045 and 042, Cudgee Creek basement granites. Ages within the plutons are reported crystallisation ages. Corresponding two-stage depleted mantle model ages are reported at the bottom of the figure. ε_{Nd} two-stage model ages are in black text and ε_{Hf} two-stage model ages are in red. ε_{Nd} two-stage model ages were calculated using formulas outlined in Champion (2013), when possible against the new ages reported in this study. Locations of the granites can be seen in Figure 5.1.

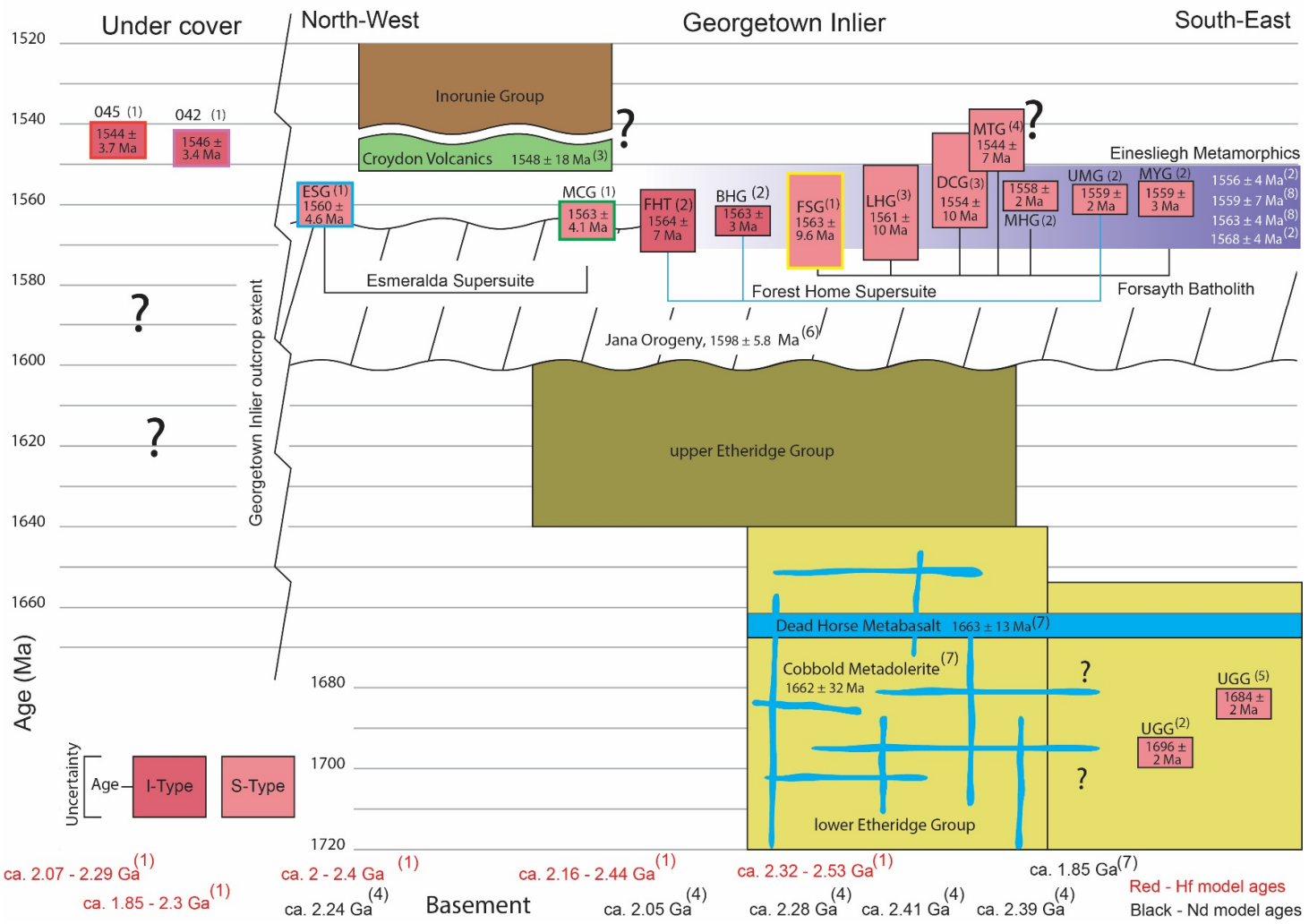
Under cover
North-West
Georgetown Inlier
South-East
Age (Ma)
1520
1540
1560
1580
1600
1620
1640
1660
1680
1700
1720
045 (1)
1544 ± 3.7 Ma
042 (1)
1546 ± 3.4 Ma
Inorunie Group
Croydon Volcanics 1548 ± 18 Ma (3)
ESG (1) 1560 ± 4.6 Ma
MCG (1) 1563 ± 4.1 Ma
FHT (2) 1564 ± 7 Ma
BHG (2) 1563 ± 3 Ma
FSG (1) 1563 ± 9.6 Ma
LHG (3) 1561 ± 10 Ma
DCG (3) 1554 ± 10 Ma
MTG (4) 1544 ± 7 Ma
1558 ± 2 Ma
MHG (2)
UMG (2) 1559 ± 2 Ma
MYG (2) 1559 ± 3 Ma
Einesliegh Metamorphics
1556 ± 4 Ma (2)
1559 ± 7 Ma (8)
1563 ± 4 Ma (8)
1568 ± 4 Ma (2)
Esmeralda Supersuite
Forest Home Supersuite
Forsayth Batholith
Jana Orogeny, 1598 ± 5.8 Ma (6)
Georgetown Inlier outcrop extent
upper Etheridge Group
Dead Horse Metabasalt 1663 ± 13 Ma (7)
Cobbold Metadolerite (7) 1662 ± 32 Ma
UGG (5) 1684 ± 2 Ma
UGG (2) 1696 ± 2 Ma
lower Etheridge Group
Uncertainty
Age
I-Type
S-Type
ca. 2.07 - 2.29 Ga (1)
ca. 1.85 - 2.3 Ga (1)
ca. 2 - 2.4 Ga (1)
ca. 2.24 Ga (4)
Basement
ca. 2.16 - 2.44 Ga (1)
ca. 2.05 Ga (4)
ca. 2.32 - 2.53 Ga (1)
ca. 2.28 Ga (4)
ca. 2.41 Ga (4)
ca. 1.85 Ga (7)
ca. 2.39 Ga (4)
Red - Hf model ages
Black - Nd model ages

The age reported for the Esmeralda Granite (1559.9 ± 4.6 Ma) is within the uncertainty of the previous 'conventional' multigrain U-Pb age of 1558 ± 4 Ma (Black and McCulloch, 1990). The Macartneys Granite is considered a component of the Esmeralda Supersuite and the age reported here of 1562.9 ± 4.1 Ma, is consistent with the Esmeralda Granite ages. These new ages are within the uncertainty of a SHRIMP U-Pb zircon age of 1548 ± 18 Ma determined by Black and Withnall (1993) for the Idalia Rhyolite within the Croydon Volcanic Group. This age has a large uncertainty and requires re-evaluation, although a previous age determination on the same sample using 'conventional' multigrain zircon dating by Black and McCulloch (1990) gave a seemingly more precise age of 1552 ± 2 Ma.

Neumann and Kositcin (2011) reported three ages from I-type granites in the Georgetown Inlier: The Forest Home Trondhjemite, Brandy Hot Granodiorite, and an unnamed monzogranite at 1564 ± 7, 1563 ± 4 and 1559 ± 2 Ma, respectively. Comparing all the Proterozoic granite ages from the Georgetown Inlier suggests no resolvable geochemical relationship with age (i.e. I- vs S-type) (Figure 5.8). Rather, these new ages suggest that magmatism occurred simultaneously within uncertainty across the whole inlier at ca. 1560 Ma (Figure 5.8). Furthermore, the granite crystallisation ages overlap with the metamorphic zircon ages (within 2σ uncertainty) from the Einasleigh Metamorphics (Black et al., 1998,2005; Neumann and Kositcin, 2011; Figure 5.8).

5.6.2 Cudgee Creek Granite drill-core samples: basement west of the Georgetown Inlier

The ages from the Cudgee Creek granites (samples 042 and 045) are the first Proterozoic ages reported from basement between the Mount Isa and Georgetown inliers. At 1545.9 ± 3.4 and 1544.2 ± 3.7 Ma, these granites from the basement are 10 to 15 Myr younger than those in the Georgetown Inlier (other than the ca. 1544 Ma age from the Mistletoe Granite). In the eastern belt of the Mount Isa Inlier, the Maramungee Granite has a similar age to the Cudgee Creek granites at 1545 ± 11 Ma and also has an I-type affinity (Figure 5.1) (Budd et al., 2001; Mark, 2001; Page and Sun, 1998; Withnall and Hutton, 2013). No zircon Lu-Hf data is available from the Maramungee Granite, but the bulk-rock ε_{Nd} value is -1.32, corresponding to a two-stage model age of 2.14 Ga, which overlaps with the zircon Lu-Hf two-stage depleted mantle model ages from the Cudgee Creek granites (042: 2. 1.85 to 2.3 Ga, and 045: 2.07 to 2.29 Ga) (Champion, 2013; Page and Sun, 1998). In fact, all ca. 1550 to 1500 Ma granites from the Mount Isa Inlier, which all occur in the eastern belt (Figure 5.1) have bulk-rock ε_{Nd} two-stage model ages between 2.1 and 2.28 Ga (Champion, 2013) which is notably less variable than those in the Georgetown Inlier (Black and McCulloch, 1990; Champion, 2013).

5.6.3 Lu-Hf data

The Lu-Hf ratios in zircon from the analysed granite samples show several trends. When comparing all samples analysed in this study, the ε_{Hf} values trend from negative to more positive values with time (Figure 5.9A), while spatially the ε_{Hf} values also

trend from negative to more positive east to west (Figure 5.9B). The difference in ε_{Hf} values between the samples might reflect the evolution of the magmatic system becoming more enriched in time, or it could reflect different aged source rocks from east to west.

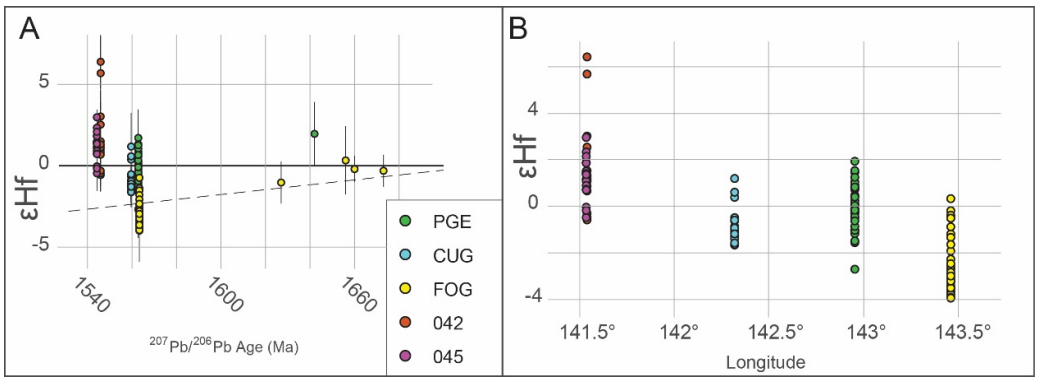

Figure 5.9: A) ε_{Hf} values vs age for the granite analysed in this study. B) ε_{Hf} value vs longitude. PGE) Macartneys Granite, CUG) Esmeralda Granite, FOG) Forsayth Granite, 042 and 045) Cudgee Creek basement granites. Black lines on (A) represent the ε_{Hf} uncertainties. Outliers have been removed from these plots.

The systematic increase in ε_{Hf} values vs age (Figure. 8) is typical for retreating accretionary orogens (Kemp et al., 2009). In the Palaeozoic Tasmanides of eastern Australia, systematic variations toward positive ε_{Hf} and ε_{Nd} values corresponded to extensional events following crustal thickening and burial of sediments. This occurred at least three times in the Tasmanides, and each time was broadly associated with the transition from S- to I- to A-type granite (Collins et al., 2019). A similar trend can be observed in Proterozoic NE Australia with the transition from S- (Esmeralda and Forsayth granites) to I- (Cudgee Creek) to A-type granites, with the latter represented by the ca. 1.55 to 1.5 Ma Williams Batholith in the eastern Mount Isa Inlier (Mark, 2001).

If the retreating orogen–Tasmanides analogy can be applied, it would suggest that the difference in ε_{Hf} values noted between the Cudgee Creek and the Georgetown Inlier granites is the result of subduction-related lithospheric stretching during ongoing west-dipping subduction between 1560–1530 Ma. However, while the trend in time is similar to the Tasmanides, the spatial extent is much greater in Proterozoic NE Australia (~500 Km compared with ~150 km in the Tasmanides). Nevertheless, if the Mesoproterozoic granites in NE Australia are the product of subduction then the most hydrous (S-type) magmas are located in the east near the arc, and the I-types are located in the back-arc region where lithospheric thinning is greatest, and the mantle contribution is highest. This back-arc extension might be responsible for the Millungera Basin, a concealed Mesoproterozoic basin observed on seismic profiles between the Georgetown and Mt Isa inliers (Korsch et al., 2012; see also Figure 5.1). Farther inboard (west), the A-type granites have a similar isotopic signature to the Forsayth Granite, suggesting they formed in normal thickness crust, beyond the stretched back arc basin, in the hinterland, far from the influence of slab derived fluids.

The only published Lu-Hf zircon data from either the Georgetown Inlier or the eastern belt of the Mount Isa Inlier are from modern stream sediments taken from catchments sourcing those terranes (Figure 5.9A and 5.9D) (Griffin et al., 2006; Murgulov et al., 2007). A compilation of these published data is presented as density contours in Figure 5.10 and compared to the Hf data from Georgetown and basement granites compiled in this study. The ε_{Hf} values from the modern stream sediments of the Georgetown Inlier are probably biased towards more extensive Forsayth

Supersuite granites because the catchments sampled are from a more easterly part of the inlier (Murgulov et al., 2007). Nevertheless, the sampled catchments cover both the Forsayth and the Forest Home supersuites, and the density plot overlaps with the Esmeralda Supersuite samples (Figure 5.10A and 5.10B) suggesting they are represented as well (CUG01 and PGE01). The catchment areas sampled for the Mount Isa Inlier are all from the eastern belt (Griffin et al., 2006), and ca. 1.55 to 1.49 Ga granites are only reported from that region of the Mount Isa Inlier (Withnall and Hutton, 2013). The ε_{Hf} values from the Cudgee Creek granite samples overlap with the published ε_{Hf} data from both the Georgetown Inlier and the Mount Isa Inlier. However, Cudgee Creek granite samples overlap directly with the highest density part of the Mount Isa Inlier, suggesting they have intruded crust more similar in Lu-Hf composition, to the eastern belt of the Mount Isa Inlier (Figure 5.10).

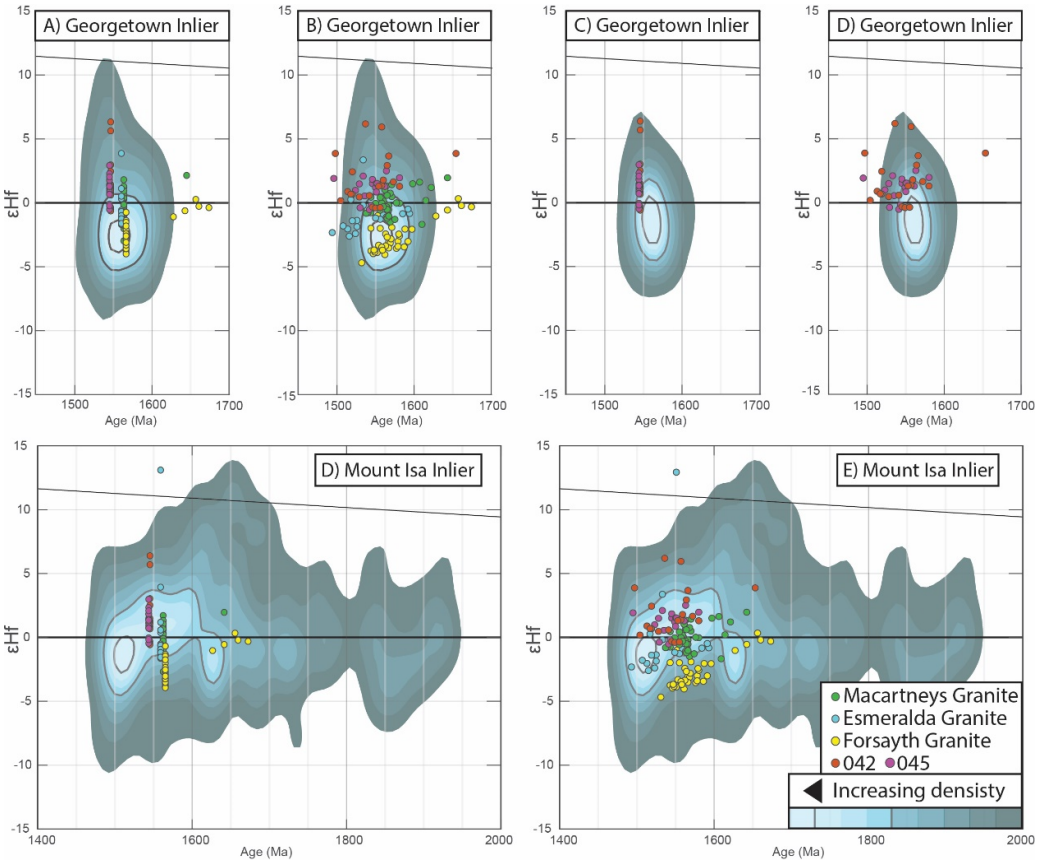

Figure 5.10: Georgetown Inlier (n=155) (Murgulov et al., 2007), and eastern Mount Isa Inlier (n=250) (Griffin et al., 2006) Age vs ε_{Hf} bivariate kernel density estimate (2dKDE) plots from modern stream sediments, overlain with the ε_{Hf} values from the granites analysed in this study. A) Georgetown Inlier stream sediment 2dKDE plots overlain with the granite ε_{Hf} values calculated to the mean weighted age. B) Georgetown Inlier stream sediment overlain by ε_{Hf} values of the granites calculated to individual grain age. C) ε_{Hf} density plot calculated including Murgulov et al. (2007) stream sediments plus the Georgetown Inlier granites from this study, overlain with the ε_{Hf} values from the basement granites calculated to the mean weighted age. D) 2dKDE plot same as (C) overlain with ε_{Hf} values from the basement granites calculated to the individual grain age. E) ε_{Hf} value 2dKDE plots of stream sediments from the eastern belt of the Mount Isa Inlier (Griffin et al., 2006), overlain with the ε_{Hf} values calculated to the mean weighted age. E) 2dKDE stream sediment plot of Mount Isa data overlain with ε_{Hf} values calculated to the individual grain age.

Crystalline basement rocks are not observed in the Georgetown Inlier: the oldest rocks exposed being metamorphosed sedimentary and mafic rocks of the lower Etheridge Group which are probably not much older than ca. 1700 Ma and intruded by ca. 1694 Ma orthogneiss (Neumann and Kositcin, 2011). Based on Nd bulk-rock

analysis of granitic rocks, Black and McCulloch (1990) argued that the basement in the Georgetown Inlier was likely composed of ca. 2.0 to 2.5 Ga igneous crust. This age is likely to be a minimum crustal-source age if any mantle-like component was involved in their genesis. While the systematic east-west variation of ε_{Nd} values in the Georgetown Inlier has not previously been reported, it has been recognised that ε_{Nd} values from sedimentary, volcanic, and granitic rocks are more variable compared to those recorded in the eastern belt of the Mount Isa Inlier (Champion, 2013). This variability with the ε_{Nd} two-stage model ages in the Georgetown Inlier may reflect an east-west variation as seen in Figure 5.8 which, like the ε_{Hf} data (Figure 5.10), broadly shows more positive ε_{Nd} values in the Esmeralda Supersuite to the west and more negative ε_{Nd} values in the granites to the east (Figure 5.8). The ε_{Hf} two-stage model age kernel density estimate (KDE) plots from the analysed granites show a significant difference from the Forsayth Granite in the east (~2.46 Ga) to the Esmeralda Batholith samples in the west (~2.33 and ~2.28 Ga) (Figure 5.11).

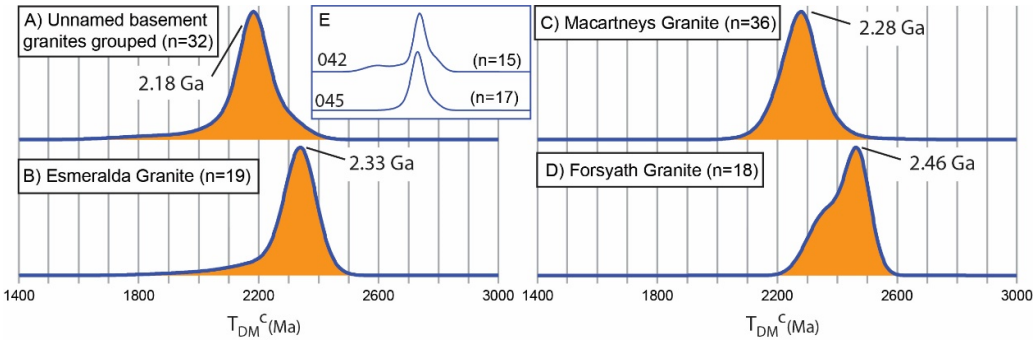

Figure 5.11: KDE plots of zircon ε_{Hf} two-stage model ages from the granites analysed in this study. A) Basement granite data grouped together. B) The Esmeralda Granite. C) Macartneys Granite. D) Forsayth Granite. E) Ungrouped basement granites.

While ε_{Hf} two-stage depleted mantle model ages should be used with caution (Payne et al., 2016), Lu-Hf compositions can provide important information about magma

sources, especially where basement rocks do not crop out and cannot be characterised. Based on deep crustal seismic data, Korsch et al. (2012) showed the Esmeralda Batholith intruding a crustal block (Numil Seismic Province) that extended from the eastern margin of the Mount Isa Inlier (the Gidyea suture) to approximately the position of the Macartneys Granite (Figure 5.1). It is possible that this crustal block is composed of younger basement compared with the Georgetown Inlier crust.

KDE plots of zircon ε_{Hf} two-stage model ages from modern sediments in the Georgetown and eastern Mount Isa inliers are significantly different (Figure 5.12). Firstly, there is a significant peak at ca. 2.58 Ga in the Georgetown data that is absent from the Mount Isa data. In the Mount Isa data, the largest peak occurs at ca. 2.22 Ma, consistent with the ε_{Nd} two-stage model ages previously reported from the eastern Mount Isa Inlier (Champion, 2013). The data also show akin to the ε_{Nd} data, a higher variability zircon ε_{Hf} two-stage model ages in Georgetown compared to Mount Isa. Intriguingly, the Georgetown stream sediment data show a subordinate population ca. 2.18 Ga, the same age as the ε_{Hf} two-stage model ages from the Cudgee Creek granites. The crystallisation ages associated with the ~24 zircon grains that characterise that ca. 2.18 Ga ε_{Hf} two-stage model age population range from 1.52 to 1.6 Ga, but only 25% of those grains have ages within the uncertainty of the Cudgee Creek granites (ages >1.5, <1.55). These zircon grains with ca. 2.18 Ga model ages either mean there are granites within the Georgetown Inlier with similar zircon Lu-Hf composition to the Cudgee Creek granites or, older granites are intruding or derived from the same basement crust (as the Cudgee Creek granites). These could include the Forest Home Supersuite for which there is currently no Lu-Hf data.

Nevertheless, ε_{Hf} two-stage model ages from the Cudgee Creek granites are more like those from the eastern Mount Isa stream sediment data than the Georgetown data (Griffin et al., 2006; Murgulov et al., 2007).

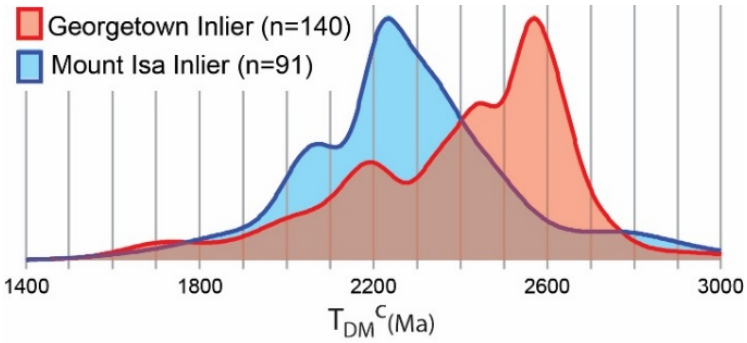

Figure 5.12: Kernel density estimate plots of zircon ε_{Hf} two-stage model ages from modern stream sediments of the eastern Mount Isa Inlier and the Georgetown Inlier (Griffin et al., 2006; Murgulov et al., 2007). Model ages are shown for grains with crystallisation ages between 1.48 and 1.61 Ga.

5.6.4 Tectonic implications

Most recently, Nordsvan et al. (2018) suggested that the Georgetown Inlier was an allochthonous terrane, derived from Laurentia when it amalgamated with the NAC at ca. 1.6 Ga. Based on a seismic profile across NE Australia, Korsch et al. (2012) suggested there were two continental ribbons concealed (by Phanerozoic sediments) between the Mount Isa and Georgetown inliers. The first, the Numil Seismic Province (Numil terrane) is bound to the west by the Gidyea Suture Zone (Figure 5.1), where it juxtaposed with the eastern Mount Isa Inlier. And the eastern boundary, the Rowe Fossil Subduction Zone, where it is in contact with the (second) Abingdon Seismic Province (Abingdon terrane). Korsch et al. (2012) suggested that west-dipping subduction drove the collision between the Numil terrane and the NAC (Mount Isa Inlier) during the Barramundi Orogeny at ca. 1.87 Ga and that the Abingdon terrane

was accreted to the NAC in a similar fashion at ca. 1.70 Ga. Betts et al. (2016) proposed a similar model where three continental ribbons, the eastern belt of the Mount Isa Inlier, the Numil terrane and Abingdon terrane were accreted from Laurentia to the eastern margin of the NAC at ca. 1.88, 1.85 and 1.80 Ga, respectively. Betts et al. (2016) suggested that the eastern margin of the eastern belt of the Mount Isa Inlier was the Gidyea Suture Zone, but Pourteau et al. (2018) reassessed the seismic profile (07GA-IG1, from Korsch et al., 2012) between Mount Isa and Georgetown and suggested this boundary might be closer to the Georgetown Inlier, cross-cutting the Numil terrane of Korsch et al. (2012) and Betts et al. (2016). In this interpretation, the Cudgee Creek granites intrude the upper plate (NAC) which is consistent with the Lu-Hf data from the Cudgee Creek granites which are more like those in the eastern Belt of the Mount Isa Inlier.

From the western Mount Isa Inlier to the Georgetown Inlier there are possibly three (or more) distinct changes identified in the isotopic model ages (ε_{Nd} and ε_{Hf}): 1) The western Mount Isa Inlier has model ages, ca. 2.5 and 2.8 Ga in age (Bierlein et al., 2011; Bierlein and Betts, 2004; Champion, 2013), 2) the eastern Mount Isa Inlier and undercover rocks at-least ~100 km east (Cudgee Creek granites), which may or may not include the western Georgetown Inlier granites (Esmeralda Supersuite) that consist of ca. 2.0 to 2.4 Ga model ages (Figure 5.11 and 5.12); and, 3) the Georgetown Inlier (possibly east of Macartneys Granite and the Numil Seismic Province), that consists of ca. 2.45 to 2.6 Ga models ages. It is proposed that these three different zones of model ages are related to the different terranes accreted to the NAC leading to the Nuna amalgamation. Further investigation is required to verify this.

5.7 Conclusion

New U-Pb ages of ca. 1545 Ma ages (042: 1545.9 ± 3.4 Ma, and 045: 1544.2 ± 3.7 Ma) were obtained for I-type granites sampled from the basement between the Mount Isa and Georgetown inliers, which are similar to ages from the I-type Maramungee Granite of the eastern Mount Isa Inlier. The ε_{Hf} values and the ε_{Hf} two-stage model ages from the basement granites are more similar to those reported from the eastern Mount Isa Inlier than the Georgetown Inlier, suggesting that the eastern Mount Isa Inlier crust extends at-least 100 km eastward of its outcrop extent. It is proposed these newly identified Proterozoic granites be titled the Cudgee Creek granites. The new granite ages from the Georgetown Inlier constrain the age of granite production across the whole inlier to ca. 1.56 Ga. The zircon Lu-Hf data from the Georgetown Inlier granites show differences between the Forsayth Granite in the east to the Esmeralda Supersuite granites in the west. The difference in ε_{Hf} and ε_{Nd} model ages across the eastern margin of the NAC might be related to different terranes accreted to the margin leading to the amalgamation of Nuna.

5.8 References

Baker, M. J., Crawford, A. J., and Withnall, I. W., 2010, Geochemical, Sm–Nd isotopic characteristics and petrogenesis of Paleoproterozoic mafic rocks from the Georgetown Inlier, north Queensland: Implications for relationship with the Broken Hill and Mount Isa Eastern Succession: Precambrian Research, v. 177, no. 1, p. 39-54.

Bennett, V., Jackson, V. A., Rivers, T., Relf, C., Horan, P., and Tubrett, M., 2005, Geology and U Pb geochronology of the Neoarchean Snare River terrane: tracking evolving tectonic regimes and crustal growth mechanisms: Canadian Journal of Earth Sciences, v. 42, no. 6, p. 895-934.

Betts, P. G., Armit, R. J., Stewart, J., Aitken, A. R. A., Ailleres, L., Donchak, P., Hutton, L., Withnall, I. W., and Giles, D., 2016, Australia and Nuna: Geological Society, London, Special Publications, v. 424, p. SP424. 422.

Bierlein, F. P., and Betts, P. G., 2004, The Proterozoic Mount Isa Fault Zone, northeastern Australia: is it really a ca. 1.9 Ga terrane-bounding suture?: Earth and Planetary Science Letters, v. 225, no. 3-4, p. 279-294.

Bierlein, F. P., Maas, R., and Woodhead, J., 2011, Pre-1.8 Ga tectono-magmatic evolution of the Kalkadoon–Leichhardt Belt: implications for the crustal architecture and metallogeny of the Mount Isa Inlier, northwest Queensland, Australia: Australian Journal of Earth Sciences, v. 58, no. 8, p. 887-915.

Black, L. P., Gregory, P., Withnall, I. W., and Bain, J. H. C., 1998, U-Pb zircon age for the Etheridge Group, Georgetown region, north Queensland: Implications for relationship with the Broken Hill and Mt Isa sequences*: Australian Journal of Earth Sciences, v. 45, no. 6, p. 925-935.

Black, L. P., and McCulloch, M. T., 1990, Isotopic evidence for the dependence of recurrent felsic magmatism on new crust formation: an example from the Georgetown region of northeastern Australia: Geochimica et Cosmochimica Acta, v. 54, no. 1, p. 183-196.

Black, L. P., and Withnall, I. W., 1993, The ages of Proterozoic granites in the Georgetown Inlier of northeastern Australia, and their relevance to the dating of tectonothermal events: AGSO Journal of Australian Geology and Geophysics, v. 14, no. 4, p. 331-341.

Black, L. P., Withnall, I. W., Gregory, P., Oversby, B. S., and Bain, J. C., 2005, U–Pb zircon ages from leucogneiss in the Etheridge Group and their significance for the early history of the Georgetown region, north Queensland: Australian Journal of Earth Sciences, v. 52, no. 3, p. 385-401.

Boger, S. D., and Hansen, D., 2004, Metamorphic evolution of the Georgetown Inlier, northeast Queensland, Australia; evidence for an accreted Palaeoproterozoic terrane?: Journal of Metamorphic Geology, v. 22, no. 6, p. 511-527.

Bouvier, A., Vervoort, J. D., and Patchett, P. J., 2008, The Lu–Hf and Sm–Nd isotopic composition of CHUR: constraints from unequilibrated chondrites and implications for the bulk composition of terrestrial planets: Earth and Planetary Science Letters, v. 273, no. 1-2, p. 48-57.

Bowring, S. A., and Podosek, F. A., 1989, Nd isotopic evidence from Wopmay orogen for 2.0–2.4 Ga crust in western North America: Earth and Planetary Science Letters, v. 94, no. 3-4, p. 217-230.

Budd, A. R., Wyborn, L. A. I., and Bastrakova, I. V., 2001, The metallogenic potential of Australian Proterozoic granites: Geoscience Australia, 0642466904.

Champion, D. C., 1991, The felsic granites of far north Queensland [Geology PhD]: Australian National University.

Champion, D. C., 2013, Neodymium depleted mantle model age map of Australia: explanatory notes and user guide, Canberra, Australia, Geoscience Australia, Geoscience Australia Record: 2013/44.

Cihan, M., Evins, P., Lisowiec, N., and Blake, K., 2006, Time constraints on deformation and metamorphism from EPMA dating of monazite in the Proterozoic Robertson River Metamorphics, NE Australia: Precambrian research, v. 145, no. 1, p. 1-23.

Davis, W. J., and Bleeker, W., 1999, Timing of plutonism, deformation, and metamorphism in the Yellowknife Domain, Slave Province, Canada: Canadian Journal of Earth Sciences, v. 36, no. 7, p. 1169-1187.

Etheridge, M. A., Rutland, R. W. R., and Wyborn, L. A. I., 1987, Orogenesis and tectonic process in the Early to Middle Proterozoic of northern Australia: Proterozic Lithospheric Evolution, p. 131-147.

Furlanetto, F., Thorkelson, D. J., Gibson, H. D., Marshall, D. D., Rainbird, R. H., Davis, W. J., Crowley, J. L., and Vervoort, J. D., 2013, Late Paleoproterozoic terrane accretion in northwestern Canada and the case for circum-Columbian orogenesis: Precambrian Research, v. 224, p. 512-528.

Gibson, G. M., Champion, D. C., Withnall, I. W., Neumann, N. L., and Hutton, L. J., 2018, Assembly and breakup of the Nuna supercontinent: Geodynamic

constraints from 1800 to 1600 Ma sedimentary basins and basaltic magmatism in northern Australia: Precambrian Research, v. 313, p. 148-169.

Griffin, W. L., Belousova, E. A., Walters, S. G., and O'Reilly, S. Y., 2006, Archaean and Proterozoic crustal evolution in the Eastern Succession of the Mt Isa district, Australia: U–Pb and Hf-isotope studies of detrital zircons: Australian Journal of Earth Sciences, v. 53, no. 1, p. 125-149.

Hoffman, P. F., 1991, Did the breakout of Laurentia turn Gondwanaland inside-out: Science, v. 252, no. 5011, p. 1409-1412.

Jackson, S. E., Pearson, N. J., Griffin, W. L., and Belousova, E. A., 2004, The application of laser ablation-inductively coupled plasma-mass spectrometry to in situ U–Pb zircon geochronology: Chemical Geology, v. 211, no. 1, p. 47-69.

Kinny, P. D., and Maas, R., 2003, Lu–Hf and Sm–Nd isotope systems in zircon: Reviews in mineralogy and geochemistry, v. 53, no. 1, p. 327-341.

Korsch, R. J., Huston, D. L., Henderson, R. A., Blewett, R. S., Withnall, I. W., Fergusson, C. L., Collins, W. J., Saygin, E., Kositcin, N., and Meixner, A. J., 2012, Crustal architecture and geodynamics of North Queensland, Australia: insights from deep seismic reflection profiling: Tectonophysics, v. 572, p. 76-99.

Lambeck, A., Barovich, K., Gibson, G., Huston, D., and Pisarevsky, S., 2012, An abrupt change in Nd isotopic composition in Australian basins at 1655Ma: Implications for the tectonic evolution of Australia and its place in NUNA: Precambrian Research, v. 208, p. 213-221.

Mark, G., 2001, Nd isotope and petrogenetic constraints for the origin of the Mount Angelay igneous complex: implications for the origin of intrusions in the Cloncurry district, NE Australia: Precambrian Research, v. 105, no. 1, p. 17-35.

Murgulov, V., Beyer, E., Griffin, W. L., O'Reilly, S. Y., Walters, S. G., and Stephens, D., 2007, Crustal evolution in the Georgetown Inlier, North Queensland, Australia: a detrital zircon grain study: Chemical Geology, v. 245, no. 3-4, p. 198-218.

Neumann, N. L., and Kositcin, N., 2011, New SHRIMP U-Pb zircon ages from north Queensland, 2007-2010: Geoscience Australia, 1921954450.

Nordsvan, A. R., Collins, W. J., Li, Z.-X., Spencer, C. J., Pourteau, A., Withnall, I. W., Betts, P. G., and Volante, S., 2018, Laurentian crust in northeast Australia: Implications for the assembly of the supercontinent Nuna: Geology, v. 46, no. 3, p. 251-254.

O'Dea, M. G., Lister, G. S., MacCready, T., Betts, P. G., Oliver, N. H. S., Pound, K. S., Huang, W., and Valenta, R. K., 1997, Geodynamic evolution of the Proterozoic Mount Isa terrain: Geological Society, London, Special Publications, v. 121, no. 1, p. 99-122.

Ootes, L., Davis, W. J., Jackson, V. A., and van Breemen, O., 2015, Chronostratigraphy of the Hottah terrane and Great Bear magmatic zone of Wopmay Orogen, Canada, and exploration of a terrane translation model: Canadian Journal of Earth Sciences, v. 52, no. 12, p. 1062-1092.

Page, R. W., and Sun, S. S., 1998, Aspects of geochronology and crustal evolution in the Eastern Fold Belt, Mt Isa Inlier: Australian Journal of Earth Sciences, v. 45, no. 3, p. 343-361.

Paton, C., Hellstrom, J., Paul, B., Woodhead, J., and Hergt, J., 2011, Iolite: Freeware for the visualisation and processing of mass spectrometric data: Journal of Analytical Atomic Spectrometry, v. 26, no. 12, p. 2508-2518.

Payne, J. L., McInerney, D. J., Barovich, K. M., Kirkland, C. L., Pearson, N. J., and Hand, M., 2016, Strengths and limitations of zircon Lu-Hf and O isotopes in modelling crustal growth: Lithos, v. 248, p. 175-192.

Petrus, J. A., and Kamber, B. S., 2012, VizualAge: A novel approach to laser ablation ICP-MS U-Pb geochronology data reduction: Geostandards and Geoanalytical Research, v. 36, no. 3, p. 247-270.

Pourteau, A., Smit, M. A., Li, Z.-X., Collins, W. J., Nordsvan, A. R., Volante, S., and Li, J., 2018, 1.6 Ga crustal thickening along the final Nuna suture: Geology, v. 46, no. 11, p. 959-962.

Scherer, E., Münker, C., and Mezger, K., 2001, Calibration of the lutetium-hafnium clock: Science, v. 293, no. 5530, p. 683-687.

Stern, R. A., Bodorkos, S., Kamo, S. L., Hickman, A. H., and Corfu, F., 2009, Measurement of SIMS instrumental mass fractionation of Pb isotopes during zircon dating: Geostandards and Geoanalytical Research, v. 33, no. 2, p. 145-168.

van Breemen, O., Davis, W. J., and King, J. E., 1992, Temporal distribution of granitoid plutonic rocks in the Archean Slave Province, northwest Canadian Shield: Canadian Journal of Earth Sciences, v. 29, no. 10, p. 2186-2199.

Vermeesch, P., 2018, IsoplotR: A free and open toolbox for geochronology: Geoscience Frontiers, v. 9, no. 5, p. 1479-1493.

Wiedenbeck, M., Alle, P., Corfu, F., Griffin, W. L., Meier, M., Oberli, F. v., Quadt, A. v., Roddick, J. C., and Spiegel, W., 1995, Three natural zircon standards for U-Th-Pb, Lu-Hf, trace element and REE analyses: Geostandards newsletter, v. 19, no. 1, p. 1-23.

Withnall, I. W., Bain, J. H. C., Draper, J. J., MacKenzie, D. E., and Oversby, B. S., 1988, Proterozoic stratigraphy and tectonic history of the Georgetown Inlier, northeastern Queensland: Precambrian Research, v. 40, p. 429-446.

Withnall, I. W., and Henderson, R. A., 2012, Accretion on the long-lived continental margin of northeastern Australia: Episodes, v. 35, no. 1, p. 166-176.

Withnall, I. W., and Hutton, L. J., 2013, Proterozoic–North Australian Craton, *in* Jell, P. A., ed., Geology of Queensland: Brisbane, Australia, Geological Survey of Queensland, p. 23-112.

.

Chapter 6: Conclusion

Proterozoic rocks in NE Australia have a strong affinity to Laurentia. The Georgetown Inlier (along with Coen, Dargalong and Yambo) is the most north-easterly Proterozoic terrain in Australia and detrital zircon from ca. 1.7 to 1.65 Ga sediments in the inlier are similar to those deposited in Laurentia during the same period and contrast with sediments deposited at the same time in the Mount Isa Inlier. Up-sequence there is a provenance shift, and sediments have a unimodal ca. 1655 Ma detrital zircon population attributed to a proximal volcanic arc, likely correlative with Bonnetia Arc (Nielsen et al., 2013).

One possible tectonic model is that roll-back of the subduction zone associated with this arc system rifted the Georgetown Inlier from the western margin of Laurentia. The Georgetown Inlier then collided with Australia during the ca. 1.6 Ga Isan Orogen at the final stages of Nuna amalgamation. Evidence for this putative subduction zone in Laurentia either does not exist or is cryptic. Alternatively, subduction only occurred at the Australian margin and the Georgetown Inlier was a rifted block from the passive margin of Laurentia. In this alternative model, the ca. 1655 Ma zircon population noted in the upper Etheridge Group is not related to a proximal arc and would need further explanation. Either way, the Georgetown Inlier is a piece of Laurentian crust. But how far does the Laurentian crust extend westward into Australia?

Paleo- to Mesoproterozoic sedimentary rocks in the Mount Isa Inlier, previously thought to correlate across different structural domains, have been used as evidence

to argue they were deposited at a passive margin (or back-arc basin) deepening to the east. However, no detailed sedimentological data has been presented to support this hypothesis, and sedimentological data, such as facies and paleocurrent analysis reported from the eastern belt of the inlier, contradicts this model (Beardsmore et al., 1988; Laing and Beardsmore, 1986; Hatton, 2004). In chapter four, evidence is provided to show that deposition of the Mary Kathleen Group in the central belt was associated with N-S extension. Most recent tectonic models (Betts et al., 2016, Gibson et al., 2018, 2019) developed to explain the Mount Isa Inlier tectonic evolution overlook N-S extension in favour of E-W extension. While E-W extension is significant in the Mount Isa Inlier, N-S directed extension should be accounted for in any tectonic model. The N-S directed extension identified in the Mary Kathleen Domain likely correlates with the Myally Supersequence of the western belt, which correlates with a period of N-S directed extension in the McArthur Basin, and was likely associated with roll-back of a north-dipping subduction zone in central Australia (Giles et al., 2002; Scott et al., 2000). Nevertheless, evidence for N-S extensional events that correlate with the events described in the western and central belts have not been widely reported from the eastern belt of the Mount Isa Inlier.

In addition, new detrital zircon data and contrasting stratigraphy (chapter 4), along with differences in volcanic ages suggest that the eastern Mount Isa Inlier evolved independently of the NAC and might be an allochthonous terrane. Structural complexities in the Mitakoodi Domain of the eastern belt impede understanding the complete basin evolution of the Malbon Group. However, the stratigraphy is notably different from the Leichhardt Superbasin sediments in the western belt that they are

proposed to be correlative with (Chapter 4). The ca. 2.58 Ga detrital zircon population observed in every Malbon Group sample collected during this study (or from any previous study) cannot be accounted for in any source rock in Australia. Furthermore, this population is rarely observed in any Proterozoic sedimentary rocks across the NAC. A possible source terrane could be Laurentia. Both the Slave and Rae cratons of northern Canada have abundant ca. 2.58 Ga source rocks. Furthermore, these Laurentia cratons are the most likely source terranes for the lower Etheridge Group sediments in the Georgetown Inlier. Nonetheless, if the eastern belt of the Mount Isa Inlier is an allochthonous terrane then understanding its origin is related to the tectonic significance of pre-1.85 Ga Barramundi Orogeny.

The oldest rocks observed in the Mount Isa Inlier are related to the ca. 1.9 to 1.85 Ga Barramundi Orogeny, which is characterised by a significant northeast–southwest to east–west compressive events that can be observed across multiple terranes in northern Australia (Etheridge et al., 1987). However, the tectonic significance of the Barramundi Orogeny is poorly understood. One possibility is that the Barramundi Orogeny correlates with the similarly aged Wopmay orogen of NW Canada and represents a collision between Australia and Laurentia. If so, the eastern Mount Isa Inlier (terrane) represents crust generated between Laurentia and Australia leading to this Barramundi aged collisional event. Following the collision, Australia and Laurentia have to separate to accommodate ca. 1.75 Ga passive margin sedimentation in western Laurentia (i.e. Wernecke Supergroup, Muskwa Assemblage, etc.), and by ca. 1.8 Ga sedimentation in eastern Australia (the Mount Isa Inlier superbasins). During post-Barramundi rifting, the eastern belt (Mount Isa

Inlier) remains part of Laurentia and accommodates the Malbon Group sedimentation. The eastern belt would then be amalgamated either during the ca. 1.74 Ga east-west compressional event recorded across the whole Mount Isa Inlier or at ca. 1.6 Ga during the Isan Orogeny.

The alternative explanation is that the Barramundi Orogeny, rather than representing a collision with Laurentia, signifies a terrane accretion event. Indeed, the evidence for subduction in the whole-rock geochemistry from ca. 1.85 Ga igneous rocks from both the western fold belt and the Kalkadoon-Leichhardt Belt (central belt, Mount Isa Inlier), suggests that arc magmatism occurred relatively quickly following the ca. 1.87 to 1.85 Ga Barramundi Orogeny (Bierlein et al., 2011; Bierlein et al., 2008). In this case, if the Barramundi Orogen represents a terrane accretion event, then it would require a terrane to have collided with the NAC. Previously, both the central and eastern belts of the Mount Isa Inlier, or allochthonous terranes further east (i.e. Numil Seismic Province) have been proposed to have collided with the NAC during the Barramundi Orogeny. Bierlein and Betts (2004) demonstrated that basement rocks in the western belt of the Mount Isa Inlier have the same densities as basement rocks from elsewhere in the NAC, suggesting they are likely the same crust. Moreover, Bierlein et al. (2011) established that the western and central belts of the Mount Isa Inlier consist of the same basement rocks and that their pre-1.8 Ga tectonic evolution was similar. In contrast to the western and central belts of the Mount Isa Inlier, ε_{Hf} and ε_{Nd} two-stage model ages from the eastern belt indicate comprising of younger basement rocks (Bierlein et al., 2011; Bierlein et al., 2008; Champion, 2013; Griffin et al., 2006; Mark, 2001; Page and Sun, 1998). This led several authors to

suggest that the eastern belt of the Mount Isa Inlier is allochthonous and that it might have collided with the NAC during the Barramundi Orogeny (Betts et al., 2016; Bierlein et al., 2011; Laing and Beardsmore, 1986; Page and Sun, 1998). However, the data presented in chapter 4 suggests that the eastern belt of the Mount Isa Inlier was allochthonous during deposition of the Malbon Group at ca. 1.75 Ga. Therefore, if the Barramundi Orogeny represents a terrane accretion event, rather than being a collision between the eastern belt of the Mount Isa Inlier and the NAC, it would have been between the NAC and the central belt of the inlier (the Kalkadoon-Leichhardt Domain). To account for the similarities between the NAC and the central belt, it is possible the central belt was rifted away during subduction roll-back and reaccreted later during the Barramundi Orogeny ca. 1.87 to 1.85 Ga (Bierlein et al., 2011). Thus, the eastern belt of the Mount Isa Inlier would represent a piece of Laurentian crust, probably transferred to Australia in a similar fashion to that of the Georgetown Inlier (Chapter 3).

In either scenario, it is likely the eastern belt of the Mount Isa Inlier was allochthonous during deposition of the Malbon Group ca. 1.75 Ga (chapter 4). Post ca. 1.75 Ga there are two major east-west directed shortening events recognised across the Mount Isa Inlier that might reflect the amalgamation between the eastern belt with the central and western belts of the inlier. The most probable event is the ca. 1.74 to 1.71 Ga Big event (Blaikie et al., 2017). If the eastern belt was amalgamated with the rest of the Mount Isa Inlier (and the NAC) during this event, then the sediments deposited afterwards should be correlative across the Mount Isa Inlier. While there are depositional models that suggest the Calvert and Isa superbasins correlate across the

whole inlier (Neumann et al., 2009; Southgate et al., 2013), only minor sedimentological work has been done in the eastern belt to support this (Hatton, 2004). Furthermore, detrital zircon geochronology from the western and eastern belts notably different and the timing of deposition is ambiguous during both the Calvert and Isa superbasins (Neumann et al., 2009). Nevertheless, if current depositional models (Southgate et al., 2013) for the Calvert and Isa superbasins are correct, and the sedimentary systems correlate across the whole inlier, then they constrain the timing of amalgamation between the eastern belt of the Mount Isa Inlier and the NAC between ca. 1.75 and 1.72 Ga, the timing of the Big Event (Blaikie et al., 2017).

The extent to which the eastern belt of the Mount Isa Inlier might extend towards the east is uncertain. Both Korsch et al. (2012) and Betts et al. (2016) suggested that the eastern boundary of Mount Isa Inlier is the Gudiya Suture, a crustal-scale break imaged in seismic and other geophysical datasets, interpreted as a suture zone that marked the amalgamation of the Numil seismic province with the NAC pre-1.80 Ga. Nevertheless, two-stage model ages from ε_{Hf} in zircon from the ca. 1.54 Ga Cudgee Creek granites intruding the basement (Numil seismic province) east of the Gudiya Suture between Mount Isa and Georgetown inliers are the same as whole-rock ε_{Nd} two-stage model ages from the ca. 1.54 Ga Maramungee Granite of the eastern belt of the Mount Isa Inlier. While not conclusive this suggests that the eastern part of the Mount Isa Inlier terrane might extent much further east then the location of the Gudiya Suture, closer to the Georgetown Inlier.

To advance our understanding of the tectonic evolution of Proterozoic NE Australia and the amalgamation of Nuna the following needs to be further evaluated: 1) Further structural, metamorphic and geochemistry work needs to be done on the Barramundi Orogeny to fully comprehend its importance. If the Barramundi Orogeny truly represents an early attempt at Nuna amalgamation or if it was just a terrane accretion event is not entirely clear. Both scenarios have implications of the post-1.8 Ga evolution of NE Australia and global geodynamics; 2) To reevaluate the Gudiya Suture and clarify the position of potential sutures considering the Laurentia affinity of the eastern Mount Isa Inlier and the Georgetown Inlier; both the geophysical data and the seismic profiles across NE Australia need should be reprocessed; 3) Additional zircon isotopic data should be obtained from the Mount Isa Inlier granites of all ages, but most importantly those from the ca. 1.55 to 1.50 Ga Williams Supersuite. This data will not only test the Laurentia affinity of the eastern Mount Isa Inlier but should also assist in clarifying the crustal evolution of the inlier, in comparison with the Georgetown Inlier; 4) It is recommended that the Calvert and Isan aged sediments in the eastern belt of the Mount Isa Inlier are re-evaluated based on this new information, and their relationship with the studies from western and central belt sediments resolved (Jackson et al., 2000; Jackson and Southgate, 2000; Jackson et al., 2005; Page et al., 2000; Southgate et al., 2000). It would be intriguing to re-evaluate the Myally Supersequence in the western belt of the inlier and the Soldiers Cap Group in the eastern belt.

6.1 References

Beardsmore, T., Newbery, S., and Laing, W., 1988, The Maronan Supergroup: an inferred early volcanosedimentary rift sequence in the Mount Isa Inlier, and its implications for ensialic rifting in the Middle Proterozoic of northwest Queensland: Precambrian Research, v. 40, p. 487-507.

Betts, P. G., Armit, R. J., Stewart, J., Aitken, A. R. A., Ailleres, L., Donchak, P., Hutton, L., Withnall, I. W., and Giles, D., 2016, Australia and Nuna: Geological Society, London, Special Publications, v. 424, p. SP 424-422.

Bierlein, F., Maas, R., and Woodhead, J., 2011, Pre-1.8 Ga tectono-magmatic evolution of the Kalkadoon–Leichhardt Belt: implications for the crustal architecture and metallogeny of the Mount Isa Inlier, northwest Queensland, Australia: Australian Journal of Earth Sciences, v. 58, no. 8, p. 887-915.

Bierlein, F. P., and Betts, P. G., 2004, The Proterozoic Mount Isa Fault Zone, northeastern Australia: is it really a ca. 1.9 Ga terrane-bounding suture?: Earth and Planetary Science Letters, v. 225, no. 3-4, p. 279-294.

Bierlein, F. P., Black, L. P., Hergt, J., and Mark, G., 2008, Evolution of Pre-1.8 Ga basement rocks in the western Mt Isa Inlier, northeastern Australia—insights from SHRIMP U–Pb dating and in-situ Lu–Hf analysis of zircons: Precambrian Research, v. 163, no. 1-2, p. 159-173.

Blaikie, T., Betts, P., Armit, R., and Ailleres, L., 2017, The ca. 1740–1710 Ma Leichhardt Event: Inversion of a continental rift and revision of the tectonic evolution of the North Australian Craton: Precambrian Research, v. 292, p. 75-92.

Borg, S. G., and DePaolo, D. J., 1994, Laurentia, Australia, and Antarctica as a Late Proterozoic supercontinent: constraints from isotopic mapping: Geology, v. 22, no. 4, p. 307-310.

Champion, D. C., 2013, Neodymium depleted mantle model age map of Australia: explanatory notes and user guide, Geoscience Australia.

Etheridge, M., Rutland, R., and Wyborn, L., 1987, Orogenesis and tectonic process in the Early to Middle Proterozoic of northern Australia: Proterozoic Lithospheric Evolution, p. 131-147.

Giles, D., Betts, P. G., and Lister, G. S., 2002, Far-field continental backarc setting for the 1.80–1.67 Ga basins of northeastern Australia: Geology, v. 30, no. 9, p. 823-826.

Griffin, W., Belousova, E., Walters, S., and O'Reilly, S., 2006, Archaean and Proterozoic crustal evolution in the Eastern Succession of the Mt Isa district, Australia: U–Pb and Hf-isotope studies of detrital zircons: Australian Journal of Earth Sciences, v. 53, no. 1, p. 125-149.

Jackson, M., Scott, D., and Rawlings, D., 2000, Stratigraphic framework for the Leichhardt and Calvert Superbasins: review and correlations of the pre-1700 Ma successions between Mt Isa and McArthur River: Australian Journal of Earth Sciences, v. 47, no. 3, p. 381-403.

Jackson, M., and Southgate, P., 2000, Evolution of three unconformity-bounded sandy carbonate successions in the McArthur River region of northern Australia: The Lawn, Wide and Doom Supersequences in a proximal part of the Isa Superbasin: Australian Journal of Earth Sciences, v. 47, no. 3, p. 625-635.

Jackson, M., Southgate, P., Black, L., Blake, P., and Domagala, J., 2005, Overcoming Proterozoic quartzite sand-body miscorrelations: integrated sequence stratigraphy and SHRIMP U–Pb dating of the Surprise Creek Formation, Torpedo Creek and Warrina Park Quartzites, Mt Isa Inlier: Australian Journal of Earth Sciences, v. 52, no. 1, p. 1-25.

Korsch, R., Huston, D., Henderson, R., Blewett, R., Withnall, I., Fergusson, C. L., Collins, W. J., Saygin, E., Kositcin, N., and Meixner, A., 2012, Crustal architecture and geodynamics of North Queensland, Australia: insights from deep seismic reflection profiling: Tectonophysics, v. 572, p. 76-99.

Laing, W., and Beardsmore, T., Stratigraphic rationalisation of the eastern Mount Isa block, recognition of key correlations with Georgetown and Broken Hill Blocks in an Eastern Australian Proterozoic terrain, and their metallogenic implications, in Proceedings Geological Society of Australia Abstracts1986, Volume 15, p. 114-115.

Mark, G., 2001, Nd isotope and petrogenetic constraints for the origin of the Mount Angelay igneous complex: implications for the origin of intrusions in the Cloncurry district, NE Australia: Precambrian Research, v. 105, no. 1, p. 17-35.

Neumann, N. L., Southgate, P. N., and Gibson, G. M., 2009, Defining unconformities in Proterozoic sedimentary basins using detrital geochronology and basin analysis—An example from the Mount Isa Inlier, Australia: Precambrian Research, v. 168, no. 3, p. 149-166.

Nielsen, A. B., Thorkelson, D. J., Gibson, H. D., and Marshall, D. D., 2013, The Wernecke igneous clasts in Yukon, Canada: fragments of the Paleoproterozoic volcanic arc terrane Bonnetia: Precambrian Research, v. 238, p. 78-92.

Page, R. W., Jackson, M. J., and Krassay, A. A., 2000, Constraining sequence stratigraphy in north Australian basins: SHRIMP U–Pb zircon geochronology between Mt Isa and McArthur River: Australian Journal of Earth Sciences, v. 47, no. 3, p. 431-459.

Page, R. W., and Sun, S. S., 1998, Aspects of geochronology and crustal evolution in the Eastern Fold Belt, Mt Isa Inlier: Australian Journal of Earth Sciences, v. 45, no. 3, p. 343-361.

Scott, D., Rawlings, D., Page, R., Tarlowski, C., Idnurm, M., Jackson, M., and Southgate, P., 2000, Basement framework and geodynamic evolution of the Palaeoproterozoic superbasins of north-central Australia: An integrated review of geochemical, geochronological and geophysical data: Australian Journal of Earth Sciences, v. 47, no. 3, p. 341-380.

Southgate, P., Scott, D., Sami, T., Domagala, J., Jackson, M., James, N., and Kyser, T., 2000, Basin shape and sediment architecture in the Gun Supersequence: a strike-slip model for Pb–Zn–Ag ore genesis at Mt Isa: Australian Journal of Earth Sciences, v. 47, no. 3, p. 509-531.

Chapter 7: Bibliography

Abbott, S. T., and Sweet, I. P., 2000, Tectonic control on third-order sequences in a siliciclastic ramp-style basin: an example from the Roper Superbasin (Mesoproterozoic), northern Australia: Australian Journal of Earth Sciences, v. 47, no. 3, p. 637-657.

Abbott, S. T., Sweet, I. P., Plumb, K. A., Young, D. A., Cutovinos, A., Ferenczi, P. A., Brakel, A. T., and Pietsch, B. A., 2001, Roper Region: Urapunga - Roper River, Northern Territory: combined explanatory notes.

Ahmad, M., Dunster, J. N., and Munson, T. J., 2013, Chapter 15: McArthur Basin, *in* M, A., and T.J., M., eds., Geology and mineral resources of the Northern Territory, Volume 5: Darwin, Australia, Northern Territory Geological Survey: Special Publication.

Alonso-Torres, D., Beauchamp, B., Guest, B., Hadlari, T., and Matthews, W., 2018, Late Paleozoic to Triassic arc magmatism north of the Sverdrup Basin in the Canadian Arctic: Evidence from detrital zircon U-Pb geochronology: Lithosphere, v. 10, no. 3, p. 426-445.

Armistead, S. E., Collins, A. S., Payne, J. L., Foden, J. D., De Waele, B., Shaji, E., and Santosh, M., 2018, A re-evaluation of the Kumta Suture in western peninsular India and its extension into Madagascar: Journal of Asian Earth Sciences, v. 157, p. 317-328.

Bain, J. H. C., Heinrich, C. A., and Henderson, G. A. M., 1992, Stratigraphy, structure, and metasomatism of the Haslingden Group, east Moondarra area, Mount Isa: a deformed and mineralised Proterozoic multistage rift-sag sequence, *in* Stewart, A. J., and Blake, D. H., eds., Detailed Studies of the Mount Isa Inlier, Volume 243: Canberra, Australia, AGSO Bulletin, p. 125-136.

Baker, M. J., Crawford, A. J., and Withnall, I. W., 2010, Geochemical, Sm–Nd isotopic characteristics and petrogenesis of Paleoproterozoic mafic rocks from the Georgetown Inlier, north Queensland: Implications for relationship with the Broken Hill and Mount Isa Eastern Succession: Precambrian Research, v. 177, no. 1, p. 39-54.

Barham, M., Kirkland, C. L., and Hollis, J., 2019, Spot the difference: Zircon disparity tracks crustal evolution: Geology, v. 47, no. 5, p. 435–439.

Beardsmore, T. J., Newbery, S. P., and Laing, W. P., 1988, The Maronan Supergroup: an inferred early volcanosedimentary rift sequence in the Mount Isa Inlier, and its implications for ensialic rifting in the Middle Proterozoic of northwest Queensland: Precambrian Research, v. 40, p. 487-507.

Bell, R. T., and Jefferson, C. W., An hypothesis for an Australian-Canadian connection in the Late Proterozoic and the birth of the Pacific Ocean, *in* Proceedings Proceedings, Pacific Rim Congress1987, Volume 87, p. 39-50.

Bennett, V., Jackson, V. A., Rivers, T., Relf, C., Horan, P., and Tubrett, M., 2005, Geology and U Pb geochronology of the Neoarchean Snare River terrane: tracking evolving tectonic regimes and crustal growth mechanisms: Canadian Journal of Earth Sciences, v. 42, no. 6, p. 895-934.

Bennett, V. C., and DePaolo, D. J., 1987, Proterozoic crustal history of the western United States as determined by neodymium isotopic mapping: Geological Society of America Bulletin, v. 99, no. 5, p. 674-685.

Betts, P. G., Armit, R. J., Stewart, J., Aitken, A. R. A., Ailleres, L., Donchak, P., Hutton, L., Withnall, I. W., and Giles, D., 2016, Australia and Nuna: Geological Society, London, Special Publications, v. 424, p. SP424. 422.

Betts, P. G., and Giles, D., 2006, The 1800–1100 Ma tectonic evolution of Australia: Precambrian Research, v. 144, no. 1-2, p. 92-125.

Betts, P. G., Giles, D., Mark, G., Lister, G. S., Goleby, B. R., and Ailleres, L., 2006, Synthesis of the Proterozoic evolution of the Mt Isa Inlier: Australian Journal of Earth Sciences, v. 53, no. 1, p. 187-211.

Betts, P. G., Giles, D., and Schaefer, B. F., 2008, Comparing 1800–1600Ma accretionary and basin processes in Australia and Laurentia: possible geographic connections in Columbia: Precambrian Research, v. 166, no. 1, p. 81-92.

Beyer, E. E., Hollis, J. A., Whelan, J. A., Glass, L. M., Donnellan, N., Yaxley, G., Armstrong, R., Allen, C., and Scherstén, A., 2012, Summary of results. NTGS

laser ablation ICPMS and SHRIMP U-Pb, Hf and O geochronology project: Pine Creek Orogen, Arunta Region, Georgina Basin and McArthur Basin, July 2008–May 2011.

Bickford, M. E., and Hill, B. M., 2007, Does the arc accretion model adequately explain the Paleoproterozoic evolution of southern Laurentia?: An expanded interpretation: Geology, v. 35, no. 2, p. 167-170.

Bierlein, F. P., and Betts, P. G., 2004, The Proterozoic Mount Isa Fault Zone, northeastern Australia: is it really a ca. 1.9 Ga terrane-bounding suture?: Earth and Planetary Science Letters, v. 225, no. 3-4, p. 279-294.

Bierlein, F. P., Maas, R., and Woodhead, J., 2011, Pre-1.8 Ga tectono-magmatic evolution of the Kalkadoon–Leichhardt Belt: implications for the crustal architecture and metallogeny of the Mount Isa Inlier, northwest Queensland, Australia: Australian Journal of Earth Sciences, v. 58, no. 8, p. 887-915.

Black, L. P., Gregory, P., Withnall, I. W., and Bain, J. H. C., 1998, U-Pb zircon age for the Etheridge Group, Georgetown region, north Queensland: Implications for relationship with the Broken Hill and Mt Isa sequences*: Australian Journal of Earth Sciences, v. 45, no. 6, p. 925-935.

Black, L. P., and McCulloch, M. T., 1990, Isotopic evidence for the dependence of recurrent felsic magmatism on new crust formation: an example from the Georgetown region of northeastern Australia: Geochimica et Cosmochimica Acta, v. 54, no. 1, p. 183-196.

Black, L. P., and Withnall, I. W., 1993, The ages of Proterozoic granites in the Georgetown Inlier of northeastern Australia, and their relevance to the dating of tectonothermal events: AGSO Journal of Australian Geology and Geophysics, v. 14, no. 4, p. 331-341.

Black, L. P., Withnall, I. W., Gregory, P., Oversby, B. S., and Bain, J. C., 2005, U–Pb zircon ages from leucogneiss in the Etheridge Group and their significance for the early history of the Georgetown region, north Queensland: Australian Journal of Earth Sciences, v. 52, no. 3, p. 385-401.

Blaikie, T. N., Betts, P. G., Armit, R. J., and Ailleres, L., 2017, The ca. 1740–1710 Ma Leichhardt Event: Inversion of a continental rift and revision of the tectonic evolution of the North Australian Craton: Precambrian Research, v. 292, p. 75-92.

Blair, T. C., 1987, Tectonic and hydrologic controls on cyclic alluvial fan, fluvial, and lacustrine rift-basin sedimentation, Jurassic-Lowermost Cretaceous Todos Santos Formation, Chiapas, Mexico: Journal of Sedimentary Research, v. 57, no. 5, p. 845-862.

Blake, D. H., 1987, Geology of the Mount Isa inlier and environs, Queensland and Northern Territory, Australian Govt. Pub. Service.

Blake, D. H., 1996, Structural interpretations of the Wonga Belt in the Proterozoic Mount Isa Inlier of northwest Queensland-A review: AGSO Journal of Australian Geology and Geophysics, v. 16, no. 4, p. 609.

Blake, D. H., and Stewart, A. J., 1992, Stratigraphic and tectonic framework, Mount Isa inlier, *in* Stewart, A. J., and Blake, D. H., eds., Detailed study of the Mount Isa Inlier, Volume 243: Canberra, Australia, AGSO Bulletin, p. 1-12.

Blichert-Toft, J., and Albarède, F., 1997, The Lu-Hf isotope geochemistry of chondrites and the evolution of the mantle-crust system: Earth and Planetary Science Letters, v. 148, no. 1-2, p. 243-258.

Boger, S. D., and Hansen, D., 2004, Metamorphic evolution of the Georgetown Inlier, northeast Queensland, Australia; evidence for an accreted Palaeoproterozoic terrane?: Journal of Metamorphic Geology, v. 22, no. 6, p. 511-527.

Borg, I., and Groenen, P., 2003, Modern multidimensional scaling: Theory and applications: Journal of Educational Measurement, v. 40, no. 3, p. 277-280.

Borg, S. G., and DePaolo, D. J., 1994, Laurentia, Australia, and Antarctica as a Late Proterozoic supercontinent: constraints from isotopic mapping: Geology, v. 22, no. 4, p. 307-310.

Bouvier, A., Vervoort, J. D., and Patchett, P. J., 2008, The Lu–Hf and Sm–Nd isotopic composition of CHUR: constraints from unequilibrated chondrites and

implications for the bulk composition of terrestrial planets: Earth and Planetary Science Letters, v. 273, no. 1-2, p. 48-57.

Bowring, S. A., and Podosek, F. A., 1989, Nd isotopic evidence from Wopmay orogen for 2.0–2.4 Ga crust in western North America: Earth and Planetary Science Letters, v. 94, no. 3-4, p. 217-230.

Budd, A. R., Wyborn, L. A. I., and Bastrakova, I. V., 2001, The metallogenic potential of Australian Proterozoic granites: Geoscience Australia, 0642466904.

Bull, S. W., and Rogers, J. R., Recognition and significance of an early compressional deformation event in the Tawallah Group, McArthur Basin, NT, *in* Proceedings MIC'96: New developments in metallogenic research1996, Volume 55, p. 28-32.

Carson, C., 2013, GA Sample No - 1987412: Geoscience Australia Geochron Delivery System, Geoscience Australia.

Carson, C. J., Hutton, L. J., Withnall, I. W., and Perkins, W. G., 2008, Joint GSQ-GA-NGA geochronology project Mount Isa region, 2007–2008: Geological Survey of Queensland.

Catuneanu, O., 2006, Principles of sequence stratigraphy, Amsterdam, The Netherlands, Elsevier Science, v. 1st, 386 p.:

Champion, D. C., 1991, The felsic granites of far north Queensland [Geology PhD]: Australian National University.

Champion, D. C., 2013, Neodymium depleted mantle model age map of Australia: explanatory notes and user guide, Canberra, Australia, Geoscience Australia, Geoscience Australia Record: 2013/44.

Chorowicz, J., 2005, The east African rift system: Journal of African Earth Sciences, v. 43, no. 1-3, p. 379-410.

Cihan, M., Evins, P., Lisowiec, N., and Blake, K., 2006, Time constraints on deformation and metamorphism from EPMA dating of monazite in the Proterozoic Robertson River Metamorphics, NE Australia: Precambrian Research, v. 145, no. 1, p. 1-23.

Collins, W. J., and Shaw, R. D., 1995, Geochronological constraints on orogenic events in the Arunta Inlier: a review: Precambrian Research, v. 71, no. 1-4, p. 315-346.

Cox, T. F., and Cox, M. A. A., 2000, Multidimensional scaling, Boca Raton, FL, Chapman and Hall/CRC.

Dalziel, I. W., 1991, Pacific margins of Laurentia and East Antarctica-Australia as a conjugate rift pair: Evidence and implications for an Eocambrian supercontinent: Geology, v. 19, no. 6, p. 598-601.

Davis, B. J., Berman, R. G., Nadeau, L., and Percival, J. A., 2014, U-Pb Zircon Geochronology of a Transect Across Thelon Tectonic Zone, Queen Maud Region, and Adjacent Rae Craton, Kitikmeot Region, Nunavut: Natural Resources Canada.

Davis, B. J., Pehrsson, S. J., and Percival, J. A., 2015, Results of a U-Pb zircon geochronology transect across the southern Rae craton, Northwest Territories, Canada: Geological Survey of Canada.

Davis, W. J., and Bleeker, W., 1999, Timing of plutonism, deformation, and metamorphism in the Yellowknife Domain, Slave Province, Canada: Canadian Journal of Earth Sciences, v. 36, no. 7, p. 1169-1187.

Day, R. W., 1983, Queensland Geology: A companion volume to the 1: 2,500,000 scale geological map (1975), Geological Survey of Queensland, v. 383.

De Leeuw, J., and Meulman, J., 1986, A special jackknife for multidimensional scaling: Journal of Classification, v. 3, no. 1, p. 97-112.

Derrick, G. M., Wilson, I. H., and Hill, R. M., 1976, Revision of stratigraphic nomenclature in the Precambrian of northwestern Queensland, IV: Malbon Group: Queensl. Gov. Min. J., v. 77, p. 515-517.

Derrick, G. M., Wilson, I. H., and Sweet, I. P., 1980, The Quilalar and Surprise Creek Formations—new Proterozoic units from the Mount Isa inlier: Their regional sedimentology and application to regional correlation: BMR Journal of Australian Geology & Geophysics, v. 5, p. 215-223.

Doe, M. F., Jones, J. V., Karlstrom, K. E., Dixon, B., Gehrels, G., and Pecha, M., 2013, Using detrital zircon ages and Hf isotopes to identify 1.48–1.45 Ga sedimentary basins and fingerprint sources of exotic 1.6–1.5 Ga grains in southwestern Laurentia: Precambrian Research, v. 231, p. 409-421.

Doe, M. F., Jones, J. V., Karlstrom, K. E., Thrane, K., Frei, D., Gehrels, G., and Pecha, M., 2012, Basin formation near the end of the 1.60–1.45 Ga tectonic gap in southern Laurentia: Mesoproterozoic Hess Canyon Group of Arizona and implications for ca. 1.5 Ga supercontinent configurations: Lithosphere, v. 4, no. 1, p. 77-88.

Domagala, J., Southgate, P. N., McConachie, B. A., and Pidgeon, B. A., 2000, Evolution of the Palaeoproterozoic Prize, Gun and lower Loretta Supersequences of the Surprise Creek Formation and Mt Isa Group: Australian Journal of Earth Sciences, v. 47, no. 3, p. 485-507.

Eglington, B. M., Pehrsson, S. J., Ansdell, K. M., Lescuyer, J.-L., Quirt, D., Milesi, J.-P., and Brown, P., 2013, A domain-based digital summary of the evolution of the Palaeoproterozoic of North America and Greenland and associated unconformity-related uranium mineralization: Precambrian Research, v. 232, p. 4-26.

Eriksson, K. A., Simpson, E. L., and Jackson, M. J., 1994, Stratigraphical Evolution of a Proterozoic Syn-Rift to Post-Rift Basin: Constraints on the Nature of Lithospheric Extension in the Mount Isa Inlier, Australia, *in* A, F. K., and J, S. R., eds., Tectonic controls and signatures in sedimentary successions: London, UK, The International Association of Sedimentologists, p. 203-221.

Etheridge, M. A., Rutland, R. W. R., and Wyborn, L. A. I., 1987, Orogenesis and tectonic process in the Early to Middle Proterozoic of northern Australia: Proterozoic Lithospheric Evolution, p. 131-147.

Evans, D. A. D., and Mitchell, R. N., 2011, Assembly and breakup of the core of Paleoproterozoic–Mesoproterozoic supercontinent Nuna: Geology, v. 39, no. 5, p. 443-446.

Fedo, C. M., Sircombe, K. N., and Rainbird, R. H., 2003, Detrital zircon analysis of the sedimentary record: Reviews in Mineralogy and Geochemistry, v. 53, no. 1, p. 277-303.

Foster, D. A., Mueller, P. A., Mogk, D. W., Wooden, J. L., and Vogl, J. J., 2006, Proterozoic evolution of the western margin of the Wyoming craton: Implications for the tectonic and magmatic evolution of the northern Rocky Mountains: Canadian Journal of Earth Sciences, v. 43, no. 10, p. 1601-1619.

Foster, D. R. W., and Austin, J. R., 2008, The 1800–1610 Ma stratigraphic and magmatic history of the Eastern Succession, Mount Isa Inlier, and correlations with adjacent Paleoproterozoic terranes: Precambrian Research, v. 163, no. 1-2, p. 7-30.

Furlanetto, F., Thorkelson, D. J., Gibson, H. D., Marshall, D. D., Rainbird, R. H., Davis, W. J., Crowley, J. L., and Vervoort, J. D., 2013, Late Paleoproterozoic terrane accretion in northwestern Canada and the case for circum-Columbian orogenesis: Precambrian Research, v. 224, p. 512-528.

Furlanetto, F., Thorkelson, D. J., Rainbird, R. H., Davis, W. J., Gibson, H. D., and Marshall, D. D., 2016, The Paleoproterozoic Wernecke Supergroup of Yukon, Canada: Relationships to orogeny in northwestern Laurentia and basins in North America, East Australia, and China: Gondwana Research, v. 39, p. 14-40.

Gehrels, G., 2011, Detrital zircon U-Pb geochronology: Current methods and new opportunities, Tectonics of sedimentary basins: Recent advances, Blackwell Publishing Ltd, p. 45-62.

-, 2014, Detrital zircon U-Pb geochronology applied to tectonics: Annual Review of Earth and Planetary Sciences, v. 42, p. 127-149.

Gibson, G. M., Champion, D. C., Withnall, I. W., Neumann, N. L., and Hutton, L. J., 2018, Assembly and breakup of the Nuna supercontinent: Geodynamic constraints from 1800 to 1600 Ma sedimentary basins and basaltic magmatism in northern Australia: Precambrian Research, v. 313, p. 148-169.

Gibson, G. M., Henson, P. A., Neumann, N. L., Southgate, P. N., and Hutton, L. J., 2012, Paleoproterozoic-earliest Mesoproterozoic basin evolution in the Mount Isa region, northern Australia and implications for reconstructions of the Nuna and Rodinia supercontinents: Episodes, v. 35, no. 1, p. 131-141.

Gibson, G. M., Hutton, L. J., and Holzschuh, J., 2017, Basin inversion and supercontinent assembly as drivers of sediment-hosted Pb–Zn mineralization in the Mount Isa region, northern Australia: Journal of the Geological Society, p. jgs2016-2105.

Gibson, G. M., Rubenach, M. J., Neumann, N. L., Southgate, P. N., and Hutton, L. J., 2008, Syn-and post-extensional tectonic activity in the Palaeoproterozoic sequences of Broken Hill and Mount Isa and its bearing on reconstructions of Rodinia: Precambrian Research, v. 166, no. 1-4, p. 350-369.

Giles, D., Betts, P. G., and Lister, G. S., 2002, Far-field continental backarc setting for the 1.80–1.67 Ga basins of northeastern Australia: Geology, v. 30, no. 9, p. 823-826.

Giles, D., and Nutman, A. P., 2002, SHRIMP U–Pb monazite dating of 1600–1580 Ma amphibolite facies metamorphism in the southeastern Mt Isa Block, Australia: Australian Journal of Earth Sciences, v. 49, no. 3, p. 455-465.

Griffin, W. L., Belousova, E. A., Walters, S. G., and O'Reilly, S. Y., 2006, Archaean and Proterozoic crustal evolution in the Eastern Succession of the Mt Isa district, Australia: U–Pb and Hf-isotope studies of detrital zircons: Australian Journal of Earth Sciences, v. 53, no. 1, p. 125-149.

Hahn, K., Rainbird, R., and Cousens, B., 2013, Sequence stratigraphy, provenance, C and O isotopic composition, and correlation of the late Paleoproterozoic–early Mesoproterozoic upper Hornby Bay and lower Dismal Lakes groups, NWT and Nunavut: Precambrian Research, v. 232, p. 209-225.

Hampson, G. J., and Storms, J. E. A., 2003, Geomorphological and sequence stratigraphic variability in wave-dominated, shoreface-shelf parasequences: Sedimentology, v. 50, no. 4, p. 667-701.

Hand, M., Reid, A., and Jagodzinski, L., 2007, Tectonic framework and evolution of the Gawler Craton, Southern Australia: Economic Geology, v. 102, no. 8, p. 1377-1395.

Helland-Hansen, W., and Hampson, G. J., 2009, Trajectory analysis: concepts and applications: Basin Research, v. 21, no. 5, p. 454-483.

Helland-Hansen, W., and Martinsen, O. J., 1996, Shoreline trajectories and sequences: description of variable depositional-dip scenarios: Journal of Sedimentary Research, v. 66, no. 4.

Hoffman, P. F., 1989, Precambrian geology and tectonic history of North America, *in* Albert W. Bally, and Palmer, A. R., eds., The Geology of North America—An Overview: Boulder, United States of America, Geological Society of America, Inc., p. 447-512.

-, 1991, Did the breakout of Laurentia turn Gondwanaland inside-out: Science, v. 252, no. 5011, p. 1409-1412.

Hoffman, P. F., 1997, Tectonic genealogy of North America, *in* Marshak, S., and Van der Pluijm, B. A., eds., Earth structure: An introduction to structural geology and tectonics.: New York, United States of America, McGraw-Hill, p. 459-464.

Holcombe, R. J., Pearson, P. J., and Oliver, N. H. S., 1992, Structure of the Mary Kathleen fold belt, *in* Stewart, A. J., and Blake, D. H., eds., Detailed Studies of the Mount Isa Inlier: Canberra, Australia, AGSO Bulletin, p. 257-287.

Hollis, J. A., Carson, C. J., Glass, L. M., Kositcin, N., Scherstén, A., Worden, K. E., Armstrong, R. A., Yaxley, G. M., and Kemp, A. I. S., 2014, Detrital zircon U–Pb–Hf and O isotope character of the Cahill Formation and Nourlangie Schist, Pine Creek Orogen: Implications for the tectonic correlation and evolution of the North Australian Craton: Precambrian Research, v. 246, p. 35-53.

Ibañez-Mejia, M., Pullen, A., Pepper, M., Urbani, F., Ghoshal, G., and Ibañez-Mejia, J. C., 2018, Use and abuse of detrital zircon U-Pb geochronology—A case from the Río Orinoco delta, eastern Venezuela: Geology, v. 46, no. 11, p. 1019-1022.

Idnurm, M., and Giddings, J. W., 1995, Paleoproterozoic-Neoproterozoic North America–Australia link: new evidence from paleomagnetism: Geology, v. 23, no. 2, p. 149-152.

Jackson, M. J., Scott, D. L., and Rawlings, D. J., 2000, Stratigraphic framework for the Leichhardt and Calvert Superbasins: review and correlations of the pre-1700 Ma successions between Mt Isa and McArthur River: Australian Journal of Earth Sciences, v. 47, no. 3, p. 381-403.

Jackson, M. J., Simpson, E. L., and Eriksson, K. A., 1990, Facies and sequence stratigraphic analysis in an intracratonic, thermal-relaxation basin: the Early Proterozoic, Lower Quilalar Formation and Ballara Quartzite, Mount Isa Inlier, Australia: Sedimentology, v. 37, no. 6, p. 1053-1078.

Jackson, M. J., and Southgate, P. N., 2000, Evolution of three unconformity-bounded sandy carbonate successions in the McArthur River region of northern Australia: The Lawn, Wide and Doom Supersequences in a proximal part of the Isa Superbasin: Australian Journal of Earth Sciences, v. 47, no. 3, p. 625-635.

Jackson, M. J., Southgate, P. N., Black, L. P., Blake, P. R., and Domagala, J., 2005, Overcoming Proterozoic quartzite sand-body miscorrelations: integrated sequence stratigraphy and SHRIMP U–Pb dating of the Surprise Creek Formation, Torpedo Creek and Warrina Park Quartzites, Mt Isa Inlier: Australian Journal of Earth Sciences, v. 52, no. 1, p. 1-25.

Jackson, S. E., Pearson, N. J., Griffin, W. L., and Belousova, E. A., 2004, The application of laser ablation-inductively coupled plasma-mass spectrometry to in situ U–Pb zircon geochronology: Chemical Geology, v. 211, no. 1, p. 47-69.

Jackson, V. A., van Breemen, O., Ootes, L., Bleeker, W., Bennett, V., Davis, W. J., Ketchum, J. W. F., and Smar, L., 2013, U–Pb zircon ages and field relationships of Archean basement and Proterozoic intrusions, south-central Wopmay Orogen, NWT: implications for tectonic assignments: Canadian Journal of Earth Sciences, v. 50, no. 10, p. 979-1006.

Jacoby, W. G., and Armstrong, D. A., 2014, Bootstrap confidence regions for multidimensional scaling solutions: American Journal of Political Science, v. 58, no. 1, p. 264-278.

Jagodzinski, E. A., 2005, Compilation of SHRIMP U-Pb geochronological data, Olympic Domain, Gawler Craton, South Australia, 2001-2003.

Jefferson, C. W., Correlation of Middle and Upper Proterozoic strata between northwestern Canada and south and central Australia, *in* Proceedings Geological Association of Canada: Abstracts1978, Volume 13, p. 429.

Jessup, M. J., Karlstrom, K. E., Connelly, J., Williams, M., Livaccari, R., Tyson, A., Rogers, S. A., and Keller, G., 2005, Complex Proterozoic crustal assembly of southwestern North America in an arcuate subduction system: The Black Canyon of the Gunnison, southwestern Colorado: Lithospheric structure and evolution of the Rocky Mountains: American Geophysical Union Geophysical Monograph, v. 154, p. 21-38.

Johnson, J. P., and Cross, K. C., 1995, U-Pb geochronological constraints on the genesis of the Olympic Dam Cu-U-Au-Ag deposit, South Australia: Economic Geology, v. 90, no. 5, p. 1046-1063.

Jolivet, L., Gorini, C., Smit, J., and Leroy, S., 2015, Continental breakup and the dynamics of rifting in back-arc basins: The Gulf of Lion margin: Tectonics, v. 34, no. 4, p. 662-679.

Kinny, P. D., and Maas, R., 2003, Lu–Hf and Sm–Nd isotope systems in zircon: Reviews in mineralogy and geochemistry, v. 53, no. 1, p. 327-341.

Kirkland, C. L., Strachan, R. A., and Prave, A. R., 2008, Detrital zircon signature of the Moine Supergroup, Scotland: Contrasts and comparisons with other Neoproterozoic successions within the circum-North Atlantic region: Precambrian Research, v. 163, no. 3-4, p. 332-350.

Korsch, R. J., Huston, D. L., Henderson, R. A., Blewett, R. S., Withnall, I. W., Fergusson, C. L., Collins, W. J., Saygin, E., Kositcin, N., and Meixner, A. J., 2012, Crustal architecture and geodynamics of North Queensland, Australia: insights from deep seismic reflection profiling: Tectonophysics, v. 572, p. 76-99.

Kositcin, N., Munson, T. J., and Whelan, J. A., 2017, Summary of results. Joint NTGS-GA geochronology project: greater McArthur Basin, July 2016-June 2017.

Kositcin, N., Whelan, J. A., and Edgoose, C. J., 2015, Summary of results. Joint NTGS-GA geochronology project: McArthur Basin, July 2014-June 2015: Northern Territory Geological Survey, 0724572988.

Kruskal, J. B., 1964, Nonmetric multidimensional scaling: a numerical method: Psychometrika, v. 29, no. 2, p. 115-129.

Kuiper, N. H., Tests concerning random points on a circle, *in* Proceedings Nederl. Akad. Wetensch. Proc. Ser. A1960, Volume 63, p. 38-47.

Lambeck, A., Barovich, K., Gibson, G., Huston, D., and Pisarevsky, S., 2012, An abrupt change in Nd isotopic composition in Australian basins at 1655Ma: Implications for the tectonic evolution of Australia and its place in NUNA: Precambrian Research, v. 208, p. 213-221.

Li, Z.-X., and Zhong, S., 2009, Supercontinent–superplume coupling, true polar wander and plume mobility: plate dominance in whole-mantle tectonics: Physics of the Earth and Planetary Interiors, v. 176, no. 3, p. 143-156.

MacCready, T., Goleby, B. R., Goncharov, A., Drummond, B. J., and Lister, G. S., 1998, A framework of overprinting orogens based on interpretation of the Mount Isa deep seismic transect: Economic Geology, v. 93, no. 8, p. 1422-1434.

Magee, C. W., Withnall, I. W., Hutton, L. J., Perkins, W. G., Donchak, P. J. T., Parson, A., Blake, P. R., Sweet, I. P., and Carson, C. J., 2012, Joint GSQ–GA geochronology project, Mount Isa Region, 2008–2009: Queensland Geological Record 2012/07.

Mair, P., Borg, I., and Rusch, T., 2016, Goodness-of-fit assessment in multidimensional scaling and unfolding: Multivariate behavioral research, v. 51, no. 6, p. 772-789.

Mark, G., 2001, Nd isotope and petrogenetic constraints for the origin of the Mount Angelay igneous complex: implications for the origin of intrusions in the Cloncurry district, NE Australia: Precambrian Research, v. 105, no. 1, p. 17-35.

Martins-Neto, M. A., and Catuneanu, O., 2010, Rift sequence stratigraphy: Marine and Petroleum Geology, v. 27, no. 1, p. 247-253.

Massey, F. J., 1951, The Kolmogorov-Smirnov test for goodness of fit: Journal of the American Statistical Association, v. 46, no. 253, p. 68-78.

McDonald, G. D., Collerson, K. D., and Kinny, P. D., 1997, Late Archean and early Proterozoic crustal evolution of the Mount Isa block, northwest Queensland, Australia: Geology, v. 25, no. 12, p. 1095-1098.

Meara, K., Robin, F., and Sireci, S. G., 2000, Using multidimensional scaling to assess the dimensionality of dichotomous item data: Multivariate Behavioral Research, v. 35, no. 2, p. 229-259.

Medig, K. P. R., Thorkelson, D. J., Davis, W. J., Rainbird, R. H., Gibson, H. D., Turner, E. C., and Marshall, D. D., 2014, Pinning northeastern Australia to northwestern Laurentia in the Mesoproterozoic: Precambrian Research, v. 249, p. 88-99.

Moores, E. M., 1991, Southwest US-East Antarctic (SWEAT) connection: a hypothesis: Geology, v. 19, no. 5, p. 425-428.

Munson, T. J., Thompson, J. M., Zhukova, I., Meffre, S., Beyer, E. E., Woodhead, J. D., and Whelan, J. A., 2018, Summary of results. NTGS laser ablation ICP-MS U-Pb and Lu-Hf geochronology project: Roper Group (McArthur Basin), overlying ungrouped units (Beetaloo Sub-basin), Renner Group (Tomkinson Province), and Tijunna Group (Birrindudu Basin), 1443-1149.

Murgulov, V., Beyer, E., Griffin, W. L., O'Reilly, S. Y., Walters, S. G., and Stephens, D., 2007, Crustal evolution in the Georgetown Inlier, North Queensland, Australia: a detrital zircon grain study: Chemical Geology, v. 245, no. 3-4, p. 198-218.

Murphy, J. B., and Nance, R. D., 2003, Do supercontinents introvert or extrovert?: Sm-Nd isotope evidence: Geology, v. 31, no. 10, p. 873-876.

Muto, T., and Steel, R. J., 2001, Autostepping during the transgressive growth of deltas: results from flume experiments: Geology, v. 29, no. 9, p. 771-774.

Nance, R. D., Murphy, J. B., and Santosh, M., 2014, The supercontinent cycle: a retrospective essay: Gondwana Research, v. 25, no. 1, p. 4-29.

Nance, R. D., Worsley, T. R., and Moody, J. B., 1988, The supercontinent cycle: Scientific American, v. 259, no. 1, p. 72-79.

Neumann, N., 2016, GA Sample No - 1925975: Geoscience Australia Geochron Delivery System, Geoscience Australia.

-, 2016, GA Sample No - 1925976: Geoscience Australia Geochron Delivery System, Geoscience Australia.

Neumann, N. L., and Fraser, G. L., 2007, Geochronological synthesis and time-space plots for Proterozoic Australia, Canberra, Australia, Geoscience Australia.

Neumann, N. L., Gibson, G. M., and Southgate, P. N., 2009, New SHRIMP age constraints on the timing and duration of magmatism and sedimentation in the Mary Kathleen Fold Belt, Mt Isa Inlier, Australia: Australian Journal of Earth Sciences, v. 56, no. 7, p. 965-983.

Neumann, N. L., and Kositcin, N., 2011, New SHRIMP U-Pb zircon ages from north Queensland, 2007-2010: Geoscience Australia, 1921954450.

Neumann, N. L., Southgate, P. N., and Gibson, G. M., 2009, Defining unconformities in Proterozoic sedimentary basins using detrital geochronology and basin analysis—An example from the Mount Isa Inlier, Australia: Precambrian Research, v. 168, no. 3, p. 149-166.

Neumann, N. L., Southgate, P. N., Gibson, G. M., and McIntyre, A., 2006, New SHRIMP geochronology for the Western Fold Belt of the Mt Isa Inlier: developing a 1800–1650 Ma event framework∗: Australian Journal of Earth Sciences, v. 53, no. 6, p. 1023-1039.

Nielsen, A. B., Thorkelson, D. J., Gibson, H. D., and Marshall, D. D., 2013, The Wernecke igneous clasts in Yukon, Canada: fragments of the Paleoproterozoic volcanic arc terrane Bonnetia: Precambrian Research, v. 238, p. 78-92.

Nilsen, T. H., 1982, Alluvial fan deposits, *in* Scholle, P. A., and Spearing, D., eds., Sandstone Depositional Environments: Tulsa, United States of America, American Association of Petroleum Geologists, p. 49-86.

Nordsvan, A. R., Collins, W. J., Li, Z.-X., Spencer, C. J., Pourteau, A., Withnall, I. W., Betts, P. G., and Volante, S., 2018, Laurentian crust in northeast Australia:

Implications for the assembly of the supercontinent Nuna: Geology, v. 46, no. 3, p. 251-254.

O'Dea, M. G., Betts, P. G., MacCready, T., and Aillères, L., 2006, Sequential development of a mid-crustal fold-thrust complex: evidence from the Mitakoodi Culminationin the eastern Mt Isa Inlier, Australia: Australian Journal of Earth Sciences, v. 53, no. 1, p. 69-90.

O'Dea, M. G., Lister, G. S., Betts, P. G., and Pound, K. S., 1997, A shortened intraplate rift system in the Proterozoic Mount Isa terrane, NW Queensland, Australia: Tectonics, v. 16, no. 3, p. 425-441.

O'Dea, M. G., Lister, G. S., MacCready, T., Betts, P. G., Oliver, N. H. S., Pound, K. S., Huang, W., and Valenta, R. K., 1997, Geodynamic evolution of the Proterozoic Mount Isa terrain: Geological Society, London, Special Publications, v. 121, no. 1, p. 99-122.

Oliver, N. H. S., Holcombe, R. J., Hill, E. J., and Pearson, P. J., 1991, Tectono-metamorphic evolution of the Mary Kathleen Fold Belt, northwest Queensland: a reflection of mantle plume processes?: Australian Journal of Earth Sciences, v. 38, no. 4, p. 425-455.

Ootes, L., Davis, W. J., Jackson, V. A., and van Breemen, O., 2015, Chronostratigraphy of the Hottah terrane and Great Bear magmatic zone of Wopmay Orogen, Canada, and exploration of a terrane translation model: Canadian Journal of Earth Sciences, v. 52, no. 12, p. 1062-1092.

Page, R. W., 1983, Timing of superposed volcanism in the Proterozoic Mount Isa inlier, Australia: Precambrian Research, v. 21, no. 3-4, p. 223-245.

Page, R. W., Jackson, M. J., and Krassay, A. A., 2000, Constraining sequence stratigraphy in north Australian basins: SHRIMP U–Pb zircon geochronology between Mt Isa and McArthur River: Australian Journal of Earth Sciences, v. 47, no. 3, p. 431-459.

Page, R. W., and Sun, S. S., 1998, Aspects of geochronology and crustal evolution in the Eastern Fold Belt, Mt Isa Inlier: Australian Journal of Earth Sciences, v. 45, no. 3, p. 343-361.

Page, R. W., Sun, S.-S., and MacCready, T. C., New Geochronological Results in the Central and Eastern Mount Isa Inlier & Implications for Mineral Exploration, *in* Proceedings Geodynamics and Ore Deposits Conference1997.

Paton, C., Hellstrom, J., Paul, B., Woodhead, J., and Hergt, J., 2011, Iolite: Freeware for the visualisation and processing of mass spectrometric data: Journal of Analytical Atomic Spectrometry, v. 26, no. 12, p. 2508-2518.

Payne, J. L., Hand, M., Barovich, K. M., Reid, A., and Evans, D. A. D., 2009, Correlations and reconstruction models for the 2500-1500 Ma evolution of the Mawson Continent: Geological Society, London, Special Publications, v. 323, no. 1, p. 319-355.

Payne, J. L., McInerney, D. J., Barovich, K. M., Kirkland, C. L., Pearson, N. J., and Hand, M., 2016, Strengths and limitations of zircon Lu-Hf and O isotopes in modelling crustal growth: Lithos, v. 248, p. 175-192.

Pearson, P. J., Holcombe, R. J., and Page, R. W., 1992, Synkinematic emplacement of the Middle Proterozoic Wonga batholith into a midcrustal extensional shear zone, Mount Isa Inlier, Queensland, Australia, *in* Stewart, A. J., and Blake, D. H., eds., Detailed Studies of the Mount Isa Inlier: Canberra, Australia, AGSO Bulletin, p. 289-328.

Pehrsson, S. J., Eglington, B. M., Evans, D. A. D., Huston, D., and Reddy, S. M., 2016, Metallogeny and its link to orogenic style during the Nuna supercontinent cycle: Geological Society, London, Special Publications, v. 424, no. 1, p. 83-94.

Petrus, J. A., and Kamber, B. S., 2012, VizualAge: A novel approach to laser ablation ICP-MS U-Pb geochronology data reduction: Geostandards and Geoanalytical Research, v. 36, no. 3, p. 247-270.

Pisarevsky, S. A., Elming, S. Å., Pesonen, L. J., and Li, Z.-X., 2014, Mesoproterozoic paleogeography: supercontinent and beyond: Precambrian Research, v. 244, p. 207-225.

Posamentier, H. W., Jervey, M. T., and Vail, P. R., 1988, Eustatic controls on clastic deposition I—conceptual framework, *in* Wilgus, C. K., Hastings, B. S., Posamentier, H. W., Van Wagoner, J. C., Ross, C. A., and Kendall, C. G. S. C.,

eds., Sea-Level Changes: An Integrated Approach, Volume 42: Oklahoma, United States of America, Society of Economic Paleontologists and Mineralogists (SEPM), p. 110–124.

Potma, W. A., and Betts, P. G., 2006, Extension-related structures in the Mitakoodi Culmination: implications for the nature and timing of extension, and effect on later shortening in the eastern Mt Isa Inlier: Australian Journal of Earth Sciences, v. 53, no. 1, p. 55-67.

Pourteau, A., Smit, M. A., Li, Z.-X., Collins, W. J., Nordsvan, A. R., Volante, S., and Li, J., 2018, 1.6 Ga crustal thickening along the final Nuna suture: Geology, v. 46, no. 11, p. 959-962.

Rainbird, R. H., and Davis, W. J., 2007, U-Pb detrital zircon geochronology and provenance of the late Paleoproterozoic Dubawnt Supergroup: Linking sedimentation with tectonic reworking of the western Churchill Province, Canada: Geological Society of America Bulletin, v. 119, no. 3-4, p. 314-328.

Rainbird, R. H., Hadlari, T., Aspler, L. B., Donaldson, J. A., LeCheminant, A. N., and Peterson, T. D., 2003, Sequence stratigraphy and evolution of the Paleoproterozoic intracontinental Baker Lake and Thelon basins, western Churchill Province, Nunavut, Canada: Precambrian Research, v. 125, no. 1-2, p. 21-53.

Rainbird, R. H., Stern, R. A., Rayner, N., and Jefferson, C. W., 2007, Age, provenance, and regional correlation of the Athabasca Group, Saskatchewan and Alberta, constrained by igneous and detrital zircon geochronology, *in* W, J. C., and G, D., eds., EXTECH IV - geology and uranium EXploration TECHnology of the Proterozoic Athabasca Basin, Saskatchewan and Alberta, Volume 588, Geological Survey of Canada Bulletin, p. 193–209.

Ramsay, J. O., 1977, Maximum likelihood estimation in multidimensional scaling: Psychometrika, v. 42, no. 2, p. 241-266.

Rawlings, D. J., 1999, Stratigraphic resolution of a multiphase intracratonic basin system: the McArthur Basin, northern Australia: Australian Journal of Earth Sciences, v. 46, no. 5, p. 703-723.

Rawlings, D. J., and Scott, D., Geodynamics of the Redbank package, basal McArthur Basin, *in* Proceedings Annual geoscience exploration seminar (AGES),2002, Northern Territory Geological Survey.

Rogers, J. J. W., and Santosh, M., 2002, Configuration of Columbia, a Mesoproterozoic supercontinent: Gondwana Research, v. 5, no. 1, p. 5-22.

Ross, G. M., Parrish, R. R., and Winston, D., 1992, Provenance and U-Pb geochronology of the Mesoproterozoic Belt Supergroup (northwestern United States): Implications for age of deposition and pre-Panthalassa plate reconstructions: Earth and Planetary Science Letters, v. 113, no. 1-2, p. 57-76.

Ross, G. M., and Villeneuve, M., 2003, Provenance of the Mesoproterozoic (1.45 Ga) Belt basin (western North America): Another piece in the pre-Rodinia paleogeographic puzzle: Geological Society of America Bulletin, v. 115, no. 10, p. 1191-1217.

Ross, G. M., Villeneuve, M. E., and Theriault, R. J., 2001, Isotopic provenance of the lower Muskwa assemblage (Mesoproterozoic, Rocky Mountains, British Columbia): New clues to correlation and source areas: Precambrian Research, v. 111, no. 1, p. 57-77.

Satkoski, A. M., Wilkinson, B. H., Hietpas, J., and Samson, S. D., 2013, Likeness among detrital zircon populations—An approach to the comparison of age frequency data in time and space: Bulletin, v. 125, no. 11-12, p. 1783-1799.

Saylor, J. E., Stockli, D. F., Horton, B. K., Nie, J., and Mora, A., 2012, Discriminating rapid exhumation from syndepositional volcanism using detrital zircon double dating: Implications for the tectonic history of the Eastern Cordillera, Colombia: Bulletin, v. 124, no. 5-6, p. 762-779.

Saylor, J. E., and Sundell, K. E., 2016, Quantifying comparison of large detrital geochronology data sets: Geosphere, v. 12, no. 1, p. 203-220.

Saylor, J. E., Sundell, K. E., and Sharman, G. R., 2019, Characterizing sediment sources by non-negative matrix factorization of detrital geochronological data: Earth and Planetary Science Letters, v. 512, p. 46-58.

Scherer, E., Münker, C., and Mezger, K., 2001, Calibration of the lutetium-hafnium clock: Science, v. 293, no. 5530, p. 683-687.

Scott, D. L., Rawlings, D. J., Page, R. W., Tarlowski, C. Z., Idnurm, M., Jackson, M. J., and Southgate, P. N., 2000, Basement framework and geodynamic evolution of the Palaeoproterozoic superbasins of north-central Australia: An integrated review of geochemical, geochronological and geophysical data: Australian Journal of Earth Sciences, v. 47, no. 3, p. 341-380.

Sircombe, K. N., and Hazelton, M. L., 2004, Comparison of detrital zircon age distributions by kernel functional estimation: Sedimentary Geology, v. 171, no. 1-4, p. 91-111.

Southgate, P. N., Neumann, N. L., and Gibson, G. M., 2013, Depositional systems in the Mt Isa Inlier from 1800 Ma to 1640 Ma: Implications for Zn–Pb–Ag mineralisation: Australian Journal of Earth Sciences, v. 60, no. 2, p. 157-173.

Stern, R. A., Bodorkos, S., Kamo, S. L., Hickman, A. H., and Corfu, F., 2009, Measurement of SIMS instrumental mass fractionation of Pb isotopes during zircon dating: Geostandards and Geoanalytical Research, v. 33, no. 2, p. 145-168.

Stewart, A. J., 1992, Stratigraphy, extension, and contraction in the Ballara-Mount Frosty area, Mount Isa Inlier, Queensland, *in* Stewart, A. J., and Blake, D. H., eds., Detailed Studies in the Mount Isa Inlier, Volume 243: Canberra, Australia, AGSO Bulletin, p. 209-228.

Tapani Rämö, O., and Calzia, J. P., 1998, Nd isotopic composition of cratonic rocks in the southern Death Valley region: Evidence for a substantial Archean source component in Mojavia: Geology, v. 26, no. 10, p. 891-894.

Thériault, R. J., St-Onge, M. R., and Scott, D. J., 2001, Nd isotopic and geochemical signature of the Paleoproterozoic Trans-Hudson Orogen, southern Baffin Island, Canada: implications for the evolution of eastern Laurentia: Precambrian Research, v. 108, no. 1-2, p. 113-138.

Thorkelson, D. J., Abbott, J. G., Mortensen, J. K., Creaser, R. A., Villeneuve, M. E., McNicoll, V. J., and Layer, P. W., 2005, Early and middle Proterozoic evolution

of Yukon, Canada: Canadian Journal of Earth Sciences, v. 42, no. 6, p. 1045-1071.

Thorkelson, D. J., and Laughton, J. R., 2015, Paleoproterozoic closure of an Australia–Laurentia seaway revealed by megaclasts of an obducted volcanic arc in Yukon, Canada: Gondwana Research, v. 33, p. 115-133.

Thorkelson, D. J., Mortensen, J. K., Creaser, R. A., Davidson, G. J., and Abbott, J. G., 2001, Early Proterozoic magmatism in Yukon, Canada: constraints on the evolution of northwestern Laurentia: Canadian Journal of Earth Sciences, v. 38, no. 10, p. 1479-1494.

Thorkelson, D. J., Mortensen, J. K., Davidson, G. J., Creaser, R. A., Perez, W. A., and Abbott, J. G., 2001, Early Mesoproterozoic intrusive breccias in Yukon, Canada: the role of hydrothermal systems in reconstructions of North America and Australia: Precambrian Research, v. 111, no. 1-4, p. 31-55.

Torgerson, W. S., 1952, Multidimensional scaling: I. Theory and method: Psychometrika, v. 17, no. 4, p. 401-419.

van Breemen, O., Davis, W. J., and King, J. E., 1992, Temporal distribution of granitoid plutonic rocks in the Archean Slave Province, northwest Canadian Shield: Canadian Journal of Earth Sciences, v. 29, no. 10, p. 2186-2199.

Van Wagoner, J. C., Posamentier, H. W., Mitchum, R. M. J., Vail, P. R., Sarg, J. F., Loutit, T. S., and Hardenbol, J., 1988, An overview of the fundamentals of sequence stratigraphy and key definitions.

Verbaas, J., Thorkelson, D. J., Crowley, J., Davis, W. J., Foster, D. A., Gibson, H. D., Marshall, D. D., and Milidragovic, D., 2018, A sedimentary overlap assemblage links Australia to northwestern Laurentia at 1.6 Ga: Precambrian Research, v. 305, p. 19-39.

Vermeesch, P., 2012, On the visualisation of detrital age distributions: Chemical Geology, v. 312, p. 190-194.

-, 2013, Multi-sample comparison of detrital age distributions: Chemical Geology, v. 341, p. 140-146.

-, 2018, Dissimilarity measures in detrital geochronology: Earth-Science Reviews, v. 178, p. 310-321.

-, 2018, IsoplotR: A free and open toolbox for geochronology: Geoscience Frontiers, v. 9, no. 5, p. 1479-1493.

Vervoort, J. D., and Blichert-Toft, J., 1999, Evolution of the depleted mantle: Hf isotope evidence from juvenile rocks through time: Geochimica et Cosmochimica Acta, v. 63, no. 3-4, p. 533-556.

Whitmeyer, S. J., and Karlstrom, K. E., 2007, Tectonic model for the Proterozoic growth of North America: Geosphere, v. 3, no. 4, p. 220-259.

Wiedenbeck, M., Alle, P., Corfu, F., Griffin, W. L., Meier, M., Oberli, F. v., Quadt, A. v., Roddick, J. C., and Spiegel, W., 1995, Three natural zircon standards for U-Th-Pb, Lu-Hf, trace element and REE analyses: Geostandards newsletter, v. 19, no. 1, p. 1-23.

Williams, P. R., 1989, Nature and timing of early extensional structures in the Mitakoodi Quartzite, Mount Isa Inlier, northwest Queensland: Australian Journal of Earth Sciences, v. 36, no. 2, p. 283-296.

Wilson, I. H., Derrick, G. M., and Perkin, D. J., 1984, Eastern Creek Volcanics-their geochemistry and possible role in copper mineralization at Mount Isa, Queensland: BMR Journal of Australian Geology & Geophysics, v. 9, no. 4, p. 317-328.

Wissink, G. K., Wilkinson, B. H., and Hoke, G. D., 2018, Pairwise sample comparisons and multidimensional scaling of detrital zircon ages with examples from the North American platform, basin, and passive margin settings: Lithosphere, v. 10, no. 3, p. 478-491.

Withnall, I. W., Bain, J. H. C., Draper, J. J., MacKenzie, D. E., and Oversby, B. S., 1988, Proterozoic stratigraphy and tectonic history of the Georgetown Inlier, northeastern Queensland: Precambrian Research, v. 40, p. 429-446.

Withnall, I. W., and Henderson, R. A., 2012, Accretion on the long-lived continental margin of northeastern Australia: Episodes, v. 35, no. 1, p. 166-176.

Withnall, I. W., and Hutton, L. J., 2013, Proterozoic–North Australian Craton, *in* Jell, P. A., ed., Geology of Queensland: Brisbane, Australia, Geological Survey of Queensland, p. 23-112.

Wygralak, A. S., Ahmad, M., and Hallenstein, C. P., 1988, Sedimentology of the Westmoreland Conglomerate, southern McArthur Basin, Northern Territory, Australia: Journal of the Geological Society of Australia, v. 35, no. 2, p. 195-207.

Yang, B., Smith, T. M., Collins, A. S., Munson, T. J., Schoemaker, B., Nicholls, D., Cox, G., Farkas, J., and Glorie, S., 2018, Spatial and temporal variation in detrital zircon age provenance of the hydrocarbon-bearing upper Roper group, Beetaloo sub-basin, Northern Territory, Australia: Precambrian Research, v. 304, p. 140-155.

Zecchin, M., and Catuneanu, O., 2013, High-resolution sequence stratigraphy of clastic shelves I: units and bounding surfaces: Marine and Petroleum Geology, v. 39, no. 1, p. 1-25.

Zhang, S., Li, Z.-X., Evans, D. A. D., Wu, H., Li, H., and Dong, J., 2012, Pre-Rodinia supercontinent Nuna shaping up: a global synthesis with new paleomagnetic results from North China: Earth and Planetary Science Letters, v. 353, p. 145-155.

Zhao, G., Cawood, P. A., Wilde, S. A., and Sun, M., 2002, Review of global 2.1–1.8 Ga orogens: implications for a pre-Rodinia supercontinent: Earth-Science Reviews, v. 59, no. 1, p. 125-162.

Zhao, G., Sun, M., Wilde, S. A., and Li, S., 2004, A Paleo-Mesoproterozoic supercontinent: assembly, growth and breakup: Earth-Science Reviews, v. 67, no. 1, p. 91-123.

Every reasonable effort has been made to acknowledge the owners of copyright material. I would be pleased to hear from any copyright owner who has been omitted or incorrectly acknowledged.

Appendix A: Statement of Authorship

Chapter 2: SOA

Title of Paper: *Caveats for multidimensional scaling in detrital zircon geochronology: an example from the Proterozoic McArthur Basin, north Australia*

Publication Status: *Under review at scientific journal: Earth Science Reviews*

Author Contributions

By signing the Statement of Authorship, the principal author certifies the contribution made to the manuscript by *Adam R. Nordsvan* is accurate and that permission is granted for the publication to be included in the candidate's thesis.

Name of Principal Author: *Adam R. Nordsvan* (Candidate)

Contributions to the Paper: *Led all aspects of the research, noted the problem and made corrections to the Matlab script to address them. Wrote the manuscript, drafted all the figures, collected the data and did the analysis.*

Overall Contribution: *65%*

Signature: Date: 3/7/2019

Name of Co-Author: *Uwe Kirscher*

Contributions to the Paper: *Assisted with the ideas, and editing of the manuscript*

Overall Contribution: *10%*

Signature: Date: 3/7/2019

Name of Co-Author: *Chris Kirkland*

Contributions to the Paper: *Assisted with the ideas, and editing of the manuscript*

Overall Contribution: 10*%*

Signature: Date: 3/7/2019

Name of Co-Author: *Milo Barham*

Contributions to the Paper: *Assisted with the ideas, and editing of the manuscript*

Overall Contribution: 10*%*

Signature:  Date: 3/7/2019

Name of Co-Author: *Danial Brennan*

Contributions to the Paper: *Assisted with the ideas, and editing of the manuscript*

Overall Contribution: 5*%*

Signature: 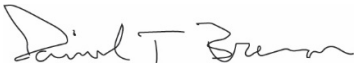 Date: 11/7/2019

Chapter 3: SOA

Statement of Authorship

Title of Paper: *Laurentian crust in northeast Australia: Implications for the assembly of the supercontinent Nuna*
Publication Status: Published
Publication Reference: Nordsvan, A. R., Collins, W. J., Li, Z.-X., Spencer, C. J., Pourteau, A., Withnall, I. W., Betts, P. G., and Volante, S., 2018, Laurentian crust in northeast Australia: Implications for the assembly of the supercontinent Nuna: Geology, v. 46, no. 3, p. 251-254.

Author Contributions

By signing the Statement of Authorship, the principal author certifies the contribution made to the manuscript by *Adam R. Nordsvan* is accurate and that permission is granted for the publication to be included in the candidate's thesis.

Name of Principal Author: *Adam R. Nordsvan* (Candidate)

Contributions to the Paper: *Led all aspects of the research, LA-ICP-MS data collection, data reduction of new isotopic analyses, compiled published data included within the study, all statistical analyses and data treatment, reporting and interpretation of results, drafted all figures, drafted and revised the manuscript*

Overall Contribution: *61%*

Signature: Date: 3/7/2019

Name of Co-Author: *William J. Collins*

Contributions to the Paper: *Assisted with the interpretation of results, clarification of ideas, and editing of the manuscript*

Overall Contribution: *7%*

Signature: Date: 25/7/2019

Name of Co-Author: *Zheng-Xiang Li*

Contributions to the Paper: *Assisted with the interpretation of results, clarification of ideas, and editing of the manuscript*

Overall Contribution: *7%*

Signature:  Date: 4 July 2019

Name of Co-Author: *Christopher J. Spencer*

Contributions to the Paper: *Assisted with the interpretation of results, clarification of ideas, and editing of the manuscript*

Overall Contribution: 5%

Signature:  Date: 3 July 2019

Name of Co-Author: *Amaury Pourteau*

Contributions to the Paper: *Assisted with the interpretation of results, clarification of ideas, and editing of the manuscript*

Overall Contribution: 5%

Signature: Date: 3 July 2019

Name of Co-Author: *Ian W. Withnall*

Contributions to the Paper: *Assisted with the interpretation of results, clarification of ideas, and editing of the manuscript*

Overall Contribution: 5%

Signature: Date: 4 July 2019

Name of Co-Author: *Peter G. Betts*

Contributions to the Paper: *Assisted with the interpretation of results, clarification of ideas, and editing of the manuscript*

Overall Contribution: 5%

Signature: Date: 3rd July 2019

Name of Co-Author: *Silvia Volante*

Contributions to the Paper: *Assisted with the interpretation of results, clarification of ideas, and editing of the manuscript*

Overall Contribution: 5%

Signature: Date: 3 July 2019

Appendix B: Chapter 2, supplementary file

Example 1 and 2,

To generate synthetic data the NORMINV function in excel was used with a random variable.

How much does the difference in uncertainty between samples change the K-S-D-Value?

In this simple experiment, we take a single population of 1000 Ma with n=1000 with 5 myr uncertainty and compared the resulting K-S-D-value against the same 1000 Ma population with increasing uncertainty from 10 to 70 myr (Table 3). Figure 1 shows the results of comparing the 5 myr uncertainty vs (x) myr uncertainty sample D-values. It appears that above a difference of 25 myr the rate of difference in uncertainty reduces for the 5 myr sample. Figure 2 shows the K-S-D-Value from every sample compares with all other samples. Figure 2 shows that lower sample uncertainty equates to larger shifts in D-values when the uncertainties are different. In other words, it is the proportion of the difference in the uncertainty rather than the difference itself that will cause bigger changes to the D-values. Figure 3 and 4 show this relationship. Figure 5 not only demonstrates the difference in uncertainty between igneous and detrital grains but the variability of uncertainty within detrital zircons. This difference in uncertainty will lead to miscorrelations within MDS analysis.

Table 3: Synthetic samples used to test the increase in D-values with increasing difference in uncertainty. This data was used from Figure 1 to Figure 4.

Sample	population (mean)	Std.dev

a5	1000	5
a10	1000	10
a20	1000	20
a30	1000	30
a40	1000	40
a50	1000	50
a60	1000	60
a70	1000	70

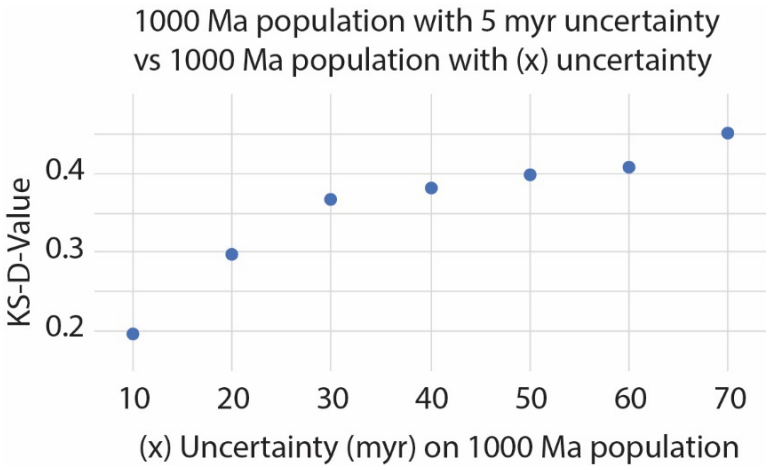

Figure 1: Results of comparing the K-S-D-value with increasing the difference in uncertainty within a single population. The difference in D-value does not increase at the same rate above 30 myr, a difference of 25 myr.

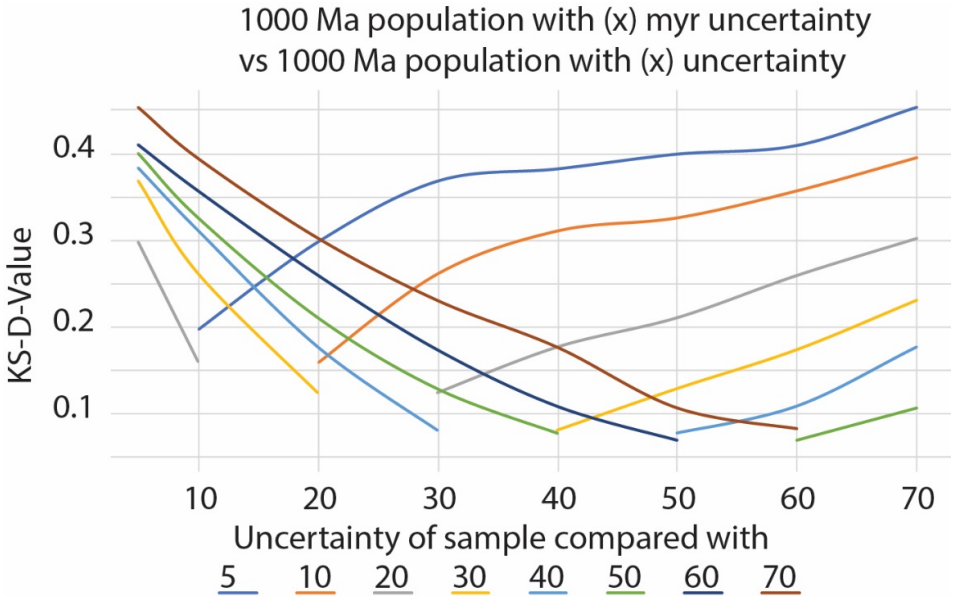

Figure 2: Comparing the difference in K-S-D-Values from all samples with different uncertainties. Note, that a difference in uncertainty of 10 myr has a larger effect on samples with lower uncertainties.

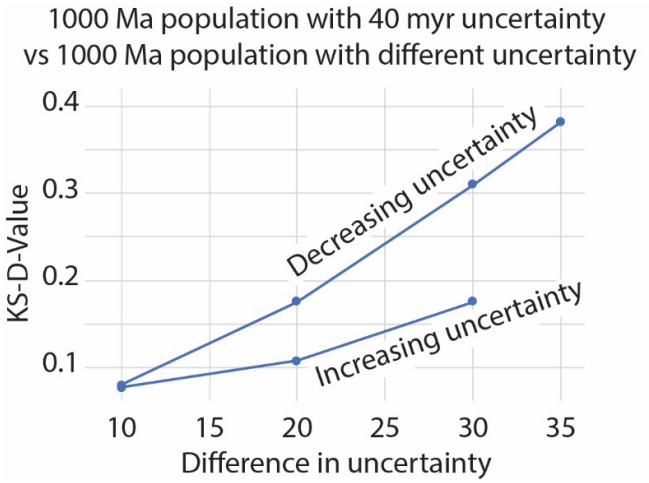

Figure 3: 1000 Ma population with 40 myr uncertainty compared with 1000 Ma population with increasing and decreasing uncertainties. This figure demonstrates that it is the proportion of the difference in uncertainty rather than the difference in the uncertainty that affects the K-S-D-value.

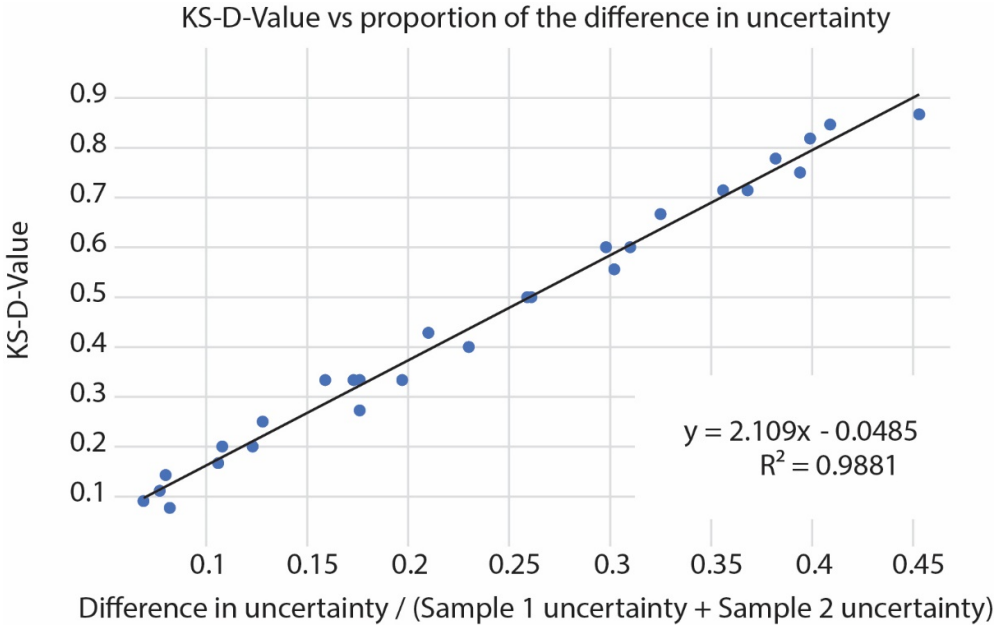

Figure 4: K-S-D-value vs the proportion of the difference in uncertainty between samples.

Kuiper statistical test

The Kuiper statistical test was achieved by modifying the K-Stest2 script in Matlab, blindly altering this script can cause issues. Please email authors for a full description of this method.

The effect of sample size on the D-Value

To generate synthetic data, we use the NORMINV function in excel with a random probability we emulated the populations from sample s1 of example 1 and replicated it 10*10 times from n=100 to n=1000.

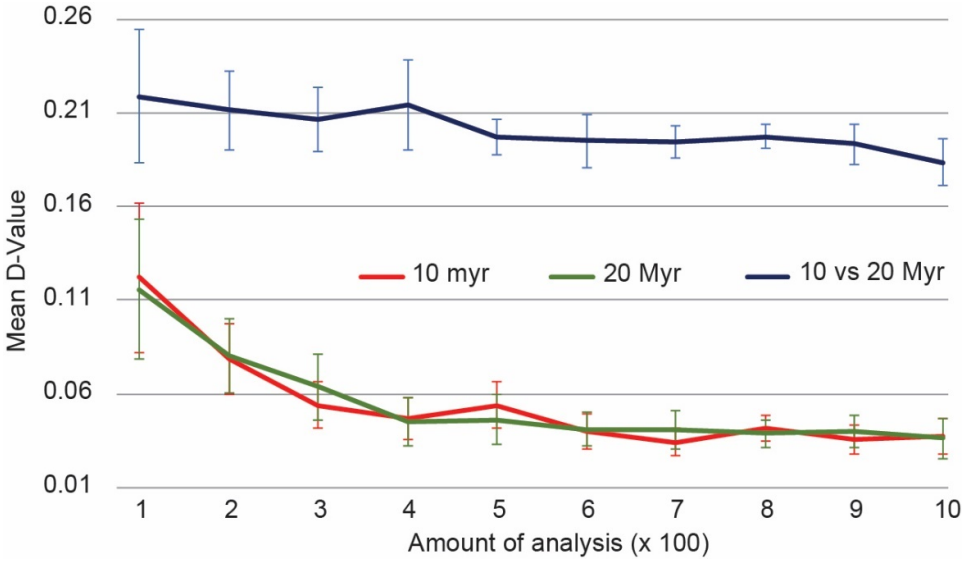

Figure 5: summary of the K-S- D-values against sample size.

Supplementary data

Table 1a: Detrital zircon samples from the McArthur Basin

Phelp	Reported uncertainty	Limmen	Reported uncertainty	Crawford	Reported uncertainty	Arnold	Reported uncertainty	Hodgson	Reported uncertainty	Bessie	Reported uncertainty	Moroak	Reported uncertainty
1625	44	1615	50	1711	16	1589	40	1595	26	1385	116	1406	78
1668	30	1622	34	1719	32	1660	64	1609	36	1464	40	1550	34
1705	68	1646	42	1745	48	1682	64	1666	36	1522	38	1565	34
1735	28	1753	28	1755	26	1695	54	1666	40	1536	58	1568	46
1740	38	1800	34	1761	28	1712	42	1721	36	1546	54	1581	26
1750	22	1803	44	1762	34	1717	64	1728	46	1553	74	1587	54
1758	32	1803	32	1763	40	1724	28	1728	32	1561	70	1624	34
1758	30	1805	34	1765	28	1727	34	1738	32	1568	54	1624	54
1762	22	1810	38	1777	34	1731	46	1739	32	1578	36	1625	44
1764	26	1815	24	1783	28	1731	34	1739	40	1590	34	1645	36
1771	24	1817	38	1793	44	1731	66	1739	38	1593	54	1650	28
1774	48	1820	24	1803	50	1732	30	1743	36	1594	38	1652	36
1779	24	1846	28	1806	30	1732	38	1744	36	1604	30	1680	48
1779	62	1848	38	1814	34	1734	104	1745	56	1622	42	1710	40
1787	46	1849	70	1821	22	1735	28	1745	26	1625	32	1732	56
1793	30	1858	50	1879	40	1737	42	1745	32	1634	44	1733	46
1799	40	1860	46	2432	26	1738	66	1746	44	1635	92	1737	30
1801	44	1872	26	2631	20	1743	30	1746	24	1637	62	1738	36
1805	42	1875	38			1743	46	1746	28	1646	30	1742	26
1811	38	1885	34			1743	22	1747	44	1649	32	1747	40
1811	30	1911	44			1743	26	1749	28	1663	32	1752	34
1813	36	1921	50			1744	40	1750	34	1666	28	1753	30
1813	48	1934	44			1745	32	1751	24	1671	54	1755	30
1815	68	1961	40			1746	34	1752	46	1695	32	1756	32
1816	32	2030	30			1746	32	1753	30	1715	34	1758	28
1818	30	2229	36			1747	28	1754	26	1726	38	1763	24

1819	30	2496	44
1826	70	2528	22
1828	42	2933	38
1834	44		
1835	38		
1839	40		
1840	24		
1843	34		
1844	34		
1851	36		
1851	26		
1872	26		
1872	42		
1873	34		
1874	32		
1877	50		
1877	32		
1879	24		
1879	100		
1887	48		
1890	28		
1900	30		
1913	38		
1918	62		
1921	48		
1929	76		
1985	72		
1989	38		
1996	30		
2030	22		
2068	26		

1748	34	1757	30	1735	66	1765	26
1749	34	1758	24	1738	56	1769	26
1750	30	1759	38	1744	46	1769	38
1750	74	1760	34	1753	30	1771	34
1754	64	1764	26	1754	34	1772	56
1755	22	1765	28	1765	26	1776	46
1757	58	1765	28	1766	30	1777	56
1758	38	1767	26	1767	26	1783	54
1758	34	1769	20	1768	32	1786	48
1759	26	1770	32	1775	34	1786	26
1760	64	1772	38	1777	30	1787	36
1760	48	1776	32	1778	106	1804	34
1761	24	1777	28	1783	28	1807	40
1762	40	1778	26	1787	36	1809	64
1762	36	1784	32	1791	34	1817	48
1765	34	1786	28	1791	40	1825	40
1765	48	1788	38	1794	44	1826	40
1767	32	1791	58	1798	74	1829	24
1767	24	1792	32	1803	46	1829	30
1768	36	1794	24	1805	24	1831	32
1768	30	1794	32	1806	36	1834	42
1768	42	1796	32	1808	26	1837	30
1770	82	1796	30	1812	30	1841	56
1770	68	1797	30	1812	24	1842	26
1771	34	1798	22	1813	38	1847	24
1772	30	1807	32	1820	48	1853	24
1773	26	1816	60	1821	48	1862	32
1773	26	1825	38	1822	28	1868	26
1774	34	1825	38	1822	74	1882	22
1775	28	1832	40	1825	38	1883	32
1776	32	1835	54	1826	30	1896	44

2131	38
2192	24
2204	42
2293	30
2304	40
2444	22
2481	30
2486	34
2503	20
2515	22
2519	28
2530	36
2543	22
2545	32
2575	34
2579	28
2626	18
2681	56
2713	24
2823	18

1776	44
1777	50
1779	34
1779	30
1784	32
1784	48
1786	42
1789	34
1796	42
1796	52
1797	34
1800	34
1815	30
1815	40
1817	30
1821	36
1835	34
1850	32
1857	30
1899	50
2003	36
2009	22
2453	44
2528	22
2542	32
2629	54
2816	16
2819	22

1972	52
2972	22

1829	24
1836	36
1849	52
1849	34
1860	60
1861	42
1863	44
1864	52
1894	50
1906	42
1967	40
2305	26
2406	38
2452	32
2528	52
2533	30
2777	32
2817	44

1908	32
1931	26
2024	28
2480	26
2617	34
2885	16

Table 1b: Detrital zircon samples from the McArthur Basin

Bukalorkmi	Reported uncertainty

1353	44
1510	42
1563	24
1564	34
1589	30
1609	42
1644	40
1688	48
1721	24
1747	20
1751	58
1753	38
1780	24
1789	32
1793	28
1794	24
1811	22
1816	30
1828	62
1837	32
1840	32
1851	36
1855	42
1874	44
1886	26
1888	24
1902	48
2011	28
2493	32

Appendix C: Chapter 3, supplementary file

Data acquisition

Compiled Data

Data from the Georgetown and Mt. Isa Inliers were compiled from Geoscience Australia's Geochron Delivery system (http://www.ga.gov.au/geochron-sapub-web/geochronology/shrimp/search.htm). Additional data from the Georgetown Inlier were obtained from Lambeck (2011). Data from the Wernecke Supergroup were obtained from Furlanetto et al. (2016).

Sample collection (IG01)

A sample from the Inorunie Group was collected from a road cutting on Gulf Development Rd (IG01).

Sample Preparation

Zircons were separated from the sample at Curtin University and University of Newcastle. Zircon grains were hand-picked and mounted in 25 mm diameter epoxy resin discs and polished to approximately half grain thickness then cleaned, and carbon coated at the University of Newcastle. The discs were carbon coated for backscattered, secondary electron and cathodoluminescence (CL) imaging on JEOL JSM- 6480 LA scanning electron microscope (SEM) at Macquarie University using an accelerating voltage of 10 kV at a working distance of 15 mm.

LA-ICP-MS analysis: U–Pb dating

Sample IG01 was analysed on 2 different occasions.

1-IG01a

LA-ICP-MS data were collected at the University of Newcastle using an NWR UP-213 Nd: YAG laser ablation system, coupled with an Agilent 7700× ICP-MS. Zircon spots were chosen using CL and transmitted light imaging in order to avoid rims, boundaries and inclusions. A repetition rate of 5 Hz was used for all analyses. Helium gas was used as the laser ablation carrier gas. A single analysis was 1 s (2 Hz) pre-ablation, 30 s washout time, 30 s background and 50 s sample analyses with a 40 μm spot size. Between every 10 unknown grains GJ-1, 91500 and Plešovice zircon standards were used. GJ-1, with a 207Pb/206Pb age of 608.5 ± 0.4 Ma (Jackson et al., 2004), was used as the primary standard for data reduction.

2-IG01b

LA-ICP-MS data were collected at the GeoHistory Facility in the John de Laeter Centre, Curtin University using a COMPex 102 excimer laser with an Agilent 7700× ICP-MS. Zircon spots were chosen using CL and transmitted light imaging in order to avoid rims, boundaries and inclusions. A repetition rate of 7 Hz was used for all analyses. A single analysis was 1 s (2 Hz) pre-ablation, 20 s background and 30 s sample analyses with a 50 μm spot size. Between every 10 unknown grains GJ-1, 91500 and Plešovice zircon standards were used. GJ-1, with a 207Pb/206Pb age of 608.5 ± 0.4 Ma (Jackson et al., 2004),

was used as the primary standard for data reduction. Zircon standards OG1 and R33 were used as additional checks.

Detrital zircon age spectrum

Kernel density estimates (Vermeesch, 2012) are used to visualise the detrital zircon U-Pb data. Both negatively and positively discordant data outside >5% Concordia was omitted. Data was plotted using DensityPlotter 7.3. (http://www.ucl.ac.uk/~ucfbpve/densityplotter/) using an adaptive bandwidth of 15.

Magmatic ages (Figure 2)

Magmatic ages for Laurentia were obtained from Natural Resources Canada (http://atlas.gc.ca/geochron/en/) and Condie et al. (2009). Magmatic ages from the NAC were attained from Geoscience Australia (http://www.ga.gov.au/geochron-sapub-web/geochronology/shrimp/search.htm) and Neumann and Fraser (2007).

The magmatic geochronological data was plotted using DensityPlotter 7.3 and compared to detrital samples.

Paleocurrent Measurements

From the lower Etheridge Group paleocurrent measurements were taken in 5 locations from current ripples in the sandy deltaic facies (Withnall et al., 1988). In the lower Etheridge Group measurements were corrected for the dip of the beds using Stereonet 7 software (http://www.geo.cornell.edu/geology/faculty/RWA/programs/stereonet-7-for-

windows.html). From 4 locations in the Inorunie Group, measurements were taken from trough crossbedding in delta plain facies and planar and trough crossbeds in fluvial facies.

Data

Table 1: data from the lower Etheridge Group detrital zircon

lower Etheridge Group detrital zircon													
Sample 2007169004 (1937153), Corbett Formation					New SHRIMP U-Pb zircon ages from north Queensland, 2007–2010					Neumann and Kositcin, 2011			
Grain ID	206Pbc(%)1	U (ppm)	Th (ppm)	232Th/238U	238U/206Pb	± 1σ (%)	207Pb/206Pb	± 1σ (%)	207Pb/206Pb Age (Ma)	± 1σ (Ma)	Disc (%)		
B.1.1.1	0.02	242	111	0.48	2.6016	1.3	0.1334	0.4	2143	7	2		
B.11.1.1	0.01	282	179	0.66	1.8584	1.4	0.2049	0.3	2866	4	3		
B.12.1.1	0.06	259	138	0.55	2.4755	1.3	0.1471	0.4	2313	7	5		
B.14.1.1	0.07	197	110	0.58	2.7576	1.3	0.1211	0.5	1973	9	-1		
B.15.1.1	0.05	127	184	1.5	2.0373	1.6	0.1749	0.4	2605	7	1		
B.16.1.1	0.02	511	655	1.33	3.0869	1.2	0.1166	0.3	1905	6	5		
B.2.1.1	0.12	23	15	0.69	2.1234	1.9	0.1614	1.2	2471	20	-1		
B.21.1.1	0.02	284	203	0.74	3.1102	1.2	0.1128	0.5	1845	8	3		
B.22.1.1	0.01	298	72	0.25	1.4934	1.2	0.2643	0.5	3273	8	-1		
B.23.1.1	0.06	516	266	0.53	2.8166	1.2	0.1237	0.3	2010	6	3		
B.24.1.1	0.03	336	108	0.33	2.9755	1.3	0.1203	0.5	1961	8	5		
B.26.1.1	0.07	146	63	0.45	1.6613	1.3	0.2362	0.3	3095	5	2		
B.3.1.1	0.02	213	71	0.35	1.9495	1.3	0.1854	0.3	2701	5	1		
B.37.1.1	0.07	167	116	0.72	2.0485	1.3	0.1761	0.5	2617	8	2		
B.4.1.1	0.02	234	165	0.73	2.0239	1.3	0.1746	0.3	2602	5	1		
B.46.1.1	0.06	228	67	0.3	2.0107	1.3	0.1807	0.4	2660	7	2		
B.47.1.1	0.05	384	212	0.57	2.0548	1.3	0.1835	0.3	2685	5	5		
B.48.1.1	0.02	428	170	0.41	2.135	1.3	0.1664	0.3	2522	5	2		

B.49.1.1	0.02	766	267	0.36	3.0279	1.2	0.1154	0.3	1886	6	2		
B.5.1.1	0.01	416	174	0.43	2.0723	1.2	0.1738	0.2	2595	4	2		
B.50.1.1	0.02	352	83	0.24	1.8405	1.3	0.2091	0.3	2899	4	3		
B.52.1.1	0.07	278	35	0.13	3.0496	1.3	0.1176	0.5	1919	9	5		
B.53.1.1	0.02	413	98	0.25	3.0529	1.3	0.1176	0.4	1920	7	5		
B.54.1.1	0.05	240	73	0.31	2.1066	1.3	0.1745	0.4	2602	7	4		
B.55.1.1	0.04	201	95	0.49	2.0946	1.3	0.1728	0.4	2585	7	3		
B.56.1.1	0.02	573	299	0.54	2.1469	1.2	0.1628	0.3	2485	5	1		
B.57.1.1	0.04	274	155	0.58	1.9872	1.3	0.1748	0.4	2604	6	-1		
B.58.1.1	0.02	582	123	0.22	2.1505	1.5	0.1704	0.9	2562	15	4		
B.59.1.1	0.01	552	56	0.1	2.2548	1.2	0.1585	0.3	2440	5	3		
B.6.1.1	0.02	295	302	1.06	2.4496	1.5	0.149	0.3	2335	5	5		
B.61.1.1	0.04	259	61	0.24	2.0928	1.3	0.1722	0.4	2579	6	2		
B.62.1.1	0.03	351	209	0.62	2.123	1.5	0.1624	0.4	2481	6	0		
B.63.1.1	0.08	296	134	0.47	2.8155	1.3	0.1202	0.5	1959	9	0		
B.65.1.1	0.2	101	85	0.87	2.8199	1.8	0.1226	1	1994	17	2		
B.66.1.1	0.03	232	129	0.57	2.1362	1.3	0.1609	0.4	2465	7	0		
B.67.1.1	0.03	440	138	0.32	2.2383	1.4	0.16	1.6	2455	27	3		
B.68.1.1	0.05	164	130	0.82	1.9528	1.4	0.187	0.5	2716	8	2		
B.69.1.1	0.07	220	161	0.76	3.0484	1.3	0.1171	0.7	1912	12	4		
B.7.1.1	0.02	347	303	0.9	2.145	1.2	0.1604	0.3	2460	5	0		
B.71.1.1	0.07	610	228	0.39	2.1374	1.2	0.1735	0.3	2592	4	5		
B.72.1.1	0.03	483	505	1.08	3.1465	1.2	0.1127	0.4	1843	7	3		
B.75.1.1	0.07	135	45	0.35	1.7158	1.4	0.219	0.5	2974	7	0		
B.76.1.1	0.03	335	106	0.33	2.0911	1.3	0.1657	0.4	2515	6	0		
B.77.1.1	0.19	341	129	0.39	3.0532	1.3	0.1181	0.6	1928	10	5		
B.78.1.1	0.02	517	281	0.56	2.1356	1.2	0.1665	0.3	2523	5	2		
B.79.1.1	0.02	931	37	0.04	2.0947	1.3	0.1749	0.2	2605	3	3		
B.8.1.1	0.03	100	63	0.65	1.8105	1.4	0.2121	0.4	2922	7	3		

B.80.1.1	-0.03	88	75	0.89	2.6856	1.5	0.1235	0.9	2008	15	-2		
B.81.1.1	0.12	101	204	2.1	2.8265	1.4	0.1183	0.8	1931	14	-1		
B.82.1.1	0.07	115	49	0.44	1.93	1.4	0.1817	0.5	2669	9	-1		
B.83.1.1	0.07	229	131	0.59	2.1764	1.3	0.1715	0.4	2572	7	5		
B.84.1.1	0.02	464	201	0.45	2.6931	1.3	0.1238	0.4	2012	6	-1		
B.85.1.1	0.03	313	176	0.58	2.0891	1.3	0.1684	0.3	2542	6	1		
B.86.1.1	0.04	181	244	1.39	1.9389	1.3	0.1851	0.4	2699	7	1		
B.9.1.1	0.02	439	242	0.57	2.1823	1.2	0.1634	0.2	2491	4	2		
Sample 2007169003 (1937152), Daniel Creek Formation					New SHRIMP U-Pb zircon ages from north Queensland, 2007–2010					Neumann and Kositcin, 2011			
Grain ID	206Pbc(%)1	U (ppm)	Th (ppm)	232Th/238U	238U/206Pb	± 1σ (%)	207Pb/206Pb	± 1σ (%)	207Pb/206Pb Age (Ma)	± 1σ (Ma)	Disc (%)		
C.1.1.1	0.03	447	314	0.73	2.1539	1.3	0.1664	0.3	2521	5	2		
C.13.1.1	0.03	162	173	1.1	1.8672	1.4	0.1881	0.5	2726	8	-1		
C.14.1.1	0.31	151	74	0.51	2.3652	1.4	0.146	0.7	2300	12	1		
C.15.1.1	0.04	233	191	0.85	1.9581	1.3	0.1872	0.4	2718	7	2		
C.16.1.1	0.02	287	118	0.43	2.5714	1.3	0.1398	0.4	2224	7	5		
C.17.1.1	0.05	88	41	0.49	1.3717	2.1	0.3065	0.5	3503	7	-1		
C.18.1.1	0.05	343	251	0.76	2.1207	1.3	0.1627	0.4	2484	6	0		
C.19.1.1	0.07	194	143	0.76	2.3437	1.3	0.1459	0.5	2298	9	0		
C.2.1.1	0.09	253	221	0.9	2.0865	1.3	0.1812	0.4	2664	6	5		
C.20.1.1	0.04	285	179	0.65	2.008	1.3	0.1854	0.3	2702	6	4		
C.22.1.1	0.01	487	254	0.54	2.3152	1.2	0.1504	0.3	2351	5	2		
C.23.1.1	0.03	531	195	0.38	2.3128	1.2	0.1477	0.3	2319	5	0		
C.24.1.1	0.04	305	206	0.7	2.196	1.3	0.1658	0.4	2516	6	4		
C.25.1.1	0.04	1668	7	0	2.4047	1.9	0.1513	1.4	2361	24	5		
C.26.1.1	0.13	96	40	0.43	2.2583	1.4	0.1599	0.7	2455	11	4		
C.27.1.1	0.18	132	58	0.45	2.9311	1.4	0.1169	0.8	1909	14	1		
C.28.1.1	0.12	79	31	0.41	1.7587	1.5	0.2225	0.6	2999	10	3		

C.29.1.1	0.04	230	72	0.32	1.8723	1.3	0.1881	0.3	2725	6	-1		
C.30.1.1	0.04	390	219	0.58	1.9966	1.2	0.1736	0.3	2593	5	-1		
C.31.1.1	0.03	193	64	0.34	1.8866	1.4	0.1866	0.4	2712	6	-1		
C.32.1.1	0.07	613	316	0.53	2.8962	1.2	0.1205	0.3	1963	6	3		
C.33.1.1	0.05	107	63	0.61	1.8124	1.4	0.2114	0.5	2917	7	3		
C.35.1.1	0.02	352	167	0.49	2.181	1.2	0.1642	0.3	2500	5	3		
C.36.1.1	0.04	322	167	0.54	2.0233	1.3	0.1759	0.3	2614	5	1		
C.37.1.1	0.05	181	127	0.72	2.6328	1.4	0.1336	0.5	2145	9	3		
C.38.1.1	0.06	396	52	0.14	3.0742	1.2	0.1174	0.4	1916	7	5		
C.40.1.1	0.13	37	53	1.47	2.169	1.7	0.1699	1.6	2557	26	4		
C.43.1.1	0.04	256	142	0.57	2.2354	1.3	0.1542	0.4	2393	6	0		
C.44.1.1	0.05	210	231	1.13	2.0595	1.6	0.1742	0.4	2599	6	2		
C.45.1.1	0.19	317	125	0.41	2.2191	1.2	0.1622	0.4	2478	6	3		
C.47.1.1	0.03	333	254	0.79	2.1596	1.2	0.1617	0.3	2473	5	1		
C.48.1.1	0.04	281	157	0.58	2.0576	1.4	0.1735	0.3	2592	6	1		
C.49.1.1	0.15	120	99	0.85	2.1668	1.4	0.1645	0.6	2503	10	2		
C.5.1.1	-0.01	218	76	0.36	2.066	1.5	0.1787	0.8	2641	13	4		
C.50.1.1	0.02	546	229	0.43	2.1157	0.9	0.163	0.3	2487	4	0		
C.51.1.1	0	449	228	0.52	3.022	0.9	0.1149	0.4	1878	7	2		
C.52.1.1	0.04	271	216	0.82	1.9419	1	0.1865	0.3	2711	6	1		
C.53.1.1	0.02	430	674	1.62	1.9891	0.9	0.1773	0.3	2628	5	0		
C.54.1.1	0.07	299	200	0.69	2.0448	1	0.1747	0.4	2604	6	1		
C.55.1.1	0.06	195	73	0.39	2.3769	1.1	0.1473	0.5	2315	8	2		
C.56.1.1	0.03	110	208	1.96	1.9739	1.1	0.1866	0.5	2713	9	3		
C.57.1.1	0.06	238	239	1.04	2.9102	1	0.1185	0.5	1934	10	2		
C.59.1.1	0.02	593	92	0.16	2.1606	1	0.1671	0.2	2529	4	3		
C.6.1.1	0.04	252	201	0.82	2.3487	1.3	0.1484	0.4	2327	7	2		
C.60.1.1	0.19	98	59	0.62	1.9988	1.2	0.1809	0.6	2661	10	2		
C.61.1.1	0.05	467	323	0.71	2.1703	1	0.1717	0.3	2574	5	5		

C.62.1.1	0.06	244	160	0.68	1.9386	1	0.1879	0.3	2724	6	2		
C.63.1.1	0.13	408	366	0.93	2.6463	0.9	0.1365	0.4	2184	6	5		
C.64.1.1	0.06	507	140	0.28	3.0892	1	0.1119	0.4	1831	7	1		
C.65.1.1	0.05	312	161	0.53	2.2194	1	0.1554	0.4	2407	6	0		
C.66.1.1	0.1	126	149	1.22	2.0318	1.1	0.1745	0.5	2601	9	1		
C.68.1.1	0.24	131	86	0.68	2.8991	1.1	0.1202	0.8	1960	15	3		
C.69.1.1	0.04	269	135	0.52	2.0361	1	0.1754	0.3	2610	6	1		
C.7.1.1	0.08	204	156	0.79	2.7803	1.3	0.1222	0.6	1988	10	0		
C.70.1.1	0.03	625	118	0.19	2.2416	0.9	0.1639	0.2	2496	4	5		
C.71.1.1	0.02	582	254	0.45	2.3801	0.9	0.1509	0.3	2356	4	4		
C.72.1.1	0.05	281	72	0.27	2.7619	1.1	0.1277	0.4	2066	8	4		
C.73.1.1	0.01	382	133	0.36	1.9319	0.9	0.1895	0.3	2738	4	2		
C.74.1.1	0.03	539	415	0.8	2.1858	0.9	0.1638	0.3	2496	4	3		
C.77.1.1	0.16	94	103	1.13	2.7596	1.2	0.1266	1	2051	17	3		
C.78.1.1	0.03	232	131	0.59	3.208	1	0.1122	0.6	1835	10	5		
C.79.1.1	0.03	224	73	0.34	1.9403	1	0.1878	0.4	2723	6	2		
C.8.1.1	0.08	170	133	0.81	2.11	1.4	0.1758	0.7	2613	11	4		
C.80.1.1	0.04	203	59	0.3	1.9894	1.6	0.1821	0.7	2672	12	2		
C.81.1.1	0.01	193	159	0.85	1.9233	1	0.1842	0.5	2691	9	0		
C.82.1.1	0.06	347	177	0.53	2.0052	1	0.1844	1.3	2693	22	3		
C.83.1.1	0.05	268	134	0.52	2.2201	1.2	0.1578	0.4	2432	7	1		
C.84.1.1	0.04	473	264	0.58	2.1174	1	0.1633	0.3	2490	5	0		
C.85.1.1	0.05	228	86	0.39	2.9877	1	0.1159	0.6	1894	10	2		
C.86.1.1	0.01	508	222	0.45	2.0943	0.9	0.1682	0.3	2540	4	1		
C.87.1.1	0.01	674	239	0.37	2.2491	0.9	0.1558	0.2	2411	4	2		
Sample 2007169004 (1937153), Corbett Formation					New SHRIMP U-Pb zircon ages from north Queensland, 2007–2010					Neumann and Kositcin, 2011			
Grain ID	206Pbc(%)1	U (ppm)	Th (ppm)	232Th/238U	238U/206Pb	± 1σ (%)	207Pb/206Pb	± 1σ (%)	207Pb/206Pb Age (Ma)	± 1σ (Ma)	Disc (%)		

D.1.1.1	0.04	90	49	0.56	2.6857	1.6	0.1292	0.8	2086	14	2		
D.10.1.1	0.03	250	160	0.66	2.3637	1.4	0.1506	0.3	2353	6	3		
D.11.1.1	0.03	309	180	0.6	2.0726	1.4	0.1746	0.3	2602	4	2		
D.12.1.1	0.08	228	106	0.48	3.2019	1.4	0.1092	0.5	1785	10	2		
D.13.1.1	0.01	356	144	0.42	2.2177	1.4	0.164	0.3	2497	4	4		
D.14.1.1	-0.02	236	125	0.55	2.477	1.6	0.1353	0.4	2167	6	-1		
D.15.1.1	0	204	85	0.43	3.0745	1.4	0.113	0.4	1849	8	2		
D.17.1.1	0.04	346	32	0.09	2.9057	0.9	0.1202	0.4	1959	7	3		
D.18.1.1	0.21	55	66	1.24	2.1381	1.3	0.1677	0.7	2535	12	2		
D.19.1.1	0.05	269	101	0.39	2.9622	1	0.1164	0.5	1902	8	1		
D.2.1.1	0.03	188	91	0.5	2.3889	1.6	0.1486	0.5	2330	9	3		
D.20.1.1	0.04	429	217	0.52	2.98	1.1	0.1151	0.4	1881	6	1		
D.21.1.1	0.05	460	427	0.96	2.9479	0.9	0.1173	0.4	1915	6	2		
D.22.1.1	0.02	501	167	0.34	2.0284	0.9	0.1743	0.2	2599	4	1		
D.23.1.1	0.05	308	307	1.03	1.9761	1	0.1871	0.3	2717	5	3		
D.25.1.1	0.05	402	11	0.03	2.7534	0.9	0.125	0.4	2028	7	2		
D.27.1.1	0.04	351	416	1.23	2.8106	0.9	0.1225	0.4	1993	7	2		
D.28.1.1	0.08	238	251	1.09	2.7484	1	0.1256	0.5	2038	9	2		
D.29.1.1	0.02	102	32	0.32	1.8055	1.1	0.2112	0.5	2914	8	3		
D.3.1.1	0.08	169	50	0.31	1.9487	1.5	0.1973	0.4	2804	7	5		
D.30.1.1	0.05	407	139	0.35	2.1091	0.9	0.1752	0.3	2608	5	4		
D.31.1.1	0.07	264	186	0.73	2.9412	1	0.1158	0.5	1892	9	0		
D.32.1.1	0.17	81	43	0.55	2.0553	1.5	0.1647	0.7	2504	12	-2		
D.33.1.1	0.11	353	175	0.51	3.1103	1.3	0.1162	0.5	1898	8	5		
D.34.1.1	0.08	118	59	0.52	2.676	1.4	0.13	0.7	2098	13	2		
D.35.1.1	0.05	190	80	0.44	2.4948	1.6	0.1354	0.5	2169	9	0		
D.36.1.1	0.03	316	81	0.26	2.5984	1.3	0.1303	0.4	2103	7	0		
D.37.1.1	0.05	132	67	0.52	2.136	1.4	0.1637	0.5	2495	9	1		
D.38.1.1	0.12	129	54	0.43	2.3756	1.4	0.1467	0.6	2308	10	2		

D.39.1.1	0.01	514	100	0.2	2.0243	1.3	0.1765	0.4	2621	6	1		
D.4.1.1	0.06	167	150	0.93	2.1189	1.5	0.1677	0.5	2534	8	2		
D.40.1.1	0.03	281	102	0.37	3.1701	1.4	0.109	0.5	1782	9	1		
D.41.1.1	0.05	191	112	0.61	2.0362	1.4	0.171	0.4	2568	7	0		
D.42.1.1	0.05	270	103	0.39	2.7514	1.3	0.1231	0.5	2002	8	0		
D.43.1.1	0.03	306	110	0.37	1.4791	1.3	0.2735	0.2	3326	4	0		
D.44.1.1	0.2	82	47	0.6	2.9329	1.5	0.1164	1	1902	18	1		
D.45.1.1	0.01	318	137	0.45	2.0216	1.3	0.1745	0.3	2602	5	0		
D.46.1.1	0.03	216	92	0.44	2.0343	1.3	0.174	0.4	2596	6	1		
D.47.1.1	0.07	121	32	0.28	2.7954	1.4	0.1225	0.8	1992	13	1		
D.48.1.1	0.1	81	44	0.56	1.8827	1.5	0.1866	0.6	2713	11	-1		
D.49.1.1	0.11	126	46	0.38	2.9403	1.7	0.1181	0.7	1927	13	2		
D.5.1.1	0.05	128	114	0.92	1.9071	1.5	0.1902	0.4	2744	6	1		
D.50.1.1	0.32	87	43	0.52	3.0047	1.5	0.1148	1.2	1877	21	1		
D.51.1.1	0.06	453	143	0.33	3.058	1.3	0.1144	0.4	1870	6	2		
D.52.1.1	0.16	86	49	0.59	2.0916	1.4	0.1708	0.6	2566	10	2		
D.53.1.1	0.3	72	67	0.96	2.7769	1.5	0.1224	1.1	1992	20	0		
D.54.1.1	0.07	124	78	0.65	2.0491	1.4	0.1747	0.5	2604	8	2		
D.56.1.1	0.15	248	249	1.04	3.0506	1.3	0.1108	0.6	1812	10	-1		
D.57.1.1	0.09	86	41	0.5	1.828	1.4	0.2125	0.5	2924	9	4		
D.58.1.1	0.08	314	124	0.41	2.8344	1.3	0.1216	0.4	1980	8	2		
D.59.1.1	0.03	357	166	0.48	2.8086	1.3	0.1196	0.4	1950	7	-1		
D.6.1.1	0	305	36	0.12	2.1298	1.4	0.1709	0.3	2566	4	3		
D.60.1.1	0.13	77	31	0.41	2.9339	1.5	0.1191	0.9	1943	17	3		
D.61.1.1	0.07	385	172	0.46	3.0091	1.3	0.115	0.4	1880	8	2		
D.62.1.1	0.05	185	169	0.95	2.5047	1.3	0.1392	0.5	2217	9	2		
D.63.1.1	0.14	145	67	0.48	2.9029	1.4	0.1178	0.7	1924	13	1		
D.64.1.1	0	161	129	0.83	1.917	1.3	0.1845	0.4	2694	7	0		
D.65.1.1	0.15	265	119	0.46	2.8867	1.3	0.1233	0.5	2005	9	4		

D.66.1.1	0.05	109	39	0.37	2.871	1.4	0.116	1	1895	17	-2		
D.67.1.1	0.04	147	188	1.32	2.0378	1.4	0.1755	0.5	2611	8	1		
D.68.1.1	0	118	118	1.04	1.861	1.4	0.1884	0.6	2728	10	-2		
D.69.1.1	0.06	84	60	0.73	1.8189	1.5	0.1976	0.6	2807	9	-1		
D.7.1.1	-0.01	268	134	0.52	2.0326	1.4	0.1752	0.3	2608	5	1		
D.70.1.1	0.05	320	164	0.53	2.1011	1.3	0.1617	0.3	2474	6	-1		
D.71.1.1	0.07	249	118	0.49	3.0715	1.3	0.1093	0.6	1788	11	-2		
D.72.1.1	0.08	213	151	0.73	2.7816	1.5	0.1212	0.6	1975	10	0		
D.73.1.1	0.06	301	261	0.89	2.7311	1.3	0.1223	0.5	1990	8	-1		
D.74.1.1	0.13	53	20	0.39	1.8952	1.6	0.19	0.8	2742	13	0		
D.8.1.1	0.02	190	163	0.89	1.9583	1.5	0.1858	0.3	2705	5	2		
D.9.1.1	0.02	161	72	0.46	2.0763	1.5	0.1747	0.4	2603	6	3		
GA sample ID 1977852, Lane Creek Formation					Basin analysis and the geochemical signature of Paleoproterozoic sedimentary successions in northern Australia: Constraints on basin development in respect to mineralisation and paleoreconstruction models							Lambeck, 2011	
Grain ID	206Pbc(%)1	U (ppm)	Th (ppm)	232Th/238U	238U/206Pb	± 1σ (%)	207Pb/206Pb	± 1σ (%)	206Pb/238U Age (Ma)	± 1σ (%)	207Pb/206Pb Age (Ma)	± 1σ (Ma)	Disc (%)
852.61.1.1	0.02	906	298	0.34	3.2208	1.31	0.1087	0.3	1743	20.8	1775	5.5	3
852.22.1.1	0.02	439	237	0.56	3.1215	1.35	0.1093	0.4	1791	22.6	1785	7.9	2
852.20.1.1	0.04	239	102	0.44	3.2034	1.68	0.1095	0.6	1750	27.2	1785	11.1	2
852.25.1.1	-0.01	434	172	0.41	3.1904	1.35	0.1092	0.4	1757	21.8	1787	7.8	2
852.5.1.1	0	327	133	0.42	3.2237	1.38	0.1093	0.5	1743	22.2	1788	9	1
852.81.1.1	0.03	294	104	0.37	3.1155	1.4	0.1097	0.5	1794	23	1790	10.5	2
852.8.1.1	-0.01	478	395	0.86	3.1536	1.34	0.1094	0.5	1777	23.3	1792	8.5	0
852.57.1.1	0.05	147	61	0.43	3.1089	1.5	0.1109	1.1	1796	24.8	1806	20.7	0
852.84.1.1	0.22	82	44	0.55	3.0951	1.69	0.1124	1	1805	28.6	1807	22.7	1
852.49.1.1	0.14	81	63	0.8	3.0252	1.66	0.1121	0.9	1845	29.7	1815	21.9	2
852.53.1.1	0.04	138	75	0.56	2.982	1.51	0.1114	1.1	1863	26.3	1817	21.2	0
852.55.1.1	-0.07	237	88	0.38	3.1333	1.57	0.1107	0.6	1785	25.8	1820	11	1

852.66.1.1	0.41	56	54	1	3.0784	1.83	0.1151	1.2	1807	33.4	1824	30.8	1
852.10.1.1	0.05	267	94	0.36	3.0805	1.39	0.1122	0.5	1812	23	1828	10.5	1
852.46.2.1	0.13	85	63	0.76	3.0532	1.72	0.1129	0.9	1835	30.3	1829	20.7	3
852.82.1.1	-0.01	458	129	0.29	3.0383	1.63	0.1117	0.4	1836	26.9	1829	7.4	1
852.47.1.1	0.01	645	349	0.56	3.0939	1.32	0.1119	0.3	1805	22.3	1829	6.4	2
852.54.1.1	0.05	227	92	0.42	3.0417	1.42	0.1122	0.6	1831	23.9	1829	10.8	3
852.71.1.1	0.14	83	60	0.75	3.001	1.76	0.1131	0.9	1856	31.4	1830	22.3	3
852.59.1.1	0.03	577	50	0.09	3.0492	1.41	0.1123	0.4	1829	22.8	1833	6.7	1
852.41.1.1	-0.01	424	304	0.74	3.1077	1.35	0.1121	0.4	1797	23.3	1835	7.5	1
852.31.1.1	0.01	315	330	1.08	3.0753	1.38	0.1122	0.5	1817	25.2	1835	8.8	0
852.11.1.1	0.13	107	44	0.43	3.0492	1.57	0.1134	0.8	1827	26.3	1837	17.6	1
852.64.1.1	0.04	60	42	0.72	2.9861	1.88	0.1128	1.1	1857	33.5	1838	20.5	0
852.40.1.1	0.01	1175	92	0.08	3.032	1.3	0.1129	0.2	1837	20.9	1845	4.5	1
852.56.1.1	-0.01	252	101	0.41	3.0444	1.41	0.1128	0.5	1831	23.6	1847	9.7	0
852.29.1.1	0	282	166	0.61	3.0578	1.39	0.113	0.5	1824	23.9	1848	9	0
852.33.1.1	0.01	449	57	0.13	3.0426	1.34	0.1132	0.4	1831	21.7	1851	7.2	0
852.32.1.1	0.02	728	272	0.39	3.0338	1.32	0.1136	0.3	1837	22.2	1855	5.8	1
852.14.1.1	0.07	95	54	0.59	3.0407	1.6	0.1144	0.8	1821	27.7	1861	16.9	-1
852.73.1.1	0.02	433	108	0.26	3.0746	1.35	0.1141	0.4	1814	22.1	1864	7.9	1
852.18.1.1	-0.02	485	229	0.49	3.001	1.34	0.1144	0.4	1852	22.9	1873	6.7	-1
852.43.1.1	0.04	449	120	0.28	2.9888	1.34	0.115	0.4	1862	22.4	1874	7.7	-1
852.21.1.1	0.01	88	12	0.14	2.9412	1.62	0.1148	0.9	1886	27	1875	15.7	1
852.50.1.1	0.04	385	216	0.58	2.9252	1.36	0.1151	0.4	1894	24	1877	7.9	-3
852.42.1.1	-0.02	159	127	0.83	3.0599	1.48	0.1148	0.7	1822	26.2	1880	12.3	1
852.63.2.1	0.24	36	36	1.03	2.7862	2.05	0.1173	1.3	1972	40.3	1883	39.5	2
852.27.1.1	0.01	54	21	0.41	3.0535	1.81	0.1157	1.2	1823	30.4	1890	21.5	2
852.16.1.1	-0.01	156	30	0.2	2.9676	1.48	0.1159	0.7	1872	24.7	1896	11.9	-1
852.4.1.1	0.04	304	246	0.84	2.935	1.39	0.117	0.5	1886	25.4	1906	9.3	1
852.3.1.1	0.07	125	75	0.62	2.9383	1.54	0.1178	0.8	1890	27.4	1914	14.6	1

852.9.1.1	0.13	134	201	1.55	2.9421	1.51	0.1187	0.8	1881	31	1919	16.8	-1
852.28.1.1	0.04	351	179	0.53	2.9459	1.36	0.118	0.4	1884	23.8	1921	8	3
852.13.1.1	0.02	336	184	0.57	2.9053	1.36	0.1182	0.4	1907	24.2	1927	8.1	2
852.17.1.1	0	426	197	0.48	2.8941	1.35	0.118	0.4	1912	23.6	1927	7	1
852.44.1.1	0.05	152	83	0.57	2.8646	1.48	0.1186	0.7	1929	26.6	1928	12.9	1
852.19.1.1	0.01	713	265	0.38	2.8792	1.32	0.1182	0.3	1921	22.9	1928	5.5	1
852.30.1.1	0.09	166	222	1.38	2.8877	1.47	0.119	0.7	1916	29.5	1930	13.4	3
852.48.1.1	-0.07	75	49	0.68	2.9053	1.69	0.1187	0.9	1906	30.4	1947	17.6	0
852.52.1.1	-0.05	133	67	0.52	2.928	1.51	0.1193	0.9	1894	26.6	1953	17.3	0
852.62.1.1	0.01	197	189	0.99	2.8797	1.44	0.121	0.6	1918	27.3	1970	10.2	-5
852.67.1.1	-0.02	285	196	0.71	2.7704	1.39	0.1225	0.5	1985	25.9	1995	8.3	0
852.12.1.1	0.28	63	55	0.89	2.6767	1.74	0.128	1	2045	34.4	2036	23	3
852.85.1.1	0.14	173	93	0.55	2.6314	1.48	0.1282	0.6	2076	28.1	2056	12.6	0
852.80.1.1	0.11	433	143	0.34	2.5578	1.36	0.1294	0.4	2125	25.7	2077	7.6	2
852.65.1.1	0.02	439	193	0.45	2.6165	1.35	0.1288	0.4	2087	25.3	2078	6.5	-1
852.38.1.1	0.03	150	59	0.41	2.6572	1.48	0.1298	0.8	2058	27.4	2092	14.7	0
852.26.1.1	-0.03	88	46	0.54	2.6888	1.62	0.1296	0.8	2038	30.3	2096	14.2	-2
852.60.1.1	0.01	618	328	0.55	2.3327	1.41	0.1473	0.3	2300	29	2314	4.8	1
852.6.1.1	0.04	129	119	0.95	2.3262	1.53	0.1533	0.6	2301	33.3	2378	11.3	3
852.70.1.1	0.03	246	109	0.46	2.2041	1.41	0.1613	0.4	2413	29.8	2467	7.4	2
852.34.1.1	-0.08	49	22	0.47	2.2283	2.88	0.1604	0.9	2387	60.6	2467	15.6	3
852.39.1.1	0.01	287	127	0.46	2.1698	1.38	0.1623	0.4	2443	29.6	2479	6.2	1
852.23.1.1	0.03	83	36	0.44	2.0995	1.63	0.1689	0.7	2514	35.7	2543	11.4	1
852.15.1.1	0.05	122	85	0.72	2.0446	1.52	0.1717	0.5	2563	35	2570	9.3	0
852.51.1.1	0.02	291	104	0.37	2.0463	1.54	0.1725	0.6	2564	33.9	2581	10.2	1
852.76.1.1	-0.01	522	411	0.81	2.0433	1.34	0.1734	0.3	2567	31	2591	4.4	1
852.77.1.1	0	382	112	0.3	2.0165	1.36	0.1735	0.3	2596	30	2592	5.2	0
852.72.1.1	0.01	76	36	0.5	2.0499	1.7	0.1737	0.7	2557	37.9	2593	11.7	1
852.7.1.1	0.01	416	62	0.15	2.0449	1.37	0.1738	0.3	2566	29.5	2594	4.9	1

852.75.1.1	0.01	202	93	0.47	1.9985	1.49	0.1738	0.4	2616	33.6	2594	7.2	-1
852.45.1.1	0.02	353	289	0.84	2.0573	1.37	0.177	0.7	2549	31.7	2624	12.4	3
852.1.1.1	0.02	521	85	0.17	1.9939	1.5	0.1785	0.3	2620	32.8	2637	4.4	1
852.36.1.1	0.05	172	58	0.35	1.9738	1.49	0.181	1.2	2645	33.5	2658	19.5	1
852.35.1.1	0	160	96	0.62	1.9693	1.47	0.1819	0.4	2647	34.1	2670	7.4	1
852.83.1.1	0.03	222	76	0.35	2.0015	1.43	0.1836	0.4	2616	31.8	2684	6.7	3
852.69.1.1	0.02	391	218	0.57	1.9852	1.35	0.1851	0.3	2624	31	2697	5.4	3
852.37.1.1	0.01	250	177	0.73	1.9368	1.39	0.1873	0.3	2687	33.1	2718	5.8	1
852.68.1.1	0.88	85	67	0.81	1.8887	1.64	0.1957	1.3	2741	40.4	2723	42.1	0
852.78.1.1	0.03	109	78	0.74	1.911	1.57	0.1918	0.5	2714	37.7	2755	9.2	2
852.74.1.1	0.02	430	51	0.12	1.9328	1.35	0.1933	0.6	2689	30.1	2769	9.3	3
852.2.1.1	0	278	321	1.19	1.9279	1.69	0.1957	0.3	2693	42.5	2791	5.7	4
852.79.1.1	0.03	110	33	0.31	1.7525	1.58	0.2033	0.5	2909	38.2	2851	8.7	-2
852.24.1.1	0.12	82	75	0.94	1.7719	1.63	0.2098	0.6	2879	42	2896	9.9	1

Table 2: data from the upper Etheridge- and Langlovale groups detrital zircon

upper Etheridge- and Langlovale Group detrital zircon											
Sample 2007169005 (1937154), Townley Formation					New SHRIMP U-Pb zircon ages from north Queensland, 2007–2010					Neumann and Kositcin, 2011	
Grain ID	206Pbc(%)1	U (ppm)	Th (ppm)	232Th/238U	238U/206Pb	± 1σ (%)	207Pb/206Pb	± 1σ(%)	207Pb/206Pb Age (Ma)	± 1σ (Ma)	Disc (%)
E.1.1.1	0.17	69	53	0.8	3.0816	1.7	0.1115	1	1823	18	1
E.10.1.1	0.07	289	94	0.34	3.3721	1.2	0.1076	0.4	1759	8	5
E.11.1.1	0.04	178	133	0.77	2.5566	1.3	0.1365	0.4	2183	7	3
E.12.1.1	0.08	90	23	0.27	3.2217	1.4	0.1119	0.8	1830	14	5
E.13.1.1	0.01	118	33	0.28	2.066	1.3	0.1795	0.4	2648	7	4
E.14.1.1	0.11	121	104	0.89	2.8656	1.3	0.124	0.6	2015	11	4
E.15.1.1	-0.02	99	45	0.47	2.9724	1.4	0.1213	0.6	1976	11	5
E.16.1.1	0.07	338	221	0.67	3.448	1.2	0.1017	0.5	1656	8	1
E.18.1.1	0.02	352	84	0.25	2.0537	1.2	0.1842	0.2	2691	4	5
E.19.1.1	0.16	73	91	1.28	3.4072	1.4	0.1006	0.9	1635	17	-1

E.2.1.1	0.02	226	152	0.7	1.4738	1.3	0.2763	0.2	3342	4	0
E.20.1.1	0.05	193	34	0.18	3.113	1.3	0.1127	0.5	1843	9	3
E.26.1.1	0.08	180	62	0.36	3.2559	1.3	0.1084	0.5	1773	10	3
E.27.1.1	0.09	206	144	0.72	3.4457	1.3	0.1016	0.5	1653	10	1
E.28.1.1	0.03	217	228	1.08	2.1055	1.2	0.1746	0.3	2602	5	4
E.3.1.1	0.12	89	26	0.3	3.1844	1.4	0.1082	0.8	1769	15	0
E.30.1.1	0.01	178	98	0.57	2.0662	1.3	0.1715	0.4	2572	6	1
E.31.1.1	0.07	523	84	0.17	3.0564	1.2	0.1125	0.4	1841	7	1
E.32.1.1	0.2	195	88	0.46	2.8011	1.3	0.1204	0.8	1963	14	0
E.33.1.1	0.1	196	147	0.78	3.5449	1.3	0.1013	0.6	1648	11	3
E.37.1.1	0.13	117	55	0.49	2.4951	1.3	0.1436	1.2	2271	21	4
E.4.1.1	0.14	55	20	0.37	2.0217	1.5	0.1868	0.6	2714	10	5
E.42.1.1	0.16	95	77	0.84	3.519	1.4	0.1007	0.9	1636	17	1
E.43.1.1	0.07	385	310	0.83	3.3863	1.2	0.1012	0.4	1646	8	-1
E.44.1.1	0.06	151	80	0.55	2.2987	1.8	0.1469	0.4	2310	8	-1
E.45.1.1	0.04	239	116	0.5	2.0158	1.3	0.1715	0.3	2573	5	-1
E.46.1.1	0.09	181	53	0.3	1.8983	1.3	0.2018	0.5	2841	8	4
E.47.1.1	0.05	155	79	0.53	1.7972	1.3	0.2185	0.3	2970	5	4
E.49.1.1	0.22	112	84	0.78	3.5592	1.4	0.1004	1.1	1632	20	2
E.5.1.1	0.04	267	319	1.23	3.5883	1.3	0.1015	0.5	1651	9	4
E.50.1.1	0.07	218	149	0.71	3.4775	1.3	0.102	0.6	1661	11	2
E.51.1.1	0.18	91	102	1.16	3.6856	1.4	0.1007	1	1637	19	5
E.56.1.1	0.11	124	55	0.46	3.0639	1.4	0.112	0.8	1832	15	1
E.57.1.1	0.14	201	238	1.22	3.0354	1.3	0.1128	0.6	1846	11	1
E.58.1.1	0.09	127	67	0.54	2.9866	1.4	0.1119	0.8	1830	14	-2
E.59.1.1	0.03	341	97	0.29	3.218	1.2	0.1075	0.4	1757	8	1
E.6.1.1	0.04	182	118	0.67	3.5344	1.4	0.1017	0.6	1656	10	3
E.60.1.1	0.13	133	61	0.47	2.6699	1.4	0.1283	0.7	2075	13	1
E.61.1.1	0.06	132	118	0.93	3.5462	1.3	0.1028	0.7	1676	13	4

E.66.1.1	0.03	347	143	0.43	3.2581	1.3	0.1109	0.5	1815	9	5
E.67.1.1	0.08	223	168	0.78	3.4651	1.3	0.1006	0.7	1635	13	0
E.68.1.1	0.09	99	73	0.76	3.4873	1.5	0.1032	1.1	1682	20	3
E.69.1.1	0.02	208	219	1.09	3.4734	1.7	0.1019	0.8	1658	14	2
E.7.1.1	0.07	221	55	0.26	3.2027	1.4	0.1087	0.5	1779	9	2
E.70.1.1	0.01	270	168	0.64	2.0386	1.3	0.1726	0.4	2583	6	0
E.71.1.1	0.03	354	266	0.78	3.4138	1.3	0.1013	0.6	1647	10	-1
E.8.1.1	0.01	268	383	1.48	2.9371	1.3	0.1197	0.4	1952	7	3
Sample 2007169006 (1937155), Heliman Formation					New SHRIMP U-Pb zircon ages from north Queensland, 2007–2010					Neumann and Kositcin, 2011	
Grain ID	206Pbc(%)1	U (ppm)	Th (ppm)	232Th/238U	238U/206Pb	± 1σ (%)	207Pb/206Pb	± 1σ(%)	207Pb/206Pb Age (Ma)	± 1σ (Ma)	Disc (%)
C.1.1.1	0.08	231	85	0.38	3.3211	1.2	0.1081	0.6	1767	12	4
C.10.1.1	0.04	430	157	0.38	3.1848	1.2	0.107	0.4	1749	7	-1
C.11.1.1	0.09	298	205	0.71	3.4428	1.2	0.1019	0.5	1658	9	1
C.12.1.1	0.08	164	115	0.72	3.4913	1.2	0.1012	0.7	1647	13	1
C.13.1.1	0.13	192	169	0.91	3.4628	1.2	0.1002	0.8	1627	14	-1
C.14.1.1	0.21	687	538	0.81	3.596	1.1	0.1013	0.4	1647	8	4
C.15.1.1	0.15	443	140	0.33	3.0393	1.1	0.1132	0.4	1851	7	1
C.17.1.1	0.3	125	157	1.29	3.4666	1.3	0.0999	1	1622	19	-1
C.18.1.1	0.11	225	232	1.06	3.4936	1.2	0.1009	0.6	1640	12	1
C.19.1.1	0.03	269	316	1.22	3.4481	1.2	0.1014	0.5	1650	9	0
C.2.1.1	0.07	169	157	0.96	3.5658	1.2	0.1025	0.7	1669	13	5
C.20.1.1	0.02	113	173	1.58	3.4053	1.4	0.1021	0.9	1663	16	0
C.21.1.1	0.08	224	325	1.5	3.5518	1.2	0.1015	0.7	1651	14	3
C.22.1.1	0.05	163	52	0.33	3.2834	1.3	0.1089	0.9	1782	16	4
C.25.1.1	0.02	134	82	0.63	1.9511	1.2	0.1834	0.4	2684	7	1
C.26.1.1	0.1	190	201	1.09	3.4711	1.2	0.1013	0.7	1648	13	1
C.27.1.1	0.04	523	373	0.74	3.4089	1.1	0.1015	0.4	1652	7	0

C.3.1.1	0.02	136	101	0.77	3.4462	1.3	0.1028	0.7	1676	13	2
C.30.1.1	0.04	151	151	1.03	3.4634	1.2	0.1023	0.6	1666	11	2
C.31.1.1	-0.01	309	201	0.67	3.5636	1.2	0.1025	0.4	1670	8	5
C.32.1.1	0.03	418	163	0.4	2.6399	1.1	0.1343	0.4	2155	6	4
C.33.1.1	0.14	100	74	0.76	3.4818	1.9	0.1029	1	1676	19	3
C.36.1.1	0.1	322	96	0.31	3.2119	1.2	0.1081	0.5	1768	9	1
C.38.1.1	0.01	407	118	0.3	2.9545	1.3	0.112	0.4	1833	7	-3
C.39.1.1	0.04	229	232	1.05	3.4434	1.2	0.1017	0.5	1654	10	1
C.4.1.1	0.04	335	431	1.33	3.395	1.2	0.1014	0.5	1651	9	-1
C.41.1.1	0.17	173	146	0.88	3.4682	1.2	0.1005	0.8	1633	14	0
C.42.1.1	0	127	48	0.39	3.5808	1.3	0.1028	0.7	1675	12	5
C.44.1.1	0.1	172	144	0.86	3.4713	1.2	0.1016	0.7	1654	14	1
C.45.1.1	0.03	136	123	0.94	3.5102	1.3	0.1019	0.7	1659	13	3
C.47.1.1	-0.05	134	119	0.92	3.5898	1.3	0.1019	0.7	1659	13	5
C.48.1.1	0.08	276	275	1.03	3.3535	1.2	0.1006	0.5	1635	10	-3
C.49.1.1	0.04	247	230	0.96	3.4888	1.2	0.1014	0.5	1650	9	2
C.5.1.1	0.01	389	462	1.23	3.6195	1.1	0.1017	0.4	1655	8	5
C.50.1.1	0.06	241	267	1.14	3.4005	1.3	0.1017	0.5	1656	10	0
C.51.1.1	0.04	384	138	0.37	2.7402	1.1	0.1237	0.4	2010	7	0
C.52.1.1	0.01	229	143	0.65	3.4804	1.2	0.1023	0.6	1666	11	2
C.53.1.1	0.13	236	356	1.56	3.4029	1.2	0.101	0.6	1642	12	-1
C.54.1.1	0.02	327	359	1.13	3.4986	1.2	0.1018	0.4	1657	8	2
C.55.1.1	0.06	436	360	0.85	2.8863	1.1	0.12	0.3	1956	6	2
C.56.1.1	0.16	141	155	1.13	3.5166	1.2	0.1011	0.8	1645	15	2
C.57.1.1	0.14	604	358	0.61	2.9406	1.1	0.1149	0.4	1879	6	0
C.58.1.1	0.16	272	177	0.67	3.4055	1.2	0.1013	0.6	1649	11	-1
C.59.1.1	0.06	219	229	1.08	3.4358	1.2	0.1018	0.7	1658	13	1
C.6.1.1	0.2	142	147	1.08	3.6576	1.3	0.1006	0.9	1636	17	5
C.60.1.1	0.02	263	144	0.56	1.6447	1.2	0.2189	0.3	2972	4	-3

C.61.1.1	0.02	279	308	1.14	1.9114	1.2	0.1893	0.3	2736	4	1
C.62.1.1	0	162	204	1.3	3.475	1.2	0.102	0.5	1661	10	2
C.63.1.1	0.02	443	126	0.29	3.0833	1.3	0.1151	0.4	1881	7	4
C.64.1.1	0.07	221	79	0.37	3.3123	1.2	0.1093	0.6	1789	11	5
C.66.1.1	0.02	293	135	0.48	3.0207	1.2	0.113	0.4	1848	7	0
C.67.1.1	-0.02	208	340	1.69	3.5263	1.2	0.1027	0.5	1673	10	4
C.68.1.1	0.1	183	41	0.23	3.4052	1.2	0.1042	0.6	1701	11	2
C.69.1.1	0.11	173	167	1	3.4005	1.3	0.1008	0.8	1640	15	-1
C.7.1.1	0.03	174	46	0.27	3.2614	1.2	0.1076	0.6	1759	11	2
C.70.1.1	0.06	263	300	1.18	3.5694	1.2	0.1019	0.5	1659	9	4
C.71.1.1	0.03	668	278	0.43	3.0433	1.1	0.1148	0.3	1877	5	2
C.72.1.1	0.47	41	92	2.3	2.4783	1.9	0.1408	1.4	2237	24	2
C.74.1.1	0.11	131	121	0.95	3.4412	1.3	0.1009	0.8	1641	15	0
C.75.1.1	0.05	212	104	0.51	3.0011	1.2	0.1143	0.5	1869	9	1
C.76.1.1	0.16	198	133	0.69	3.5414	1.2	0.1013	0.7	1648	13	3
C.79.1.1	0.05	274	62	0.23	3.3364	1.2	0.1089	0.5	1782	9	5
C.8.1.1	0.16	330	362	1.13	3.4654	1.2	0.1019	0.5	1660	10	2
C.80.1.1	0.05	184	178	1	3.4779	1.2	0.1024	0.6	1667	12	2
C.81.1.1	0.02	647	258	0.41	2.7889	1.1	0.1235	0.3	2007	5	2
C.82.1.1	0.07	215	155	0.74	3.5068	1.3	0.1019	0.6	1658	11	2
C.9.1.1	0.02	600	439	0.76	3.079	1.1	0.1146	0.3	1873	5	3
Sample 2007169007 (1937156), Langdon River Mudstone					New SHRIMP U-Pb zircon ages from north Queensland, 2007–2010					Neumann and Kositcin, 2011	
Grain ID	206Pbc(%)1	U (ppm)	Th (ppm)	232Th/238U	238U/206Pb	± 1σ (%)	207Pb/206Pb	± 1σ(%)	207Pb/206Pb Age (Ma)	± 1σ (Ma)	Disc (%)
D.1.1.1	0.1	334	518	1.6	3.4899	1.2	0.0994	0.5	1612	9	-1
D.10.1.1	0.03	447	74	0.17	3.2284	1.1	0.1089	0.3	1782	6	2
D.11.1.1	0.11	166	152	0.95	3.2669	1.2	0.1038	0.7	1693	13	-2
D.12.1.1	0.06	421	263	0.64	3.1603	1.1	0.1105	0.4	1808	7	2

D.14.1.1	0.08	236	281	1.23	3.3659	1.2	0.0994	0.6	1613	11	-4
D.16.1.1	0.11	128	67	0.54	2.5556	1.3	0.1275	0.6	2064	11	-3
D.17.1.1	0.02	864	11	0.01	3.0623	1.1	0.11	0.2	1799	4	-1
D.18.1.1	0.06	140	91	0.67	3.2892	1.3	0.1041	0.7	1699	13	-1
D.19.1.1	0.15	301	202	0.69	3.4846	1.2	0.1016	0.5	1653	10	2
D.2.1.1	0	385	151	0.41	3.2877	1.1	0.1056	0.4	1725	7	1
D.20.1.1	0.02	65	56	0.9	3.4023	1.4	0.1015	1.1	1652	21	-1
D.21.1.1	0.08	159	100	0.65	2.1338	1.2	0.162	0.4	2476	7	0
D.22.1.1	0.12	166	219	1.36	3.4447	1.3	0.0996	0.8	1617	14	-2
D.25.1.1	0.06	228	141	0.64	3.4084	1.2	0.1005	0.5	1633	10	-2
D.26.1.1	0.13	350	422	1.25	3.5918	1.2	0.1002	0.5	1627	10	3
D.27.1.1	0.07	598	280	0.48	3.1296	1.1	0.1081	0.3	1768	6	-1
D.4.1.1	0.02	176	88	0.52	2.7176	1.2	0.1263	0.4	2048	8	1
D.6.1.1	0.04	200	261	1.34	3.3615	1.2	0.1006	0.5	1635	10	-3
D.9.1.1	0.15	91	58	0.66	3.3042	1.3	0.1025	1.7	1669	32	-2
Sample 2007169009 (1937158), Malacura Sandstone					New SHRIMP U-Pb zircon ages from north Queensland, 2007–2010					Neumann and Kositcin, 2011	
Grain ID	206Pbc(%)1	U (ppm)	Th (ppm)	232Th/238U	238U/206Pb	± 1σ (%)	207Pb/206Pb	± 1σ(%)	207Pb/206Pb Age (Ma)	± 1σ (Ma)	Disc (%)
A.1.1.1	0.04	261	288	1.14	3.515	1.2	0.1013	0.5	1647	9	2
A.10.1.1	0.03	282	163	0.6	3.446	1.2	0.104	0.5	1697	9	3
A.11.1.1	0.12	288	204	0.73	3.5826	1.2	0.101	0.5	1643	9	3
A.12.1.1	0.05	188	157	0.86	3.4704	1.2	0.1009	0.6	1642	12	1
A.13.1.1	0.04	215	184	0.89	3.4782	1.2	0.1015	0.6	1652	11	1
A.14.1.1	0.06	103	92	0.93	3.6294	1.3	0.1017	0.8	1655	14	5
A.15.1.1	0.06	97	71	0.75	3.6436	1.3	0.1005	0.9	1633	16	4
A.16.1.1	0.37	223	85	0.4	2.9582	1.2	0.1127	1.9	1843	34	-2
A.17.1.1	-0.02	264	190	0.74	3.5788	1.2	0.1003	0.4	1630	8	3
A.18.1.1	0.1	149	80	0.56	3.2551	1.2	0.1044	0.6	1703	11	-1

A.19.1.1	0.03	506	304	0.62	3.5117	1.1	0.1044	0.4	1705	7	5
A.22.1.1	0.03	441	192	0.45	3.4939	1.1	0.0996	0.3	1617	6	0
A.23.1.1	-0.02	252	64	0.26	3.4013	1.2	0.107	0.5	1748	9	5
A.24.1.1	-0.01	345	390	1.17	3.7043	1.3	0.0998	0.4	1620	7	5
A.25.1.1	0.01	137	166	1.25	3.2525	1.2	0.1057	0.8	1726	15	0
A.26.1.1	0.13	127	86	0.7	3.2672	1.2	0.1015	0.8	1652	14	-4
A.27.1.1	0.06	318	248	0.81	3.6477	1.2	0.1007	0.5	1637	9	5
A.28.1.1	-0.01	234	262	1.15	3.5844	1.3	0.0999	0.5	1622	9	2
A.29.1.1	0	303	292	1	3.265	1.5	0.1059	0.4	1729	7	0
A.3.1.1	-0.14	71	69	1	3.4938	1.4	0.1033	1.3	1685	23	4
A.30.1.1	0.11	262	10	0.04	3.2773	1.2	0.1046	0.5	1708	9	-1
A.31.1.1	0.04	174	156	0.93	3.4802	1.2	0.1002	0.6	1628	12	0
A.32.1.1	0.06	156	90	0.6	3.4612	1.2	0.1022	0.6	1664	11	2
A.33.1.1	0.02	255	194	0.79	3.3748	1.2	0.1028	0.5	1675	9	0
A.34.1.1	0.25	87	78	0.93	3.367	1.3	0.1018	1	1658	19	-1
A.35.1.1	0.07	391	194	0.51	3.1454	1.1	0.113	0.4	1849	7	4
A.37.1.1	-0.02	292	171	0.61	3.198	1.1	0.1099	0.4	1798	7	2
A.38.1.1	0.02	114	81	0.73	3.4016	1.2	0.1039	0.7	1696	12	2
A.39.1.1	0.02	201	78	0.4	3.5743	1.2	0.0999	0.6	1623	12	2
A.40.1.1	0.08	325	360	1.15	3.2616	1.1	0.1051	0.4	1716	8	0
A.41.1.1	0.18	158	64	0.42	3.4623	1.2	0.1016	0.7	1654	14	1
A.44.1.1	0.06	141	124	0.91	3.5558	1.4	0.1001	0.7	1627	14	2
A.45.1.1	0.03	230	189	0.85	3.5754	1.2	0.1001	0.6	1625	11	2
A.46.1.1	0.06	586	204	0.36	2.1422	1.1	0.1758	0.2	2613	3	5
A.47.1.1	0.09	242	170	0.73	3.2001	1.2	0.1068	0.5	1745	9	0
A.48.1.1	0.03	245	256	1.08	3.6632	1.2	0.099	0.5	1606	9	3
A.49.1.1	0.07	420	273	0.67	3.5004	1.1	0.1018	0.4	1657	7	2
A.50.1.1	0.16	111	91	0.85	3.5233	1.3	0.1001	0.9	1626	17	1
A.52.1.1	0.08	234	86	0.38	3.0926	1.2	0.1124	0.5	1839	9	2

A.53.1.1	0.08	138	101	0.76	3.4409	1.2	0.1016	0.7	1653	13	1
A.54.1.1	0.16	228	262	1.18	3.5902	1.3	0.0984	0.7	1594	12	1
A.56.1.1	0.08	283	356	1.3	3.4229	1.2	0.1021	0.5	1663	9	1
A.57.1.1	0.11	138	197	1.47	3.6831	1.2	0.1	0.8	1624	16	5
A.58.1.1	0.17	108	90	0.86	3.4676	1.3	0.0997	0.9	1618	17	-1
A.59.1.1	0.05	248	193	0.8	3.3815	1.2	0.1031	0.5	1680	9	1
A.6.1.1	0.13	201	163	0.84	3.4508	1.2	0.0998	0.7	1621	12	-1
A.61.1.1	0.04	286	256	0.92	3.5525	1.2	0.1002	0.5	1628	9	2
A.62.1.1	0.07	221	184	0.86	3.3531	1.2	0.1034	0.5	1686	10	0
A.63.1.1	0.07	174	71	0.42	3.5085	1.2	0.1012	0.7	1646	13	2
A.64.1.1	0.05	307	204	0.69	3.3638	1.2	0.1032	0.4	1682	8	0
A.65.1.1	0.08	612	424	0.72	3.43	1.2	0.1053	0.3	1719	6	4
A.66.1.1	0.01	219	42	0.2	3.1857	1.2	0.1095	0.4	1792	8	2
A.67.1.1	0.11	150	77	0.53	3.506	1.4	0.0985	0.7	1595	14	-1
A.68.1.1	0.02	486	452	0.96	3.4391	1.1	0.1006	0.4	1636	7	-1
A.69.1.1	-0.01	195	243	1.29	3.4213	1.2	0.1034	0.5	1686	9	2
A.7.1.1	0.08	259	154	0.62	3.4032	1.2	0.1036	0.5	1690	9	2
A.70.1.1	0.02	173	202	1.21	3.4806	1.2	0.1011	0.6	1644	11	1
A.71.1.1	0.06	178	63	0.36	3.3949	1.2	0.1047	0.6	1709	11	3
A.72.1.1	0	329	331	1.04	3.5247	1.1	0.101	0.4	1642	7	2
A.74.1.1	0.16	192	154	0.83	3.3637	1.3	0.102	0.6	1661	12	-1
A.75.1.1	0.03	305	276	0.94	3.3148	1.1	0.1049	0.6	1713	12	1
A.77.1.1	0.07	177	229	1.34	3.5759	1.2	0.1001	0.6	1626	12	2
A.78.1.1	0.01	562	778	1.43	3.4678	1.1	0.1009	0.3	1641	6	0
A.79.1.1	0.16	136	119	0.91	3.6223	1.2	0.0993	0.9	1612	17	3
A.8.1.1	0.18	97	144	1.54	3.495	1.3	0.0984	1	1594	19	-2
A.80.1.1	-0.08	144	128	0.91	3.5229	1.2	0.1017	0.7	1656	12	3

Table 3: data from the Inorunie Group detrital zircon

Inorunie Group detrital zircon											
GA Sample ID: 2008 83 7023 (unpublished)					Inorunie Group		Sample prepared and processed by Dr. Richard Wormald				
Grain ID	206Pb$_c$ (%)	U (ppm)	Th (ppm)	Th/U	206Pb/^{238}U	± (%)	207Pb/^{206}Pb	± (%)	207Pb/^{206}Pb Age (Ma)	±Ma (1sig)	Disc (%)
7023-1		209.91	80.84	0.385	0.317	0.003	0.106	0.001	1732.9	22.32	-2.4
7023-2		139.63	82.08	0.588	0.284	0.002	0.099	0.001	1602.7	23.38	-0.6
7023-6		239.28	99.83	0.417	0.473	0.004	0.161	0.002	2469.6	20.8	-1.1
7023-7		207.53	125.12	0.603	0.318	0.003	0.107	0.001	1745.4	24.34	-1.8
7023-9		273.38	144.91	0.53	0.301	0.003	0.101	0.001	1647	24.82	-2.9
7023-12		92.87	42.28	0.455	0.299	0.003	0.105	0.002	1717.3	28.65	1.8
7023-13		160.67	204.55	1.273	0.329	0.003	0.107	0.001	1755.2	23.57	-4.2
7023-15		268.09	107.47	0.401	0.314	0.003	0.107	0.001	1742.8	23.11	-1.1
7023-16		106.48	61.4	0.577	0.344	0.003	0.109	0.002	1774.6	28.12	-6.9
7023-17		186.1	154.24	0.829	0.317	0.003	0.106	0.002	1724	25.92	-2.9
7023-19		168.06	113.65	0.676	0.318	0.003	0.108	0.001	1766.6	23.65	-0.9
7023-22		96.5	103.52	1.073	0.307	0.003	0.107	0.001	1757	25.12	1.8
7023-23		252.28	144.04	0.571	0.33	0.003	0.106	0.001	1734	23.26	-5.6
7023-24		332.43	161.02	0.484	0.304	0.003	0.111	0.002	1814.5	27	6.1
ss7023-25		213.57	102.52	0.48	0.511	0.004	0.173	0.002	2585.6	22.12	-2.9
7023-28		568.42	198.55	0.349	0.31	0.003	0.108	0.002	1767.2	25.95	1.5
7023-31		78.82	84.9	1.077	0.303	0.003	0.1	0.002	1618.6	28.48	-5.1
7023-33		161.36	74.37	0.461	0.315	0.003	0.108	0.002	1761.8	27.28	-0.2
7023-34		157.87	249.27	1.579	0.306	0.003	0.106	0.001	1735.4	25.55	0.8
7023-41		243.35	88.4	0.363	0.324	0.003	0.106	0.001	1726.4	24.16	-4.6
7023-43		425.61	222.02	0.522	0.452	0.004	0.164	0.002	2493.6	22.28	3.7
7023-47		99.52	58.74	0.59	0.29	0.003	0.102	0.002	1652	29.07	0.8
7023-49		158.32	119.45	0.754	0.315	0.003	0.105	0.002	1712.9	26.17	-3
7023-50		183.53	216.72	1.181	0.311	0.003	0.104	0.002	1700.8	26.29	-2.5

7023-51		145.92	71.79	0.492	0.462	0.004	0.164	0.002	2495.3	23.64	2
7023-52		123.08	75.09	0.61	0.491	0.004	0.158	0.002	2434	25.61	-5.4
7023-54		159.2	211.51	1.329	0.332	0.003	0.106	0.002	1737	26.7	-5.9
Sample collected by Adam Nordsvan						Sample preperation done at Curtin University and University of Newcastle					
SAMPLE - IG01a	Processed at University of Newcastle				7/10/2016	Inorunie Group			Coord (UTM, 54) 677603 / 7978521		
Grain ID	206Pbc (%)	U (ppm)	Th (ppm)	Th/U	206Pb/238U	± (%)	207Pb/206Pb	± (%)	207Pb/206Pb Age (Ma)	±Ma (1sig)	Disc (%)
IG01-02.d		430	94	6.400	0.445	0.004	0.158	0.001	2439	17	2.4
IG01-07.d		485.7	213.9	2.258	0.319	0.003	0.104	0.001	1703	15	-4.9
IG01-08.d		275.9	145	1.891	0.284	0.002	0.098	0.001	1582	12	-1.9
IG01-09.d		144.9	111.5	1.296	0.312	0.004	0.107	0.001	1742	20	-0.5
IG01-10.d		117	85.5	1.374	0.295	0.003	0.104	0.001	1696	20	2.2
IG01-11.d		274.7	174.8	1.563	0.309	0.003	0.108	0.001	1696	14	-4.4
IG01-12.d		258.6	126.8	2.018	0.323	0.003	0.105	0.001	1743	14	-4.4
IG01-15.d		464	357	1.296	0.320	0.004	0.112	0.001	1861	14	1.7
IG01-18.d		243.7	143.5	1.690	0.317	0.002	0.104	0.001	1739	18	4.9
IG01-19.d		119.9	78.2	1.544	0.321	0.003	0.106	0.001	1533	20	-5.1
IG01-22.d		92.8	143.4	0.645	0.327	0.002	0.107	0.001	1749	37	1.5
IG01-24.d		185.4	107.5	1.727	0.328	0.003	0.114	0.001	1775	18	-3.4
IG01-25.d		86.3	112.4	0.739	0.293	0.002	0.107	0.001	1855	22	4.2
IG01-29.d		189.7	257	0.764	0.285	0.002	0.096	0.001	1669	15	-5.4
IG01-34.d		303.8	186.8	1.600	0.307	0.006	0.108	0.002	1690	12	-2.5
IG01-35.d		194.5	137.3	1.449	0.330	0.004	0.109	0.001	1616	19	-0.9
IG01-36.d		304	174.2	1.715	0.318	0.003	0.114	0.001	1740	15	-3.4
IG01-37.d		168.9	76.5	2.210	0.315	0.002	0.103	0.001	2406	11	-2.9
IG01-38.d		303.4	333.5	0.902	0.309	0.003	0.104	0.001	1788	16	2.1
IG01-39.d		623	280.9	2.207	0.288	0.003	0.100	0.001	1544	14	-4.5
IG01-42.d		569	246.2	2.360	0.323	0.003	0.107	0.001	1586	11	-4.1

IG01-44.d		253.1	195.8	1.286	0.469	0.003	0.156	0.001	1763	18	0.1
IG01-46.d		110.8	83.7	1.377	0.312	0.003	0.110	0.001	1608	18	-3.6
IG01-47.d		239.9	224.7	1.057	0.285	0.002	0.096	0.001	1717	13	0.4
IG01-48.d		301.7	311	0.978	0.293	0.002	0.098	0.001	1720	13	-1.9
IG01-52.d		324	307	1.013	0.314	0.003	0.108	0.001	1788	14	-3.7
IG01-55.d		242	238	0.939	0.296	0.003	0.099	0.001	1741	13	-2.2
IG01-58.d		650	429.5	1.485	0.304	0.002	0.105	0.001	1774	14	5.1
IG01-63.d		600	670	0.883	0.313	0.002	0.105	0.001	1723	11	-2.8
IG01-64.d		324	214	1.540	0.334	0.003	0.110	0.001	1756	15	0.9
IG01-66.d		897	227.4	3.890	0.318	0.003	0.107	0.001	1703.8	10	0.4
IG01-67.d		456.5	145	3.360	0.299	0.003	0.109	0.001	1723	12	-1.8
IG01-72.d		113	202.2	0.571	0.317	0.003	0.106	0.001	1586	27	0.3
IG01-73.d		290.2	116.4	2.481	0.310	0.003	0.108	0.001	1723	12	-5.4
IG01-74.d		461.7	268.5	1.713	0.301	0.002	0.105	0.001	2580.6	8	-1.4
IG01-80.d		470.4	205.6	2.286	0.313	0.002	0.106	0.001	1748	12	1.0
IG01-81.d		209.3	114.5	1.980	0.278	0.003	0.099	0.001	1752	20	3.7
IG01-83.d		509.4	204	3.300	0.327	0.003	0.106	0.001	2441	11	2.5
IG01-88.d		172.5	121.9	1.426	0.501	0.003	0.172	0.001	1622	18	-0.7
IG01-89.d		522.7	49.3	11.440	0.308	0.003	0.107	0.001	2402	10	-1.7
IG01-95.d		893	338	2.760	0.300	0.003	0.107	0.001	1734	21	2.7
IG01-98.d		158.3	119.6	1.316	0.447	0.005	0.159	0.001	1604	20	-4.9
IG01-101.d		444	418	1.062	0.288	0.003	0.100	0.001	1761	14	1.3
IG01-102.d		149.1	135.3	1.120	0.461	0.003	0.155	0.001	1706	19	-5.4
IG01-103.d		158.3	160.7	1.041	0.300	0.005	0.106	0.001	1829	21	2.3
IG01-110.d		368.5	207.3	1.737	0.299	0.002	0.099	0.001	1724	12	-4.1
Sample collected by Adam Nordsvan						Sample preperation done at Curtin University and University of Newcastle					
SAMPLE - IG01b	Processed at Curtin University				7/04/2017	Inorunie Group			Coord (UTM, 54) 677603 / 7978521		

Grain ID	206Pbc (%)	U (ppm)	Th (ppm)	Th/U	206Pb/238U	± (%)	207Pb/206Pb	± (%)	207Pb/206Pb Age (Ma)	±Ma (1sig)	Disc (%)
IG01 - 1		296	203.00	1.428	0.310	0.002	0.105	0.001	1705	22	-1.9
IG01 - 2		115.2	107.80	1.047	0.278	0.003	0.099	0.003	1597	54	1.2
IG01 - 5		12.05	0.29	72	0.334	0.016	0.114	0.010	1830	150	-1.5
IG01 - 6		92.4	125.00	0.737	0.311	0.004	0.105	0.002	1706	43	-2.5
IG01 - 8		79.4	-0.01	-8520	0.306	0.010	0.101	0.004	1636	77	-4.8
IG01 - 11		231	185.10	1.22	0.311	0.003	0.103	0.002	1680	29	-3.8
IG01 - 12		194	183.00	1.045	0.315	0.003	0.105	0.001	1719	23	-2.5
IG01 - 14		16.12	0.03	-830	0.315	0.010	0.111	0.008	1790	130	1.5
IG01 - 16		31.8	0.09	-830	0.335	0.014	0.117	0.004	1892	66	1.7
IG01 - 19		62.6	2.42	69	0.300	0.008	0.104	0.004	1693	65	0.3
IG01 - 28		26.62	0.00	-1520	0.351	0.007	0.113	0.004	1844	70	-4.9
IG01 - 30		664	1790.00	0.368	0.297	0.005	0.108	0.002	1768	36	5.4
IG01 - 32		616	193.00	3.24	0.307	0.002	0.106	0.001	1726	14	0.1
IG01 - 34		187	182.00	1.032	0.284	0.003	0.098	0.002	1591	33	-1.2
IG01 - 35		490	299.00	1.67	0.307	0.004	0.105	0.001	1713	24	-0.6
IG01 - 36		175.3	164.40	1.066	0.282	0.003	0.098	0.002	1588	35	-0.7
IG01 - 38		160	122.10	1.33	0.304	0.004	0.105	0.002	1709	30	0.0
IG01 - 39		12.37	0.00	-500	0.352	0.015	0.115	0.007	1860	120	-4.2
IG01 - 40		386	188.60	2.035	0.282	0.002	0.097	0.002	1561	29	-2.6
IG01 - 42		508	77.00	9	0.466	0.006	0.159	0.002	2448	16	-0.8
IG01 - 44		7.78	0.65	30	0.358	0.016	0.132	0.013	2080	180	5.5
IG01 - 45		263	246.00	1.085	0.304	0.003	0.104	0.002	1687	33	-1.4
IG01 - 52		268	164.80	1.655	0.316	0.003	0.107	0.002	1738	33	-1.8
IG01 - 53		422	297.00	1.52	0.425	0.006	0.156	0.001	2410	10	5.5
IG01 - 54		179	147.70	1.233	0.280	0.002	0.099	0.002	1597	36	0.4
IG01 - 56		141	92.70	1.556	0.283	0.003	0.098	0.002	1578	35	-1.6
IG01 - 57		22.78	0.00	-1520	0.325	0.010	0.110	0.008	1770	130	-2.3

IG01 - 59		261.4	192.30	1.391	0.315	0.003	0.105	0.001	1720	22	-2.5
IG01 - 65		3.53	0.10	32	0.327	0.020	0.112	0.014	1760	220	-3.3
IG01 - 69		33.21	0.05	-500	0.315	0.007	0.108	0.011	1750	170	-1.0
IG01 - 71		214	148.20	1.458	0.309	0.003	0.104	0.002	1685	27	-2.9
IG01 - 76		215	200.00	1.082	0.295	0.002	0.108	0.002	1755	28	5.2
IG01 - 80		184	166.00	1.131	0.293	0.006	0.105	0.005	1711	84	3.2
IG01 - 81		126.5	155.00	0.834	0.279	0.003	0.098	0.002	1575	39	-0.5
IG01 - 82		316	167.60	1.92	0.335	0.002	0.113	0.001	1850	16	-0.6
IG01 - 83		189.7	189.30	1.022	0.308	0.003	0.106	0.001	1725	25	-0.3
IG01 - 84		1.07	0.16	17	0.424	0.064	0.157	0.042	2320	390	2.2
IG01 - 88		456	254.00	1.95	0.314	0.006	0.106	0.001	1729	22	-1.8
IG01 - 90		195.6	200.30	0.994	0.289	0.003	0.099	0.002	1604	30	-2.0
IG01 - 91		306	196.40	1.596	0.309	0.005	0.105	0.003	1705	51	-1.7
IG01 - 93		295	404.00	0.746	0.324	0.006	0.116	0.004	1892	61	4.7
IG01 - 95		292	167.00	1.821	0.315	0.004	0.106	0.001	1734	24	-1.7
IG01 - 96		175.7	425.00	0.429	0.279	0.003	0.097	0.002	1571	35	-0.8
IG01 - 99		24.68	0.53	-320	0.317	0.008	0.108	0.007	1750	120	-1.3
IG01 - 100		347	287.00	1.247	0.283	0.005	0.098	0.001	1583	21	-1.4
IG01a - 4		309	184.00	1.685	0.315	0.003	0.104	0.001	1700	20	-3.7
IG01a - 5		406	534.00	0.756	0.316	0.002	0.108	0.002	1769	34	0.1
IG01a - 9		295	240.00	1.231	0.299	0.003	0.107	0.001	1750	18	3.7
IG01a - 10		213	71.50	2.99	0.480	0.006	0.162	0.002	2479	18	-1.8
IG01a - 13		538	261.70	2.06	0.296	0.003	0.106	0.001	1721	22	3.0
IG01a - 15		107.5	74.70	1.441	0.277	0.003	0.099	0.002	1591	43	0.9
IG01a - 18		80.7	115.20	0.69	0.330	0.006	0.114	0.006	1854	91	0.9
IG01a - 21		172.1	131.00	1.342	0.309	0.004	0.105	0.001	1714	24	-1.1
IG01a - 22		166	309.00	0.5413	0.431	0.005	0.156	0.002	2413	20	4.4

References

Condie, K.C., Belousova, E., Griffin, W.L., and Sircombe, K.N., 2009, Granitoid events in space and time: constraints from igneous and detrital zircon age spectra: Gondwana Research, v. 15, no. 3, p. 228-242.

Furlanetto, F., Thorkelson, D.J., Rainbird, R.H., Davis, W.J., Gibson, H.D., and Marshall, D.D., 2016, The Paleoproterozoic Wernecke Supergroup of Yukon, Canada: Relationships to orogeny in northwestern Laurentia and basins in North America, East Australia, and China: Gondwana Research, v. 39, p. 14-40.

Jackson, S.E., Pearson, N.J., Griffin, W.L., and Belousova, E.A., 2004, The application of laser ablation-inductively coupled plasma-mass spectrometry to in situ U-Pb zircon geochronology: Chemical Geology, v. 211, no. 1, p. 47-69.

Lambeck, A., 2011, Basin analysis and the geochemical signature of Paleoproterozoic sedimentary successions in northern Australia: Constraints on basin development in respect to mineralisation and paleoreconstruction models: School of Earth and Environmental Sciences The University of Adelaide This thesis is submitted in fulfilment of the requirements for the degree of Doctor of Philosophy in the Faculty of Science, University of Adelaide.

Neumann, N.L., and Fraser, G.L., 2007, Geochronological synthesis and time-space plots for Proterozoic Australia, Geoscience Australia.

Vermeesch, P., 2012, On the visualisation of detrital age distributions: Chemical Geology, v. 312, p. 190-194.

Withnall, I., Bain, J., Draper, J., MacKenzie, D., and Oversby, B., 1988, Proterozoic stratigraphy and tectonic history of the Georgetown Inlier, northeastern Queensland: Precambrian Research, v. 40, p. 429-446.

Appendix D: Chapter 4, supplementary file

Paleocurrent measurements are reported from the alluvial fan facies at locations B1. Measurements were corrected for the dip of the beds using Stereonet 7 software: (http://www.geo.cornell.edu/geology/faculty/RWA/programs/stereonet-7-for-windows.html).

Measured sections used in chapter 4 for the composite sections. See main text for facies descriptions. Note that sections are different scales.

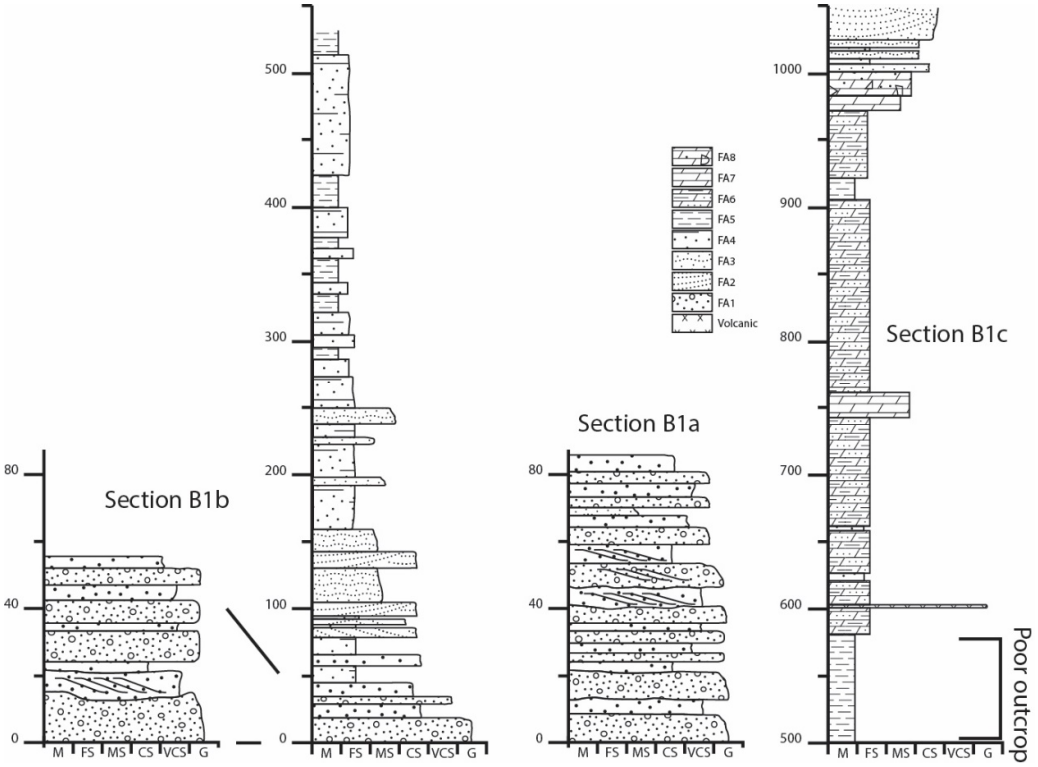

Figure 1: Sections at location B1. B1a: 20°25'28.71"S, 139°52'34.89"E at 086°. B1a: 20°24'57.29"S, 139°52'24.13"E at 086°. B1c: 20°24'33.92"S, 139°52'46.92"E at 078°.

Figure 2: Sections at location B2. B2a: 20°29'35.90"S, 139°50'51.47"E at 087°. B2b: 20°29'32.45"S, 139°50'54.38"E at 102°. B2c: 20°29'43.85"S, 139°51'1.38"E at 084°.

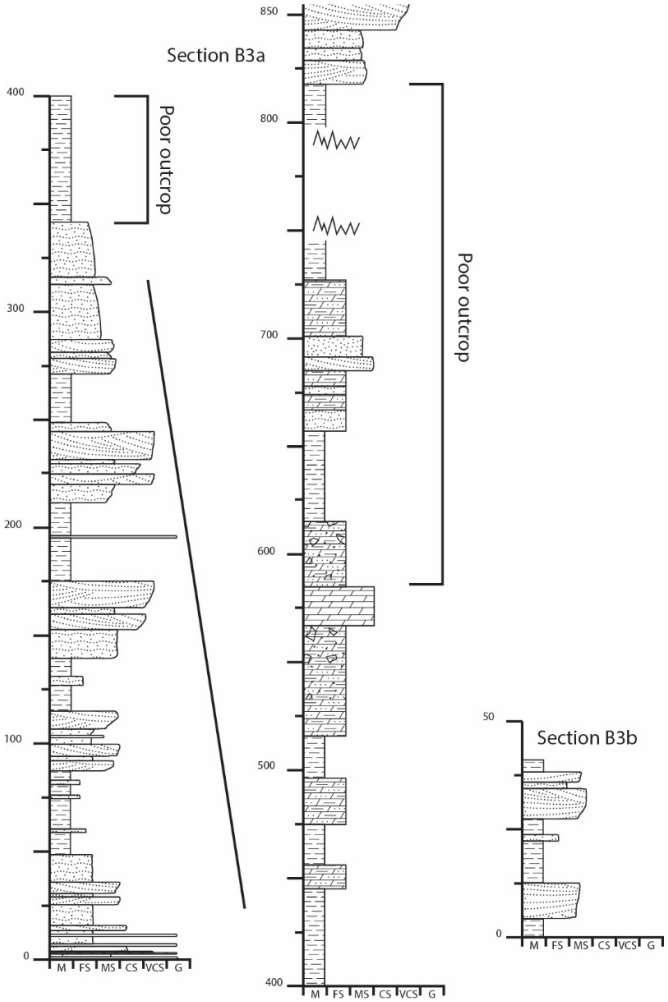

Figure 3: Sections at location B3. B3a: 20°33'30.01"S, 139°48'26.62"E at 076°. B3b: 20°33'31.34"S, 139°48'34.64"E at 081°.

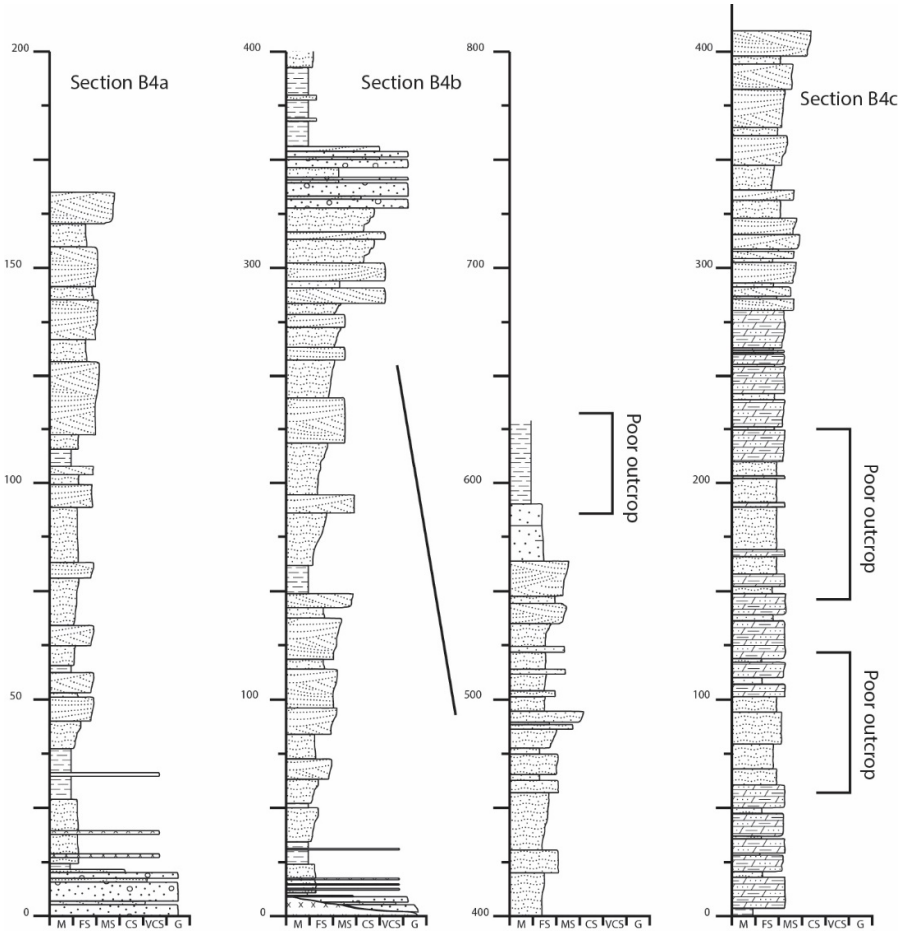

Figure 4: Sections at location B4. B4a: 20°44'26.03"S, 139°51'17.53"E at 075°. B4b: 20°44'2.65"S, 139°51'12.23"E at 073°. B4c: 20°45'9.07"S, 139°52'9.14"E at 083°.

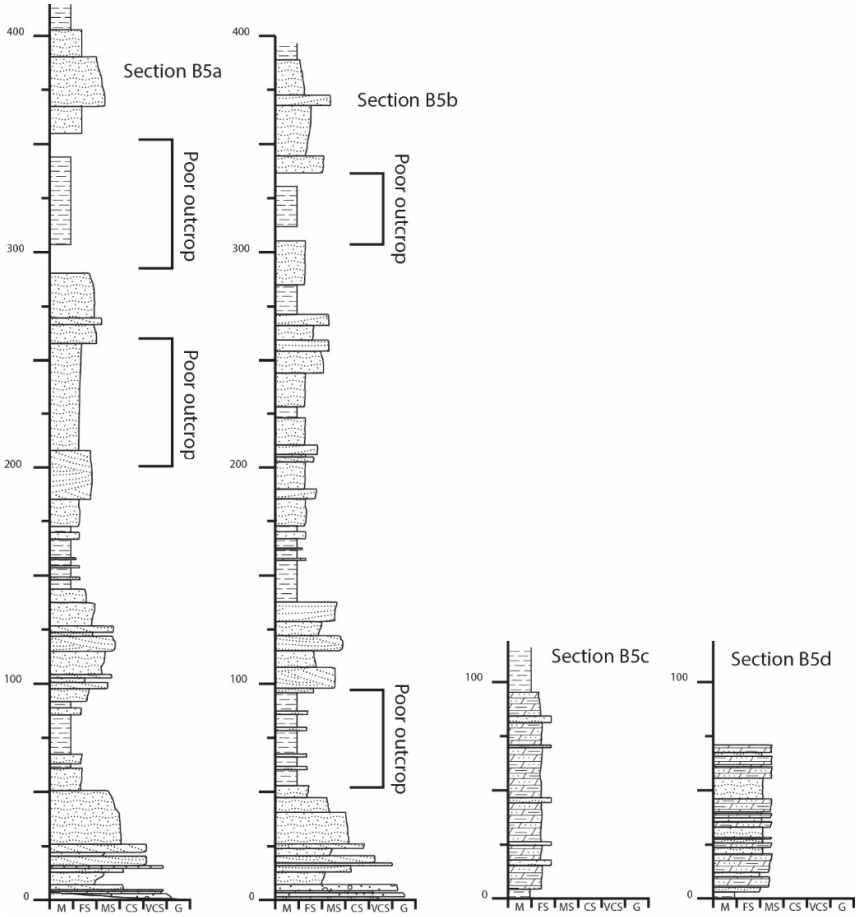

Figure 5: Sections at location B5. B5a: 20°45'7.02"S, 139°49'9.86"E at 071°. B5b: 20°45'50.92"S, 139°49'23.57"E at 083°. B5c: 20°45'30.48"S, 139°49'56.16"E at 084°. B5d: 20°45'37.12"S, 139°50'19.61"E at 082°.

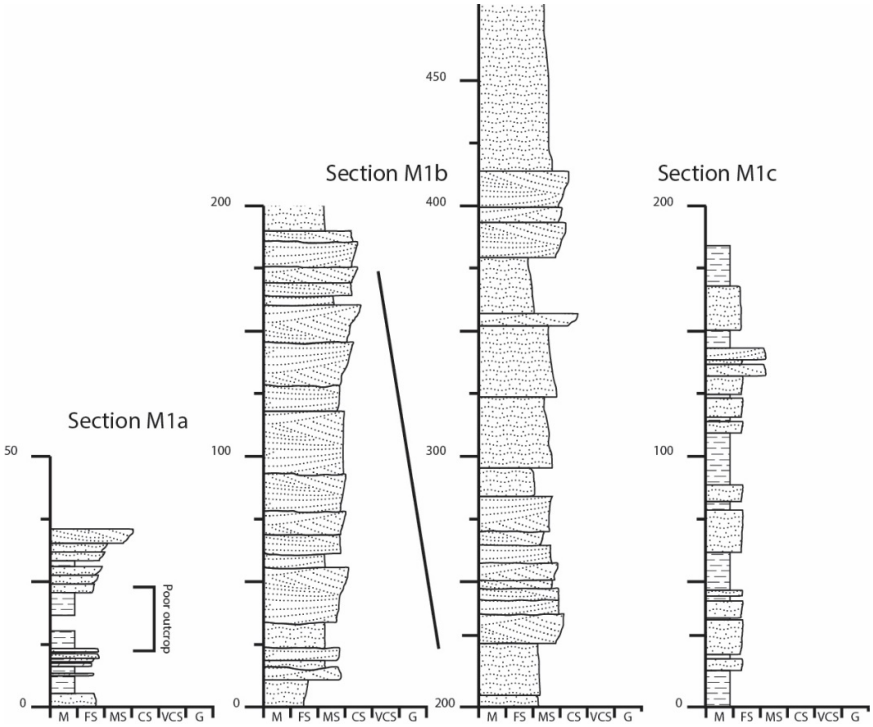

Figure 6: Sections at location M1. M1a: 20°48'31.11"S, 140° 8'43.15"E at 318°. B5b: 20°48'7.25"S, 140° 9'17.00"E at 310°. M1c: 20°47'36.82"S, 140° 9'14.63"E at 334°.

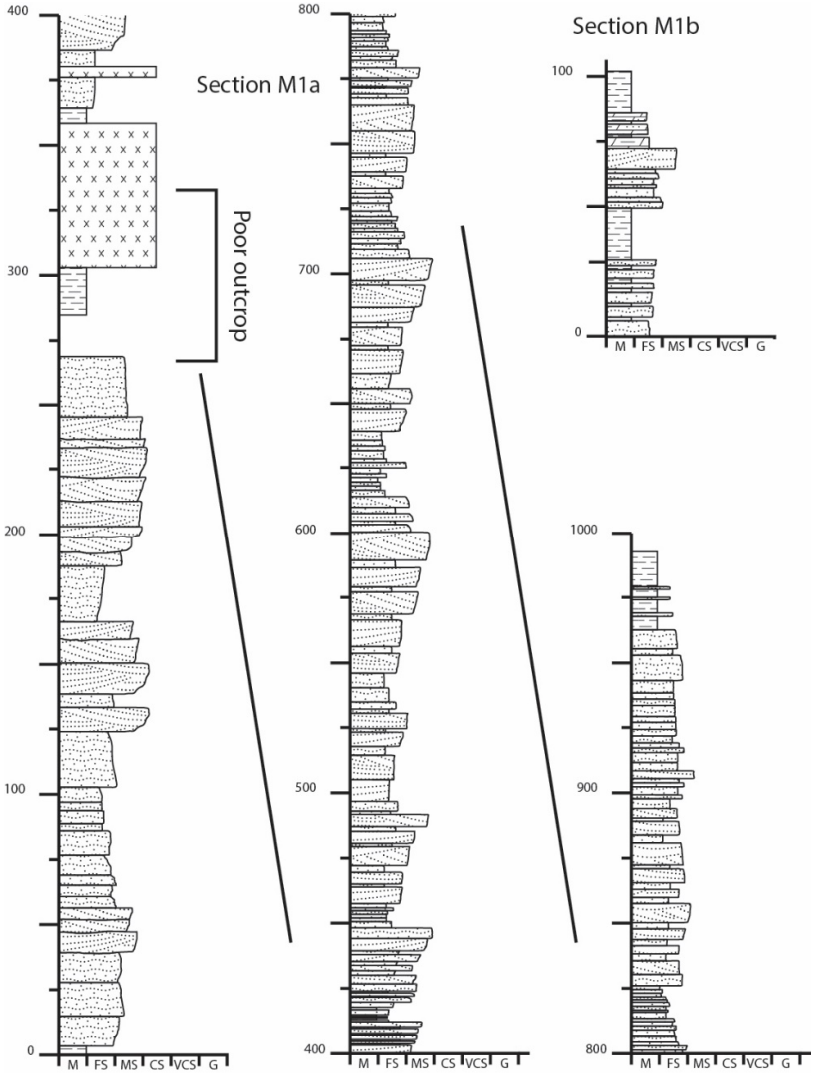

Figure 7: Sections at location M2. M2a, see also Figure 8, 20°53'13.97"S, 140°19'26.55"E at 084°. M1b: 20°57'44.74"S, 140°21'18.08"E at 052°.

Figure 7: Location of the M2a measured section. All colours are the Mitakoodi Quartzite. White line is the smoothed composite GPS path for the measured section. Triangle was the start position. Image taken from Google Earth. Geological units taken from the Queensland Geological Survey.

Table 1: Dissimilarity matrixes used for the sample MDS analysis in Figure 4.13c. The top is the K-S value, the bottom is the Kuiper values.

K-S	MQ01	MQ02	MIT1701	BAL1701	BAL1703	BAL1706	COR1702e	COR1701	MIT05A
MQ01	0.00	0.13	0.11	0.61	0.53	0.63	0.64	0.43	0.15
MQ02	0.13	0.00	0.13	0.62	0.53	0.63	0.66	0.45	0.16
MIT1701	0.11	0.13	0.00	0.64	0.52	0.63	0.64	0.45	0.15
BAL1701	0.61	0.62	0.64	0.00	0.25	0.12	0.21	0.27	0.65
BAL1703	0.53	0.53	0.52	0.25	0.00	0.23	0.18	0.17	0.52
BAL1706	0.63	0.63	0.63	0.12	0.23	0.00	0.21	0.28	0.63
COR1702e	0.64	0.66	0.64	0.21	0.18	0.21	0.00	0.22	0.60
COR1701	0.43	0.45	0.45	0.27	0.17	0.28	0.22	0.00	0.45
MIT05A	0.15	0.16	0.15	0.65	0.52	0.63	0.60	0.45	0.00

Kuiper	MQ01	MQ02	MIT1701	BAL1701	BAL1703	BAL1706	COR1702e	COR1701	MIT05A
MQ01	0.00	0.18	0.21	0.61	0.53	0.63	0.66	0.43	0.21
MQ02	0.18	0.00	0.16	0.62	0.53	0.65	0.68	0.47	0.29
MIT1701	0.21	0.16	0.00	0.64	0.52	0.64	0.66	0.47	0.22
BAL1701	0.61	0.62	0.64	0.00	0.28	0.16	0.25	0.29	0.65
BAL1703	0.53	0.53	0.52	0.28	0.00	0.28	0.28	0.21	0.52
BAL1706	0.63	0.65	0.64	0.16	0.28	0.00	0.26	0.31	0.63
COR1702e	0.66	0.68	0.66	0.25	0.28	0.26	0.00	0.28	0.60
COR1701	0.43	0.47	0.47	0.29	0.21	0.31	0.28	0.00	0.45
MIT05A	0.21	0.29	0.22	0.65	0.52	0.63	0.60	0.45	0.00

Table 2: Dissimilarity matrixes used for the MDS and dendrogram analysis in Figure 4.20. The top is the K-S value, the bottom is the Kuiper values.

K-S	Mitakoodi	Ballara	Corella	Pine C	Pine C1	Pine C2	Halls C	Halls C1	Halls C2	Mount I	Mount I1	Mount I2	Arn	Arn1	Arn2	Aru	Aru1	Aru2	Murp	Murp1	Murp2	Ten	Ten1	Ten2
Mitakoodi	0.00	0.59	0.55	0.59	0.52	0.42	0.66	0.64	0.61	0.79	0.74	0.69	0.53	0.52	0.52	0.80	0.80	0.79	0.53	0.47	0.48	0.75	0.70	0.63
Ballara	0.59	0.00	0.18	0.50	0.50	0.48	0.37	0.35	0.30	0.25	0.20	0.13	0.45	0.42	0.35	0.23	0.22	0.21	0.56	0.55	0.47	0.43	0.41	0.38
Corella	0.55	0.18	0.00	0.40	0.38	0.33	0.24	0.23	0.19	0.29	0.25	0.22	0.29	0.26	0.22	0.39	0.36	0.33	0.44	0.39	0.32	0.27	0.25	0.24
Pine C	0.59	0.50	0.40	0.00	0.14	0.20	0.47	0.45	0.43	0.43	0.49	0.54	0.37	0.33	0.31	0.72	0.70	0.70	0.29	0.24	0.22	0.46	0.40	0.40
Pine C1	0.52	0.50	0.38	0.14	0.00	0.13	0.36	0.37	0.33	0.42	0.41	0.49	0.27	0.21	0.25	0.71	0.70	0.68	0.17	0.20	0.19	0.36	0.28	0.30
Pine C2	0.42	0.48	0.33	0.20	0.13	0.00	0.31	0.29	0.26	0.41	0.40	0.43	0.19	0.16	0.15	0.69	0.66	0.63	0.21	0.12	0.13	0.38	0.32	0.25
Halls C	0.66	0.37	0.24	0.47	0.36	0.31	0.00	0.05	0.09	0.36	0.34	0.34	0.21	0.21	0.20	0.57	0.54	0.50	0.44	0.39	0.33	0.21	0.16	0.10
Halls C1	0.64	0.35	0.23	0.45	0.37	0.29	0.05	0.00	0.08	0.34	0.33	0.32	0.21	0.21	0.20	0.56	0.53	0.48	0.43	0.37	0.33	0.20	0.14	0.09
Halls C2	0.61	0.30	0.19	0.43	0.33	0.26	0.09	0.08	0.00	0.29	0.27	0.28	0.20	0.20	0.20	0.50	0.47	0.43	0.39	0.35	0.30	0.17	0.15	0.09
Mount I	0.79	0.25	0.29	0.43	0.42	0.41	0.36	0.34	0.29	0.00	0.07	0.14	0.41	0.39	0.34	0.32	0.31	0.30	0.46	0.45	0.43	0.40	0.37	0.36
Mount I1	0.74	0.20	0.25	0.49	0.41	0.40	0.34	0.33	0.27	0.07	0.00	0.09	0.39	0.37	0.33	0.32	0.30	0.27	0.49	0.45	0.42	0.38	0.35	0.34
Mount I2	0.69	0.13	0.22	0.54	0.49	0.43	0.34	0.32	0.28	0.14	0.09	0.00	0.39	0.36	0.33	0.27	0.25	0.20	0.57	0.52	0.41	0.37	0.34	0.33
Arn	0.53	0.45	0.29	0.37	0.27	0.19	0.21	0.21	0.20	0.41	0.39	0.39	0.00	0.07	0.12	0.65	0.63	0.59	0.30	0.26	0.24	0.23	0.20	0.18
Arn1	0.52	0.42	0.26	0.33	0.21	0.16	0.21	0.21	0.20	0.39	0.37	0.36	0.07	0.00	0.09	0.62	0.59	0.55	0.28	0.25	0.20	0.25	0.21	0.19
Arn2	0.52	0.35	0.22	0.31	0.25	0.15	0.20	0.20	0.20	0.34	0.33	0.33	0.12	0.09	0.00	0.55	0.52	0.49	0.32	0.24	0.18	0.26	0.22	0.21

Aru	0.80	0.23	0.39	0.72	0.71	0.69	0.57	0.56	0.50	0.32	0.32	0.27	0.65	0.62	0.55	0.00	0.05	0.10	0.77	0.76	0.67	0.63	0.61	0.58
Aru1	0.80	0.22	0.36	0.70	0.70	0.66	0.54	0.53	0.47	0.31	0.30	0.25	0.63	0.59	0.52	0.05	0.00	0.06	0.77	0.74	0.64	0.60	0.58	0.55
Aru2	0.79	0.21	0.33	0.70	0.68	0.63	0.50	0.48	0.43	0.30	0.27	0.20	0.59	0.55	0.49	0.10	0.00	0.06	0.76	0.71	0.60	0.56	0.54	0.50
Murp	0.53	0.56	0.44	0.29	0.27	0.21	0.44	0.43	0.39	0.46	0.49	0.57	0.30	0.28	0.22	0.77	0.77	0.76	0.00	0.21	0.21	0.30	0.30	0.26
Murp1	0.47	0.55	0.39	0.24	0.20	0.12	0.39	0.37	0.35	0.45	0.45	0.52	0.26	0.25	0.24	0.67	0.64	0.61	0.21	0.00	0.21	0.34	0.33	0.32
Murp2	0.48	0.47	0.32	0.22	0.19	0.13	0.33	0.33	0.30	0.43	0.42	0.41	0.24	0.20	0.18	0.67	0.64	0.61	0.21	0.21	0.00	0.27	0.26	0.25
Ten	0.75	0.43	0.27	0.46	0.43	0.38	0.31	0.30	0.27	0.40	0.38	0.37	0.35	0.32	0.30	0.63	0.60	0.56	0.30	0.43	0.40	0.00	0.26	0.23
Ten1	0.70	0.41	0.25	0.40	0.38	0.32	0.26	0.24	0.21	0.37	0.35	0.34	0.30	0.28	0.27	0.60	0.58	0.54	0.30	0.34	0.31	0.26	0.00	0.19
Ten2	0.63	0.38	0.24	0.40	0.38	0.35	0.29	0.28	0.26	0.36	0.34	0.33	0.28	0.26	0.25	0.56	0.54	0.50	0.36	0.33	0.27	0.23	0.19	0.00

Kuiper	Mitakoodi	Ballara	Corella	Pine C	Pine C1	Pine C2	Halls C	Halls C1	Halls C2	Mount I	Mount I1	Mount I2	Arn	Arn1	Arn2	Aru	Aru1	Aru2	Murp	Murp1	Murp2	Ten	Ten1	Ten2
Mitakoodi	0.00	0.59	0.55	0.68	0.62	0.50	0.61	0.64	0.61	0.79	0.74	0.69	0.56	0.55	0.53	0.80	0.80	0.79	0.56	0.50	0.51	0.75	0.70	0.63
Ballara	0.59	0.00	0.19	0.56	0.51	0.48	0.44	0.44	0.43	0.36	0.30	0.20	0.45	0.42	0.40	0.53	0.50	0.48	0.56	0.55	0.47	0.63	0.60	0.58
Corella	0.55	0.19	0.00	0.52	0.48	0.40	0.44	0.43	0.40	0.31	0.27	0.23	0.43	0.39	0.37	0.49	0.47	0.45	0.46	0.42	0.34	0.62	0.59	0.57
Pine C	0.68	0.56	0.52	0.00	0.25	0.39	0.38	0.37	0.36	0.43	0.49	0.54	0.48	0.45	0.44	0.57	0.55	0.54	0.44	0.39	0.40	0.66	0.63	0.61
Pine C1	0.62	0.51	0.48	0.25	0.00	0.26	0.32	0.31	0.30	0.42	0.41	0.49	0.45	0.42	0.41	0.54	0.52	0.51	0.30	0.32	0.35	0.66	0.63	0.61
Pine C2	0.50	0.48	0.40	0.39	0.26	0.00	0.29	0.26	0.25	0.41	0.40	0.43	0.43	0.41	0.40	0.53	0.51	0.50	0.39	0.23	0.25	0.68	0.65	0.63

Halls C	0.66	0.48	0.44	0.48	0.36	0.32	0.00	0.09	0.15	0.41	0.35	0.35	0.21	0.21	0.24	0.63	0.60	0.55	0.45	0.40	0.35	0.34	0.27	0.20
Halls C1	0.64	0.44	0.43	0.47	0.37	0.29	0.09	0.00	0.12	0.39	0.34	0.33	0.21	0.21	0.23	0.62	0.59	0.54	0.44	0.38	0.33	0.32	0.24	0.17
Halls C2	0.61	0.36	0.36	0.46	0.34	0.26	0.15	0.12	0.00	0.30	0.28	0.28	0.20	0.20	0.20	0.56	0.53	0.49	0.40	0.35	0.31	0.33	0.27	0.17
Mount I	0.79	0.36	0.31	0.43	0.42	0.41	0.41	0.39	0.30	0.00	0.13	0.25	0.41	0.39	0.34	0.39	0.39	0.39	0.46	0.45	0.44	0.46	0.38	0.37
Mount I1	0.74	0.30	0.27	0.49	0.41	0.40	0.35	0.34	0.28	0.13	0.00	0.16	0.39	0.37	0.33	0.39	0.36	0.34	0.49	0.45	0.42	0.41	0.36	0.35
Mount I2	0.69	0.20	0.23	0.54	0.49	0.43	0.35	0.33	0.28	0.25	0.16	0.00	0.39	0.36	0.33	0.36	0.30	0.26	0.57	0.52	0.41	0.45	0.37	0.34
Arn	0.56	0.45	0.33	0.48	0.35	0.23	0.21	0.21	0.20	0.41	0.39	0.39	0.00	0.14	0.18	0.65	0.63	0.59	0.39	0.35	0.34	0.32	0.22	0.18
Arn1	0.55	0.42	0.29	0.45	0.30	0.21	0.21	0.21	0.20	0.39	0.37	0.36	0.14	0.00	0.14	0.63	0.59	0.55	0.38	0.34	0.29	0.30	0.23	0.19
Arn2	0.53	0.35	0.24	0.45	0.36	0.20	0.24	0.23	0.20	0.34	0.33	0.33	0.18	0.14	0.00	0.55	0.52	0.49	0.42	0.34	0.28	0.35	0.30	0.25
Aru	0.80	0.27	0.42	0.72	0.71	0.69	0.63	0.62	0.56	0.39	0.39	0.36	0.65	0.63	0.55	0.00	0.08	0.18	0.78	0.76	0.68	0.67	0.65	0.61
Aru1	0.80	0.23	0.38	0.71	0.70	0.66	0.60	0.59	0.53	0.39	0.36	0.30	0.63	0.59	0.52	0.08	0.00	0.11	0.78	0.75	0.65	0.64	0.62	0.59
Aru2	0.79	0.22	0.34	0.70	0.68	0.63	0.55	0.54	0.49	0.39	0.34	0.26	0.59	0.55	0.49	0.18	0.11	0.00	0.77	0.72	0.60	0.60	0.58	0.54
Murp	0.56	0.56	0.46	0.44	0.30	0.39	0.45	0.44	0.40	0.46	0.49	0.57	0.39	0.38	0.42	0.78	0.78	0.77	0.00	0.42	0.42	0.30	0.31	0.36
Murp1	0.50	0.55	0.42	0.39	0.32	0.23	0.40	0.38	0.35	0.45	0.45	0.52	0.35	0.34	0.34	0.76	0.75	0.72	0.42	0.00	0.32	0.43	0.35	0.33
Murp2	0.51	0.47	0.34	0.40	0.35	0.25	0.35	0.33	0.31	0.44	0.42	0.41	0.34	0.29	0.28	0.68	0.65	0.60	0.42	0.32	0.00	0.48	0.37	0.29
Ten	0.75	0.63	0.52	0.46	0.36	0.38	0.34	0.32	0.33	0.46	0.41	0.45	0.32	0.30	0.35	0.67	0.64	0.60	0.30	0.43	0.48	0.00	0.20	0.29
Ten1	0.70	0.56	0.46	0.41	0.29	0.32	0.27	0.24	0.27	0.38	0.36	0.37	0.22	0.23	0.30	0.65	0.62	0.58	0.31	0.35	0.37	0.20	0.00	0.18

Ten2	0.63	0.47	0.44	0.40	0.30	0.25	0.20	0.17	0.17	0.37	0.35	0.34	0.18	0.19	0.25	0.61	0.59	0.54	0.36	0.33	0.29	0.29	0.18	0.00

Table 3: U-Pb data generated for this study.

Sample: BAL1701A

Grain ID	*207Pb/232Th*	*207Pb/232Th prop2SE*	*206Pb/238U*	*206Pb/238U prop2SE*	*207Pb/206Pb*	*207Pb/206Pb prop2SE*	*206Pb/238Pb Age (Ma)*	*± 1σ(Ma)*	*207Pb/206Pb Age (Ma)*	*± 1σ (Ma)*	*Disc (%)*
BAL1701a.1.01	4.98	0.16	0.3285	0.0056	0.1089	0.0038	1831	27	1780	64	3%
BAL1701a.1.02	2.545	0.099	0.1588	0.0053	0.1148	0.0017	950	29	1876	27	-49%
BAL1701a.1.03	3.38	0.15	0.223	0.011	0.1085	0.0027	1298	58	1774	46	-27%
BAL1701a.1.04	3.452	0.091	0.2301	0.0046	0.1083	0.0018	1335	24	1770	30	-25%
BAL1701a.1.05	4.722	0.1	0.3159	0.0048	0.1075	0.0018	1770	24	1757	31	1%
BAL1701a.1.06	4.666	0.075	0.312	0.0033	0.1075	0.0014	1751	16	1757	24	0%
BAL1701a.1.07	0.807	0.02	0.0495	0.0012	0.1174	0.002	311.5	7.4	1916	31	-84%
BAL1701a.1.08	2.637	0.097	0.1638	0.0063	0.1158	0.0016	978	35	1892	25	-48%
BAL1701a.1.09	1.739	0.052	0.1127	0.0028	0.1109	0.0016	688	16	1813	26	-62%
BAL1701a.1.10	3.28	0.13	0.2068	0.0082	0.1142	0.0018	1212	44	1866	29	-35%
BAL1701a.1.11	1.75	0.082	0.1166	0.0059	0.108	0.0025	711	34	1765	42	-60%
BAL1701a.1.12	2.379	0.067	0.1485	0.0037	0.115	0.0018	893	21	1879	28	-52%
BAL1701a.1.13	4.713	0.11	0.3016	0.0048	0.1123	0.0021	1699	24	1836	34	-7%
BAL1701a.1.14	1.904	0.056	0.1244	0.004	0.1102	0.002	756	23	1802	33	-58%

BAL1701a.1.15	3.707	0.093	0.2313	0.0056	0.1154	0.0016	1341	29	1885	25	-29%
BAL1701a.1.16	2.842	0.1	0.1779	0.0058	0.1145	0.0015	1055	32	1871	24	-44%
BAL1701a.1.17	1.508	0.029	0.0937	0.0021	0.1154	0.002	577	12	1885	31	-69%
BAL1701a.1.18	2.389	0.068	0.1493	0.0021	0.1147	0.0031	897	12	1874	49	-52%
BAL1701a.1.19	1.768	0.029	0.1285	0.0022	0.099	0.0017	779	13	1605	32	-51%
BAL1701a.1.20	4.76	0.15	0.3146	0.0089	0.1096	0.0038	1763	44	1792	63	-2%
BAL1701a.1.21	3.407	0.072	0.2064	0.0029	0.1186	0.002	1210	16	1934	30	-37%
BAL1701a.1.22	4.898	0.064	0.3197	0.0034	0.1107	0.0014	1788	17	1810	23	-1%
BAL1701a.1.23	5.07	0.36	0.331	0.029	0.1104	0.0035	1840	140	1805	58	2%
BAL1701a.1.24	1.427	0.03	0.0854	0.0018	0.1201	0.0022	528	11	1957	33	-73%
BAL1701a.1.25	1.327	0.074	0.0831	0.0047	0.1146	0.0016	515	28	1873	25	-73%
BAL1701a.1.26	1.202	0.043	0.0778	0.0025	0.1108	0.0015	483	15	1812	25	-73%
BAL1701a.1.27	5.02	0.13	0.3257	0.0074	0.1105	0.0022	1818	36	1807	36	1%
BAL1701a.1.28	1.95	0.049	0.121	0.0028	0.1159	0.0015	736	16	1893	23	-61%
BAL1701a.1.29	1.96	0.15	0.1267	0.0082	0.1106	0.0026	769	47	1808	43	-57%
BAL1701a.1.30	5.47	0.11	0.3445	0.0048	0.1144	0.0017	1908	23	1870	27	2%
BAL1701a.1.31	4.887	0.1	0.3167	0.0047	0.11091	0.0014	1774	23	1814	23	-2%
BAL1701a.1.32	2.212	0.063	0.1324	0.0032	0.1203	0.0017	802	18	1960	25	-59%
BAL1701a.1.33	1.982	0.049	0.1275	0.0028	0.1123	0.0015	774	16	1836	24	-58%
BAL1701a.4.01	3.97	0.14	0.2558	0.0098	0.1069	0.0025	1468	50	1746	43	-16%
BAL1701a.4.02	5.47	0.17	0.3446	0.013	0.1151	0.0023	1909	62	1881	36	1%
BAL1701a.4.03	4.69	0.18	0.3154	0.014	0.1081	0.0018	1767	69	1767	31	0%
BAL1701a.4.04	4.405	0.14	0.2734	0.012	0.117	0.0019	1558	61	1910	29	-18%
BAL1701a.4.05	3.043	0.12	0.1975	0.0094	0.1118	0.0019	1162	51	1828	31	-36%

BAL1701a.4.06	3.14	0.15	0.2093	0.01	0.109	0.0024	1225	53	1782	40	-31%
BAL1701a.4.07	4.78	0.18	0.3147	0.013	0.1114	0.0037	1764	64	1822	60	-3%
BAL1701a.4.08	4.96	0.15	0.3211	0.012	0.1127	0.0022	1795	59	1843	35	-3%
BAL1701a.4.09	2.58	0.12	0.1657	0.0083	0.1131	0.0024	988	46	1849	38	-47%
BAL1701a.4.10	5.167	0.15	0.334	0.013	0.1125	0.0016	1858	63	1839	26	1%
BAL1701a.4.11	5.04	0.22	0.3226	0.013	0.1138	0.0027	1802	63	1860	43	-3%
BAL1701a.4.12	3.71	0.15	0.2403	0.012	0.1125	0.0022	1388	62	1839	36	-25%
BAL1701a.4.13	4.71	0.19	0.3197	0.014	0.1079	0.0029	1788	68	1763	49	1%
BAL1701a.4.14	5.27	0.17	0.3385	0.013	0.1144	0.0026	1879	63	1870	41	0%
BAL1701a.4.15	5.71	0.18	0.2507	0.01	0.1668	0.002	1442	52	2525	20	-43%
BAL1701a.4.16	1.669	0.075	0.1005	0.0045	0.1219	0.002	617	26	1983	29	-69%
BAL1701a.4.17	5.54	0.17	0.3529	0.014	0.115	0.0019	1948	67	1879	30	4%
BAL1701a.4.18	5.24	0.24	0.335	0.018	0.1148	0.0018	1863	87	1876	28	-1%
BAL1701a.4.19	9.31	0.3	0.4444	0.017	0.1536	0.0021	2370	76	2386	24	-1%
BAL1701a.4.20	1.679	0.06	0.1086	0.0046	0.1132	0.0018	665	27	1851	29	-64%
BAL1701a.4.21	4.82	0.17	0.32	0.012	0.1105	0.0023	1790	59	1807	38	-1%
BAL1701a.4.22	4.66	0.16	0.3032	0.012	0.1131	0.0029	1707	59	1849	46	-8%
BAL1701a.4.23	5.49	0.25	0.3447	0.016	0.1168	0.0027	1909	77	1907	42	0%
BAL1701a.4.24	5.09	0.22	0.3296	0.013	0.1133	0.0035	1836	63	1852	56	-1%
BAL1701a.4.25	3.33	0.13	0.2086	0.0095	0.117	0.0016	1221	51	1910	25	-36%
BAL1701a.4.26	4.87	0.16	0.3109	0.013	0.1148	0.0019	1745	64	1876	30	-7%
BAL1701a.4.27	5.521	0.16	0.3529	0.013	0.1144	0.0019	1948	62	1870	30	4%
BAL1701a.4.28	0.972	0.038	0.0596	0.0026	0.1191	0.0028	373	16	1942	42	-81%
BAL1701a.4.29	3	0.15	0.2017	0.01	0.1083	0.0031	1184	54	1770	52	-33%
BAL1701a.4.30	5.408	0.14	0.3422	0.013	0.1155	0.0017	1897	62	1887	27	1%

BAL1701a.4.31	2.547	0.075	0.1619	0.0062	0.1149	0.002	967	34	1878	32	-49%
BAL1701a.4.32	4.72	0.17	0.3013	0.012	0.1139	0.0027	1698	59	1862	43	-9%
BAL1701a.4.33	4.736	0.14	0.3173	0.013	0.1088	0.0023	1777	64	1779	39	0%
BAL1701a.4.34	4.68	0.16	0.3154	0.013	0.1078	0.0027	1767	64	1762	46	0%
BAL1701a.4.35	1.91	0.14	0.116	0.0094	0.1194	0.0017	707	54	1946	26	-64%
BAL1701a.4.36	6.34	0.2	0.2707	0.011	0.1704	0.0024	1544	56	2561	24	-40%
BAL1701a.4.37	2.568	0.08	0.1627	0.0064	0.1147	0.0021	972	35	1874	33	-48%
BAL1701a.4.38	4.663	0.14	0.3033	0.011	0.1114	0.002	1708	54	1822	33	-6%
BAL1701a.4.39	4.89	0.15	0.3238	0.013	0.1094	0.0023	1808	63	1789	38	1%
BAL1701a.4.40	4.917	0.13	0.3224	0.013	0.1105	0.0018	1801	63	1807	30	0%
BAL1701a.4.41	5.31	0.2	0.3398	0.014	0.1132	0.0029	1886	67	1851	46	2%
BAL1701a.4.42	2.943	0.12	0.1807	0.0084	0.1174	0.0022	1071	46	1916	34	-44%
BAL1701a.4.43	3.48	0.14	0.1046	0.0053	0.2249	0.0035	641	31	3015	25	-79%
BAL1701a.4.44	4.788	0.15	0.318	0.012	0.1085	0.0022	1780	59	1774	37	0%
BAL1701a.4.45	4.6	0.23	0.3099	0.014	0.107	0.0044	1740	69	1748	75	0%
BAL1701a.4.46	5.005	0.15	0.3284	0.013	0.1099	0.0016	1831	63	1797	27	2%
BAL1701a.4.47	6	0.19	0.3608	0.015	0.12	0.0013	1986	71	1955	20	2%
BAL1701a.4.48	3.88	0.18	0.1485	0.007	0.1876	0.0045	893	39	2720	40	-67%
BAL1701a.4.49	4.74	0.21	0.283	0.015	0.1199	0.0029	1606	75	1954	43	-18%
BAL1701a.4.50	4.22	0.18	0.2771	0.012	0.1099	0.0035	1577	61	1797	58	-12%
BAL1701a.4.51	5.728	0.16	0.3489	0.013	0.1182	0.0013	1929	62	1928	20	0%
BAL1701a.4.52	5.47	0.17	0.3417	0.013	0.1154	0.0018	1895	62	1885	28	1%
BAL1701a.4.53	4.39	0.16	0.2703	0.011	0.11	0.0024	1542	56	1799	40	-14%
BAL1701a.4.54	4.75	0.15	0.3221	0.013	0.1063	0.0016	1800	63	1736	28	4%
BAL1701a.4.55	5.16	0.19	0.3292	0.013	0.1127	0.004	1835	63	1843	64	0%

BAL1701a.4.56	5.28	0.18	0.3295	0.013	0.1158	0.0012	1836	63	1892	19	-3%
BAL1701a.4.57	4.33	0.22	0.2879	0.013	0.1086	0.0044	1631	65	1775	74	-8%
BAL1701a.4.58	5.59	0.22	0.3428	0.014	0.1175	0.0035	1900	67	1918	54	-1%
BAL1701a.4.59	5.42	0.17	0.3416	0.014	0.1147	0.0019	1894	67	1874	30	1%
BAL1701a.4.60	5.276	0.16	0.3167	0.012	0.1201	0.0019	1774	59	1957	28	-9%
BAL1701a.4.61	4.96	0.2	0.3196	0.012	0.1117	0.0034	1788	59	1826	55	-2%
BAL1701a.4.62	5.02	0.23	0.3253	0.015	0.1118	0.0039	1816	73	1828	63	-1%
BAL1701a.4.63	5.42	0.2	0.3377	0.014	0.116	0.0034	1876	67	1895	53	-1%
BAL1701a.4.64	5.31	0.18	0.3345	0.013	0.1147	0.0023	1860	63	1874	36	-1%
BAL1701a.4.65	1.807	0.057	0.1114	0.0044	0.1174	0.0016	681	26	1916	25	-64%
BAL1701a.4.66	5.52	0.28	0.3464	0.015	0.1156	0.0051	1917	72	1888	79	2%
BAL1701a.4.67	5.74	0.2	0.3528	0.015	0.1173	0.0019	1948	71	1915	29	2%
BAL1701a.4.68	5.33	0.18	0.3358	0.013	0.1147	0.0024	1866	63	1874	38	0%
BAL1701a.4.69	5.47	0.17	0.3404	0.013	0.1163	0.0025	1889	63	1899	39	-1%
BAL1701a.4.70	5.35	0.17	0.3372	0.013	0.1147	0.0021	1873	63	1874	33	0%
BAL1701a.4.71	9.98	0.77	0.46	0.025	0.157	0.0062	2440	110	2423	67	1%
BAL1701a.4.72	4.87	0.25	0.3193	0.013	0.1103	0.0049	1786	64	1804	81	-1%
BAL1701a.4.73	5.33	0.16	0.3351	0.013	0.115	0.0017	1863	63	1879	27	-1%
BAL1701a.4.74	1.945	0.082	0.1191	0.0055	0.118	0.0028	725	32	1925	43	-62%
BAL1701a.4.75	11.38	0.41	0.44	0.019	0.1874	0.0024	2351	85	2719	21	-14%
BAL1701a.4.76	1.998	0.1	0.1308	0.0066	0.1099	0.0045	792	38	1797	75	-56%
BAL1701a.4.77	5.85	0.18	0.3662	0.015	0.1151	0.0011	2011	71	1881	17	7%
BAL1701a.4.78	2.68	0.12	0.1778	0.0087	0.1085	0.0025	1055	48	1774	42	-41%
BAL1701a.4.79	3.529	0.11	0.2202	0.0084	0.1158	0.0025	1283	44	1892	39	-32%
BAL1701a.4.80	4.64	0.16	0.3027	0.013	0.1107	0.0023	1705	64	1810	38	-6%

BAL1701a.4.81	5.64	0.25	0.346	0.016	0.1177	0.0038	1915	77	1921	58	0%
BAL1701a.4.82	4.86	0.17	0.3174	0.013	0.1103	0.0019	1777	64	1804	31	-1%
BAL1701a.4.83	4.91	0.18	0.3212	0.013	0.1101	0.0023	1796	63	1800	38	0%
BAL1701a.4.84	1.632	0.053	0.0636	0.0026	0.1849	0.0035	397	16	2697	31	-85%
BAL1701a.4.85	5.16	0.17	0.3264	0.013	0.114	0.0019	1821	63	1863	30	-2%
BAL1701a.4.86	5.62	0.19	0.3444	0.013	0.1173	0.0024	1908	62	1915	37	0%

Sample: BAL1701B

Grain ID	*207Pb/232Th*	*207Pb/232Th prop2SE*	*206Pb/238U*	*206Pb/238U prop2SE*	*207Pb/206Pb*	*207Pb/206Pb prop2SE*	*206Pb/238Pb Age (Ma)*	*± 1σ(Ma)*	*207Pb/206Pb Age (Ma)*	*± 1σ (Ma)*	*Disc (%)*
BAL1701b.4.01	1.38	0.14	0.0869	0.009	0.1077	0.0044	537	53	1760	75	69%
BAL1701b.4.02	4.65	0.15	0.3117	0.013	0.108	0.0022	1749	64	1765	37	1%
BAL1701b.4.03	1.799	0.083	0.1185	0.0057	0.1097	0.0018	722	33	1794	30	60%
BAL1701b.4.04	4.91	0.17	0.3244	0.013	0.109	0.0028	1811	63	1782	47	-2%
BAL1701b.4.05	4.56	0.18	0.3052	0.012	0.1079	0.0024	1717	59	1763	41	3%
BAL1701b.4.06	4.22	0.14	0.2806	0.011	0.1085	0.0019	1594	55	1774	32	10%
BAL1701b.4.07	4.88	0.16	0.3219	0.013	0.1095	0.002	1799	63	1790	33	-1%
BAL1701b.4.08	4.892	0.14	0.3258	0.013	0.1085	0.0022	1818	63	1774	37	-2%
BAL1701b.4.09	4.61	0.25	0.312	0.019	0.107	0.0022	1751	93	1748	38	0%
BAL1701b.4.10	4.872	0.14	0.3215	0.012	0.1093	0.0018	1797	59	1787	30	-1%
BAL1701b.4.11	4.905	0.14	0.3227	0.012	0.1097	0.0017	1803	58	1794	28	-1%
BAL1701b.4.12	4.66	0.21	0.312	0.015	0.108	0.0034	1751	74	1765	58	1%
BAL1701b.4.13	4.855	0.14	0.3225	0.013	0.1087	0.0019	1802	63	1777	32	-1%
BAL1701b.4.14	2.67	0.18	0.1658	0.012	0.1089	0.0022	989	66	1780	37	44%
BAL1701b.4.15	4.06	0.17	0.274	0.015	0.1073	0.0021	1561	76	1753	36	11%

BAL1701b.4.16	1.88	0.079	0.1202	0.0056	0.1128	0.0022	732	32	1844	35	60%
BAL1701b.4.17	5.07	0.16	0.3332	0.014	0.1099	0.002	1854	68	1797	33	-3%
BAL1701b.4.18	3.594	0.12	0.2215	0.0094	0.1106	0.0015	1290	50	1808	25	29%
BAL1701b.4.19	4.86	0.18	0.3223	0.013	0.1089	0.0019	1801	63	1780	32	-1%
BAL1701b.4.20	2.77	0.1	0.1714	0.0076	0.1105	0.0023	1020	42	1807	38	44%
BAL1701b.4.21	4.91	0.17	0.3264	0.013	0.1086	0.0022	1821	63	1775	37	-3%
BAL1701b.4.22	4.09	0.16	0.2602	0.012	0.1083	0.0021	1491	61	1770	36	16%
BAL1701b.4.23	4.2	0.15	0.2803	0.011	0.1083	0.0024	1593	55	1770	41	10%
BAL1701b.4.24	4.62	0.16	0.3084	0.012	0.1084	0.0027	1733	59	1772	46	2%
BAL1701b.4.25	4.832	0.14	0.3209	0.013	0.109	0.0021	1794	63	1782	35	-1%
BAL1701b.4.26	4.755	0.14	0.3169	0.012	0.1085	0.0018	1775	59	1774	30	0%
BAL1701b.4.27	4.786	0.15	0.317	0.012	0.1092	0.0021	1775	59	1785	35	1%
BAL1701b.4.28	4.79	0.17	0.3209	0.013	0.1078	0.0029	1794	63	1762	49	-2%
BAL1701b.4.29	4.279	0.13	0.2866	0.011	0.1079	0.0019	1625	55	1763	32	8%
BAL1701b.4.30	4.78	0.16	0.3222	0.012	0.1076	0.0025	1800	59	1758	43	-2%
BAL1701b.4.31	4.317	0.14	0.2884	0.011	0.1085	0.002	1634	55	1774	34	8%
BAL1701b.4.32	4.658	0.13	0.3122	0.012	0.1081	0.0018	1752	59	1767	31	1%
BAL1701b.4.33	4.57	0.14	0.3077	0.012	0.108	0.0014	1729	59	1765	24	2%

Sample: BAL1703A

Grain ID	*207Pb/232Th*	*207Pb/232Th prop2SE*	*206Pb/238U*	*206Pb/238U prop2SE*	*207Pb/206Pb*	*207Pb/206Pb prop2SE*	*206Pb/238Pb Age (Ma)*	*± 1σ(Ma)*	*207Pb/206Pb Age (Ma)*	*± 1σ (Ma)*	*Disc (%)*
BAL1703a.4.01	3.042	0.089	0.1859	0.0076	0.1199	0.0017	1099	41	1954	25	44%
BAL1703a.4.02	2.326	0.089	0.1689	0.0075	0.1007	0.0014	1006	41	1636	26	39%
BAL1703a.4.03	3.78	0.14	0.2635	0.013	0.1051	0.0013	1508	66	1715	23	12%

BAL1703a.4.04	1.631	0.077	0.1053	0.0058	0.1132	0.0019	645	34	1851	30	65%
BAL1703a.4.05	3.421	0.12	0.2103	0.0095	0.1125	0.0021	1230	51	1839	34	33%
BAL1703a.4.06	3.353	0.11	0.2245	0.0093	0.1091	0.001	1306	49	1784	17	27%
BAL1703a.4.07	1.021	0.044	0.0697	0.0033	0.1072	0.0019	434	20	1752	33	75%
BAL1703a.4.08	4.59	0.15	0.3114	0.014	0.1079	0.0014	1748	69	1763	24	1%
BAL1703a.4.09	4.5	0.15	0.2924	0.013	0.1126	0.0029	1654	65	1841	47	10%
BAL1703a.4.10	4.697	0.13	0.3233	0.013	0.1061	0.0014	1806	63	1733	24	-4%
BAL1703a.4.11	4.35	0.16	0.2676	0.012	0.1184	0.0026	1529	61	1931	39	21%
BAL1703a.4.12	4.44	0.18	0.2936	0.013	0.1105	0.0017	1659	65	1807	28	8%
BAL1703a.4.13	6.93	0.27	0.3515	0.015	0.1434	0.0019	1942	72	2268	23	14%
BAL1703a.4.14	5.94	0.37	0.31	0.019	0.1399	0.0037	1741	94	2225	46	22%
BAL1703a.4.15	3.95	0.16	0.2478	0.011	0.1158	0.0025	1427	57	1892	39	25%
BAL1703a.4.16	2.78	0.14	0.1716	0.0088	0.1176	0.0029	1021	48	1919	44	47%
BAL1703a.4.17	4.931	0.15	0.3289	0.013	0.1089	0.0018	1833	63	1780	30	-3%
BAL1703a.4.18	4.6	0.15	0.3098	0.013	0.1076	0.0022	1740	64	1758	37	1%
BAL1703a.4.19	2.023	0.066	0.1309	0.0055	0.1123	0.0016	793	31	1836	26	57%
BAL1703a.4.20	7.32	0.27	0.397	0.016	0.1334	0.0023	2155	74	2142	30	-1%
BAL1703a.4.21	4.84	0.18	0.3179	0.015	0.1103	0.002	1779	73	1804	33	1%
BAL1703a.4.22	8.94	0.33	0.3814	0.016	0.1697	0.0027	2083	75	2554	27	18%
BAL1703a.4.23	0.63	0.032	0.0406	0.0034	0.1134	0.0045	257	21	1854	72	86%
BAL1703a.4.24	5.697	0.16	0.3581	0.013	0.1152	0.0018	1973	62	1882	28	-5%
BAL1703a.4.25	5.36	0.17	0.3381	0.014	0.1147	0.0014	1878	67	1874	22	0%
BAL1703a.4.26	3.66	0.12	0.2392	0.011	0.1109	0.0022	1383	57	1813	36	24%
BAL1703a.4.27	4.93	0.17	0.3039	0.014	0.1176	0.0029	1711	69	1919	44	11%
BAL1703a.4.28	1.423	0.051	0.0739	0.0037	0.1396	0.0027	460	22	2221	34	79%

BAL1703a.4.29	3.918	0.13	0.2558	0.01	0.111	0.0029	1468	51	1815	48	19%
BAL1703a.4.30	4.804	0.15	0.3201	0.012	0.1084	0.0018	1790	59	1772	30	-1%
BAL1703a.4.31	4.756	0.13	0.3163	0.012	0.1086	0.0015	1772	59	1775	25	0%
BAL1703a.4.32	2.989	0.1	0.1331	0.0063	0.1624	0.0021	806	36	2480	22	68%
BAL1703a.4.33	5.1	0.17	0.3279	0.013	0.1124	0.0022	1828	63	1838	36	1%
BAL1703a.4.34	2.454	0.11	0.1697	0.0083	0.1048	0.0045	1010	46	1710	79	41%
BAL1703a.4.35	5.03	0.16	0.3272	0.013	0.1112	0.0035	1825	63	1818	57	0%
BAL1703a.4.36	4	0.55	0.18	0.024	0.1589	0.0027	1070	130	2443	29	56%
BAL1703a.4.37	3.946	0.13	0.2448	0.0094	0.1161	0.0023	1412	49	1896	36	26%
BAL1703a.4.38	4.02	0.19	0.2578	0.013	0.1128	0.0036	1479	67	1844	58	20%
BAL1703a.4.39	4.4	0.22	0.2744	0.014	0.1158	0.0023	1563	71	1892	36	17%
BAL1703a.4.40	2.311	0.098	0.076	0.0035	0.2196	0.004	472	21	2977	30	84%
BAL1703a.4.41	0.86	0.037	0.0507	0.0023	0.1224	0.0022	319	14	1991	32	84%
BAL1703a.4.42	1.683	0.069	0.0902	0.004	0.1148	0.0021	557	24	1876	33	70%
BAL1703a.4.43	2.283	0.066	0.1666	0.0066	0.0991	0.0019	993	36	1606	36	38%
BAL1703a.4.44	2.895	0.095	0.1766	0.0079	0.1185	0.0026	1048	43	1933	39	46%
BAL1703a.4.45	4.84	0.16	0.3136	0.014	0.1113	0.0029	1758	69	1820	47	3%
BAL1703a.4.46	1.615	0.072	0.085	0.0041	0.1372	0.003	526	24	2191	38	76%
BAL1703a.4.47	1.6	0.049	0.095	0.004	0.1217	0.0022	585	24	1980	32	70%
BAL1703a.4.48	4.91	0.19	0.3229	0.015	0.1093	0.0025	1804	73	1787	42	-1%
BAL1703a.4.49	4.53	0.17	0.2877	0.011	0.114	0.0029	1630	55	1863	46	13%
BAL1703a.4.50	2.45	0.16	0.143	0.0089	0.1241	0.0033	862	50	2015	47	57%
BAL1703a.4.51	6.03	0.32	0.361	0.024	0.1205	0.0034	1990	110	1963	50	-1%
BAL1703a.4.52	1.933	0.071	0.0921	0.0042	0.1519	0.0033	568	25	2367	37	76%
BAL1703a.4.53	5.3	0.18	0.335	0.013	0.1142	0.0028	1863	63	1866	44	0%

BAL1703a.4.54	1.743	0.06	0.1033	0.0043	0.1218	0.0038	634	25	1982	56	68%
BAL1703a.4.55	4.07	0.16	0.2551	0.01	0.1153	0.0022	1465	51	1884	34	22%
BAL1703a.4.56	5.14	0.21	0.3179	0.014	0.1169	0.0023	1779	68	1909	35	7%
BAL1703a.4.57	2.882	0.097	0.1657	0.008	0.1208	0.0038	988	44	1967	56	50%
BAL1703a.4.58	1.519	0.067	0.0883	0.0038	0.1242	0.0037	545	23	2017	53	73%
BAL1703a.4.59	4.49	0.19	0.2724	0.014	0.1196	0.0033	1553	71	1949	49	20%
BAL1703a.4.60	4.917	0.13	0.3209	0.012	0.1109	0.0015	1794	59	1813	25	1%
BAL1703a.4.61	4.77	0.18	0.3062	0.013	0.113	0.0034	1722	64	1847	55	7%
BAL1703a.4.62	3.03	0.14	0.1748	0.0083	0.126	0.0027	1039	46	2042	38	49%
BAL1703a.4.63	4.77	0.18	0.2966	0.014	0.1171	0.002	1674	70	1912	31	12%
BAL1703a.4.64	4.87	0.16	0.3222	0.014	0.1097	0.0011	1800	68	1794	18	0%
BAL1703a.4.65	4.36	0.15	0.279	0.012	0.1139	0.0021	1586	60	1862	33	15%
BAL1703a.4.66	4.23	0.16	0.2779	0.012	0.1107	0.0024	1581	61	1810	40	13%
BAL1703a.4.67	4.51	0.15	0.2946	0.011	0.1114	0.0023	1664	55	1822	38	9%
BAL1703a.4.68	5.44	0.19	0.3414	0.015	0.116	0.0022	1893	72	1895	34	0%
BAL1703a.4.69	3.22	0.14	0.2027	0.0094	0.116	0.0022	1190	50	1895	34	37%
BAL1703a.4.70	4.519	0.14	0.29	0.011	0.1137	0.002	1642	55	1859	32	12%
BAL1703a.4.71	1.344	0.043	0.0636	0.0034	0.1549	0.0037	397	21	2400	41	83%
BAL1703a.4.72	9.31	0.37	0.349	0.017	0.1947	0.0019	1930	81	2782	16	31%
BAL1703a.4.73	5.325	0.16	0.3369	0.013	0.1153	0.0019	1872	63	1884	30	1%
BAL1703a.4.74	5.27	0.22	0.3282	0.014	0.1173	0.0027	1830	68	1915	41	4%
BAL1703a.4.75	4.83	0.2	0.3114	0.013	0.1127	0.0042	1748	64	1843	68	5%
BAL1703a.4.76	3.37	0.14	0.1958	0.011	0.1257	0.0047	1153	59	2038	66	43%
BAL1703a.4.77	4.08	0.18	0.2538	0.013	0.1177	0.003	1458	67	1921	46	24%
BAL1703a.4.78	1.626	0.068	0.0942	0.0047	0.1264	0.0037	580	28	2048	52	72%

BAL1703a.4.79	9.91	0.29	0.4428	0.017	0.1637	0.002	2363	76	2493	21	5%
BAL1703a.4.80	2.727	0.11	0.125	0.0053	0.1582	0.004	759	30	2436	43	69%
BAL1703a.4.81	5.201	0.14	0.3211	0.012	0.118	0.0016	1795	59	1925	24	7%
BAL1703a.4.82	4.19	0.14	0.2532	0.011	0.1142	0.0034	1455	57	1866	54	22%
BAL1703a.4.83	3.54	0.18	0.1796	0.0091	0.1439	0.0038	1065	50	2274	46	53%
BAL1703a.4.84	2.465	0.08	0.119	0.0067	0.1518	0.0041	725	39	2366	46	69%
BAL1703a.4.85	5.11	0.28	0.3218	0.014	0.1155	0.0045	1799	68	1887	70	5%
BAL1703a.4.86	5.34	0.17	0.3385	0.013	0.1155	0.0029	1879	63	1887	45	0%
BAL1703a.4.87	3.901	0.13	0.2439	0.011	0.1168	0.0013	1407	57	1907	20	26%
BAL1703a.4.88	4.81	0.18	0.3167	0.013	0.1109	0.0024	1774	64	1813	39	2%
BAL1703a.4.89	3.42	0.28	0.228	0.018	0.1087	0.0021	1324	94	1777	35	25%
BAL1703a.4.90	3.81	0.15	0.2283	0.012	0.1221	0.0026	1326	63	1986	38	33%
BAL1703a.4.91	4.93	0.16	0.3174	0.012	0.113	0.0024	1777	59	1847	39	4%
BAL1703a.4.92	5.11	0.2	0.3235	0.014	0.1152	0.002	1807	68	1882	31	4%
BAL1703a.4.93	3.12	0.16	0.2004	0.012	0.1135	0.0016	1177	64	1855	26	37%
BAL1703a.4.94	1.072	0.032	0.04629	0.0019	0.1686	0.0025	292	12	2543	25	89%
BAL1703a.4.95	4.93	0.15	0.323	0.013	0.1109	0.0015	1804	63	1813	25	0%
BAL1703a.4.96	5.41	0.14	0.3388	0.013	0.1156	0.0016	1881	63	1888	25	0%
BAL1703a.4.97	4.573	0.14	0.3026	0.013	0.1101	0.0021	1704	64	1800	35	5%
BAL1703a.4.98	4.919	0.15	0.3218	0.012	0.1112	0.0018	1799	59	1818	30	1%
BAL1703a.4.99	4.28	0.15	0.2819	0.011	0.1105	0.0029	1601	55	1807	48	11%
BAL1703a.4.100	3.361	0.096	0.2336	0.0098	0.1042	0.0018	1353	51	1699	32	20%
BAL1703a.4.101	2.05	0.12	0.1127	0.0066	0.1316	0.0036	688	38	2119	48	68%
BAL1703a.4.102	1.768	0.076	0.1141	0.005	0.1126	0.0025	697	29	1841	40	62%
BAL1703a.4.103	1.243	0.044	0.0714	0.0031	0.1263	0.0019	445	19	2046	27	78%

BAL1703a.4.104	3.29	0.13	0.2252	0.011	0.1061	0.0016	1309	58	1733	28	24%
BAL1703a.4.105	2.24	0.13	0.1286	0.0072	0.1258	0.0034	780	41	2039	48	62%
BAL1703a.4.106	3.13	0.13	0.1977	0.0091	0.1149	0.0031	1163	49	1878	49	38%
BAL1703a.4.107	4.51	0.17	0.285	0.014	0.115	0.0022	1616	70	1879	35	14%
BAL1703a.5.01	4.17	0.13	0.2697	0.0085	0.1128	0.0028	1539	43	1844	45	17%
BAL1703a.5.02	8.94	0.51	0.405	0.021	0.161	0.002	2192	96	2465	21	11%
BAL1703a.5.03	5.421	0.087	0.3403	0.0054	0.1156	0.001	1888	26	1888	16	0%
BAL1703a.5.04	9.15	0.18	0.4186	0.0092	0.1582	0.0028	2254	42	2436	30	7%
BAL1703a.5.05	4.879	0.099	0.3211	0.0049	0.1098	0.0023	1795	24	1795	38	0%
BAL1703a.5.06	5.44	0.11	0.3447	0.0058	0.1145	0.0026	1909	28	1871	41	-2%
BAL1703a.5.07	3.94	0.2	0.2686	0.0098	0.1056	0.0023	1534	50	1724	40	11%
BAL1703a.5.08	5.424	0.08	0.3425	0.0052	0.1148	0.0014	1899	25	1876	22	-1%
BAL1703a.5.09	3.5	0.13	0.237	0.0065	0.1069	0.0034	1371	34	1746	58	21%
BAL1703a.5.10	4.33	0.12	0.2648	0.0082	0.1185	0.0025	1514	42	1933	38	22%
BAL1703a.5.11	4.566	0.072	0.3031	0.0041	0.1093	0.0023	1707	20	1787	38	4%
BAL1703a.5.12	11.78	0.16	0.5051	0.0064	0.1682	0.002	2636	27	2539	20	-4%
BAL1703a.5.13	3.94	0.087	0.2564	0.0076	0.1109	0.0027	1471	39	1813	44	19%
BAL1703a.5.14	4.99	0.14	0.3228	0.0066	0.1124	0.0035	1803	32	1838	56	2%
BAL1703a.5.15	5.3	0.11	0.3348	0.0079	0.1155	0.0024	1862	38	1887	38	1%
BAL1703a.5.16	2.96	0.11	0.2053	0.0079	0.1052	0.0023	1204	42	1717	40	30%
BAL1703a.5.17	2.314	0.058	0.1495	0.0057	0.1119	0.0023	898	32	1830	37	51%
BAL1703a.5.18	11.27	0.28	0.482	0.011	0.1707	0.003	2536	48	2564	30	1%
BAL1703a.5.19	4.471	0.076	0.286	0.0058	0.1146	0.0011	1622	29	1873	18	13%
BAL1703a.5.20	1.754	0.041	0.1176	0.0027	0.1077	0.0038	717	16	1760	65	59%

BAL1703a.5.21	1.93	0.15	0.087	0.0023	0.1594	0.0086	538	14	2449	91	78%
BAL1703a.5.22	6.42	0.1	0.3755	0.0049	0.1239	0.0011	2055	23	2012	16	-2%
BAL1703a.5.23	4.216	0.061	0.2846	0.0046	0.1074	0.0015	1614	23	1755	26	8%

Sample: BAL1706a

Grain ID	*207Pb/232Th*	*207Pb/232Th prop2SE*	*206Pb/238U*	*206Pb/238U prop2SE*	*207Pb/206Pb*	*207Pb/206Pb prop2SE*	*206Pb/238Pb Age (Ma)*	*± 1σ(Ma)*	*207Pb/206Pb Age (Ma)*	*± 1σ (Ma)*	*Disc (%)*
BAL1706a.4.01	2.033	0.072	0.1167	0.0051	0.1279	0.0018	712	29	2069	25	66%
BAL1706a.4.02	4.75	0.15	0.3197	0.012	0.1089	0.0018	1788	59	1780	30	0%
BAL1706a.4.03	4.47	0.19	0.2929	0.012	0.1119	0.0031	1656	60	1830	50	10%
BAL1706a.4.04	4.74	0.17	0.3008	0.012	0.1157	0.0027	1695	59	1890	42	10%
BAL1706a.4.05	7.15	0.41	0.3571	0.016	0.1464	0.0065	1968	76	2304	76	15%
BAL1706a.4.06	4.93	0.2	0.3249	0.014	0.1109	0.0027	1814	68	1813	44	0%
BAL1706a.4.07	4.83	0.22	0.323	0.017	0.1095	0.0019	1804	83	1790	32	-1%
BAL1706a.4.08	4.851	0.15	0.3247	0.013	0.1095	0.0024	1813	63	1790	40	-1%
BAL1706a.4.09	5.23	0.21	0.2526	0.013	0.1515	0.0023	1452	67	2362	26	39%
BAL1706a.4.10	4.783	0.14	0.3188	0.012	0.1096	0.0015	1784	59	1792	25	0%
BAL1706a.4.11	5.13	0.18	0.3164	0.013	0.1185	0.0026	1772	64	1933	39	8%
BAL1706a.4.12	3.015	0.11	0.1856	0.0077	0.1189	0.0021	1097	42	1939	32	43%
BAL1706a.4.13	3.4	0.097	0.1999	0.008	0.1234	0.0015	1175	43	2005	22	41%
BAL1706a.4.14	5.44	0.18	0.3446	0.013	0.1151	0.0019	1909	62	1881	30	-1%
BAL1706a.4.15	2.857	0.099	0.1458	0.0061	0.1429	0.0029	877	34	2262	35	61%
BAL1706a.4.16	4.686	0.15	0.3156	0.012	0.1082	0.0021	1768	59	1769	36	0%
BAL1706a.4.17	3.28	0.19	0.1871	0.0094	0.1278	0.0042	1106	51	2067	58	46%
BAL1706a.4.18	4.64	0.21	0.312	0.016	0.1085	0.0017	1751	79	1774	29	1%

BAL1706a.4.19	4.77	0.18	0.3179	0.013	0.1091	0.002	1779	64	1784	34	0%
BAL1706a.4.20	5.01	0.16	0.327	0.014	0.1116	0.0015	1824	68	1825	25	0%
BAL1706a.4.21	5.28	0.17	0.337	0.013	0.1138	0.0024	1872	63	1860	38	-1%
BAL1706a.4.22	4.31	0.16	0.2989	0.011	0.105	0.0027	1686	55	1713	47	2%
BAL1706a.4.23	7.36	0.27	0.3882	0.016	0.1381	0.0024	2114	74	2203	30	4%
BAL1706a.4.24	5.405	0.16	0.3438	0.013	0.1141	0.0016	1905	62	1865	25	-2%
BAL1706a.4.25	3.44	0.13	0.1887	0.0077	0.1325	0.0019	1114	42	2131	25	48%
BAL1706a.4.26	4.97	0.16	0.3274	0.013	0.1103	0.0019	1826	63	1804	31	-1%
BAL1706a.4.27	5.29	0.17	0.3358	0.013	0.1144	0.0019	1866	63	1870	30	0%
BAL1706a.4.28	5.5	0.19	0.3456	0.015	0.1154	0.0017	1914	72	1885	27	-2%
BAL1706a.4.29	4.78	0.16	0.3183	0.012	0.1088	0.0021	1781	59	1779	35	0%
BAL1706a.4.30	4.21	0.15	0.2674	0.011	0.1144	0.0029	1528	56	1870	46	18%
BAL1706a.4.31	5.39	0.19	0.3385	0.013	0.1154	0.0026	1879	63	1885	41	0%
BAL1706a.4.32	3.01	0.12	0.1833	0.01	0.1194	0.0027	1085	54	1946	41	44%
BAL1706a.4.33	4	0.21	0.239	0.014	0.1162	0.0041	1381	73	1898	64	27%
BAL1706a.4.34	3.969	0.12	0.2648	0.011	0.1087	0.0014	1514	56	1777	24	15%
BAL1706a.4.35	5.51	0.22	0.3439	0.013	0.1163	0.0033	1905	62	1899	51	0%
BAL1706a.4.36	4.87	0.18	0.3179	0.013	0.1109	0.0032	1779	64	1813	52	2%
BAL1706a.4.37	5.57	0.21	0.343	0.014	0.1176	0.0019	1901	67	1919	29	1%
BAL1706a.4.38	4.381	0.12	0.2725	0.011	0.1162	0.0025	1553	56	1898	39	18%
BAL1706a.4.39	5.15	0.17	0.3347	0.013	0.1113	0.0025	1861	63	1820	41	-2%
BAL1706a.4.40	4.82	0.16	0.3324	0.013	0.105	0.0027	1850	63	1713	47	-8%
BAL1706a.4.41	5.54	0.19	0.3477	0.014	0.1154	0.0023	1924	67	1885	36	-2%
BAL1706a.4.42	4.65	0.22	0.315	0.016	0.1072	0.0022	1765	78	1752	38	-1%
BAL1706a.4.43	11.08	0.33	0.4855	0.02	0.1655	0.0022	2551	87	2512	23	-2%

BAL1706a.4.44	2.414	0.078	0.1315	0.0053	0.1327	0.0022	796	30	2133	29	63%
BAL1706a.4.45	4.84	0.17	0.3217	0.013	0.1089	0.0021	1798	63	1780	35	-1%
BAL1706a.4.46	4.702	0.14	0.3125	0.012	0.10842	0.00096	1753	59	1772	16	1%
BAL1706a.4.47	4.67	0.16	0.3108	0.012	0.1087	0.0025	1745	59	1777	42	2%

Sample: BAL1706B

Grain ID	*207Pb/232Th*	*207Pb/232Th prop2SE*	*206Pb/238U*	*206Pb/238U prop2SE*	*207Pb/206Pb*	*207Pb/206Pb prop2SE*	*206Pb/238Pb Age (Ma)*	*± 1σ(Ma)*	*207Pb/206Pb Age (Ma)*	*± 1σ (Ma)*	*Disc (%)*
BAL1706b.3.01	2.266	0.098	0.1354	0.0046	0.1211	0.004	819	26	1972	59	58%
BAL1706b.3.02	3.348	0.093	0.2114	0.0062	0.1146	0.0029	1236	33	1873	46	34%
BAL1706b.3.03	4.93	0.2	0.3234	0.0076	0.1104	0.0046	1806	37	1805	76	0%
BAL1706b.3.04	4.29	0.13	0.2808	0.0072	0.1095	0.0036	1595	36	1790	60	11%
BAL1706b.3.05	1.857	0.08	0.1118	0.0042	0.1202	0.0033	683	24	1958	49	65%
BAL1706b.3.06	3.076	0.1	0.1901	0.0074	0.1161	0.0035	1122	40	1896	54	41%
BAL1706b.3.07	1.513	0.039	0.0872	0.0021	0.1257	0.0038	539	12	2038	54	74%
BAL1706b.3.08	2.03	0.12	0.1241	0.0074	0.1185	0.0033	754	42	1933	50	61%
BAL1706b.3.09	4.65	0.17	0.3048	0.01	0.1105	0.0033	1715	49	1807	54	5%
BAL1706b.3.10	4.55	0.15	0.2978	0.0082	0.1105	0.0035	1680	41	1807	58	7%
BAL1706b.3.11	4.65	0.16	0.2927	0.0093	0.1141	0.0028	1655	46	1865	44	11%
BAL1706b.3.12	3.037	0.11	0.1968	0.0053	0.1119	0.0038	1158	29	1830	62	37%
BAL1706b.3.13	3.011	0.088	0.1414	0.0038	0.1546	0.0043	853	21	2397	47	64%
BAL1706b.3.14	2.085	0.065	0.1284	0.0033	0.118	0.0037	779	19	1925	56	60%
BAL1706b.3.15	4.91	0.16	0.3011	0.011	0.1184	0.003	1697	55	1931	45	12%
BAL1706b.3.16	2.52	0.17	0.151	0.011	0.1198	0.0041	907	62	1952	61	54%
BAL1706b.3.17	1.813	0.046	0.1093	0.0026	0.1204	0.0032	669	15	1961	48	66%

BAL1706b.3.18	1.62	0.056	0.0785	0.0029	0.1499	0.0045	487	17	2344	51	79%
BAL1706b.3.19	5.04	0.18	0.3257	0.0094	0.1123	0.0035	1818	46	1836	57	1%
BAL1706b.3.20	5.21	0.15	0.3323	0.0077	0.1139	0.0033	1850	37	1862	52	1%
BAL1706b.3.21	1.645	0.05	0.091	0.0034	0.1313	0.0033	561	20	2115	44	73%
BAL1706b.3.22	1.872	0.054	0.1108	0.0029	0.1227	0.0034	677	17	1995	49	66%
BAL1706b.3.23	4.47	0.14	0.2947	0.0068	0.1101	0.0033	1665	34	1800	55	8%
BAL1706b.3.24	2.946	0.095	0.1738	0.0062	0.123	0.0032	1033	34	1999	46	48%
BAL1706b.3.25	10.27	0.23	0.4656	0.01	0.1601	0.004	2464	44	2456	42	0%
BAL1706b.3.26	4.28	0.14	0.2536	0.007	0.1223	0.0038	1457	36	1989	55	27%
BAL1706b.3.27	4.808	0.12	0.3207	0.007	0.1091	0.0027	1793	34	1784	45	-1%
BAL1706b.3.28	0.952	0.03	0.0489	0.0018	0.1414	0.0046	308	11	2244	56	86%
BAL1706b.3.29	3.932	0.12	0.2385	0.0058	0.1196	0.0036	1379	30	1949	54	29%
BAL1706b.3.30	4.736	0.11	0.3154	0.0071	0.1088	0.0026	1767	35	1779	44	1%
BAL1706b.3.31	5.02	0.15	0.3242	0.0088	0.1122	0.0029	1810	43	1835	47	1%
BAL1706b.3.32	6.73	0.65	0.29	0.029	0.1677	0.0041	1640	140	2534	41	35%
BAL1706b.3.33	1.058	0.034	0.0484	0.0021	0.1588	0.0049	305	13	2442	52	88%
BAL1706b.3.34	3.466	0.093	0.2151	0.0054	0.1155	0.0029	1256	29	1887	45	33%
BAL1706b.3.35	2.33	0.062	0.133	0.0039	0.127	0.0032	805	22	2056	45	61%
BAL1706b.3.36	2.595	0.075	0.1472	0.0047	0.1278	0.0038	885	26	2067	53	57%
BAL1706b.3.37	11.35	0.42	0.481	0.013	0.1709	0.0057	2532	57	2566	56	1%
BAL1706b.3.38	2.268	0.091	0.1309	0.0053	0.1255	0.0048	793	30	2035	68	61%
BAL1706b.3.39	4.728	0.12	0.3161	0.0075	0.1081	0.0028	1771	37	1767	47	0%
BAL1706b.3.40	5.02	0.14	0.3291	0.0074	0.1104	0.0031	1834	36	1805	51	-2%
BAL1706b.3.41	5.44	0.15	0.3415	0.0077	0.1153	0.0033	1894	37	1884	52	-1%
BAL1706b.3.42	1.425	0.057	0.0937	0.003	0.1099	0.0032	577	18	1797	53	68%

BAL1706b.3.43	2.93	0.089	0.1813	0.0064	0.1172	0.0047	1074	35	1913	72	44%
BAL1706b.3.44	4.05	0.15	0.2515	0.0095	0.1165	0.0032	1446	49	1902	49	24%
BAL1706b.3.45	2.326	0.089	0.1371	0.0048	0.1225	0.0034	828	27	1992	49	58%
BAL1706b.3.46	1.948	0.058	0.1205	0.0028	0.1167	0.0037	733	16	1905	57	62%
BAL1706b.3.47	1.72	0.054	0.1103	0.004	0.1126	0.0028	674	23	1841	45	63%
BAL1706b.4.01	3.42	0.13	0.2078	0.0085	0.1147	0.0041	1217	45	1874	65	35%
BAL1706b.4.02	4.34	0.18	0.2788	0.012	0.113	0.0029	1585	60	1847	47	14%
BAL1706b.4.03	4.803	0.14	0.3201	0.012	0.1088	0.0017	1790	59	1779	29	-1%
BAL1706b.4.04	3.01	0.16	0.1305	0.0083	0.1676	0.0025	791	47	2533	25	69%
BAL1706b.4.05	4.98	0.16	0.3278	0.013	0.1101	0.002	1828	63	1800	33	-2%
BAL1706b.4.06	3.42	0.13	0.2053	0.0096	0.1212	0.004	1204	51	1973	59	39%
BAL1706b.4.07	1.936	0.077	0.1288	0.0063	0.1093	0.002	781	36	1787	33	56%
BAL1706b.4.08	2.712	0.097	0.1531	0.0062	0.1284	0.0018	918	35	2075	25	56%
BAL1706b.4.09	0.868	0.032	0.0572	0.0033	0.1108	0.0031	359	20	1812	51	80%
BAL1706b.4.10	1.232	0.078	0.0702	0.0049	0.1278	0.0026	437	30	2067	36	79%
BAL1706b.4.11	1.531	0.051	0.1026	0.0046	0.1081	0.0024	630	27	1767	41	64%
BAL1706b.4.12	3.29	0.13	0.1959	0.011	0.1225	0.0026	1153	59	1992	38	42%
BAL1706b.4.13	4.54	0.19	0.3027	0.012	0.1091	0.0032	1705	59	1784	54	4%
BAL1706b.4.14	4.11	0.14	0.2563	0.011	0.1168	0.0016	1471	56	1907	25	23%
BAL1706b.4.15	1.548	0.085	0.0938	0.0063	0.1198	0.0027	578	37	1952	40	70%
BAL1706b.4.16	1.448	0.064	0.0899	0.005	0.1175	0.0027	555	30	1918	41	71%
BAL1706b.4.17	1.49	0.11	0.0759	0.0041	0.1426	0.0048	472	25	2258	58	79%
BAL1706b.4.18	4.556	0.14	0.3033	0.013	0.1096	0.0029	1708	64	1792	48	5%
BAL1706b.4.19	1.492	0.077	0.1006	0.0053	0.1081	0.0015	618	31	1767	26	65%

BAL1706b.4.20	5.83	0.17	0.3537	0.014	0.1203	0.0015	1952	67	1960	22	0%
BAL1706b.4.21	5.33	0.18	0.3389	0.014	0.1147	0.0015	1881	67	1874	24	0%
BAL1706b.4.22	4.88	0.15	0.3241	0.013	0.1099	0.0016	1810	63	1797	27	-1%
BAL1706b.4.23	4.92	0.15	0.3234	0.012	0.1105	0.0015	1806	58	1807	25	0%
BAL1706b.4.24	1.48	0.11	0.0898	0.0061	0.12	0.0028	554	36	1955	42	72%
BAL1706b.4.25	0.891	0.038	0.0532	0.0024	0.122	0.0022	334	15	1985	32	83%
BAL1706b.4.26	2.83	0.21	0.1613	0.0086	0.1279	0.0054	964	48	2069	74	53%
BAL1706b.4.27	4.582	0.14	0.2868	0.011	0.1171	0.002	1626	55	1912	31	15%
BAL1706b.4.28	2.41	0.095	0.1432	0.0065	0.1156	0.0025	863	37	1888	39	54%
BAL1706b.4.29	2.06	0.12	0.1147	0.008	0.1324	0.003	700	46	2129	40	67%
BAL1706b.4.30	4.07	0.2	0.2687	0.013	0.1109	0.0032	1534	66	1813	52	15%
BAL1706b.4.31	10.33	0.3	0.4691	0.019	0.1611	0.0018	2480	83	2466	19	-1%
BAL1706b.4.32	2.18	0.095	0.1257	0.0062	0.119	0.0024	763	36	1940	36	61%
BAL1706b.4.33	8.91	0.97	0.402	0.022	0.162	0.013	2180	100	2480	140	12%
BAL1706b.4.34	1.898	0.087	0.1209	0.0062	0.115	0.0014	736	36	1879	22	61%
BAL1706b.4.35	14.85	0.39	0.5489	0.022	0.1986	0.0031	2821	92	2814	26	0%
BAL1706b.4.36	3.49	0.12	0.2311	0.0091	0.1108	0.0029	1340	48	1812	48	26%
BAL1706b.4.37	4.58	0.21	0.314	0.013	0.1068	0.0034	1760	64	1745	58	-1%
BAL1706b.4.38	2.527	0.098	0.1506	0.0068	0.1162	0.0025	904	38	1898	39	52%
BAL1706b.4.39	4.02	0.14	0.2499	0.01	0.1182	0.0024	1438	52	1928	36	25%
BAL1706b.4.40	2.759	0.097	0.1161	0.0052	0.1743	0.0023	708	30	2599	22	73%
BAL1706b.4.41	1.502	0.058	0.0929	0.0044	0.1178	0.0022	573	26	1922	34	70%
BAL1706b.4.42	3.59	0.16	0.2198	0.0099	0.123	0.0069	1281	52	1999	100	36%
BAL1706b.4.43	3.155	0.095	0.1393	0.006	0.1662	0.0031	841	34	2519	32	67%

Sample: COR1702e

Grain ID	*207Pb/232Th*	*207Pb/232Th prop2SE*	*206Pb/238U*	*206Pb/238U prop2SE*	*207Pb/206Pb*	*207Pb/206Pb prop2SE*	*206Pb/238Pb Age (Ma)*	*± 1σ(Ma)*	*207Pb/206Pb Age (Ma)*	*± 1σ (Ma)*	*Disc (%)*
COR1702e.5.01	4.86	0.12	0.3242	0.0076	0.1085	0.0017	1810	37	1774	29	-2%
COR1702e.5.02	0.492	0.013	0.02404	0.00042	0.1479	0.0036	153.1	2.6	2321	42	93%
COR1702e.5.03	4.82	0.1	0.3229	0.0041	0.1081	0.002	1804	20	1767	34	-2%
COR1702e.5.04	3.088	0.074	0.2092	0.0044	0.1068	0.0012	1225	23	1745	21	30%
COR1702e.5.05	5.12	0.2	0.332	0.012	0.1118	0.0017	1848	58	1828	28	-1%
COR1702e.5.06	10.99	0.18	0.4864	0.0066	0.1631	0.0027	2555	29	2487	28	-3%
COR1702e.5.07	1.59	0.18	0.109	0.013	0.1059	0.0018	667	76	1729	31	61%
COR1702e.5.08	4.5	0.13	0.3075	0.0057	0.1068	0.003	1728	28	1745	52	1%
COR1702e.5.09	6.12	0.14	0.3588	0.0073	0.1235	0.002	1976	35	2007	29	2%
COR1702e.5.10	5.046	0.069	0.3331	0.0054	0.11	0.0014	1853	26	1799	23	-3%
COR1702e.5.11	9.74	0.25	0.4503	0.0085	0.1578	0.0038	2397	38	2431	41	1%
COR1702e.5.12	4.14	0.14	0.2509	0.007	0.1188	0.0021	1443	36	1937	32	26%
COR1702e.5.13	6.12	0.15	0.3699	0.0086	0.1204	0.0021	2029	40	1961	31	-3%
COR1702e.5.14	3.655	0.095	0.2323	0.007	0.1144	0.0021	1347	37	1870	33	28%
COR1702e.5.15	0.721	0.048	0.0467	0.0023	0.1111	0.0032	294	14	1817	52	84%
COR1702e.5.16	1.352	0.057	0.0859	0.0037	0.1142	0.0035	531	22	1866	55	72%
COR1702e.5.17	5.19	0.15	0.333	0.01	0.1134	0.0016	1853	48	1854	26	0%
COR1702e.5.18	4.56	0.1	0.29	0.0047	0.1138	0.0018	1642	24	1860	29	12%
COR1702e.5.19	4.524	0.084	0.2903	0.0057	0.1132	0.0014	1643	28	1851	23	11%
COR1702e.5.20	2.014	0.082	0.1297	0.0051	0.1122	0.002	786	29	1835	32	57%
COR1702e.5.21	4.71	0.12	0.3185	0.0056	0.1073	0.0025	1782	27	1753	43	-2%
COR1702e.5.22	22.39	0.28	0.6388	0.0081	0.2552	0.0039	3184	32	3217	24	1%

COR1702e.5.23	2.179	0.065	0.1357	0.0044	0.1162	0.0028	820	25	1898	43	57%
COR1702e.5.24	13.08	0.33	0.5211	0.0097	0.1821	0.0027	2704	41	2671	25	-1%
COR1702e.5.25	3.92	0.12	0.2561	0.006	0.1102	0.0017	1470	31	1802	28	18%
COR1702e.5.26	4.39	0.18	0.293	0.012	0.109	0.003	1657	60	1782	50	7%
COR1702e.5.27	4.39	0.12	0.2852	0.0058	0.1109	0.002	1617	29	1813	33	11%
COR1702e.5.28	6.02	0.14	0.3577	0.0078	0.1222	0.0016	1971	37	1988	23	1%
COR1702e.5.29	1.921	0.047	0.1278	0.0031	0.1088	0.0016	775	18	1779	27	56%
COR1702e.5.30	3.847	0.09	0.2558	0.0051	0.1085	0.0028	1468	26	1774	47	17%
COR1702e.5.31	5.1	0.12	0.3305	0.0042	0.1123	0.0029	1841	20	1836	47	0%
COR1702e.5.32	3.89	0.15	0.2577	0.0078	0.1097	0.0022	1478	40	1794	37	18%
COR1702e.5.33	4.69	0.11	0.317	0.0056	0.1075	0.0021	1775	27	1757	36	-1%
COR1702e.5.34	5.45	0.11	0.3467	0.006	0.1138	0.0018	1919	29	1860	29	-3%
COR1702e.5.35	3.45	0.25	0.223	0.013	0.1117	0.005	1298	69	1826	81	29%
COR1702e.5.36	5.08	0.14	0.3263	0.0077	0.1124	0.0031	1820	37	1838	50	1%
COR1702e.5.37	2.89	0.15	0.2011	0.0089	0.1045	0.002	1181	48	1705	35	31%
COR1702e.5.38	1.523	0.027	0.1092	0.0019	0.101	0.0015	668	11	1642	28	59%
COR1702e.5.39	0.662	0.018	0.03609	0.0008	0.1327	0.0027	228.6	5	2133	36	89%
COR1702e.5.40	1.72	0.25	0.114	0.016	0.1093	0.004	696	93	1787	67	61%
COR1702e.5.41	10.09	0.34	0.438	0.013	0.1662	0.0027	2342	58	2519	27	7%
COR1702e.5.42	5.344	0.091	0.3407	0.0041	0.1137	0.0015	1890	20	1859	24	-2%
COR1702e.5.43	4.97	0.11	0.3208	0.0055	0.1117	0.0028	1794	27	1826	46	2%
COR1702e.5.44	5.164	0.098	0.3305	0.0057	0.1141	0.0021	1841	28	1865	33	1%
COR1702e.5.45	4.6	0.11	0.3178	0.0062	0.1054	0.0021	1779	30	1720	37	-3%
COR1702e.5.46	4.4	0.16	0.2754	0.009	0.1151	0.0028	1568	45	1881	44	17%
COR1702e.5.47	4.379	0.098	0.2893	0.0068	0.1093	0.0022	1638	34	1787	37	8%

COR1702e.5.48	4.76	0.12	0.3041	0.0052	0.1132	0.0018	1712	26	1851	29	8%
COR1702e.5.49	1.955	0.049	0.1269	0.0023	0.111	0.0022	770	13	1815	36	58%
COR1702e.5.50	4.782	0.099	0.32	0.0042	0.1083	0.0017	1790	21	1770	29	-1%
COR1702e.5.51	3.57	0.11	0.2313	0.0073	0.1116	0.0019	1341	38	1825	31	27%
COR1702e.5.52	2.953	0.096	0.1973	0.007	0.1087	0.0029	1161	38	1777	49	35%
COR1702e.5.53	4.95	0.11	0.3178	0.0047	0.1133	0.0032	1779	23	1852	51	4%
COR1702e.5.54	5.332	0.08	0.3397	0.005	0.1136	0.0012	1885	24	1857	19	-2%
COR1702e.5.55	4.053	0.085	0.2776	0.005	0.1056	0.0013	1579	25	1724	23	8%
COR1702e.5.56	10.94	0.24	0.4811	0.0096	0.1649	0.001	2532	42	2506	11	-1%
COR1702e.5.57	3.146	0.083	0.2052	0.003	0.1108	0.003	1203	16	1812	49	34%
COR1702e.5.58	4.88	0.14	0.3074	0.0064	0.1144	0.0023	1728	32	1870	36	8%
COR1702e.5.59	4.653	0.098	0.3139	0.0041	0.1073	0.0021	1760	20	1753	36	0%
COR1702e.5.60	4.81	0.2	0.3086	0.0059	0.1122	0.0037	1734	29	1835	60	6%
COR1702e.5.61	4.22	0.1	0.2759	0.0061	0.1108	0.0017	1571	31	1812	28	13%
COR1702e.5.62	4.89	0.11	0.3221	0.0046	0.1094	0.0018	1800	22	1789	30	-1%
COR1702e.5.63	1.58	0.058	0.0995	0.0031	0.1148	0.0022	611	18	1876	35	67%
COR1702e.5.64	2.179	0.077	0.1448	0.0043	0.1093	0.002	872	24	1787	33	51%
COR1702e.5.65	6.01	0.21	0.311	0.0092	0.1396	0.0028	1746	45	2221	35	21%
COR1702e.5.66	4.84	0.11	0.3147	0.0056	0.1112	0.0018	1764	27	1818	30	3%
COR1702e.5.67	5.44	0.2	0.3403	0.0071	0.1154	0.004	1888	34	1885	62	0%
COR1702e.5.68	5.52	0.27	0.249	0.014	0.1615	0.0043	1433	72	2471	45	42%
COR1702e.5.69	0.768	0.03	0.0504	0.0023	0.1109	0.0023	317	14	1813	38	83%
COR1702e.5.70	4.21	0.11	0.2751	0.0052	0.1103	0.0028	1567	26	1804	46	13%
COR1702e.5.71	3.28	0.2	0.2151	0.0064	0.1099	0.0047	1256	34	1797	78	30%
COR1702e.5.72	2.142	0.062	0.1436	0.003	0.1081	0.0035	865	17	1767	59	51%

COR1702e.5.73	4.84	0.11	0.3243	0.0063	0.1087	0.0017	1811	31	1777	29	-2%
COR1702e.5.74	1.208	0.031	0.0713	0.0016	0.1224	0.0032	444	9.6	1991	47	78%
COR1702e.5.75	5.332	0.093	0.3389	0.0057	0.1142	0.0017	1881	27	1866	27	-1%
COR1702e.5.76	1.446	0.047	0.0917	0.0023	0.1144	0.0034	566	14	1870	54	70%
COR1702e.5.77	4.45	0.11	0.2849	0.0065	0.1133	0.0017	1616	33	1852	27	13%
COR1702e.5.78	5.01	0.12	0.3275	0.0043	0.1111	0.0026	1826	21	1817	43	0%
COR1702e.5.79	5.33	0.097	0.3424	0.0041	0.1131	0.0016	1898	20	1849	26	-3%
COR1702e.5.80	5.31	0.24	0.3183	0.0093	0.1204	0.0048	1781	45	1961	71	9%
COR1702e.5.81	5.9	0.28	0.354	0.012	0.1206	0.0026	1954	57	1964	39	1%
COR1702e.5.82	4.89	0.14	0.3285	0.0064	0.1074	0.0032	1831	31	1755	55	-4%
COR1702e.5.83	5.3	0.092	0.3436	0.0052	0.1118	0.0014	1904	25	1828	23	-4%
COR1702e.5.84	5.512	0.097	0.3545	0.0054	0.1128	0.0013	1956	26	1844	21	-6%
COR1702e.5.85	4.71	0.1	0.3158	0.0044	0.1083	0.0022	1769	22	1770	37	0%
COR1702e.5.86	0.93	0.029	0.051	0.0013	0.133	0.0044	320.7	8	2137	58	85%
COR1702e.5.87	8.26	0.19	0.3615	0.0089	0.1668	0.0022	1989	42	2525	22	21%
COR1702e.5.88	4.69	0.14	0.3046	0.0052	0.1115	0.0027	1714	26	1823	44	6%
COR1702e.5.89	1.385	0.047	0.0936	0.003	0.107	0.0024	577	18	1748	41	67%
COR1702e.5.90	3.74	0.097	0.2439	0.0063	0.1108	0.0019	1407	33	1812	31	22%
COR1702e.5.91	5.88	0.17	0.354	0.012	0.1207	0.0021	1954	57	1966	31	1%
COR1702e.5.92	2.77	0.17	0.1871	0.0098	0.1069	0.0037	1106	53	1746	63	37%
COR1702e.5.93	4.68	0.12	0.3126	0.005	0.1085	0.0028	1753	25	1774	47	1%
COR1702e.5.94	3.82	0.12	0.262	0.007	0.1057	0.0022	1500	36	1726	38	13%
COR1702e.5.95	5.4	0.091	0.3442	0.0045	0.1138	0.0015	1907	22	1860	24	-3%
COR1702e.5.96	5.101	0.082	0.3326	0.005	0.1111	0.0013	1851	24	1817	21	-2%
COR1702e.5.97	4.887	0.091	0.3257	0.0055	0.1088	0.002	1818	27	1779	34	-2%

COR1702e.5.98	4.07	0.13	0.2637	0.01	0.1123	0.0029	1509	51	1836	47	18%
COR1702e.5.99	3.98	0.13	0.2577	0.0084	0.1121	0.0011	1478	43	1833	18	19%
COR1702e.5.100	6.09	0.14	0.3619	0.0057	0.1218	0.0022	1991	27	1982	32	0%
COR1702e.5.101	3.857	0.089	0.2475	0.0056	0.1132	0.0014	1426	29	1851	23	23%
COR1702e.5.102	5.13	0.11	0.3306	0.0049	0.1124	0.0018	1841	24	1838	29	0%
COR1702e.5.103	4.947	0.079	0.3337	0.0036	0.1073	0.0016	1856	17	1753	27	-6%
COR1702e.5.104	4.009	0.096	0.2676	0.0053	0.1081	0.0017	1529	27	1767	29	13%
COR1702e.5.105	5	0.13	0.3254	0.0062	0.1112	0.0022	1816	30	1818	36	0%
COR1702e.5.106	4.932	0.077	0.3017	0.0042	0.1184	0.0016	1700	21	1931	24	12%
COR1702e.5.107	5.003	0.087	0.3292	0.0066	0.1102	0.0013	1835	32	1802	22	-2%
COR1702e.5.108	4.76	0.11	0.3173	0.0063	0.1088	0.0015	1777	31	1779	25	0%
COR1702e.5.109	5.412	0.086	0.3395	0.009	0.1164	0.0023	1884	43	1901	36	1%
COR1702e.5.110	5.5	0.12	0.3433	0.0046	0.116	0.0024	1903	22	1895	37	0%
COR1702e.5.111	4.92	0.14	0.2993	0.0072	0.1194	0.0038	1688	36	1946	57	13%
COR1702e.5.112	4.45	0.14	0.2958	0.0068	0.1087	0.0025	1670	34	1777	42	6%
COR1702e.5.113	4.24	0.12	0.2799	0.0066	0.11	0.0026	1591	33	1799	43	12%
COR1702e.5.114	4.966	0.068	0.3272	0.0044	0.11	0.0013	1825	21	1799	22	-1%
COR1702e.5.115	5.09	0.12	0.3293	0.0076	0.112	0.0015	1835	37	1831	24	0%
COR1702e.5.116	5.432	0.082	0.3525	0.0044	0.1116	0.0011	1947	21	1825	18	-7%
COR1702e.5.117	10.04	0.2	0.4582	0.0089	0.1597	0.0017	2432	39	2452	18	1%
COR1702e.5.118	4.89	0.13	0.3226	0.0077	0.1099	0.0024	1802	38	1797	40	0%
COR1702e.5.119	1.234	0.046	0.0906	0.0035	0.0987	0.0011	559	21	1599	21	65%
COR1702e.5.120	4.71	0.1	0.3139	0.0065	0.1095	0.0016	1760	32	1790	27	2%
COR1702e.5.121	8.41	0.1	0.4012	0.0058	0.1526	0.0019	2175	27	2374	21	8%
COR1702e.5.122	4.16	0.13	0.2745	0.0099	0.1105	0.0023	1564	50	1807	38	13%

COR1702e.5.123	4.84	0.22	0.3031	0.0091	0.1153	0.0033	1707	45	1884	52	9%
COR1702e.5.124	11.29	0.34	0.483	0.012	0.1692	0.0032	2540	52	2549	32	0%
COR1702e.5.125	4.99	0.19	0.324	0.012	0.1113	0.0015	1809	58	1820	25	1%
COR1702e.5.126	5.395	0.067	0.3414	0.0042	0.114	0.0017	1893	20	1863	27	-2%
COR1702e.5.127	10.98	0.27	0.479	0.012	0.166	0.0015	2523	52	2517	16	0%
COR1702e.5.128	1.041	0.024	0.068	0.002	0.1118	0.0036	424	12	1828	58	77%
COR1702e.5.129	4.23	0.19	0.2765	0.0076	0.1118	0.0037	1574	38	1828	60	14%
COR1702e.5.130	4.58	0.12	0.3054	0.0038	0.1089	0.0029	1718	19	1780	49	3%
COR1702e.5.131	5.23	0.12	0.335	0.0051	0.1134	0.0023	1863	25	1854	37	0%

Sample: COR1701a

Grain ID	*207Pb/232Th*	*207Pb/232Th prop2SE*	*206Pb/238U*	*206Pb/238U prop2SE*	*207Pb/206Pb*	*207Pb/206Pb prop2SE*	*206Pb/238Pb Age (Ma)*	*± 1σ(Ma)*	*207Pb/206Pb Age (Ma)*	*± 1σ (Ma)*	*Disc (%)*
COR1701a.3.01	4.86	0.19	0.3126	0.0084	0.1118	0.005	1753	41	1828	81	4%
COR1701a.3.02	3.53	0.16	0.225	0.017	0.1131	0.0047	1308	89	1849	75	29%
COR1701a.3.03	5.33	0.23	0.3358	0.009	0.1142	0.0059	1866	43	1866	93	0%
COR1701a.3.04	4.3	0.12	0.2725	0.0067	0.1134	0.0033	1553	34	1854	53	16%
COR1701a.3.05	2.517	0.081	0.1519	0.0057	0.1192	0.0031	912	32	1943	47	53%
COR1701a.3.06	2.84	0.13	0.178	0.0073	0.1145	0.0034	1056	40	1871	54	44%
COR1701a.3.07	5.961	0.12	0.3583	0.0078	0.1196	0.0026	1974	37	1949	39	-1%
COR1701a.3.08	2.75	0.12	0.1826	0.0075	0.1072	0.0028	1081	41	1752	48	38%
COR1701a.3.09	4.26	0.16	0.2732	0.011	0.1121	0.0035	1557	56	1833	57	15%
COR1701a.3.10	5.67	0.16	0.337	0.0083	0.1211	0.0031	1872	40	1972	46	5%
COR1701a.3.11	1.648	0.05	0.0729	0.002	0.1626	0.0044	454	12	2482	46	82%
COR1701a.3.12	2.428	0.18	0.1482	0.012	0.1176	0.0029	891	67	1919	44	54%

COR1701a.3.13	2.099	0.095	0.1232	0.0062	0.1227	0.0029	749	36	1995	42	62%
COR1701a.3.14	5.322	0.13	0.3283	0.0071	0.1147	0.0029	1830	34	1874	46	2%
COR1701a.3.15	2.98	0.15	0.1893	0.0099	0.1125	0.0032	1118	54	1839	52	39%
COR1701a.3.16	1.656	0.049	0.0974	0.0026	0.1222	0.0031	599	15	1988	45	70%
COR1701a.3.17	1.37	0.086	0.0778	0.005	0.1274	0.003	483	30	2062	42	77%
COR1701a.3.18	4.671	0.12	0.3127	0.0074	0.1076	0.0027	1754	36	1758	46	0%
COR1701a.3.19	4.75	0.13	0.3048	0.0073	0.1123	0.003	1715	36	1836	48	7%
COR1701a.3.20	8.63	0.22	0.3747	0.0088	0.1658	0.004	2051	41	2515	41	18%
COR1701a.3.21	5.16	0.26	0.286	0.011	0.1295	0.0047	1622	55	2090	64	22%
COR1701a.3.22	4.45	0.14	0.287	0.0081	0.1118	0.0033	1627	41	1828	54	11%
COR1701a.3.23	11.75	0.22	0.4632	0.01	0.1826	0.0043	2454	44	2676	39	8%
COR1701a.3.24	4.91	0.13	0.3123	0.0085	0.1132	0.0034	1752	42	1851	54	5%
COR1701a.3.25	6	0.16	0.3582	0.0095	0.1207	0.0027	1974	45	1966	40	0%
COR1701a.3.26	5.44	0.18	0.3391	0.0088	0.1155	0.0038	1882	42	1887	59	0%
COR1701a.3.27	3.77	0.13	0.2403	0.012	0.113	0.0048	1388	62	1847	77	25%
COR1701a.3.28	2.329	0.074	0.1352	0.0051	0.1241	0.0034	817	29	2015	49	59%
COR1701a.3.29	14.62	0.83	0.346	0.018	0.3009	0.0065	1915	86	3474	34	45%
COR1701a.3.30	2.415	0.075	0.1174	0.0035	0.1482	0.004	716	20	2324	46	69%
COR1701a.3.31	2.5	0.16	0.1221	0.0048	0.1457	0.0061	743	28	2295	72	68%
COR1701a.3.32	3.94	0.12	0.2443	0.0079	0.1161	0.003	1409	41	1896	47	26%
COR1701a.3.33	1.719	0.064	0.0807	0.0039	0.1535	0.0043	500	23	2385	48	79%
COR1701a.3.34	5.59	0.16	0.3458	0.0085	0.1163	0.0031	1915	41	1899	48	-1%
COR1701a.3.35	5.466	0.11	0.3415	0.0074	0.1152	0.0026	1894	36	1882	41	-1%
COR1701a.3.36	4.5	0.23	0.263	0.013	0.1232	0.0038	1505	66	2002	55	25%
COR1701a.3.37	1.476	0.09	0.0876	0.0053	0.1215	0.0033	541	31	1978	48	73%

COR1701a.3.38	7.75	0.24	0.3341	0.011	0.1673	0.0038	1858	53	2530	38	27%
COR1701a.3.39	4.88	0.12	0.3213	0.0069	0.1095	0.0026	1796	34	1790	43	0%
COR1701a.3.40	5.381	0.13	0.3233	0.0096	0.1198	0.0036	1806	47	1952	54	7%
COR1701a.3.41	3.11	0.21	0.178	0.012	0.1256	0.0031	1056	66	2036	44	48%
COR1701a.3.42	1.437	0.052	0.0621	0.003	0.1675	0.005	388	18	2532	50	85%
COR1701a.3.43	5.56	0.16	0.345	0.0078	0.1155	0.0035	1911	37	1887	55	-1%
COR1701a.3.44	4.28	0.12	0.2728	0.0087	0.1148	0.0036	1555	44	1876	57	17%
COR1701a.3.45	5.25	0.15	0.3347	0.0087	0.113	0.0028	1861	42	1847	45	-1%
COR1701a.3.46	1.784	0.043	0.0869	0.0021	0.1479	0.0039	537	12	2321	45	77%
COR1701a.3.47	3.35	0.12	0.202	0.0055	0.1195	0.0034	1186	30	1948	51	39%
COR1701a.3.48	3.817	0.11	0.2302	0.0061	0.1195	0.0029	1336	32	1948	43	31%
COR1701a.3.49	2.324	0.08	0.1364	0.0047	0.1231	0.0037	824	27	2001	53	59%
COR1701a.3.50	5.05	0.15	0.326	0.0088	0.1118	0.0028	1819	43	1828	46	0%
COR1701a.3.51	1.093	0.036	0.0604	0.0022	0.1307	0.0038	378	13	2107	51	82%
COR1701a.3.52	1.49	0.074	0.0817	0.0044	0.1318	0.0034	506	26	2121	45	76%
COR1701a.3.53	3.32	0.13	0.2097	0.0076	0.1144	0.003	1227	41	1870	47	34%
COR1701a.3.54	2.685	0.076	0.1578	0.0042	0.1226	0.0029	945	23	1994	42	53%
COR1701a.3.55	5.3	0.14	0.3338	0.008	0.1145	0.0036	1857	39	1871	57	1%
COR1701a.3.56	4.82	0.18	0.2717	0.011	0.1269	0.0062	1549	56	2055	86	25%
COR1701a.3.57	3.88	0.13	0.2294	0.0063	0.1221	0.0038	1331	33	1986	55	33%
COR1701a.3.58	4.96	0.17	0.3228	0.0075	0.1108	0.004	1803	37	1812	66	0%
COR1701a.3.59	3.63	0.13	0.2164	0.0064	0.1211	0.0032	1263	34	1972	47	36%
COR1701a.3.60	11.29	0.26	0.4853	0.011	0.168	0.0037	2550	48	2537	37	-1%
COR1701a.3.61	4.79	0.24	0.315	0.012	0.11	0.0037	1765	59	1799	61	2%
COR1701a.3.62	1.89	0.07	0.0833	0.0031	0.1639	0.0038	516	18	2496	39	79%

COR1701a.3.63	2.91	0.26	0.182	0.018	0.1167	0.0033	1078	98	1905	51	43%
COR1701a.3.64	1.792	0.077	0.1051	0.0044	0.1231	0.0035	644	26	2001	51	68%
COR1701a.3.65	2.79	0.11	0.1625	0.0068	0.124	0.003	971	38	2014	43	52%
COR1701a.3.66	4.46	0.15	0.2909	0.008	0.1107	0.0036	1646	40	1810	59	9%
COR1701a.3.67	4.6	0.16	0.2962	0.007	0.1123	0.0037	1672	35	1836	60	9%
COR1701a.3.68	1.384	0.056	0.0776	0.0024	0.1288	0.0041	482	14	2081	56	77%
COR1701a.3.69	4.83	0.22	0.279	0.013	0.125	0.0027	1586	66	2028	38	22%
COR1701a.3.70	4.958	0.11	0.3249	0.0076	0.1103	0.0026	1814	37	1804	43	-1%
COR1701a.3.71	5.68	0.14	0.3474	0.0077	0.1182	0.003	1922	37	1928	46	0%
COR1701a.3.72	2.07	0.12	0.1203	0.0068	0.1247	0.0034	732	39	2024	48	64%
COR1701a.3.73	4.8	0.13	0.319	0.0073	0.1089	0.0029	1785	36	1780	49	0%
COR1701a.3.74	5.606	0.13	0.3446	0.0079	0.1176	0.0029	1909	38	1919	44	1%
COR1701a.3.75	1.461	0.053	0.0834	0.0031	0.1268	0.0031	516	18	2053	43	75%
COR1701a.3.76	1.237	0.049	0.0747	0.0031	0.1198	0.0028	464	19	1952	42	76%
COR1701a.3.77	1.92	0.16	0.1116	0.0098	0.1249	0.0036	682	57	2027	51	66%
COR1701a.3.78	1.16	0.054	0.0646	0.0026	0.1299	0.0037	404	16	2096	50	81%

Sample: COR1701b

Grain ID	*207Pb/232Th*	*207Pb/232Th prop2SE*	*206Pb/238U*	*206Pb/238U prop2SE*	*207Pb/206Pb*	*207Pb/206Pb prop2SE*	*206Pb/238Pb Age (Ma)*	*± 1σ(Ma)*	*207Pb/206Pb Age (Ma)*	*± 1σ (Ma)*	*Disc (%)*
COR1701b.4.01	5.4	0.17	0.3387	0.013	0.1141	0.0019	1880	63	1865	30	-1%
COR1701b.4.02	4.84	0.18	0.2956	0.012	0.1166	0.003	1669	60	1904	46	12%
COR1701b.4.03	5.84	0.19	0.3419	0.013	0.1218	0.0023	1896	62	1982	34	4%
COR1701b.4.04	2.686	0.081	0.1327	0.0053	0.1439	0.0023	803	30	2274	28	65%
COR1701b.4.05	5.36	0.21	0.3359	0.014	0.1134	0.0029	1867	68	1854	46	-1%

COR1701b.4.06	2.302	0.1	0.1366	0.0062	0.1198	0.0027	825	35	1952	40	58%
COR1701b.4.07	4.91	0.17	0.3229	0.013	0.1086	0.0028	1804	63	1775	47	-2%
COR1701b.4.08	4.93	0.16	0.3158	0.012	0.1112	0.002	1769	59	1818	33	3%
COR1701b.4.09	2.127	0.08	0.13	0.0054	0.1168	0.0028	788	31	1907	43	59%
COR1701b.4.10	4.858	0.14	0.3183	0.012	0.1087	0.0017	1781	59	1777	29	0%
COR1701b.4.11	16.97	0.69	0.574	0.025	0.211	0.0046	2920	100	2913	35	0%
COR1701b.4.12	10.3	0.31	0.4453	0.017	0.1648	0.0022	2374	76	2505	23	5%
COR1701b.4.13	3.87	0.16	0.231	0.012	0.114	0.0019	1340	63	1863	30	28%
COR1701b.4.14	2.442	0.11	0.14	0.0076	0.1165	0.0031	845	43	1902	48	56%
COR1701b.4.15	2.887	0.099	0.1683	0.0068	0.122	0.0024	1003	38	1985	35	49%
COR1701b.4.16	3.93	0.17	0.2476	0.013	0.1134	0.002	1426	67	1854	32	23%
COR1701b.4.17	4.5	0.2	0.28	0.014	0.1149	0.0014	1591	71	1878	22	15%
COR1701b.4.18	5.474	0.15	0.3404	0.013	0.1146	0.0022	1889	63	1873	35	-1%
COR1701b.4.19	4.67	0.26	0.3062	0.014	0.1088	0.0046	1722	69	1779	77	3%
COR1701b.4.20	4.61	0.22	0.2814	0.012	0.1168	0.0033	1598	60	1907	51	16%
COR1701b.4.21	2.99	0.15	0.1738	0.0078	0.1158	0.003	1033	43	1892	47	45%
COR1701b.4.22	3.878	0.12	0.2307	0.0094	0.1203	0.0022	1338	49	1960	33	32%
COR1701b.4.23	1.957	0.064	0.1158	0.0048	0.1208	0.0023	706	28	1967	34	64%
COR1701b.4.24	8.87	0.27	0.3212	0.013	0.1721	0.0023	1796	63	2577	23	30%
COR1701b.4.25	11.58	0.45	0.483	0.021	0.1712	0.0028	2540	91	2569	28	1%
COR1701b.4.26	5.53	0.17	0.3367	0.013	0.1176	0.0016	1871	63	1919	25	3%
COR1701b.4.27	2.99	0.13	0.1872	0.01	0.1148	0.0024	1106	54	1876	38	41%
COR1701b.4.28	4.11	0.17	0.2623	0.012	0.1126	0.0034	1502	61	1841	55	18%
COR1701b.4.29	5.39	0.26	0.227	0.014	0.1711	0.0027	1319	74	2568	27	49%
COR1701b.4.30	5.9	0.29	0.3587	0.014	0.118	0.0038	1976	66	1925	58	-3%

COR1701b.4.31	4.98	0.17	0.3191	0.013	0.1124	0.0032	1785	64	1838	52	3%
COR1701b.4.32	4.74	0.18	0.2952	0.012	0.1156	0.0034	1667	60	1888	53	12%
COR1701b.4.33	2.341	0.088	0.1388	0.0062	0.1216	0.0026	838	35	1979	38	58%
COR1701b.4.34	1.904	0.078	0.109	0.0052	0.1259	0.0025	667	30	2041	35	67%
COR1701b.4.35	3.275	0.1	0.214	0.0087	0.1103	0.0018	1250	46	1804	30	31%
COR1701b.4.36	4.27	0.15	0.2688	0.012	0.1145	0.0024	1535	61	1871	38	18%
COR1701b.4.37	0.841	0.032	0.1012	0.004	0.0601	0.0017	621	23	606	61	-2%
COR1701b.4.38	5.84	0.19	0.3534	0.014	0.1198	0.0024	1951	67	1952	36	0%
COR1701b.4.39	7.4	0.23	0.3312	0.013	0.162	0.0023	1844	63	2476	24	26%
COR1701b.4.40	4.85	0.16	0.3178	0.013	0.1106	0.0024	1779	64	1808	40	2%
COR1701b.4.41	1.857	0.063	0.1118	0.0046	0.1205	0.0025	683	27	1963	37	65%
COR1701b.4.42	2.59	0.075	0.1378	0.0062	0.1363	0.0023	832	35	2180	30	62%
COR1701b.4.43	4.226	0.12	0.1905	0.0075	0.1623	0.0018	1124	41	2479	19	55%
COR1701b.4.44	4.83	0.16	0.326	0.013	0.108	0.0021	1819	63	1765	36	-3%
COR1701b.4.45	2.66	0.094	0.1648	0.0069	0.1176	0.0021	983	38	1919	32	49%
COR1701b.4.46	3.12	0.13	0.1953	0.0089	0.1158	0.0027	1150	48	1892	42	39%
COR1701b.4.47	1.43	0.28	0.067	0.013	0.1555	0.0018	418	79	2407	20	83%
COR1701b.4.48	4.18	0.16	0.2781	0.012	0.11	0.0031	1582	61	1799	51	12%
COR1701b.4.49	5.21	0.17	0.3378	0.013	0.1126	0.0027	1876	63	1841	44	-2%
COR1701b.4.50	6.17	0.32	0.366	0.017	0.1226	0.0037	2011	80	1994	54	-1%
COR1701b.4.51	20.95	0.63	0.5527	0.022	0.2771	0.0035	2836	91	3346	20	15%
COR1701b.4.52	6.19	0.37	0.3123	0.014	0.1451	0.0063	1752	69	2288	75	23%
COR1701b.4.53	2.6	0.12	0.1495	0.007	0.1274	0.0029	898	39	2062	40	56%
COR1701b.4.54	2.852	0.1	0.1836	0.0079	0.1138	0.0019	1087	43	1860	30	42%
COR1701b.4.55	4.749	0.13	0.3169	0.012	0.11	0.0014	1775	59	1799	23	1%

COR1701b.4.56	2.726	0.11	0.1564	0.0067	0.1275	0.0039	937	37	2063	54	55%
COR1701b.4.57	2.206	0.086	0.133	0.0061	0.1211	0.0018	805	35	1972	27	59%
COR1701b.4.58	1.481	0.078	0.0819	0.0049	0.1323	0.0025	507	29	2128	33	76%
COR1701b.4.59	2.48	0.074	0.1613	0.0067	0.1126	0.0026	964	37	1841	42	48%
COR1701b.4.60	4.51	0.16	0.3062	0.012	0.1081	0.0022	1722	59	1767	37	3%
COR1701b.4.61	5.19	0.2	0.333	0.014	0.1152	0.0026	1853	68	1882	41	2%
COR1701b.4.62	3.53	0.19	0.2386	0.012	0.1085	0.0022	1379	62	1774	37	22%
COR1701b.4.63	7.9	0.39	0.331	0.018	0.1665	0.0027	1843	87	2522	27	27%
COR1701b.4.64	5.82	0.18	0.3658	0.014	0.1165	0.0019	2010	66	1902	29	-6%

Sample: MQ01

Grain ID	*207Pb/232Th*	*207Pb/232Th prop2SE*	*206Pb/238U*	*206Pb/238U prop2SE*	*207Pb/206Pb*	*207Pb/206Pb prop2SE*	*206Pb/238Pb Age (Ma)*	*± 1σ(Ma)*	*207Pb/206Pb Age (Ma)*	*± 1σ (Ma)*	*Disc (%)*
MQ01.1.01	4.04	0.45	0.225	0.027	0.1332	0.0025	1310	140	2140	33	39%
MQ01.1.02	6.03	0.13	0.3483	0.0068	0.1269	0.0021	1926	33	2055	29	6%
MQ01.1.03	11.44	0.22	0.4792	0.0063	0.1738	0.0027	2524	27	2594	26	3%
MQ01.1.04	3.46	0.13	0.1348	0.0052	0.1865	0.0025	815	30	2711	22	70%
MQ01.1.05	5.99	0.12	0.3563	0.0049	0.1224	0.0022	1965	23	1991	32	1%
MQ01.1.06	5.29	0.14	0.3288	0.0087	0.1164	0.0035	1833	42	1901	54	4%
MQ01.1.07	8.39	0.18	0.3458	0.0053	0.1762	0.0028	1915	25	2617	27	27%
MQ01.1.08	2.36	0.28	0.13	0.019	0.1412	0.0078	790	110	2241	96	65%
MQ01.1.09	2.199	0.078	0.1182	0.0051	0.1326	0.0027	720	29	2132	36	66%
MQ01.1.10	3.69	0.25	0.159	0.011	0.1683	0.0026	951	61	2540	26	63%
MQ01.1.11	4.77	0.12	0.1997	0.0049	0.1698	0.0022	1174	26	2555	22	54%
MQ01.1.12	5.96	0.12	0.3533	0.0068	0.12319	0.0014	1950	32	2002	20	3%

MQ01.1.13	2.87	0.1	0.0902	0.0033	0.2295	0.0034	557	20	3048	24	82%
MQ01.1.14	2.102	0.037	0.06323	0.00081	0.2406	0.0032	395.2	4.9	3123	21	87%
MQ01.1.15	4.64	0.31	0.231	0.015	0.1455	0.0036	1340	79	2293	43	42%
MQ01.1.16	5.42	0.11	0.3293	0.0053	0.1195	0.0019	1835	26	1948	29	6%
MQ01.1.17	5.51	0.14	0.3413	0.0061	0.1175	0.0022	1893	29	1918	34	1%
MQ01.1.18	9.38	0.17	0.399	0.0075	0.1704	0.0022	2164	35	2561	22	16%
MQ01.1.19	5.93	0.4	0.239	0.017	0.1793	0.0018	1381	88	2646	17	48%
MQ01.1.20	4.126	0.084	0.1608	0.0032	0.1858	0.0021	961	18	2705	19	64%
MQ01.1.21	8.59	0.27	0.3469	0.0086	0.1785	0.0029	1920	41	2638	27	27%
MQ01.1.22	1.724	0.044	0.0672	0.0015	0.1856	0.0024	419.3	9.1	2703	22	84%
MQ01.1.23	2.268	0.066	0.1044	0.0032	0.1568	0.0037	640	19	2421	40	74%
MQ01.1.24	5.1	0.13	0.3178	0.0077	0.1165	0.0019	1779	38	1902	29	6%
MQ01.1.25	5.526	0.11	0.3458	0.0053	0.1149	0.0024	1915	25	1878	38	-2%
MQ01.1.26	5.53	0.12	0.3448	0.0071	0.116	0.0014	1910	34	1895	22	-1%
MQ01.1.27	5.25	0.17	0.3045	0.0049	0.124	0.0034	1714	24	2014	49	15%
MQ01.1.28	5.87	0.11	0.3486	0.0049	0.1215	0.0022	1928	23	1978	32	3%
MQ01.1.29	5.22	0.12	0.3286	0.0045	0.1149	0.0028	1832	22	1878	44	2%
MQ01.1.30	5.306	0.11	0.3348	0.0044	0.1142	0.0021	1862	21	1866	33	0%
MQ01.1.31	5.922	0.1	0.3551	0.0051	0.1206	0.0016	1959	24	1964	24	0%
MQ01.1.32	5.93	0.11	0.347	0.0069	0.124	0.0022	1920	33	2014	32	5%
MQ01.1.33	8.33	0.18	0.3961	0.006	0.1527	0.0027	2151	28	2376	30	9%
MQ01.1.34	2.333	0.066	0.1117	0.0049	0.1525	0.0028	683	28	2373	31	71%
MQ01.1.35	3.099	0.082	0.1791	0.0051	0.1252	0.0019	1062	28	2031	27	48%
MQ01.1.36	2.484	0.066	0.1353	0.0049	0.1332	0.0028	818	28	2140	37	62%
MQ01.1.37	1.374	0.028	0.0711	0.0012	0.1394	0.0018	442.8	7.2	2219	23	80%

MQ01.1.38	2.87	0.11	0.1197	0.0045	0.1726	0.0037	729	26	2582	36	72%
MQ01.1.39	10.96	0.2	0.4713	0.0053	0.1688	0.0028	2489	23	2545	28	2%
MQ01.1.40	11.09	0.16	0.4824	0.0053	0.1661	0.0021	2538	23	2518	21	-1%
MQ01.1.41	2.62	0.1	0.1552	0.0058	0.1228	0.0031	930	32	1997	45	53%
MQ01.1.42	5.034	0.096	0.3217	0.0044	0.1133	0.002	1798	21	1852	32	3%
MQ01.1.43	2.115	0.037	0.0927	0.0014	0.165	0.0021	571.5	8.3	2507	22	77%
MQ01.1.44	7.08	0.22	0.2752	0.0084	0.1862	0.0022	1567	42	2708	20	42%
MQ01.1.45	1.68	0.084	0.0906	0.0053	0.1353	0.003	559	31	2167	39	74%
MQ01.1.46	5.08	0.21	0.3176	0.009	0.1156	0.0037	1778	44	1888	58	6%
MQ01.1.47	20.68	0.48	0.6264	0.0096	0.2404	0.0043	3135	38	3122	29	0%
MQ01.1.48	2.326	0.063	0.1291	0.0031	0.1297	0.0017	783	18	2093	23	63%
MQ01.1.49	3.08	0.11	0.1804	0.0072	0.124	0.0017	1069	39	2014	24	47%
MQ01.1.50	2.882	0.082	0.1783	0.0045	0.1174	0.0029	1058	25	1916	44	45%
MQ01.1.51	3.31	0.15	0.1868	0.0092	0.1289	0.0017	1104	50	2082	23	47%
MQ01.1.52	6.25	0.14	0.3634	0.0078	0.1252	0.0018	1998	37	2031	26	2%
MQ01.1.53	5.1	0.12	0.3229	0.0045	0.1145	0.0022	1804	22	1871	35	4%
MQ01.1.54	5.591	0.1	0.3548	0.0048	0.1149	0.0018	1957	23	1878	28	-4%
MQ01.1.55	5.183	0.096	0.3291	0.0036	0.1144	0.0018	1834	17	1870	29	2%
MQ01.1.56	1.85	0.12	0.0725	0.0056	0.1841	0.0041	451	34	2689	37	83%
MQ01.1.57	5.172	0.09	0.3346	0.0055	0.1124	0.0014	1861	27	1838	23	-1%
MQ01.1.58	8.61	0.26	0.3783	0.0073	0.1655	0.0029	2068	34	2512	30	18%
MQ01.1.59	12.05	0.18	0.5076	0.006	0.1727	0.0019	2646	26	2583	19	-2%
MQ01.1.60	11.15	0.19	0.4715	0.0058	0.1726	0.0025	2490	25	2582	24	4%
MQ01.1.61	12.95	0.28	0.5197	0.0089	0.1815	0.0031	2698	38	2666	28	-1%
MQ01.1.62	2.767	0.064	0.1483	0.0036	0.1367	0.0021	891	20	2185	27	59%

MQ01.1.63	5.388	0.1	0.3423	0.0049	0.1145	0.0017	1898	24	1871	27	-1%
MQ01.1.64	2.035	0.047	0.1019	0.0016	0.1452	0.0026	625.5	9.4	2289	31	73%
MQ01.1.65	5.83	0.15	0.3276	0.0058	0.129	0.0028	1827	28	2084	38	12%
MQ01.1.66	2.458	0.042	0.1367	0.0022	0.1304	0.0019	826	12	2103	26	61%
MQ01.1.67	10.32	0.23	0.4288	0.007	0.1749	0.0027	2300	32	2604	26	12%
MQ01.1.68	4.04	0.081	0.1734	0.0032	0.1693	0.0026	1031	18	2550	26	60%
MQ01.1.69	2.958	0.088	0.1685	0.0048	0.1278	0.0021	1004	26	2067	29	51%
MQ01.1.70	2.76	0.17	0.154	0.01	0.1305	0.0021	923	56	2104	28	56%
MQ01.1.71	2.936	0.049	0.1494	0.0019	0.1428	0.0018	898	11	2261	22	60%
MQ01.1.72	3.6	0.08	0.2109	0.0039	0.124	0.0021	1234	21	2014	30	39%
MQ01.1.73	5.462	0.096	0.3468	0.0037	0.1146	0.002	1919	18	1873	32	-2%
MQ01.1.74	8.15	0.21	0.372	0.01	0.1593	0.0021	2039	47	2447	23	17%
MQ01.1.75	5.91	0.22	0.2226	0.0077	0.1925	0.0023	1296	41	2763	20	53%
MQ01.1.76	2.457	0.057	0.0951	0.0021	0.1877	0.0028	586	12	2721	25	78%
MQ01.1.77	10.7	0.23	0.4351	0.0076	0.1789	0.0025	2329	34	2642	23	12%
MQ01.1.78	4.108	0.077	0.2397	0.0045	0.1247	0.0016	1385	23	2024	23	32%
MQ01.1.79	2.85	0.072	0.1617	0.0046	0.1282	0.0017	966	26	2073	24	53%
MQ01.1.80	5.17	0.33	0.1865	0.0068	0.199	0.0067	1102	37	2817	55	61%
MQ01.1.81	8.6	0.16	0.3557	0.0066	0.1759	0.0025	1962	31	2614	24	25%
MQ01.1.82	15.11	0.29	0.5523	0.01	0.1996	0.0041	2835	42	2822	34	0%
MQ01.1.83	6.636	0.11	0.3848	0.0041	0.125	0.0022	2099	19	2028	31	-4%
MQ01.1.84	11.36	0.17	0.4806	0.0065	0.1718	0.002	2530	28	2575	20	2%
MQ01.1.85	4.822	0.095	0.296	0.0057	0.1187	0.0024	1671	28	1936	36	14%
MQ01.1.86	3.4	0.26	0.188	0.014	0.1317	0.0035	1111	76	2120	47	48%
MQ01.1.87	4.61	0.13	0.2847	0.009	0.1181	0.0024	1615	45	1927	37	16%

MQ01.1.88	11.54	0.33	0.4814	0.009	0.1733	0.0033	2533	39	2589	32	2%
MQ01.1.89	7.05	0.15	0.3853	0.0061	0.1331	0.0025	2101	28	2138	33	2%
MQ01.1.90	3.601	0.096	0.1459	0.0049	0.1799	0.0048	878	28	2651	44	67%
MQ01.1.91	7.97	0.16	0.3218	0.005	0.1793	0.0031	1799	24	2646	29	32%
MQ01.1.92	16.33	0.56	0.5	0.013	0.2355	0.0046	2614	56	3089	31	15%
MQ01.1.93	5.173	0.085	0.2087	0.0025	0.1791	0.0027	1222	13	2644	25	54%
MQ01.1.94	5.64	0.17	0.227	0.007	0.1759	0.003	1319	37	2614	29	50%
MQ01.1.95	6.23	0.33	0.3638	0.0064	0.1231	0.006	2000	30	2001	87	0%
MQ01.1.96	5.48	0.15	0.3167	0.0064	0.1252	0.0029	1774	31	2031	41	13%
MQ01.1.97	6.155	0.11	0.3541	0.0043	0.1252	0.0021	1954	20	2031	30	4%
MQ01.1.98	12.2	0.24	0.5024	0.0082	0.1756	0.0025	2624	35	2611	24	0%
MQ01.1.99	5.43	0.089	0.3413	0.0035	0.1149	0.0017	1893	17	1878	27	-1%
MQ01.1.100	5.16	0.13	0.3137	0.0061	0.1191	0.0017	1759	30	1942	26	9%
MQ01.1.101	12.17	0.22	0.5004	0.0058	0.1756	0.0026	2616	25	2611	25	0%
MQ01.1.102	5.718	0.11	0.3508	0.0036	0.1176	0.0019	1938	17	1919	29	-1%
MQ01.1.103	3.32	0.12	0.1693	0.0048	0.1411	0.0027	1008	26	2240	33	55%
MQ01.1.104	4.22	0.079	0.2534	0.0048	0.1203	0.002	1456	25	1960	30	26%
MQ01.1.105	5.447	0.1	0.3397	0.0044	0.1157	0.0017	1885	21	1890	27	0%
MQ01.2.01	7	0.45	0.289	0.019	0.176	0.0042	1637	95	2615	40	37%
MQ01.2.02	6.15	0.3	0.249	0.011	0.1783	0.0036	1433	57	2636	34	46%
MQ01.2.03	7.3	0.25	0.3014	0.0072	0.1751	0.004	1698	36	2606	38	35%
MQ01.2.04	8.04	0.71	0.23	0.014	0.249	0.0097	1334	73	3178	62	58%
MQ01.2.05	2.92	0.17	0.101	0.0028	0.2078	0.008	620	16	2888	63	79%
MQ01.2.06	4.05	0.17	0.238	0.012	0.1235	0.0042	1376	62	2007	60	31%

MQ01.2.07	5.12	0.16	0.3176	0.0061	0.1165	0.0025	1778	30	1902	39	7%
MQ01.2.08	5.51	0.23	0.2228	0.008	0.1791	0.0047	1297	42	2644	44	51%
MQ01.2.09	5.405	0.13	0.34	0.0043	0.1151	0.0026	1887	21	1881	41	0%
MQ01.2.10	5.01	0.24	0.306	0.01	0.1189	0.0042	1721	49	1939	63	11%
MQ01.2.11	7.11	0.27	0.3183	0.0073	0.1618	0.005	1781	36	2474	52	28%
MQ01.2.12	6.15	0.2	0.262	0.0053	0.1708	0.0039	1500	27	2565	38	42%
MQ01.2.13	4.29	0.15	0.2796	0.0057	0.1113	0.0033	1589	29	1820	54	13%
MQ01.2.14	9.35	0.33	0.3953	0.0071	0.1712	0.0048	2147	33	2569	47	16%
MQ01.2.15	2.345	0.089	0.09	0.0023	0.1892	0.0049	556	14	2734	43	80%
MQ01.2.16	2.478	0.091	0.1305	0.0035	0.1379	0.003	791	20	2200	38	64%
MQ01.2.17	5.48	0.28	0.325	0.011	0.1224	0.0049	1814	54	1991	71	9%
MQ01.2.18	8.29	0.36	0.368	0.0079	0.1645	0.0052	2020	37	2502	53	19%
MQ01.2.19	4.61	0.26	0.279	0.016	0.1197	0.0024	1586	81	1951	36	19%
MQ01.2.20	5.15	0.16	0.3091	0.0049	0.1212	0.003	1736	24	1973	44	12%
MQ01.2.21	3.87	0.13	0.2343	0.0072	0.1208	0.0026	1357	38	1967	38	31%
MQ01.2.22	10.7	0.32	0.4632	0.0052	0.1685	0.0042	2454	23	2542	42	3%
MQ01.2.23	3.44	0.092	0.196	0.0027	0.1283	0.0031	1154	15	2074	43	44%
MQ01.2.24	7.73	0.24	0.3327	0.0069	0.1695	0.0039	1851	33	2552	39	27%
MQ01.2.25	2.65	0.23	0.146	0.013	0.1336	0.0033	879	73	2145	43	59%
MQ01.2.26	4.55	0.21	0.283	0.012	0.1169	0.0032	1606	60	1909	49	16%
MQ01.2.27	4.942	0.12	0.3097	0.004	0.1162	0.0025	1739	20	1898	39	8%
MQ01.2.28	no value	NAN	no value	NAN	0.1302	0.0043					#DIV/0!
MQ01.2.29	5.28	0.15	0.3361	0.0051	0.1146	0.0026	1868	25	1873	41	0%
MQ01.2.30	4.8	0.16	0.3026	0.0048	0.1163	0.003	1704	24	1899	46	10%
MQ01.2.31	9.09	0.25	0.4153	0.0059	0.1605	0.0034	2239	27	2460	36	9%

MQ01.2.32	5.93	0.19	0.3589	0.0043	0.1208	0.0033	1977	20	1967	49	-1%
MQ01.2.33	7.06	0.24	0.2836	0.0087	0.181	0.0043	1609	44	2661	40	40%
MQ01.2.34	11	0.31	0.4689	0.0057	0.1716	0.004	2479	25	2573	39	4%
MQ01.2.35	1.734	0.059	0.0912	0.0027	0.1392	0.0029	563	16	2216	36	75%
MQ01.2.36	8.03	0.36	0.34	0.014	0.1765	0.0035	1887	67	2620	33	28%
MQ01.2.37	5.97	0.18	0.3246	0.0052	0.1336	0.0038	1812	25	2145	50	16%
MQ01.2.38	5.62	0.17	0.3463	0.0037	0.1183	0.0032	1917	18	1930	49	1%
MQ01.2.39	18.13	0.61	0.574	0.011	0.2287	0.0064	2924	45	3042	45	4%
MQ01.2.40	5.04	0.19	0.2805	0.0071	0.1313	0.0038	1594	36	2115	51	25%
MQ01.2.41	3.54	0.16	0.1888	0.0095	0.1369	0.0035	1115	52	2188	45	49%
MQ01.2.42	6.27	0.18	0.3659	0.007	0.1246	0.0026	2010	33	2022	37	1%
MQ01.2.43	1.87	0.064	0.0944	0.002	0.1465	0.0034	582	12	2305	40	75%
MQ01.2.44	12.03	0.31	0.4987	0.0048	0.1749	0.0036	2608	21	2604	34	0%
MQ01.2.45	4.028	0.13	0.2338	0.0042	0.1274	0.0029	1354	22	2062	40	34%
MQ01.2.46	5.06	0.16	0.3191	0.0046	0.1148	0.0028	1785	23	1876	44	5%
MQ01.2.47	1.352	0.071	0.0653	0.003	0.1531	0.0038	408	18	2380	42	83%
MQ01.2.48	5.99	0.2	0.3473	0.0043	0.1245	0.0031	1922	21	2021	44	5%
MQ01.2.49	11.83	0.4	0.4955	0.01	0.1732	0.004	2594	43	2588	39	0%
MQ01.2.50	2.61	0.12	0.139	0.0053	0.1356	0.0027	839	30	2171	35	61%
MQ01.2.51	5.67	0.18	0.3487	0.0092	0.118	0.0036	1928	44	1925	55	0%
MQ01.2.52	5.58	0.24	0.3456	0.0052	0.117	0.0039	1914	25	1910	60	0%
MQ01.2.53	6	0.18	0.3583	0.0046	0.1212	0.003	1974	22	1973	44	0%
MQ01.2.54	5.15	0.16	0.3315	0.0041	0.1126	0.0029	1846	20	1841	47	0%
MQ01.2.55	5.97	0.2	0.2451	0.0057	0.1767	0.0038	1413	30	2621	36	46%
MQ01.2.56	11.44	0.31	0.4807	0.0082	0.1727	0.004	2530	36	2583	39	2%

MQ01.2.57	5.17	0.19	0.3246	0.0074	0.1149	0.0031	1812	36	1878	49	4%
MQ01.2.58	5.3	0.19	0.3357	0.0054	0.1137	0.0035	1866	26	1859	56	0%
MQ01.2.59	5.8	0.18	0.3504	0.0053	0.12	0.0028	1937	25	1955	42	1%
MQ01.2.60	5.37	0.25	0.2239	0.0095	0.1746	0.0042	1302	50	2601	40	50%
MQ01.2.61	no value	NAN	no value	NAN		0.1817	0.0039				
MQ01.2.62	11.26	0.32	0.4608	0.0075	0.1766	0.0042	2443	33	2620	40	7%
MQ01.2.63	5.128	0.14	0.32	0.0039	0.1159	0.0027	1790	19	1893	42	5%
MQ01.2.64	6.37	0.22	0.334	0.012	0.1391	0.0054	1858	58	2215	67	16%
MQ01.2.65	6.01	0.18	0.3596	0.0045	0.1208	0.0027	1980	21	1967	40	-1%
MQ01.2.66	5.47	0.16	0.3379	0.0046	0.1173	0.0028	1877	22	1915	43	2%

Sample: MQ02

Grain ID	*207Pb/232Th*	*207Pb/232Th prop2SE*	*206Pb/238U*	*206Pb/238U prop2SE*	*207Pb/206Pb*	*207Pb/206Pb prop2SE*	*206Pb/238Pb Age (Ma)*	*± 1σ(Ma)*	*207Pb/206Pb Age (Ma)*	*± 1σ (Ma)*	*Disc (%)*
MQ02.1.01	3.25	0.2	0.1325	0.0082	0.1718	0.0036	802	47	2575	35	69%
MQ02.1.02	6.04	0.27	0.256	0.011	0.1692	0.002	1469	56	2549	20	42%
MQ02.1.03	4.81	0.16	0.2949	0.0091	0.1164	0.0021	1666	45	1901	33	12%
MQ02.1.04	5.463	0.11	0.3381	0.0051	0.1164	0.0018	1878	25	1901	28	1%
MQ02.1.05	5.011	0.089	0.3078	0.0046	0.1175	0.0017	1730	23	1918	26	10%
MQ02.1.06	8.49	0.45	0.361	0.019	0.1697	0.0019	1987	90	2554	19	22%
MQ02.1.07	6.1	0.17	0.3623	0.0084	0.1219	0.0024	1993	40	1983	35	-1%
MQ02.1.08	5.59	0.081	0.3465	0.0035	0.1167	0.0015	1918	17	1905	23	-1%
MQ02.1.09	2.066	0.04	0.1196	0.002	0.1246	0.0021	728	12	2022	30	64%
MQ02.1.10	5.356	0.08	0.3384	0.0038	0.1143	0.0015	1879	18	1868	24	-1%
MQ02.1.11	7.67	0.17	0.3454	0.0064	0.1611	0.0021	1913	31	2466	22	22%

MQ02.1.12	5.347	0.11	0.3349	0.0038	0.1159	0.0022	1862	18	1893	34	2%
MQ02.1.13	1.122	0.028	0.0586	0.0016	0.1393	0.0022	367.1	9.7	2218	28	83%
MQ02.1.14	2.73	0.4	0.119	0.017	0.1657	0.0026	725	98	2514	27	71%
MQ02.1.15	5.16	0.17	0.3271	0.0076	0.1151	0.0024	1824	37	1881	38	3%
MQ02.1.16	6.244	0.1	0.368	0.0038	0.1234	0.0016	2020	18	2005	23	-1%
MQ02.1.17	5.19	0.12	0.3264	0.005	0.1156	0.0024	1821	24	1888	37	4%
MQ02.1.18	6.47	0.24	0.278	0.01	0.1693	0.0019	1581	50	2550	19	38%
MQ02.1.19	5.42	0.14	0.344	0.0074	0.1146	0.003	1906	36	1873	47	-2%
MQ02.1.20	4.7	0.14	0.2593	0.0064	0.1319	0.0024	1486	33	2123	32	30%
MQ02.1.21	5.41	0.11	0.3419	0.0045	0.1163	0.0025	1896	22	1899	39	0%
MQ02.1.22	9.87	0.31	0.396	0.013	0.1828	0.0029	2151	60	2678	26	20%
MQ02.1.23	5.93	0.13	0.3567	0.0052	0.1219	0.0021	1967	25	1983	31	1%
MQ02.1.24	10.79	0.2	0.4768	0.0056	0.166	0.0022	2513	24	2517	23	0%
MQ02.1.25	1.759	0.032	0.1034	0.0017	0.1244	0.002	634.3	9.9	2019	29	69%
MQ02.1.26	5.53	0.12	0.3467	0.0061	0.1167	0.002	1919	29	1905	31	-1%
MQ02.1.27	10.21	0.16	0.4726	0.005	0.158	0.0021	2495	22	2434	23	-3%
MQ02.1.28	1.662	0.033	0.0946	0.0014	0.128	0.0019	582.7	8.3	2070	26	72%
MQ02.1.29	8.38	0.34	0.425	0.011	0.1446	0.0054	2283	50	2282	64	0%
MQ02.1.30	5.32	0.25	0.337	0.014	0.1153	0.0046	1872	68	1884	72	1%
MQ02.1.31	4.75	0.15	0.3016	0.0064	0.1153	0.0027	1699	32	1884	42	10%
MQ02.1.32	12.18	0.31	0.498	0.012	0.1787	0.0024	2605	52	2640	23	1%
MQ02.1.33	5.31	0.12	0.3384	0.0065	0.1143	0.0016	1879	31	1868	25	-1%
MQ02.1.34	11.6	1.2	0.446	0.024	0.1872	0.0086	2380	110	2717	76	12%
MQ02.1.35	5.41	0.12	0.3411	0.0041	0.116	0.0023	1892	20	1895	36	0%
MQ02.1.36	7.2	0.15	0.3931	0.006	0.1341	0.0029	2137	28	2152	38	1%

MQ02.1.37	6.7	0.21	0.38	0.0098	0.1294	0.0025	2076	46	2089	34	1%
MQ02.1.38	6.9	0.22	0.39	0.01	0.1286	0.003	2123	46	2078	41	-2%
MQ02.1.39	3.67	0.17	0.1613	0.0071	0.1656	0.0021	964	39	2513	22	62%
MQ02.1.40	11.43	0.16	0.4747	0.0057	0.1751	0.002	2504	25	2606	19	4%
MQ02.1.41	5.257	0.087	0.3361	0.0034	0.1143	0.0018	1868	16	1868	29	0%
MQ02.1.42	5.1	0.087	0.3236	0.005	0.1148	0.0018	1807	24	1876	28	4%
MQ02.1.43	10.35	0.18	0.4669	0.0059	0.162	0.0028	2470	26	2476	29	0%
MQ02.1.44	6.276	0.11	0.3681	0.0042	0.1244	0.0022	2020	20	2019	31	0%
MQ02.1.45	4.98	0.13	0.3154	0.0071	0.1149	0.0021	1767	35	1878	33	6%
MQ02.1.46	5.352	0.11	0.3412	0.0038	0.114	0.0021	1892	18	1863	33	-2%
MQ02.1.47	2.49	0.12	0.1457	0.0078	0.1248	0.002	877	44	2025	29	57%
MQ02.1.48	4.77	0.15	0.291	0.0046	0.1191	0.0031	1647	23	1942	47	15%
MQ02.1.49	3.58	0.15	0.2096	0.0093	0.1246	0.0018	1227	50	2022	26	39%
MQ02.1.50	4.4	0.11	0.2753	0.0079	0.117	0.0028	1568	40	1910	43	18%
MQ02.1.51	11.29	0.18	0.4878	0.0065	0.1685	0.0019	2561	28	2542	19	-1%
MQ02.1.52	5.18	0.16	0.3378	0.0053	0.1119	0.0033	1876	26	1830	54	-3%
MQ02.1.53	6	0.15	0.3591	0.0068	0.122	0.0025	1978	32	1985	37	0%
MQ02.1.54	1.444	0.03	0.0702	0.0011	0.1497	0.0021	437.4	6.6	2342	24	81%
MQ02.1.55	5.35	0.097	0.3379	0.0043	0.1155	0.0019	1877	21	1887	30	1%
MQ02.1.56	10.65	0.18	0.4571	0.0057	0.17	0.0022	2427	25	2557	22	5%
MQ02.1.57	5.34	0.11	0.3403	0.0035	0.1144	0.0022	1888	17	1870	35	-1%
MQ02.1.58	2.77	0.16	0.1226	0.0065	0.1635	0.003	746	37	2491	31	70%
MQ02.1.59	9.58	0.22	0.4514	0.0088	0.1546	0.0019	2401	39	2397	21	0%
MQ02.1.60	5.3	0.18	0.3382	0.0066	0.1148	0.0036	1878	32	1876	57	0%
MQ02.1.61	5.58	0.12	0.3515	0.0053	0.1158	0.002	1942	25	1892	31	-3%

MQ02.1.62	5.9	0.17	0.3504	0.0079	0.1231	0.0023	1937	38	2001	33	3%
MQ02.1.63	8.08	0.19	0.3906	0.0079	0.1506	0.0021	2126	37	2352	24	10%
MQ02.1.64	9.4	0.51	0.384	0.022	0.1784	0.0022	2090	100	2637	21	21%
MQ02.1.65	5.159	0.11	0.3328	0.0046	0.1127	0.0023	1852	22	1843	37	0%
MQ02.1.66	1.564	0.079	0.0704	0.0037	0.1622	0.0022	439	22	2478	23	82%
MQ02.1.67	5.36	0.13	0.3421	0.0047	0.1137	0.0025	1897	23	1859	40	-2%
MQ02.1.68	5.11	0.35	0.203	0.015	0.1835	0.0026	1191	80	2684	24	56%
MQ02.1.69	2.29	0.11	0.1369	0.0065	0.1221	0.0021	827	37	1986	31	58%
MQ02.1.70	5.26	0.21	0.334	0.013	0.1155	0.0024	1858	63	1887	38	2%
MQ02.1.71	11.37	0.17	0.487	0.0061	0.1695	0.002	2558	26	2552	20	0%
MQ02.1.72	5.47	0.17	0.3405	0.0058	0.1174	0.0029	1889	28	1916	44	1%
MQ02.1.73	5.537	0.11	0.3444	0.0043	0.1173	0.0022	1908	21	1915	34	0%
MQ02.1.74	7.12	0.15	0.3909	0.0052	0.1328	0.0021	2127	24	2135	28	0%
MQ02.1.75	5.451	0.1	0.3426	0.004	0.116	0.0018	1899	19	1895	28	0%
MQ02.1.76	5.297	0.099	0.3373	0.0046	0.1137	0.0021	1874	22	1859	33	-1%
MQ02.1.77	5.004	0.11	0.3192	0.0037	0.1147	0.0024	1786	18	1874	38	5%
MQ02.1.78	9.18	0.16	0.4416	0.0053	0.1516	0.0023	2358	24	2363	26	0%
MQ02.1.79	5.24	0.11	0.3127	0.0049	0.1225	0.0021	1754	24	1992	31	12%
MQ02.1.80	4.6	0.13	0.2814	0.0057	0.1192	0.0033	1598	29	1943	50	18%
MQ02.1.81	5.562	0.1	0.3464	0.0051	0.117	0.0015	1917	24	1910	23	0%
MQ02.1.82	10.8	0.39	0.472	0.014	0.167	0.0033	2492	61	2527	33	1%
MQ02.1.83	6.23	0.14	0.363	0.0056	0.1255	0.002	1996	27	2035	28	2%
MQ02.1.84	4.889	0.11	0.3012	0.0048	0.1183	0.0024	1697	24	1930	36	12%
MQ02.1.85	5.214	0.11	0.328	0.0057	0.1163	0.0026	1829	28	1899	40	4%
MQ02.1.86	10.28	0.19	0.4304	0.0064	0.1739	0.0028	2308	29	2595	27	11%

MQ02.1.87	9.15	0.13	0.3919	0.0049	0.1696	0.0017	2132	23	2553	17	16%
MQ02.1.88	4.11	0.13	0.2575	0.0077	0.1161	0.0022	1477	39	1896	34	22%
MQ02.1.89	5.15	0.11	0.3193	0.0036	0.1176	0.0025	1786	18	1919	38	7%
MQ02.1.90	12.05	0.2	0.4987	0.0058	0.1755	0.0027	2608	25	2610	26	0%
MQ02.1.91	5.277	0.085	0.3349	0.0046	0.1147	0.0016	1862	22	1874	25	1%
MQ02.1.92	9.08	0.54	0.384	0.022	0.1718	0.0018	2090	100	2575	18	19%
MQ02.1.93	4.8	0.34	0.203	0.014	0.1707	0.0023	1191	75	2564	23	54%
MQ02.1.94	3.55	0.11	0.2044	0.0059	0.1255	0.0016	1199	32	2035	23	41%
MQ02.1.95	2.209	0.068	0.1214	0.004	0.132	0.0017	739	23	2124	23	65%
MQ02.1.96	5.17	0.33	0.217	0.014	0.1718	0.0021	1266	74	2575	21	51%
MQ02.1.97	12.22	0.18	0.5065	0.0061	0.1743	0.0021	2642	26	2599	20	-2%
MQ02.1.98	2.168	0.069	0.0958	0.0026	0.1628	0.0029	590	15	2484	30	76%
MQ02.1.99	3.16	0.2	0.1321	0.008	0.1723	0.0022	800	46	2579	22	69%
MQ02.1.100	4.759	0.07	0.2793	0.0032	0.1213	0.0017	1588	16	1975	25	20%
MQ02.1.101	6.02	0.11	0.3577	0.0046	0.1217	0.0019	1971	22	1980	28	0%
MQ02.1.102	10.25	0.28	0.4619	0.006	0.1603	0.0036	2448	26	2458	38	0%
MQ02.1.103	5.67	0.12	0.3428	0.0045	0.1196	0.002	1900	22	1949	30	3%
MQ02.1.104	11.41	0.25	0.48	0.0089	0.1718	0.0019	2527	39	2575	19	2%
MQ02.1.105	5.71	0.15	0.3501	0.0056	0.1181	0.0029	1935	27	1927	44	0%
MQ02.1.106	12.11	0.19	0.4973	0.0055	0.1759	0.0029	2602	24	2614	28	0%
MQ02.1.107	2.15	0.12	0.1277	0.0069	0.122	0.0023	775	39	1985	34	61%
MQ02.1.108	7.32	0.15	0.3029	0.0049	0.1747	0.0027	1706	24	2602	26	34%
MQ02.1.109	5.18	0.11	0.3198	0.0076	0.1149	0.0016	1789	37	1878	25	5%
MQ02.1.110	6.31	0.16	0.3671	0.0061	0.1242	0.0026	2016	29	2017	37	0%
MQ02.1.111	1.99	0.24	0.11	0.014	0.1313	0.0035	673	81	2115	47	68%

MQ02.1.112	5.258	0.098	0.3238	0.0043	0.1173	0.0018	1808	21	1915	28	6%
MQ02.1.113	11.99	0.33	0.496	0.0072	0.1753	0.0044	2597	31	2608	42	0%
MQ02.1.114	5.385	0.1	0.3361	0.0043	0.1165	0.0022	1868	21	1902	34	2%
MQ02.1.115	5.125	0.084	0.3205	0.0042	0.1163	0.0018	1792	21	1899	28	6%
MQ02.1.116	5.57	0.12	0.3369	0.0058	0.1197	0.0016	1872	28	1951	24	4%
MQ02.1.117	11.26	0.26	0.4846	0.008	0.1683	0.0027	2547	35	2540	27	0%
MQ02.1.118	10.62	0.18	0.4452	0.0076	0.1724	0.0028	2374	34	2580	27	8%
MQ02.1.119	3.999	0.087	0.2463	0.0067	0.1157	0.0022	1419	35	1890	34	25%
MQ02.1.120	2.272	0.047	0.1358	0.0026	0.1211	0.0019	821	15	1972	28	58%
MQ02.1.121	5.38	0.11	0.3381	0.0045	0.1158	0.0022	1878	22	1892	34	1%
MQ02.1.122	11.57	0.22	0.4933	0.0077	0.1698	0.0022	2585	33	2555	22	-1%
MQ02.1.123	6.003	0.11	0.3593	0.0041	0.1212	0.002	1979	19	1973	30	0%
MQ02.1.124	5.33	0.16	0.3378	0.0079	0.1144	0.0021	1876	38	1870	33	0%
MQ02.1.125	5.31	0.14	0.3347	0.0047	0.1149	0.003	1861	23	1878	47	1%
MQ02.1.126	5.49	0.11	0.3423	0.0048	0.1164	0.0016	1898	23	1901	25	0%
MQ02.1.127	5.58	0.1	0.345	0.0039	0.1183	0.0019	1911	19	1930	29	1%
MQ02.1.128	2.471	0.074	0.0925	0.0026	0.1944	0.0025	570	15	2779	21	79%
MQ02.2.01	2.25	0.13	0.1397	0.006	0.1181	0.0034	843	34	1927	52	56%
MQ02.2.02	11.97	0.3	0.4987	0.0052	0.1753	0.0038	2608	22	2608	36	0%
MQ02.2.03	3.897	0.13	0.246	0.004	0.1161	0.0038	1418	21	1896	59	25%
MQ02.2.04	2.63	0.074	0.154	0.0017	0.1254	0.0032	923.3	9.5	2034	45	55%
MQ02.2.05	9.18	0.26	0.3687	0.0057	0.1822	0.0039	2023	27	2672	36	24%
MQ02.2.06	0.979	0.07	0.0386	0.0024	0.189	0.0047	244	15	2733	41	91%
MQ02.2.07	7.16	0.34	0.318	0.013	0.1648	0.0032	1780	64	2505	33	29%

MQ02.2.08	4.46	0.22	0.2763	0.009	0.1181	0.0033	1573	45	1927	50	18%
MQ02.2.09	4.74	0.14	0.2509	0.0057	0.1384	0.0035	1443	29	2207	44	35%
MQ02.2.10	1.93	0.084	0.0825	0.0026	0.1707	0.004	511	15	2564	39	80%
MQ02.2.11	5.46	0.18	0.3414	0.005	0.1162	0.0029	1893	24	1898	45	0%
MQ02.2.12	13.1	0.41	0.516	0.011	0.1847	0.0041	2682	47	2695	37	0%
MQ02.2.13	7.15	0.2	0.3178	0.005	0.1628	0.0038	1779	24	2484	39	28%

Sample: MIT1701d

Grain ID	*207Pb/232Th*	*207Pb/232Th prop2SE*	*206Pb/238U*	*206Pb/238U prop2SE*	*207Pb/206Pb*	*207Pb/206Pb prop2SE*	*206Pb/238Pb Age (Ma)*	*± 1σ(Ma)*	*207Pb/206Pb Age (Ma)*	*± 1σ (Ma)*	*Disc (%)*
MIT1701d.3.01	5.56	0.14	0.3452	0.0085	0.1166	0.0034	1912	41	1904	52	0%
MIT1701d.3.02	11.12	0.25	0.4639	0.01	0.1733	0.0043	2457	44	2589	42	5%
MIT1701d.3.03	12.22	0.3	0.5156	0.012	0.1712	0.0041	2680	51	2569	40	-4%
MIT1701d.3.04	5.338	0.12	0.3351	0.0075	0.1151	0.0028	1863	36	1881	44	1%
MIT1701d.3.05	5.294	0.14	0.3302	0.008	0.1158	0.0029	1839	39	1892	45	3%
MIT1701d.3.06	6.57	0.2	0.3752	0.0091	0.1261	0.0033	2054	43	2044	46	0%
MIT1701d.3.07	5.694	0.13	0.349	0.0094	0.1178	0.0029	1930	45	1922	44	0%
MIT1701d.3.08	5.32	0.19	0.337	0.0083	0.1142	0.0045	1872	40	1866	71	0%
MIT1701d.3.09	5.8	0.16	0.3369	0.0081	0.123	0.0031	1872	39	1999	45	6%
MIT1701d.3.10	5.23	0.19	0.3337	0.0087	0.1132	0.0039	1856	42	1851	62	0%
MIT1701d.3.11	6.48	0.15	0.3718	0.0082	0.1256	0.0031	2038	39	2036	44	0%
MIT1701d.3.12	10.39	0.3	0.462	0.012	0.1624	0.0048	2448	53	2480	50	1%
MIT1701d.3.13	6.15	0.15	0.3607	0.0077	0.123	0.0031	1985	36	1999	45	1%
MIT1701d.3.14	5.3	0.12	0.3063	0.0088	0.1249	0.003	1722	43	2027	43	15%
MIT1701d.3.15	13.14	0.31	0.5128	0.011	0.1847	0.0042	2669	47	2695	38	1%

MIT1701d.3.16	9.56	0.24	0.4354	0.0096	0.1565	0.0038	2330	43	2417	41	4%
MIT1701d.3.17	5.27	0.16	0.3341	0.008	0.1135	0.0033	1858	39	1855	53	0%
MIT1701d.3.18	12.38	0.3	0.5143	0.012	0.1735	0.0039	2675	51	2591	38	-3%
MIT1701d.3.19	11.62	0.23	0.4839	0.011	0.1725	0.0039	2544	48	2581	38	1%
MIT1701d.3.20	5.394	0.13	0.3382	0.0072	0.1145	0.0029	1878	35	1871	46	0%
MIT1701d.3.21	4.1	0.14	0.2128	0.0082	0.1384	0.0034	1244	44	2207	43	44%
MIT1701d.3.22	5.537	0.13	0.3429	0.0078	0.1159	0.0028	1901	37	1893	44	0%
MIT1701d.3.23	11.64	0.28	0.484	0.012	0.1726	0.0042	2545	52	2582	41	1%
MIT1701d.3.24	5.802	0.16	0.3464	0.0078	0.1202	0.0032	1917	37	1958	48	2%
MIT1701d.3.25	11.94	0.36	0.49	0.016	0.1749	0.0042	2571	69	2604	40	1%
MIT1701d.3.26	11.87	0.28	0.48	0.011	0.1773	0.0045	2527	48	2627	42	4%
MIT1701d.3.27	5.184	0.12	0.3075	0.0072	0.1209	0.0027	1728	36	1969	40	12%
MIT1701d.3.28	6.782	0.15	0.3692	0.008	0.1303	0.0028	2026	38	2101	38	4%
MIT1701d.3.29	5.43	0.15	0.3388	0.0073	0.1149	0.0032	1881	35	1878	50	0%
MIT1701d.3.30	13.85	0.3	0.535	0.012	0.1856	0.0041	2762	50	2703	37	-2%
MIT1701d.3.31	11.67	0.32	0.495	0.015	0.1689	0.0042	2592	65	2546	42	-2%
MIT1701d.3.32	5.6	0.26	0.338	0.013	0.1191	0.0051	1877	63	1942	77	3%
MIT1701d.3.33	7.03	0.2	0.319	0.01	0.158	0.0037	1785	49	2434	40	27%
MIT1701d.3.34	5.706	0.14	0.3469	0.0075	0.1177	0.0028	1920	36	1921	43	0%
MIT1701d.3.35	6	0.16	0.3435	0.0076	0.1245	0.0033	1903	36	2021	47	6%
MIT1701d.3.36	5.93	0.15	0.3452	0.009	0.1231	0.0038	1912	43	2001	55	4%
MIT1701d.3.37	6.09	0.18	0.3581	0.011	0.1219	0.0033	1973	52	1983	48	1%
MIT1701d.3.38	11.54	0.36	0.481	0.017	0.1722	0.0054	2532	74	2578	52	2%
MIT1701d.3.39	5.39	0.15	0.3361	0.0073	0.115	0.0036	1868	35	1879	56	1%
MIT1701d.3.40	5.61	0.14	0.3472	0.008	0.1157	0.0029	1921	38	1890	45	-2%

MIT1701d.3.41	5.35	0.29	0.3376	0.011	0.1135	0.0056	1875	53	1855	89	-1%
MIT1701d.3.42	5.21	0.14	0.2975	0.0087	0.1256	0.0034	1679	43	2036	48	18%
MIT1701d.3.43	5.52	0.14	0.338	0.0081	0.1169	0.0033	1877	39	1909	51	2%
MIT1701d.3.44	5.81	0.16	0.3485	0.0085	0.1195	0.0035	1927	41	1948	52	1%
MIT1701d.3.45	10.25	0.26	0.464	0.012	0.1582	0.0036	2457	53	2436	39	-1%
MIT1701d.3.46	5.45	0.17	0.3391	0.0077	0.115	0.0037	1882	37	1879	58	0%
MIT1701d.3.47	6.34	0.15	0.3683	0.0079	0.1232	0.0033	2021	37	2002	48	-1%
MIT1701d.3.48	5.43	0.37	0.339	0.014	0.1148	0.0067	1882	67	1880	110	0%
MIT1701d.3.49	5.18	0.18	0.32	0.0082	0.1147	0.004	1790	40	1874	63	4%
MIT1701d.3.50	10.63	0.33	0.447	0.016	0.1687	0.004	2382	71	2544	40	6%
MIT1701d.3.51	5.5	0.19	0.341	0.0088	0.1156	0.0039	1891	42	1888	61	0%
MIT1701d.3.52	12.03	0.27	0.4988	0.012	0.1727	0.0039	2609	52	2583	38	-1%
MIT1701d.3.53	10.85	0.32	0.4509	0.012	0.1726	0.0053	2399	53	2582	51	7%
MIT1701d.3.54	12.59	0.24	0.5239	0.011	0.1722	0.0037	2716	47	2578	36	-5%
MIT1701d.3.55	11.47	0.27	0.4855	0.012	0.1693	0.0043	2551	52	2550	43	0%
MIT1701d.3.56	6.02	0.17	0.3581	0.01	0.1205	0.0042	1973	47	1963	62	-1%
MIT1701d.3.57	5.3	0.14	0.3258	0.0086	0.1156	0.0035	1818	42	1888	55	4%
MIT1701d.3.58	5.52	0.18	0.3392	0.0082	0.1166	0.004	1883	39	1904	62	1%
MIT1701d.3.59	5.13	0.13	0.3119	0.0084	0.1166	0.003	1750	41	1904	46	8%
MIT1701d.3.60	11.75	0.27	0.4877	0.012	0.1729	0.0042	2561	52	2585	41	1%
MIT1701d.3.61	5.41	0.14	0.3383	0.0077	0.1146	0.0029	1878	37	1873	46	0%
MIT1701d.3.62	5.828	0.13	0.3364	0.0081	0.1242	0.0027	1869	39	2017	39	7%
MIT1701d.3.63	5.46	0.16	0.3315	0.0082	0.1184	0.0038	1846	40	1931	58	4%
MIT1701d.3.64	9.29	0.34	0.441	0.017	0.15142	0.0032	2355	76	2361	36	0%
MIT1701d.3.65	5.6	0.14	0.3467	0.0095	0.1158	0.0034	1919	45	1892	53	-1%

MIT1701d.3.66	6.17	0.38	0.268	0.018	0.1654	0.0041	1531	92	2511	42	39%
MIT1701d.3.67	11.92	0.24	0.4987	0.01	0.1715	0.0036	2608	43	2572	35	-1%
MIT1701d.3.68	11.69	0.31	0.4887	0.011	0.1718	0.0041	2565	48	2575	40	0%
MIT1701d.3.69	5.648	0.13	0.3459	0.0072	0.1174	0.0029	1915	35	1916	44	0%
MIT1701d.3.70	5.481	0.12	0.3421	0.0082	0.1151	0.0026	1897	39	1881	41	-1%

Sample: MIT1701e

Grain ID	*207Pb/232Th*	*207Pb/232Th prop2SE*	*206Pb/238U*	*206Pb/238U prop2SE*	*207Pb/206Pb*	*207Pb/206Pb prop2SE*	*206Pb/238Pb Age (Ma)*	*± 1σ(Ma)*	*207Pb/206Pb Age (Ma)*	*± 1σ (Ma)*	*Disc (%)*
MIT1701e.3.01	6.15	0.16	0.3717	0.0089	0.1202	0.0029	2037	42	1958	43	-4%
MIT1701e.3.02	11.81	0.37	0.494	0.018	0.1736	0.0045	2588	78	2592	43	0%
MIT1701e.3.03	11.56	0.24	0.4787	0.01	0.1756	0.0042	2522	44	2611	40	3%
MIT1701e.3.04	11.09	0.28	0.4688	0.013	0.172	0.0038	2478	57	2576	37	4%
MIT1701e.3.05	12.31	0.29	0.4999	0.011	0.1792	0.0041	2613	47	2645	38	1%
MIT1701e.3.06	5.36	0.12	0.336	0.0073	0.1162	0.0027	1867	35	1898	42	2%
MIT1701e.3.07	5.67	0.14	0.3502	0.0084	0.118	0.0028	1936	40	1925	43	-1%
MIT1701e.3.08	9.16	0.31	0.3825	0.012	0.1745	0.0049	2088	56	2601	47	20%
MIT1701e.3.09	5.34	0.13	0.3423	0.0073	0.1138	0.003	1898	35	1860	48	-2%
MIT1701e.3.10	11.79	0.28	0.4919	0.012	0.1749	0.0044	2579	52	2604	42	1%
MIT1701e.3.11	5.63	0.16	0.3463	0.0084	0.1187	0.003	1917	40	1936	45	1%
MIT1701e.3.12	5.34	0.18	0.3395	0.009	0.115	0.0032	1884	43	1879	50	0%
MIT1701e.3.13	5.349	0.13	0.341	0.0077	0.1146	0.0028	1891	37	1873	44	-1%
MIT1701e.3.14	5.39	0.16	0.3426	0.0088	0.115	0.0028	1899	42	1879	44	-1%
MIT1701e.3.15	5.8	0.14	0.3542	0.008	0.1199	0.003	1955	38	1954	45	0%
MIT1701e.3.16	5.709	0.13	0.3492	0.0078	0.1197	0.0031	1931	37	1951	46	1%

MIT1701e.3.17	9.08	0.23	0.4023	0.011	0.1653	0.0039	2180	51	2510	40	13%
MIT1701e.3.18	5.96	0.15	0.3601	0.008	0.1213	0.0031	1983	38	1975	46	0%
MIT1701e.3.19	5.526	0.13	0.3296	0.0071	0.123	0.003	1836	34	1999	43	8%
MIT1701e.3.20	5.05	0.14	0.3175	0.0072	0.1167	0.0034	1778	35	1905	52	7%
MIT1701e.3.21	5.78	0.15	0.3609	0.0086	0.1173	0.003	1986	41	1915	46	-4%
MIT1701e.3.22	5.53	0.14	0.3463	0.0087	0.117	0.0029	1917	42	1910	45	0%
MIT1701e.3.23	5.89	0.16	0.3556	0.0082	0.1217	0.0034	1961	39	1980	50	1%
MIT1701e.3.24	12.19	0.27	0.5057	0.012	0.1772	0.0042	2638	51	2626	40	0%
MIT1701e.3.25	5.36	0.2	0.3394	0.0082	0.1159	0.0035	1884	39	1893	54	0%
MIT1701e.3.26	5.59	0.15	0.3499	0.0081	0.1174	0.0031	1934	39	1916	47	-1%
MIT1701e.3.27	5.302	0.13	0.3406	0.0075	0.1145	0.0027	1890	36	1871	43	-1%
MIT1701e.3.28	6.23	0.15	0.2662	0.0062	0.1722	0.0042	1521	32	2578	41	41%
MIT1701e.3.29	4.848	0.1	0.3057	0.0069	0.1166	0.0027	1720	34	1904	42	10%
MIT1701e.3.30	5.97	0.15	0.3602	0.0094	0.1221	0.0031	1983	45	1986	45	0%
MIT1701e.3.31	5.22	0.2	0.3356	0.012	0.1142	0.0029	1865	58	1866	46	0%
MIT1701e.3.32	4.27	0.13	0.2478	0.0094	0.1269	0.0028	1427	49	2055	39	31%
MIT1701e.3.33	11.34	0.25	0.4811	0.011	0.1714	0.004	2532	48	2571	39	2%
MIT1701e.3.34	5.31	0.17	0.3391	0.0095	0.1138	0.003	1882	46	1860	48	-1%
MIT1701e.3.35	5.717	0.12	0.3392	0.007	0.124	0.003	1883	34	2014	43	7%
MIT1701e.3.36	5.352	0.11	0.3446	0.0072	0.1142	0.0027	1909	35	1866	43	-2%
MIT1701e.3.37	5.394	0.13	0.3401	0.0078	0.1157	0.0033	1887	38	1890	51	0%
MIT1701e.3.38	11.82	0.36	0.503	0.014	0.1726	0.0047	2627	60	2582	46	-2%
MIT1701e.3.39	5.389	0.13	0.3403	0.0073	0.1163	0.003	1888	35	1899	46	1%
MIT1701e.3.40	6.23	0.22	0.3664	0.0093	0.1249	0.0038	2012	44	2027	54	1%
MIT1701e.3.41	11.93	0.26	0.4958	0.01	0.1767	0.0041	2596	43	2621	39	1%

MIT1701e.3.42	5.78	0.17	0.3525	0.0085	0.1203	0.0031	1947	41	1960	46	1%
MIT1701e.3.43	6.323	0.12	0.3798	0.0077	0.1222	0.0026	2075	36	1988	38	-4%
MIT1701e.3.44	11.48	0.25	0.5005	0.01	0.1677	0.0037	2616	43	2534	37	-3%
MIT1701e.3.45	5.19	0.16	0.3328	0.0096	0.1141	0.0032	1852	46	1865	51	1%
MIT1701e.3.46	8.05	0.24	0.369	0.015	0.1593	0.004	2025	71	2447	43	17%
MIT1701e.3.47	12.31	0.3	0.5115	0.012	0.1757	0.0044	2663	51	2612	42	-2%
MIT1701e.3.48	16.95	0.4	0.5911	0.015	0.2096	0.005	2994	61	2902	39	-3%
MIT1701e.3.49	5.799	0.14	0.3677	0.008	0.1153	0.003	2019	38	1884	47	-7%
MIT1701e.3.50	11.54	0.22	0.5079	0.01	0.166	0.0036	2648	43	2517	37	-5%
MIT1701e.3.51	6.268	0.13	0.3809	0.0085	0.1203	0.0028	2080	40	1960	42	-6%
MIT1701e.3.52	3.38	0.18	0.2411	0.0079	0.1023	0.0041	1392	41	1665	74	16%
MIT1701e.3.53	5.35	0.13	0.3407	0.0077	0.1146	0.0029	1890	37	1873	46	-1%
MIT1701e.3.54	5.388	0.14	0.3415	0.0077	0.1151	0.0029	1894	37	1881	45	-1%
MIT1701e.3.55	5.36	0.2	0.3377	0.0083	0.1155	0.0036	1876	40	1887	56	1%
MIT1701e.3.56	5.39	0.14	0.3394	0.0077	0.1155	0.0029	1884	37	1887	45	0%
MIT1701e.3.57	5.62	0.15	0.3512	0.0076	0.1164	0.0032	1940	36	1901	49	-2%
MIT1701e.3.58	5.4	0.16	0.3397	0.0082	0.1155	0.0034	1885	39	1887	53	0%
MIT1701e.3.59	5.32	0.14	0.341	0.0076	0.1134	0.003	1891	37	1854	48	-2%
MIT1701e.3.60	6.12	0.18	0.3639	0.0087	0.1224	0.0041	2001	41	1991	60	-1%
MIT1701e.3.61	11.7	0.27	0.4935	0.011	0.1722	0.0038	2586	47	2578	37	0%
MIT1701e.3.62	10.84	0.42	0.453	0.014	0.1735	0.006	2409	62	2591	58	7%
MIT1701e.3.63	5.44	0.15	0.342	0.0082	0.1155	0.0031	1896	39	1887	48	0%
MIT1701e.3.64	9.01	0.28	0.3778	0.011	0.1713	0.0044	2066	51	2570	43	20%
MIT1701e.3.65	5.33	0.2	0.3338	0.0078	0.116	0.0045	1857	38	1895	70	2%
MIT1701e.3.66	5.536	0.12	0.348	0.0074	0.1154	0.0027	1925	35	1885	42	-2%

MIT1701e.3.67	5.317	0.13	0.3356	0.0081	0.1147	0.0029	1865	39	1874	46	0%
MIT1701e.3.68	6.17	0.17	0.2771	0.0064	0.161	0.004	1577	32	2465	42	36%
MIT1701e.3.69	5.722	0.13	0.3484	0.0077	0.1188	0.0029	1927	37	1937	44	1%
MIT1701e.3.70	5.56	0.16	0.3313	0.0087	0.1213	0.0032	1845	42	1975	47	7%

Sample: MIT1703e

Grain ID	*207Pb/232Th*	*207Pb/232Th prop2SE*	*206Pb/238U*	*206Pb/238U prop2SE*	*207Pb/206Pb*	*207Pb/206Pb prop2SE*	*206Pb/238Pb Age (Ma)*	*± 1σ(Ma)*	*207Pb/206Pb Age (Ma)*	*± 1σ (Ma)*	*Disc (%)*
MIT1703e.4.01	0.914	0.042	0.0504	0.0025	0.123	0.0037	317	15	1999	54	84%
MIT1703e.4.02	2.431	0.1	0.1101	0.006	0.1594	0.0029	673	35	2449	31	73%
MIT1703e.4.03	5.29	0.21	0.3074	0.014	0.1242	0.0021	1728	69	2017	30	14%
MIT1703e.4.04	1.955	0.058	0.1046	0.0041	0.1345	0.0024	641	24	2157	31	70%
MIT1703e.4.05	0.936	0.042	0.056	0.0035	0.1205	0.0037	351	21	1963	55	82%
MIT1703e.4.06	3.48	0.14	0.2041	0.011	0.1228	0.0031	1197	59	1997	45	40%
MIT1703e.4.07	2.21	0.12	0.0968	0.0063	0.1644	0.0035	596	37	2501	36	76%
MIT1703e.4.08	0.979	0.073	0.0364	0.0029	0.1661	0.0024	230	18	2518	25	91%
MIT1703e.4.09	3.95	0.25	0.244	0.015	0.1173	0.0051	1407	78	1915	78	27%
MIT1703e.4.10	3.223	0.1	0.1972	0.0091	0.1182	0.0028	1160	49	1928	43	40%
MIT1703e.4.11	10.02	0.33	0.3908	0.015	0.1734	0.0035	2127	70	2590	34	18%
MIT1703e.4.12	2.201	0.11	0.1283	0.0076	0.1238	0.0025	778	43	2011	36	61%
MIT1703e.4.13	3.52	0.2	0.2075	0.012	0.1158	0.0024	1215	64	1892	37	36%
MIT1703e.4.14	2.94	0.12	0.1857	0.0089	0.1145	0.0023	1098	48	1871	36	41%
MIT1703e.4.15	0.837	0.033	0.0525	0.0023	0.1151	0.0019	330	14	1881	30	82%
MIT1703e.4.16	4.75	0.16	0.2801	0.011	0.1224	0.0014	1592	55	1991	21	20%
MIT1703e.4.17	23.71	0.73	0.6539	0.025	0.2627	0.0051	3243	97	3262	31	1%

MIT1703e.4.18	5.29	0.2	0.332	0.016	0.1141	0.0016	1848	77	1865	25	1%
MIT1703e.4.19	3.05	0.2	0.1319	0.01	0.1683	0.0042	799	57	2540	42	69%
MIT1703e.4.20	3.43	0.22	0.1458	0.01	0.1702	0.0045	877	56	2559	44	66%
MIT1703e.4.21	4.61	0.18	0.2867	0.013	0.1166	0.0025	1625	65	1904	39	15%
MIT1703e.4.22	4.52	0.15	0.2697	0.011	0.1139	0.002	1539	56	1862	32	17%
MIT1703e.4.23	3.35	0.21	0.146	0.0089	0.1657	0.0023	879	50	2514	24	65%
MIT1703e.4.24	2.845	0.1	0.1182	0.0051	0.1741	0.0035	720	29	2597	34	72%
MIT1703e.4.25	1.383	0.087	0.0841	0.0053	0.1193	0.0034	521	32	1945	51	73%
MIT1703e.4.26	3.31	0.16	0.1961	0.0093	0.1223	0.0022	1154	50	1989	32	42%
MIT1703e.4.27	2.271	0.086	0.1064	0.0047	0.155	0.0013	652	27	2401	15	73%
MIT1703e.4.28	2.174	0.11	0.1326	0.0083	0.1196	0.0023	803	47	1949	34	59%
MIT1703e.4.29	10.88	0.37	0.468	0.02	0.1697	0.0033	2475	88	2554	33	3%
MIT1703e.4.30	1.981	0.095	0.1162	0.0065	0.1179	0.0034	709	38	1924	52	63%
MIT1703e.4.31	4.41	0.2	0.273	0.015	0.1178	0.0014	1556	76	1922	22	19%
MIT1703e.4.32	3.67	0.16	0.2028	0.0083	0.1236	0.0024	1190	44	2008	35	41%
MIT1703e.4.33	1.664	0.066	0.0815	0.0037	0.1486	0.0025	505	22	2329	29	78%
MIT1703e.4.34	4.49	0.18	0.2608	0.012	0.1251	0.0023	1494	61	2029	33	26%
MIT1703e.4.35	1.055	0.052	0.0517	0.003	0.1386	0.0022	325	18	2209	28	85%
MIT1703e.4.36	0.77	0.028	0.0446	0.002	0.1257	0.002	281	12	2038	28	86%
MIT1703e.4.37	2.238	0.091	0.1296	0.0068	0.1259	0.0026	786	39	2041	37	61%
MIT1703e.4.38	9.21	0.32	0.3017	0.014	0.2225	0.0022	1700	69	2998	16	43%
MIT1703e.4.39	3.544	0.11	0.2017	0.0088	0.1199	0.003	1184	47	1954	45	39%
MIT1703e.4.40	6.16	0.2	0.2618	0.01	0.1368	0.0034	1499	51	2186	43	31%
MIT1703e.4.41	1.883	0.056	0.0878	0.0034	0.1556	0.0024	543	20	2408	26	77%
MIT1703e.4.42	5.43	0.17	0.343	0.014	0.1153	0.0024	1901	67	1884	38	-1%

MIT1703e.4.43	11.37	0.35	0.475	0.019	0.1741	0.0028	2505	83	2597	27	4%
MIT1703e.4.44	2.586	0.11	0.1486	0.0083	0.1268	0.0032	893	47	2053	45	57%
MIT1703e.4.45	1.754	0.052	0.0905	0.0037	0.1405	0.0015	558	22	2233	19	75%
MIT1703e.4.46	5.04	0.2	0.3148	0.015	0.1164	0.0017	1764	74	1901	26	7%
MIT1703e.4.47	5.89	0.25	0.2559	0.013	0.1661	0.002	1469	67	2518	20	42%
MIT1703e.4.48	5.59	0.28	0.3472	0.015	0.116	0.0049	1921	72	1895	76	-1%
MIT1703e.4.49	2.52	0.12	0.1427	0.0078	0.1192	0.0026	860	44	1943	39	56%
MIT1703e.4.50	2.474	0.099	0.1568	0.0076	0.1135	0.0017	939	42	1855	27	49%
MIT1703e.4.51	1.728	0.08	0.0977	0.0051	0.1278	0.0022	601	30	2067	30	71%
MIT1703e.4.52	0.27	0.012	0.01453	0.00075	0.1341	0.0027	93	4.8	2152	35	96%
MIT1703e.4.53	0.99	0.04	0.0613	0.0028	0.1162	0.0016	384	17	1898	25	80%
MIT1703e.4.54	1.599	0.052	0.0803	0.0033	0.1431	0.0016	498	20	2264	20	78%
MIT1703e.4.55	1.228	0.062	0.0592	0.003	0.1487	0.0033	371	18	2330	38	84%
MIT1703e.4.56	1.363	0.083	0.0833	0.0057	0.1178	0.0012	516	34	1922	18	73%
MIT1703e.4.57	0.352	0.014	0.01934	0.001	0.1304	0.0023	123.5	6.3	2103	31	94%
MIT1703e.4.58	5.39	0.15	0.3388	0.013	0.1143	0.002	1881	63	1868	32	-1%
MIT1703e.4.59	2.862	0.12	0.1453	0.0069	0.1408	0.002	875	39	2236	25	61%
MIT1703e.4.60	6.07	0.22	0.2601	0.012	0.1674	0.0024	1490	61	2531	24	41%
MIT1703e.4.61	0.817	0.034	0.0501	0.0025	0.1164	0.002	315	15	1901	31	83%
MIT1703e.4.62	1.567	0.062	0.0729	0.0033	0.1536	0.0021	454	20	2386	24	81%
MIT1703e.4.63	6.72	0.3	0.279	0.014	0.1718	0.0024	1586	71	2575	24	38%
MIT1703e.4.64	6.08	0.18	0.3598	0.014	0.1207	0.0022	1981	66	1966	33	-1%
MIT1703e.4.65	2.88	0.17	0.178	0.014	0.1163	0.0034	1056	77	1899	53	44%
MIT1703e.4.66	4.78	0.16	0.2951	0.012	0.1158	0.0013	1667	60	1892	20	12%
MIT1703e.4.67	3.155	0.12	0.178	0.0081	0.1268	0.0025	1056	44	2053	35	49%

MIT1703e.4.68	2.58	0.15	0.1439	0.0094	0.1194	0.0029	867	53	1946	44	55%
MIT1703e.4.69	7	0.3	0.288	0.013	0.1733	0.005	1632	65	2589	48	37%
MIT1703e.4.70	10.85	0.39	0.469	0.019	0.1656	0.0031	2479	83	2513	32	1%
MIT1703e.4.71	5.15	0.22	0.318	0.017	0.1161	0.0028	1780	83	1896	43	6%
MIT1703e.4.72	2.317	0.096	0.136	0.0056	0.1215	0.0036	822	32	1978	53	58%
MIT1703e.4.73	4.06	0.19	0.2544	0.013	0.1144	0.0024	1461	67	1870	38	22%
MIT1703e.4.74	6.07	0.24	0.3577	0.016	0.1214	0.0039	1971	76	1976	57	0%
MIT1703e.4.75	7.3	0.29	0.3083	0.014	0.1699	0.0026	1732	69	2556	26	32%
MIT1703e.4.76	1.854	0.078	0.1084	0.005	0.1157	0.0015	663	29	1890	24	65%
MIT1703e.4.77	1.976	0.11	0.0858	0.006	0.1663	0.0035	531	36	2520	36	79%
MIT1703e.4.78	5.23	0.18	0.3318	0.013	0.1134	0.0029	1847	63	1854	46	0%
MIT1703e.4.79	5.47	0.16	0.3468	0.013	0.1137	0.0026	1919	62	1859	41	-3%
MIT1703e.4.80	10.23	0.32	0.4603	0.019	0.1599	0.0016	2441	84	2454	17	1%
MIT1703e.4.81	5.56	0.19	0.3483	0.014	0.115	0.0024	1926	67	1879	38	-3%
MIT1703e.4.82	2.76	0.16	0.1681	0.011	0.1187	0.002	1002	61	1936	30	48%
MIT1703e.4.83	12.03	0.46	0.493	0.022	0.1759	0.0029	2584	95	2614	28	1%
MIT1703e.4.84	1.574	0.056	0.0947	0.004	0.1199	0.0022	583	24	1954	33	70%
MIT1703e.4.85	5.37	0.17	0.3367	0.013	0.1155	0.0016	1871	63	1887	25	1%
MIT1703e.4.86	0.769	0.042	0.0459	0.0025	0.1213	0.0022	289	15	1975	32	85%
MIT1703e.4.87	4.83	0.19	0.2144	0.009	0.1634	0.003	1252	48	2490	31	50%
MIT1703e.4.88	0.514	0.019	0.02978	0.0012	0.1254	0.0023	189.2	7.5	2034	33	91%
MIT1703e.4.89	1.214	0.068	0.0588	0.0035	0.15	0.0024	368	21	2345	28	84%
MIT1703e.4.90	5.09	0.89	0.217	0.037	0.1691	0.0024	1270	200	2548	24	50%
MIT1703e.4.91	1.463	0.054	0.0752	0.0034	0.1424	0.0026	467	20	2256	32	79%
MIT1703e.4.92	0.738	0.041	0.046	0.0025	0.1179	0.0023	290	15	1924	35	85%

MIT1703e.4.93	1.094	0.052	0.0697	0.0036	0.1149	0.0032	434	22	1878	50	77%
MIT1703e.4.94	1.104	0.053	0.0689	0.0037	0.1179	0.003	430	22	1924	46	78%
MIT1703e.4.95	5.07	0.22	0.3276	0.013	0.1139	0.0041	1827	63	1862	65	2%
MIT1703e.4.96	5.46	0.19	0.3403	0.014	0.118	0.0024	1888	67	1925	37	2%
MIT1703e.4.97	5.37	0.22	0.2257	0.01	0.1746	0.0035	1312	53	2601	34	50%
MIT1703e.4.98	1.448	0.067	0.0696	0.0036	0.153	0.0018	434	22	2379	20	82%
MIT1703e.4.99	5.86	0.2	0.2677	0.011	0.1612	0.0017	1529	56	2468	18	38%
MIT1703e.4.100	1.414	0.052	0.0855	0.0043	0.1156	0.0023	529	26	1888	36	72%
MIT1703e.4.101	5.855	0.17	0.3545	0.014	0.122	0.0015	1956	67	1985	22	1%
MIT1703e.4.102	10.64	0.27	0.4728	0.018	0.1666	0.0014	2496	79	2523	14	1%
MIT1703e.4.103	2.128	0.066	0.0964	0.0038	0.163	0.0021	593	22	2486	22	76%
MIT1703e.4.104	4.35	0.14	0.2727	0.011	0.1182	0.0022	1554	56	1928	33	19%
MIT1703e.4.105	17.98	0.75	0.566	0.028	0.234	0.004	2890	120	3079	28	6%
MIT1703e.4.106	7.33	0.25	0.477	0.021	0.1136	0.0013	2514	92	1857	21	-35%
MIT1703e.4.107	3.42	0.18	0.2161	0.012	0.1169	0.0035	1261	64	1909	54	34%
MIT1703e.4.108	10.89	0.46	0.466	0.022	0.1722	0.0035	2466	97	2578	34	4%
MIT1703e.4.109	0.579	0.021	0.03503	0.0015	0.1233	0.0016	222	9.3	2004	23	89%
MIT1703e.4.110	1.135	0.059	0.0711	0.0052	0.1188	0.0039	443	31	1937	59	77%
MIT1703e.4.111	0.815	0.047	0.0537	0.0038	0.1128	0.0019	337	23	1844	31	82%
MIT1703e.4.112	9.95	0.33	0.4226	0.018	0.1742	0.0031	2272	82	2598	30	13%
MIT1703e.4.113	0.698	0.024	0.04033	0.0016	0.1279	0.0024	254.9	9.9	2069	33	88%
MIT1703e.4.114	1.36	0.052	0.0824	0.0036	0.122	0.002	510	21	1985	29	74%
MIT1703e.4.115	4.76	0.14	0.3005	0.013	0.117	0.0016	1694	64	1910	25	11%
MIT1703e.4.116	1.919	0.075	0.0959	0.0047	0.1476	0.0017	590	28	2318	20	75%
MIT1703e.4.117	5.13	0.16	0.3314	0.013	0.114	0.002	1845	63	1863	32	1%

MIT1703e.4.118	3.5	0.13	0.1498	0.0068	0.1725	0.0016	900	38	2581	16	65%
MIT1703e.4.119	5.265	0.16	0.3354	0.013	0.1154	0.0018	1865	63	1885	28	1%
MIT1703e.4.120	5.48	0.21	0.3393	0.014	0.1184	0.0023	1883	67	1931	35	2%
MIT1703e.4.121	4.986	0.14	0.3148	0.012	0.1162	0.0014	1764	59	1898	22	7%
MIT1703e.4.122	1.995	0.096	0.1187	0.0058	0.115	0.0026	723	33	1879	41	62%
MIT1703e.4.123	1.837	0.091	0.1111	0.0049	0.1206	0.0028	679	28	1964	42	65%
MIT1703e.4.124	0.2228	0.0078	0.01191	0.00055	0.1368	0.0028	76.3	3.5	2186	36	97%
MIT1703e.4.125	0.344	0.02	0.01592	0.0011	0.1343	0.0031	101.8	7	2154	40	95%
MIT1703e.4.126	11.61	0.36	0.488	0.019	0.174	0.0026	2562	82	2596	25	1%
MIT1703e.4.127	5.2	0.19	0.3291	0.013	0.1152	0.0029	1834	63	1882	45	3%
MIT1703e.4.128	11.16	0.47	0.476	0.022	0.1707	0.0049	2510	96	2564	48	2%
MIT1703e.4.129	0.977	0.037	0.0571	0.0026	0.1243	0.0017	358	16	2018	24	82%
MIT1703e.4.130	12.17	0.47	0.4612	0.019	0.1914	0.003	2445	84	2753	26	11%
MIT1703e.4.131	1.713	0.084	0.1124	0.0058	0.1108	0.0024	687	34	1812	39	62%
MIT1703e.4.132	9.28	0.3	0.3958	0.016	0.1699	0.0022	2150	74	2556	22	16%
MIT1703e.4.133	2.223	0.088	0.1213	0.0054	0.1326	0.0029	738	31	2132	38	65%
MIT1703e.4.134	5.11	0.22	0.2159	0.011	0.1718	0.0023	1260	58	2575	23	51%
MIT1703e.4.135	5.45	0.2	0.3404	0.014	0.1149	0.0027	1889	67	1878	42	-1%
MIT1703e.4.136	4.95	0.16	0.2881	0.012	0.1166	0.0017	1632	60	1904	26	14%
MIT1703e.4.137	1.07	0.053	0.0648	0.0036	0.1189	0.0024	405	22	1939	36	79%
MIT1703e.4.138	0.593	0.027	0.0339	0.0019	0.1259	0.0028	215	12	2041	39	89%
MIT1703e.4.139	11.1	0.49	0.431	0.019	0.1849	0.0056	2310	86	2697	50	14%
MIT1703e.4.140	4.118	0.13	0.2525	0.01	0.1168	0.0014	1451	51	1907	22	24%
MIT1703e.4.141	1.803	0.094	0.1094	0.0056	0.118	0.0031	669	33	1925	47	65%
MIT1703e.4.142	1.196	0.047	0.068	0.0037	0.1261	0.0025	424	22	2044	35	79%

Table 4: Lu-Hf data generated for this study.

Sample: BAL1701A

Grain ID	*207Pb/206Pb Age (Ma)*	*± 1σ (Ma)*	*Disc (%)*	*176Hf/177Hf*	*± 1SE(abs)*	*176Lu/177Hf*	*176Yb/177Hf*	*εHf (t)*	*εHf ± 1SE*	*TDM Crustal (Ga)*
BAL1701a.1.01	1780	64	3%	0.281584	0.000057	0.0003793	0.01342	-3.31	2.00	2.65
BAL1701a.1.02	1876	27	-49%	0.281503	0.000073	0.001679	0.0682	-5.67	2.56	2.88
BAL1701a.1.03	1774	46	-27%	0.281629	0.000058	0.000752	0.0313	-2.29	2.03	2.58
BAL1701a.1.04	1770	30	-25%	0.281594	0.000072	0.00151	0.0636	-4.52	2.52	2.72
BAL1701a.1.05	1757	31	1%	0.281734	0.000053	0.0008323	0.03164	0.97	1.86	2.36
BAL1701a.1.06	1757	24	0%	0.281625	0.000047	0.000664	0.0251	-2.71	1.65	2.60
BAL1701a.1.07	1916	31	-84%	0.281447	0.000086	0.004732	0.2198	-10.74	3.01	3.23
BAL1701a.1.08	1892	25	-48%	0.281521	0.000059	0.001446	0.0628	-4.39	2.07	2.81
BAL1701a.1.09	1813	26	-62%	0.281564	0.000067	0.002574	0.1116	-5.96	2.35	2.85
BAL1701a.1.10	1866	29	-35%	0.281545	0.000054	0.00189	0.0779	-4.66	1.89	2.80
BAL1701a.1.11	1765	42	-60%	0.281567	0.000059	0.00129	0.0545	-5.33	2.07	2.77
BAL1701a.1.12	1879	28	-52%	0.281449	0.000061	0.00186	0.0819	-7.75	2.14	3.01
BAL1701a.1.13	1836	34	-7%	0.281546	0.000056	0.000739	0.02806	-3.84	1.96	2.73
BAL1701a.1.14	1802	33	-58%	0.281437	0.000057	0.00277	0.1192	-10.93	2.00	3.15
BAL1701a.1.15	1885	25	-29%	0.281451	0.000072	0.000893	0.0354	-6.32	2.52	2.92
BAL1701a.1.16	1871	24	-44%	0.281553	0.000063	0.00181	0.078	-4.17	2.21	2.78
BAL1701a.1.17	1885	31	-69%	0.281471	0.000067	0.00319	0.147	-8.53	2.35	3.06
BAL1701a.1.18	1874	49	-52%	0.281532	0.000067	0.00221	0.0925	-5.35	2.35	2.85
BAL1701a.1.19	1605	32	-51%	0.281687	0.000053	0.00187	0.0743	-5.18	1.86	2.64
BAL1701a.1.20	1792	63	-2%	0.281581	0.000055	0.0003948	0.01404	-3.16	1.93	2.65

BAL1701a.1.21	1934	30	-37%	0.28151	0.000063	0.00145	0.061	-3.87	2.21	2.81
BAL1701a.1.22	1810	23	-1%	0.281659	0.000057	0.001076	0.0411	-0.82	2.00	2.52
BAL1701a.1.23	1805	58	2%	0.281554	0.000044	0.00212	0.093	-5.93	1.54	2.84
BAL1701a.1.24	1957	33	-73%	0.281492	0.000057	0.00251	0.11	-5.41	2.00	2.92
BAL1701a.1.25	1873	25	-73%	0.281493	0.00006	0.00252	0.109	-7.15	2.10	2.97
BAL1701a.1.26	1812	25	-73%	0.281487	0.000056	0.00298	0.131	-9.21	1.96	3.05
BAL1701a.1.27	1807	36	1%	0.281706	0.000055	0.001026	0.0405	0.84	1.93	2.41
BAL1701a.1.28	1893	23	-61%	0.281501	0.000058	0.00209	0.0896	-5.90	2.03	2.90
BAL1701a.1.29	1808	43	-57%	0.281621	0.000078	0.00147	0.0633	-2.69	2.73	2.63
BAL1701a.1.30	1870	27	2%	0.281489	0.000044	0.000456	0.01623	-4.75	1.54	2.81
BAL1701a.1.31	1814	23	-2%	0.281675	0.000045	0.000974	0.03768	-0.04	1.58	2.47
BAL1701a.1.32	1960	25	-59%	0.281517	0.000064	0.00254	0.11	-4.49	2.24	2.87
BAL1701a.1.33	1836	24	-58%	0.281545	0.000057	0.002683	0.1136	-6.28	2.00	2.88
BAL1701a.4.01	1746	43	-16%	0.281423	0.000035	0.000937	0.0312	-10.44	1.23	3.08
BAL1701a.4.02	1881	36	1%	0.281583	0.000043	0.0008629	0.026993	-1.69	1.51	2.63
BAL1701a.4.03	1767	31	0%	0.281575	0.000032	0.0004859	0.01602	-4.05	1.12	2.69
BAL1701a.4.04	1910	29	-18%	0.281553	0.000042	0.000709	0.02292	-1.91	1.47	2.66
BAL1701a.4.05	1828	31	-36%	0.281611	0.000038	0.00002065	0.00086	-0.83	1.33	2.53
BAL1701a.4.06	1782	40	-31%	0.281575	0.000038	0.001295	0.04486	-4.68	1.33	2.74
BAL1701a.4.07	1822	60	-3%	0.281521	0.000048	0.000465	0.01489	-4.71	1.68	2.77
BAL1701a.4.08	1843	35	-3%	0.28165	0.000035	0.001382	0.0479	-0.79	1.23	2.54
BAL1701a.4.09	1849	38	-47%	0.281597	0.000033	0.0004716	0.01524	-1.41	1.16	2.58
BAL1701a.4.10	1839	26	1%	0.281505	0.000049	0.00423	0.162	-9.56	1.72	3.09
BAL1701a.4.11	1860	43	-3%	0.281396	0.000038	0.00549	0.207	-14.59	1.33	3.43
BAL1701a.4.12	1839	36	-25%	0.281579	0.000045	0.001056	0.0355	-3.00	1.58	2.68
BAL1701a.4.13	1763	49	1%	0.281631	0.000039	0.0009	0.0296	-2.64	1.37	2.60
BAL1701a.4.14	1870	41	0%	0.281437	0.000034	0.0007268	0.022812	-6.94	1.19	2.95
BAL1701a.4.15	2525	20	-43%	0.281178	0.000042	0.00181	0.066	-3.32	1.47	3.23
BAL1701a.4.16	1983	29	-69%	0.281534	0.000052	0.0008165	0.02441	-1.10	1.82	2.67
BAL1701a.4.17	1879	30	4%	0.281422	0.000044	0.0003965	0.01221	-6.86	1.54	2.95

BAL1701a.4.18	1876	28	-1%	0.281411	0.000062	0.000427	0.0143	-7.35	2.17	2.98
BAL1701a.4.19	2386	24	-1%	0.281233	0.000033	0.0003345	0.00982	-2.01	1.16	3.04
BAL1701a.4.20	1851	29	-64%	0.281516	0.000045	0.00416	0.1515	-8.84	1.58	3.06
BAL1701a.4.21	1807	38	-1%	0.281694	0.000046	0.001266	0.041	0.13	1.61	2.45
BAL1701a.4.22	1849	46	-8%	0.281525	0.000043	0.000758	0.02495	-4.32	1.51	2.77
BAL1701a.4.23	1907	42	0%	0.281424	0.000051	0.00091	0.02759	-6.82	1.79	2.97
BAL1701a.4.24	1852	56	-1%	0.281612	0.000046	0.000946	0.02882	-1.40	1.61	2.59
BAL1701a.4.25	1910	25	-36%	0.281502	0.000048	0.002247	0.0792	-5.70	1.68	2.90
BAL1701a.4.26	1876	30	-7%	0.281636	0.000043	0.000652	0.02148	0.35	1.51	2.49
BAL1701a.4.27	1870	30	4%	0.281576	0.000039	0.0006435	0.01989	-1.90	1.37	2.63
BAL1701a.4.28	1942	42	-81%	0.281377	0.000059	0.00689	0.2603	-15.54	2.07	3.55
BAL1701a.4.29	1770	52	-33%	0.281684	0.000034	0.00147	0.0511	-1.28	1.19	2.52
BAL1701a.4.30	1887	27	1%	0.281559	0.000038	0.0010841	0.033497	-2.69	1.33	2.70
BAL1701a.4.31	1878	32	-49%	0.281517	0.00004	0.001985	0.074	-5.52	1.40	2.87
BAL1701a.4.32	1862	43	-9%	0.281609	0.000037	0.000691	0.0228	-0.97	1.30	2.57
BAL1701a.4.33	1779	39	0%	0.281568	0.000041	0.0005852	0.01887	-4.14	1.44	2.70
BAL1701a.4.34	1762	46	0%	0.28162	0.000039	0.000493	0.0157	-2.57	1.37	2.59
BAL1701a.4.35	1946	26	-64%	0.281388	0.000064	0.0029	0.109	-9.84	2.24	3.19
BAL1701a.4.36	2561	24	-40%	0.281074	0.000062	0.001529	0.0575	-5.75	2.17	3.41
BAL1701a.4.37	1874	33	-48%	0.281598	0.000046	0.00262	0.0975	-3.53	1.61	2.74
BAL1701a.4.38	1822	33	-6%	0.281633	0.000048	0.0007051	0.02228	-1.02	1.68	2.54
BAL1701a.4.39	1789	38	1%	0.281667	0.000031	0.000694	0.02256	-0.54	1.09	2.48
BAL1701a.4.40	1807	30	0%	0.281668	0.000041	0.001332	0.04265	-0.88	1.44	2.52
BAL1701a.4.41	1851	46	2%	0.281518	0.000033	0.0006908	0.021657	-4.44	1.16	2.78
BAL1701a.4.42	1916	34	-44%	0.281532	0.00005	0.002052	0.0749	-4.26	1.75	2.82
BAL1701a.4.43	3015	25	-79%	0.280632	0.000052	0.0031	0.119	-14.67	1.82	4.32
BAL1701a.4.44	1774	37	0%	0.281679	0.000045	0.001081	0.0366	-0.91	1.58	2.49
BAL1701a.4.45	1748	75	0%	0.281568	0.000035	0.000571	0.01866	-4.82	1.23	2.72
BAL1701a.4.46	1797	27	2%	0.281654	0.000042	0.0008363	0.02769	-0.99	1.47	2.52
BAL1701a.4.47	1955	20	2%	0.281413	0.00004	0.000677	0.01785	-5.84	1.40	2.95
BAL1701a.4.48	2720	40	-67%	0.281127	0.000069	0.00349	0.1275	-3.98	2.42	3.42

BAL1701a.4.49	1954	43	-18%	0.281633	0.000045	0.001879	0.06075	0.37	1.58	2.55
BAL1701a.4.50	1797	58	-12%	0.281678	0.000044	0.001069	0.03635	-0.42	1.54	2.48
BAL1701a.4.51	1928	20	0%	0.281535	0.000042	0.00014997	0.005054	-1.42	1.47	2.65
BAL1701a.4.52	1885	28	1%	0.281538	0.000049	0.000533	0.01745	-2.78	1.72	2.70
BAL1701a.4.53	1799	40	-14%	0.281697	0.00003	0.001075	0.036	0.29	1.05	2.44
BAL1701a.4.54	1736	28	4%	0.281559	0.000037	0.0004459	0.01424	-5.26	1.30	2.74
BAL1701a.4.55	1843	64	0%	0.281674	0.000045	0.000707	0.02297	0.90	1.58	2.43
BAL1701a.4.56	1892	19	-3%	0.281558	0.000046	0.00188	0.0604	-3.63	1.61	2.76
BAL1701a.4.57	1775	74	-8%	0.281567	0.00004	0.000879	0.02825	-4.62	1.40	2.73
BAL1701a.4.58	1918	54	-1%	0.281651	0.000042	0.000675	0.02137	1.79	1.47	2.43
BAL1701a.4.59	1874	30	1%	0.281544	0.000037	0.000499	0.0151	-2.77	1.30	2.69
BAL1701a.4.60	1957	28	-9%	0.281638	0.000029	0.001241	0.039	1.46	1.02	2.49
BAL1701a.4.61	1826	55	-2%	0.281542	0.00004	0.000429	0.0143	-3.83	1.40	2.72
BAL1701a.4.62	1828	63	-1%	0.281559	0.000054	0.0017	0.0577	-4.74	1.89	2.78
BAL1701a.4.63	1895	53	-1%	0.28137	0.000042	0.0005601	0.01693	-8.55	1.47	3.07
BAL1701a.4.64	1874	36	-1%	0.281486	0.000042	0.001163	0.0369	-5.66	1.47	2.87
BAL1701a.4.65	1916	25	-64%	0.281489	0.000054	0.002346	0.0823	-6.16	1.89	2.94
BAL1701a.4.66	1888	79	2%	0.281542	0.00004	0.0006021	0.01807	-2.65	1.40	2.69
BAL1701a.4.67	1915	29	2%	0.281514	0.00004	0.000604	0.01808	-3.05	1.40	2.74
BAL1701a.4.68	1874	38	0%	0.281591	0.000032	0.000559	0.01621	-1.17	1.12	2.59
BAL1701a.4.69	1899	39	-1%	0.281546	0.000045	0.00075	0.02115	-2.46	1.58	2.69
BAL1701a.4.70	1874	33	0%	0.281517	0.000027	0.000508	0.01471	-3.74	0.95	2.75
BAL1701a.4.71	2423	67	1%	0.281707	0.000036	0.00108	0.0324	14.46	1.26	2.01
BAL1701a.4.72	1804	81	-1%	0.281563	0.000038	0.000567	0.01632	-3.74	1.33	2.70
BAL1701a.4.73	1879	27	-1%	0.281564	0.000036	0.0006157	0.01763	-2.09	1.26	2.65
BAL1701a.4.74	1925	43	-62%	0.281472	0.000047	0.003176	0.1066	-7.65	1.65	3.04
BAL1701a.4.75	2719	21	-14%	0.281022	0.000048	0.000967	0.0273	-3.07	1.68	3.36
BAL1701a.4.76	1797	75	-56%	0.281511	0.000044	0.00289	0.0987	-8.56	1.54	3.00
BAL1701a.4.77	1881	17	7%	0.281602	0.000053	0.001086	0.03158	-1.29	1.86	2.60
BAL1701a.4.78	1774	42	-41%	0.281566	0.000041	0.001927	0.0572	-5.93	1.44	2.81
BAL1701a.4.79	1892	39	-32%	0.281503	0.000046	0.001967	0.0627	-5.69	1.61	2.89

BAL1701a.4.80	1810	38	-6%	0.281571	0.000029	0.001452	0.044	-4.40	1.02	2.74
BAL1701a.4.81	1921	58	0%	0.281534	0.000033	0.0006452	0.01829	-2.26	1.16	2.69
BAL1701a.4.82	1804	31	-1%	0.28169	0.000034	0.001424	0.04184	-0.27	1.19	2.48
BAL1701a.4.83	1800	38	0%	0.281648	0.000037	0.0007214	0.02035	-1.00	1.30	2.52
BAL1701a.4.84	2697	31	-85%	0.280616	0.000059	0.0089	0.3006	-32.57	2.07	5.19
BAL1701a.4.85	1863	30	-2%	0.281593	0.000068	0.001131	0.0281	-2.07	2.38	2.64
BAL1701a.4.86	1915	37	0%	0.281487	0.000037	0.00079	0.0223	-4.25	1.30	2.82

Sample: BAL1701B

Grain ID	*207Pb/206Pb Age (Ma)*	*± 1σ (Ma)*	*Disc (%)*	*176Hf/177Hf*	*± 1SE(abs)*	*176Lu/177Hf*	*176Yb/177Hf*	*εHf (t)*	*εHf ± 1SE*	*TDM Crustal (Ga)*
BAL1701b.4.01	1760	75	69%	0.281656	0.000066	0.00397	0.161	-5.45	2.31	2.77
BAL1701b.4.02	1765	37	1%	0.281738	0.000041	0.00118	0.0392	0.87	1.44	2.37
BAL1701b.4.03	1794	30	60%	0.281627	0.000043	0.001953	0.0773	-3.37	1.51	2.67
BAL1701b.4.04	1782	47	-2%	0.281628	0.000038	0.0005836	0.01887	-1.95	1.33	2.57
BAL1701b.4.05	1763	41	3%	0.281683	0.000043	0.001439	0.0491	-1.43	1.51	2.52
BAL1701b.4.06	1774	32	10%	0.281628	0.000036	0.00155	0.0594	-3.28	1.26	2.65
BAL1701b.4.07	1790	33	-1%	0.281677	0.00004	0.000649	0.0218	-0.11	1.40	2.46
BAL1701b.4.08	1774	37	-2%	0.28167	0.000049	0.000871	0.0277	-0.98	1.72	2.50
BAL1701b.4.09	1748	38	0%	0.281693	0.000043	0.00197	0.0699	-2.03	1.51	2.55
BAL1701b.4.10	1787	30	-1%	0.28168	0.000042	0.0009937	0.03169	-0.48	1.47	2.48
BAL1701b.4.11	1794	28	-1%	0.281662	0.000043	0.001335	0.044	-1.38	1.51	2.54
BAL1701b.4.12	1765	58	1%	0.281663	0.000045	0.00176	0.062	-2.48	1.58	2.59
BAL1701b.4.13	1777	32	-1%	0.281667	0.000041	0.001417	0.04609	-1.67	1.44	2.55
BAL1701b.4.14	1780	37	44%	0.281637	0.000044	0.00237	0.086	-3.81	1.54	2.68
BAL1701b.4.15	1753	36	11%	0.281674	0.000034	0.0016	0.0553	-2.16	1.19	2.56
BAL1701b.4.16	1844	35	60%	0.281647	0.000044	0.003656	0.1267	-3.70	1.54	2.73
BAL1701b.4.17	1797	33	-3%	0.281671	0.000043	0.000889	0.0274	-0.45	1.51	2.48
BAL1701b.4.18	1808	25	29%	0.281629	0.000031	0.001358	0.0432	-2.27	1.09	2.61
BAL1701b.4.19	1780	32	-1%	0.281693	0.000043	0.001526	0.0476	-0.81	1.51	2.49
BAL1701b.4.20	1807	38	44%	0.28169	0.000039	0.001068	0.03368	0.22	1.37	2.45

BAL1701b.4.21	1775	37	-3%	0.281699	0.00003	0.001371	0.042	-0.52	1.05	2.47
BAL1701b.4.22	1770	36	16%	0.28167	0.000038	0.00143	0.0443	-1.73	1.33	2.54
BAL1701b.4.23	1770	41	10%	0.281684	0.000041	0.000997	0.0309	-0.72	1.44	2.48
BAL1701b.4.24	1772	46	2%	0.281674	0.000036	0.000749	0.02218	-0.73	1.26	2.48
BAL1701b.4.25	1782	35	-1%	0.281679	0.000044	0.001356	0.0418	-1.06	1.54	2.51
BAL1701b.4.26	1774	30	0%	0.281654	0.000038	0.00095	0.0286	-1.64	1.33	2.54
BAL1701b.4.27	1785	35	1%	0.281711	0.000035	0.000996	0.0301	0.57	1.23	2.41
BAL1701b.4.28	1762	49	-2%	0.281697	0.000041	0.000955	0.0293	-0.38	1.44	2.45
BAL1701b.4.29	1763	32	8%	0.281706	0.000036	0.001625	0.0526	-0.84	1.26	2.48
BAL1701b.4.30	1758	43	-2%	0.281649	0.000041	0.000834	0.02522	-2.03	1.44	2.55
BAL1701b.4.31	1774	34	8%	0.281703	0.000035	0.001259	0.0396	-0.27	1.23	2.45
BAL1701b.4.32	1767	31	1%	0.281749	0.000033	0.002105	0.06398	0.21	1.16	2.42
BAL1701b.4.33	1765	24	2%	0.281737	0.000046	0.001508	0.04745	0.45	1.61	2.40

Sample: BAL1703A

Grain ID	*207Pb/206Pb Age (Ma)*	*± 1σ (Ma)*	*Disc (%)*	*176Hf/177Hf*	*± 1SE(abs)*	*176Lu/177Hf*	*176Yb/177Hf*	*εHf (t)*	*εHf ± 1SE*	*TDM Crustal (Ga)*
BAL1703a.4.01	1954	25	44%	0.281563	0.000039	0.001767	0.0641	-1.97	1.37	2.70
BAL1703a.4.02	1636	26	39%	0.281668	0.000042	0.0009479	0.03133	-4.18	1.47	2.60
BAL1703a.4.03	1715	23	12%	0.28165	0.000051	0.001083	0.03645	-3.24	1.79	2.60
BAL1703a.4.04	1851	30	65%	0.281672	0.000043	0.001004	0.03467	0.63	1.51	2.46
BAL1703a.4.05	1839	34	33%	0.281652	0.00004	0.001109	0.0393	-0.47	1.40	2.52
BAL1703a.4.06	1784	17	27%	0.281614	0.000047	0.001191	0.03961	-3.13	1.65	2.64
BAL1703a.4.07	1752	33	75%	0.281634	0.000039	0.001791	0.0625	-3.83	1.37	2.66
BAL1703a.4.08	1763	24	1%	0.281637	0.000044	0.000672	0.0212	-2.16	1.54	2.57
BAL1703a.4.09	1841	47	10%	0.281497	0.000045	0.00093	0.03486	-5.71	1.58	2.85
BAL1703a.4.10	1733	24	-4%	0.281666	0.000044	0.0007116	0.02295	-1.84	1.54	2.52
BAL1703a.4.11	1931	39	21%	0.281449	0.000034	0.00089	0.0344	-5.37	1.19	2.90
BAL1703a.4.12	1807	28	8%	0.281623	0.000052	0.000712	0.02333	-1.72	1.82	2.57
BAL1703a.4.13	2268	23	14%	0.281327	0.000094	0.000754	0.0266	-2.00	3.29	2.95
BAL1703a.4.14	2225	46	22%	0.281691	0.000042	0.000798	0.02408	9.91	1.47	2.15

BAL1703a.4.15	1892	39	25%	0.281566	0.000049	0.00178	0.0644	-3.21	1.72	2.73
BAL1703a.4.16	1919	44	47%	0.281654	0.000041	0.00203	0.0702	0.17	1.44	2.54
BAL1703a.4.17	1780	30	-3%	0.281662	0.000033	0.0007609	0.02581	-1.00	1.16	2.50
BAL1703a.4.18	1758	37	1%	0.281609	0.000043	0.000793	0.0251	-3.40	1.51	2.64
BAL1703a.4.19	1836	26	57%	0.281551	0.000056	0.0008639	0.026779	-3.82	1.96	2.73
BAL1703a.4.20	2142	30	-1%	0.281303	0.000042	0.000349	0.01011	-5.08	1.47	3.04
BAL1703a.4.21	1804	33	1%	0.281696	0.000036	0.001057	0.0364	0.38	1.26	2.44
BAL1703a.4.22	2554	27	18%	0.281052	0.00003	0.000714	0.02341	-5.27	1.05	3.37
BAL1703a.4.23	1854	72	86%	0.281503	0.000047	0.00803	0.327	-14.08	1.65	3.39
BAL1703a.4.24	1882	28	-5%	0.281648	0.000037	0.000551	0.01823	1.04	1.30	2.45
BAL1703a.4.25	1874	22	0%	0.281576	0.000036	0.0006291	0.01993	-1.79	1.26	2.63
BAL1703a.4.26	1813	36	24%	0.281697	0.000044	0.001258	0.04015	0.37	1.54	2.44
BAL1703a.4.27	1919	44	11%	0.281541	0.00004	0.0005308	0.01748	-1.90	1.40	2.67
BAL1703a.4.28	2221	34	79%	0.281558	0.00005	0.00478	0.1895	-0.89	1.75	2.84
BAL1703a.4.29	1815	48	19%	0.281713	0.000053	0.001635	0.0541	0.52	1.86	2.44
BAL1703a.4.30	1772	30	-1%	0.281672	0.000039	0.000679	0.02238	-0.72	1.37	2.48
BAL1703a.4.31	1775	25	0%	0.281635	0.000038	0.0006401	0.020199	-1.92	1.33	2.56
BAL1703a.4.32	2480	22	68%	0.281173	0.000044	0.003996	0.158	-8.16	1.54	3.50
BAL1703a.4.33	1838	36	1%	0.28168	0.000044	0.001161	0.036	0.44	1.54	2.46
BAL1703a.4.34	1710	79	41%	0.281665	0.000036	0.001134	0.03798	-2.87	1.26	2.57
BAL1703a.4.35	1818	57	0%	0.281659	0.00005	0.000619	0.01878	-0.08	1.75	2.48
BAL1703a.4.36	2443	29	56%	0.281076	0.000055	0.001235	0.0439	-7.78	1.93	3.45
BAL1703a.4.37	1896	36	26%	0.281562	0.000034	0.001001	0.03313	-2.27	1.19	2.68
BAL1703a.4.38	1844	58	20%	0.28156	0.00003	0.000543	0.0176	-2.92	1.05	2.68
BAL1703a.4.39	1892	36	17%	0.281491	0.000042	0.001481	0.0466	-5.50	1.47	2.88
BAL1703a.4.40	2977	30	84%	0.281412	0.000053	0.001331	0.03753	15.89	1.86	2.34
BAL1703a.4.41	1991	32	84%	0.281394	0.00004	0.001802	0.05584	-7.22	1.40	3.06
BAL1703a.4.42	1876	33	70%	0.281709	0.000039	0.00298	0.084	0.00	1.37	2.52
BAL1703a.4.43	1606	36	38%	0.281651	0.000048	0.00129	0.03995	-5.81	1.68	2.68
BAL1703a.4.44	1933	39	46%	0.281659	0.000041	0.00115	0.0366	1.79	1.44	2.45
BAL1703a.4.45	1820	47	3%	0.281675	0.000034	0.0006152	0.018717	0.53	1.19	2.44

BAL1703a.4.46	2191	38	76%	0.281691	0.000038	0.001878	0.04198	7.55	1.33	2.28
BAL1703a.4.47	1980	32	70%	0.281618	0.000049	0.002867	0.1051	-0.92	1.72	2.65
BAL1703a.4.48	1787	42	-1%	0.281656	0.00004	0.0007103	0.02171	-0.99	1.40	2.51
BAL1703a.4.49	1863	46	13%	0.281634	0.000031	0.001319	0.04372	-0.85	1.09	2.56
BAL1703a.4.50	2015	47	57%	0.281507	0.000048	0.00244	0.1006	-3.55	1.68	2.85
BAL1703a.4.51	1963	50	-1%	0.28156	0.000043	0.000705	0.02259	-0.47	1.51	2.61
BAL1703a.4.52	2367	37	76%	0.28148	0.000048	0.00449	0.177	-0.33	1.68	2.92
BAL1703a.4.53	1866	44	0%	0.281534	0.000039	0.0006437	0.0206	-3.48	1.37	2.73
BAL1703a.4.54	1982	56	68%	0.281633	0.000036	0.001847	0.0682	1.02	1.26	2.53
BAL1703a.4.55	1884	34	22%	0.281734	0.000038	0.001828	0.0606	2.52	1.33	2.36
BAL1703a.4.56	1909	35	7%	0.281519	0.000045	0.000794	0.0257	-3.25	1.58	2.75
BAL1703a.4.57	1967	56	50%	0.281664	0.000041	0.001685	0.0583	2.01	1.44	2.46
BAL1703a.4.58	2017	53	73%	0.281642	0.000042	0.001044	0.03469	3.18	1.47	2.42
BAL1703a.4.59	1949	49	20%	0.281677	0.000039	0.001725	0.0591	2.03	1.37	2.44
BAL1703a.4.60	1813	25	1%	0.281632	0.000036	0.001408	0.04694	-2.12	1.26	2.60
BAL1703a.4.61	1847	55	7%	0.281671	0.000035	0.000754	0.026	0.82	1.23	2.44
BAL1703a.4.62	2042	38	49%	0.281512	0.000054	0.001408	0.0484	-1.38	1.89	2.73
BAL1703a.4.63	1912	31	12%	0.281552	0.000048	0.0008353	0.02714	-2.06	1.68	2.67
BAL1703a.4.64	1794	18	0%	0.281693	0.000043	0.0009532	0.03169	0.18	1.51	2.44
BAL1703a.4.65	1862	33	15%	0.281712	0.000045	0.001057	0.03704	2.23	1.58	2.36
BAL1703a.4.66	1810	40	13%	0.281634	0.000032	0.000915	0.0327	-1.51	1.12	2.56
BAL1703a.4.67	1822	38	9%	0.281673	0.000045	0.001291	0.04539	-0.32	1.58	2.49
BAL1703a.4.68	1895	34	0%	0.28169	0.000039	0.000735	0.025	2.59	1.37	2.37
BAL1703a.4.69	1895	34	37%	0.281672	0.000046	0.00098	0.03574	1.64	1.61	2.43
BAL1703a.4.70	1859	32	12%	0.281689	0.000038	0.0007136	0.02455	1.78	1.33	2.39
BAL1703a.4.71	2400	41	83%	0.28157	0.000051	0.00357	0.1396	5.03	1.79	2.60
BAL1703a.4.72	2782	16	31%	0.280847	0.000037	0.0010286	0.03058	-8.00	1.30	3.72
BAL1703a.4.73	1884	30	1%	0.281549	0.000036	0.0005731	0.0191	-2.46	1.26	2.68
BAL1703a.4.74	1915	41	4%	0.281494	0.000046	0.000733	0.02551	-3.92	1.61	2.80
BAL1703a.4.75	1843	68	5%	0.281641	0.000051	0.00093	0.0311	-0.55	1.79	2.53
BAL1703a.4.76	2038	66	43%	0.281722	0.000039	0.001144	0.04	6.35	1.37	2.23

BAL1703a.4.77	1921	46	24%	0.281505	0.000037	0.000742	0.02706	-3.41	1.30	2.77
BAL1703a.4.78	2048	52	72%	0.281603	0.000045	0.00251	0.0989	0.46	1.58	2.62
BAL1703a.4.79	2493	21	5%	0.281327	0.000037	0.0009089	0.03046	2.80	1.30	2.81
BAL1703a.4.80	2436	43	69%	0.281488	0.000047	0.00355	0.1617	2.88	1.65	2.76
BAL1703a.4.81	1925	24	7%	0.281624	0.000029	0.001056	0.0362	0.50	1.02	2.52
BAL1703a.4.82	1866	54	22%	0.281623	0.000032	0.000839	0.02835	-0.57	1.12	2.54
BAL1703a.4.83	2274	46	53%	0.281514	0.000041	0.00218	0.0896	2.59	1.44	2.66
BAL1703a.4.84	2366	46	69%	0.281604	0.000058	0.00655	0.268	0.76	2.03	2.85
BAL1703a.4.85	1887	70	5%	0.281676	0.000049	0.000796	0.02732	1.84	1.72	2.41
BAL1703a.4.86	1887	45	0%	0.28154	0.000031	0.00051053	0.017836	-2.63	1.09	2.69
BAL1703a.4.87	1907	20	26%	0.281561	0.000041	0.00113	0.0413	-2.23	1.44	2.68
BAL1703a.4.88	1813	39	2%	0.281663	0.00003	0.000909	0.0311	-0.41	1.05	2.49
BAL1703a.4.89	1777	35	25%	0.281679	0.000043	0.000999	0.0319	-0.74	1.51	2.49
BAL1703a.4.90	1986	38	33%	0.281568	0.000043	0.001405	0.0507	-0.61	1.51	2.64
BAL1703a.4.91	1847	39	4%	0.281662	0.000043	0.0006502	0.02197	0.63	1.51	2.45
BAL1703a.4.92	1882	31	4%	0.281589	0.000049	0.001575	0.0543	-2.35	1.72	2.67
BAL1703a.4.93	1855	26	37%	0.281603	0.000033	0.00067	0.02246	-1.31	1.16	2.58
BAL1703a.4.94	2543	25	89%	0.281512	0.000045	0.005137	0.2131	3.20	1.58	2.83
BAL1703a.4.95	1813	25	0%	0.281674	0.000043	0.0011318	0.03361	-0.29	1.51	2.49
BAL1703a.4.96	1888	25	0%	0.281585	0.000041	0.0006331	0.02125	-1.17	1.44	2.60
BAL1703a.4.97	1800	35	5%	0.281664	0.000039	0.001043	0.03594	-0.82	1.37	2.51
BAL1703a.4.98	1818	30	1%	0.281498	0.000041	0.001223	0.04203	-6.54	1.44	2.89
BAL1703a.4.99	1807	48	11%	0.281695	0.00003	0.000966	0.0308	0.53	1.05	2.43
BAL1703a.4.100	1699	32	20%	0.281687	0.000049	0.001108	0.03548	-2.30	1.72	2.53
BAL1703a.4.101	2119	48	68%	0.281602	0.000044	0.003103	0.1238	1.07	1.54	2.63
BAL1703a.4.102	1841	40	62%	0.281651	0.000047	0.00202	0.0733	-1.59	1.65	2.59
BAL1703a.4.103	2046	27	78%	0.28136	0.000043	0.003798	0.1533	-10.00	1.51	3.28
BAL1703a.4.104	1733	28	24%	0.28164	0.000043	0.001058	0.035	-3.17	1.51	2.61
BAL1703a.4.105	2039	48	62%	0.281594	0.000053	0.00316	0.1283	-0.95	1.86	2.70
BAL1703a.4.106	1878	49	38%	0.281659	0.000047	0.001357	0.0455	0.32	1.65	2.50
BAL1703a.4.107	1879	35	14%	0.281646	0.000043	0.000884	0.03064	0.48	1.51	2.49

Sample: BAL1706a

Grain ID	207Pb/206Pb Age (Ma)	± 1σ (Ma)	Disc (%)	176Hf/177Hf	± 1SE(abs)	176Lu/177Hf	176Yb/177Hf	εHf (t)	εHf ± 1SE	TDM Crustal (Ga)
BAL1706a.4.01	2069	25	66%	0.281495	0.000046	0.00352	0.1511	-4.35	1.61	2.94
BAL1706a.4.02	1780	30	0%	0.281475	0.000033	0.0019328	0.06719	-9.04	1.16	3.01
BAL1706a.4.03	1830	50	10%	0.281516	0.000041	0.000816	0.02626	-5.14	1.44	2.81
BAL1706a.4.04	1890	42	10%	0.281523	0.000034	0.000685	0.02407	-3.39	1.19	2.74
BAL1706a.4.05	2304	76	15%	0.281647	0.000037	0.0007251	0.02492	10.23	1.30	2.19
BAL1706a.4.06	1813	44	0%	0.281697	0.00006	0.00112	0.0397	0.54	2.10	2.43
BAL1706a.4.07	1790	32	-1%	0.281667	0.000031	0.000775	0.02527	-0.61	1.09	2.49
BAL1706a.4.08	1790	40	-1%	0.281525	0.000046	0.001711	0.0558	-6.78	1.61	2.88
BAL1706a.4.09	2362	26	39%	0.281091	0.00006	0.00107	0.0391	-8.78	2.10	3.45
BAL1706a.4.10	1792	25	0%	0.28165	0.000027	0.0006031	0.02029	-0.96	0.95	2.51
BAL1706a.4.11	1933	39	8%	0.281532	0.000043	0.000853	0.02879	-2.33	1.51	2.71
BAL1706a.4.12	1939	32	43%	0.28147	0.000042	0.001647	0.0634	-5.44	1.47	2.91
BAL1706a.4.13	2005	22	41%	0.281645	0.000042	0.001625	0.0634	2.24	1.47	2.47
BAL1706a.4.14	1881	30	-1%	0.281536	0.00005	0.00085	0.02833	-3.34	1.75	2.73
BAL1706a.4.15	2262	35	61%	0.281615	0.000046	0.0029	0.1198	4.82	1.61	2.51
BAL1706a.4.16	1769	36	0%	0.281659	0.000037	0.0006142	0.020414	-1.17	1.30	2.51
BAL1706a.4.17	2067	58	46%	0.281527	0.00005	0.002194	0.0839	-1.40	1.75	2.75
BAL1706a.4.18	1774	29	1%	0.281705	0.000047	0.001674	0.0568	-0.69	1.65	2.48
BAL1706a.4.19	1784	34	0%	0.281661	0.000053	0.000701	0.02356	-0.87	1.86	2.50
BAL1706a.4.20	1825	25	0%	0.281636	0.000045	0.001266	0.0419	-1.54	1.58	2.57
BAL1706a.4.21	1860	38	-1%	0.281547	0.00003	0.000531	0.0178	-3.01	1.05	2.70
BAL1706a.4.22	1713	47	2%	0.281642	0.000037	0.00077	0.0269	-3.20	1.30	2.59
BAL1706a.4.23	2203	30	4%	0.281452	0.000045	0.001903	0.0653	-0.72	1.58	2.81
BAL1706a.4.24	1865	25	-2%	0.281543	0.000044	0.000874	0.029	-3.47	1.54	2.73
BAL1706a.4.25	2131	25	48%	0.281438	0.000057	0.00332	0.135	-4.82	2.00	3.02
BAL1706a.4.26	1804	31	-1%	0.281678	0.000043	0.0008244	0.02797	0.03	1.51	2.46
BAL1706a.4.27	1870	30	0%	0.281506	0.000041	0.001109	0.03754	-4.97	1.44	2.83

BAL1706a.4.28	1885	27	-2%	0.281568	0.000043	0.001009	0.03384	-2.32	1.51	2.67
BAL1706a.4.29	1779	35	0%	0.281668	0.000044	0.000977	0.0346	-1.06	1.54	2.51
BAL1706a.4.30	1870	46	18%	0.281674	0.000035	0.001335	0.0501	0.71	1.23	2.47
BAL1706a.4.31	1885	41	0%	0.281523	0.000048	0.0005496	0.01838	-3.33	1.68	2.73
BAL1706a.4.32	1946	41	44%	0.281656	0.000062	0.00298	0.1186	-0.43	2.17	2.60
BAL1706a.4.33	1898	64	27%	0.281547	0.000054	0.00265	0.105	-4.87	1.89	2.84
BAL1706a.4.34	1777	24	15%	0.281662	0.000051	0.001317	0.0436	-1.73	1.79	2.55
BAL1706a.4.35	1899	51	0%	0.28154	0.000033	0.0003258	0.0106	-2.13	1.16	2.67
BAL1706a.4.36	1813	52	2%	0.281612	0.000034	0.0004265	0.01454	-1.63	1.19	2.57
BAL1706a.4.37	1919	29	1%	0.281513	0.000032	0.0006547	0.02311	-3.06	1.12	2.74
BAL1706a.4.38	1898	39	18%	0.281635	0.000034	0.00086	0.03201	0.54	1.19	2.50
BAL1706a.4.39	1820	41	-2%	0.281555	0.000033	0.0005473	0.01856	-3.64	1.16	2.70
BAL1706a.4.40	1713	47	-8%	0.281635	0.000034	0.000753	0.0248	-3.43	1.19	2.61
BAL1706a.4.41	1885	36	-2%	0.281522	0.000037	0.0006226	0.021377	-3.46	1.30	2.74
BAL1706a.4.42	1752	38	-1%	0.281726	0.000041	0.001305	0.0486	0.01	1.44	2.42
BAL1706a.4.43	2512	23	-2%	0.28111	0.000042	0.0004869	0.016103	-3.77	1.47	3.25
BAL1706a.4.44	2133	29	63%	0.281326	0.000039	0.002259	0.0848	-7.23	1.37	3.17
BAL1706a.4.45	1780	35	-1%	0.281717	0.000035	0.000866	0.0296	0.83	1.23	2.39
BAL1706a.4.46	1772	16	1%	0.281676	0.00004	0.000982	0.0328	-0.94	1.40	2.50
BAL1706a.4.47	1777	42	2%	0.281708	0.000036	0.001599	0.0577	-0.43	1.26	2.47

Sample: BAL1706b

Grain ID	*207Pb/206Pb Age (Ma)*	*± 1σ (Ma)*	*Disc (%)*	*176Hf/177Hf*	*± 1SE(abs)*	*176Lu/177Hf*	*176Yb/177Hf*	*εHf (t)*	*εHf ± 1SE*	*TDM Crustal (Ga)*
BAL1706b.3.01	1972	59	58%	0.28154	0.000053	0.0045	0.1774	-6.03	1.86	2.97
BAL1706b.3.02	1873	46	34%	0.281641	0.000044	0.00179	0.0681	-0.97	1.54	2.58
BAL1706b.3.03	1805	76	0%	0.281629	0.000037	0.0011	0.0369	-2.02	1.30	2.59
BAL1706b.3.04	1790	60	11%	0.28166	0.000037	0.001235	0.0429	-1.42	1.30	2.54
BAL1706b.3.05	1958	49	65%	0.281486	0.000035	0.004541	0.1765	-8.28	1.23	3.10
BAL1706b.3.06	1896	54	41%	0.281634	0.000037	0.00193	0.0754	-0.91	1.30	2.59
BAL1706b.3.07	2038	54	74%	0.281481	0.00005	0.00758	0.3155	-11.06	1.75	3.34

BAL1706b.3.08	1933	50	61%	0.281578	0.000039	0.00585	0.239	-7.21	1.37	3.02
BAL1706b.3.09	1807	54	5%	0.281619	0.000042	0.001673	0.0582	-3.03	1.47	2.66
BAL1706b.3.10	1807	58	7%	0.281724	0.00004	0.001524	0.0478	0.88	1.40	2.41
BAL1706b.3.11	1865	44	11%	0.281534	0.000043	0.001357	0.0475	-4.40	1.51	2.79
BAL1706b.3.12	1830	62	37%	0.281573	0.000044	0.00301	0.116	-5.82	1.54	2.85
BAL1706b.3.13	2397	47	64%	0.280938	0.000062	0.00786	0.322	-24.48	2.17	4.46
BAL1706b.3.14	1925	56	60%	0.281615	0.00005	0.00443	0.182	-4.20	1.75	2.82
BAL1706b.3.15	1931	45	12%	0.281536	0.000034	0.0014	0.0523	-2.94	1.19	2.75
BAL1706b.3.16	1952	61	54%	0.281425	0.000043	0.00387	0.153	-9.68	1.51	3.19
BAL1706b.3.17	1961	48	66%	0.28153	0.000047	0.00587	0.2367	-8.42	1.65	3.12
BAL1706b.3.18	2344	51	79%	0.281391	0.00004	0.00529	0.2301	-5.22	1.40	3.21
BAL1706b.3.19	1836	57	1%	0.281526	0.000046	0.00157	0.0539	-5.58	1.61	2.84
BAL1706b.3.20	1862	52	1%	0.281525	0.000033	0.000933	0.03215	-4.25	1.16	2.78
BAL1706b.3.21	2115	44	73%	0.281075	0.000029	0.00446	0.1908	-19.67	1.02	3.94
BAL1706b.3.22	1995	49	66%	0.281555	0.000042	0.004305	0.1807	-4.78	1.47	2.91
BAL1706b.3.23	1800	55	8%	0.281671	0.000034	0.000807	0.02729	-0.29	1.19	2.48
BAL1706b.3.24	1999	46	48%	0.281557	0.00004	0.00246	0.098	-2.14	1.40	2.75
BAL1706b.3.25	2456	42	0%	0.281332	0.000041	0.000858	0.02666	2.24	1.44	2.82
BAL1706b.3.26	1989	55	27%	0.281484	0.000057	0.001481	0.0546	-3.63	2.00	2.83
BAL1706b.3.27	1784	45	-1%	0.281677	0.000037	0.0006237	0.02065	-0.21	1.30	2.46
BAL1706b.3.28	2244	56	86%	0.281365	0.000082	0.01104	0.466	-16.81	2.87	3.86
BAL1706b.3.29	1949	54	29%	0.281564	0.000044	0.00173	0.072	-1.99	1.54	2.70
BAL1706b.3.30	1779	44	1%	0.281665	0.00004	0.000664	0.02187	-0.80	1.40	2.49
BAL1706b.3.31	1835	47	1%	0.281602	0.000038	0.000674	0.02234	-1.80	1.33	2.60
BAL1706b.3.32	2534	41	35%	0.281035	0.000055	0.0067	0.274	-16.63	1.93	4.07
BAL1706b.3.33	2442	52	88%	0.281151	0.00007	0.01289	0.5497	-24.45	2.45	4.49
BAL1706b.3.34	1887	45	33%	0.281466	0.000056	0.00233	0.091	-7.57	1.96	3.00
BAL1706b.3.35	2056	45	61%	0.281453	0.000056	0.00493	0.2045	-8.06	1.96	3.17
BAL1706b.3.36	2067	53	57%	0.281543	0.000042	0.003121	0.1335	-2.13	1.47	2.80
BAL1706b.3.37	2566	56	1%	0.281026	0.000039	0.000655	0.0226	-5.82	1.37	3.42
BAL1706b.3.38	2035	68	61%	0.28166	0.000043	0.00463	0.1875	-0.71	1.51	2.68

BAL1706b.3.39	1767	47	0%	0.281699	0.000038	0.00069	0.02332	0.11	1.33	2.42
BAL1706b.3.40	1805	51	-2%	0.281683	0.00004	0.0006708	0.02123	0.41	1.40	2.43
BAL1706b.3.41	1884	52	-1%	0.281581	0.000036	0.000848	0.0271	-1.67	1.26	2.63
BAL1706b.3.42	1797	53	68%	0.281428	0.000051	0.00504	0.2023	-14.10	1.79	3.35
BAL1706b.3.43	1913	72	44%	0.281637	0.000034	0.00179	0.0706	-0.25	1.19	2.56
BAL1706b.3.44	1902	49	24%	0.281589	0.000052	0.002501	0.0911	-3.11	1.82	2.73
BAL1706b.3.45	1992	49	58%	0.281439	0.000044	0.00286	0.1238	-7.02	1.54	3.05
BAL1706b.3.46	1905	57	62%	0.281487	0.000046	0.004125	0.1673	-8.75	1.61	3.09
BAL1706b.3.47	1841	45	63%	0.281512	0.000047	0.00497	0.2035	-10.19	1.65	3.13
BAL1706b.4.01	1874	65	35%	0.281477	0.000042	0.00291	0.125	-8.19	1.47	3.03
BAL1706b.4.02	1847	47	14%	0.281492	0.000036	0.00192	0.0756	-6.99	1.26	2.94
BAL1706b.4.03	1779	29	-1%	0.281673	0.000034	0.00086	0.0296	-0.75	1.19	2.49
BAL1706b.4.04	2533	25	69%	0.28085	0.000071	0.00681	0.3002	-23.42	2.49	4.50
BAL1706b.4.05	1800	33	-2%	0.281638	0.000049	0.000647	0.02137	-1.27	1.72	2.54
BAL1706b.4.06	1973	59	39%	0.281523	0.000039	0.001935	0.0813	-3.20	1.37	2.79
BAL1706b.4.07	1787	33	56%	0.281326	0.000047	0.00207	0.087	-14.34	1.65	3.35
BAL1706b.4.08	2075	25	56%	0.281576	0.000048	0.00507	0.2109	-3.52	1.68	2.89
BAL1706b.4.09	1812	51	80%	0.281544	0.000053	0.00729	0.307	-12.44	1.86	3.25
BAL1706b.4.10	2067	36	79%	0.28149	0.000063	0.00703	0.303	-9.47	2.21	3.26
BAL1706b.4.11	1767	41	64%	0.281545	0.000051	0.004401	0.1833	-9.77	1.79	3.05
BAL1706b.4.12	1992	38	42%	0.281467	0.000044	0.00294	0.1273	-6.13	1.54	3.00
BAL1706b.4.13	1784	54	4%	0.281672	0.000035	0.000846	0.02967	-0.65	1.23	2.49
BAL1706b.4.14	1907	25	23%	0.281476	0.000051	0.00136	0.0549	-5.55	1.79	2.89
BAL1706b.4.15	1952	40	70%	0.281567	0.000051	0.00627	0.263	-7.80	1.79	3.07
BAL1706b.4.16	1918	41	71%	0.281524	0.000039	0.00479	0.2037	-8.04	1.37	3.06
BAL1706b.4.17	2258	58	79%	0.28131	0.000059	0.01247	0.544	-20.73	2.07	4.12
BAL1706b.4.18	1792	48	5%	0.281662	0.000039	0.001321	0.048	-1.41	1.37	2.54
BAL1706b.4.19	1767	26	65%	0.281565	0.000043	0.00469	0.1991	-9.40	1.51	3.03
BAL1706b.4.20	1960	22	0%	0.281577	0.000024	0.0006	0.02083	0.20	0.84	2.57
BAL1706b.4.21	1874	24	0%	0.281545	0.000033	0.000846	0.0288	-3.17	1.16	2.72

BAL1706b.4.22	1797	27	-1%	0.281724	0.000036	0.00266	0.0913	-0.71	1.26	2.50
BAL1706b.4.23	1807	25	0%	0.281713	0.000043	0.001387	0.0502	0.65	1.51	2.42
BAL1706b.4.24	1955	42	72%	0.28144	0.000074	0.00732	0.309	-13.64	2.59	3.44
BAL1706b.4.25	1985	32	83%	0.281425	0.000066	0.00978	0.4315	-16.93	2.31	3.67
BAL1706b.4.26	2069	74	53%	0.28143	0.000061	0.00336	0.145	-6.43	2.14	3.07
BAL1706b.4.27	1912	31	15%	0.281702	0.00004	0.000987	0.0389	3.07	1.40	2.35
BAL1706b.4.28	1888	39	54%	0.281603	0.000035	0.00261	0.1123	-3.04	1.23	2.72
BAL1706b.4.29	2129	40	67%	0.281384	0.000056	0.00559	0.247	-10.04	1.96	3.35
BAL1706b.4.30	1813	52	15%	0.281702	0.000033	0.001103	0.0394	0.74	1.16	2.42
BAL1706b.4.31	2466	19	-1%	0.281119	0.000045	0.000813	0.02714	-5.04	1.58	3.29
BAL1706b.4.32	1940	36	61%	0.281645	0.000039	0.00287	0.121	-0.80	1.37	2.62
BAL1706b.4.33	2480	140	12%	0.281505	0.000042	0.000573	0.02003	9.41	1.47	2.38
BAL1706b.4.34	1879	22	61%	0.281473	0.000049	0.00461	0.1993	-10.38	1.72	3.18
BAL1706b.4.35	2814	26	0%	0.280951	0.000036	0.0019942	0.07347	-5.43	1.26	3.58
BAL1706b.4.36	1812	48	26%	0.281668	0.000039	0.000801	0.0289	-0.12	1.37	2.47
BAL1706b.4.37	1745	58	-1%	0.281622	0.000042	0.0004963	0.01698	-2.88	1.47	2.60
BAL1706b.4.38	1898	39	52%	0.281674	0.000041	0.001784	0.0758	0.74	1.44	2.49
BAL1706b.4.39	1928	36	25%	0.281603	0.000031	0.00204	0.081	-1.46	1.09	2.65
BAL1706b.4.40	2599	22	73%	0.280551	0.000046	0.0041	0.1789	-28.06	1.61	4.84
BAL1706b.4.41	1922	34	70%	0.281511	0.00005	0.005554	0.2419	-9.41	1.75	3.15
BAL1706b.4.42	1999	100	36%	0.281504	0.000038	0.001505	0.0586	-2.74	1.33	2.78
BAL1706b.4.43	2519	32	67%	0.281089	0.000059	0.00627	0.275	-14.25	2.07	3.91

Sample: COR1701a

Grain ID	*207Pb/206Pb Age (Ma)*	*± 1σ (Ma)*	*Disc (%)*	*176Hf/177Hf*	*± 1SE(abs)*	*176Lu/177Hf*	*176Yb/177Hf*	*εHf (t)*	*εHf ± 1SE*	*TDM Crustal (Ga)*
COR1701a.3.01	1828	81	4%	0.281636	0.000042	0.001032	0.034	-1.19	1.47	2.55
COR1701a.3.02	1849	75	29%	0.281571	0.000039	0.001296	0.0442	-3.36	1.37	2.71
COR1701a.3.03	1866	93	0%	0.281588	0.000042	0.000375	0.01176	-1.23	1.47	2.59
COR1701a.3.04	1854	53	16%	0.281558	0.000039	0.001845	0.0648	-4.40	1.37	2.78
COR1701a.3.05	1943	47	53%	0.281563	0.000042	0.00186	0.0658	-2.33	1.47	2.72

COR1701a.3.06	1871	54	44%	0.281559	0.000054	0.001116	0.03907	-3.08	1.89	2.71
COR1701a.3.07	1949	39	-1%	0.281476	0.000029	0.00057268	0.0184	-3.59	1.02	2.80
COR1701a.3.08	1752	48	38%	0.281648	0.000039	0.002007	0.07162	-3.58	1.37	2.65
COR1701a.3.09	1833	57	15%	0.281516	0.000045	0.001207	0.0406	-5.55	1.58	2.84
COR1701a.3.10	1972	46	5%	0.281613	0.000034	0.00088	0.0291	1.38	1.19	2.50
COR1701a.3.11	2482	46	82%	0.281543	0.00005	0.002674	0.1036	7.26	1.75	2.52
COR1701a.3.12	1919	44	54%	0.281574	0.000039	0.00197	0.0723	-2.59	1.37	2.71
COR1701a.3.13	1995	42	62%	0.281557	0.000043	0.00357	0.1332	-3.72	1.51	2.84
COR1701a.3.14	1874	46	2%	0.281608	0.00004	0.000772	0.0259	-0.84	1.40	2.57
COR1701a.3.15	1839	52	39%	0.281647	0.000046	0.001469	0.0489	-1.09	1.61	2.56
COR1701a.3.16	1988	45	70%	0.281557	0.000045	0.00465	0.172	-5.31	1.58	2.94
COR1701a.3.17	2062	42	77%	0.281552	0.000041	0.00327	0.1293	-2.12	1.44	2.79
COR1701a.3.18	1758	46	0%	0.281618	0.000038	0.000505	0.01577	-2.74	1.33	2.60
COR1701a.3.19	1836	48	7%	0.281641	0.000041	0.000844	0.02736	-0.60	1.44	2.52
COR1701a.3.20	2515	41	18%	0.281199	0.000043	0.001229	0.03989	-1.80	1.51	3.12
COR1701a.3.21	2090	64	22%	0.281558	0.000047	0.0027	0.106	-0.52	1.65	2.71
COR1701a.3.22	1828	54	11%	0.281666	0.000044	0.000671	0.0218	0.32	1.54	2.46
COR1701a.3.23	2676	39	8%	0.28115	0.000042	0.000541	0.01587	1.29	1.47	3.05
COR1701a.3.24	1851	54	5%	0.281632	0.000039	0.001116	0.03552	-0.93	1.37	2.56
COR1701a.3.25	1966	40	0%	0.28153	0.000045	0.00064	0.0205	-1.39	1.58	2.67
COR1701a.3.26	1887	59	0%	0.281576	0.000036	0.00132	0.0413	-2.38	1.26	2.68
COR1701a.3.27	1847	77	25%	0.281594	0.000043	0.00136	0.0474	-2.67	1.51	2.66
COR1701a.3.28	2015	49	59%	0.281482	0.000051	0.001957	0.0691	-3.79	1.79	2.86
COR1701a.3.29	3474	34	45%	0.280412	0.000042	0.00167	0.0589	-9.36	1.47	4.34
COR1701a.3.30	2324	46	69%	0.281476	0.000038	0.00559	0.236	-3.06	1.33	3.06
COR1701a.3.31	2295	72	68%	0.281641	0.000042	0.00225	0.08	7.45	1.47	2.36
COR1701a.3.32	1896	47	26%	0.281668	0.000048	0.000947	0.0299	1.56	1.68	2.43
COR1701a.3.33	2385	48	79%	0.281584	0.000053	0.00528	0.191	2.45	1.86	2.75
COR1701a.3.34	1899	48	-1%	0.281506	0.000042	0.001098	0.0321	-4.32	1.47	2.81
COR1701a.3.35	1882	41	-1%	0.28164	0.000049	0.0000523	0.00218	1.39	1.72	2.43
COR1701a.3.36	2002	55	25%	0.281554	0.000046	0.00147	0.0489	-0.85	1.61	2.67

COR1701a.3.37	1978	48	73%	0.281543	0.000043	0.00327	0.11	-4.17	1.51	2.86
COR1701a.3.38	2530	38	27%	0.280954	0.000041	0.000661	0.0219	-9.21	1.44	3.60
COR1701a.3.39	1790	43	0%	0.281641	0.000039	0.001392	0.0416	-2.28	1.37	2.59
COR1701a.3.40	1952	54	7%	0.281549	0.000044	0.00089	0.0309	-1.35	1.54	2.66
COR1701a.3.41	2036	44	48%	0.281588	0.000035	0.001766	0.0554	0.69	1.23	2.59
COR1701a.3.42	2532	50	85%	0.281558	0.000042	0.00347	0.1168	7.49	1.47	2.54
COR1701a.3.43	1887	55	-1%	0.281595	0.000043	0.000712	0.01979	-0.93	1.51	2.58
COR1701a.3.44	1876	57	17%	0.281609	0.000045	0.000722	0.02157	-0.69	1.58	2.56
COR1701a.3.45	1847	45	-1%	0.281685	0.000042	0.001456	0.0395	0.44	1.47	2.46
COR1701a.3.46	2321	45	77%	0.281622	0.000035	0.002159	0.0695	7.47	1.23	2.38
COR1701a.3.47	1948	51	39%	0.281645	0.000054	0.002021	0.0593	0.48	1.89	2.54
COR1701a.3.48	1948	43	31%	0.281602	0.00004	0.00198	0.06	-0.99	1.40	2.63
COR1701a.3.49	2001	53	59%	0.281533	0.000041	0.001314	0.0463	-1.41	1.44	2.70
COR1701a.3.50	1828	46	0%	0.281641	0.000035	0.000977	0.027	-0.94	1.23	2.54
COR1701a.3.51	2107	51	82%	0.281583	0.000054	0.003904	0.1244	-0.99	1.89	2.76
COR1701a.3.52	2121	45	76%	0.281518	0.000048	0.003602	0.1184	-2.58	1.68	2.87
COR1701a.3.53	1870	47	34%	0.281757	0.000046	0.003076	0.0902	1.46	1.61	2.42
COR1701a.3.54	1994	42	53%	0.281563	0.000043	0.00337	0.1018	-3.26	1.51	2.81
COR1701a.3.55	1871	57	1%	0.281537	0.000035	0.0006312	0.01669	-3.25	1.23	2.72
COR1701a.3.56	2055	86	25%	0.281343	0.000032	0.001305	0.0326	-6.96	1.12	3.10
COR1701a.3.57	1986	55	33%	0.281544	0.00004	0.001276	0.0355	-1.29	1.40	2.68
COR1701a.3.58	1812	66	0%	0.281694	0.000038	0.000956	0.02546	0.61	1.33	2.43
COR1701a.3.59	1972	47	36%	0.281595	0.000042	0.001856	0.056	-0.56	1.47	2.63
COR1701a.3.60	2537	37	-1%	0.281247	0.000054	0.001043	0.0263	0.71	1.89	2.98
COR1701a.3.61	1799	61	2%	0.281664	0.000055	0.001124	0.03141	-0.94	1.93	2.52
COR1701a.3.62	2496	39	79%	0.280997	0.000044	0.00336	0.1186	-13.02	1.54	3.82
COR1701a.3.63	1905	51	43%	0.281677	0.000037	0.00166	0.0504	1.16	1.30	2.46
COR1701a.3.64	2001	51	68%	0.281548	0.000061	0.002555	0.0847	-2.55	2.14	2.77
COR1701a.3.65	2014	43	52%	0.281571	0.000043	0.002233	0.068	-1.02	1.51	2.69
COR1701a.3.66	1810	59	9%	0.281627	0.000036	0.000828	0.0237	-1.65	1.26	2.57
COR1701a.3.67	1836	60	9%	0.2817	0.000058	0.001391	0.0399	0.82	2.03	2.43

COR1701a.3.68	2081	56	77%	0.281282	0.000045	0.00613	0.214	-15.34	1.58	3.64
COR1701a.3.69	2028	38	22%	0.281042	0.00004	0.001763	0.0582	-18.87	1.40	3.82
COR1701a.3.70	1804	43	-1%	0.281625	0.000049	0.001076	0.03132	-2.16	1.72	2.60
COR1701a.3.71	1928	46	0%	0.281502	0.000037	0.000779	0.0226	-3.41	1.30	2.77
COR1701a.3.72	2024	48	64%	0.281575	0.000039	0.002134	0.07321	-0.53	1.37	2.66
COR1701a.3.73	1780	49	0%	0.281609	0.000033	0.00088	0.02631	-3.02	1.16	2.63
COR1701a.3.74	1919	44	1%	0.281559	0.00004	0.000901	0.02885	-1.74	1.40	2.66
COR1701a.3.75	2053	43	75%	0.281547	0.000044	0.001739	0.0614	-0.36	1.54	2.68
COR1701a.3.76	1952	42	76%	0.28158	0.000049	0.002466	0.0903	-2.33	1.72	2.72
COR1701a.3.77	2027	51	66%	0.281556	0.000044	0.00301	0.1045	-2.34	1.54	2.78
COR1701a.3.78	2096	50	81%	0.281434	0.000062	0.003759	0.1369	-6.30	2.17	3.09

Sample: COR1701b

Grain ID	*207Pb/206Pb Age (Ma)*	*± 1σ (Ma)*	*Disc (%)*	*176Hf/177Hf*	*± 1SE(abs)*	*176Lu/177Hf*	*176Yb/177Hf*	*εHf (t)*	*εHf ± 1SE*	*TDM Crustal (Ga)*
COR1701b.4.01	1865	30	-1%	0.281531	0.000036	0.0008133	0.02791	-3.82	1.26	2.75
COR1701b.4.02	1904	46	12%	0.281582	0.00005	0.001178	0.04066	-1.62	1.75	2.64
COR1701b.4.03	1982	34	4%	0.281475	0.000043	0.0005526	0.01847	-2.86	1.51	2.78
COR1701b.4.04	2274	28	65%	0.281471	0.000045	0.001383	0.0533	2.29	1.58	2.68
COR1701b.4.05	1854	46	-1%	0.281505	0.00003	0.0002223	0.006957	-4.25	1.05	2.77
COR1701b.4.06	1952	40	58%	0.281572	0.000043	0.001398	0.051	-1.20	1.51	2.65
COR1701b.4.07	1775	47	-2%	0.281645	0.000046	0.000728	0.02295	-1.67	1.61	2.54
COR1701b.4.08	1818	33	3%	0.281621	0.00004	0.001052	0.0336	-1.96	1.40	2.60
COR1701b.4.09	1907	43	59%	0.281647	0.000053	0.001843	0.06552	-0.10	1.86	2.55
COR1701b.4.10	1777	29	0%	0.281609	0.000038	0.000759	0.02451	-2.94	1.33	2.63
COR1701b.4.11	2913	35	0%	0.280913	0.000037	0.00054	0.01713	-1.73	1.30	3.42
COR1701b.4.12	2505	23	5%	0.281265	0.000054	0.001012	0.03204	0.69	1.89	2.96
COR1701b.4.13	1863	30	28%	0.281675	0.000058	0.00187	0.0661	-0.08	2.03	2.51
COR1701b.4.14	1902	48	56%	0.281666	0.000046	0.001175	0.0412	1.33	1.61	2.45
COR1701b.4.15	1985	35	49%	0.281456	0.000047	0.001046	0.0384	-4.13	1.65	2.86
COR1701b.4.16	1854	32	23%	0.2817	0.000045	0.00104	0.0359	1.65	1.58	2.39

COR1701b.4.17	1878	22	15%	0.281297	0.000058	0.00116	0.0407	-12.28	2.03	3.29
COR1701b.4.18	1873	35	-1%	0.281518	0.000049	0.000513	0.01647	-3.73	1.72	2.75
COR1701b.4.19	1779	77	3%	0.281606	0.000046	0.000344	0.00966	-2.51	1.61	2.60
COR1701b.4.20	1907	51	16%	0.281464	0.000042	0.000951	0.0322	-5.45	1.47	2.89
COR1701b.4.21	1892	47	45%	0.281502	0.000045	0.000632	0.0252	-4.02	1.58	2.78
COR1701b.4.22	1960	33	32%	0.28161	0.000041	0.000997	0.03499	0.85	1.44	2.53
COR1701b.4.23	1967	34	64%	0.281676	0.000057	0.00304	0.115	0.64	2.00	2.55
COR1701b.4.24	2577	23	30%	0.281135	0.000037	0.00171	0.0577	-3.54	1.30	3.28
COR1701b.4.25	2569	28	1%	0.281209	0.000041	0.0007746	0.0252	0.55	1.44	3.01
COR1701b.4.26	1919	25	3%	0.281506	0.000037	0.000983	0.03174	-3.73	1.30	2.79
COR1701b.4.27	1876	38	41%	0.28166	0.000035	0.001307	0.04625	0.38	1.23	2.49
COR1701b.4.28	1841	55	18%	0.281691	0.000049	0.001211	0.0414	0.83	1.72	2.44
COR1701b.4.29	2568	27	49%	0.281051	0.000042	0.001068	0.0405	-5.61	1.47	3.41
COR1701b.4.30	1925	58	-3%	0.281481	0.000043	0.000746	0.0246	-4.18	1.51	2.82
COR1701b.4.31	1838	52	3%	0.281676	0.000038	0.000736	0.02367	0.82	1.33	2.43
COR1701b.4.32	1888	53	12%	0.281641	0.000041	0.001263	0.0425	0.02	1.44	2.52
COR1701b.4.33	1979	38	58%	0.281513	0.00006	0.00151	0.0509	-2.86	2.10	2.78
COR1701b.4.34	2041	35	67%	0.281526	0.000057	0.002019	0.07644	-1.75	2.00	2.75
COR1701b.4.35	1804	30	31%	0.281652	0.000047	0.001348	0.04389	-1.53	1.65	2.56
COR1701b.4.36	1871	38	18%	0.281589	0.000047	0.0007015	0.02289	-1.49	1.65	2.61
COR1701b.4.37	606	61	-2%	0.281986	0.000045	0.00057	0.0197	-15.16	1.58	2.49
COR1701b.4.38	1952	36	0%	0.281536	0.000047	0.0002408	0.007885	-0.96	1.65	2.64
COR1701b.4.39	2476	24	26%	0.281268	0.000054	0.001057	0.0325	0.07	1.89	2.97
COR1701b.4.40	1808	40	2%	0.281661	0.000039	0.001068	0.0349	-0.78	1.37	2.51
COR1701b.4.41	1963	37	65%	0.281623	0.000062	0.002256	0.07725	-0.29	2.17	2.60
COR1701b.4.42	2180	30	62%	0.281439	0.000055	0.001822	0.06954	-1.56	1.93	2.85
COR1701b.4.43	2479	19	55%	0.280966	0.000039	0.001716	0.06002	-11.71	1.37	3.72
COR1701b.4.44	1765	36	-3%	0.281549	0.000033	0.000483	0.01564	-5.01	1.16	2.75
COR1701b.4.45	1919	32	49%	0.28158	0.000045	0.001504	0.0535	-1.78	1.58	2.66
COR1701b.4.46	1892	42	39%	0.281518	0.00004	0.001713	0.0603	-4.83	1.40	2.84
COR1701b.4.47	2407	20	83%	0.28121	0.000041	0.00349	0.135	-7.50	1.44	3.40

COR1701b.4.48	1799	51	12%	0.281545	0.000044	0.000875	0.0288	-4.87	1.54	2.77
COR1701b.4.49	1841	44	-2%	0.281414	0.000038	0.0006224	0.02124	-8.27	1.33	3.01
COR1701b.4.50	1994	54	-1%	0.281519	0.000042	0.000382	0.01104	-0.80	1.47	2.66
COR1701b.4.51	3346	20	15%	0.280794	0.000048	0.00277	0.0944	-1.13	1.68	3.72
COR1701b.4.52	2288	75	23%	0.281715	0.000056	0.000794	0.02571	12.18	1.96	2.05
COR1701b.4.53	2062	40	56%	0.281496	0.000036	0.00158	0.0581	-1.75	1.26	2.77
COR1701b.4.54	1860	30	42%	0.281651	0.000038	0.001917	0.0648	-1.06	1.33	2.57
COR1701b.4.55	1799	23	1%	0.281657	0.000046	0.0008269	0.02715	-0.83	1.61	2.51
COR1701b.4.56	2063	54	55%	0.281348	0.000066	0.001365	0.0505	-6.69	2.31	3.09
COR1701b.4.57	1972	27	59%	0.281485	0.00005	0.001548	0.05857	-4.06	1.75	2.85
COR1701b.4.58	2128	33	76%	0.281604	0.00005	0.002726	0.1032	1.87	1.75	2.59
COR1701b.4.59	1841	42	48%	0.281614	0.000043	0.000939	0.03235	-1.57	1.51	2.59
COR1701b.4.60	1767	37	3%	0.281695	0.000046	0.0010543	0.03608	-0.46	1.61	2.46
COR1701b.4.61	1882	41	2%	0.281519	0.000045	0.0003141	0.01055	-3.24	1.58	2.73
COR1701b.4.62	1774	37	22%	0.281596	0.000062	0.000835	0.0306	-3.56	2.17	2.66
COR1701b.4.63	2522	27	27%	0.281367	0.000055	0.001047	0.0356	4.64	1.93	2.72
COR1701b.4.64	1902	29	-6%	0.281459	0.000046	0.000445	0.01431	-5.09	1.61	2.86

Sample: MQ01

Grain ID	*207Pb/206Pb Age (Ma)*	*± 1σ (Ma)*	*Disc (%)*	*176Hf/177Hf*	*± 1SE(abs)*	*176Lu/177Hf*	*176Yb/177Hf*	*εHf (t)*	*εHf ± 1SE*	*TDM Crustal (Ga)*
MQ01.1.01	2140	33	39%	0.281543	0.000046	0.000298	0.000298	3.47	1.61	2.50
MQ01.1.02	2055	29	6%	0.281525	0.000067	0.000519	0.000519	0.60	2.35	2.62
MQ01.1.03	2594	26	3%	0.281229	0.000066	0.000894	0.000894	1.61	2.31	2.97
MQ01.1.04	2711	22	70%	0.281242	0.000073	0.000667	0.000667	5.13	2.56	2.83
MQ01.1.05	1991	32	1%	0.281484	0.000054	0.000529	0.000529	-2.31	1.89	2.75
MQ01.1.06	1901	54	4%	0.281529	0.000047	0.0003229	0.0003229	-2.47	1.65	2.69
MQ01.1.07	2617	27	27%	0.281266	0.000066	0.001092	0.001092	3.09	2.31	2.89
MQ01.1.08	2241	96	65%	0.281597	0.000087	0.00163	0.00163	5.67	3.05	2.43
MQ01.1.09	2132	36	66%	0.281555	0.000046	0.000907	0.000907	2.84	1.61	2.53
MQ01.1.10	2540	26	63%	0.281133	0.000071	0.001192	0.001192	-3.53	2.49	3.25

MQ01.1.11	2555	22	54%	0.28123	0.000062	0.001008	0.001008	0.57	2.17	3.00
MQ01.1.12	2002	20	3%	0.281668	0.000055	0.0002723	0.0002723	4.82	1.93	2.30
MQ01.1.13	3048	24	82%	0.281065	0.000083	0.00227	0.00227	3.17	2.91	3.21
MQ01.1.14	3123	21	87%	0.281203	0.000063	0.001354	0.001354	11.68	2.21	2.72
MQ01.1.15	2293	43	42%	0.281325	0.000063	0.00032	0.00032	-0.83	2.21	2.89
MQ01.1.16	1948	29	6%	0.281521	0.00005	0.00089	0.00089	-2.44	1.75	2.73
MQ01.1.17	1918	34	1%	0.281568	0.000061	0.000716	0.000716	-1.21	2.14	2.63
MQ01.1.18	2561	22	16%	0.281025	0.000044	0.000652	0.000652	-5.96	1.54	3.42
MQ01.1.19	2646	17	48%	0.281186	0.000051	0.000998	0.000998	1.07	1.79	3.04
MQ01.1.20	2705	19	64%	0.281162	0.000095	0.001161	0.001161	1.24	3.33	3.08
MQ01.1.21	2638	27	27%	0.281235	0.000053	0.001163	0.001163	2.33	1.86	2.95
MQ01.1.22	2703	22	84%	0.281145	0.000082	0.001855	0.001855	-0.69	2.87	3.20
MQ01.1.23	2421	40	74%	0.2816	0.000074	0.00115	0.00115	10.50	2.59	2.26
MQ01.1.24	1902	29	6%	0.281658	0.000049	0.000451	0.000451	1.97	1.72	2.41
MQ01.1.25	1878	38	-2%	0.281597	0.000051	0.000489	0.000489	-0.78	1.79	2.57
MQ01.1.26	1895	22	-1%	0.28151	0.00006	0.001426	0.001426	-4.69	2.10	2.83
MQ01.1.27	2014	49	15%	0.281657	0.000065	0.000659	0.000659	4.17	2.28	2.36
MQ01.1.28	1978	32	3%	0.281465	0.000062	0.000701	0.000701	-3.51	2.17	2.82
MQ01.1.29	1878	44	2%	0.281638	0.000039	0.000215	0.000215	1.02	1.37	2.45
MQ01.1.30	1866	33	0%	0.281665	0.000055	0.000427	0.000427	1.44	1.93	2.42
MQ01.1.31	1964	24	0%	0.281529	0.000055	0.000546	0.000546	-1.34	1.93	2.67
MQ01.1.32	2014	32	5%	0.281534	0.000067	0.000502	0.000502	0.02	2.35	2.62
MQ01.1.33	2376	30	9%	0.28137	0.000048	0.0005093	0.0005093	2.35	1.68	2.75
MQ01.1.34	2373	31	71%	0.281546	0.000054	0.0007722	0.0007722	8.12	1.89	2.38
MQ01.1.35	2031	27	48%	0.281704	0.000066	0.000956	0.000956	5.82	2.31	2.26
MQ01.1.36	2140	37	62%	0.281368	0.000057	0.000995	0.000995	-3.75	2.00	2.96
MQ01.1.37	2219	23	80%	0.281684	0.000078	0.001525	0.001525	8.44	2.73	2.24
MQ01.1.38	2582	36	72%	0.281559	0.000061	0.000675	0.000675	13.46	2.14	2.19
MQ01.1.39	2545	28	2%	0.281173	0.00004	0.0008	0.0008	-1.32	1.40	3.12
MQ01.1.40	2518	21	-1%	0.281165	0.000077	0.000515	0.000515	-1.72	2.70	3.12
MQ01.1.41	1997	45	53%	0.281609	0.000053	0.000632	0.000632	2.13	1.86	2.47

MQ01.1.42	1852	32	3%	0.281548	0.000049	0.000637	0.000637	-3.29	1.72	2.71
MQ01.1.43	2507	22	77%	0.281189	0.000067	0.001409	0.001409	-2.64	2.35	3.17
MQ01.1.44	2708	20	42%	0.281216	0.000055	0.002159	0.002159	1.39	1.93	3.07
MQ01.1.45	2167	39	74%	0.281662	0.000068	0.001212	0.001212	6.97	2.38	2.29
MQ01.1.46	1888	58	6%	0.281506	0.000047	0.000531	0.000531	-3.84	1.65	2.77
MQ01.1.47	3122	29	0%	0.280848	0.000056	0.0003306	0.0003306	1.20	1.96	3.40
MQ01.1.48	2093	23	63%	0.281665	0.000056	0.001041	0.001041	5.69	1.96	2.32
MQ01.1.49	2014	24	47%	0.281633	0.000054	0.00067	0.00067	3.31	1.89	2.41
MQ01.1.50	1916	44	45%	0.281539	0.000058	0.00063	0.00063	-2.17	2.03	2.68
MQ01.1.51	2082	23	47%	0.281599	0.000058	0.000419	0.000419	3.98	2.03	2.42
MQ01.1.52	2031	26	2%	0.281736	0.000058	0.000818	0.000818	7.14	2.03	2.18
MQ01.1.53	1871	35	4%	0.281637	0.000062	0.00030421	0.00030421	0.71	2.17	2.47
MQ01.1.54	1878	28	-4%	0.281468	0.000059	0.0007603	0.0007603	-5.71	2.07	2.88
MQ01.1.55	1870	29	2%	0.281656	0.000046	0.000453	0.000453	1.18	1.61	2.44
MQ01.1.56	2689	37	83%	0.281125	0.000068	0.00271	0.00271	-3.27	2.38	3.35
MQ01.1.57	1838	23	-1%	0.281549	0.000055	0.0000119	0.0000119	-2.79	1.93	2.66
MQ01.1.58	2512	30	18%	0.281256	0.000062	0.000745	0.000745	0.98	2.17	2.94
MQ01.1.59	2583	19	-2%	0.281143	0.000048	0.0002344	0.0002344	-0.54	1.68	3.09
MQ01.1.60	2582	24	4%	0.281264	0.000054	0.000378	0.000378	3.49	1.89	2.84
MQ01.1.61	2666	28	-1%	0.281172	0.000045	0.0000693	0.0000693	2.70	1.58	2.95
MQ01.1.62	2185	27	59%	0.281493	0.000062	0.001187	0.001187	1.40	2.17	2.66
MQ01.1.63	1871	27	-1%	0.281526	0.000052	0.000543	0.000543	-3.53	1.82	2.74
MQ01.1.64	2289	31	73%	0.281676	0.000074	0.001838	0.001838	9.20	2.59	2.24
MQ01.1.65	2084	38	12%	0.281608	0.000064	0.000639	0.000639	4.03	2.24	2.42
MQ01.1.66	2103	26	61%	0.281591	0.000065	0.000888	0.000888	3.50	2.28	2.47
MQ01.1.67	2604	26	12%	0.281094	0.000067	0.000707	0.000707	-2.63	2.35	3.24
MQ01.1.68	2550	26	60%	0.281238	0.000066	0.000741	0.000741	1.21	2.31	2.96
MQ01.1.69	2067	29	51%	0.281617	0.000066	0.001137	0.001137	3.27	2.31	2.45
MQ01.1.70	2104	28	56%	0.281499	0.000051	0.0007	0.0007	0.52	1.79	2.66
MQ01.1.71	2261	22	60%	0.281545	0.000067	0.001034	0.001034	5.17	2.35	2.48
MQ01.1.72	2014	30	39%	0.281515	0.000053	0.0006875	0.0006875	-0.91	1.86	2.68

MQ01.1.73	1873	32	-2%	0.281539	0.000046	0.0003488	0.0003488	-2.78	1.61	2.69
MQ01.1.74	2447	23	17%	0.281377	0.000072	0.001276	0.001276	2.94	2.52	2.77
MQ01.1.75	2763	20	53%	0.281026	0.000063	0.001826	0.001826	-3.56	2.21	3.43
MQ01.1.76	2721	25	78%	0.281284	0.000053	0.001279	0.001279	5.72	1.86	2.80
MQ01.1.77	2642	23	12%	0.281207	0.000058	0.000958	0.000958	1.80	2.03	2.99
MQ01.1.78	2024	23	32%	0.281657	0.00006	0.000753	0.000753	4.27	2.10	2.36
MQ01.1.79	2073	24	53%	0.28156	0.000047	0.000836	0.000836	1.80	1.65	2.55
MQ01.1.80	2817	55	61%	0.281149	0.000081	0.001739	0.001739	2.17	2.84	3.10
MQ01.1.81	2614	24	25%	0.281146	0.000053	0.000748	0.000748	-0.63	1.86	3.12
MQ01.1.82	2822	34	0%	0.280924	0.000064	0.000874	0.000874	-4.06	2.24	3.50
MQ01.1.83	2028	31	-4%	0.281636	0.000051	0.000496	0.000496	3.97	1.79	2.38
MQ01.1.84	2575	20	2%	0.281198	0.000062	0.00091	0.00091	0.05	2.17	3.05
MQ01.1.85	1936	36	14%	0.281615	0.000067	0.00079	0.00079	0.77	2.35	2.51
MQ01.1.86	2120	47	48%	0.281454	0.000054	0.000785	0.000785	-0.84	1.89	2.76
MQ01.1.87	1927	37	16%	0.281527	0.000056	0.00089	0.00089	-2.69	1.96	2.73
MQ01.1.88	2589	32	2%	0.281207	0.000052	0.000891	0.000891	0.72	1.82	3.02
MQ01.1.89	2138	33	2%	0.281406	0.00006	0.0004166	0.0004166	-1.61	2.10	2.82
MQ01.1.90	2651	44	67%	0.281161	0.000048	0.00147	0.00147	-0.56	1.68	3.15
MQ01.1.91	2646	29	32%	0.281136	0.000046	0.000514	0.000514	0.16	1.61	3.10
MQ01.1.92	3089	31	15%	0.281026	0.000095	0.0006701	0.0006701	6.06	3.33	3.06
MQ01.1.93	2644	25	54%	0.281255	0.000048	0.00102	0.00102	3.44	1.68	2.89
MQ01.1.94	2614	29	50%	0.281067	0.000062	0.000839	0.000839	-3.60	2.17	3.31
MQ01.1.95	2001	87	0%	0.281528	0.000053	0.000655	0.000655	-0.69	1.86	2.66
MQ01.1.96	2031	41	13%	0.281494	0.000052	0.000674	0.000674	-1.26	1.82	2.72
MQ01.1.97	2031	30	4%	0.281548	0.000076	0.000672	0.000672	0.67	2.66	2.59
MQ01.1.98	2611	24	0%	0.281163	0.000049	0.000575	0.000575	0.21	1.72	3.07
MQ01.1.99	1878	27	-1%	0.281525	0.000048	0.0003573	0.0003573	-3.17	1.68	2.72
MQ01.1.100	1942	26	9%	0.281697	0.000044	0.0004771	0.0004771	4.22	1.54	2.30
MQ01.1.101	2611	25	0%	0.281168	0.000061	0.0004711	0.0004711	0.58	2.14	3.05
MQ01.1.102	1919	29	-1%	0.28155	0.000065	0.000473	0.000473	-1.51	2.28	2.65
MQ01.1.103	2240	33	55%	0.281648	0.000055	0.000483	0.000483	9.20	1.93	2.21

MQ01.1.104	1960	30	26%	0.281075	0.000058	0.000484	0.000484	-17.47	2.03	3.68
MQ01.1.105	1890	27	0%	0.281633	0.000053	0.0003275	0.0003275	0.97	1.86	2.46
MQ01.2.01	2615	40	37%	0.281339	0.000074	0.00095	0.0337	-4.61	2.59	3.02
MQ01.2.02	2636	34	46%	0.281694	0.000039	0.0004622	0.01571	3.87	1.37	2.31
MQ01.2.03	2606	38	35%	0.280843	0.000051	0.00084	0.0275	-1.89	1.79	3.53
MQ01.2.04	3178	62	58%	0.281694	0.000072	0.000479	0.01636	8.01	2.52	2.19
MQ01.2.05	2888	63	79%	0.281583	0.000068	0.001238	0.0432	4.59	2.38	2.46
MQ01.2.06	2007	60	31%	0.281514	0.000053	0.0001733	0.00539	-0.06	1.86	2.63
MQ01.2.07	1902	39	7%	0.281561	0.000038	0.000858	0.02918	6.99	1.33	2.40
MQ01.2.08	2644	44	51%	0.281294	0.000048	0.001149	0.04	3.70	1.68	2.84
MQ01.2.09	1881	41	0%	0.281583	0.00005	0.000922	0.0324	2.25	1.75	2.52
MQ01.2.10	1939	63	11%	0.281561	0.000067	0.000841	0.0302	-2.55	2.35	2.68
MQ01.2.11	2474	52	28%	0.281607	0.000066	0.000681	0.0239	10.59	2.31	2.22
MQ01.2.12	2565	38	42%	0.281546	0.000045	0.00076	0.0266	0.25	1.58	2.61
MQ01.2.13	1820	54	13%	0.281161	0.000058	0.000519	0.017	-0.28	2.03	3.08
MQ01.2.14	2569	47	16%	0.28157	0.000045	0.000944	0.03207	4.19	1.58	2.48
MQ01.2.15	2734	43	80%	0.281723	0.000057	0.000766	0.0266	4.39	2.00	2.27
MQ01.2.16	2200	38	64%	0.281542	0.000066	0.0005289	0.01599	-2.07	2.31	2.67
MQ01.2.17	1991	71	9%	0.281288	0.000052	0.0001777	0.00622	-9.21	1.82	3.17
MQ01.2.18	2502	53	19%	0.281645	0.000051	0.000824	0.0285	-0.32	1.79	2.51
MQ01.2.19	1951	36	19%	0.281216	0.00006	0.00126	0.0409	1.11	2.10	3.02
MQ01.2.20	1973	44	12%	0.281137	0.000052	0.000517	0.0178	-1.25	1.82	3.14
MQ01.2.21	1967	38	31%	0.281685	0.00006	0.001109	0.0388	1.56	2.10	2.42
MQ01.2.22	2542	42	3%	0.281544	0.000033	0.000424	0.0148	-3.01	1.16	2.69
MQ01.2.23	2074	43	44%	0.281487	0.000052	0.0007073	0.02467	-3.25	1.82	2.78
MQ01.2.24	2552	39	27%	0.281193	0.00005	0.000591	0.02009	1.02	1.75	3.01
MQ01.2.25	2145	43	59%	0.281148	0.000047	0.000767	0.0248	-57.89	1.65	4.61
MQ01.2.26	1909	49	16%	0.281204	0.00005	0.000668	0.02292	1.71	1.75	2.98
MQ01.2.27	1898	39	8%	0.281559	0.000059	0.000611	0.0212	-1.95	2.07	2.65
MQ01.2.28			#DIV/0!	0.281434	0.000058	0.000654	0.0224	0.77	2.03	2.73

MQ01.2.29	1873	41	0%	0.281573	0.000053	0.000364	0.0121	0.53	1.86	2.55
MQ01.2.30	1899	46	10%	0.281719	0.000053	0.000676	0.0241	4.14	1.86	2.28
MQ01.2.31	2460	36	9%	0.281279	0.000072	0.001537	0.0455	2.72	2.52	2.91
MQ01.2.32	1967	49	-1%	0.281228	0.000061	0.000912	0.0267	2.49	2.14	2.94
MQ01.2.33	2661	40	40%	0.281206	0.000044	0.001049	0.0312	0.79	1.54	3.03
MQ01.2.34	2573	39	4%	0.281251	0.000063	0.00129	0.0299	14.76	2.21	2.57
MQ01.2.35	2216	36	75%	0.28122	0.000069	0.001966	0.0577	5.82	2.42	2.92
MQ01.2.36	2620	33	28%	0.281657	0.000052	0.000783	0.02383	3.85	1.82	2.37
MQ01.2.37	2145	50	16%	0.281661	0.000054	0.000775	0.02448	1.66	1.89	2.43
MQ01.2.38	1930	49	1%	0.281045	0.000074	0.000803	0.0252	-3.64	2.59	3.34
MQ01.2.39	3042	45	4%	0.281652	0.000057	0.0005442	0.01732	1.17	2.00	2.44
MQ01.2.40	2115	51	25%	0.281437	0.000043	0.000596	0.0192	-5.23	1.51	2.90
MQ01.2.41	2188	45	49%	0.281248	0.000057	0.000439	0.0131	0.36	2.00	2.95
MQ01.2.42	2022	37	1%	0.281382	0.000059	0.000857	0.02607	6.47	2.07	2.63
MQ01.2.43	2305	40	75%	0.281543	0.000042	0.000616	0.01938	-4.15	1.47	2.74
MQ01.2.44	2604	34	0%	0.281229	0.000051	0.000599	0.01854	1.56	1.79	2.95
MQ01.2.45	2062	40	34%	0.281199	0.000059	0.00136	0.0464	2.83	2.07	3.00
MQ01.2.46	1876	44	5%	0.281614	0.000057	0.0007718	0.02552	6.65	2.00	2.34
MQ01.2.47	2380	42	83%	0.281487	0.000048	0.00021257	0.006364	-1.78	1.68	2.72
MQ01.2.48	2021	44	5%	0.281431	0.000052	0.00109	0.0345	6.40	1.82	2.59
MQ01.2.49	2588	39	0%	0.281535	0.000058	0.00056	0.0174	-1.44	2.03	2.67
MQ01.2.50	2171	35	61%	0.281472	0.00005	0.0007185	0.02431	-3.39	1.75	2.81
MQ01.2.51	1925	55	0%	0.281535	0.00006	0.001	0.0338	-1.66	2.10	2.69
MQ01.2.52	1910	60	0%	0.281215	0.000046	0.00069	0.0229	0.30	1.61	3.01
MQ01.2.53	1973	44	0%	0.281678	0.00004	0.001073	0.03649	5.69	1.40	2.30
MQ01.2.54	1841	47	0%	0.281313	0.000047	0.001002	0.03178	3.47	1.65	2.81
MQ01.2.55	2621	36	46%	0.28165	0.000044	0.000308	0.0115	7.37	1.54	2.25
MQ01.2.56	2583	39	2%	0.281629	0.000049	0.000646	0.0221	0.85	1.72	2.49
MQ01.2.57	1878	49	4%	0.28164	0.000051	0.0004786	0.01582	1.21	1.79	2.46
MQ01.2.58	1859	56	0%	0.281539	0.000059	0.00071	0.0244	-44.06	2.07	3.79
MQ01.2.59	1955	42	1%	0.281681	0.000047	0.0005219	0.01774	2.05	1.65	2.38

MQ01.2.60	2601	40	50%	0.281688	0.000047	0.000618	0.02126	2.76	1.65	2.36
MQ01.2.61				0.281322	0.000046	0.000935	0.0309	1.84	1.61	2.85
MQ01.2.62	2620	40	7%	0.281573	0.000043	0.0006008	0.02008	0.22	1.51	2.57
MQ01.2.63	1893	42	5%	0.281218	0.000051	0.000403	0.01291	3.62	1.79	2.89
MQ01.2.64	2215	67	16%	0.281312	0.000042	0.001175	0.04036	3.60	1.47	2.82
MQ01.2.65	1967	40	-1%	0.281669	0.00005	0.000652	0.0206	9.15	1.75	2.19
MQ01.2.66	1915	43	2%	0.281245	0.000044	0.001206	0.0435	2.21	1.54	2.95

Sample: MQ02

Grain ID	*207Pb/206Pb Age (Ma)*	*± 1σ (Ma)*	*Disc (%)*	*176Hf/177Hf*	*± 1SE(abs)*	*176Lu/177Hf*	*176Yb/177Hf*	*εHf (t)*	*εHf ± 1SE*	*TDM Crustal (Ga)*
MQ02.1.01	2575	35	69%	0.281184	0.000047	0.00173	0.074	-1.88	1.65	3.17
MQ02.1.02	2549	20	42%	0.281179	0.000059	0.001047	0.0405	-1.44	2.07	3.13
MQ02.1.03	1901	33	12%	0.281642	0.000045	0.001045	0.0394	0.62	1.58	2.50
MQ02.1.04	1901	28	1%	0.281603	0.000048	0.000679	0.0249	-0.30	1.68	2.55
MQ02.1.05	1918	26	10%	0.281494	0.00004	0.0008	0.0297	-3.94	1.40	2.80
MQ02.1.06	2554	19	22%	0.28119	0.000056	0.00094	0.0348	-0.75	1.96	3.09
MQ02.1.07	1983	35	-1%	0.28088	0.000048	0.000854	0.0339	-24.38	1.68	4.13
MQ02.1.08	1905	23	-1%	0.281386	0.000034	0.0003624	0.01268	-7.51	1.19	3.01
MQ02.1.09	2022	30	64%	0.281641	0.000064	0.001258	0.0522	2.97	2.24	2.44
MQ02.1.10	1868	24	-1%	0.281612	0.000061	0.000474	0.0163	-0.45	2.14	2.54
MQ02.1.11	2466	22	22%	0.281302	0.00006	0.000634	0.0216	1.77	2.10	2.86
MQ02.1.12	1893	34	2%	0.28168	0.000045	0.000482	0.017	2.51	1.58	2.37
MQ02.1.13	2218	28	83%	0.281429	0.000057	0.002308	0.0994	-1.82	2.00	2.90
MQ02.1.14	2514	27	71%	0.281081	0.000043	0.00275	0.122	-8.62	1.51	3.55
MQ02.1.15	1881	38	3%	0.281573	0.000044	0.000474	0.01781	-1.55	1.54	2.62
MQ02.1.16	2005	23	-1%	0.281481	0.000038	0.0003734	0.01257	-1.89	1.33	2.74
MQ02.1.17	1888	37	4%	0.281452	0.000062	0.000724	0.02552	-6.01	2.17	2.91
MQ02.1.18	2550	19	38%	0.281179	0.00004	0.001313	0.0553	-1.88	1.40	3.16
MQ02.1.19	1873	47	-2%	0.281562	0.000063	0.000375	0.01322	-1.99	2.21	2.64
MQ02.1.20	2123	32	30%	0.281402	0.000052	0.001019	0.0402	-2.96	1.82	2.89

MQ02.1.21	1899	39	0%	0.281527	0.000059	0.0005388	0.01915	-2.86	2.07	2.72
MQ02.1.22	2678	26	20%	0.281191	0.000062	0.0008	0.0296	2.32	2.17	2.99
MQ02.1.23	1983	31	1%	0.281472	0.000043	0.0004439	0.01531	-2.80	1.51	2.78
MQ02.1.24	2517	23	0%	0.281194	0.000051	0.0003763	0.012405	-0.48	1.79	3.04
MQ02.1.25	2019	29	69%	0.281647	0.000062	0.002452	0.102	1.49	2.17	2.53
MQ02.1.26	1905	31	-1%	0.281556	0.000045	0.000427	0.01397	-1.55	1.58	2.64
MQ02.1.27	2434	23	-3%	0.28136	0.000045	0.000702	0.0235	2.99	1.58	2.75
MQ02.1.28	2070	26	72%	0.281379	0.000067	0.002358	0.1003	-6.82	2.35	3.10
MQ02.1.29	2282	64	0%	0.281274	0.000057	0.000419	0.01371	-3.05	2.00	3.02
MQ02.1.30	1884	72	1%	0.281532	0.00006	0.000647	0.0221	-3.16	2.10	2.72
MQ02.1.31	1884	42	10%	0.281556	0.000065	0.0004277	0.01542	-2.03	2.28	2.65
MQ02.1.32	2640	23	1%	0.281191	0.000054	0.000866	0.0315	1.35	1.89	3.02
MQ02.1.33	1868	25	-1%	0.281595	0.000063	0.000511	0.01766	-1.10	2.21	2.58
MQ02.1.34	2717	76	12%	0.281391	0.000055	0.0006144	0.02216	10.66	1.93	2.48
MQ02.1.35	1895	36	0%	0.281574	0.000056	0.000607	0.02011	-1.37	1.96	2.62
MQ02.1.36	2152	38	1%	0.281346	0.000059	0.000954	0.03713	-4.21	2.07	3.00
MQ02.1.37	2089	34	1%							
MQ02.1.38	2078	41	-2%	0.281411	0.000046	0.0002595	0.00883	-2.57	1.61	2.83
MQ02.1.39	2513	22	62%	0.281174	0.000067	0.001651	0.0691	-3.46	2.35	3.23
MQ02.1.40	2606	19	4%	0.281177	0.000051	0.000978	0.0357	-0.12	1.79	3.09
MQ02.1.41	1868	29	0%	0.281658	0.00005	0.000681	0.02503	0.92	1.75	2.45
MQ02.1.42	1876	28	4%	0.281441	0.000047	0.000625	0.02258	-6.54	1.65	2.93
MQ02.1.43	2476	29	0%	0.281284	0.000037	0.000711	0.02465	1.22	1.30	2.90
MQ02.1.44	2019	31	0%	0.28148	0.000053	0.00066	0.02327	-2.00	1.86	2.75
MQ02.1.45	1878	33	6%	0.281619	0.000045	0.0007026	0.02598	-0.27	1.58	2.53
MQ02.1.46	1863	33	-2%	0.281487	0.000056	0.0004047	0.0147	-4.92	1.96	2.82
MQ02.1.47	2025	29	57%	0.281516	0.00004	0.00159	0.0632	-1.86	1.40	2.75
MQ02.1.48	1942	47	15%	0.281534	0.000063	0.000669	0.02415	-1.82	2.21	2.68
MQ02.1.49	2022	26	39%	0.281539	0.000061	0.000983	0.0395	-0.28	2.14	2.65
MQ02.1.50	1910	43	18%	0.281695	0.000045	0.000464	0.017	3.45	1.58	2.32
MQ02.1.51	2542	19	-1%	0.281194	0.00006	0.000406	0.01435	0.04	2.10	3.03

MQ02.1.52	1830	54	-3%	0.281556	0.000052	0.000435	0.0151	-3.25	1.82	2.69
MQ02.1.53	1985	37	0%	0.281545	0.000056	0.000477	0.0172	-0.21	1.96	2.61
MQ02.1.54	2342	24	81%	0.281059	0.000067	0.00342	0.1607	-14.09	2.35	3.77
MQ02.1.55	1887	30	1%	0.281527	0.000057	0.000377	0.0133	-2.92	2.00	2.71
MQ02.1.56	2557	22	5%	0.281204	0.000056	0.000687	0.02302	0.25	1.96	3.02
MQ02.1.57	1870	35	-1%	0.281475	0.000054	0.000291	0.00998	-5.04	1.89	2.83
MQ02.1.58	2491	31	70%	0.28117	0.000053	0.001859	0.0762	-4.43	1.86	3.27
MQ02.1.59	2397	21	0%	0.281331	0.000043	0.000738	0.0252	1.07	1.51	2.85
MQ02.1.60	1876	57	0%	0.281505	0.00005	0.000545	0.01862	-4.16	1.75	2.78
MQ02.1.61	1892	31	-3%	0.281499	0.000061	0.0001852	0.00587	-3.56	2.14	2.75
MQ02.1.62	2001	33	3%	0.281565	0.000066	0.000755	0.0287	0.49	2.31	2.58
MQ02.1.63	2352	24	10%	0.281252	0.000051	0.000517	0.01686	-2.40	1.79	3.04
MQ02.1.64	2637	21	21%	0.281189	0.000071	0.00079	0.0308	1.34	2.49	3.02
MQ02.1.65	1843	37	0%	0.281502	0.000065	0.0003846	0.013861	-4.81	2.28	2.80
MQ02.1.66	2478	23	82%	0.281259	0.000061	0.00226	0.0995	-2.22	2.14	3.12
MQ02.1.67	1859	40	-2%	0.28152	0.000055	0.000435	0.01509	-3.87	1.93	2.75
MQ02.1.68	2684	24	56%	0.281166	0.000071	0.00145	0.0558	0.38	2.49	3.11
MQ02.1.69	1986	31	58%	0.281654	0.000057	0.001335	0.0563	2.54	2.00	2.44
MQ02.1.70	1887	38	2%	0.281649	0.000054	0.000492	0.01814	1.26	1.89	2.44
MQ02.1.71	2552	20	0%	0.281102	0.000058	0.0005718	0.02078	-3.29	2.03	3.25
MQ02.1.72	1916	44	1%	0.281532	0.000058	0.000445	0.01579	-2.18	2.03	2.69
MQ02.1.73	1915	34	0%	0.281398	0.000053	0.000397	0.01352	-6.90	1.86	2.98
MQ02.1.74	2135	28	0%	0.281482	0.000061	0.000298	0.0098	1.19	2.14	2.64
MQ02.1.75	1895	28	0%	0.281523	0.00006	0.0005581	0.018942	-3.12	2.10	2.73
MQ02.1.76	1859	33	-1%	0.281518	0.000062	0.000468	0.01678	-3.99	2.17	2.76
MQ02.1.77	1874	38	5%	0.281535	0.000047	0.000544	0.0191	-3.14	1.65	2.71
MQ02.1.78	2363	26	0%	0.281291	0.00004	0.0003796	0.01302	-0.54	1.40	2.93
MQ02.1.79	1992	31	12%	0.281573	0.000064	0.0006913	0.0261	0.65	2.24	2.56
MQ02.1.80	1943	50	18%	0.281563	0.000067	0.000637	0.0235	-0.72	2.35	2.61
MQ02.1.81	1910	23	0%	0.281451	0.000048	0.000862	0.0284	-5.73	1.68	2.91
MQ02.1.82	2527	33	1%	0.28083	0.000049	0.0002351	0.00843	-12.95	1.72	3.84

MQ02.1.83	2035	28	2%	0.28162	0.000048	0.0005347	0.01844	3.50	1.68	2.41
MQ02.1.84	1930	36	12%	0.281512	0.000068	0.000527	0.01905	-2.68	2.38	2.73
MQ02.1.85	1899	40	4%	0.281737	0.000068	0.001006	0.0399	4.00	2.38	2.28
MQ02.1.86	2595	27	11%	0.281151	0.000071	0.001014	0.03798	-1.35	2.49	3.16
MQ02.1.87	2553	17	16%	0.281223	0.000064	0.002071	0.0742	-1.56	2.24	3.14
MQ02.1.88	1896	34	22%	0.28167	0.000062	0.000705	0.0261	1.94	2.17	2.41
MQ02.1.89	1919	38	7%	0.281546	0.000041	0.000503	0.01692	-1.69	1.44	2.66
MQ02.1.90	2610	26	0%	0.281172	0.000064	0.0003519	0.01169	0.91	2.24	3.02
MQ02.1.91	1874	25	1%	0.281481	0.00005	0.00034	0.0111	-4.80	1.75	2.82
MQ02.1.92	2575	18	19%	0.281191	0.000075	0.000867	0.0342	-0.12	2.63	3.06
MQ02.1.93	2564	23	54%	0.281159	0.000075	0.0015	0.067	-2.61	2.63	3.21
MQ02.1.94	2035	23	41%	0.281269	0.000074	0.001011	0.042	-9.62	2.59	3.25
MQ02.1.95	2124	23	65%	0.281371	0.000083	0.001	0.0416	-4.01	2.91	2.96
MQ02.1.96	2575	21	51%	0.281188	0.000062	0.00186	0.0755	-1.96	2.17	3.18
MQ02.1.97	2599	20	-2%	0.28119	0.000042	0.000377	0.01333	1.25	1.47	2.99
MQ02.1.98	2484	30	76%	0.281084	0.000059	0.00149	0.063	-7.02	2.07	3.43
MQ02.1.99	2579	22	69%	0.28118	0.000062	0.00206	0.0848	-2.51	2.17	3.22
MQ02.1.100	1975	25	20%	0.281461	0.000064	0.00095	0.036	-4.05	2.24	2.85
MQ02.1.101	1980	28	0%	0.28157	0.000049	0.0003633	0.01277	0.72	1.72	2.55
MQ02.1.102	2458	38	0%	0.280868	0.000053	0.0002651	0.009262	-13.23	1.86	3.80
MQ02.1.103	1949	30	3%	0.281563	0.000042	0.0005708	0.02042	-0.50	1.47	2.60
MQ02.1.104	2575	19	2%	0.2812	0.000045	0.0005439	0.0192	0.77	1.58	3.01
MQ02.1.105	1927	44	0%	0.281486	0.000068	0.0002645	0.00893	-3.33	2.38	2.77
MQ02.1.106	2614	28	0%	0.281207	0.000051	0.001072	0.03994	0.96	1.79	3.02
MQ02.1.107	1985	34	61%	0.281559	0.000051	0.001473	0.0548	-1.05	1.79	2.67
MQ02.1.108	2602	26	34%	0.281172	0.000068	0.00131	0.053	-0.97	2.38	3.14
MQ02.1.109	1878	25	5%	0.28169	0.000054	0.000315	0.0117	2.74	1.89	2.34
MQ02.1.110	2017	37	0%	0.281516	0.000048	0.000937	0.03476	-1.15	1.68	2.70
MQ02.1.111	2115	47	68%	0.281499	0.000047	0.00199	0.085	-1.08	1.65	2.77
MQ02.1.112	1915	28	6%	0.281653	0.000054	0.00053	0.0188	1.98	1.89	2.42
MQ02.1.113	2608	42	0%	0.281172	0.000048	0.00088	0.0318	-0.08	1.68	3.08

MQ02.1.114	1902	34	2%	0.281532	0.000039	0.000776	0.0274	-2.92	1.37	2.72
MQ02.1.115	1899	28	6%	0.281563	0.000058	0.000538	0.0175	-1.58	2.03	2.63
MQ02.1.116	1951	24	4%	0.281439	0.000039	0.0000714	0.00316	-4.20	1.37	2.84
MQ02.1.117	2540	27	0%	0.28108	0.000053	0.000415	0.01448	-4.07	1.86	3.29
MQ02.1.118	2580	27	8%	0.281168	0.000063	0.000823	0.0302	-0.75	2.21	3.11
MQ02.1.119	1890	34	25%	0.281211	0.000059	0.00088	0.0363	-14.72	2.07	3.46
MQ02.1.120	1972	28	58%	0.281505	0.000059	0.000695	0.0272	-2.21	2.07	2.73
MQ02.1.121	1892	34	1%	0.281486	0.000056	0.000556	0.019	-4.49	1.96	2.81
MQ02.1.122	2555	22	-1%	0.28113	0.000057	0.0005655	0.01866	-2.22	2.00	3.18
MQ02.1.123	1973	30	0%	0.281442	0.000051	0.001119	0.03568	-4.99	1.79	2.91
MQ02.1.124	1870	33	0%	0.281501	0.000041	0.0002905	0.00946	-4.12	1.44	2.77
MQ02.1.125	1878	47	1%	0.281516	0.000062	0.0003984	0.013799	-3.54	2.17	2.74
MQ02.1.126	1901	25	0%	0.281591	0.000048	0.0000738	0.00307	0.05	1.68	2.53
MQ02.1.127	1930	29	1%	0.281573	0.000062	0.00042564	0.01424	-0.38	2.17	2.58
MQ02.1.128	2779	21	79%	0.281112	0.000075	0.00238	0.107	-1.19	2.63	3.29
MQ02.2.01	1927	52	56%	0.281493	0.000073	0.00135	0.051	-4.49	2.56	2.84
MQ02.2.02	2608	36	0%	0.281187	0.000056	0.000685	0.0239	0.80	1.96	3.03
MQ02.2.03	1896	59	25%	0.281652	0.000052	0.000866	0.0352	1.09	1.82	2.46
MQ02.2.04	2034	45	55%	0.2816	0.000052	0.00131	0.0498	1.70	1.82	2.53
MQ02.2.05	2672	36	24%	0.281204	0.000061	0.0017	0.0579	1.01	2.14	3.06
MQ02.2.06	2733	41	91%	0.281039	0.00005	0.00168	0.071	-3.48	1.75	3.40
MQ02.2.07	2505	33	29%	0.281184	0.000041	0.00075	0.0253	-1.74	1.44	3.11
MQ02.2.08	1927	50	18%	0.281586	0.000051	0.000723	0.02385	-0.38	1.79	2.58
MQ02.2.09	2207	44	35%	0.281136	0.00004	0.00085	0.03392	-10.29	1.40	3.42
MQ02.2.10	2564	39	80%	0.281144	0.000069	0.00389	0.1599	-7.30	2.42	3.51
MQ02.2.11	1898	45	0%	0.281559	0.000048	0.0003704	0.011603	-1.53	1.68	2.63
MQ02.2.12	2695	37	0%	0.281215	0.000044	0.000395	0.01294	4.30	1.54	2.87
MQ02.2.13	2484	39	28%	0.281237	0.000049	0.000789	0.0291	-0.40	1.72	3.01

Sample: MIT1701d

Grain ID	207Pb/206Pb Age (Ma)	± 1σ (Ma)	Disc (%)	176Hf/177Hf	± 1SE(abs)	176Lu/177Hf	176Yb/177Hf	εHf (t)	εHf ± 1SE	TDM Crustal (Ga)
MIT1701d.3.01	1904	52	0%	0.281479	0.000033	0.0002867	0.00867	-4.13	1.16	2.80
MIT1701d.3.02	2589	42	5%	0.281162	0.000037	0.002	0.0582	-2.83	1.30	3.25
MIT1701d.3.03	2569	40	-4%	0.281085	0.000035	0.000822	0.0262	-3.95	1.23	3.30
MIT1701d.3.04	1881	44	1%	0.281695	0.000033	0.0007384	0.02335	2.45	1.16	2.36
MIT1701d.3.05	1892	45	3%	0.281516	0.000033	0.0004492	0.013	-3.29	1.16	2.74
MIT1701d.3.06	2044	46	0%	0.281515	0.000035	0.0006645	0.02001	-0.21	1.23	2.66
MIT1701d.3.07	1922	44	0%	0.28152	0.000033	0.0010732	0.03101	-3.29	1.16	2.76
MIT1701d.3.08	1866	71	0%	0.281518	0.000035	0.0005152	0.015779	-3.89	1.23	2.76
MIT1701d.3.09	1999	45	6%	0.281067	0.000031	0.000658	0.01806	-17.12	1.09	3.69
MIT1701d.3.10	1851	62	0%	0.281562	0.000031	0.001216	0.03792	-3.54	1.09	2.72
MIT1701d.3.11	2036	44	0%	0.281519	0.000038	0.0012071	0.03619	-0.99	1.33	2.70
MIT1701d.3.12	2480	50	1%	0.281268	0.000029	0.000924	0.02887	0.39	1.02	2.96
MIT1701d.3.13	1999	45	1%	0.281451	0.000026	0.0003597	0.01078	-3.07	0.91	2.81
MIT1701d.3.14	2027	43	15%	0.281602	0.000042	0.000655	0.0233	2.52	1.47	2.47
MIT1701d.3.15	2695	38	1%	0.281201	0.000042	0.00157	0.0461	1.65	1.47	3.04
MIT1701d.3.16	2417	41	4%	0.281352	0.000037	0.000504	0.01462	2.65	1.30	2.76
MIT1701d.3.17	1855	53	0%	0.281491	0.000048	0.000502	0.01571	-5.08	1.68	2.82
MIT1701d.3.18	2591	38	-3%	0.281153	0.000037	0.0009362	0.02758	-1.23	1.30	3.15
MIT1701d.3.19	2581	38	1%	0.281144	0.000039	0.0005396	0.01644	-1.08	1.37	3.13
MIT1701d.3.20	1871	46	0%	0.281217	0.000035	0.0006711	0.02129	-14.66	1.23	3.44
MIT1701d.3.21	2207	43	44%	0.28161	0.000046	0.002555	0.0887	4.00	1.61	2.52
MIT1701d.3.22	1893	44	0%	0.281485	0.000049	0.0007301	0.02121	-4.73	1.72	2.83
MIT1701d.3.23	2582	41	1%	0.281174	0.00004	0.000955	0.0298	-0.72	1.40	3.11
MIT1701d.3.24	1958	48	2%	0.281552	0.000046	0.000295	0.00927	-0.33	1.61	2.60
MIT1701d.3.25	2604	40	1%	0.281163	0.000034	0.000935	0.029	-0.58	1.19	3.11
MIT1701d.3.26	2627	42	4%	0.28117	0.000035	0.000642	0.0195	0.71	1.23	3.05
MIT1701d.3.27	1969	40	12%	0.281645	0.000044	0.001285	0.0407	1.91	1.54	2.47
MIT1701d.3.28	2101	38	4%	0.281287	0.000034	0.000898	0.0265	-7.36	1.19	3.16
MIT1701d.3.29	1878	50	0%	0.281621	0.000037	0.000423	0.01301	0.15	1.30	2.51

MIT1701d.3.30	2703	37	-2%	0.281066	0.000039	0.0006417	0.016838	-1.27	1.37	3.23
MIT1701d.3.31	2546	42	-2%	0.281178	0.000045	0.0009701	0.02963	-1.41	1.58	3.12
MIT1701d.3.32	1942	77	3%	0.281536	0.000034	0.0006116	0.01929	-1.67	1.19	2.67
MIT1701d.3.33	2434	40	27%	0.281208	0.00004	0.001925	0.0617	-4.43	1.40	3.23
MIT1701d.3.34	1921	43	0%	0.281437	0.00004	0.000963	0.0308	-6.11	1.40	2.94
MIT1701d.3.35	2021	47	6%	0.281518	0.000032	0.0006008	0.01874	-0.53	1.12	2.66
MIT1701d.3.36	2001	55	4%	0.281542	0.00005	0.000894	0.0275	-0.52	1.75	2.65
MIT1701d.3.37	1983	48	1%	0.281548	0.000037	0.000373	0.0103	-0.01	1.30	2.60
MIT1701d.3.38	2578	52	2%	0.281176	0.000035	0.000826	0.0247	-0.51	1.23	3.09
MIT1701d.3.39	1879	56	1%	0.281505	0.000031	0.0004014	0.01261	-3.92	1.09	2.77
MIT1701d.3.40	1890	45	-2%	0.281452	0.000039	0.001058	0.03214	-6.39	1.37	2.93
MIT1701d.3.41	1855	89	-1%	0.281469	0.000035	0.0003413	0.01065	-5.66	1.23	2.86
MIT1701d.3.42	2036	48	18%	0.281665	0.000052	0.00226	0.075	2.75	1.82	2.46
MIT1701d.3.43	1909	51	2%	0.28147	0.000032	0.0003423	0.00979	-4.41	1.12	2.82
MIT1701d.3.44	1948	52	1%	0.281492	0.000024	0.0000802	0.002073	-2.40	0.84	2.72
MIT1701d.3.45	2436	39	-1%	0.281201	0.000059	0.000872	0.02587	-2.90	2.07	3.13
MIT1701d.3.46	1879	58	0%	0.281512	0.000029	0.0008895	0.028627	-4.28	1.02	2.79
MIT1701d.3.47	2002	48	-1%	0.281499	0.000036	0.001002	0.0307	-2.17	1.26	2.75
MIT1701d.3.48	1880	110	0%	0.281487	0.000035	0.000694	0.0214	-4.90	1.23	2.83
MIT1701d.3.49	1874	63	4%	0.28162	0.00004	0.000685	0.021	-0.30	1.40	2.53
MIT1701d.3.50	2544	40	6%	0.281166	0.000042	0.001217	0.0388	-2.31	1.47	3.18
MIT1701d.3.51	1888	61	0%	0.281559	0.000035	0.00002257	0.000804	-1.31	1.23	2.61
MIT1701d.3.52	2583	38	-1%	0.281174	0.000039	0.00114	0.0354	-1.02	1.37	3.13
MIT1701d.3.53	2582	51	7%	0.281167	0.000038	0.0006586	0.02022	-0.45	1.33	3.09
MIT1701d.3.54	2578	36	-5%	0.281168	0.000044	0.001286	0.03908	-1.60	1.54	3.16
MIT1701d.3.55	2550	43	0%	0.281065	0.000039	0.0004336	0.01305	-4.41	1.37	3.32
MIT1701d.3.56	1963	62	-1%	0.281512	0.000031	0.00032	0.00975	-1.67	1.09	2.69
MIT1701d.3.57	1888	55	4%	0.281546	0.000049	0.00112	0.03558	-3.17	1.72	2.73
MIT1701d.3.58	1904	62	1%	0.281515	0.000033	0.0003929	0.01219	-2.99	1.16	2.73
MIT1701d.3.59	1904	46	8%	0.281516	0.000037	0.000824	0.0266	-3.50	1.30	2.76
MIT1701d.3.60	2585	41	1%	0.281172	0.000036	0.001142	0.0369	-1.05	1.26	3.13

MIT1701d.3.61	1873	46	0%	0.281531	0.000039	0.000687	0.0211	-3.49	1.37	2.74
MIT1701d.3.62	2017	39	7%	0.281648	0.000051	0.00147	0.0475	2.82	1.79	2.44
MIT1701d.3.63	1931	58	4%	0.28148	0.000037	0.00048	0.01502	-3.74	1.30	2.80
MIT1701d.3.64	2361	36	0%	0.281409	0.000049	0.00244	0.0712	0.31	1.72	2.87
MIT1701d.3.65	1892	53	-1%	0.281519	0.000043	0.001119	0.035	-4.04	1.51	2.79
MIT1701d.3.66	2511	42	39%	0.281344	0.000049	0.00475	0.163	-2.74	1.72	3.18
MIT1701d.3.67	2572	35	-1%	0.281127	0.000029	0.0007479	0.02441	-2.26	1.02	3.20
MIT1701d.3.68	2575	40	0%	0.281215	0.00003	0.001495	0.0471	-0.36	1.05	3.08
MIT1701d.3.69	1916	44	0%	0.281556	0.000035	0.000624	0.01928	-1.56	1.23	2.65
MIT1701d.3.70	1881	41	-1%	0.281467	0.000032	0.001097	0.0355	-6.10	1.12	2.91

Sample: MIT1701e

Grain ID	*207Pb/206Pb Age (Ma)*	*± 1σ (Ma)*	*Disc (%)*	*176Hf/177Hf*	*± 1SE(abs)*	*176Lu/177Hf*	*176Yb/177Hf*	*εHf (t)*	*εHf ± 1SE*	*TDM Crustal (Ga)*
MIT1701e.3.01	1958	43	-4%	0.28156	0.000034	0.0005944	0.02004	-0.44	1.19	2.61
MIT1701e.3.02	2592	43	0%	0.281188	0.000036	0.0007477	0.024392	0.37	1.26	3.04
MIT1701e.3.03	2611	40	3%	0.281171	0.000038	0.0003502	0.01013	0.90	1.33	3.02
MIT1701e.3.04	2576	37	4%	0.281212	0.00004	0.001337	0.0484	-0.17	1.40	3.07
MIT1701e.3.05	2645	38	1%	0.281172	0.00004	0.000799	0.0281	0.90	1.40	3.05
MIT1701e.3.06	1898	42	2%	0.281655	0.000025	0.00006347	0.002598	2.27	0.88	2.39
MIT1701e.3.07	1925	43	-1%	0.281692	0.000031	0.000617	0.0201	3.48	1.09	2.33
MIT1701e.3.08	2601	47	20%	0.281174	0.000036	0.0008109	0.02625	-0.04	1.26	3.08
MIT1701e.3.09	1860	48	-2%	0.281537	0.000032	0.0004247	0.014113	-3.24	1.12	2.71
MIT1701e.3.10	2604	42	1%	0.281095	0.000033	0.000737	0.02456	-2.65	1.16	3.25
MIT1701e.3.11	1936	45	1%	0.281608	0.000025	0.00023	0.00953	1.25	0.88	2.48
MIT1701e.3.12	1879	50	0%	0.281646	0.000041	0.0004041	0.01338	1.09	1.44	2.45
MIT1701e.3.13	1873	44	-1%	0.281603	0.000037	0.0005536	0.01818	-0.76	1.30	2.56
MIT1701e.3.14	1879	44	-1%	0.281478	0.000038	0.000608	0.0194	-5.14	1.33	2.84
MIT1701e.3.15	1954	45	0%	0.281343	0.000036	0.0001219	0.00406	-7.61	1.26	3.06
MIT1701e.3.16	1951	46	1%	0.281577	0.000035	0.000826	0.02845	-0.30	1.23	2.59
MIT1701e.3.17	2510	40	13%	0.281207	0.000041	0.000959	0.0308	-1.17	1.44	3.08

MIT1701e.3.18	1975	46	0%	0.281434	0.000037	0.000566	0.0155	-4.50	1.30	2.88
MIT1701e.3.19	1999	43	8%	0.281348	0.000037	0.000931	0.0311	-7.50	1.30	3.09
MIT1701e.3.20	1905	52	7%	0.28154	0.000033	0.0006797	0.02162	-2.44	1.16	2.69
MIT1701e.3.21	1915	46	-4%	0.281512	0.000038	0.000813	0.02705	-3.39	1.33	2.76
MIT1701e.3.22	1910	45	0%	0.281574	0.000033	0.000202	0.00672	-0.51	1.16	2.57
MIT1701e.3.23	1980	50	1%	0.281064	0.000034	0.00032421	0.010356	-17.20	1.19	3.68
MIT1701e.3.24	2626	40	0%	0.281186	0.000038	0.00098	0.0312	0.65	1.33	3.05
MIT1701e.3.25	1893	54	0%	0.281481	0.000046	0.00041262	0.013481	-4.47	1.61	2.81
MIT1701e.3.26	1916	47	-1%	0.281245	0.000039	0.000775	0.024627	-12.80	1.37	3.36
MIT1701e.3.27	1871	43	-1%	0.281374	0.00004	0.000642	0.019247	-9.05	1.40	3.09
MIT1701e.3.28	2578	41	41%	0.281202	0.00003	0.000984	0.0343	0.13	1.05	3.05
MIT1701e.3.29	1904	42	10%	0.281486	0.000052	0.0006183	0.02324	-4.31	1.82	2.81
MIT1701e.3.30	1986	45	0%	0.28101	0.000028	0.00054514	0.01771	-19.28	0.98	3.82
MIT1701e.3.31	1866	46	0%	0.28158	0.000043	0.00169	0.05219	-3.16	1.51	2.71
MIT1701e.3.32	2055	39	31%	0.281595	0.000047	0.000452	0.0174	3.18	1.65	2.45
MIT1701e.3.33	2571	39	2%	0.281208	0.000031	0.00091	0.0289	0.32	1.09	3.03
MIT1701e.3.34	1860	48	-1%	0.281486	0.00004	0.000745	0.0236	-5.45	1.40	2.85
MIT1701e.3.35	2014	43	7%	0.281513	0.000033	0.000882	0.0288	-1.24	1.16	2.70
MIT1701e.3.36	1866	43	-2%	0.281488	0.000034	0.000381	0.01287	-4.79	1.19	2.81
MIT1701e.3.37	1890	51	0%	0.281447	0.000029	0.0002717	0.008572	-5.56	1.02	2.88
MIT1701e.3.38	2582	46	-2%	0.281076	0.000033	0.000793	0.02164	-3.92	1.16	3.31
MIT1701e.3.39	1899	46	1%	0.281411	0.000031	0.000707	0.0222	-7.19	1.09	2.99
MIT1701e.3.40	2027	54	1%	0.281577	0.000034	0.0005996	0.017233	1.71	1.19	2.52
MIT1701e.3.41	2621	39	1%	0.281202	0.000037	0.000871	0.0241	1.30	1.30	3.01
MIT1701e.3.42	1960	46	1%	0.281292	0.000028	0.000451	0.01363	-9.72	0.98	3.20
MIT1701e.3.43	1988	38	-4%	0.281597	0.000036	0.0012163	0.03881	0.71	1.26	2.56
MIT1701e.3.44	2534	37	-3%	0.281182	0.000029	0.0007278	0.02214	-1.12	1.02	3.09
MIT1701e.3.45	1865	51	1%	0.281521	0.000038	0.000637	0.01868	-3.96	1.33	2.76
MIT1701e.3.46	2447	43	17%	0.281231	0.000043	0.000939	0.0267	-1.69	1.51	3.06
MIT1701e.3.47	2612	42	-2%	0.281146	0.000041	0.000541	0.01488	-0.31	1.44	3.10
MIT1701e.3.48	2902	39	-3%	0.280848	0.000041	0.0003117	0.00957	-3.84	1.44	3.55

MIT1701e.3.49	1884	47	-7%	0.281556	0.000043	0.000534	0.01714	-2.16	1.51	2.66
MIT1701e.3.50	2517	37	-5%	0.281252	0.000035	0.0006036	0.01584	1.20	1.23	2.93
MIT1701e.3.51	1960	42	-6%	0.281632	0.000049	0.000636	0.01949	2.11	1.72	2.45
MIT1701e.3.52	1665	74	16%	0.281639	0.000042	0.000614	0.01847	-4.20	1.47	2.62
MIT1701e.3.53	1873	46	-1%	0.281628	0.00003	0.00003591	0.001423	0.78	1.05	2.46
MIT1701e.3.54	1881	45	-1%	0.281657	0.000037	0.0006823	0.02177	1.17	1.30	2.44
MIT1701e.3.55	1887	56	1%	0.281542	0.000029	0.000613	0.01896	-2.69	1.02	2.70
MIT1701e.3.56	1887	45	0%	0.281452	0.000034	0.000268	0.00709	-5.45	1.19	2.87
MIT1701e.3.57	1901	49	-2%	0.281423	0.000032	0.0009339	0.02914	-7.01	1.12	2.98
MIT1701e.3.58	1887	53	0%	0.281621	0.000034	0.0002644	0.00795	0.56	1.19	2.49
MIT1701e.3.59	1854	48	-2%	0.281535	0.000029	0.0005108	0.01637	-3.55	1.02	2.72
MIT1701e.3.60	1991	60	-1%	0.281545	0.000032	0.0007979	0.02592	-0.51	1.12	2.64
MIT1701e.3.61	2578	37	0%	0.281168	0.000028	0.0007716	0.02462	-0.70	0.98	3.10
MIT1701e.3.62	2591	58	7%	0.281158	0.000037	0.000763	0.02378	-0.75	1.30	3.11
MIT1701e.3.63	1887	48	0%	0.281404	0.00003	0.0008326	0.02492	-7.87	1.05	3.02
MIT1701e.3.64	2570	43	20%	0.28114	0.000042	0.0006	0.01872	-1.58	1.47	3.15
MIT1701e.3.65	1895	70	2%	0.281562	0.000032	0.0005012	0.01492	-1.66	1.12	2.64
MIT1701e.3.66	1885	42	-2%	0.281606	0.000028	0.000678	0.02173	-0.54	0.98	2.56
MIT1701e.3.67	1874	46	0%	0.281652	0.000046	0.00074	0.0229	0.76	1.61	2.47
MIT1701e.3.68	2465	42	36%	0.281379	0.000055	0.000901	0.0417	4.04	1.93	2.71
MIT1701e.3.69	1937	44	1%	0.281585	0.000029	0.0000729	0.003146	0.66	1.02	2.52
MIT1701e.3.70	1975	47	7%	0.281532	0.000048	0.000949	0.0308	-1.52	1.68	2.69

Sample: MIT1703e

Grain ID	*207Pb/206Pb Age (Ma)*	*± 1σ (Ma)*	*Disc (%)*	*176Hf/177Hf*	*± 1SE(abs)*	*176Lu/177Hf*	*176Yb/177Hf*	*εHf (t)*	*εHf ± 1SE*	*TDM Crustal (Ga)*
MIT1703e.4.01	1999	54	84%	0.281597	0.000056	0.00294	0.1012	-1.37	1.96	2.70
MIT1703e.4.02	2449	31	73%	0.281115	0.000046	0.00288	0.0933	-9.00	1.61	3.53
MIT1703e.4.03	2017	30	14%	0.281638	0.000045	0.002485	0.0741	1.08	1.58	2.56
MIT1703e.4.04	2157	31	70%	0.281325	0.000038	0.002325	0.075	-6.85	1.33	3.17
MIT1703e.4.05	1963	55	82%	0.281447	0.000049	0.00415	0.1451	-9.05	1.72	3.16

MIT1703e.4.06	1997	45	40%	0.281582	0.000043	0.000665	0.0212	1.12	1.51	2.54
MIT1703e.4.07	2501	36	76%	0.281083	0.000059	0.00292	0.0989	-9.11	2.07	3.58
MIT1703e.4.08	2518	25	91%	0.281151	0.000081	0.00582	0.196	-11.29	2.84	3.73
MIT1703e.4.09	1915	78	27%	0.281539	0.000037	0.00095	0.0298	-2.61	1.30	2.71
MIT1703e.4.10	1928	43	40%	0.281421	0.000039	0.00202	0.0639	-7.90	1.37	3.06
MIT1703e.4.11	2590	34	18%	0.281227	0.000037	0.0006872	0.02067	1.82	1.30	2.95
MIT1703e.4.12	2011	36	61%	0.281615	0.000051	0.00195	0.067	0.86	1.79	2.56
MIT1703e.4.13	1892	37	36%	0.281609	0.000052	0.000748	0.02413	-0.37	1.82	2.55
MIT1703e.4.14	1871	36	41%	0.281604	0.000052	0.001442	0.0473	-1.89	1.82	2.63
MIT1703e.4.15	1881	30	82%	0.281206	0.000055	0.005037	0.1896	-20.37	1.93	3.80
MIT1703e.4.16	1991	21	20%	0.281506	0.000034	0.0008364	0.02714	-1.94	1.19	2.73
MIT1703e.4.17	3262	31	1%	0.280741	0.000046	0.0003923	0.01114	0.49	1.61	3.55
MIT1703e.4.18	1865	25	1%	0.281679	0.000045	0.001007	0.0323	1.19	1.58	2.43
MIT1703e.4.19	2540	42	69%	0.28113	0.000039	0.001635	0.0574	-4.40	1.37	3.31
MIT1703e.4.20	2559	44	66%	0.281246	0.00005	0.002	0.068	-0.49	1.75	3.07
MIT1703e.4.21	1904	39	15%	0.281644	0.000058	0.001608	0.0544	0.03	2.03	2.54
MIT1703e.4.22	1862	32	17%	0.281651	0.000055	0.000908	0.03039	0.25	1.93	2.49
MIT1703e.4.23	2514	24	65%	0.281199	0.000059	0.0032	0.12	-5.19	2.07	3.34
MIT1703e.4.24	2597	34	72%	0.281041	0.000059	0.00247	0.0913	-7.79	2.07	3.57
MIT1703e.4.25	1945	51	73%	0.281558	0.000047	0.00219	0.0843	-2.89	1.65	2.75
MIT1703e.4.26	1989	32	42%	0.281546	0.000044	0.00199	0.0766	-2.11	1.54	2.74
MIT1703e.4.27	2401	15	73%	0.281154	0.000038	0.002544	0.0948	-8.07	1.33	3.43
MIT1703e.4.28	1949	34	59%	0.281535	0.000033	0.001615	0.0637	-2.87	1.16	2.75
MIT1703e.4.29	2554	33	3%	0.281114	0.000037	0.001016	0.0333	-3.59	1.30	3.27
MIT1703e.4.30	1924	52	63%	0.281509	0.000051	0.001363	0.0538	-4.01	1.79	2.81
MIT1703e.4.31	1922	22	19%	0.281649	0.000037	0.000684	0.0241	1.80	1.30	2.44
MIT1703e.4.32	2008	35	41%	0.281478	0.00004	0.001644	0.0625	-3.65	1.40	2.85
MIT1703e.4.33	2329	29	78%	0.281219	0.000054	0.002913	0.104	-7.87	1.89	3.37
MIT1703e.4.34	2029	33	26%	0.281549	0.000058	0.00172	0.05846	-0.78	2.03	2.68
MIT1703e.4.35	2209	28	85%	0.281228	0.000053	0.00443	0.172	-12.33	1.86	3.55
MIT1703e.4.36	2038	28	86%	0.281471	0.000057	0.00646	0.2635	-9.88	2.00	3.27

MIT1703e.4.37	2041	37	61%	0.281618	0.000044	0.001785	0.0683	1.84	1.54	2.53
MIT1703e.4.38	2998	16	43%	0.280867	0.000059	0.00509	0.182	-10.74	2.07	4.06
MIT1703e.4.39	1954	45	39%	0.281469	0.000049	0.00173	0.0626	-5.26	1.72	2.91
MIT1703e.4.40	2186	43	31%	0.281569	0.000035	0.001403	0.0344	3.81	1.23	2.51
MIT1703e.4.41	2408	26	77%	0.281062	0.000042	0.00312	0.1193	-12.14	1.47	3.70
MIT1703e.4.42	1884	38	-1%	0.281667	0.000044	0.000882	0.02931	1.34	1.54	2.44
MIT1703e.4.43	2597	27	4%	0.28113	0.000029	0.0010258	0.0344	-2.07	1.02	3.20
MIT1703e.4.44	2053	45	57%	0.281298	0.000035	0.000835	0.02925	-7.95	1.23	3.16
MIT1703e.4.45	2233	19	75%	0.281245	0.000046	0.00285	0.1123	-8.86	1.61	3.35
MIT1703e.4.46	1901	26	7%	0.281575	0.000044	0.000405	0.0151	-0.94	1.54	2.59
MIT1703e.4.47	2518	20	42%	0.281166	0.000041	0.001291	0.0457	-3.02	1.44	3.20
MIT1703e.4.48	1895	76	-1%	0.281141	0.000034	0.0002933	0.00905	-16.34	1.19	3.56
MIT1703e.4.49	1943	39	56%	0.281673	0.000055	0.001934	0.0711	1.48	1.93	2.47
MIT1703e.4.50	1855	27	49%	0.281616	0.00005	0.001942	0.0712	-2.44	1.75	2.65
MIT1703e.4.51	2067	30	71%	0.281407	0.000056	0.00254	0.0949	-6.15	1.96	3.05
MIT1703e.4.52	2152	35	96%	0.280938	0.00006	0.0079	0.2983	-28.82	2.10	4.54
MIT1703e.4.53	1898	25	80%	0.281553	0.000054	0.00451	0.1679	-7.04	1.89	2.98
MIT1703e.4.54	2264	20	78%	0.281311	0.000052	0.004271	0.1666	-8.05	1.82	3.33
MIT1703e.4.55	2330	38	84%	0.281145	0.000046	0.00504	0.1772	-13.84	1.61	3.74
MIT1703e.4.56	1922	18	73%	0.281547	0.00005	0.00334	0.1297	-5.26	1.75	2.89
MIT1703e.4.57	2103	31	94%	0.28137	0.000079	0.01075	0.405	-18.37	2.77	3.85
MIT1703e.4.58	1868	32	-1%	0.281421	0.000041	0.000378	0.01214	-7.12	1.44	2.96
MIT1703e.4.59	2236	25	61%	0.281111	0.000055	0.001614	0.0613	-11.69	1.93	3.53
MIT1703e.4.60	2531	24	41%	0.281192	0.000045	0.001226	0.044	-1.69	1.58	3.13
MIT1703e.4.61	1901	31	83%	0.281433	0.000063	0.00465	0.1789	-11.42	2.21	3.26
MIT1703e.4.62	2386	24	81%	0.281117	0.00006	0.00423	0.163	-12.43	2.10	3.70
MIT1703e.4.63	2575	24	38%	0.281199	0.000058	0.00139	0.04446	-0.75	2.03	3.10
MIT1703e.4.64	1966	33	-1%	0.28149	0.000038	0.0001751	0.00619	-2.19	1.33	2.72
MIT1703e.4.65	1899	53	44%	0.281621	0.00005	0.00191	0.0716	-1.28	1.75	2.61
MIT1703e.4.66	1892	20	12%	0.281589	0.000037	0.000757	0.0241	-1.09	1.30	2.60
MIT1703e.4.67	2053	35	49%	0.28152	0.000044	0.00213	0.0876	-1.86	1.54	2.77

MIT1703e.4.68	1946	44	55%	0.28153	0.000048	0.001115	0.0391	-2.46	1.68	2.73
MIT1703e.4.69	2589	48	37%	0.281111	0.000045	0.000899	0.03157	-2.71	1.58	3.24
MIT1703e.4.70	2513	32	1%	0.281137	0.000035	0.0009635	0.03208	-3.60	1.23	3.24
MIT1703e.4.71	1896	43	6%	0.28163	0.000035	0.000705	0.0243	0.52	1.23	2.50
MIT1703e.4.72	1978	53	58%	0.281201	0.000043	0.001698	0.0577	-14.21	1.51	3.49
MIT1703e.4.73	1870	38	22%	0.281633	0.00003	0.00106	0.038	-0.40	1.05	2.54
MIT1703e.4.74	1976	57	0%	0.281468	0.000037	0.000848	0.0266	-3.64	1.30	2.82
MIT1703e.4.75	2556	26	32%	0.281166	0.000044	0.001432	0.0538	-2.42	1.54	3.19
MIT1703e.4.76	1890	24	65%	0.281981	0.000052	0.000933	0.0399	12.56	1.82	1.72
MIT1703e.4.77	2520	36	79%	0.280943	0.000054	0.00338	0.1369	-14.48	1.89	3.93
MIT1703e.4.78	1854	46	0%	0.281605	0.000027	0.000416	0.01351	-0.94	0.95	2.56
MIT1703e.4.79	1859	41	-3%	0.281685	0.000039	0.0005061	0.01683	1.90	1.37	2.38
MIT1703e.4.80	2454	17	1%	0.281365	0.000048	0.00212	0.0681	1.26	1.68	2.88
MIT1703e.4.81	1879	38	-3%	0.281687	0.000031	0.000897	0.031	1.92	1.09	2.40
MIT1703e.4.82	1936	30	48%	0.281585	0.000039	0.0015	0.0586	-1.23	1.37	2.64
MIT1703e.4.83	2614	28	1%	0.281143	0.000037	0.000784	0.02705	-0.80	1.30	3.14
MIT1703e.4.84	1954	33	70%	0.28152	0.000034	0.00191	0.0739	-3.68	1.19	2.81
MIT1703e.4.85	1887	25	1%	0.281606	0.000052	0.000518	0.01756	-0.30	1.82	2.54
MIT1703e.4.86	1975	32	85%	0.281477	0.000043	0.00361	0.143	-7.02	1.51	3.04
MIT1703e.4.87	2490	31	50%	0.281147	0.000044	0.0011634	0.04596	-4.10	1.54	3.25
MIT1703e.4.88	2034	33	91%	0.281479	0.000061	0.00475	0.1907	-7.32	2.14	3.10
MIT1703e.4.89	2345	28	84%	0.281157	0.000052	0.0043	0.165	-11.95	1.82	3.63
MIT1703e.4.90	2548	24	50%	0.281109	0.00005	0.00148	0.056	-4.70	1.75	3.33
MIT1703e.4.91	2256	32	79%	0.281101	0.000055	0.0025	0.0966	-12.96	1.93	3.63
MIT1703e.4.92	1924	35	85%	0.281562	0.000042	0.00425	0.1707	-5.87	1.47	2.93
MIT1703e.4.93	1878	50	77%	0.281258	0.000046	0.001373	0.0564	-13.94	1.61	3.40
MIT1703e.4.94	1924	46	78%	0.281598	0.00005	0.0023	0.0895	-2.06	1.75	2.68
MIT1703e.4.95	1862	65	2%	0.281546	0.000036	0.000656	0.022	-3.16	1.26	2.71
MIT1703e.4.96	1925	37	2%	0.281551	0.000038	0.0004159	0.01407	-1.27	1.33	2.63
MIT1703e.4.97	2601	34	50%	0.281217	0.000039	0.001418	0.0519	0.42	1.37	3.05
MIT1703e.4.98	2379	20	82%	0.281155	0.000059	0.005115	0.2045	-12.65	2.07	3.71

MIT1703e.4.99	2468	18	38%	0.281154	0.000049	0.0013	0.0461	-4.57	1.72	3.26
MIT1703e.4.100	1888	36	72%	0.281666	0.000044	0.00173	0.0716	0.31	1.54	2.50
MIT1703e.4.101	1985	22	1%	0.281407	0.000043	0.0004524	0.01537	-5.08	1.51	2.92
MIT1703e.4.102	2523	14	1%	0.28103	0.000036	0.000708	0.0238	-6.74	1.26	3.44
MIT1703e.4.103	2486	22	76%	0.281062	0.000065	0.003045	0.1218	-10.38	2.28	3.64
MIT1703e.4.104	1928	33	19%	0.28165	0.000044	0.00123	0.044	1.26	1.54	2.48
MIT1703e.4.105	3079	28	6%	0.280892	0.000041	0.000625	0.0199	1.15	1.44	3.37
MIT1703e.4.106	1857	21	-35%	0.281639	0.00004	0.0009667	0.03344	-0.36	1.40	2.52
MIT1703e.4.107	1909	54	34%	0.281561	0.000038	0.00162	0.0627	-2.82	1.33	2.72
MIT1703e.4.108	2578	34	4%	0.281129	0.000038	0.000616	0.02114	-1.82	1.33	3.17
MIT1703e.4.109	2004	23	89%	0.281452	0.00005	0.00362	0.1516	-7.34	1.75	3.08
MIT1703e.4.110	1937	59	77%	0.281528	0.000051	0.00454	0.1836	-7.20	1.79	3.02
MIT1703e.4.111	1844	31	82%	0.281516	0.000041	0.00337	0.1326	-8.00	1.44	3.00
MIT1703e.4.112	2598	30	13%	0.281173	0.000042	0.000739	0.02395	-0.02	1.47	3.07
MIT1703e.4.113	2069	33	88%	0.281428	0.000057	0.00421	0.1728	-7.69	2.00	3.15
MIT1703e.4.114	1985	29	74%	0.281521	0.000052	0.003996	0.1527	-5.78	1.82	2.97
MIT1703e.4.115	1910	25	11%	0.281514	0.000034	0.000611	0.01917	-3.17	1.19	2.74
MIT1703e.4.116	2318	20	75%	0.281223	0.000041	0.00239	0.0945	-7.14	1.44	3.31
MIT1703e.4.117	1863	32	1%	0.281588	0.00005	0.000767	0.02646	-1.79	1.75	2.62
MIT1703e.4.118	2581	16	65%	0.281136	0.000061	0.002472	0.1008	-4.76	2.14	3.36
MIT1703e.4.119	1885	28	1%	0.281606	0.000032	0.000793	0.0263	-0.69	1.12	2.57
MIT1703e.4.120	1931	35	2%	0.281542	0.000042	0.0011665	0.0353	-2.43	1.47	2.71
MIT1703e.4.121	1898	22	7%	0.28149	0.000044	0.00098	0.0336	-4.76	1.54	2.84
MIT1703e.4.122	1879	41	62%	0.281668	0.000045	0.000993	0.037	1.12	1.58	2.45
MIT1703e.4.123	1964	42	65%	0.281526	0.000029	0.00333	0.133	-5.14	1.02	2.91
MIT1703e.4.124	2186	36	97%	0.281303	0.000067	0.007812	0.315	-15.12	2.35	3.71
MIT1703e.4.125	2154	40	95%	0.281348	0.00006	0.00504	0.216	-10.05	2.10	3.37
MIT1703e.4.126	2596	25	1%	0.281211	0.000039	0.001636	0.0584	-0.29	1.37	3.09
MIT1703e.4.127	1882	45	3%	0.281519	0.000039	0.000987	0.0326	-4.09	1.37	2.78
MIT1703e.4.128	2564	48	2%	0.28123	0.000038	0.001244	0.0434	0.36	1.33	3.02
MIT1703e.4.129	2018	24	82%	0.281452	0.000048	0.00536	0.2133	-9.42	1.68	3.22

MIT1703e.4.130	2753	26	11%	0.281159	0.000045	0.000949	0.0319	2.60	1.58	3.02
MIT1703e.4.131	1812	39	62%	0.281435	0.000051	0.00239	0.0903	-10.33	1.79	3.12
MIT1703e.4.132	2556	22	16%	0.28118	0.000042	0.000928	0.03322	-1.04	1.47	3.11
MIT1703e.4.133	2132	38	65%	0.281448	0.000054	0.00276	0.1042	-3.63	1.89	2.94
MIT1703e.4.134	2575	23	51%	0.280887	0.000054	0.00121	0.0484	-11.53	1.89	3.79
MIT1703e.4.135	1878	42	-1%	0.281552	0.000039	0.0006063	0.01941	-2.53	1.37	2.68
MIT1703e.4.136	1904	26	14%	0.281702	0.000046	0.000834	0.0288	3.09	1.61	2.34
MIT1703e.4.137	1939	36	79%	0.281526	0.00005	0.002472	0.0986	-4.53	1.75	2.85
MIT1703e.4.138	2041	39	89%	0.281565	0.000051	0.00355	0.147	-2.47	1.79	2.80
MIT1703e.4.139	2697	50	14%	0.281202	0.000051	0.00124	0.0393	2.34	1.79	3.00
MIT1703e.4.140	1907	22	24%	0.281462	0.000035	0.0009083	0.03138	-5.46	1.23	2.89
MIT1703e.4.141	1925	47	65%	0.281624	0.000056	0.0017	0.0689	-0.34	1.96	2.58
MIT1703e.4.142	2044	35	79%	0.281555	0.000038	0.00218	0.0845	-0.88	1.33	2.70

Appendix E: Chapter 5, supplementary file

Table 1: U-Pb data generated for this study.

Sample: FOG01

Grain ID	*207Pb/232Th*	*207Pb/232Th prop2SE*	*206Pb/238U*	*206Pb/238U prop2SE*	*207Pb/206Pb*	*207Pb/206Pb prop2SE*	*206Pb/238Pb Age (Ma)*	*± 1σ(Ma)*	*207Pb/206Pb Age (Ma)*	*± 1σ (Ma)*	*Disc (%)*
FOG01.1.01	3.55	0.13	0.2575	0.0095	0.1002	0.0027	1477	49	1627	50	10%
FOG01.1.02	3.655	0.1	0.2745	0.0046	0.097	0.0021	1564	23	1566	41	0%
FOG01.1.03	3.705	0.088	0.2772	0.0026	0.09715	0.0019	1577	13	1569	37	-1%
FOG01.1.04	3.669	0.1	0.2749	0.0054	0.09693	0.0019	1566	27	1565	37	0%
FOG01.1.05	3.91	0.14	0.2577	0.0054	0.1105	0.0025	1478	28	1807	41	22%
FOG01.1.06	2.087	0.075	0.1583	0.006	0.09645	0.002	947	33	1556	39	64%
FOG01.1.07	7.66	0.37	0.299	0.0069	0.1901	0.0071	1686	34	2742	62	63%
FOG01.1.08	3.05	0.14	0.226	0.0098	0.0981	0.0019	1314	52	1587	36	21%
FOG01.1.09	3.59	0.15	0.2671	0.0077	0.0981	0.0019	1526	39	1587	36	4%
FOG01.1.10	2.82	0.12	0.1872	0.0069	0.10928	0.0021	1106	37	1787	35	62%
FOG01.1.11	12.6	1.4	0.249	0.02	0.364	0.017	1430	100	3766	71	163%
FOG01.1.12	3.232	0.11	0.2364	0.0061	0.09905	0.002	1368	32	1605	38	17%
FOG01.1.13	2.421	0.091	0.1658	0.0037	0.1055	0.0023	989	20	1722	40	74%
FOG01.1.14	3.541	0.082	0.2681	0.0022	0.09582	0.0018	1531	11	1543	35	1%
FOG01.1.15	9.73	0.83	0.2894	0.0095	0.241	0.013	1639	48	3126	86	91%
FOG01.1.16	3.66	0.13	0.256	0.007	0.10351	0.002	1469	36	1687	36	15%
FOG01.1.17	2.86	0.25	0.207	0.016	0.1001	0.0023	1213	85	1625	43	34%
FOG01.1.18	3.692	0.11	0.2767	0.0051	0.09678	0.0018	1575	26	1562	35	-1%
FOG01.1.19	3.26	0.14	0.2067	0.0047	0.1145	0.0029	1211	25	1871	46	55%
FOG01.1.20	4.34	0.17	0.2321	0.0038	0.1356	0.0052	1345	20	2171	67	61%
FOG01.1.21	3.634	0.095	0.2655	0.0036	0.09857	0.0019	1518	18	1596	36	5%
FOG01.1.22	3.509	0.087	0.263	0.0035	0.0958	0.0021	1505	18	1543	41	3%
FOG01.1.23	3.44	0.26	0.251	0.021	0.0988	0.0028	1440	110	1601	53	11%
FOG01.1.24	4.24	0.21	0.3	0.012	0.1018	0.0026	1691	60	1656	47	-2%
FOG01.1.25	3.311	0.09	0.2347	0.0038	0.1016	0.002	1359	20	1653	37	22%
FOG01.1.26	3.56	0.13	0.2636	0.0067	0.09678	0.002	1508	34	1562	39	4%
FOG01.1.27	2.794	0.11	0.1989	0.0067	0.10162	0.002	1169	36	1653	37	41%

360

FOG01.1.28	2.858	0.082	0.2051	0.003	0.1002	0.0024	1203	16	1627	45	35%
FOG01.1.29	3.454	0.1	0.2569	0.0053	0.0963	0.0023	1474	27	1553	45	5%
FOG01.1.30	6.24	0.46	0.301	0.016	0.1484	0.0046	1696	79	2327	53	37%
FOG01.1.31	3.55	0.15	0.2059	0.0066	0.1238	0.0047	1207	35	2011	67	67%
FOG01.1.32	3.743	0.091	0.2744	0.0029	0.09761	0.0018	1563	15	1578	35	1%
FOG01.1.33	3.708	0.11	0.2735	0.0047	0.0971	0.0021	1559	24	1568	41	1%
FOG01.1.34	3.739	0.11	0.2775	0.0066	0.0969	0.0019	1579	33	1564	37	-1%
FOG01.1.35	3.6	0.13	0.2686	0.0071	0.09596	0.0019	1534	36	1546	37	1%
FOG01.1.36	3.23	0.15	0.2376	0.0088	0.0973	0.0022	1374	46	1572	42	14%
FOG01.1.37	3.55	0.12	0.2626	0.0072	0.09642	0.0019	1503	37	1555	37	3%
FOG01.1.38	3.601	0.11	0.2568	0.0058	0.1012	0.0021	1473	30	1645	39	12%
FOG01.1.39	3.284	0.11	0.2445	0.0057	0.09626	0.0019	1410	30	1552	37	10%
FOG01.1.40	3.475	0.091	0.2507	0.0031	0.099	0.0022	1442	16	1605	42	11%
FOG01.3.01	3.309	0.051	0.241	0.0038	0.0985	0.005	1392	20	1595	95	15%
FOG01.3.02	3.767	0.057	0.2799	0.0037	0.096	0.0049	1591	19	1547	96	-3%
FOG01.3.03	3.926	0.05	0.2838	0.0022	0.098	0.005	1610	11	1586	95	-1%
FOG01.3.04	3.85	0.12	0.2677	0.0048	0.1022	0.0056	1529	24	1660	100	9%
FOG01.3.05	3.43	0.16	0.2186	0.004	0.1115	0.0067	1274	21	1820	110	43%
FOG01.3.06	4.37	0.14	0.2837	0.0027	0.109	0.0064	1610	14	1780	110	11%
FOG01.3.07	6.07	0.43	0.2797	0.0085	0.154	0.011	1590	43	2390	120	50%
FOG01.3.08	3.785	0.052	0.2796	0.0033	0.09608	0.0048	1589	17	1548	94	-3%
FOG01.3.09	3.783	0.09	0.2791	0.0031	0.0962	0.005	1587	16	1551	98	-2%
FOG01.3.10	3.829	0.085	0.2798	0.0027	0.0975	0.0053	1590	14	1580	100	-1%
FOG01.3.11	3.57	0.11	0.2606	0.0069	0.0971	0.005	1493	35	1568	97	5%
FOG01.3.12	3.832	0.078	0.2821	0.0052	0.09659	0.0049	1602	26	1558	95	-3%
FOG01.3.13	4.426	0.094	0.3233	0.0052	0.0972	0.0051	1806	25	1570	98	-13%
FOG01.3.14	3.849	0.064	0.2821	0.0057	0.09765	0.0049	1602	29	1579	94	-1%
FOG01.3.15	4.66	0.14	0.2817	0.0037	0.1168	0.0064	1600	19	1907	98	19%
FOG01.3.16	3.9	0.11	0.2682	0.0059	0.1027	0.0053	1532	30	1673	95	9%
FOG01.3.17	3.556	0.071	0.2544	0.0032	0.0983	0.005	1461	16	1591	95	9%

FOG01.3.18	3.052	0.044	0.2312	0.0032	0.09346	0.0047	1341	17	1496	95	12%
FOG01.3.19	9.7	1	0.314	0.013	0.221	0.019	1760	64	2990	140	70%
FOG01.3.20	6.7	1.2	0.306	0.012	0.153	0.022	1721	59	2380	250	38%

Sample: PGE01

Grain ID	*207Pb/232Th*	*207Pb/232Th prop2SE*	*206Pb/238U*	*206Pb/238U prop2SE*	*207Pb/206Pb*	*207Pb/206Pb prop2SE*	*206Pb/238Pb Age (Ma)*	*± 1σ(Ma)*	*207Pb/206Pb Age (Ma)*	*± 1σ (Ma)*	*Disc (%)*
PGE01.1.01	3.83	0.14	0.283	0.0053	0.0972	0.0034	1606	27	1570	66	-2%
PGE01.1.02	3.721	0.12	0.2759	0.0044	0.0964	0.0028	1571	22	1555	55	-1%
PGE01.1.03	3.76	0.14	0.2771	0.0041	0.0968	0.0033	1577	21	1563	64	-1%
PGE01.1.04	3.78	0.14	0.2793	0.0042	0.0962	0.0025	1588	21	1551	49	-2%
PGE01.1.05	3.787	0.12	0.2736	0.0043	0.0995	0.0025	1559	22	1614	47	4%
PGE01.1.06	3.952	0.14	0.2872	0.0058	0.0986	0.0025	1628	29	1597	47	-2%
PGE01.1.07	3.76	0.14	0.2779	0.0043	0.0967	0.0032	1581	22	1561	62	-1%
PGE01.1.08	3.897	0.11	0.2761	0.0038	0.101	0.0025	1572	19	1642	46	4%
PGE01.1.09	3.735	0.11	0.2776	0.0039	0.0969	0.0025	1579	20	1564	48	-1%
PGE01.1.10	3.749	0.12	0.2789	0.0036	0.0961	0.003	1586	18	1549	59	-2%
PGE01.1.11	3.6	0.13	0.2645	0.0041	0.0967	0.0029	1513	21	1561	56	3%
PGE01.1.12	3.72	0.14	0.2736	0.004	0.0972	0.0031	1559	20	1570	60	1%
PGE01.1.13	3.658	0.1	0.2734	0.0026	0.0958	0.0023	1558	13	1543	45	-1%
PGE01.1.14	3.703	0.13	0.2742	0.0041	0.0964	0.0029	1562	21	1555	57	0%
PGE01.1.15	3.756	0.11	0.2765	0.0032	0.0974	0.0024	1574	16	1574	46	0%
PGE01.1.16	3.774	0.11	0.2786	0.0036	0.097	0.0024	1584	18	1566	46	-1%
PGE01.1.17	3.621	0.11	0.2722	0.0031	0.0955	0.0025	1552	16	1537	49	-1%
PGE01.1.18	3.71	0.11	0.274	0.0038	0.0966	0.0025	1561	19	1559	49	0%
PGE01.1.19	3.704	0.094	0.2751	0.0034	0.0969	0.0021	1567	17	1564	41	0%
PGE01.1.20	3.686	0.11	0.2739	0.0042	0.0968	0.0027	1561	21	1563	52	0%
PGE01.1.21	3.737	0.11	0.2756	0.0032	0.0975	0.0027	1569	16	1576	52	0%
PGE01.1.22	3.79	0.11	0.2785	0.0031	0.0971	0.0028	1584	16	1568	54	-1%
PGE01.1.23	3.64	0.14	0.2672	0.0037	0.0968	0.0033	1527	19	1563	64	2%

PGE01.1.24	3.668	0.12	0.2706	0.0036	0.0969	0.0029	1544	18	1564	56	1%
PGE01.1.25	3.71	0.11	0.2748	0.003	0.097	0.0026	1565	15	1566	50	0%
PGE01.1.26	3.713	0.11	0.2757	0.0034	0.0965	0.0027	1570	17	1557	53	-1%
PGE01.1.27	3.674	0.12	0.2732	0.005	0.0966	0.0027	1557	25	1559	53	0%
PGE01.1.28	3.83	0.15	0.2772	0.0044	0.0999	0.0035	1577	22	1621	65	3%
PGE01.1.29	3.687	0.096	0.2733	0.0033	0.0968	0.002	1558	17	1563	39	0%
PGE01.1.30	3.844	0.11	0.2795	0.0027	0.09923	0.002	1589	14	1609	38	1%
PGE01.1.31	3.74	0.12	0.2707	0.0036	0.0991	0.0029	1544	18	1606	55	4%
PGE01.1.32	3.68	0.11	0.274	0.003	0.0971	0.0028	1561	15	1568	54	0%
PGE01.1.33	3.625	0.11	0.272	0.0027	0.0956	0.0025	1551	14	1539	49	-1%
PGE01.1.34	3.585	0.13	0.2573	0.0047	0.1004	0.0026	1476	24	1631	48	11%
PGE01.1.35	3.634	0.19	0.272	0.004	0.0958	0.0033	1551	20	1543	65	-1%
PGE01.1.36	3.737	0.12	0.2755	0.0039	0.0977	0.0028	1569	20	1580	54	1%
PGE01.1.37	3.539	0.12	0.264	0.0037	0.097	0.0026	1510	19	1566	50	4%
PGE01.5.01	3.685	0.12	0.277	0.009	0.09676	0.00052	1576	45	1562	10	-1%
PGE01.5.02	3.714	0.13	0.2778	0.0098	0.09763	0.00061	1580	49	1578	12	0%
PGE01.5.03	3.623	0.12	0.2702	0.0088	0.09713	0.00051	1542	45	1569	10	2%
PGE01.5.04	3.651	0.12	0.2746	0.0089	0.09657	0.00046	1564	45	1558	9.4	0%
PGE01.5.05	3.499	0.11	0.2646	0.0086	0.09623	0.00044	1513	44	1551.4	9	3%
PGE01.5.06	3.593	0.12	0.2684	0.0089	0.09731	0.00051	1533	45	1572	10	3%
PGE01.5.07	3.76	0.15	0.2813	0.012	0.097	0.0011	1598	60	1566	21	-2%
PGE01.5.08	3.61	0.12	0.2702	0.0091	0.09688	0.00047	1542	46	1564.1	9.5	1%
PGE01.5.09	3.524	0.12	0.2668	0.0095	0.09634	0.00042	1525	48	1553.6	8.6	2%
PGE01.5.10	4.004	0.14	0.3035	0.012	0.09642	0.00045	1709	59	1555.1	9.2	-9%

Sample: CUG01

Grain ID	*207Pb/232Th*	*207Pb/232Th prop2SE*	*206Pb/238U*	*206Pb/238U prop2SE*	*207Pb/206Pb*	*207Pb/206Pb prop2SE*	*206Pb/238Pb Age (Ma)*	*± 1σ(Ma)*	*207Pb/206Pb Age (Ma)*	*± 1σ (Ma)*	*Disc (%)*
CUG01.2.01	4.11	0.25	0.2944	0.0085	0.0964	0.0044	1663	42	1555	86	6%
CUG01.2.02	0.371	0.025	0.0499	0.001	0.0528	0.0032	313.9	6.1	320	140	-2%

CUG01.2.03	3.8	0.12	0.2791	0.0059	0.0949	0.0023	1587	30	1525	46	4%
CUG01.2.04	3.92	0.12	0.2929	0.0048	0.094	0.0023	1656	24	1507	46	9%
CUG01.2.05	3.619	0.099	0.2681	0.0035	0.0945	0.0026	1531	18	1517	52	1%
CUG01.2.06	3.855	0.081	0.2839	0.0041	0.0944	0.0021	1611	21	1515	42	6%
CUG01.2.07	3.81	0.11	0.2809	0.0038	0.0962	0.0029	1596	19	1551	57	3%
CUG01.2.08	3.631	0.061	0.2529	0.0026	0.1007	0.0013	1453	13	1636	24	-13%
CUG01.2.09	0.39	0.031	0.0471	0.001	0.056	0.0052	296.7	6.2	450	210	-52%
CUG01.2.10	0.302	0.096	0.0402	0.0018	0.057	0.018	254	11	490	700	-93%
CUG01.2.11	0.31	0.025	0.0426	0.00056	0.0503	0.0038	268.9	3.5	210	180	22%
CUG01.2.12	0.286	0.024	0.03686	0.00084	0.0556	0.0051	233.3	5.2	440	200	-89%
CUG01.2.13	3.956	0.064	0.2904	0.0027	0.0948	0.0023	1644	14	1523	46	7%
CUG01.2.14	3.99	0.084	0.2859	0.0037	0.0983	0.0028	1621	19	1591	53	2%
CUG01.2.15	3.831	0.087	0.283	0.0034	0.0953	0.0018	1606	17	1533	36	5%
CUG01.2.16	9.41	0.34	0.4278	0.0085	0.1571	0.006	2296	38	2424	65	-6%
CUG01.2.17	0.145	0.062	0.0193	0.0012	0.052	0.023	123.2	7.6	280	1010	-127%
CUG01.2.18	3.71	0.15	0.2685	0.0087	0.0996	0.0026	1533	44	1616	49	-5%
CUG01.2.19	0.338	0.019	0.0488	0.0012	0.0508	0.003	307.2	7.4	230	140	25%
CUG01.2.20	3.67	0.13	0.2798	0.0042	0.0953	0.0033	1590	21	1533	65	4%
CUG01.2.21	3.54	0.1	0.2727	0.0049	0.0933	0.0031	1554	25	1493	63	4%
CUG01.2.22	0.318	0.019	0.04363	0.00047	0.0521	0.0033	275.3	2.9	290	140	-5%
CUG01.2.23	3.695	0.092	0.2784	0.0046	0.0966	0.0027	1583	23	1559	53	2%
CUG01.2.24	3.52	0.14	0.2713	0.0042	0.0949	0.0031	1547	21	1525	62	1%
CUG01.2.25	3.77	0.11	0.2804	0.0033	0.0968	0.0025	1593	17	1563	49	2%
CUG01.2.26	3.728	0.08	0.2807	0.0055	0.0984	0.0019	1595	28	1593	36	0%
CUG01.2.27	3.608	0.072	0.277	0.0032	0.0943	0.0018	1576	16	1513	36	4%
CUG01.2.28	0.324	0.021	0.04666	0.0009	0.0533	0.0031	294	5.5	340	130	-16%
CUG01.2.29	2.679	0.067	0.1985	0.0042	0.1002	0.002	1167	23	1627	37	-39%
CUG01.2.30	3.65	0.14	0.2822	0.0046	0.0946	0.0032	1602	23	1519	64	5%
CUG01.2.31	3.55	0.064	0.2756	0.0053	0.0961	0.0022	1569	27	1549	43	1%
CUG01.2.32	3.77	0.11	0.2875	0.005	0.0979	0.0029	1629	25	1584	55	3%
CUG01.2.33	3.359	0.066	0.2562	0.0027	0.0969	0.0018	1470	14	1564	35	-6%

CUG01.5.01	3.59	0.18	0.2687	0.013	0.0968	0.00059	1534	66	1563	12	-2%
CUG01.5.02	3.539	0.18	0.265	0.013	0.09701	0.0006	1515	66	1567	12	-3%
CUG01.5.03	3.641	0.19	0.272	0.013	0.09728	0.00061	1551	66	1572	12	-1%
CUG01.5.04	3.614	0.18	0.2712	0.013	0.09658	0.00061	1547	66	1558	12	-1%
CUG01.5.05	0.3173	0.016	0.04376	0.0021	0.05256	0.00039	276	13	309	17	-12%
CUG01.5.06	5.455	0.28	0.338	0.016	0.11713	0.00075	1877	77	1912	12	-2%
CUG01.5.07	4.277	0.22	0.2968	0.014	0.10475	0.00063	1675	70	1709	11	-2%
CUG01.5.08	3.637	0.18	0.271	0.013	0.09741	0.00062	1546	66	1574	12	-2%
CUG01.5.09	3.579	0.18	0.26764	0.013	0.09688	0.0006	1529	66	1564	12	-2%
CUG01.5.10	11.97	0.62	0.4312	0.021	0.20108	0.0012	2311	95	2834	10	-23%
CUG01.5.11	0.2976	0.017	0.04032	0.002	0.05354	0.00085	255	12	351	36	-38%
CUG01.5.12	3.885	0.2	0.2925	0.014	0.09645	0.00058	1654	70	1556	12	6%
CUG01.5.13	3.577	0.18	0.2706	0.013	0.09583	0.0006	1544	66	1544	12	0%
CUG01.5.14	3.659	0.19	0.2759	0.013	0.09632	0.00061	1571	66	1553	12	1%
CUG01.5.15	3.708	0.19	0.2799	0.013	0.09613	0.0006	1591	65	1549	12	3%
CUG01.6.01	0.33	0.12	0.037	0.0024	0.059	0.023	234	15	570	850	-144%
CUG01.6.02	18.88	0.72	0.59	0.011	0.2332	0.0053	2989	45	3073	36	-3%
CUG01.6.03	3.631	0.1	0.2729	0.0042	0.0971	0.0022	1556	21	1568	43	-1%
CUG01.6.04	0.301	0.051	0.047	0.0015	0.0472	0.0081	296.1	9.2	58	409	80%
CUG01.6.05	0.405	0.066	0.0456	0.0019	0.067	0.011	287	12	840	340	-193%
CUG01.6.06	3.72	0.21	0.2739	0.0051	0.0984	0.005	1561	26	1593	95	-2%
CUG01.6.07	1.98	0.16	0.1829	0.0074	0.0776	0.0068	1083	40	1140	170	-5%
CUG01.6.08	0.324	0.05	0.0474	0.0014	0.0515	0.0069	298.5	8.6	260	310	13%
CUG01.6.09	1.74	0.12	0.1403	0.0058	0.089	0.0052	846	33	1400	110	-65%
CUG01.6.10	3.544	0.13	0.2614	0.0033	0.0982	0.0029	1497	17	1589	55	-6%
CUG01.6.11	3.69	0.17	0.2753	0.0051	0.0988	0.0047	1568	26	1601	89	-2%

Sample: 042

Grain ID	*207Pb/232Th*	*207Pb/232Th prop2SE*	*206Pb/238U*	*206Pb/238U prop2SE*	*207Pb/206Pb*	*207Pb/206Pb prop2SE*	*206Pb/238Pb Age (Ma)*	*± 1σ(Ma)*	*207Pb/206Pb Age (Ma)*	*± 1σ (Ma)*	*Disc (%)*
042.4.01	3.575	0.063	0.269	0.0052	0.0959	0.0023	1536	26	1545	45	1%
042.4.02	3.55	0.094	0.2585	0.0049	0.1016	0.0018	1482	25	1653	33	12%
042.4.03	3.545	0.096	0.2499	0.0023	0.0946	0.0028	1438	12	1519	56	6%
042.4.04	3.529	0.078	0.269	0.003	0.0961	0.0018	1536	15	1549	35	1%
042.4.05	3.684	0.057	0.2789	0.0021	0.0965	0.0015	1586	11	1557	29	-2%
042.4.06	3.334	0.063	0.2562	0.0034	0.09505	0.0018	1470	17	1528	36	4%
042.4.07	3.594	0.042	0.2774	0.0026	0.09451	0.0012	1578	13	1517	24	-4%
042.4.08	3.007	0.044	0.2058	0.0037	0.0977	0.0022	1206	20	1580	42	31%
042.4.09	3.525	0.045	0.2674	0.0028	0.0963	0.0014	1528	14	1553	27	2%
042.4.10	3.475	0.083	0.2488	0.0048	0.095	0.0019	1432	25	1527	38	7%
042.4.11	2.485	0.066	0.1718	0.0038	0.097	0.002	1022	21	1566	39	53%
042.4.12	2.882	0.055	0.225	0.0032	0.0943	0.0016	1308	17	1513	32	16%
042.4.13	3.009	0.046	0.2345	0.0028	0.09386	0.0013	1358	15	1504	26	11%
042.4.14	3.57	0.1	0.2722	0.0041	0.0965	0.0027	1552	21	1557	53	0%
042.4.15	2.706	0.067	0.216	0.0028	0.0913	0.0019	1261	15	1452	40	15%
042.4.16	0.4006	0.007	0.05473	0.00095	0.0529	0.00081	343.5	5.8	323	35	-6%
042.4.17	3.643	0.073	0.2804	0.0072	0.0957	0.0019	1593	36	1541	37	-3%
042.4.18	3.412	0.081	0.2625	0.005	0.0969	0.0027	1503	26	1564	52	4%
042.4.19	3.515	0.067	0.2618	0.0045	0.09546	0.0014	1499	23	1536	28	2%
042.4.20	3.592	0.091	0.2723	0.0038	0.0946	0.0022	1552	19	1519	44	-2%
042.4.21	3.736	0.1	0.275	0.0045	0.0966	0.002	1566	23	1559	39	0%
042.4.22	3.488	0.082	0.2642	0.006	0.0973	0.0021	1511	31	1572	41	4%
042.4.23	3.384	0.065	0.2553	0.0048	0.0964	0.0022	1466	25	1555	43	6%
042.4.24	2.919	0.076	0.2274	0.0044	0.0935	0.0018	1321	23	1497	37	13%
042.4.25	0.428	0.0074	0.0581	0.001	0.0543	0.0015	364.1	6.1	383	62	5%
042.5.01	3.472	0.11	0.2635	0.0086	0.09574	0.00043	1508	44	1541.8	8.9	2%
042.5.02	3.592	0.12	0.2729	0.009	0.09614	0.00049	1556	46	1549.7	10	0%
042.5.03	3.484	0.12	0.2638	0.0089	0.09612	0.00049	1509	45	1549.3	10	3%

042.5.04	3.455	0.11	0.26306	0.0085	0.09539	0.00042	1505	43	1534.9	8.7	2%
042.5.05	3.532	0.11	0.268	0.0087	0.09575	0.00048	1531	44	1542	9.8	1%
042.5.06	3.594	0.11	0.272	0.0088	0.09614	0.00048	1551	45	1549.7	9.8	0%
042.5.07	3.53	0.11	0.2683	0.0089	0.09555	0.00042	1532	45	1538.1	8.7	0%
042.5.08	3.642	0.12	0.2751	0.0089	0.09644	0.00049	1567	45	1555.5	9.9	-1%
042.5.09	3.443	0.11	0.2627	0.0085	0.09511	0.00047	1504	43	1529.4	9.7	2%
042.5.10	3.43	0.11	0.2592	0.0085	0.09611	0.00043	1486	44	1549.1	8.8	4%
042.5.11	3.612	0.12	0.2723	0.0091	0.0961	0.00044	1552	46	1548.9	9	0%
042.5.12	3.508	0.11	0.265	0.0086	0.09627	0.00049	1515	44	1552.2	9.9	2%
042.5.13	3.662	0.12	0.2766	0.009	0.09637	0.00046	1574	45	1554.2	9.4	-1%
042.5.14	3.656	0.12	0.2746	0.009	0.09657	0.00066	1564	46	1558	13	0%
042.5.15	3.545	0.11	0.2688	0.0087	0.09557	0.00052	1535	44	1538	11	0%
042.5.16	3.53	0.13	0.2677	0.01	0.09574	0.00044	1529	51	1541.8	9.1	1%
042.5.17	3.463	0.11	0.26317	0.0085	0.09565	0.00046	1506	43	1540.1	9.5	2%
042.5.18	3.704	0.13	0.2782	0.0093	0.09666	0.00063	1582	47	1560	13	-1%
042.5.19	3.624	0.12	0.2737	0.0089	0.09647	0.00046	1560	45	1556.1	9.4	0%

Sample: 045

Grain ID	*207Pb/232Th*	*207Pb/232Th prop2SE*	*206Pb/238U*	*206Pb/238U prop2SE*	*207Pb/206Pb*	*207Pb/206Pb prop2SE*	*206Pb/238Pb Age (Ma)*	*± 1σ(Ma)*	*207Pb/206Pb Age (Ma)*	*± 1σ (Ma)*	*Disc (%)*
045.4.01	3.438	0.053	0.2424	0.0028	0.09503	0.0014	1399	15	1528	28	9%
045.4.02	3.496	0.074	0.2677	0.0058	0.0948	0.0014	1529	30	1523	28	0%
045.4.03	3.42	0.11	0.2644	0.0053	0.0951	0.002	1512	27	1529	40	1%
045.4.04	3.468	0.064	0.2428	0.0043	0.0957	0.0015	1401	22	1541	30	10%
045.4.05	3.486	0.066	0.255	0.0019	0.0961	0.0015	1464.2	9.8	1549	29	6%
045.4.06	2.48	0.045	0.1741	0.003	0.09506	0.0013	1035	16	1528	26	48%
045.4.07	3.618	0.076	0.2731	0.0042	0.0962	0.002	1557	21	1551	39	0%
045.4.08	0.477	0.011	0.06352	0.00072	0.0552	0.0014	397	4.4	419	57	6%
045.4.09	2.64	0.13	0.1844	0.0094	0.1022	0.0025	1091	51	1664	45	53%
045.4.10	3.306	0.064	0.2362	0.0032	0.0934	0.0014	1367	17	1495	28	9%
045.4.11	2.834	0.086	0.2188	0.004	0.0948	0.0019	1276	21	1523	38	19%

045.4.12	3.02	0.14	0.2247	0.0035	0.0987	0.0033	1307	18	1599	62	22%
045.4.13	3.41	0.11	0.2618	0.004	0.0959	0.0024	1499	20	1545	47	3%
045.4.14	2.68	0.036	0.2011	0.0017	0.0934	0.0016	1181.2	9.1	1495	33	27%
045.4.15	3.578	0.068	0.2716	0.0028	0.09616	0.0016	1549	14	1550	31	0%
045.4.16	3.548	0.08	0.2696	0.0038	0.0968	0.0016	1539	19	1563	31	2%
045.4.17	3.184	0.052	0.2455	0.0026	0.0953	0.0014	1415	13	1533	28	8%
045.4.18	2.75	0.045	0.1949	0.0016	0.0938	0.0015	1147.9	8.7	1503	30	31%
045.4.19	3.611	0.064	0.2716	0.0029	0.0958	0.0018	1549	15	1543	35	0%
045.4.20	3.537	0.071	0.2511	0.0031	0.0977	0.0019	1444	16	1580	36	9%
045.4.21	3.046	0.15	0.2154	0.0063	0.099	0.0022	1258	33	1605	42	28%
045.4.22	3.509	0.071	0.2685	0.0056	0.09618	0.0015	1533	28	1550	29	1%
045.4.23	3.205	0.074	0.2277	0.0036	0.1004	0.0024	1322	19	1631	45	23%
045.4.24	3.332	0.089	0.234	0.0029	0.0954	0.0023	1355	15	1535	45	13%
045.4.25	3.57	0.09	0.2671	0.0028	0.0954	0.0025	1526	14	1535	49	1%
045.4.26	3.551	0.062	0.27	0.0027	0.0967	0.0019	1541	14	1561	37	1%
045.4.27	2.415	0.76	0.1827	0.042	0.0979	0.0038	1080	230	1584	73	47%
045.4.28	3.243	0.13	0.2443	0.0056	0.0973	0.0047	1409	29	1572	91	12%
045.4.29	3.306	0.058	0.2511	0.0037	0.0959	0.0016	1444	19	1545	31	7%
045.4.30	3.331	0.072	0.2386	0.0041	0.09591	0.0014	1379	21	1545	28	12%
045.4.31	4.16	0.19	0.2388	0.0044	0.1288	0.007	1380	23	2081	96	51%
045.5.01	3.625	0.12	0.2727	0.009	0.09666	0.00047	1554	46	1559.8	9.5	0%
045.5.02	3.684	0.12	0.2766	0.0092	0.09653	0.00048	1574	46	1557.3	9.7	-1%
045.5.03	2.169	0.073	0.1675	0.0056	0.09425	0.00052	998	31	1512	11	34%
045.5.04	3.417	0.11	0.2596	0.0085	0.09568	0.00044	1488	44	1540.7	9.1	3%
045.5.05	-0.00155	0.00021	-0.0000217	0.0000029	0.5199	0.0034					
045.5.06	3.743	0.14	0.2823	0.011	0.09667	0.00054	1603	55	1560	11	-3%
045.5.07	-0.001011	0.000064	-0.00001293	0.00000081	0.5684	0.0039					
045.5.08	3.56	0.12	0.27	0.0098	0.09587	0.00048	1541	50	1544.4	9.8	0%

045.5.09	-0.000868	0.000058	-0.00001069	0.00000071	0.591	0.0046					
045.5.10	3.457	0.11	0.2631	0.0085	0.09509	0.00046	1506	43	1529	9.5	2%
045.5.11	3.448	0.11	0.2629	0.0087	0.09505	0.00044	1505	44	1528.2	9.1	2%
045.5.12	-0.00186	0.0003	-0.0000258	0.0000041	0.5223	0.0038					
045.5.13	3.367	0.11	0.2566	0.0084	0.09523	0.00044	1472	43	1531.8	9.1	4%
045.5.14	3.525	0.11	0.2673	0.0086	0.09601	0.00048	1527	44	1547.1	9.8	1%
045.5.15	-0.000371	0.000033	-0.00000503	0.00000042	0.5349	0.0049					
045.5.16	3.548	0.11	0.2679	0.0087	0.09621	0.00047	1530	44	1551	9.6	1%
045.5.17	3.511	0.11	0.2665	0.0086	0.09554	0.00046	1523	44	1537.9	9.5	1%
045.5.18	3.274	0.1	0.25012	0.0081	0.09496	0.00045	1439	42	1526.4	9.3	6%
045.5.19	3.462	0.11	0.2628	0.0088	0.09554	0.00043	1504	45	1537.9	8.9	2%
045.5.20	3.544	0.12	0.2658	0.0091	0.09664	0.0005	1519	46	1559	10	3%

Table 2: Lu-Hf data generated for this study.

Sample: FOG01

Grain ID	*207Pb/206Pb Age (Ma)*	*± 1σ (Ma)*	*Disc (%)*	*176Hf/177Hf*	*± 1SE(abs)*	*176Lu/177Hf*	*176Yb/177Hf*	*εHf (t)*	*εHf ± 1SE*	*TDM Crustal (Ga)*
FOG01.1.01	1627	50	10%	0.281733	0.000037	0.001096	0.03765	-1.03	1.30	2.95
FOG01.1.02	1566	41	0%	0.281702	0.000056	0.000576	0.01899	-3.52	1.96	3.19
FOG01.1.03	1569	37	-1%	0.28172	0.000039	0.000663	0.02112	-2.81	1.37	3.11
FOG01.1.04	1565	37	0%	0.281782	0.000044	0.000872	0.0264	-0.70	1.54	2.88
FOG01.1.05	1807	41	22%	0.281731	0.000058	0.000676	0.0217	2.98	2.03	2.62
FOG01.1.06	1556	39	64%	0.281694	0.000051	0.002108	0.0733	-4.03	1.79	3.24
FOG01.1.07	2742	62	63%	0.281707	0.000052	0.00096	0.0328	23.62	1.82	0.82
FOG01.1.08	1587	36	21%	0.281725	0.000044	0.00129	0.043	-2.22	1.54	3.06
FOG01.1.09	1587	36	4%	0.28173	0.000046	0.001138	0.03831	-2.05	1.61	3.04
FOG01.1.10	1787	35	62%	0.281771	0.000044	0.002047	0.0655	3.95	1.54	2.50

FOG01.1.11	3766	71	163%	0.28167	0.0001	0.001855	0.0581	46.39	3.50	-1.32
FOG01.1.12	1605	38	17%	0.281717	0.000057	0.001683	0.06097	-2.10	2.00	3.05
FOG01.1.13	1722	40	74%	0.281719	0.000073	0.001558	0.05086	0.62	2.56	2.83
FOG01.1.14	1543	35	1%	0.28171	0.000041	0.000563	0.01622	-3.75	1.44	3.20
FOG01.1.15	3126	86	91%	0.281688	0.000057	0.001312	0.0442	31.91	2.00	0.07
FOG01.1.16	1687	36	15%	0.281727	0.000052	0.000885	0.0281	0.11	1.82	2.86
FOG01.1.17	1625	43	34%	0.281784	0.000032	0.000861	0.0302	0.73	1.12	2.76
FOG01.1.18	1562	35	-1%	0.281709	0.000056	0.000687	0.0206	-3.36	1.96	3.17
FOG01.1.19	1871	46	55%	0.281671	0.000057	0.00152	0.051	2.31	2.00	2.73
FOG01.1.20	2171	67	61%	0.281699	0.000059	0.001129	0.0357	10.16	2.07	2.03
FOG01.1.21	1596	36	5%	0.281724	0.000075	0.001088	0.0347	-2.06	2.63	3.04
FOG01.1.22	1543	41	3%	0.28176	0.000042	0.0008	0.0236	-1.98	1.47	3.00
FOG01.1.23	1601	53	11%	0.281729	0.000056	0.001709	0.0555	-1.77	1.96	3.02
FOG01.1.24	1656	47	-2%	0.281753	0.00006	0.00128	0.0389	0.33	2.10	2.82
FOG01.1.25	1653	37	22%	0.281715	0.000071	0.001133	0.0368	-1.08	2.49	2.97
FOG01.1.26	1562	39	4%	0.281735	0.000053	0.00098	0.03081	-2.43	1.86	3.06
FOG01.1.27	1653	37	41%	0.281697	0.000056	0.00162	0.056	-1.72	1.96	3.04
FOG01.1.28	1627	45	35%	0.281719	0.000039	0.001898	0.0602	-1.53	1.37	3.01
FOG01.1.29	1553	45	5%	0.281716	0.000044	0.00042	0.01189	-3.31	1.54	3.16
FOG01.1.30	2327	53	37%	0.281757	0.000065	0.001391	0.0459	15.80	2.28	1.48
FOG01.1.31	2011	67	67%	0.281736	0.000061	0.001553	0.0494	7.81	2.14	2.20
FOG01.1.32	1578	35	1%	0.281709	0.000041	0.000931	0.02815	-3.00	1.44	3.14
FOG01.1.33	1568	41	1%	0.281764	0.00004	0.00074	0.0218	-1.27	1.40	2.94
FOG01.1.34	1564	37	-1%	0.281727	0.000055	0.000923	0.02641	-2.67	1.93	3.09
FOG01.1.35	1546	37	1%	0.281702	0.000052	0.001061	0.0315	-3.97	1.82	3.22
FOG01.1.36	1572	42	14%	0.281746	0.000065	0.000942	0.0273	-1.82	2.28	3.00
FOG01.1.37	1555	37	3%	0.281752	0.000045	0.000751	0.0224	-1.99	1.58	3.01
FOG01.1.38	1645	39	12%	0.281666	0.00005	0.00044	0.0134	-3.00	1.75	3.18
FOG01.1.39	1552	37	10%	0.281782	0.00006	0.001021	0.0285	-0.99	2.10	2.90
FOG01.1.40	1605	42	11%	0.281758	0.000049	0.000766	0.0214	-0.65	1.72	2.89

FOG01.3.01	1595	95	15%	0.28173	0.000027	0.001351	0.04697	-1.89	0.95	2.42
FOG01.3.02	1547	96	-3%	0.28171	0.000019	0.000592	0.0196	-3.68	0.67	2.50
FOG01.3.03	1586	95	-1%	0.281692	0.000025	0.0009321	0.03245	-3.44	0.88	2.51
FOG01.3.04	1660	100	9%	0.281736	0.000023	0.001082	0.03783	-0.21	0.81	2.36
FOG01.3.05	1820	110	43%	0.281717	0.000026	0.001466	0.0519	2.75	0.91	2.30
FOG01.3.06	1780	110	11%	0.281705	0.000027	0.000908	0.0344	1.41	0.95	2.35
FOG01.3.07	2390	120	50%	0.28171	0.00003	0.001729	0.0681	15.53	1.05	1.91
FOG01.3.08	1548	94	-3%	0.281705	0.000024	0.000801	0.03027	-3.84	0.84	2.51
FOG01.3.09	1551	98	-2%	0.281702	0.000021	0.000728	0.02815	-3.88	0.74	2.51
FOG01.3.10	1580	100	-1%	0.28172	0.000022	0.0001021	0.00459	-2.58	0.77	2.45
FOG01.3.11	1568	97	5%	0.281712	0.000028	0.001132	0.04536	-3.14	0.98	2.48
FOG01.3.12	1558	95	-3%	0.281703	0.000025	0.000828	0.03221	-3.69	0.88	2.50
FOG01.3.13	1570	98	-13%	0.281742	0.00003	0.00138	0.0561	-2.04	1.05	2.41
FOG01.3.14	1579	94	-1%	0.281725	0.000029	0.000964	0.03776	-2.44	1.02	2.44
FOG01.3.15	1907	98	19%	0.281696	0.000026	0.00096	0.03586	3.98	0.91	2.29
FOG01.3.16	1673	95	9%	0.281725	0.000028	0.001057	0.0427	-0.31	0.98	2.38
FOG01.3.17	1591	95	9%	0.281701	0.000025	0.000855	0.03414	-3.01	0.88	2.49
FOG01.3.18	1496	95	12%	0.281702	0.000029	0.001134	0.04501	-5.13	1.02	2.55
FOG01.3.19	2990	140	70%	0.281723	0.000022	0.000917	0.0338	29.93	0.77	1.43
FOG01.3.20	2380	250	38%	0.281716	0.000039	0.001155	0.0448	15.50	1.37	1.91

Sample: PGE01

Grain ID	*207Pb/206Pb Age (Ma)*	*± 1σ (Ma)*	*Disc (%)*	*176Hf/177Hf*	*± 1SE(abs)*	*176Lu/177Hf*	*176Yb/177Hf*	*εHf (t)*	*εHf ± 1SE*	*TDM Crustal (Ga)*
PGE01.1.01	1570	66	-2%	0.281825	0.000043	0.000427	0.0128	0.49	1.51	2.25
PGE01.1.02	1555	55	-1%	0.281819	0.00006	0.00092	0.027	-0.57	2.10	2.30
PGE01.1.03	1563	64	-1%	0.281795	0.000031	0.000794	0.0239	-1.12	1.09	2.34
PGE01.1.04	1551	49	-2%	0.281876	0.00005	0.000835	0.0252	1.45	1.75	2.17
PGE01.1.05	1614	47	4%	0.281807	0.000053	0.001023	0.03029	0.19	1.86	2.30
PGE01.1.06	1597	47	-2%	0.281851	0.000043	0.000917	0.0276	1.49	1.51	2.20

PGE01.1.07	1561	62	-1%	0.281826	0.000062	0.000795	0.0236	-0.06	2.17	2.28
PGE01.1.08	1642	46	4%	0.281834	0.000056	0.000846	0.0253	1.96	1.96	2.21
PGE01.1.09	1564	48	-1%	0.281844	0.000054	0.000847	0.0254	0.59	1.89	2.24
PGE01.1.10	1549	59	-2%	0.281845	0.000041	0.00117	0.0343	-0.04	1.44	2.27
PGE01.1.11	1561	56	3%	0.281861	0.000046	0.000944	0.0282	1.02	1.61	2.21
PGE01.1.12	1570	60	1%	0.281863	0.00005	0.000822	0.0245	1.42	1.75	2.19
PGE01.1.13	1543	45	-1%	0.281852	0.000048	0.000821	0.0244	0.44	1.68	2.23
PGE01.1.14	1555	57	0%	0.281836	0.000048	0.000544	0.0159	0.42	1.68	2.24
PGE01.1.15	1574	46	0%	0.281782	0.000062	0.000747	0.0226	-1.29	2.17	2.36
PGE01.1.16	1566	46	-1%	0.281801	0.000052	0.000979	0.0295	-1.03	1.82	2.34
PGE01.1.17	1537	49	-1%	0.281823	0.00004	0.000906	0.0271	-0.81	1.40	2.31
PGE01.1.18	1559	49	0%	0.281827	0.000047	0.001019	0.0299	-0.30	1.65	2.29
PGE01.1.19	1564	41	0%	0.281809	0.000053	0.001367	0.0404	-1.20	1.86	2.35
PGE01.1.20	1563	52	0%	0.281798	0.000059	0.000875	0.02645	-1.10	2.07	2.34
PGE01.1.21	1576	52	0%	0.281817	0.000045	0.000748	0.0223	0.00	1.58	2.28
PGE01.1.22	1568	54	-1%	0.281781	0.000035	0.000779	0.02385	-1.49	1.23	2.37
PGE01.1.23	1563	64	2%	0.281865	0.000049	0.000827	0.02478	1.33	1.72	2.19
PGE01.1.24	1564	56	1%	0.281812	0.000045	0.000812	0.02447	-0.51	1.58	2.31
PGE01.1.25	1566	50	0%	0.281809	0.000045	0.000773	0.02328	-0.53	1.58	2.31
PGE01.1.26	1557	53	-1%	0.281826	0.00006	0.000667	0.02	-0.02	2.10	2.27
PGE01.1.27	1559	53	0%	0.281837	0.000052	0.0009	0.0269	0.17	1.82	2.26
PGE01.1.28	1621	65	3%	0.281823	0.000056	0.000758	0.0221	1.20	1.96	2.24
PGE01.1.29	1563	39	0%	0.281838	0.000052	0.001478	0.04499	-0.31	1.82	2.29
PGE01.1.30	1609	38	1%	0.281773	0.00005	0.001533	0.0453	-1.68	1.75	2.42
PGE01.1.31	1606	55	4%	0.281844	0.000053	0.000752	0.02279	1.62	1.86	2.20
PGE01.1.32	1568	54	0%	0.281848	0.000042	0.0009	0.0281	0.76	1.47	2.23
PGE01.1.33	1539	49	-1%	0.281828	0.000045	0.001085	0.0337	-0.78	1.58	2.30
PGE01.1.34	1631	48	11%	0.281804	0.000057	0.00081	0.0243	0.69	2.00	2.28
PGE01.1.35	1543	65	-1%	0.281835	0.000051	0.001403	0.042	-0.77	1.79	2.31
PGE01.1.36	1580	54	1%	0.281814	0.000049	0.000756	0.0233	-0.03	1.72	2.29
PGE01.1.37	1566	50	4%	0.281821	0.000035	0.00087	0.0267	-0.21	1.23	2.29

Sample: CUG01

Grain ID	*207Pb/206Pb Age (Ma)*	*± 1σ (Ma)*	*Disc (%)*	*176Hf/177Hf*	*± 1SE(abs)*	*176Lu/177Hf*	*176Yb/177Hf*	*εHf (t)*	*εHf ± 1SE*	*TDM Crustal (Ga)*
CUG01.2.01	1555	86	6%	0.281802	0.000027	0.001023	0.0378	-0.49	0.95	2.33
CUG01.2.02	320	140	-2%	0.282635	0.000019	0.0013	0.0466	1.29	0.67	1.22
CUG01.2.03	1525	46	4%	0.281811	0.000029	0.001255	0.0494	-1.08	1.02	2.34
CUG01.2.04	1507	46	9%	0.281815	0.000025	0.00095	0.03539	-1.36	0.88	2.33
CUG01.2.05	1517	52	1%	0.281883	0.000059	0.00151	0.0566	1.58	2.07	2.18
CUG01.2.06	1515	42	6%	0.281797	0.000027	0.001282	0.0485	-1.45	0.95	2.37
CUG01.2.07	1551	57	3%	0.28221	0.00092	0.001219	0.0465	12.95	32.20	1.43
CUG01.2.08	1636	24	-13%	0.281813	0.000017	0.00188	0.0734	-0.34	0.60	2.34
CUG01.2.09	450	210	-52%	0.282548	0.000022	0.001396	0.0551	-2.06	0.77	1.42
CUG01.2.10	490	700	-93%	0.282808	0.000028	0.000372	0.01158	6.51	0.98	0.85
CUG01.2.11	210	180	22%	0.282554	0.000029	0.001154	0.0445	-2.46	1.02	1.42
CUG01.2.12	440	200	-89%	0.282825	0.000034	0.00157	0.0569	6.29	1.19	0.84
CUG01.2.13	1523	46	7%	0.281816	0.000025	0.001915	0.0727	-1.36	0.88	2.37
CUG01.2.14	1591	53	2%	0.281801	0.000031	0.00099	0.0404	-1.99	1.09	2.37
CUG01.2.15	1533	36	5%	0.28196	0.00019	0.00149	0.057	2.67	6.65	2.06
CUG01.2.16	2424	65	-6%	0.281144	0.000026	0.000411	0.0154	-4.43	0.91	3.22
CUG01.2.17	280	1010	-127%	0.282879	0.000026	0.00159	0.0573	25.27	0.91	0.23
CUG01.2.18	1616	49	-5%	0.2799	0.0061	0.00219	0.092	-69.72	213.50	6.55
CUG01.2.19	230	140	25%	0.282808	0.000027	0.001122	0.0439	7.40	0.95	0.83
CUG01.2.20	1533	65	4%	0.281847	0.000031	0.001054	0.04088	-1.12	1.09	2.29
CUG01.2.21	1493	63	4%	0.281822	0.000025	0.00141	0.0543	-2.06	0.88	2.36
CUG01.2.22	290	140	-5%	0.282835	0.000077	0.001928	0.0662	7.47	2.70	0.80
CUG01.2.23	1559	53	2%	0.281825	0.000025	0.001568	0.0585	-1.34	0.88	2.34
CUG01.2.24	1525	62	1%	0.281827	0.000026	0.00133	0.04981	-1.63	0.91	2.34
CUG01.2.25	1563	49	2%	0.281854	0.000024	0.001097	0.0424	0.18	0.84	2.25

CUG01.2.26	1593	36	0%	0.281813	0.000022	0.001745	0.0678	-1.41	0.77	2.37
CUG01.2.27	1513	36	4%	0.281821	0.000029	0.001529	0.05826	-1.61	1.02	2.35
CUG01.2.28	340	130	-16%	0.282443	0.000028	0.000277	0.01126	-6.66	0.98	1.67
CUG01.2.29	1627	37	-39%	0.281873	0.000023	0.001507	0.0571	2.13	0.81	2.18
CUG01.2.30	1519	64	5%	0.281833	0.000024	0.001441	0.0542	-0.21	0.84	2.30
CUG01.2.31	1549	43	1%	0.281826	0.00003	0.00162	0.06	-1.40	1.05	2.34
CUG01.2.32	1584	55	3%	0.281818	0.000025	0.001744	0.0627	-1.55	0.88	2.36
CUG01.2.33	1564	35	-6%	0.281818	0.000027	0.00167	0.0645	-0.90	0.95	2.34

Sample: 042

Grain ID	*207Pb/206Pb Age (Ma)*	*± 1σ (Ma)*	*Disc (%)*	*176Hf/177Hf*	*± 1SE(abs)*	*176Lu/177Hf*	*176Yb/177Hf*	*εHf (t)*	*εHf ± 1SE*	*TDM Crustal (Ga)*
042.4.01	1545	45	1%	0.281815	0.000026	0.000335	0.01259	-0.33	0.91	2.28
042.4.02	1653	33	12%	0.281869	0.000041	0.000465	0.01665	3.86	1.44	2.10
042.4.03	1519	56	6%	0.28187	0.000031	0.000702	0.02666	0.67	1.09	2.20
042.4.04	1549	35	1%	0.281814	0.000031	0.000452	0.01689	-0.40	1.09	2.29
042.4.05	1557	29	-2%	0.281869	0.000039	0.0008055	0.03135	1.36	1.37	2.18
042.4.06	1528	36	4%	0.281853	0.000031	0.000506	0.0186	0.46	1.09	2.22
042.4.07	1517	24	-4%	0.28188	0.000033	0.000994	0.03605	0.68	1.16	2.19
042.4.08	1580	42	31%	0.281857	0.000046	0.000955	0.0368	1.29	1.61	2.20
042.4.09	1553	27	2%	0.28188	0.000035	0.001155	0.045	1.30	1.23	2.18
042.4.10	1527	38	7%	0.282685	0.000091	0.001653	0.051	28.79	3.19	0.38
042.4.11	1566	39	53%	0.28194	0.000045	0.001209	0.0398	3.66	1.58	2.04
042.4.12	1513	32	16%	0.281879	0.000037	0.0006747	0.02513	0.88	1.30	2.18
042.4.13	1504	26	11%	0.281863	0.00003	0.0006195	0.01875	0.17	1.05	2.22
042.4.14	1557	53	0%	0.282003	0.000064	0.000983	0.037	5.93	2.24	1.89
042.4.15	1452	40	15%	0.282408	0.000069	0.000569	0.0203	18.40	2.42	1.00
042.4.16	323	35	-6%	0.282384	0.000031	0.00496	0.1349	-8.15	1.09	1.83
042.4.17	1541	37	-3%	0.281869	0.000038	0.001234	0.0455	0.57	1.33	2.22
042.4.18	1564	52	4%	0.281913	0.000039	0.000954	0.03461	2.92	1.37	2.09

042.4.19	1536	28	2%	0.282027	0.000047	0.00113	0.0436	6.17	1.65	1.86
042.4.20	1519	44	-2%	0.281915	0.000045	0.000536	0.01992	2.43	1.58	2.08
042.4.21	1559	39	0%	0.281884	0.00003	0.000956	0.0367	1.78	1.05	2.16
042.4.22	1572	41	4%	0.281866	0.000035	0.000757	0.0289	1.64	1.23	2.18
042.4.23	1555	43	6%	0.281824	0.000029	0.000891	0.0343	-0.37	1.02	2.29
042.4.24	1497	37	13%	0.28197	0.00003	0.000567	0.0199	3.86	1.05	1.98
042.4.25	383	62	5%	0.282381	0.000034	0.00327	0.0915	-6.70	1.19	1.78

Sample: 045

Grain ID	*207Pb/206Pb Age (Ma)*	*± 1σ (Ma)*	*Disc (%)*	*176Hf/177Hf*	*± 1SE(abs)*	*176Lu/177Hf*	*176Yb/177Hf*	*εHf (t)*	*εHf ± 1SE*	*TDM Crustal (Ga)*
045.4.01	1528	28	9%	0.281888	0.000026	0.000724	0.02728	1.48	0.91	2.15
045.4.02	1523	28	0%	0.281897	0.000033	0.00142	0.0555	0.98	1.16	2.18
045.4.03	1529	40	1%	0.28183	0.000037	0.000555	0.021	-0.38	1.30	2.27
045.4.04	1541	30	10%	0.281839	0.000031	0.00127	0.0498	-0.53	1.09	2.29
045.4.05	1549	29	6%	0.281866	0.000029	0.000695	0.02634	1.20	1.02	2.19
045.4.06	1528	26	48%	0.281915	0.000029	0.001534	0.0568	1.61	1.02	2.14
045.4.07	1551	39	0%	0.281875	0.000033	0.000748	0.0283	1.51	1.16	2.17
045.4.08	419	57	6%	0.282679	0.000096	0.00208	0.0706	4.89	3.36	1.07
045.4.09	1664	45	53%	0.281926	0.000063	0.00183	0.0617	4.61	2.21	2.06
045.4.10	1495	28	9%	0.281937	0.000048	0.001306	0.0494	1.91	1.68	2.10
045.4.11	1523	38	19%	0.281978	0.000074	0.0015	0.0581	3.77	2.59	2.00
045.4.12	1599	62	22%	0.281815	0.000031	0.0005956	0.022153	0.60	1.09	2.26
045.4.13	1545	47	3%	0.281881	0.000032	0.000508	0.01905	1.83	1.12	2.14
045.4.14	1495	33	27%	0.282014	0.000053	0.00082	0.0302	5.13	1.86	1.89
045.4.15	1550	31	0%	0.281889	0.000041	0.001836	0.073	0.85	1.44	2.21
045.4.16	1563	31	2%	0.28191	0.000021	0.00124	0.0475	2.50	0.74	2.11
045.4.17	1533	28	8%	0.281896	0.000032	0.000516	0.01873	2.09	1.12	2.12
045.4.18	1503	30	31%	0.281874	0.000026	0.0007165	0.02708	0.44	0.91	2.20
045.4.19	1543	35	0%	0.28183	0.000026	0.000682	0.0265	-0.20	0.91	2.27

045.4.20	1580	36	9%	0.28187	0.000039	0.000755	0.0293	1.96	1.37	2.16
045.4.21	1605	42	28%	0.281872	0.000039	0.00129	0.0496	2.01	1.37	2.18
045.4.22	1550	29	1%	0.281871	0.000025	0.000577	0.02202	1.52	0.88	2.17
045.4.23	1631	45	23%	0.281865	0.000038	0.000658	0.02485	3.02	1.33	2.13
045.4.24	1535	45	13%	0.281874	0.000033	0.000723	0.0285	1.14	1.16	2.18
045.4.25	1535	49	1%	0.281852	0.000031	0.000547	0.0206	0.54	1.09	2.22
045.4.26	1561	37	1%	0.281858	0.000035	0.000595	0.02283	1.28	1.23	2.19
045.4.27	1584	73	47%	0.281852	0.000033	0.0004737	0.01883	1.71	1.16	2.18
045.4.28	1572	91	12%	0.281803	0.000029	0.00096	0.0379	-0.81	1.02	2.33
045.4.29	1545	31	7%	0.281871	0.000029	0.000484	0.01808	1.50	1.02	2.16
045.4.30	1545	28	12%	0.281879	0.000027	0.00117	0.0463	1.08	0.95	2.19
045.4.31	2081	96	51%	0.281822	0.000027	0.00085	0.0328	11.27	0.95	1.95